PRESSURIZED HEAVY WATER REACTOR FUEL: INTEGRITY, PERFORMANCE AND ADVANCED CONCEPTS

The following States are Members of the International Atomic Energy Agency:

AFGHANISTAN
ALBANIA
ALGERIA
ANGOLA
ARGENTINA
ARMENIA
AUSTRALIA
AUSTRIA
AZERBAIJAN
BAHAMAS
BAHRAIN
BANGLADESH
BELARUS
BELGIUM
BELIZE
BENIN
BOLIVIA
BOSNIA AND HERZEGOVINA
BOTSWANA
BRAZIL
BRUNEI DARUSSALAM
BULGARIA
BURKINA FASO
BURUNDI
CAMBODIA
CAMEROON
CANADA
CENTRAL AFRICAN REPUBLIC
CHAD
CHILE
CHINA
COLOMBIA
CONGO
COSTA RICA
CÔTE D'IVOIRE
CROATIA
CUBA
CYPRUS
CZECH REPUBLIC
DEMOCRATIC REPUBLIC OF THE CONGO
DENMARK
DOMINICA
DOMINICAN REPUBLIC
ECUADOR
EGYPT
EL SALVADOR
ERITREA
ESTONIA
ETHIOPIA
FIJI
FINLAND
FRANCE
GABON
GEORGIA
GERMANY
GHANA
GREECE
GUATEMALA
HAITI
HOLY SEE
HONDURAS
HUNGARY
ICELAND
INDIA
INDONESIA
IRAN, ISLAMIC REPUBLIC OF
IRAQ
IRELAND
ISRAEL
ITALY
JAMAICA
JAPAN
JORDAN
KAZAKHSTAN
KENYA
KOREA, REPUBLIC OF
KUWAIT
KYRGYZSTAN
LAO PEOPLE'S DEMOCRATIC REPUBLIC
LATVIA
LEBANON
LESOTHO
LIBERIA
LIBYA
LIECHTENSTEIN
LITHUANIA
LUXEMBOURG
MADAGASCAR
MALAWI
MALAYSIA
MALI
MALTA
MARSHALL ISLANDS
MAURITANIA, ISLAMIC REPUBLIC OF
MAURITIUS
MEXICO
MONACO
MONGOLIA
MONTENEGRO
MOROCCO
MOZAMBIQUE
MYANMAR
NAMIBIA
NEPAL
NETHERLANDS
NEW ZEALAND
NICARAGUA
NIGER
NIGERIA
NORWAY
OMAN
PAKISTAN
PALAU
PANAMA
PAPUA NEW GUINEA
PARAGUAY
PERU
PHILIPPINES
POLAND
PORTUGAL
QATAR
REPUBLIC OF MOLDOVA
ROMANIA
RUSSIAN FEDERATION
RWANDA
SAN MARINO
SAUDI ARABIA
SENEGAL
SERBIA
SEYCHELLES
SIERRA LEONE
SINGAPORE
SLOVAKIA
SLOVENIA
SOUTH AFRICA
SPAIN
SRI LANKA
SUDAN
SWAZILAND
SWEDEN
SWITZERLAND
SYRIAN ARAB REPUBLIC
TAJIKISTAN
THAILAND
THE FORMER YUGOSLAV REPUBLIC OF MACEDONIA
TOGO
TRINIDAD AND TOBAGO
TUNISIA
TURKEY
UGANDA
UKRAINE
UNITED ARAB EMIRATES
UNITED KINGDOM OF GREAT BRITAIN AND NORTHERN IRELAND
UNITED REPUBLIC OF TANZANIA
UNITED STATES OF AMERICA
URUGUAY
UZBEKISTAN
VENEZUELA, BOLIVARIAN REPUBLIC OF
VIET NAM
YEMEN
ZAMBIA
ZIMBABWE

The Agency's Statute was approved on 23 October 1956 by the Conference on the Statute of the IAEA held at United Nations Headquarters, New York; it entered into force on 29 July 1957. The Headquarters of the Agency are situated in Vienna. Its principal objective is "to accelerate and enlarge the contribution of atomic energy to peace, health and prosperity throughout the world''.

IAEA-TECDOC-CD-1751

PRESSURIZED HEAVY WATER REACTOR FUEL: INTEGRITY, PERFORMANCE AND ADVANCED CONCEPTS

PROCEEDINGS OF THE TECHNICAL MEETINGS
HELD IN BUCHAREST, 24–27 SEPTEMBER 2012,
AND IN MUMBAI, 8–11 APRIL 2013

INTERNATIONAL ATOMIC ENERGY AGENCY
VIENNA, 2014

COPYRIGHT NOTICE

For further information on this publication, please contact:

Nuclear Fuel Cycle and Materials Section
International Atomic Energy Agency
Vienna International Centre
PO Box 100
1400 Vienna, Austria
Email: Official.Mail@iaea.org

Printed by the IAEA in Austria
September 2014

IAEA Library Cataloguing in Publication Data

Pressurized heavy water reactor fuel : integrity, performance and advanced concepts. — Vienna : International Atomic Energy Agency, 2014.
p. ; cm. — (IAEA-TECDOC-CD series, ISSN 1684–2073 ; no. 1751)
ISBN 978–92–0–158414–4
Includes bibliographical references.

1. Fuel burnup (Nuclear engineering). 2. Nuclear fuels. 3. Heavy water reactors. I. International Atomic Energy Agency. II. Series.

IAEAL 14–00930

FOREWORD

Seven Member States have operating pressurized heavy water reactors (PHWRs), and some of them are also planning new reactors of this type. The current type of PHWR uses natural uranium as the fuel and has an average burnup of 7000 MWd/t (megawatt days per metric tonne). To make these reactors economically competitive with other reactor types, the discharge burnup of PHWR fuel will need to be increased without affecting the integrity of the fuel pin and bundle. A significant increase in the discharge burnup of fuel is possible with the use of advanced fuel cycles in PHWRs. The advanced fuels can be slightly enriched uranium, reprocessed uranium from light water reactors, mixed oxide or thorium based fuels. At the same time, substantial savings in natural uranium resources can also be achieved through the possible extension of the discharge burnup of advanced fuels used in PHWRs without changing reactor hardware.

Following the recommendation of the Technical Working Group on Fuel Performance and Technology, two technical meetings were held: Technical Meeting on Fuel Integrity during Normal Operation and Accident Conditions in PHWRs, 24–27 September 2012, Bucharest, Romania; and Technical Meeting on Advanced Fuel Cycles in PHWRs, 8–11 April 2013, Mumbai, India. Their objective was to update information on the performance of PHWR fuels, the status and trends in the use of advanced fuels in PHWRs and the technical readiness for the deployment of such fuel cycles in these types of reactor. This publication contains the proceedings of the two technical meetings, including a record of the discussions held during the various technical sessions.

The IAEA wishes to thank Nuclearelectrica for hosting the meeting in Bucharest and Nuclear Power Corporation of India Limited for hosting the meeting in Mumbai. The IAEA is also grateful to all the participants for their contributions. The IAEA officer responsible for this publication was U. Basak of the Division of Nuclear Fuel Cycle and Waste Technology.

EDITORIAL NOTE

This publication has been prepared from the original material as submitted by the contributors and has not been edited by the editorial staff of the IAEA. The views expressed remain the responsibility of the contributors and do not necessarily represent the views of the IAEA or its Member States.

Neither the IAEA nor its Member States assume any responsibility for consequences which may arise from the use of this publication. This publication does not address questions of responsibility, legal or otherwise, for acts or omissions on the part of any person.

The use of particular designations of countries or territories does not imply any judgement by the publisher, the IAEA, as to the legal status of such countries or territories, of their authorities and institutions or of the delimitation of their boundaries.

The mention of names of specific companies or products (whether or not indicated as registered) does not imply any intention to infringe proprietary rights, nor should it be construed as an endorsement or recommendation on the part of the IAEA.

The IAEA has no responsibility for the persistence or accuracy of URLs for external or third party Internet web sites referred to in this publication and does not guarantee that any content on such web sites is, or will remain, accurate or appropriate.

CONTENTS

SUMMARY..... 1

TECHNICAL MEETING ON FUEL INTEGRITY DURING NORMAL OPERATION AND ACCIDENT CONDITIONS IN PRESSURISED HEAVY WATER REACTORS

FUEL FABRICATION AND FUEL BEHAVIOUR DURING NORMAL OPERATION (Session 1)

Nuclear fuel fabrication in Romania..... 11
D. Dina
Using advanced fuel bundles in CANDU reactors..... 15
A. Rizoiu, G. Horhoianu, I. Prodea
Fuel behaviour during large breaks in the primary heat transport circuit..... 27
C. Zălog
A regulatory perspective on the establishment of fuel safety criteria for the large loss of coolant accident in CANDU pressurized heavy water reactors..... 39
A. El-Jaby
Slightly enriched uranium core burnup study in CANDU 6 reactor..... 49
I. Prodea

FUEL INTEGRITY DURING ACCIDENT CONDITION (Session 2)

Fuel integrity assessment at KANUPP..... 61
F. Tasneem and S. E. Abbasi
Fuel cooling in absence of forced flow at shutdown condition with PHTS partially drained..... 73
L.Parasca, D. L. Pecheanu
Degradation mechanism of Zr-4 cladding during high temperature steam oxidation..... 87
T. Mele, D. Ohai
Deformation and ballooning of unirradiated Indian PHWR fuel cladding under transient heating condition..... 97
T. K. Sawarn, S. Banerjee, K. M. Pandit, S. Anantharaman, D. N. Sah

POST IRRADIATION EXAMINATION (Session 3)

Irradiation behaviour of PHWR type fuel elements containing UO_2 and $(Th,U)O_2$ pellets..... 111
G. Horhoianu, G. Olteanul, D.V. Ionescu
Application of sipping and visual inspection systems for the evaluation of spent fuel bundle integrity..... 121
Y. C. Kim, J. C.Shin, S. K. Woo, C. H. Park, T. Y. Choi
Post irradiation examination of experomental CANDU fuel elements irradiated in TRIGA-SSR reactor..... 129
S. Ionescu, M. Mincu, O. Uta, C. Gentea, M. Parvan, L. Dinu
Deformation and ballooning of irradiated PHWR fuel pins subjected to isothermal heating..... 141
P. Mishra, D.N. Sah, S. Anantharaman
FIPRED (fission product release from debris bed) Romanian project..... 153

D. Ohai, I. Dumitrescu, T. Meleg
Fission product inventory in CANDU fuel……...……. 163
C. Zălog, N. Baraitaru

FUEL CODES AND SAFETY (Session 4)

Design and performance of slightly enriched uranium fuel bundles
in Indian PHWRs…….……..…... 175
R. M. Tripathi, P. N. Prasad, A. Chauhan
CRP FUMEX PHWR cases a BaCo code point of view and its results……..…….. 183
A. C. Marino.
Three dimensional finite element modelling of a CANDU fuel pin
using the ANSYS finite element package……..…….…... 201
A. F. Williams

TECHNICAL MEETING ON ADVANCED FUEL CYCLES FOR PRESSURIZED HEAVY WATER REATOR

ADVANCED FUEL CYCLE CONCEPTS (Session 1)

Revisiting the experience with advanced fuels in the Argentine
heavy water reactors……..……. 215
L. Alvarez, A. Bussolini, P. Tripodi
Development of advanced 37-element fuel for CHF enhancement…….…..…. 225
J. H. Park, J. Yeobjung
Advanced fuel bundles for PHWRs……..……. 237
R. M. Tripathi, P. N. Prasad, A. Chauhan
INR recent contributions to Thorium-based fuel using in CANDU reactors…… 247
I. Prodea, C. A. Mărgeanu, A. Rizoiu, G. Olteanu
Utilisation of Thorium in AHWRs…….…… 261
V. Shivakumar, V. Vaze, V. Joemon, P. K. Vijayan

FUEL DESIGN AND DEVELOPMENT (Session 2)

Preliminary design studies for utilization of slightly enriched uranium
in ATUCHA-2 fuel rods……. 269
A. A. Bussolini, P. Tripodi, L. Alvarez
CARA fuel: an advanced proposal for PHWR…….…. 283
A. C. Marino, D. O. Brasnarof, C. Munoz, G. Demarco
H. Agueda, L. Juanico, J. Lago Fernandez, H. Lestani
J. E. Bergallo, G. La Mattina

FUEL FABRICATION AND PERFORMANCE (Session 3)

SEU fuel fabrication for PHWR 220 units - manufacturing experience……..……..…… 313
U. K. Aror, Sheela, N. Saibab
Research on sol–gel microsphere pelletization of UO_2 for PHWR fuel
in Indonesia……..……...… 319

Performance of slightly enriched Uranium bundles loaded in MAPS-2 equilibrium core…….. 329
S. Rathakrishnan, J. K. Sahu, R. George, D. Rajendran, R. K.Gupta, T. J. Kotteeswaran
Utilization of recycled Uranium in Indian PHWRs…….. 345
S. Mishra, M. V. Parikh, S. Ray, A. S. Pradhan, H. P. Rammohan
Status of CANDU6 fuel in KNF……. 357
K. Suk, B. J. Lee, C. H. Park

POST IRRADIATION EXAMINATION (Session 4)

Metallographic studies on irradiated PHWR fuels…….. 367
P. Mishra, V. P. Jathar, J. Banerjee S. Anantharaman
Post irradiation examination of Th-Pu and U-Pu MOX fuels……... 377
S. Anantharaman, P. Mishra, V. P.Jathar, R. S. Shriwastaw, H. N. Singh, P. M. Satheesh, P. B. Kondejkar, G. K.Mallik, J. L. Singh
Mechanical property evaluation of high burnup PHWR fuel clads…….. 389
P. K. Shah, R. S. Shriwastawa, J. S. Dubey, S. Anantharaman

ABBREVIATIONS…….. 397

LIST OF PARTICIPANTS…….. 399
.

SUMMARY

1. INTRODUCTION

Presently almost 45 pressurized heavy water reactors (PHWRs) are operating in seven countries, using mainly natural uranium fuel. These reactors operate with a fuel discharge burn-up of approximately 7000 MWd/tU. The fuel designs, fabrication facilities, reactor operation and spent fuel management are tailored to these conditions. However there is increased interest among some Member States of the International Atomic Energy Agency, namely Canada, India, Argentina, China, Republic of |Korea, Romania to introduce advanced fuels and extend the discharge burn-up of fuel assemblies in PHWRs. Substantial savings in natural uranium resources could also be achieved by extending the discharge burn-up of advanced fuels used in PHWRs without substantial changes to the hardware of the reactor.

To allow higher burn-up, the fissile content of the fuel is increased compared to natural uranium. This can lead to higher initial power, larger power ramps on refuelling and other challenging conditions for the fuel, possibly requiring changes to the design of the fuel pellets and fuel elements in order to maintain low fuel failure rates. Some lessons can be learned from the development of light water reactor (LWR) fuel, but PHWR fuels have many unique aspects to consider, such as collapsible cladding, high linear heat rating, on-power fuelling, and the absence of plenum volume. All these factors are likely to affect the integrity of fuel pin & bundle which in turn may affect the safe and economical operation of the power plants. However the integrity of fuel pin and bundle could be maintained even at high burn up operation by incorporating fuels with innovative fuel pellet design to accommodate fission gas releases, fuel swelling etc.

In some Member States, research and development activities are being carried out on the use of advanced fuels based on slightly enriched uranium (SEU) or reprocessed uranium (RepU) from LWRs or mixed uranium plutonium oxide (MOX) fuel or thorium based fuels.

In India, fuel bundle assemblies using advanced fuels based on enriched uranium, MOX and thorium have been designed, fabricated and loaded in commercial reactors. Thorium-based bundles have been loaded as a part of initial fuel charges for flux flattening for new units. Natural U - Pu MOX fuel bundles and 0.9% enriched uranium fuel bundles have been loaded as lead assemblies in operating units. Fuel pins with different MOX types were also loaded in research reactors for test irradiation. In China, natural uranium equivalent (NUE) fuel assemblies made from reprocessed uranium were loaded in two channels of a commercial PHWR as a demonstration. In Romania, experimental fuel elements containing thorium and enriched uranium were tested in a research reactor. In Canada, advanced fuels such as enriched uranium, MOX, reprocessed uranium and thoria have also been tested in research reactors and in the NPD power reactor, while advanced thermal hydraulic designs have been demonstrated in commercial power reactors. Atucha-1 NPP in Argentina is operating with full core loading of an advanced fuel cycle since the year 2000. An increase of the U enrichment from natural uranium to 0.85 % U-235 in this reactor increased the average discharge burn-up of the fuel from 5900 MWd/tU to more than 11 000 MWd/tU. The main consequence of this improvement is an important reduction of the fuel consumption and the cost of power generation.

Two Technical Meetings were proposed to the Agency by the Technical Working Group on Water Reactor Fuel Performance and Technology (TWGFPT) at its meeting in 2011 with the objective to update the information on the performances of PHWR fuels, the

status and trends in the use of advanced fuels in PHWRs and the technical readiness for the deployment of such fuel cycles in PHWRs.

The first meeting on "Fuel integrity during normal operation and accident conditions in PHWRs" was held in Bucharest, Romania from 24 to 27 September, 2012 and the second meeting on "Advanced fuels for pressurized heavy water reactors" was held in Mumbai, India from April 8 to 11, 2013.

The papers presented during the various technical sessions in the meetings have been compiled and documented in the form of this report which provides the proceedings of the two meetings.

2. FUEL INTEGRITY DURING NORMAL OPERATION AND ACCIDENT CONDITIONS IN PHWRs, BUCHAREST, ROMANIA, SEPTEMBER 24–27, 2012

2.1. Objective of the meeting

The major aim of the meeting was to understand the PHWR fuel behaviour under different operating conditions and also to generate database on the behaviour of fuel, cladding and fuel rods to understand and model the fuel pin behaviour under normal operation and accident conditions.

2.2. Meeting report

There were 24 participants from PHWR operating countries and 18 papers were presented in the meeting in four sessions covering the area of and covered fuel fabrication and fuel behaviour during normal operation, fuel integrity during accident condition, post irradiation examination and fuel codes and safety.

2.2.1. Session 1: Fuel fabrication and fuel behaviour during normal operation

In this session, 5 papers are listed & provided.

D. Dina (Romania) described the evolution of nuclear fuel manufacturing in Romania. Commercial production at Nuclear Fuel Plant – Pitesti (NFP) began in 1995, coinciding with the commissioning of the first CANDU unit at Cernavoda NPP. Since then, more than 110 000 CANDU fuel bundles have been delivered to Cernavoda NPP. The percentage of defective fuel is less than 0.09%. Encouraged by the good fuel performance achieved consistently by Cernavoda NPP, Romania is planning to complete the construction of two CANDU units on the Cernavoda site within the next decade.

A Rizoiu (Romania) presented the studies carried out using the computer Code DRAGON3.05E on the 43-element design with several fuel compositions, with the aim of assessing new reliable, economic and proliferation-resistant solution.

C Zalog (Romania) presented the methodology and results for a typical Design Basis Safety Analysis- Large LOCA with all safety system available

The paper presented by Mr. Ali El-Jabby (Canada) provided an overview of the Composite Analytical Approach for the Large LOCA analysis. This was followed by a discussion on the current status of LOCA safety margins and Design Basis Accident (DBA)

acceptance criteria, as well as the associated process to address the impact of adverse findings.

I. Prodea (Romania) presented the paper on Slightly Enriched Uranium (SEU) fuel with 1%wt ^{235}U to find out its suitability for use in CANDU reactors. The core fuel management characteristics with the use of SEU fuel in C-43 fuel bundle developed in INR Pitesti was compared with those of NU fuel in the standard 37-rod fuel bundle design.

2.2.2. Session 2: Fuel integrity during accident condition

4 papers were presented in this session.

T. Fatima (Pakistan) briefed about the fuel integrity assessment carried out at KANUPP and discussed the experiences in detecting and locating of defective fuels in the core.

L. Parasca (Romania) presented the results of the analysis performed to demonstrate fuel cooling in absence of forced flow at shut down condition with a partailly drained primary heat transport system.

T. Meleg (Romania) presented the results of isothermal oxidation tests on Zr-4 in steam-argon mixture. A theoretical model was proposed to describe the kinetic behaviour in the post-transition region more accurately. A thermo-gravimetric method to evaluate the average compressive stress developed in the oxide layer during the oxidation was proposed.

S. Anantharaman (India) presented the high temperature ballooning and deformation behavior of Indian PHWR cladding of Zircaloy-4. The details of the experimental procedure and the results obtained from the transient heating experiments carried out on internally pressurised fuel pins were presented
In his presentation,

2.2.3. *Session 3: Post Irradiation Examination*

6 papers were presented in this session.

G. Olteanu (Romania) presented the performance of the $(Th,U)O_2$ fuel element compared with UO_2 fuel element, both irradiated under similar conditions. Two elements were examined in Hot Cells of INR Pitesti. The results of this investigation like temperature-sensitive parameters were presented.

Yong-Chan KIM (Republic of Korea) presented the development of CANDU Spent Fuel Inspection Technology at KNF. Fuel inspection results carried out at Wolsung #2 and #4 was also presented.

S. Ionescu (Romania) presented the results of examinations performed in the Post Irradiation Examination Laboratory (PIEL) from INR Pitesti, on samples from a fuel element irradiated in TRIGA-SSR reactor.

P. Mishra (India) presented the study providing information on deformation and ballooning behaviour of irradiated PHWR fuel pin. The modes and mechanisms of cladding failure during ballooning were discussed.

D. Ohai (Romania) presented the scientific objectives and the main components of the FIPRED (Fission Product Release from Debris Bed) Romanian Project. It is used to evaluate

the post severe accident fission products release from debris bed under air ingress conditions, taking into account self disintegration of UO2 sintered pellets due to oxidation. The equipment, the experimental test matrix and the results obtained were also presented.

C. Zalog, (Romania) presented the work on the calculations for determining the fission products inventory and decay heat evolution within the spent fuel bundles stored in the bay. The calculation was done for a bay filled with fuel bundles up to its maximum capacity. The results obtained have provided a conservative estimation of the decay heat released and the expected temperature profile of water in the bay.

2.2.4. Session 4: Fuel codes and safety

3 papers were presented in this session.

R. M. Tripathi (India) presented the studies carried out on Slightly Enriched Uranium (SEU) with 0.9% 235 U by weight using the FUDA code (Fuel Design Analysis code). Thermo-mechanical analysis of fuel element having SEU material is carried out and the results were compared with that for similar fuel bundle element with natural uranium as fuel material.

A. C. MARINO (Argentina) presented thermo-mechanical simulation and analysis of PHWR fuel pin by CNEA developed BaCo code and also compared the results with other similar codes.

A.F. Williams (Canada) presented a 3-D thermo-mechanical model of CANDU fuel pin using ANSYS FEM (Finite Element Method) package, a deviation from the normal 2D axi-symmetric approaches to fuel modeling. The dependency of heat transfer between the pellets and cladding on both interface pressure and temperature, and the dependency of material properties of both the pellets and the sheath on temperature were considered by the model. The model also allows for the prediction of fuel pin bowing due to asymmetric thermal loads and fuel pin sagging due to overheating of the cladding, which may occur under accident conditions.

2.3. Technical visit

The visit to the Nuclear Fuel Plant – Pitesti belonging to Nuclearelectrica that fabricates fuel for Cernavoda NPP was arranged on the last day, 27th September, followed by a visit to the 14-MW TRIGA reactor–ICN and the associated PIE hotcells–SCN at Pitesti.

3. ADVANCED FUEL CYCLES FOR PRESSURIZED HEAVY WATER REATOR, MUMBAI, INDIA, APRIL 8–11, 2013.

3.1. Objective of the meeting

Research and Development is undergoing in some Member States on the use of advanced fuels based on uranium, uranium-plutonium and thorium fuels in PHWRs. The objective of the meeting is to update the information on the status and trends in the use of advanced fuels in PHWRs, their performances at high burnup and the technical readiness for the deployment of such fuel cycles in these types of reactor

3.2. Meeting report

The IAEA Technical Meeting on advanced fuel cycles in pressurized heavy water reactors was hosted by Nuclear Power Corporation of India Limiled (NPCIL) in Mumbai, India on 8–11 April 2013 with the participation of 11 members from the 6 PHWRs operating countries and 46 members from host country, India.

This meeting brought the PHWR fuel designers, manufacturers, quality inspectors, regulators, modellers, researches, safety analysts, reactor operators and post irradiation examiners together to share their knowledge and experience. 15 papers were presented in the meeting in five technical sessions.

3.2.1. Session 1: Advanced fuels for PHWRs

5 papers were presented in this session on the use of advanced fuels namely thorium, MOX and slightly enriched uranium (SEU) fuels in PHWRs.

L. Alvarez, Argentina presented a paper highlighting the use of SEU in Atucha-1. Information about the current performance of this fuel is also presented. The main consequence of the use of SEU is an important reduction of the fuel consumption and a positive impact on the reduction of the cost of power generation.

J.H.Park, ROK presented a paper on subchannel analysis to investigate the effect of the inner ring radius modification for the standard 37 element fuel bundle on the dry out power.

In his paper, R. M. Tripathi, India presented the Indian experience of advance PHWR fuels, i.e irradiation of thorium fuel bundles as a part of initial fuel charge in different units, the MOX-7 fuel bundle loading in KAPS-1 and the SEU fuel bundle loading in MAPS-2.

The paper presented by I. Prodea, Romania described the latest development to the thorium based fuel in CANDU reactors. In this paper, both lattice and CANDU core calculations using thorium fuels taking into account of the main neutron physics parameters of interest were described.

V. Shivakumar, India presented a paper on use of thorium based fuels such as (Th-Pu) MOX and (Th-U233) MOX fuels in advanced heavy water reactor (AHWR) being developed in India.

3.2.2. Session 2: Fuel design and development

2 papers were presented in this session on the design of SEU and new fuel element for reactors in Argentina.

A.A. Bussolini, Argentina presented a paper summarized the advantages of using SEU fuel. He also highlighted the design challenges and the calculations performed for a preliminary initial assessment of the fuel rod performance.

A.C. Marino, Argentina presented a paper on a new fuel element called CARA designed for two different types of heavy water reactors. This new element could match fuel requirements of Argentine HWRs namely, one CANDU and others Siemen’s design Atucha I and II.

3.2.3. Session 3: Fuel fabrication and performance experience

In this session, 5 papers were presented. One paper briefed the fabrication plan of modified 37-element fuel bundle for aged PHWRs. Three papers shared the fabrication and irradiation experience of advanced PHWR fuels namely SEU and RepU. One papper was on advanced fabrication concepts based on sol-gel route.

U.K.Arora, India presented the manufacturing experience of SEU fuel pellets and fuel elements for PHWRs. Fuel pellets were fabricated by modifying die design and optimizing compaction parameters. 51 fuel assemblies were dispatched to reactor site for testing.

M. Rachmawati, Indonesia presented a paper on the development of sol-gel microsphere pelletization technique for the fabrication of UO_2 fuel pellets using external gelation method fpr the preparation of microspheres.

S. Rathakrishnan, India presented the performance of 51 SEU fuel bundles used in operating PHWR in MAPS-2. Based on this experience, converting natural uranium core to SEU core by full core loading of SEU bundles in 220 MW_e PHWR has also been studied.

S. Mishra, India presented the analysis carried out for various possible fuel designs by mixing reprocessed PHWR uranium with reprocessed LWRs uranium in different proportions for utilization of recycled uranium.

C.K. Suk, Republic of Korea presented their experience on the manufacturing of CANDU 6 fuel in Kepco Nuclear Fuel (KNF). Some of the key manufacturing equipments were developed to improve productivity and quality.

3.2.4. Session 5: Post irradiation examination

There were 3 papers in this session which gave the experience of irradiation of advanced fuels namely ThO_2, MOX, SEU fuel bundles in commercial PHWRs in India. The fuels were irradiated to burnups of more than 20 GWd/TeU. One paper discussed the mechanical properties evaluation of clad material.

P. Mishra, India presented a paper based on post irradiation examination of natural UO2 fuels bundles discharged in the burnup range of 400–15 000 MW d/tU which included a few fuel pins. Major cause of fuel failure was identified as manufacturing related defects and handling defects.

S. Anantharaman, India presented a paper on post irradiation examinations of (Th-U)O2 and (Th-Pu)O2 fuels irradiated upto a nominal burnup of 10.2 GW.d/t in research reactor and reported that all the fuel pins were found to be intact after irradiation without any abnormal corrosion.

P.K.Shah, India presented a paper on the test procedure followed for the evaluation of mechanical properties of high burnup fuel clads. The results were also discussed based on the findings.

3.3. Conclusions

The meeting touched the efficient use of existing natural uranium fuel in PHWRs, structural modifications planned in fuel bundle designs to improve safety margins and use of advanced fuels like Th, SEU and MOX. Also the theoretical analysis to assess this and the fabrication methods to achieve this and also the operating and post irradiation experience were shared.

Development of the reliable advanced fuels will require concerted efforts on the part of the different agencies. Collaboration between countries is important and rewarding. In view of the commonality of problems and issues, sharing of information and experience on various aspects of fuel cycle could lead to quicker and less expensive redressals.

FUEL FABRICATION AND FUEL BEHAVIOUR DURING NORMAL OPERATION
(Session 1)

Chairman

N. BARAITALU
Romania

NUCLEAR FUEL FABRICATION IN ROMANIA

D. DINA
SN "Nuclearelectrica" SA,
Bucarest, Romania
Email: ddina@nuclearelectrica.ro

Abstract

This paper briefly describes the evolution of nuclear fuel manufacturing in Romania. Commercial production at Nuclear Fuel Plant – Pitesti (NFP) has started in 1995, in connection with commissioning of the first CANDU unit at Cernavoda NPP. Since then, more than 110, 000 CANDU fuel bundles have been delivered to the plant. As defective fuel represents less than 0.09% from the total, the fuel performance is very good.

1. INTRODUCTION

In the early 1970s, a political decision was taken in Romania to develop nuclear industry based on Canadian technology "CANDU". This decision was followed by consistent investments to develop techniques, technologies and equipments required for manufacturing the standard CANDU fuel bundle with 37- fuel elements.

Small scale production and testing of fuel elements begun in early 1980s at the Institute for Nuclear Power Reactors (INPR) at Piteşti. This made possible to start the mass production of fuel bundles towards the end of decade 1980s. A total of about 33, 000 fuel bundles was produced until 1990, when the production was stopped.

At the beginning of year 1992, the fuel production facility was separated from INPR and has become the Nuclear Fuel Plant. Later it was included as a branch of SN "Nuclearelectrica" SA (together with Cernavoda Nuclear Power Plant).

In 1992, a technical assessment and a technological development program assisted by Canadian companies AECL and ZPI (now CAMECO) was started. The technical specifications and the QA program were reviewed. This included the manufacture of a demonstration batch of 202 bundles under direct supervision of AECL and ZPI team in 1994. 66 bundles from this batch were included in the initial fuel charge and loaded into the Cernavoda Unit 1 reactor core. Finally, in December 1995, the Nuclear Fuel Plant was certified as a qualified CANDU-6 nuclear fuel supplier as per Canadian Standard CSA-Z-299.2.

Since the commissioning of Unit 1 at Cernavoda in 1996, NFP Piteşti has assumed the role of fuel supplier for this power plant. As result, it continuously has adapted its production to match the demand of fuel from the plant. When the decision was taken in 2001 to complete a second unit at Cernavoda NPP, fuel manufacturer has started preparations for doubling its production capacity. This meant acquisition of some new equipment, but also a new arrangement of the manufacturing process. This allowed the plant to double the quantity of fuel delivered starting with the year 2007 when Cernavoda Unit 2 was commissioned.

2. FUEL PRODUCTION

So far, the Nuclear Fuel Plant at Piteşti has produced fuel pellets exclusively from uranium dioxide powder prepared in Romania. The zircaloy cladding tubes are imported as well as the bar stock and sheet required to produce other components (i.e. end caps, end plates, spacers and bearing pads).

Initially, the production rate was calibrated to supply around 5, 500 fuel bundles per year, the quantity typically required annually for operation of a CANDU-6 unit. After 2007, the production has doubled.

High quality fuel represents the main objective of NFP-Piteşti and a strict process of quality control and surveillance is in place there to ensure compliance with technical specifications permanently. The QA system is focused on key parameters for quality of the final product, like maintaining low residual hydrogen content in the graphite coated sheaths or a high quality for the welds and the brazing process. Testing by destructive and non-destructive methods plays a major role in this processfor quality control.

3. FUEL PERFORMANCE

So far, more than 110 000 fuel bundles have been delivered to the Cernavoda NPP and have been loaded into the reactor cores.

At Unit 1 a number of 85 000 bundles were discharged from the core at an average burnup of around 167 MWh/kgU. Only 26 irradiated bundles were declared defective in over 16 years of reactor operation. This unit has achieved an excellent performance of no fuel defect recorded within a period of more than 6.5 years operation.

At Unit 2, around 25 000 bundles have been discharged from the core so far, at an average burnup of around 171 MWh/kgU. A total of 65 bundles were defective in over 5 years of operation. Most of these defects have been recorded within the first year after the reactor commissioning and power increase to full power. The in-bay inspection has revealed that about half of these defects were caused by debris fretting and confirmed that some defects were due to some manufacturing problems. It appears that the excursion of defects is strongly related to a specific batch of fuel produced in 2006 when the manufacturer has increased its production. However, the exact cause was not possible to be identified. In near future our intention is to send some of these bundles to a laboratory for post-irradiation examination. Note that after this initial excursion, the rate of fuel defects has decreased to normal values and no fuel defect was discharged from the core within the last two years.

4. FUTURE DEVELOPMENT

Encouraged by the good performances achieved constantly by Cernavoda NPP, Romania takes into account to complete the construction of other two CANDU units on the Cernavoda site within the next decade. Therefore, SN “Nuclearelectrica” SA is looking now for private investors interested to involve in such a project. A decision to proceed is expected soon.

Under these circumstances a refurbishment program for the Nuclear Fuel Plant - Piteşti is in preparation and one of its objectives is to make possible an increase of its production capacity in the future.

5. CONCLUSIONS

In the last two decades Romania has succesfuly proved its capacity to produce good quality nuclear fuel. The production rate was addapted to satify the demand of fuel for operation of one and then two CANDU-6 units at power. The performance of the fuel discharged from the reactors has constantly mantained within normal limits.

Romania has plans for completing the construction of other two CANDU units on the Cernavoda site within the next decade and takes into account to increase the production capacity at the Nuclear Fuel Plant at Pitesti in the future.

USING ADVANCED FUEL BUNDLES IN CANDU REACTORS

A. RIZOIU, G. HORHOIANU, I. PRODEA
Institute for Nuclear Research,
Mioveni, Romania
Emails: andrei.rizoiu@nuclear.ro
grigore.horhoianu@nuclear.ro

Abstract

Improving the exit fuel burnup in CANDU reactors was a long-time challenge for both bundle designers and performance analysts. Therefore, the 43-element design together with several fuel compositions was studied, in the aim of assessing new reliable, economic and proliferation-resistant solutions. Recovered Uranium (RU) fuel is intended to be used in CANDU reactors, given the important amount of slightly enriched Uranium (~0.96% w/o U235) that might be provided by the spent LWR fuel recovery plants. Though this fuel has a far too small U235 enrichment to be used in LWR's, it can be still used to fuel CANDU reactors. Plutonium based mixtures are also considered, with both natural and depleted Uranium, either for peacefully using the military grade dispositioned Plutonium or for better using Plutonium from LWR reprocessing plants. The proposed Thorium-LEU mixtures are intended to reduce the Uranium consumption per produced MW. The positive void reactivity is a major concern of any CANDU safety assessment, therefore reducing it was also a task for the present analysis. Using the 43-element bundle with a certain amount of burnable poison (e.g. Dysprosium) dissolved in the 8 innermost elements may lead to significantly reducing the void reactivity. The expected outcomes of these design improvements are: higher exit burnup, smooth/uniform radial bundle power distribution and reduced void reactivity. Since the improved fuel bundles are intended to be loaded in existing CANDU reactors, we found interesting to estimate the local reactivity effects of a mechanical control absorber (MCA) on the surrounding fuel cells. Cell parameters and neutron flux distributions, as well as macroscopic cross-sections were estimated using the transport code DRAGON and a 172-group updated nuclear data library.

1. INTRODUCTION

Increasing the exit burnup of CANDU reactors has been a challenging task for both reactor physics and fuel engineering since the early 80's. CANDU reactors can use a wide range of advanced fuels apart from the “traditional” natural Uranium fuel, e.g. RU, LEU (up to 2% U235), mixed oxide (MOX), Thorium, as well as actinide waste.

This paper is focused on using 43-element bundles, with a certain amount of Dysprosium in the innermost element(s), in the aim of obtaining negative void reactivity. Infinite cell studies were performed using the computer code DRAGON3.05E [10] and the corresponding 172-group nuclear data library [9]. The estimated cell parameters were: the maximum fuel burnup, the radial power distribution and the void reactivity.

As a starting point for further core simulations, the local reactivity effects of a mechanical control absorber (MCA) on the surrounding fuel cells were estimated, in the aim of assessing the possibility of loading the advanced fuel bundles in the existing CANDU core. The reactivity devices design and operation are supposed to be the same as in the existing CANDU reactors.

2. FUEL BUNDLES

The studied bundle projects were proposed by Grigore Horhoianu, former head of the Fuel Performance Department, based on both previous Canadian studies [1], [3], [4], [6], [2], [13] and a valuable team work of fuel design, testing and assessment in INR [7], [11], [14].

In the beginning, the "traditional" fuel was considered, containing natural Uranium dioxide - pellet density = 10.7 g/cm^3 - in standard 37-element bundle geometry:

(a) 37Nat.

For comparison purposes, a 43-element bundle also containing natural Uranium dioxide was studied:

(b) 43Nat.

The following projects were considered in the aim of directly using the existing Plutonium, either from spent fuel reprocessing and from dispositioning weapon grade Plutonium in the form of Mixed Oxide fuel (MOX). The bundles features described in [1], [3], [4] and [6] were modified in the aim of obtaining better radial power distribution and lower void reactivity:

(c) 43PuCiv: depleted Uranium - 0.2% ^{235}U - dioxide in the central element; (depleted Uranium + 1.5% Pu) dioxide in the following 7+14=21 elements; (depleted Uranium + 1% Pu) dioxide in the outmost 21 elements;
(d) 43PuCiv-Unat: depleted Uranium dioxide in the central element; (depleted Uranium + 1.5% Pu) dioxide in the following 7 elements; natural Uranium dioxide in the following 14 elements; (depleted Uranium + 1% Pu) dioxide in the outmost 21 elements;
(e) 43PuMil: depleted Uranium dioxide + 7% Dysprosium in the innermost 1+7=8 elements; depleted Uranium dioxide in the following 14 elements+ 5% Pu; (depleted Uranium + 2% Pu) dioxide in the outmost 21 elements. Then, a bundle containing recovered Uranium dioxide [2] was considered, with 0.016% ^{234}U, 0.96% ^{235}U, 0.275% ^{236}U, 98.75% ^{238}U and the same pellet density as above;
(f) 43RU.

The following fuel bundles were proposed in the aim of using uranium-thorium MOX fuels, modified from [13]:

(g) 43Th-U1.3: Thorium dioxide in the innermost 1+7=8 elements, pellet density = 10.4 g/cm^3; LEU - 1.3% ^{235}U - dioxide in the following 14+21=35 elements, pellet density = 10.7 g/cm^3 ;
(h) 43Th-U1.75: Thorium dioxide in the innermost 1+7=8 elements, pellet density = 10.4 g/cm^3; LEU - 1.75% ^{235}U - dioxide in the following 14+21=35 elements, pellet density = 10.7 g/cm^3.

3. LATTICE CELL

The studied fuel bundles are intended to be used in existing CANDU reactors, therefore the lattice cell parameters (apart from those of the fuel bundle itself) correspond to a standard CANDU lattice cell, as presented before [5], [14]. The considered cell power rating was 45 kW per kg of Heavy Element, corresponding to a bundle power of 900 kW.

4. RESULTS

- Maximum fuel burnup:

The maximum fuel burnup was defined as the maximum fuel burnup for which the cell is still critical, k_{inf} =1.0. Its values range from about 6.5 (for 37Nat) to about 16.5 MW·d/kgHE (for 43PuMil), see Figure 1.

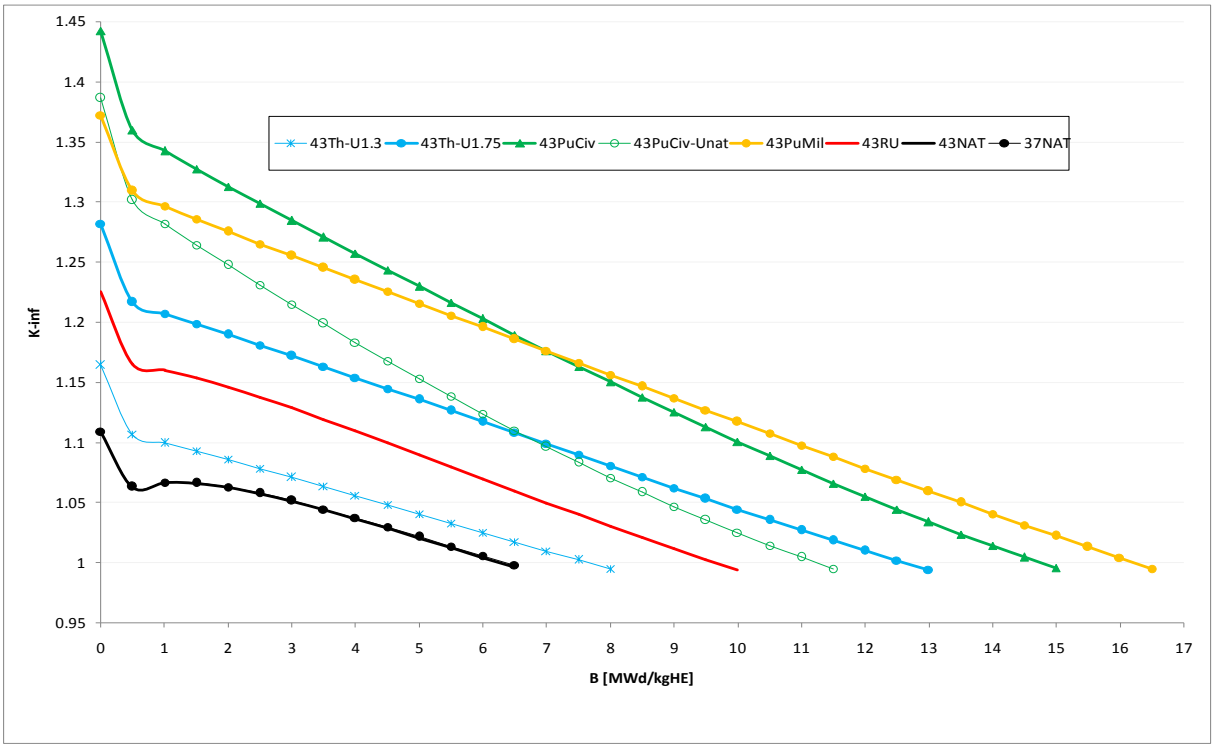

FIG. 1. K-inf evolution with burnup.

The maximum value of this parameter was obtained, as expected, for the bundles containing Pu and no Dy.

The selection criterion was a maximum burnup superior to the standard CANDU one, i.e. B > 7 MW·d/kgHE, therefore the bundles containing natural Uranium were eliminated.

The bundles intended to burn Pu confirmed a good Plutonium consumption, as the Pu239 inventory significantly diminished with burnup as shown in Fig. 2.

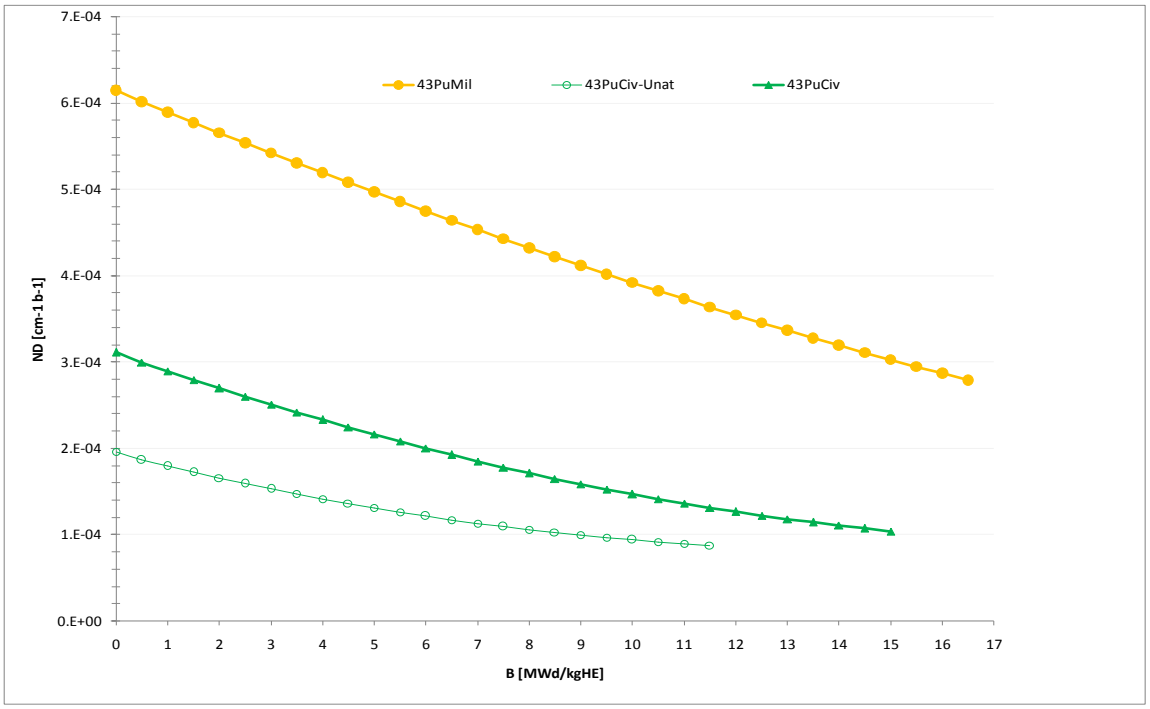

FIG. 2. Pu239 evolution with burnup.

- Radial power distribution:

The considered fuel bundles contain a central element (referred to as the 1st radial fuel region), the inner ring with 6 or 7 elements (the 2nd radial fuel region), the intermediary ring with 12 or 14 elements (the 3rd radial fuel region) and the outer ring with 18 or 21 elements (the 4th radial fuel region). The fraction of total bundle power produced by each radial fuel region only gives a global hint on the power distribution. Still, since the key parameter – from the point of view of Fuel Performance – is the power fraction produced by each element, given by its position in the bundle, a new parameter was defined for each radial fuel region, i.e. the "element linear power", ELP, related to the "power peaking factors" defined in [14]:
Since the elements situated in different radial regions have different diameters (and therefore different fuel masses), Table 1 shows ELP_r for three fuel burnup 0, 4 and 6 MW·d/kgHE. Though for 37Nat, 43Nat and 43RU the relative difference in ELP_r's lays under 60%, the presence of highly absorbing fuel mixtures severely lowers ELP_1 and ELP_2 for Pu- and Th-based MOX bundles. Element Linear Power distribution at 6 MW·d/kgHE is also shown in Fig. 3.

TABLE 1. ELEMENT LINEAR POWER (kW/m) DISTRIBUTION AT 0, 4 AND 6 MW·d/kgHE

Project Name	B=0				B=4				B=6			
	R=1	R=2	R=3	R=4	R=1	R=2	R=3	R=4	R=1	R=2	R=3	R=4
37NAT	57.333	46.246	40.863	38.978	56.684	46.794	41.591	39.721	56.232	47.098	42.216	40.445
43NAT	46.245	37.859	46.512	44.342	45.652	38.263	47.361	45.209	45.267	38.455	48.020	45.990
43RU	47.208	37.362	44.895	42.401	46.157	38.052	46.436	44.033	45.520	38.400	47.478	45.234
43PuCiv	47.591	41.265	41.293	4.931	43.889	43.492	47.265	9.679	42.339	44.050	50.367	12.723
43PuCiv-Unat	57.353	16.213	61.914	6.301	50.764	23.959	65.074	14.127	48.076	27.453	65.504	18.636
43PuMil	56.854	47.083	2.269	2.112	53.267	52.069	2.983	2.650	51.192	54.952	3.400	2.941
43Th-U1.3	58.643	45.429	0.448	0.450	54.706	44.895	11.851	10.789	52.309	44.158	19.532	17.672
43Th-U1.75	59.394	44.328	0.405	0.406	56.385	44.766	7.616	6.976	54.395	44.717	12.993	11.823

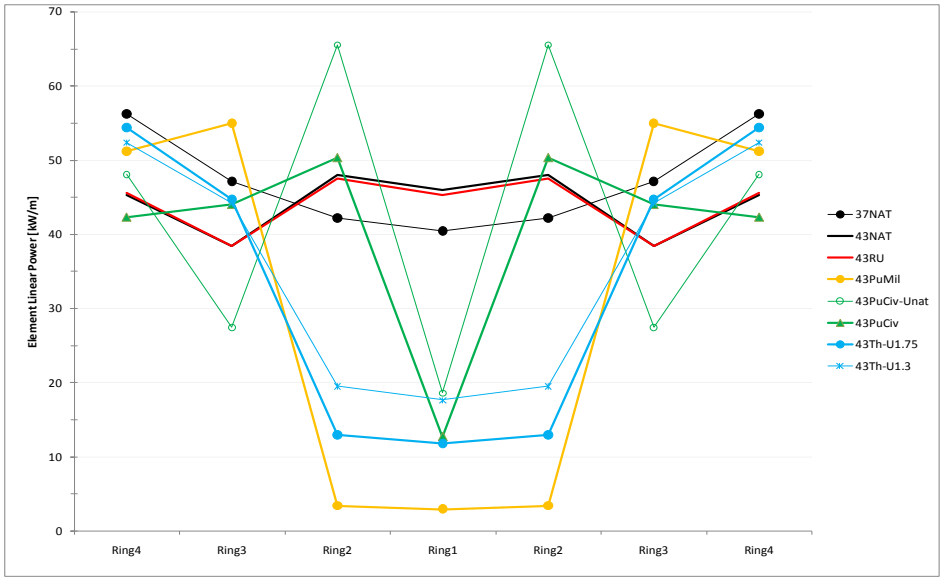

FIG. 3. Element linear power distribution at 6 MW·d/kgHE.

- Void reactivity:

The Void Reactivity (VR) previously used in [14] is a key parameter describing the cell reactivity evolution during a Loss Of Coolant Accident. The void fraction *(f)* ranges from 5 to 95%. VR is then defined as $VR(f) = \left(\frac{1}{K_{ref}} - \frac{1}{K_f} \right) \cdot 1000$ [mk], where K_{ref} is the "reference" multiplication constant corresponding to the "reference" ("cooled") cell and K_f corresponds to the void fraction ***f***.

Fig. 4 shows VR evolution with respect to *f* for the considered fuel bundles. The complete loss of coolant inserts at least 2 mk of positive reactivity. None of the studied projects could lead to a negative coefficient of void reactivity $CVR = \frac{\partial}{\partial f} VR$ [mk/%], but using absorbers (Dy or Th) in the 8 innermost elements can reduce it by more than 50%.

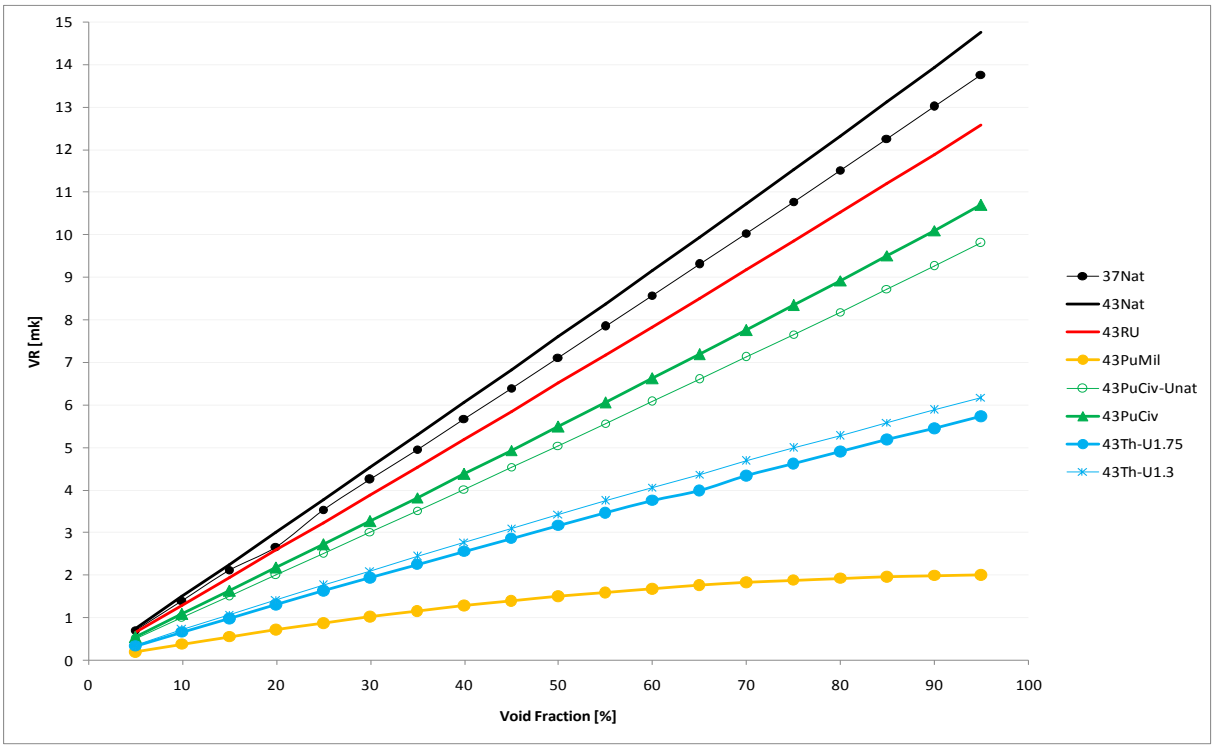

FIG. 4. Void effect on VR.

- MCA/SOR effect on the surrounding fuel cells:

As well-known in the CANDU physics community, the mechanical control absorbers (MCA's) have the most significant effect on neutron flux distribution, from all reactivity devices. Since the shut-off rods (SOR's) are similar to MCA's, we found interesting to study the neutron flux behaviour in a common MCA/SOR supercell when the CANDU fuel bundles are simply replaced by advanced ones presented before.

Fig. 5 shows the layout of the DRAGON model used for simulations, slightly modified from the supercell model proposed in [10]. The MCA and the guide tube are similar to the standard CANDU ones simulated in [12].

One should notice the horizontal fuel channel (block C) position along the Z axis and the vertical absorber (block A) insertion.

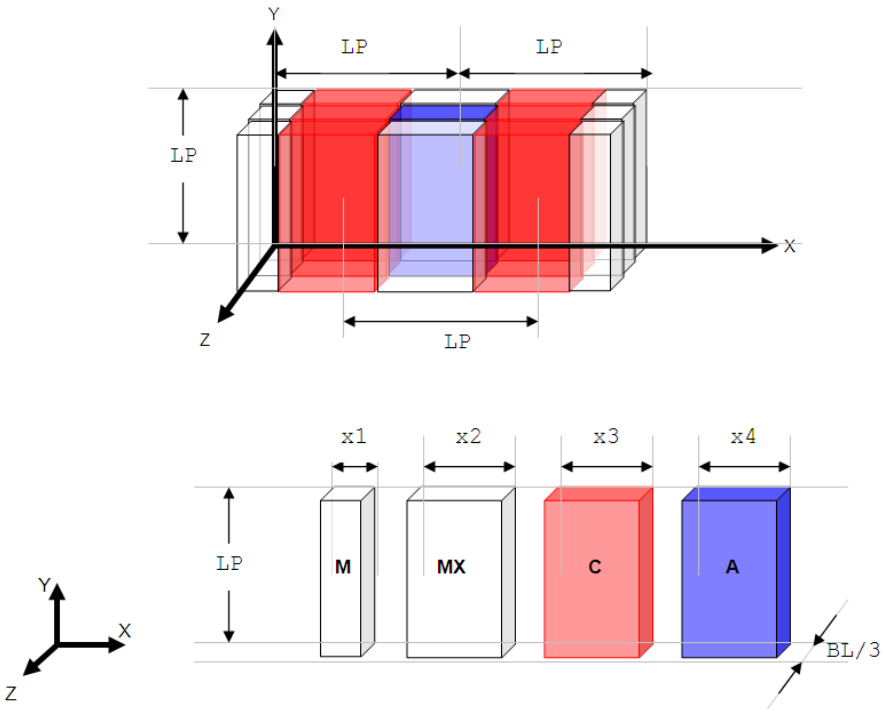

FIG. 5. DRAGON model for the MCA/SOR supercell ([12]).

In the above figure, LP is the cell lattice pitch and BL is the fuel bundle length.

The main outcome of a DRAGON supercell calculation is a consistent set of incremental cross sections (Table 2) to be used in a core flux calculation based on diffusion theory.

The following increments correspond to the supercell-averaged macroscopic cross sections related to fast neutrons transport, absorption, yield and removal, as well as to thermal neutrons transport, absorption and yield. H1 and H2 are the "power to flux ratios" estimating the fission power per unit flux for fast and thermal neutrons respectively.

TABLE 2. INCREMENTAL CROSS-SECTION FOR THE CONSIDERED SUPERCELLS

	37Nat	43Nat	43RU	43PuMil	43PuCivUnat	43PuCiv	43ThU1.75	43ThU1.3
STRN1	9.92E-04	9.91E-04	9.92E-04	9.93E-04	9.92E-04	9.92E-04	9.91E-04	9.91E-04
SABS1	1.24E-04	1.24E-04	1.24E-04	1.19E-04	1.23E-04	1.22E-04	1.24E-04	1.24E-04
NUSF1	1.42E-07	1.45E-07	8.67E-09	-4.99E-07	-5.83E-08	-2.00E-07	-2.90E-07	-1.06E-07
SREM	-1.17E-04	-1.18E-04	-1.17E-04	-1.13E-04	-1.17E-04	-1.16E-04	-1.17E-04	-1.18E-04
STRN2	-2.35E-03	-2.38E-03	-2.33E-03	-1.73E-03	-2.00E-03	-1.90E-03	-2.22E-03	-2.27E-03
SABS2	2.44E-03	2.43E-03	2.47E-03	2.92E-03	2.71E-03	2.79E-03	2.55E-03	2.50E-03
NUSF2	1.05E-04	1.03E-04	1.34E-04	4.84E-04	3.87E-04	4.51E-04	1.72E-04	1.34E-04
H1	8.08E-05	8.94E-05	-9.38E-05	-5.96E-04	-8.74E-05	-2.39E-04	-4.74E-04	-2.26E-04
H2	1.40E-01	1.37E-01	1.79E-01	5.73E-01	4.60E-01	5.35E-01	2.29E-01	1.78E-01

In most cases, the "advanced" supercells exhibit a larger incremental absorption section for thermal neutrons than the standard CANDU supercell (by up to 19.5%, therefore the reactivity worth of the MCA/SOR is expected to be more important when using other fuel than natural Uranium. Of course, this hypothesis is to be confirmed by more detailed core calculations.

The local effect of such an important neutron absorber is, as expected, a significant drop of the thermal flux in the MCA/SOR region, by a factor of 10 to 20.

Figs. 6 and 7 show the thermal flux profile across the model for a "reference" supercell without MCA/SOR inserted (but with the corresponding guide tube in place) as well as for the "perturbed" one.

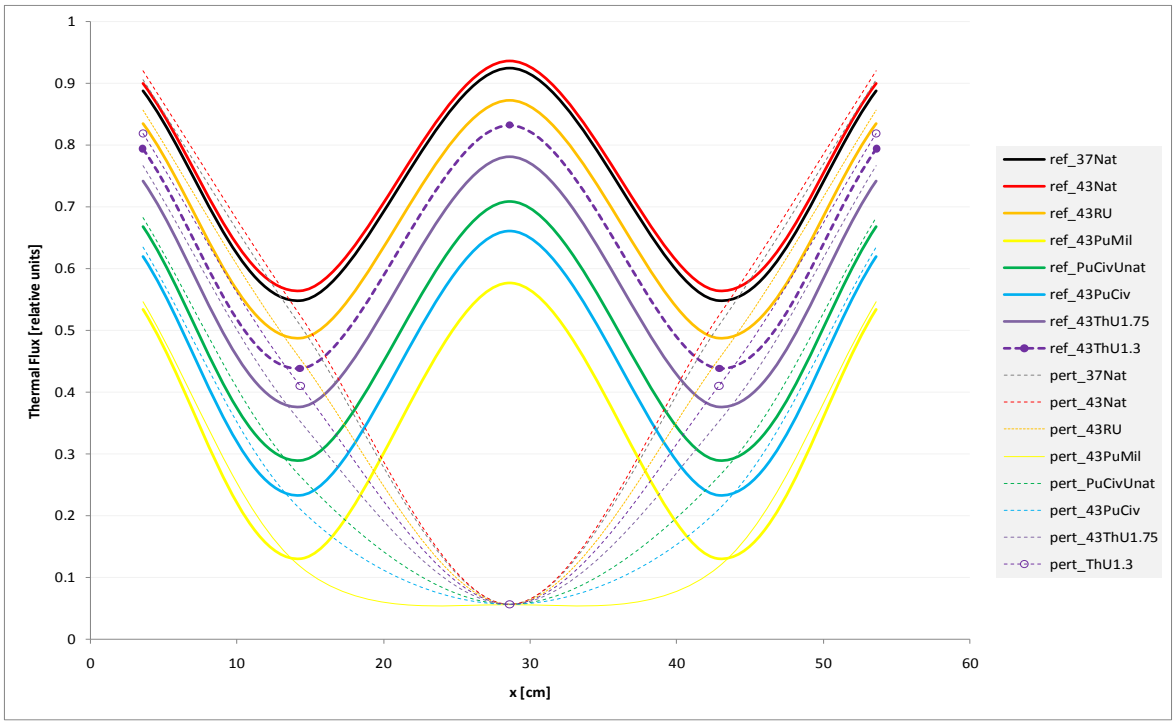

FIG. 6. Thermal flux distribution with respect to ***x*** *(see also FIG. 5).*

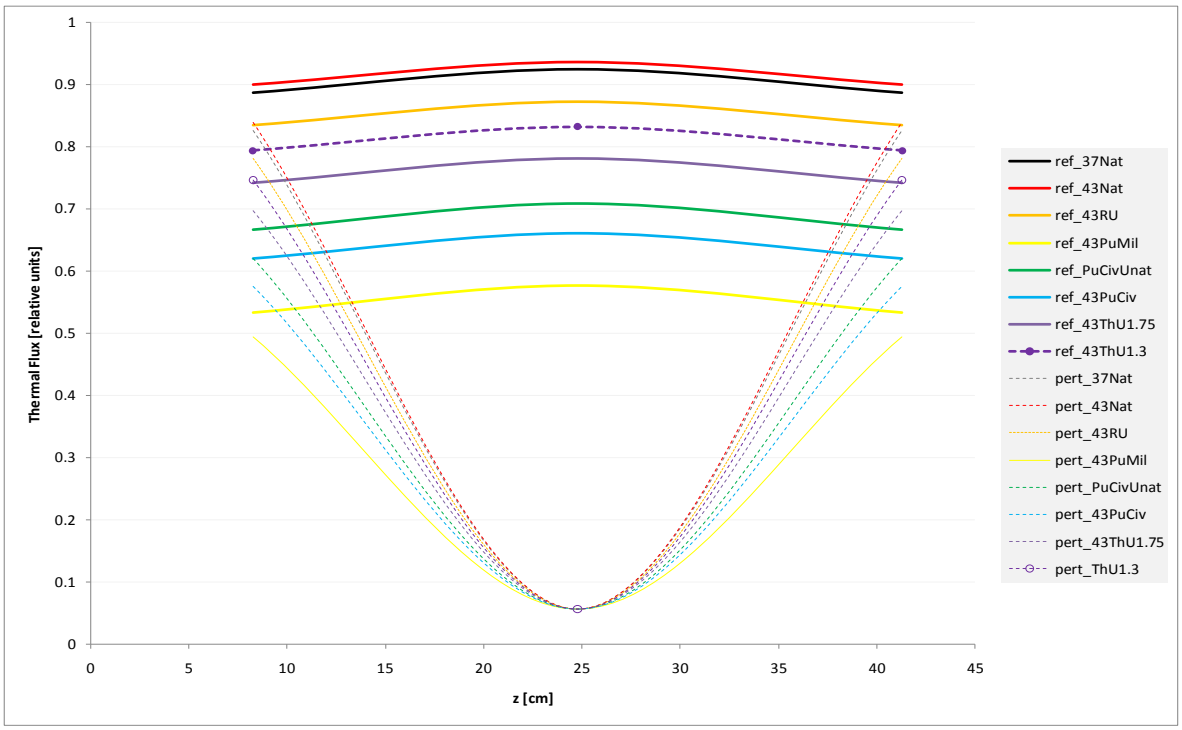

FIG. 7. Thermal flux distribution with respect to ***z*** *(see also FIG. 5).*

5. CONCLUSIONS

- Maximum fuel burnup of more than 7 MW·d/kgHE recommends bundles with RU or different MOX for further CANDU core calculations; the 43PuMil burnup is expected to be more than twice of the standard 37Nat one;
- The bundles containing Plutonium did actually consume an important part of it, during burnup, thus reducing the "sensitive" inventory;
- The selection criterion related to "uniform burnup" recommends 43-element fuel bundles without strong absorbers in the innermost elements;
- None of the studied fuel bundles could assure a safe behaviour (negative CVR) during LOCA;
- The CANDU supercell calculations with "advanced" fuel bundles lead to encouraging results with respect to ensuring the reactivity worth of the strong neutron absorbing reactivity devices, but these studies must be followed by full core simulations.

ACKNOWLEDGEMENTS

The authors acknowledge the kind help of Mr. Gheorghe Olteanu and his valuable contribution in studying and promoting the 43 elements bundle design and testing.

REFERENCES

[1] BOCZAR, P.G., HOPKIN, J.R., FEINROTH, H., LUXAT, J.C., Plutonium Disposition in CANDU, AECL-11429 (1995).

[2] D'ANTONIO, M J., DONNELLY, J.V., "Explicit core follow simulation for a CANDU® reactor fuelled with recovered uranium CANFLEX® bundles", 5th International Canadian Nuclear Society CANDU Fuel Conference, Toronto, Canada (1997).

[3] BOCZAR, P.G., GAGNON, M.J.N., CHAN, P.S.W., ELLIS, R.J., VERRALL, R.A., DASTUR, A.R., "Using weapons derived plutonium fuel in CANDU Reactors according to Atomic Energy of Canada Limited", Canadian Nuclear Society Bulletin, Vol. 18, No. 1 (1997).

[4] MAKHIJANI, A., SETH, A., The Use of Weapons Plutonium as Reactor Fuel, Institute for Energy and Environmental Research, Takoma Park, Maryland, USA (1997).

[5] DUMITRACHE, I. RIZOIU A., Benchmark Problem for a CANDU6 Lattice Cell, INR Internal report RI-5933 (2000).

[6] DIMAYUGA, F. C., "The PARALLEX project: irradiation testing and PIE of the first bundle", 8th International Conference on CANDU Fuel, Honey Harbour, Canada (September 2003).

[7] OLTEANU, G., HORHOIANU, G, ZVANCIUC, F., Updating of SEU43 Fuel Bundle Project, INR Internal Report RI-7427 (2006).

[8] NUTTIN, A., et. al., "Study of CANDU thorium based fuel cycles by deterministic and monte carlo methods", PHYSOR-2006, ANS Topical Meeting on Reactor Physics, Vancouver, Canada, (September 2006).

[9] INTERNATIONAL ATOMIC ENERGY, Report of a Coordinated Research Project: WIMS-D Library Update, IAEA, Vienna (2007).

[10] MARLEAU, G., HEBERT, A., ROY, R., A User Guide for DRAGON3.05E, IGE-174 rev.6, Institut de Génie Nucléaire, École Polytechnique de Montréal, Canada

(2007).
[11] HORHOIANU, G, PATRULESCU, I., Technical Feasibility of Using RU-43 Fuel In The CANDU-6 Reactors Of The Cernavoda NPP, in Kerntechnik 73/2008, Independent Journal for Nuclear Engineering, München, Germany (2008).
[12] RIZOIU A, PATRULESCU, I, PRODEA, I., Using DRAGON for CANDU Reactivity Devices Simulation, INR Internal Report RI-8419 (2009).
[13] ZHANG, Z., KURAN, S., "Status of development of thorium fuel cycle in CANDU reactors", AECL REUSE 4th Workshop, Toronto, Canada (2010).
[14] RIZOIU A., HORHOIANU, G, "Preliminary reactor physics studies on using advanced fuel bundles in CANDU", Nuclear 2011, 4th Annual International Conference on Sustainable Development through Nuclear Research and Education, Piteşti, Romania (2011).

FUEL BEHAVIOUR DURING LARGE BREAKS IN THE PRIMARY HEAT TRANSPORT CIRCUIT

C. ZĂLOG
Cernavoda Nuclear Power Plant,
Cernavoda, Romania
Email: czalog@cne.ro

Abstract

A large break in the Primary Heat Transport System is considered the one with a size greater than the largest feeder diameter. The break discharges coolant to the containment, causing depressurization in the affected pass and increase in containment temperature and pressure. The depressurization induces coolant voiding and, due to the positive reactivity void coefficient, power increases until reactor shuts down on a neutronic or a process conditioned trip parameter. During the power pulse, due to degraded fuel cooling, the sheath can fail. The heat transport system flow decreases faster in the core pass downstream the break. Some channels may become steam filled and others can experience stratified two phase flow, exposing some fuel elements to steam cooling, inducing fuel temperature rises. A rise in fuel temperature increases the internal fuel element gas pressure, whereas a rise in sheath temperature reduces the sheath strength. The channel coolant pressure falls below the fuel element internal gas pressure, stressing the sheath. Increased internal fuel element gas pressure, along with the decreased coolant pressure, increases fuel sheath stresses. If fuel temperature becomes high enough, sheath failure can occur in a large number of fuel bundles, releasing fission products to the coolant. One of the challenges met during the fuel analysis was to set a credible, yet conservative "image" of the in core fuel power/burnup distribution. Consequently, a statistical analysis was performed to find the best estimate plus uncertainties map for the power/burnup distribution of all in core fuel elements. For each power/burnup bin in the map, the fission product inventory and the fuel parameters at the end of the steady state irradiation stage were computed. Afterwards, for each power/burnup bin in the map, the fuel behavior is simulated during the transient. Based on the fuel failure criteria, the failed fuel elements are identified, providing the total radioactive release to the coolant circuit, base for the final dose assessment. The present paper reviews the methodology and results for a typical Design Basis Safety Analysis – Large LOCA with All Safety System Available. Methodologies used in the analysis and results are presented, focused upon fuel behavior.

1. INTRODUCTION

At CANDU reactors, a large break is defined as one with size greater than the diameter of the largest feeder from the primary heat transport system (PHTS). It corresponds to about 2.5% of the reactor inlet header cross sectional area. A large break in the PHTS could lead to a degraded fuel cooling in a large number of fuel channels causing fuel failures and, hence, a consequent release of fission products into the coolant.

For licensing purposes, analyses are performed postulating that the large breaks occur in a reactor inlet header (RIH break), in a reactor outlet header (ROH break) or in a pump suction pipe (PSH break). Wherever the postulated break is located, it causes the PHTS to lose inventory and to depressurize by discharging coolant into containment at a high rate. The PHTS depressurization causes coolant voiding and, consequently, an increase in core reactivity. As result, power increases until the reactor is automatically shut down due to a neutronic or a process-conditioned parameter exceeding its trip setpoint. The net effect is a short overpower pulse followed by power rundown to fission products decay power. Containment isolation is automatically initiated on a high reactor building pressure signal. This signal also conditions initiation of the emergency core cooling system (ECCS) injection and the steam generator crash cooldown.

PHTS flow decreases faster in the core pass downstream the break and it can reverse if the break is large enough. Under these circumstances, some fuel channels may become steam

filled and others experience stratified two phase flow, exposing some fuel pins to steam cooling. The fuel and sheath temperatures rise. As result, the internal fuel element gas pressure increases, while the sheath strength reduces. If the sheath temperature becomes high enough and coolant pressure falls below the fuel element internal gas pressure, stressing the sheath, failure can occur.

Following the reactor shutdown, fuel temperature decreases and temperature profile in the fuel pins flattens out. When the broken loop pressure falls below a pre-established level, the PHTS loops isolation and the steam generators crash cooldown are initiated and the ECCS is activated. Soon, the ECCS injection refills the broken loop. As result, fuel and sheath temperatures decrease. Depending on their initial temperatures, some fuel sheaths may fail due to the thermal shock following rewet. If fuel failures occur, some fission products are released into the coolant and are carried into containment through the break.

Long-term cooling of the broken loop is ensured by the flow of ECCS coolant through the circuit, with heat removal by ECCS heat exchangers and through the break. For the intact loop the long-term cooling is maintained by forced circulation or thermosyphoning, with heat removal by steam generators.

1. CIRCUIT THERMAL HYDRAULIC ANALYSIS

In order to simulate the plant response to Large LOCA events, a two loop, multiple average channel circuit model of the primary heat transport system was developed. The model was connected with models for ECCS and some of the secondary side systems (like steam and feedwater systems, part of the reheater drains system, etc.). On each of the four core passes, fuel channels were grouped into 7 average channels based on channel power, channel elevation and type of the feeder to header connection. Besides, the PHTS thermalhydraulic model developed at Cernavoda has accounted also for the aging effects (creep profile along fuel channels, piping roughness, etc.) affecting the plant after about 18 years of service at 85% FP.

Since the power pulse depends on voiding rate within channels located downstream the break, it is required that the circuit thermalhydraulic simulation and the core neutronic simulation to be coupled to acount for the reciprocal feedback. At Cernavoda, the transients induced by the LOCA events were simulated by coupling the thermalhydraulic code CATHENA [1] with the physics code RFSP [2] developed at AECL, Canada.

The circuit thermohydraulic analysis provides information regarding timing of major events expected to occur during the accident progression (like the moment when the reactor trips occur or when the ECC injection begins). Also it provides information about various parameters that are required as input for performing further analyses for containment, moderator, fuel or fuel channel behavior.

2. SINGLE CHANNEL ANALYSIS

In order to get more details about thermohydraulic conditions induced by the initiating event within the core channels, single channels analyses are performed using the inlet and outlet header conditions predicted from the circuit simulations as boundary conditions. Usually this investigation is done for several types of core channels, like low power channels with high or low core elevation (e.g. A10, W10) and for high power channels (e.g. O6). The limiting case is a high power channel with the power distribution modified (O6_mod), i.e. upscaled to the

maximum licensing limits allowed during plant operation (7.3 MW/channel and 935 kW/bundle, respectively).

The purpose of single channel analyses is to predict transient thermalhydraulic conditions (coolant temperature, coolant pressure and heat transfer coefficient from sheath to coolant) to which fuel from the analyzed channels is exposed to.

3. METHODOLOGY FOR FUEL BEHAVIOUER ANALYSIS

Since the intact loop is expected to be well cooled, the fuel analysis focuses on fuel behavior within the broken loop. The main objective is to determine the number of fuel elements expected to fail during the transient, the timing of these failures and the fission products inventory released to the coolant.

Activation of the shutdown systems and ECC injection ensures that the period of fuel heat up will be short during Large LOCA events and the extent of fuel failures will be limited. If the sheaths fail, fission products from failed fuel elements are available for release, especially the free gap inventory. However, examinations of fuel elements with high gas release, operated at high power, have shown deposits of some fission products on sheath inside surface. Iodine is expected to chemically combine with Cesium and be retained on fuel and sheath surfaces. Noble gases, such as krypton (Kr) and xenon (Xe), are expected to be released mostly at the time of sheath failure, since they are not chemically active. Regarding the release of fission products from grain surface or from within grains to the gap, they are temperature and time dependent. For large breaks, where fuel heat up period is not long, release of fission products from grain surface or from grain boundary is expected to be less than 1% of the total inventory contained within pellet.

TABLE 1. RESULTS OF SENSITIVE ANALYSIS ON FUEL DESIGN PARAMETERS

Parameter	Maximum Temperature	Maximum Strain	Maximum Inventory
Pellet Diameter	-	-	MAXIMUM
Dish Depth	-	minimum	minimum
Land Width	-	MAXIMUM	MAXIMUM
Pellet Density	minimum	MAXIMUM	minimum
Pellet Roughness	MAXIMUM	minimum	MAXIMUM
UO2 Grain Size	-	minimum	minimum
Pellet Stack Length	minimum	MAXIMUM	MAXIMUM
Axial Clearance	-	minimum	minimum
Radial Clearance	-	minimum	minimum
Sheath Wall Thickness	MAXIMUM	minimum	MAXIMUM
He Fraction in the filling gas	minimum	minimum	minimum
Sheath Roughness	MAXIMUM	MAXIMUM	MAXIMUM

Usually, for licensing purposes, calculation of fission products release to the coolant is done conservatively, assuming that the radioactive release from failed fuel elements consists of the total gap inventory plus 1% of grain inventory. Also, it is assumed that this release occurs at the time of sheath failure. Besides, a preliminary sensitivity analysis on fuel design parameters is done for evaluating their impact on gaseous fission products fractional release from fuel matrix to the gap. Fuel design parameters are modified within a $\pm 2\sigma$ range and the combination which maximizes the fractional release is selected to be further used in fuel behavior simulations (Table 1).

3.1. Power/burnup distribution for in core fuel elements

The fission products inventory in a fuel element and its behavior during the transient induced by the initiating event depend on the irradiation history experienced by that fuel element. During reactor operation, the in core fuel elements pass through a wide spectrum of power/burnup values, while irradiation changes continuously. If an accident analysis is to be performed at a certain instant in the core history, then several millions of simulations are required to study fuel behavior for all in core fuel elements. To avoid this, the alternative is to derive, by a statistical analysis, a "representative", yet conservative, power/burnup distribution of the fuel elements within the reactor core. Such an analysis was performed by processing the core neutronic simulations done at Cernavoda Unit 1 over a period of two years of operation. The results obtained from each simulation have been used to plot the number of fuel elements in bins for linear power and burnup. The ranges for fuel element linear power and burnup were selected to cover all possible values recorded during reactor operation at full power: 1 – 65 kW/m, in steps of 1 kW/m, for linear power and 10–270 MWh/kgU, in steps of 10 MWh/kgU, for burnup. Finally, the power/burnup Best Estimate Distribution (BED) of the in core fuel elements was obtained by plotting the average number of fuel elements in each power/burnup bin. The corresponding standard errors were also calculated to be used in obtaining the best estimate plus uncertainty map – the Limit Estimate Distribution (LED). Figure 1 gives the LED map, with a 95% level of confidence. Note that, to account for the errors in power calculation, the fuel elements powers were conservatively increased by 3%, producing the map for 103% FP, used in further fuel behavior analyses.

3.2. Limiting overpower envelope (LOE)

Both thermo-mechanical behavior and radioactive nuclide inventory of a fuel element under normal operating conditions are predicted by the ELESTRES computer code [3] and depend on irradiation history (linear power vs. burnup). Since the number of ELESTRES simulations necessary to cover all possible irradiation histories is unreasonable high, the alternative is to derive a limited set of power/burnup histories, consistent with the real ones occurring in core.

The curve plotting the maximum fuel element linear power reached in each burnup bin in the LED map is called reference overpower envelope (ROE). Since this curve is derived from a limited number of core simulations, it is possible for some fuel elements to slightly exceed it, for a short time, due to unusual or abnormal fuelling or due to short-term power control transients. However, throughout the reactor lifetime, most of the in core fuel elements are expected to have their irradiation histories bounded by ROE.

Starting from ROE, the so-called limiting overpower envelope (LOE) is produced by scaling ROE such as its peak to correspond to the linear power on an element from the outer ring of a bundle operating at the license limit of 935 Kw / bundle. Although the fuel elements

within a burnup bin can actually have different irradiation histories, all "real" histories have shapes reasonable close to the Limiting Overpower Envelope curve. Therefore, the irradiation history of each fuel element can be approximated with a curve obtained by scaling down the LOE curve (Fig. 2).

3.3. Fuel failure threshold

For a given burnup, fuel failure threshold is given by the maximum linear power for which a fuel element operating under the accident transient conditions is predicted not to fail (Figure 1). Fuel element behavior during accident is simulated by the ELOCA computer code [4] that needs as input:

- Pre-transient fuel element thermo-mechanical data supplied by elestres simulations (note that these simulations provide also the fission products inventories within gap and pellet);
- Transient thermalhydraulic boundary conditions (coolant temperature, coolant pressure and heat transfer coefficient from sheath to coolant) predicted by a single channel analysis done with CATHENA. Conservatively, it can be assumed that all in core fuel elements will experience the conditions from top, outer ring, fuel element of bundle 7, from channel O6-mod (with the power distribution upscaled to the maximum licensing limits allowed during plant operation).

For a fuel element exposed to the transient conditions induced by the initiating event, the ELOCA code calculates fuel temperature, sheath temperature and strain, pressure within gap, sheath oxidation level. Using these results, simple and conservative criteria are used to determine whether the fuel element fails or not. The criteria are derived based on experimental data and reactor operating experience. Fuel sheath is considered to remain intact if the following conditions are satisfied:

(1) No fuel centerline melting**:** A fuel element is assumed to fail if fuel centerline melting is reached. Failure occurs due to volume expansion, causing excessive sheath strain;
(2) No fuel sheath melting**:** A fuel element is assumed to fail if fuel sheath melting is reached;
(3) No excessive diametral strain**:** Uniform sheath strain shall remain less than 5% for sheath temperatures lower than 1000 ºC;
(4) No significant cracks in the oxide surface: Uniform strain shall remain below 2% for sheath temperatures higher than 1000 ºC;
(5) No oxygen embrittlement: Oxygen concentration shall remain less than 0.7 w% over half of the sheath thickness;
(6) No sheath failure by beryllium-braze penetration at bearing pad and spacer pad locations.

3.4. Transient fission product release

The radioactive release is estimated by summing the contribution from all fuel elements predicted to fail. These are all fuel elements located above the failure threshold curve.

4. RESULTS AND CONCLUSIONS

To point out the major fuel failure mechanisms, Figs 3 to 5 show the results obtained based on simulations done for three Large LOCA events: 100% ROH break, 35% RIH break and 50% PS piping break. For examplification, three burnup values were selected to study the

fuel element behavior: 60 MWh/kgU (roughly representing the burnup at the Plutonium peak), 140 MWh/kgU (typical mid-burnup at CANDU fuel) and 270 MWh/kgU (a high-burnup value at CANDU). Irradiation history was taken, conservatively, as the LOE itself. Thermalhydraulic conditions were assummed (also, conservatively) as those predicted for the upper fuel pin on the outer ring of bundle #7 from a single channel simulation performed for the channel O6-mod. Each chart gives sheath temperature and strain during the transient, with failure marked, if it occurs. Because fuel heat up period is short during a LLOCA event, oxygen embrittlement, fuel or sheaths melting are highly improbable. Hence, the most probable failure mechanisms are those related to the sheath strain (either the sheath strain exceeding 5% or exceeds 2% while the sheath temperature is over 1000C).

Fig. 6 shows the evolution of the ^{131}I release predicted during the analyzed transients. Due to late failure of mid-power fuel elements, the release is delayed following a 100% ROH break, but it is higher compared to the case of a 35% RIH or a 50%PS break. For these last two cases, the low power fuel elements do not fail. Only high power and relative high burnup fuel elements are expected to fail at the beginning of transient. Therefore, a 100% ROH break is considered to be the limiting case, because of maximum release of ^{131}I predicted.

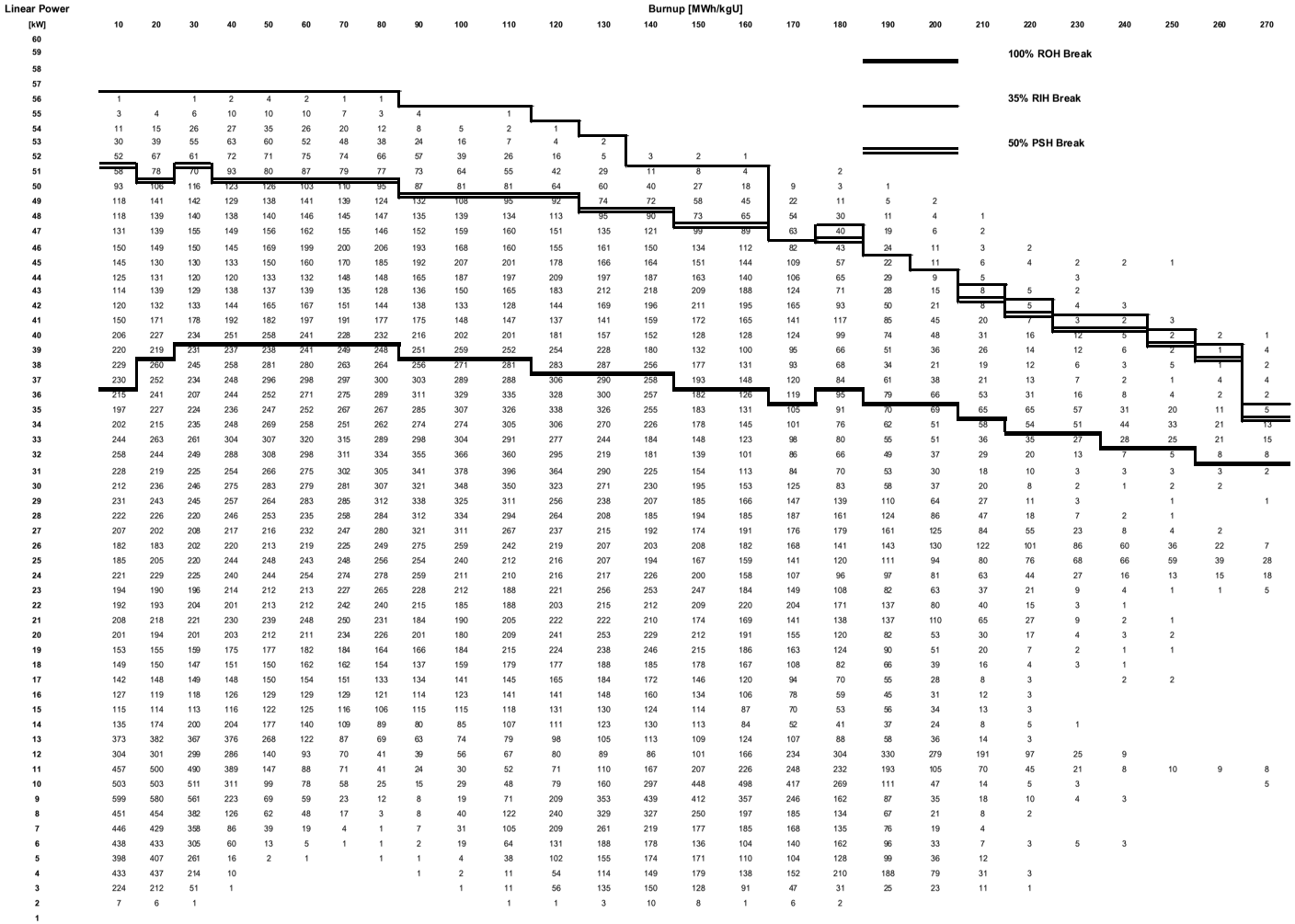

FIG. 1. Limit estimate distribution for in core fuel elements and failure threshol.

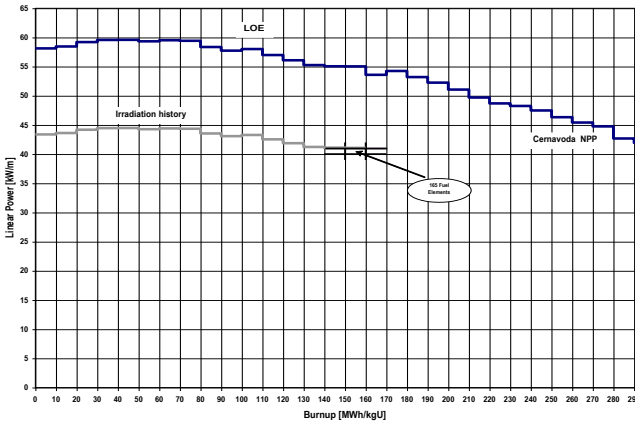

FIG. 2. Limiting overpower envelope.

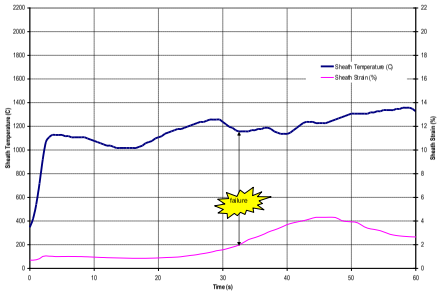

(a) Burnup: 60 MWh/kgU

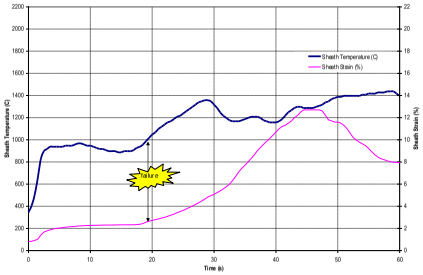

(b) Burnup: 140 MWh/kgU

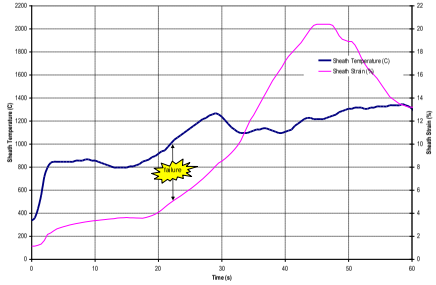

(c) Burnup: 270 MWh/kgU

FIG. 3. Sheath temperature and strain for 100% ROH break.

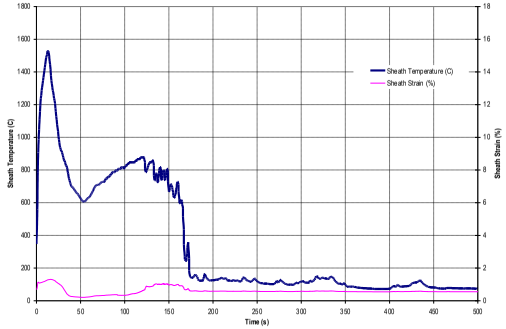

(a) Burnup:60 MWh/kgU

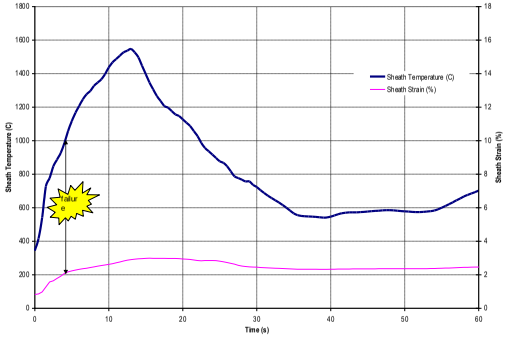

(b) burnup:140 MWh/kgU

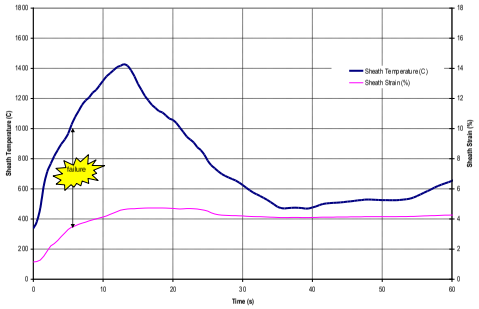

(c) burnup:270 MWh/kgU

FIG. 4. Sheath temperature and strain for35% RIH break.

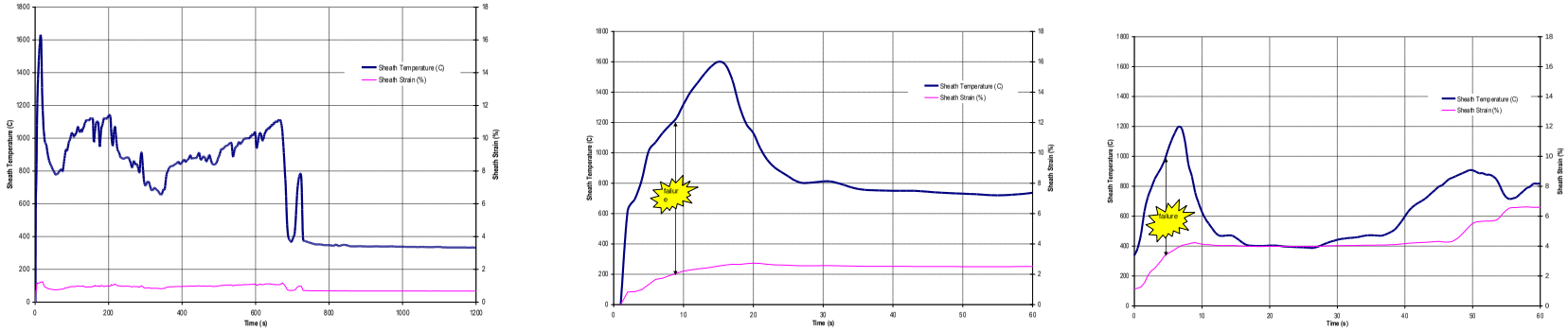

(a) burnup: 60 MWh/kgU (b) burnup: 140 MWh/kgU (c) burnup: 270 MWh/kgU

FIG. 5. Sheath temperature and strain for 50% PSH break.

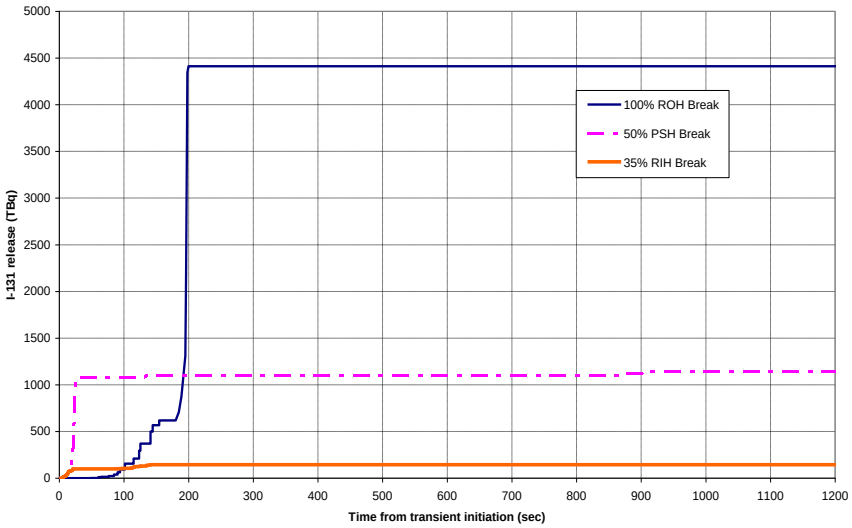

FIG. 6. ^{131}I inventory release during different accident scenarios.

REFERENCES

[1] ATOMIC ENERGY OF CANADA LIMITED, CATHENA MOD-3.5D REV. 2 Release Note, 153-112020-470-001, rev. 0 (2005).
[2] SHEN, N., JENKINS, D. A., RFSP-IST User's Manual, TTR-734, rev. 0 (2001).
[3] CHASSIE, G. G., ELESTRES-IST User's Manual, TTR-733, rev. 1 (2002).
[4] WILLIAMS, A. F., NORDIN, H. M., ELOCA-IST User's Manual, COG-00-274 (2001).

A REGULATORY PERSPECTIVE ON THE ESTABLISHMENT OF FUEL SAFETY CRITERIA FOR THE LARGE LOSS OF COOLANT ACCIDENT IN CANDU PRESSURIZED HEAVY WATER REACTORS

A. El-JABY
Canadian Nuclear Safety Commission (CNSC),
Ottawa, Ontario,
Canada
Email: Ali.El-Jaby@cnsc-ccsn.gc.ca

Abstract

The analysis of the Large Loss Of Coolant Accident (LLOCA) for CANDU Pressurized Heavy Water Reactors (PHWRs) in Canada has been affected by periodic discoveries that have impacted the predicted consequences of the event to the extent that the margins to failure have been significantly eroded. Canadian Nuclear Safety Commission (CNSC) staff is currently actively monitoring an extensive initiative by the Canadian nuclear industry to develop a new analytical framework, known as the Composite Analytical Approach (CAA), which is aimed at demonstrating that the LLOCA safety margins are much larger than those currently being predicted using a more conservative analysis methodology, which includes the use of a Limit of Operating Envelope (LOE) analysis. Part of the industry effort to demonstrate that larger safety margins exist consists of a re-evaluation of the fuel safety criteria currently being used in the LLOCA analysis. This includes a systematic process to identify the physical barriers relevant to the accident, their various failure mechanisms, and their associated failure limits. The principal output from this process is the establishment of Derived Acceptance Criteria (DAC) which are defined with a certain margin to their failure limits. This process includes a review of the existing experimental database, the identification of additional experiments needed to address gaps in knowledge, and a review of the analytical capability of the current computational toolset to demonstrate compliance to the LLOCA DAC. Pending CNSC approval for the use of the CAA, including its subsequent implementation by each licensee, the CNSC has instituted a set of interim criteria for maximum fuel enthalpy, maximum fuel centreline temperature, and maximum fuel sheath temperature. In addition, the CNSC has established a regulatory process to address any adverse findings which may impact the LLOCA safety margins under the current analysis framework.

1. INTRODUCTION

An inherent characteristic of the CANDU Pressurized Heavy Water Reactor (PHWR) core design is that it has a positive Coolant Void Reactivity (CVR) coefficient. The impact of having a positive CVR in a CANDU is most severe in the analysis of a Large Loss of Coolant Accident (LLOCA).

A LLOCA in a CANDU is postulated to occur as a result of an instantaneous failure of a large diameter pipe in the Primary Heat Transport System (PHTS). As a consequence of having a positive CVR, the rapid coolant voiding of a CANDU core under LLOCA conditions (due to the postulated large diameter pipe break) leads to a large and relatively immediate increase in reactor power. This sudden increase in reactor power is characterised by a ~2 s power pulse during which the bulk power can rise to as much as five times its nominal value. In addition, the heat generation in the hottest element of the maximum power fuel bundle can rise by as much as ten times its normal operating condition value.

The LLOCA is a low probability event which has never occurred in a CANDU PHWR. Despite the low probability of its occurrence, the LLOCA is classified as a Design Basis Accident (DBA) within the Canadian regulatory framework; and as such, it sets the requirements for the speed of the shutdown systems. In addition, the LLOCA is also used to set design requirements for the Emergency Core Cooling System (ECCS), reactor containment, and for the establishment of maximum reactor operating parameters (e.g., fuel

bundle power).

A DBA has a frequency of occurrence of 10^{-5} to 10^{-2} per reactor year. It is defined as an accident against which a nuclear power plant (NPP) is designed such that fuel damage and the release of radioactive material are kept to within authorised limits [1]. Table 1 lists the event type classification and corresponding frequency of occurrence according to Canadian Nuclear Safety Commission (CNSC) Regulatory Document 310 (RD-310) [1].

TABLE 1. EVENT CLASSIFICATION AND CORRESPONDING FREQUENCY OF OCCURRENCE

Event Type	Frequency of Occurrence [per reactor year]
Anticipated Operational Occurrence	$> 10^{-2}$
Design Basis Accident	$[10^{-5}, 10^{-2}]$
Beyond Design Basis Accident	$< 10^{-5}$

The LLOCA analysis for CANDU PHWRs in Canada has been affected by periodic discoveries that have impacted the predicted consequences of the event to the extent that the margins to failure have been significantly eroded. To address this reduction in safety margins, the Canadian nuclear industry has embarked on an extensive initiative to develop a new analytical framework aimed at demonstrating that LLOCA safety margins are much larger than those currently being predicted [2].

2. CURRENT LLOCA ANALYSIS FRAMEWORK

The current analytical framework for the LLOCA employs a Limit of Operating Envelope (LOE) analysis, which simultaneously sets all important safety and operational parameters at their allowable (most detrimental) limits in order to bound the accident consequences. Another key component of the current LLOCA analysis methodology is the assumption of an instantaneous double-ended guillotine break (DEGB) of the largest diameter pipe (e.g., an inlet header), which maximises the consequences of the accident. The high level acceptance criteria for the current LLOCA analysis are the prevention fuel channel (pressure tube) failure and meeting specified DBA dose limits.

The assumptions considered in the LOE analysis of a LLOCA are very conservative given the unlikely combination of plant conditions that are postulated prior to the initiation of the accident. Moreover, the assumption of an instantaneous DEGB of the largest diameter pipe, at a location that maximises the voiding rate, and hence the power pulse, is also a very conservative assumption.

Despite its conservative framework, the small margins predicted as a consequence of the current LLOCA analysis methodology make the resulting safety case susceptible to analytical, experimental, and operational discoveries. In response, a joint CNSC-Industry Working Group on Positive Reactivity Feedback and LLOCA Safety Margins was formed in 2008 in order to develop resolution strategies to address the erosion of the LLOCA safety

margins [2]. The working group identified two resolution strategies:

(a) The development of a new analytical framework, which may include one of, or a combination of:
    (i) Reclassification of different break-sizes into DBA and Beyond Design Basis Accident (BDBA) categories;
    (ii) Development of a more realistic model for break-opening progression;
    (iii) Further development of a more a realistic analysis methodology (e.g., Best Estimate and Analysis Uncertainty (BEAU) methodology);
    (iv) Continued use of LOE analysis.
(b) Pursuing a design change strategy, including:
    (i) Modifications to the shutdown systems;
    (ii) Implementation of Low Void Reactivity Fuel (LVRF);
    (iii) Changes to operational practices.

After considering the identified resolution strategies, the CNSC and the industry chose to pursue the option of developing a new analytical framework for resolving the LLOCA safety margin issue. This option was selected with the understanding that the design change resolution strategy (e.g., LVRF) remains as a backup option in the event that the development of a new analytical framework is unsuccessful.

3. OVERVIEW OF THE COMPOSITE ANALYTICAL APPROACH

The new analytical framework currently being developed by the industry is called the Composite Analytical Approach (CAA) [2]. The CAA is built upon four Technical Areas (TAs), each of which addresses a key component of the LLOCA analysis. Fig. 1 shows the interfaces of the four TAs for the CAA. Additional detail describing the objective of each TA is given in Table 2.

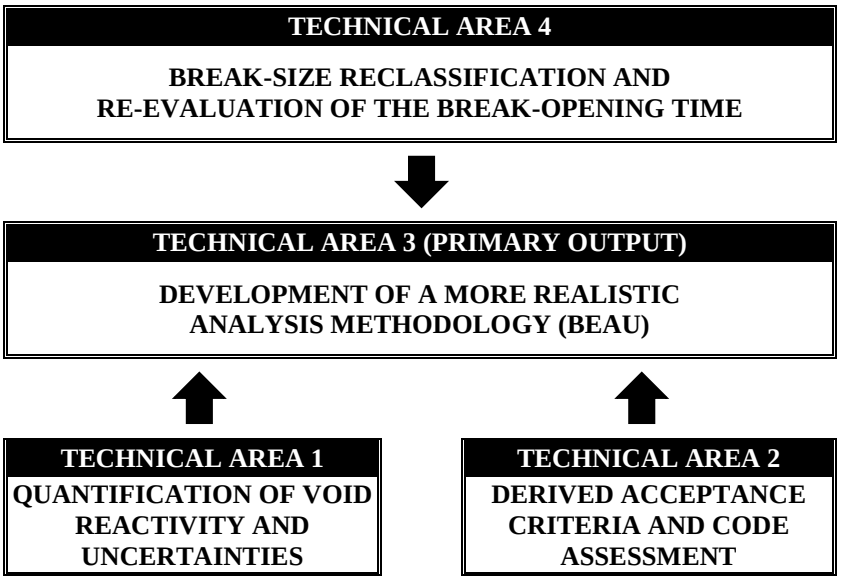

FIG. 1. Technical area interfaces for the Composite Analytical Approach [2].

An important element of the CAA is TA-2, which consists of a re-evaluation of the Derived Acceptance Criteria (DAC) and the computational toolset currently being used in the LLOCA analysis. This includes a systematic process to identify the physical barriers relevant to the accident, their various failure mechanisms, and their associated failure limits. The principal output from TA-2 is the establishment of DAC that are defined with a certain margin to their failure limits. TA-2 also includes a review of the existing experimental database, the identification of additional experiments needed to address gaps in knowledge, and a review of the analytical capability of the current computational toolset to demonstrate compliance to the newly developed DAC.

TABLE 2. TECHNICAL AREA OBJECTIVES OF THE COMPOSITE ANALYTICAL APPROACH

Technical Area	Objectives
TA-1	1. Evaluate the need for performing additional experiments in order to better quantify the CVR, as well as other reactivity feedback coefficients and physics (kinetics) parameters. Examine the possibility of using other approaches to demonstrate the applicability of the reactivity feedback coefficients (including CVR) and kinetics parameters for use in the LLOCA analysis.
TA-2	2. Systematically develop and define limits and DAC based on a re-evaluation of the current experimental database, while factoring the impact of the associated uncertainties and "unknown unknowns" may have on the margins defined by these limits and DAC. Evaluate the capability of the current computational toolset to demonstrate compliance to the newly established DAC, and to identify any phenomenological (modelling) shortcomings that may hinder an adequate analysis. Consider the need to perform additional experiments and/or validation exercises in order to address any identified gaps in the both the experimental and analytical (i.e., computational toolset) knowledge base supporting the development of the limits and DAC.
TA-3	3. Develop a more realistic BEAU methodology which reflects the improved analytical basis derived from TA-1 and TA-2, as well as the re-evaluation of the bounding characteristics of the break-frequency and break-opening time for the postulated large diameter pipe break as derived from TA-4.
TA-4	4. Quantify the likelihood (probability) of PHTS piping failures ranging from minor cracks and leaks to the limiting DEGB of the largest diameter pipe in the PHTS (e.g., inlet header). 5. Deterministically demonstrate a more realistic break-opening time for the largest diameter pipe. 6. Establish the technical basis for the potential reclassification of the LLOCA event from a DBA to BDBA.

4. CNSC EXPECTATIONS FOR THE ESTABLISHMENT OF DERIVED ACCEPTANCE CRITERIA

It is CNSC staff's position that a number of improvements are needed in the formulation of the current LLOCA DAC. For example, the margins to failure for the current DAC needs to be better defined, and the completeness of the failure mechanisms for the physical barriers needs to be confirmed. In addition, the overall experimental basis for the current DAC needs to be strengthened.

It is therefore the expectation of CNSC staff that the DAC are developed to be sufficiently robust such that they remain unaffected by experimental and/or analytical discovery issues; and more importantly, that they are independent of the analysis methodology used to demonstrate compliance. The sections that follow describe CNSC staff expectations as to how the DAC should be established.

4.1. Framework for establishing derived acceptance criteria and safety margins

Fig. 2 is the basis for defining the framework for establishing safety margins in the context of determining a DAC for a given (generic) Barrier Failure Point (BFP). The sections that follow discuss the definitions within the overall framework of Figure. 2, and are consistent with current international guidelines and practices [3–5], as well as a previous publication by CNSC staff [6].

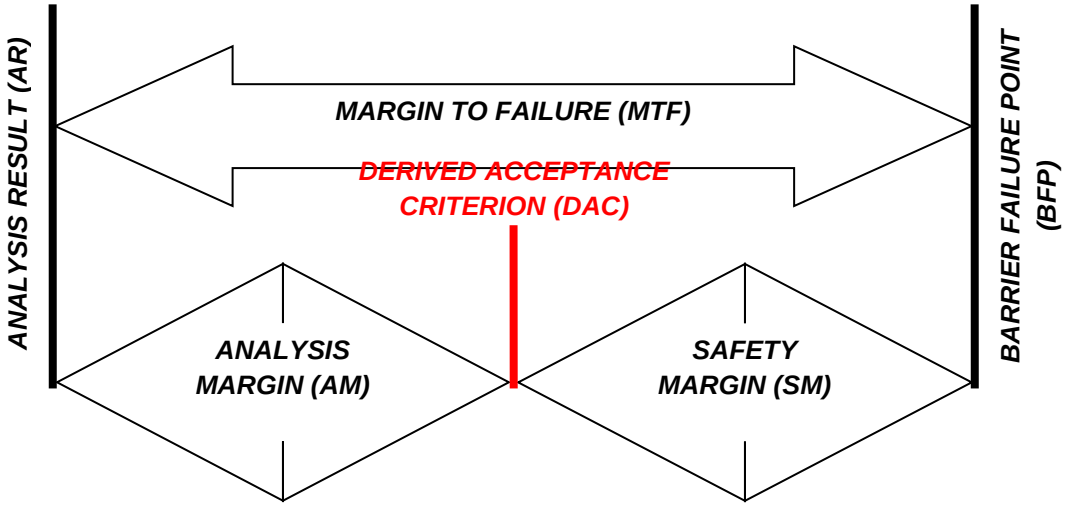

FIG. 2. Framework for establishing a derived acceptance criterion and margins.

4.2. Margin to failure

The Margin to Failure (MTF) encompasses the conditional states of a barrier ranging from the Analysis Result (AR), which reflects the state of the barrier under a certain operating condition of the NPP, to the Barrier Failure Point (BFP).

4.3. Barrier failure point

The first step in establishing a DAC is to define the BFP. A given barrier (e.g., fuel sheath or pressure tube) may have multiple failure mechanisms, each of which may be a function of a separate set of governing phenomena for a given normal operating or accident condition. The BFP is characterised by the material properties of the barrier in question, and should therefore be defined on the basis of a global evaluation of the available experimental databases (integral and separate effects) for each of the failure mechanisms that may impact the barrier for a given condition (or set of conditions).

4.4. Safety margin

The Safety Margin (SM) takes into account all experimental uncertainties associated with establishing the BFP. In addition, the SM must make allowances for "unknown unknowns" (i.e., mitigating the risk for additional discoveries) that may impact the phenomenological understanding as well as the coverage and interpretation of the experimental database(s) of the failure mechanism(s) in question.

It is important to note that due to the possible expansion of the experimental database, and the understanding thereof, the reduction or increase in the magnitude of uncertainties, as well as the potential for additional discoveries, signifies that the SM is dynamic (i.e., it may shrink or expand).

4.5. Derived acceptance criterion

The importance of clearly understanding the location of the BFP and adequately incorporating its associated uncertainties into the SM is what allows for the establishment of a robust DAC, which is defined by adjusting the BFP by the magnitude of the SM. A soundly-established DAC ensures that a barrier is never allowed to approach a state where its failure is possible within the broader operational range of the NPP subject to the analysis rules for a given event type (Table 1).

4.6. Analysis result

The AR is dependent on the analysis methodology being used, and is evaluated keeping in mind the specified requirement for meeting the DAC, as characterised by the Analysis Margin (AM).

4.7. Analysis margin

The AM incorporates all uncertainties associated with calculating the AR, including analysis methodology selection, code validation and verification, and the assignment of analytical and/or secondary conservatisms. The AM is dynamic, and may change given the potential for improvements in analysis methodologies, enhancements in computational code validation and verification, and the justified relaxation of analytical and/or secondary conservatisms.

4.8. Treatment of uncertainties

As depicted in Fig. 3, depending on the analysis methodology and the specified requirement for meeting the DAC, the AR (including associated uncertainties), as

characterised by the given probability density function, will either remain to the left of the DAC threshold (Fig. 3(a)), or, under certain circumstances, cross the threshold and extend into the area characterised by the SM, as indicated by the area shaded in red (Fig. 3(b)). The latter case, for example, would be consistent with a requirement that the DAC be met with a certain probability and confidence level. How the uncertainties are ultimately treated, and the applicability thereof with respect to the DAC, will be evaluated by CNSC staff as part of its formal review of the CAA.

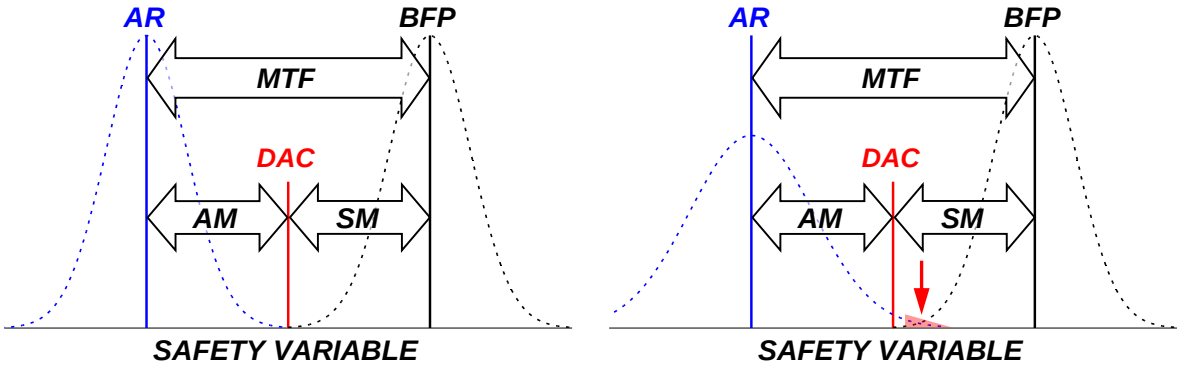

FIG.3. Treatment of uncertainties in the analysis of safety margins.

5. CURRENT STATUS OF LLOCA SAFETY MARGINS

Despite the significant reduction in LLOCA safety margins, Canadian CANDU licensees continue to meet the current acceptance criteria for the protection of fuel channels (pressure tubes) and specified DBA dose limits. Moreover, design and operational provisions are in place to mitigate the adverse effects of the positive CVR. It is therefore important to note that the safety of the current Canadian CANDU fleet as it relates to the LLOCA is not in question.

However, the current timelines associated with the completion of the development of the CAA and its implementation by licensees could potentially extend beyond 2016. In order to mitigate the risks associated with these timelines, the CNSC has developed an interim regulatory position in the event that a research, analytical, or NPP operational finding, which could have an adverse impact on the current LLOCA safety margins, emerges prior to the full implementation of the CAA.

The interim position establishes a set of action level limits and DBA acceptance criteria applicable to all Canadian CANDU NPPs irrespective of their existing LLOCA safety margins. The interim action level limits and DBA acceptance criteria, which have been developed following a series of consultations between CNSC and industry experts, serve the following purposes:

(i) Act as an **Interim Action Level Limits** in order to determine whether or not further investigation is needed following an adverse finding, or;
(ii) Act as an **Interim Acceptance Criteria** for the portion of the LLOCA that is classified

as a DBA.

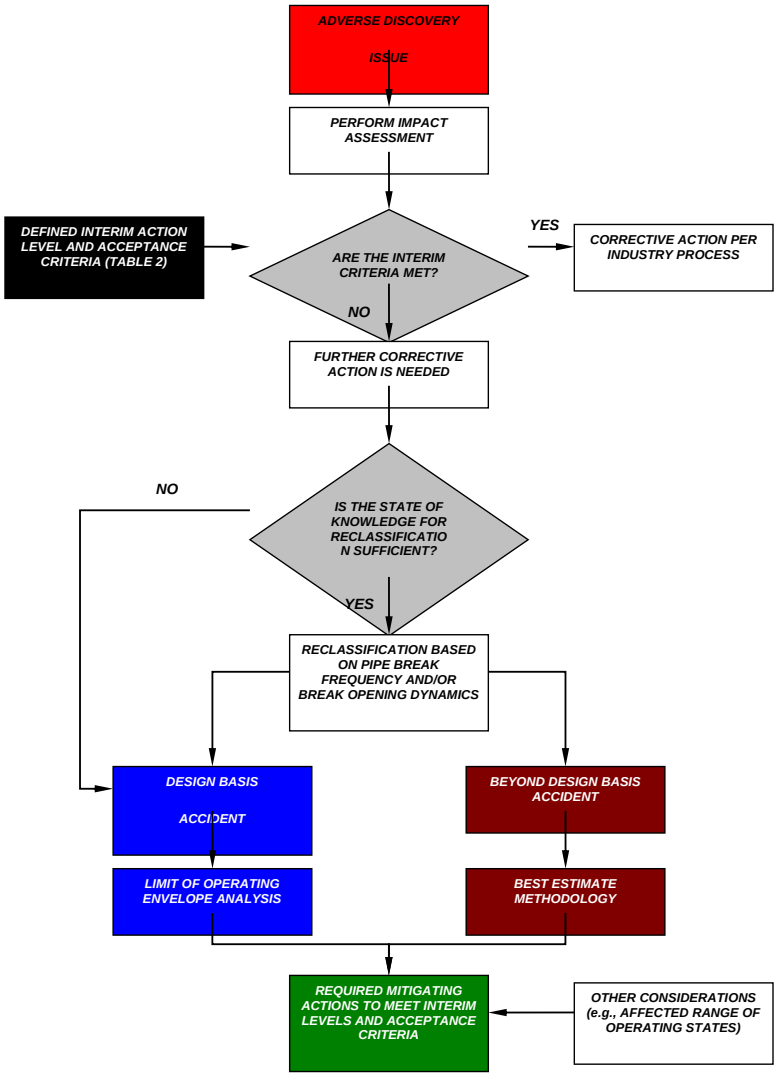

FIG. 4. LLOCA interim position assessment process decision tree.

The interim action level limits and DBA acceptance criteria are listed in Table 3, and the assessment process for the interim position is presented in Fig. 4. The interim position has been officially communicated to all Canadian CANDU licensees and is the regulatory requirement superseding the current acceptance criteria in the current safety analysis reports.

The numerical values for the interim action level limits and DBA acceptance criteria ensure that adequate safety margins remain in place until the CAA development work is complete, accepted for use by the CNSC, and implemented by industry stakeholders in their safety case.

The process described in Fig. 4 uses the interim action level limits and DBA acceptance criteria, which would be considered by CNSC staff as triggers for a decision regarding the need for further investigation and to determine the extent of corrective actions following an adverse finding. For the BDBA portion of the LLOCA, it expected that the analysis will be performed to demonstrate that the established probabilistic safety goals are met, and that the accident management programme and design provisions are effective, as defined in [1].

TABLE 3. LLOCA INTERIM ACTION LEVEL LIMITS AND DBA ACCEPTANCE CRITERIA

Safety Margin Parameter	Current Acceptance Criteria in the Safety Analysis Reports	Interim Action Level Limits and DBA Acceptance Criteria	Peak Value Range in Current Safety Analysis Reports (Licensee Specific)
Maximum Fuel Enthalpy [kJ/kg]	960	**815**	574 – 784
Maximum Fuel Centreline Temperature [°C]	2840 (melting point)	**2600**	2142 – 2546
Maximum Fuel Sheath Temperature [°C]	1760 (melting point)	**1550**	1289 – 1499
Moderator Sub-cooling Availability	Availability required		
Avoidance of fuel string axial expansion	Avoidance required		

6. CONCLUSION

The CNSC is currently actively monitoring an extensive initiative by the Canadian nuclear industry to develop the CAA, which is a new analytical framework aimed at demonstrating that the LLOCA safety margins are much larger than those currently being predicted [2].

A key component of the industry's effort to demonstrate that larger safety margins exist consists of a re-evaluation of the DAC being used in the LLOCA analysis (TA 2, Fig. 1). This includes a systematic process to identify the physical barriers relevant to the accident, their various failure mechanisms, and their associated failure limits. The principal output from TA-2 is the establishment of DAC which are defined with a SM to their respective failure limits.

Pending CNSC approval for the use of the CAA, including its subsequent implementation by each licensee, the CNSC has instituted a set of interim action level limits and DBA acceptance criteria, which includes limits on maximum fuel enthalpy, maximum

fuel centreline temperature, and maximum fuel sheath temperature. These will ensure that adequate safety margins remain in place until the LLOCA margin restoration issue is resolved. In addition, the CNSC has established a regulatory process to address any adverse findings which may impact the LLOCA safety margins under the current analysis framework.

The interim position will remain in effect until the recommendations of the industry initiative to develop the CAA are accepted by the CNSC and are fully implemented by each licensee.

ACKNOWLEDGEMENTS

The author wishes to recognise the contributions of past and present CNSC staff and colleagues in the publication of this paper.

REFERENCES

[1] CANADIAN NUCLEAR SAFETY COMMISSION, Safety Analysis for Nuclear Power Plants, RD-310, Ottawa (2008).

[2] PURDY, P., et. al., A Composite Analytical Solution for Large Break LOCA, International Conference on the Future of HWRs. Canadian CANDU Industry Steering Committee on Large Break LOCA and Positive Void Reactivity, Ottawa (2011).

[3] INTERNATIONAL ATOMIC ENERGY IAEA, Safety Margins of Operating Reactors – Analysis of Uncertainties and Implications for Decision Making, IAEA-TECDOC-1332 (2003).

[4] INTERNATIONAL ATOMIC ENERGY IAEA, Implications of Power Uprates on Safety Margins of Nuclear Power Plants, IAEA-TECDOC-1418, Vienna (2003).

[5] NUCLEAR ENERGY IAEA, Task Group on Safety Margins Action Plan (SMAP) Safety Margins Action Plan, NEA/CSNI/R(2007)9. OECD-NEA, Paris (2007).

[6] VIKTOROV, A., "Safety margins in deterministic safety analysis", 32nd Annual Canadian Nuclear Society Conference, Niagara Falls (2011).

SLIGHTLY ENRICHED URANIUM CORE BURNUP STUDY IN CANDU 6 REACTOR

I. PRODEA
RAAN-Institute for Nuclear Research,
Piteşti, Romania
Email: iosif.prodea@nuclear.ro

Abstract

CANDU reactor design also has the flexibility to use other fuel cycles than that of Natural Uranium (NU) due to the high neutron economy of its standard lattice. In this paper Slightly Enriched Uranium (SEU) fuel with 1%wt U235 is investigated in order to find out the suitability to be burnt in CANDU reactors. The core fuel management characteristics at the use of SEU fuel in C-43 fuel bundle developed in INR Pitesti are presented versus those of NU fuel in the standard 37-rod fuel bundle design. The reactor core is similar to that of Cernavoda Unit 1. The maximum channel and bundle powers are the key neutronic parameters pursued during the simulations using a 3D finite differences code - DIREN (developed in INR Pitesti). Latest developments added to the DIREN code give the possibility to simulate automatic refuelling operations for standard and advanced CANDU fuel designs. The calculations revealed that SEU fuel in C-43 bundle design allows a better power distribution control over the reactor core through more uniform Power Peaking Factors (PPFs) values over the fuel rod rings. The maximum linear powers on the outermost fuel ring are inside of operation margins. The study concludes that SEU is a viable option to be used in Romanian CANDU reactors for a better Uranium utilization.

1. INTRODUCTION

The paper continues earlier studies started to find out the possibility to use alternative fuel cycles in CANDU reactors and their influence on core integral parameters. As it is shown in [1], the Romanian Nuclear Energy Strategy foresees that the third and fourth units of the Cernavoda NPP will be commissioned by the end of actual decade. Improvements in operation and safety are expected to be applied for these Enhanced CANDU 6 (EC6) units. On the other side, it is very well known that national (actually known) Uranium reserves are not enough to cover nuclear fuel needs for more than two units in actual decade, [1]. As a result, Romania has to look for alternative fuel cycles suitable to be used in actual CANDU power reactors. One of them can be SEU fuel cycle, as it can bring economic benefits along with some safety improvements that will be revealed by the present paper. The 1%U235 fissile content of the SEU fuel taken into account makes possible its utilization in CANDU reactors. In this respect, specific core calculations must be done in order to find out the viability of SEU as fuel for actual CANDU 6 reactors.

In this paper we performed comparative calculations concerning core integral parameters estimated by both time/average and refuelling calculations in a CANDU 6 reactor. Two fuel designs were taken into account: the Natural Uranium in a 37-rods CANDU standard bundle (referred as 37Nat) and the 1%SEU in the advanced bundle design C-43 developed in Institute for Nuclear Research (referred as 43SEU**,** [2]). The CANDU reactor feature to be fuelled during operation brings additional problems for fuel burnup simulation in time steps, especially in finding fuel channel which are to be refuelled and, in the same time, satisfying nuclear safety requirements. These safety requirements are grossly given by the maximal channel powers which are to be under 7.1 MW and the powers on radial zones associated to the Zone Control Units=ZCU) which must be under 5% from their reference values obtained through a "time-average" calculation, [3]. In this respect, the 3D diffusion code DIREN [4], based on finite differences has been developed in SCN Pitesti. New options were implemented in DIREN, especially for simulation of refuelling operations and

generating burnup histories, [5], [6], [7]. Refuelling operations were performed for a sufficiently long time interval (950 days) to find out the advantages of 43SEU fuel design utilization versus the traditional CANDU 37Nat one.

2. METHODOLOGY

The two fuel design characteristics are presented in Table 1 and Figure 1.

TABLE 1. FUEL DESIGN CHARACTERISTICS

Fuel Symbol	Geometry	Configuration (Case #)	Composition by inner rings
37Nat	CANDU Standard 37 equal rods	1	CE, R1,R2,R3: Natural Uranium with 0.72%U235
43SEU	C-43 (43 rods, CANFLEX like)	2	CE, R1,R2,R3: Slightly Enriched Uranium (SEU) with 1.0 % U235

The symbols' significance in Table 1 is the following:

- CE = central element;
- R1-R3 = inner rings from inmost to outermost.

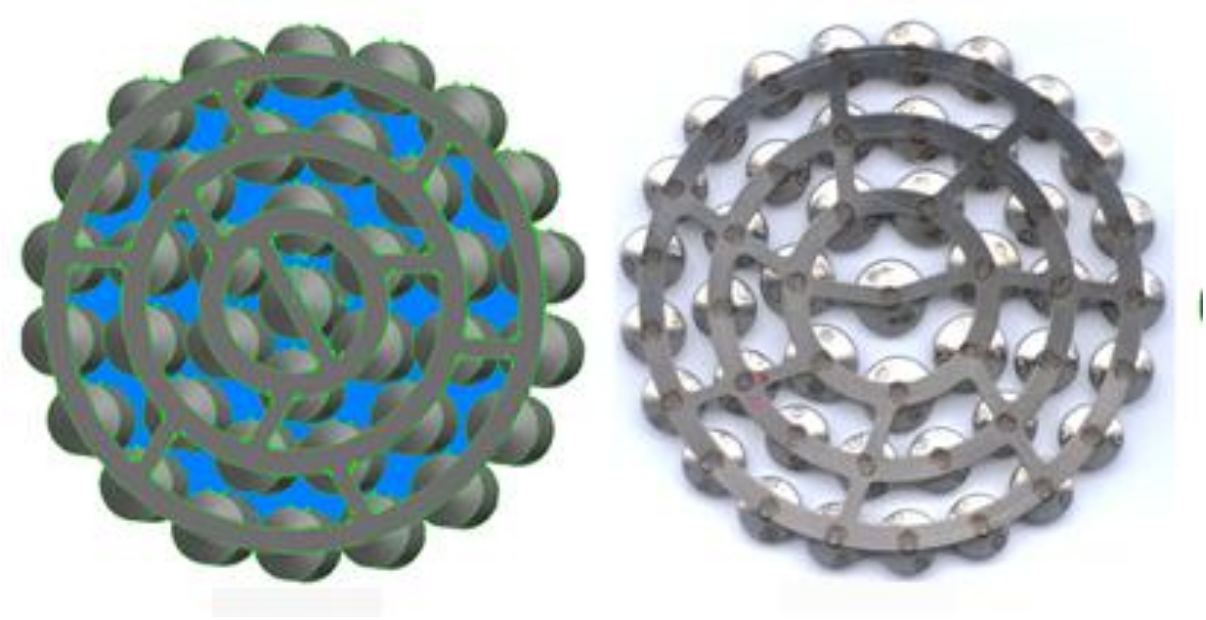

FIG. 1. 37Nat (left) and 43SEU (right) bundle designs, [8].

The 3D computer program DIREN developed in INR Pitesti in order to model CANDU reactor cores is a finite differences program based on diffusion approximation, which solves diffusion equation in a 3D geometry suitable for CANDU 6 core, where the reactivity devices are perpendicular to the fuel channels. DIREN can be used for the following type of reactor physics calculations, [5]:

- Bigroup an multigroup burnup simulation on time steps;
- Time average approximation;
- High modes of diffusion equation;
- Flux mapping;
- 3d spatial kinetics calculation using quasistatic point kinetics approximation;
- Xenon effect modelling along with zone control units (zcu) spatial and global simulation;
- Burnup histories' generation with automatic refuelling (also called "*core-follow simulations"* [9]).

To attain the proposed paper's objectives, we used the latest DIREN option.

First of all, two lattice burnup step calculations have been performed with the WIMS-D5B code [10] and an associated nuclear data library [11], in order to generate macroscopic cross sections by time steps up to 16 MW·d/kgU for 37Nat and almost double and half, 38 MW·d/kgU for 43SEU fuel design. Then, with these data for fuel and using a standard CANDU 6 core model [12], [13] adapted to the DIREN input, we performed a suite of time average calculations to find out reference data for refuelling (Block "G" in DIREN input file): reference burnup and channel power distributions along with ZCU reference radial power distribution, (in %). Varying the discharge burnup values on the four burnup regions as in Fig. 2, we achieved a symmetric ZCU radial powers and a maximum channel power value of about 6.5 MW. The seven ZCU radial power regions are defined in Fig. 3.

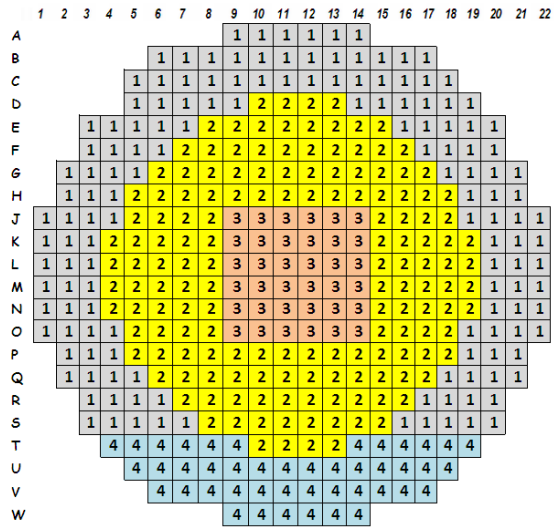

FIG. 2. The four burnup regions.

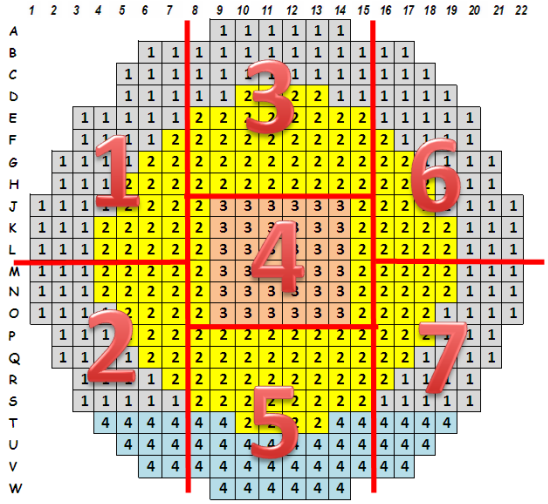

FIG. 3. The 7 zone control unit power regions.

As it is underlined in [14], the need to have symmetric up/down and left/right ZCU power distributions is mandatory to give the possibility to launch refuelling calculations. The alluded up/down and left/right differences must be under 1.5-2%, the condition being generally satisfied by the obtained values as it will be shown in the next chapter (Table 2). Another mandatory condition is getting a very good core criticality (core reactivity in the range of ± 0.5 mk), also accomplished for every fuel design, (see Table 2).

2. RESULTS

Table 2 presents core relevant parameters obtained in time average calculations.

TABLE 2. TIME/AVERAGE CORE NEUTRONIC CHARACTERISTICS

Core parameter	37Nat (0.72% U235)	43SEU (1% U235)
ZCU powers (%)	16.69 12.96 12.95 14.96 12.94 12.92 16.58	16.24 13.82 13.76 12.01 13.84 13.79 16.54
Burnup on the four regions (MW·d/kgU)	*1* *2* *3* *4* 6.35 7.0 6.5 5.95	*1* *2* *3* *4* 12.5 16.6 15.1 12.0
Average Discharge Burnup (ADB) (MW·d/kgU))	6.7	14.2
Max. channel power and location	6.54 MW P-8	6.52 MW T-8
Max.bundle power and location	804 kW S 11 - 6	779 kW T-8-8
k-effective	1.000066	0.999862
Core reactivity (mk)	0.07	-0.14

As it can be seen, all the mandatory conditions (core criticality range of ±0.5 mk, ZCU power fair symmetry and maximum channel power around of 6.5MW) have been attained. Of interest is the Average Discharge Burnup (ADB) evaluated through time/average (TA) calculations. As expected, the 43SEU fuel design supplied an ADB significantly larger than that of 43SEU fuel design, 14.2 versus to 6.7 MW·d/kgU. It is remarkable because an enrichment rising from 0.71 to 1%U235 can increase more than twice the energy generated and, in the same time, correspondingly reducing the radioactive waste amount. This means that SEU fuel cycle is a promising option to be applied in actual CANDU power reactors.

Note that, these are time average results, based on averaging of the lattice cross sections over the expected residence (dwell) time of the fuel at each point (fuel bundle position) in the reactor core, [3], [12]. This type of calculation allows for the effect of the refuelling scheme used (e.g. 8-bundle shift for 37Nat and 2&4-bundle shift for 43SEU) to be taken into account.

We will see that as a result of 950 FPD refuelling calculations with 43SEU fuel design the uranium utilization is considerably improved (Table 5).

Figs. 4 and 5 illustrate the maximum channel and bundle power evolutions during refuelling simulation interval for every fuel designs. It can be observed that the imposed values in the DIREN refuelling algorithm (935kW for maximum bundle power and 7100 kW for the maximum channel power) are not overridden in any simulation step for both fuel designs. Moreover, there is a comfortable "reserve" of 200 kW up to the channel power licence limit (7300 kW) and a smaller reserve, 21 kW up to the bundle power licence limit.

We consider these results being of a fair accuracy, knowing that our computer modelling couldn't take into account for the multitude of real field parameters involved in current operation of a power reactor, and especially for the human operator action whose decisions (for example in channel choosing for refuelling) are crucial.

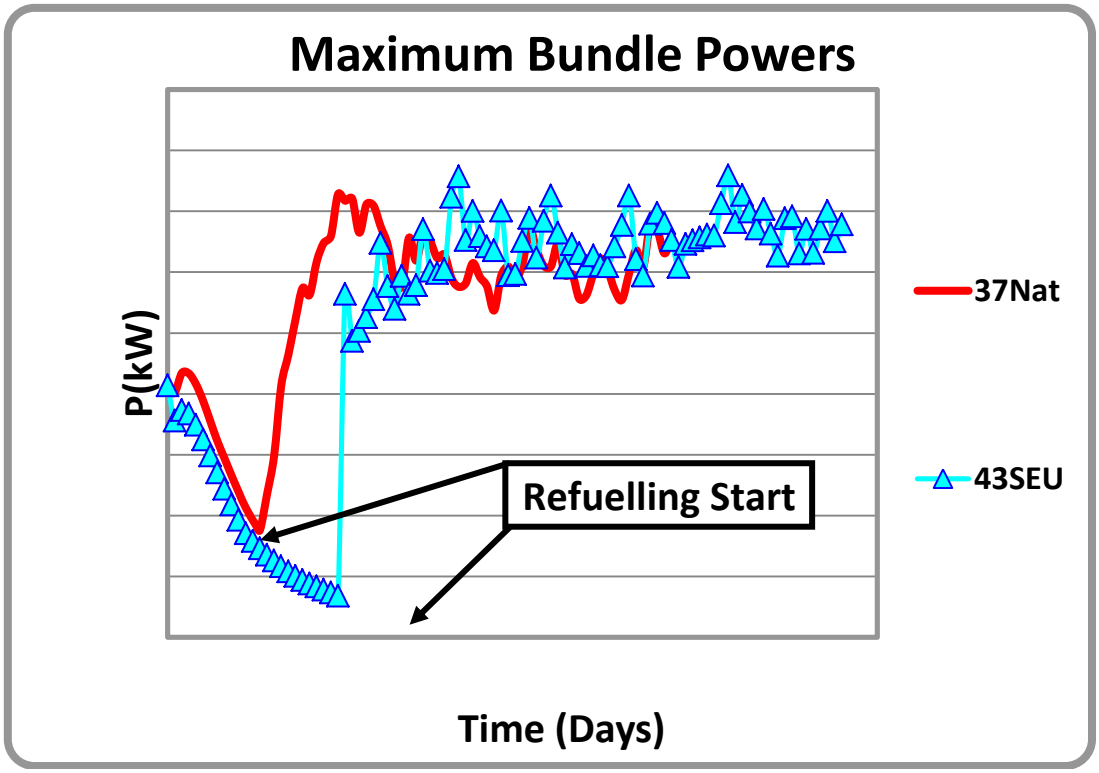

FIG. 4. Maximum bundle power evolution.

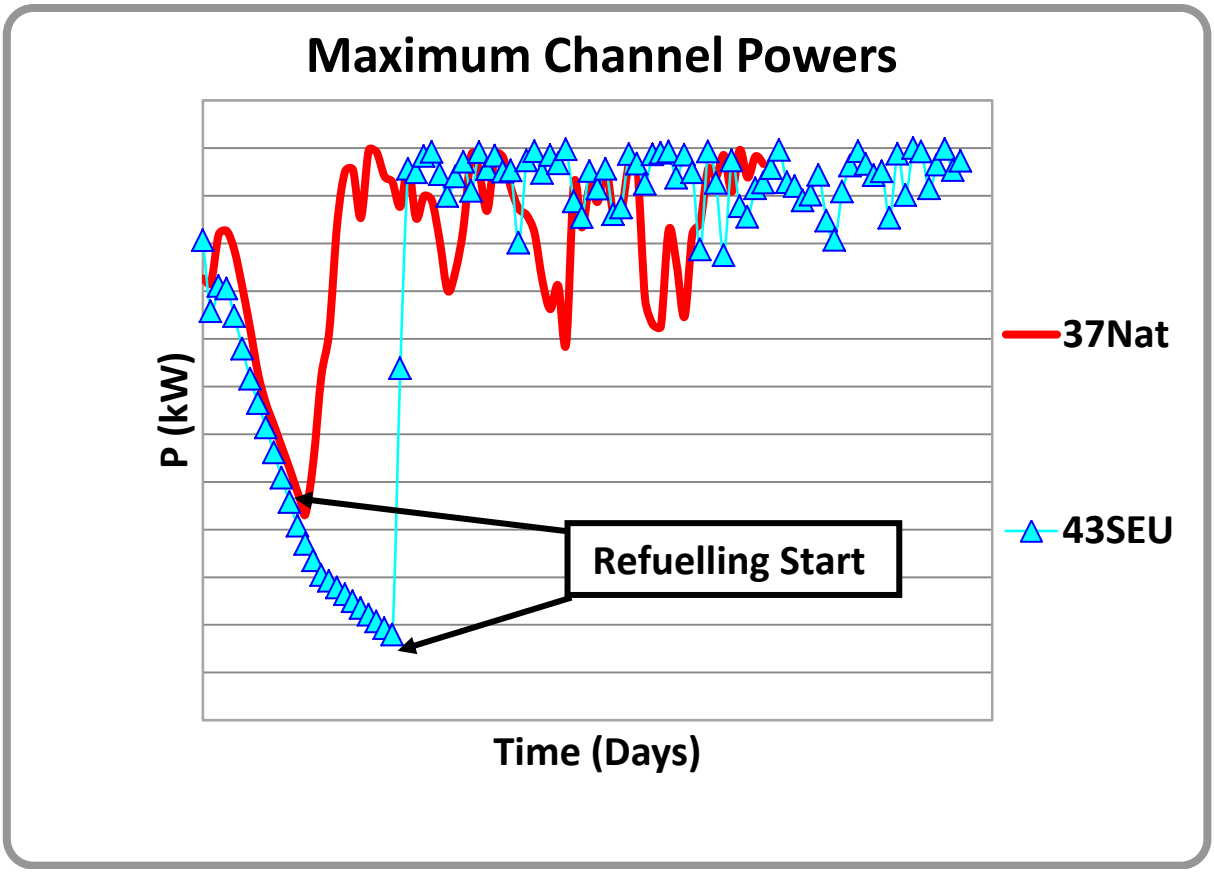

FIG. 5. Maximum channel power evolution.

On the other side, a simple calculation performed using WIMS data reveals that, even in the case of the most unfavourable situation (in the step where maximum bundle power is attained), the linear power on the outer ring of the 43SEU fuel is still lower than that of 37Nat, see Tables 3 and 4 and Fig. 6. It is well recognized and WIMS calculations show that the outer most rod ring of the 37-rods bundle is the most stressed during operation. Moreover, specific design of the C-43 bundle (with the 8 central rods thicker than the rest ones) assure a better power flattening over the bundle rings – a permanent objective of the fuel burnup management activities, see Fig. 6.

TABLE 3. LINEAR POWER THROUGH WIMS CALCULATIONS AT MID BURNUP (3.5 MW·d/kgU)

37Nat	PPF (WIMS)	Number of rods	P_{ring}/P_{bundle} (WIMS)	P (kW)	P_{lin} (kW/m)
CE	0.756	1	0.021	19.2	38.8
Ring 1	0.797	6	0.129	117.9	39.7
Ring 2	0.905	12	0.294	268.7	45.2
Ring 3	1.141	18	0.556	508.2	57.0
	Total	37	1.000	914	

TABLE 4. LINEAR POWER THROUGH WIMS CALCULATIONS AT MID BURNUP (7.0 MW·d/kgU)

43SEU	PPF (WIMS)	Number of rods	P_{ring}/P_{bundle} (WIMS)	P (kW)	P_{lin} (kW/m)
CE	0.753	1	0.025	22.35	45.2
Ring 1	0.793	7	0.179	159.94	46.2
Ring 2	0.919	14	0.285	255.06	36.8
Ring 3	1.165	21	0.511	456.83	43.9
	Total	43	1.000	894	

In Tables 3 and 4, columns 2 ("PPF") and 4 ("P_{ring}/P_{bundle}") present lattice results obtained through the WIMS calculations. The abbreviations signify:

— PPF=Power Peaking Factors=the ratio between the average power (power density) on a ring and the average power on the entire bundle (PPF are calculated in WIMS program);
— P_{ring} , P_{bundle}= the absolute power on a ring and on the bundle, respectively. The ratio P_{ring} to P_{bundle} (ring power fraction from total bundle power) is also printed in WIMS output;
— P_{lin} = the linear power on a ring.

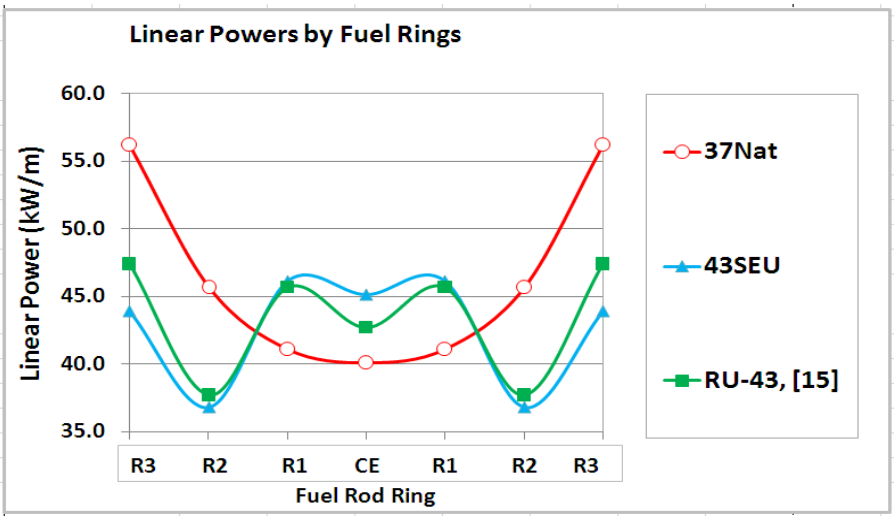

FIG. 6. Linear powers through the WIMS calculations at mid burnup [15].

The green curve in Fig. 6 corresponds to a Recovered Uranium based (0.96%U235) fuel design, "RU-43" and calculations have been performed in [15] using the same methodology. We can observe again that another slightly enriched fuel design placed in the advanced geometry bundle C-43 supplied a much better power flattening and lower linear powers by fuel rod rings.

Regarding 37Nat and 43SEU core integral parameters, these are presented in Table 5, comparatively with those of Recycled Uranium (RU-43) taken from [15]. Both 43 rods fuel designs show significant advantages on the standard 37 rods design, firstly by a significantly lower average feed rate, about a half of that of NU-37 fuel design and secondly, by a better uranium utilization.

TABLE 5. CORE INTEGRAL PARAMETERS GENERATED BY DIREN REFUELLING CALCULATIONS

Parameter	37Nat (0.72%U235)	43SEU (1%U235)	RU-43 [15] (0.96%U235)
Discharged Bundles	10,656	7700	8,068
FPD	710	950	950
Feed Rate (Bundles/FPD)	15.01	8.1	8.5
U mass/bundle.(kg)	19.3	18.6	18.6
U consumption = #Bundles*Umass/bundle (kgU/FPD)	289	151	158
Daily Energy (**DE**) = Fission Power(MWt) * 1 Day	2156 MW·d	2156 MW·d	2156 MW·d
Average Burnup = DE / Uconsumption (MW·d/kgU)	7.45	14.27	13.62
Average Discharge Burnup (Time/average Calculations) (MW·d/kgU)	6.65	14.21	13.45

We can also evaluate an Average Burnup (AB) over the entire period of simulations, in fact a measure of Uranium utilization. Through some simple calculations performed in Table 3, we obtained an average burnup of 14.27 MW·d/kgU for the "43SEU" fuel design, 13.62 MW·d/kgU for RU-43 fuel design and 7.45 MW·d/kgU for "37Nat" fuel design. The best Uranium utilization pertains to the "43SEU" fuel design (151 kg/FPD) which also benefits for a more flexible refuelling scheme. This scheme (slightly unusual face to the real operation conditions) considers a 2 bundle shift strategy in the "inner core" region and a 4 bundle strategy in the "outer core" region, as in Fig. 7.

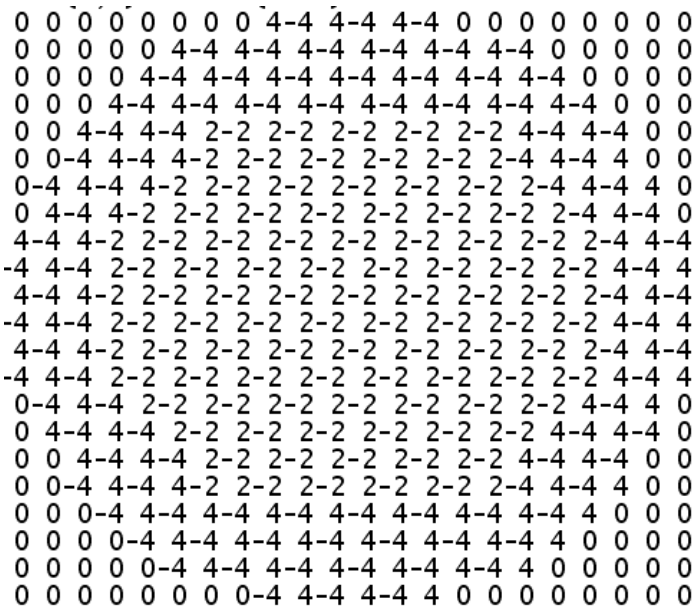

FIG. 7. Refuelling Scheme for 43SEU Fuel Design.

3. CONCLUSIONS

The DIREN code is able to be used in performing core refuelling simulations, both with natural and slightly enriched Uranium.

The maximum bundle and channel power supplied during the considered periods are situated inside of the safety limits.

The advanced SEU-43 bundle developed in INR Pitesti and fuelled with slightly enriched or recycled Uranium offers a viable fuel cycle option in CANDU reactors, this being proven by both a better radial power flattening over the bundle and a higher Uranium utilization than in the case of natural Uranium fuel cycle.

REFERENCES

[1] MINISTRY OF INDUSTRY AND TRADE, Romanian Energy Strategy for 2007–2020, www.minind.ro/presa_2007/septembrie/strategia_energetica_romania.pdf .

[2] HORHOIANU, G. et. al., Development of Romanian SEU-43 Fuel Bundle for CANDU Type Reactors, Annals of Nuclear Energy, No.16, **25** (1989) 1363–1372.

[3] ROUBEN, B., CANDU Fuel Management Course, Atomic Energy of Canada Ltd, http://canteach.candu.org/http://nuceng.mcmaster.ca/harms/harmshome.html .

[4] PATRULESCU, I., Developing of DIREN Code for Multigroup Core Calculations, Internal Report no. 5120, INR Pitesti, Romania, (1997).

[5] PATRULESCU, I., Reactor Physics Programs System for Personal Computers.

[6] PATRULESCU, I., Reactor Physics Programs System for Personal Computers. Part 4. DIREN User's Manual, Internal Technical Report, NT-308/2009, INR Pitesti.

[7] PATRULESCU, I, Reactor Physics Programs System for Personal Computers. Part 5. User's Manual for DIREN Auxiliary Programs, Internal Technical Report, NT-309/2009, INR Pitesti, Romania.

[8] CATANA, A., Thermal-hydraulics Advanced Methods for Nuclear Reactors (CFD and Subchannel Analyses for CANDU 600 Core), PhD Thesis, POLITEHNICA University of Bucharest, Power Engineering Faculty, (November 2010).

[9] D'ANTONIO, M. J., DONNELLY, J.V., "Explicit core follow simulations for a CANDU 6 reactor fuelled with recovered uranium CANFLEX Bundles", Proc. of the 5th International Conference on CANDU Fuel, ISBN 0-919784-48-8 and 0919784-50-X Set, Toronto, Canada, (21-25 Sepember 1997).

[10] WIMSD5B - NEA1507/03 Package, http://www.nea.fr/dbprog.

[11] WLUP-WIMS Library Update Project, http://wwwnds.iaea.org/wimsd/download/iaea.zip.

[12] BARAITARU, N., Description and Material Structure for Reactivity Devices and Other Components Present inside a CANDU-600 Core, Cernavoda NPP Unit 1, Reactor Physics and Safety Analysis Group, IR-03310-17, Rev.0, (7 July 2000).

[13] BARAITARU, N., A New Core Model for Neutronic Calculations with RFSP-IST (CV03M4.0), Cernavoda NPP Unit-1, Reactor Physics and Safety Analysis Group, IR-03310-34, Rev.0, (December 2004).

[14] PATRULESCU, I, Reactor Physics Programs System for Personal Computers. Part 2. Calculations' Description, Internal Technical Report, NT-306/2009, INR Pitesti.

[15] PRODEA, I., et. al., "Recovered versus natural uranium core fuel management study in a CANDU 6 Reactor", SIEN 2011, Bucharest, Romania, (16-20 October 2011).

FUEL INTREGRITY DURING ACCIDENT CONDITIONS
(Session 2)

Chairman

S. ANANTHARAMN
India

FUEL INTEGRITY ASSESSMENT AT KANUPP

F. TASNEEM and S. E. ABBASI
Karachi Nuclear Power Plant (KANUPP),
Karachi, Pakistan

Abstract

KANUPP is a pressurized heavy water reactor with gross generation capacity of 137 MWe. It has been in operation since 1972. Over 5060 full power days of operation have been completed since commissioning. The KANUPP core consists of overall 2288 fuel bundles residing in 208 fuel channels. The core is designed for flattened neutron flux profile corresponding to 100 % generator load. Currently, reactor is operating with partially flattened flux with a maximum limit upto 85% generator load. The fuel bundle generates maximum power upto 453 kW during its residence time in core that corresponds to 2.8 MW maximum channel power. The fuel management techniques are applied to keep powers of all fuel bundles residing in any fueling zone and corresponding channel powers within allowable limit. Two methods are employed at KANUPP to assess fuel integrity, namely I131 sampling in primary heat transport system and gaseous fission products' ratio (Rb88 / Cs138). After detection of fuel defect, delayed neutron scanning is used to locate the defective fuel within channel. Currently a system is being developed for the off-line measurement of inert fission gases Xe133 & Kr88 besides Rb88 & Cs138. A small fraction of primary coolant flows through the ion exchange column to remove dissolved fission products. All fission products except Xenon, Krypton and their daughter nuclides (exist in gaseous form), are assumed to be cleaned up in purification column. In the initial phase of plant operation, the core was loaded with Canadian fuel bundles. Subsequently, with attaining the capability to manufacture fuel locally, the KANUPP core has been refueled with indigenous fuel since 1980. Of more than 27,700 fuel bundles which have been irradiated in the core up to 31st August 2012, less than 0.05% have experienced failure. Few bundles experienced fuel defects at the initial stage of plant operation due to abrupt increase in power to meet grid requirement. Power increase maneuver, avoiding excessive movement of fuel bundles and removal of high burnt fuel bundles from high flux region etc were major remedial steps that ensured the fuel integrity afterward. Fuel Reliability Index is routinely calculated using I131, I134 values and purification flow. Sporadically elevated value of fuel reliability index (FRI) depicted the presence of pin holes / minor defect(s).

1. INTRODUCTION

The Karachi Nuclear power Plant (KANUPP) is the oldest CANDU power plant in operation with a total gross capacity of 1 37 000 kilowatts. KANUPP has completed 14 full power years of operation since its commissioning in 1971.

KANUPP core consists of 208 horizontal fuel channels which are arranged in a square lattice. Each fuel channel comprises of 11 fuel bundles, so overall 2288 fuel bundles are residing in the core. The 19 element fuel bundle used in KANUPP core is of the brazed split spacer design. The fuel bundle is designed to generate maximum allowable power of 453 KW that leads the central fuel channel to produce 2.8 MW. The maximum element heat rating of the fuel bundle is 52 KW/m while residing at central position of this site. The bundles attain the maximum burnup of 12 500 MW·D/TeU at the time of discharge from maximum rated channel of the central zone. The average discharge burnup of KANUPP fuel is 7400 MW·D/TeU.

KANUPP core is designed to operate with full flattened neutron flux to generate 100% reactor power. Currently, reactor is operating with partially flattened flux with a maximum limit upto 85% generator load. The core performance is evaluated by following the fueling frequency, monitoring the channel temperature, studying the variation of average core and fuel average discharge burnup and analyzing the bundle and channel powers which are derived by calculations and subsequent analysis using the parameters like absorber rod

positions, moderator level and thermal power produced. The bundle and channel powers are kept within allowable operating limit through efficient fuel management.

In the initial phase of plant operation, KANUPP core was loaded with Canadian origin fuel bundles. With the availability of locally manufactured fuel in 1980, core has been refueled with indigenous fuel since then. The locally fabricated fuel bundles were loaded in the core after satisfactory performance in out of core and in core stringent tests.

Presence of fuel defect in the reactor core is assessed through measurement of the Rb^{88} and Cs^{138} activity and their ratio using Gaseous Fission Product monitoring system and I^{131} activity in the primary heat transport system. Delayed neutron scanning system is subsequently used to locate the fuel defect after detection.

More than 27 700 fuel bundles including core resident bundles have been irradiated since commissioning. Only 13 fuel bundles had experienced fuel defect in 1973 due to abrupt reactor power cycling. KANUPP had experienced the fueling of fuel bundles with end caps manufactured out of zircaloy bars having some porosity. Iodine concentration in primary coolant remained higher in the years 2002 and 2007 when about 300 and 200 of these bundles respectively, were resided at the mid to downstream positions of fuel channels.

The high standards of quality assurance and quality control programs at the fuel fabrication stage and sound fuel management practices, coupled with well defined power maneuvering procedures that are in vogue at KANUPP are reflected in the fact that except 13 failed bundles, none of the fuel bundles have been found to have major defects so far.

2. KANUPP FUEL

The fuel for 137 MWe KANUPP heavy water reactor is brazed split spacer type. The design of the KANUPP fuel bundle is quite similar to the NPD and Douglas Point fuels as far as the envelope geometry is concerned i.e. bundle outer diameter and length. The KANUPP fuel uses brazed spacers instead of welded wire wrap to provide inter-element spacing. Three bearing pads are brazed at each outer element to space the bundle from the coolant tubes. The fuel sheath, bearing pads, end plugs, end plates and spacers are made of zircaloy-4.

KANUPP fuel assembly consists of 19 fuel elements assembled together in two concentric rings of 6 & 12 rods around a central rod (Figure 1). The fuel is designed to operate at normal power output per outer element at maximum flux position upto 52 KW/m and a thermal energy output up to 15 000 MW·D/TeU [1]. The fuel bundle design data is given in Table 1.

FIG.1. KANUPP fuel bundle.

Initially, the free space in the fuel elements is filled with Helium at standard temperature and pressure, which provides a non reactive inner atmosphere of the fuel element. It prevents fuel sheath from corrosion and hydrogen pickup by zirconium. Inside surface of KANUPP fuel sheath is provided with CANLUB graphite coatings that serve as frictionless inner surface. The graphite coating provides efficient heat transfer from UO_2 to the fuel sheath and prevents interaction between fission gas released and zircaloy sheath as well.

TABLE 1. FUEL BUNDLE DESIGN DATA

Description	Data	Remarks
Length of Bundle	19.5 inch	
Diameter of Bundle	3.219 inch	
Length of Fuel Sheath	19.396 inch	
Diameter of Fuel Sheath	0.596 inch	Outer Dia
Total weight of Bundle	16.667 Kg	
Weight of U/bundle	13.395	

3. KANUPP REACTOR CORE

The KANUPP reactor is a horizontal pressure tube type reactor fuelled by natural UO_2 with heavy water as moderator, coolant and reflector. There are 208 fuel channels, each consisting of 11 fuel bundles, arranged in a 16 x 16 square lattice to form a core. The core is contained in a cylindrical calandria shell.

CO_2 flows between Pressure tube and Calandria tube that provides insulation between coolant and moderator for transfer of heat and also used for leak detection. Boron (poison) is added in the moderator to compensate the absence of fission products at the time of startup.

4. FUEL LOADINGS AT KANUPP

Initial fuel loading of the core was carried out with fuel bundles supplied by foreign fuel vendor. Subsequent refueling also continued with imported fuel up till 1019 FPDs. Since then, capability of manufacturing local fuel enabled KANUPP to refuel with indigenous fuel. The locally fabricated fuel bundles were subjected to out-of-core thermal hydraulic tests prior to loading in the core, preferably in the outer fueling zone [2]. After satisfactory performance in the outer fueling zone of the core, four bundles were loaded in the center of the core for fuel rating and burnup tests at various axial positions of the center most channels. The test bundles were subjected to the stringent irradiation conditions corresponding to maximum design reactor rated power. One of the test bundles had produced power approaching the design maximum and experienced no defect as indicated by GFP ratio and ^{131}I activity in the primary coolant. The KANUPP core comprised of all Pakistani bundles at 1988 FPDs in August 1990.

4.1. Refuelling strategy

208 fuel channels are bunched into fourteen main rings; each ring comprises of four channels. The refueling of four channels (forming a ring) is performed simultaneously by selecting one channel from each quadrant to maintain uniformity of radial neutron flux distribution in each quadrant so as to avoid flux tilt within the core. This strategy also maintains symmetrical fuel burnup distribution, bundle / channel power and temperature in each of the quadrant. There are two zones of fueling; inner fueling zone comprising of 44 central channels refueled with single bundle, while remaining 164 channels form outer fueling zone refueled with two bundles at a time.

5. FLUX FLATTENING

KANUPP core is designed to operate with full flattened neutron flux to generate 100% reactor power. Flux flattening is imposed in the inner zone comprising of 44 central channels in order to improve the average to maximum flux ratio. However during the whole reactor operation history, the KANUPP core has gone through various neutron flux profiles in order to economize the fuel consumption rate. Full / partial flattened flux or peaked flux distribution have been prevailing since commissioning. Currently, KANUPP core has been operating with partial flattened flux profile corresponding to the 85% generator load.

6. BUNDLE POWERS AND CHANNEL POWER

The fuel is designed to be operated at power output per outer element 52 kW/m length, at reactor maximum flux position, with maximum allowable short-term power output per element is 56.6 kW/m length. The KANUPP fuel bundle can generate maximum allowable power of 453 kW that leads the central fuel channel to produce 2.8 MW [3].

However, in consequence of plant ageing and deterioration various parameters, Generator maximum output is limited to 100 MWe (78% Reactor Power) by the National Regulator. Maximum bundle powers are practically maintained around 400 kW. Bundle and channel powers are kept within the specified limits through efficient fuel management.

7. OPERATIONAL PARAMETERS

The design isotopic purity of moderator and coolant is 99.75 wt%. 16.5 inch moderator thickness above top most channels acts as reflector to control neutron leakage. The design reflector/moderator operating band is 182–188 inch. Movement of moderator within operating band provides fine control of reactivity in the core. Four 304L stainless steel absorber rods are provided for coarse control of reactivity. Moderator level touches the lower or upper band limit then absorber rods drive in/out.

However, KANUPP has not been operating with the design moderator operating band for over two decades. An appreciable loss of thermal neutrons is caused by lowering of reflector thickness. In consequence of increased neutrons leakages and a lower neutron flux at the upper end, all the channels lying at the bottom of the reactor core are generating more power and have higher burnup than the mirror channels lying at the top of the core as revealed by the Fig. 2.

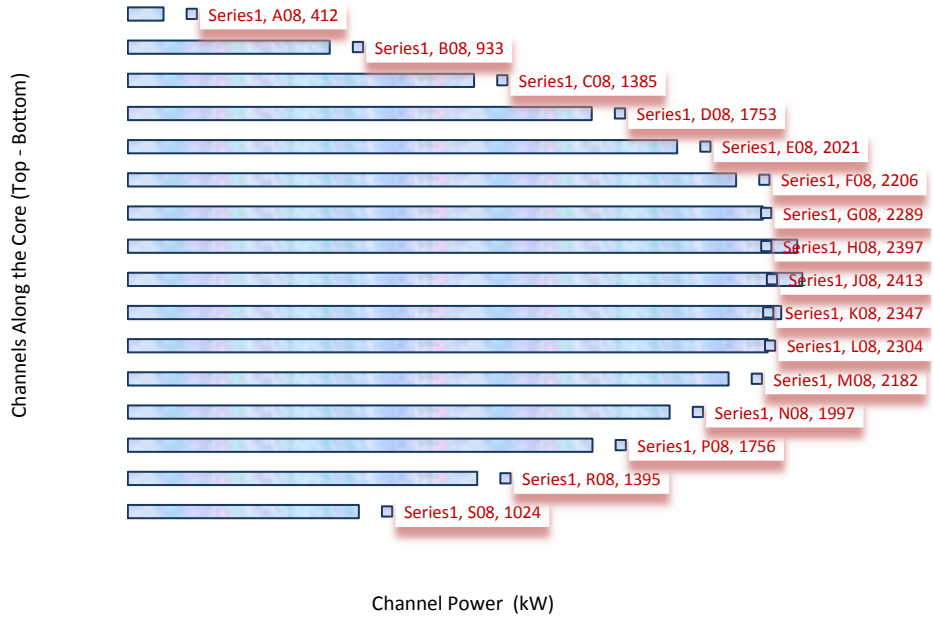

FIG. 2. Radial power flow.

8. FUEL DEFECT DETECTION SYSTEMS

8.1. GFP system

The gaseous fission products monitor measures the ratio of activities due to ^{88}Rb ($t_{1/2}$ = 17.8 m) & ^{138}Cs ($t_{1/2}$ = 32 m) in PHT produced by the beta decay of ^{88}Kr (half-life: 2.8 hrs) and ^{138}Xe (half-life 17 minutes) respectively. GFP monitoring system consists of NaI (TI) gamma ray detector coupled with power supply and amplifier. The defective fuel will cause the ratio to increase because ^{88}Kr activity increases by a factor larger than any of the short-lived gases due to the natural decay of these gases while diffusing from the fuel defects.

The maximum allowable value for GFP ratio is 1.00. If equilibrium value of the ratio increases from 0.5 to over 0.6, an alarm will be annunciated.

8.2. Iodine analysis

The ^{131}I activity in the Primary Coolant has been used to ascertain if any defect exist in the core resident fuel. ^{131}I (t1/2 = 8.05 days) is analyzed using Ge(Li) gamma ray detector connected to a multichannel analyzer. The concentration of ^{131}I in coolant provides supporting evidence for the presence of defective fuel. The sample is drawn six times a day to measure the concentration of ^{131}I in the coolant.

The maximum allowable equilibrium concentrations (in the case of a large defect), ^{131}I is 5 mCi/L. Reactor S/D will be required when the concentration of these fission products are persistently measured at the limit for more than 5 hours. The alarm limit is 500 µCi/L.

Equilibrium activity and activity in maximum rated bundle of ^{88}Rb, ^{138}Cs & ^{131}I are given in Table 2 [4].

TABLE 2. EQUILIBRIUM ACTIVITY AND ACTIVITY IN MAXIMUM RATED BUNDLE

Fission Product	Equilibrium Activity in Core (Ci)	Activity in Maximum Rated Bundle (Ci)
Rb^{88}	1.35×10^7	15700
Cs^{138}	2.08×10^7	24100
I^{131}	1.04×10^7	13410

If concentration of these fission products (^{131}I and GFP ratio) approaches to alarm limits then following actions should be taken to prevent the shutdown:

(1) Lower reactor power to reduce the fission products concentration and subsequent release rate to the coolant;
(2) Increase purification and degassing rates;
(3) Identify the channel(s) containing defective fuel(s) by DN Scanning. Move the suspected defective fuel(s) from the region of higher flux to region of lower flux or remove these defective fuels out of the reactor.

8.3. DN monitoring system

The delayed neutron (DN) monitor is used as failed fuel location system, and is able to locate the particular channel that contains the defect. The location of failed fuel bundle is determined by measuring the amount of delayed neutron activity in coolant. Sample from the outlet feeders of each of 208 fuel channels just before outlet headers are brought through sample lines into the activity monitoring rooms. The 104 sample chambers in each activity monitoring room (North and South) are monitored by 13 Boron Triflouride (BF_3) counters to give complete scan of fuel channels. 12 counters are moved on a trolley manually after each power cycle with remaining counter used as a reference in fixed sample chamber location.

The DN system detects delayed neutrons emitted from fission products, I^{137} ($t_{1/2}$ = 24 sec) and ^{87}Br ($t_{1/2}$ = 55.6 sec). A defect in cladding of a fuel element allows gaseous and volatile fission products to escape in the coolant. ^{87}Br decays to ^{87}Kr by β^- emission, that later converts to ^{86}Kr by emitting a fast neutron. This neutron is slowed down in heavy water and then detected by BF_3 detector.

9. FUEL RELIABILITY INDICATOR (FRI)

To assess the integrity of fuel bundles, Fuel Reliability Indicator (FRI) is estimated on regular basis, but reported to WANO quarterly. The FRI is the steady state I^{131} activity in coolant which has already been corrected for reactor power and tramp uranium contribution, and normalized to coolant purification rate.

A small fraction of primary coolant flows through the ion exchange column to remove dissolved fission products. All fission products except Xenon, Krypton and their daughter nuclides (exist in gaseous form), are assumed to be cleaned up in purification column.

Because of the short half-life, all of the measured I^{134} activity is assumed to result from fission of tramp material. I^{131} activity resulting from fuel defects is calculated as follows:

$$FRI = [(A131)N - k\,(A134)\,N\,] * [\,(Ln / LHGR) * (100 / Po\,)\,]^{1.5}$$

Where,

(A131)N = measured ^{131}I activity normalized to constant purification rate

(A134)N = measured ^{134}I activity normalized to constant purification rate

K = 0.0318, the tramp correction coefficient suggested by WANO.

Ln = linear heat generation rate used as basis for normalization

LHGR = linear heat generation rate at 100% reactor power (kW/m)

Po = average reactor power (percent) at the time activities were measured.

10. KANUPP EXPERIENCES IN DETECTING AND LOCATING DEFECTIVE FUEL

10.1. Stress corrosion defects

Stress corrosion defects can occur during power ramps as a result of high stresses in the zircaloy in the presence of fission products, notably Iodine.

In 1973, failed fuel monitoring system detected an increase in the Gaseous Fission Product ratio beyond normal value of 0.5, indicating fuel sheath failure. This was confirmed by analyzing the coolant sample for the presence of ^{131}I, which was approaching to the value of 6.5 mCi/Kg (Fig. 3). Further investigations revealed that fuel bundles residing at positions 5 and 6 of few channels belonging to the central zone had failed. A total of 13 fuel bundles were removed from the core. The subsequent investigation revealed that the rate of power increase was the main cause of fuel sheath failure. Power cycling between 50 to 90% generator full power preceded the appearance of the fuel defect [5]. Measurements of the concentrations of radioiodine and fission gases in the heat transport system indicated that the defect released the equivalent of 50 to 60% of these fission products contained in a single pencil of a maximum rated KANUPP fuel bundle. Major release took place rapidly from one large defect at rate of 1000 Ci/h. Subsequent measurements following the reactor shutdown indicated that smaller defects were also present which released I^{131} at rate of 45 mCi/h at shutdown.

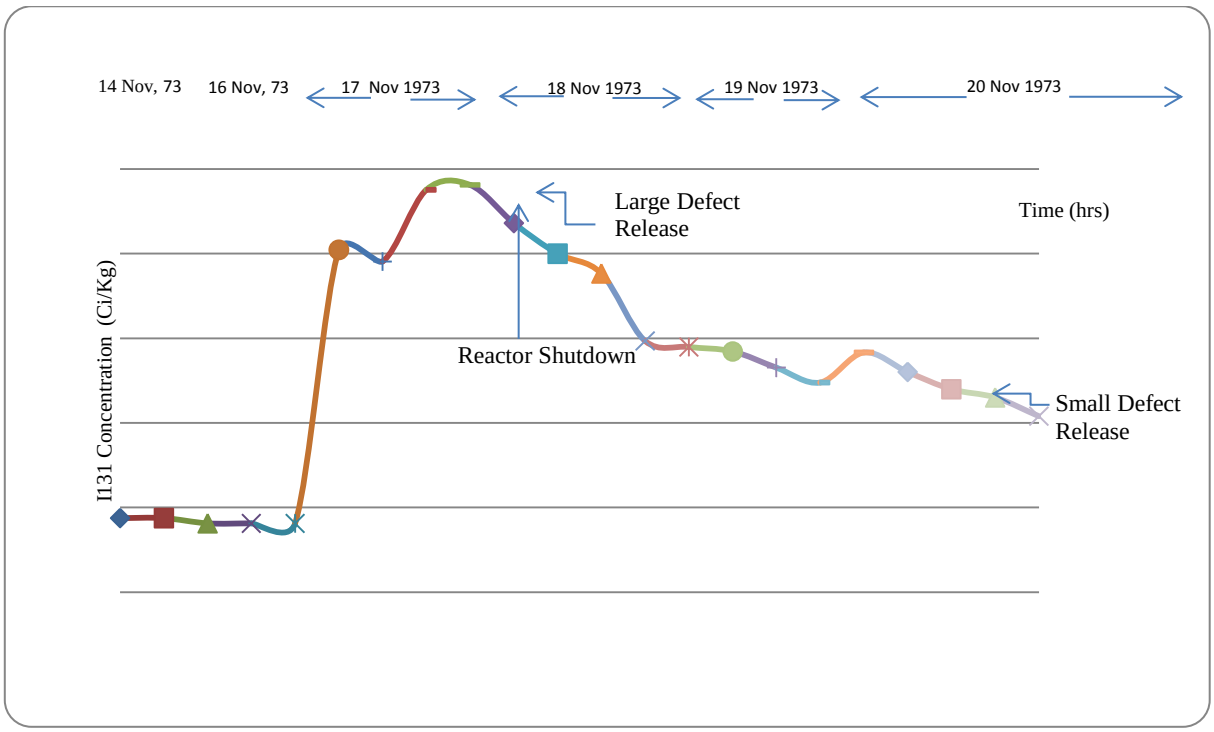

FIG. 3. Concentration of ^{131}I in heat transport system.

The in-line tritium analyzer for the boiler room atmosphere indicated an increase in airborne radioactivity (likely due to the particulate daughters of Kr^{88} and Xe^{138}) within one or two hours after fuel defect occurred.

DN scanning showed that defective fuel bundles were resident at positions 5 and 6 of few central channels [6]. After removing the defective bundles, it was found that the GFP signal had decreased by a factor of 6 and ^{131}I to 10 µCi/Kg, indicating that the defective fuel had been correctly located and removed from the core.

These bundles were stored in the cans after discharge from the reactor core. The cans are separately placed in the Inspection Area.

10.2. Experience with fuel bundles having porous end caps

KANUPP had received fuel bundles with end caps manufactured out of zircaloy bars having some porosity. These bundles (called C bundles) were fuelled into reactor core during years 2000 – 2006. The performance of these fuel bundles was not satisfactory in the region of high flux. Few typical instances are mentioned below.

Fuel bundles residing in channel K09 gained higher burnup (5430 & 6736 MW·D/TeU at bundle positions 5 & 6 respectively) than the burnup of fuel bundles lying at similar bundle positions in other central channels in year 2000. The concentration of I^{131} was reduced from 90 µCi/Kg to 27 µCi/Kg after refueling of three fresh fuel bundles in K09 as high burnt bundles were pushed to the extreme end position of this channel.

The concentration of ^{131}I was escalated to 43 µCi/l and settled in between 40–50 µCi/l in early of August, 2002. It was noticed that concentration of I^{131} was increased after refueling

of channels J07, H07 and H10, J10. Analysis became narrower by measuring the radiation level around all boilers. It was observed that radiation level around the boiler no. 1 was quite higher than the radiation level around other five boilers. Therefore, it was suspected that the channels connected at outlet header near to the boiler no.1 had defective fuel.

Bundles resided in channel J07 and J10 were shuffled with bundles resided in channels A06 and A11. While shuffling of channel J10 was in process, the concentration of I^{131} in coolant was peaked to 382 µCi/Kg. This indicated that this channel had defective fuel(s). After shuffling, the concentration of I^{131} was reduced to 23 µCi/Kg and finally stabilized below 9 µCi/Kg.

In both fuel channels K09 & J10 fuel bundles with end caps manufactured with porous zircaloy bar stock had resided at mid positions.

Iodine concentration in primary coolant also remained higher in the years 2002 and 2007 when about 300 & 200 C-bundles respectively, were present at mid to downstream positions (6th – 8th positions) of fuel channels (Fig. 4).

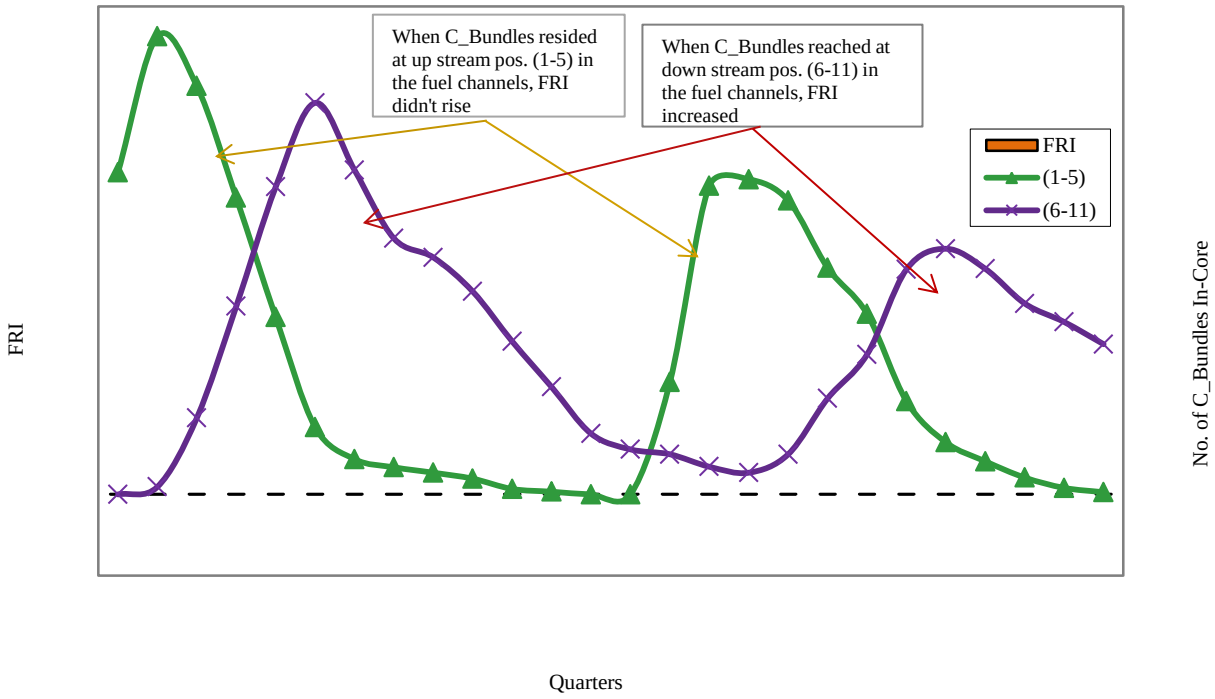

FIG. 4. Variation of FRI with number of bundles at various positions in the fuel channels.

The internal gas pressure in fuel bundles approached to maximum when resided at 7th position and 8th position (Fig. 5). At these positions, bundles too had attained higher burnup and they were generating considerable power. During these years, concentration of ^{131}I rose from prevailing value (< 9µCi/Kg) to the maximum of 91 µCi/Kg & 68 µCi/Kg respectively. ^{131}I concentration then decreased to the normal again as these bundles were shifted towards discharge end.

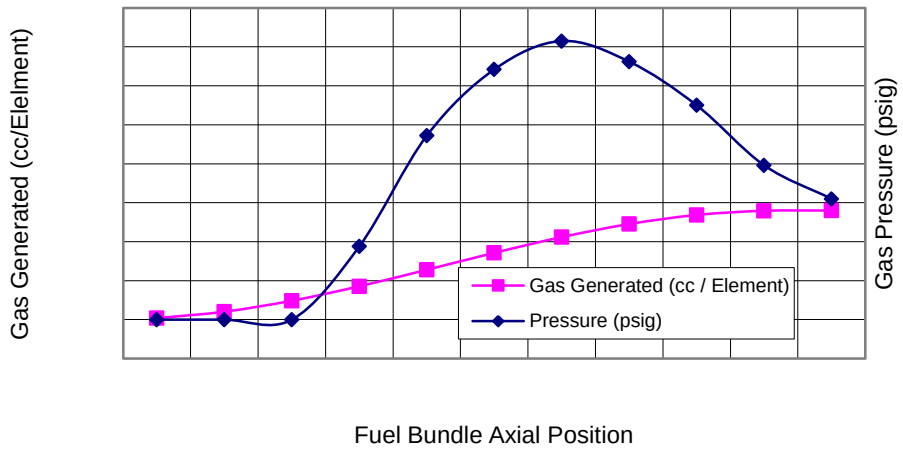

FIG. 5. Fission gas generated and internal gas pressure in KANUPP fuel bundle.

11. OPERATIONAL MEASURES TO REDUCE RISK OF FUEL FAILURE

11.1. Fuel conditioning at Kanupp

Since the incidence of failure of 13 fuel bundles at initial phase of KANUPP operation, fuel conditioning at lower power has been practiced at KANUPP. Also the load is increased at prescribed rate.

After startup of more than three days of shutdown or has been operating below 70% reactor power, the plant load is increased at any rate upto gross electrical output of 70 MWe and held at same power for at least ten hours. The power could be raised up to 88% of allowable power at 1 MWe/90 min. Afterwards it could be increased up to allowable power with any rate keeping fission product behavior in mind. The controlled rise in power after startup, prevent development of thermal stresses that could lead to fuel failure.

11.2. Bundle power vs burnup threshold

Bundle power versus burnup threshold is used to maintain the integrity of fuel bundles. This is exercised by the refueling regime. 19 element CANDU fuel bundle defect threshold line is given in Fig. 6.

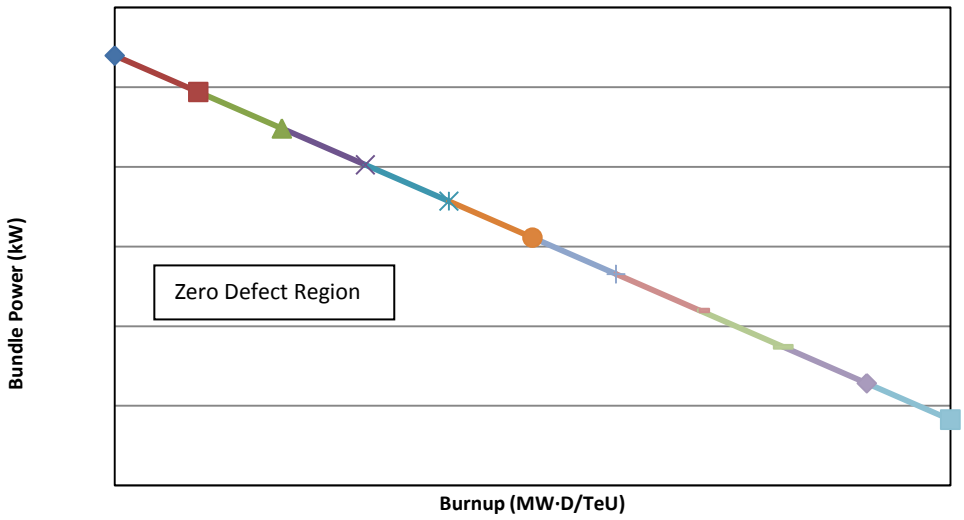

FIG. 6. Element CANDU fuel bundle defect threshold line.

11.3. Operation at power below allowable limitP

In consequence of ageing of Plant equipments, it has been decided to operate the reactor at power below 85%, the power limit allowed by the flux flattening. Therefore, prevailing bundle powers are far less than allowable limit (453 kW) and hence assist in minimizing the risk of fuel failure.

12. CONCLUSIONS

Of more than 27 700 fuel bundles (including in core fuel) irradiated up to 31st August 2012, only thirteen fuel bundles (< 0.05%) experienced major fuel defect. Minor defects (porosity) were developed in fuel bundles having end caps manufactured from porous bars. Otherwise, KANUPP fuel performance has been satisfactory during entire operational period of the reactor. High standards of quality control program, sound fuel management practices with well-defined power maneuvering procedures made it possible that no bundle had been found with major defect afterwards.

The experience and confidence gained through fueling locally fabricated fuel bundles have been considerable and proved an important milestone in country's progress towards self-reliance.

REFERENCES

[1] YUNUS, M. Y, KANUPP Fuel – Design Description, CGE R67CAP36, (1967)

[2] IQBAL AHMED, ANSAR PARVEZ, KHAWAJA GHULAM QASIM, Performance Evaluation of KNC-I Fabricated Test Fuel Bundles, KANUPP-STR-88-8.

[3] KANUPP Operating Manual, Reactor Boiler and Auxiliaries – Reactivity (Vol. I).

[4] KANUPP Final Safety Report (Original), Section 12

[5] GROOM, S. H., Failed Fuel Detection at KANUPP for Fuel Defect, Report No. CAR 15 (1973).

[6] GROOM, S. H., Failed Fuel Detection at KANUPP for Fuel Defect, Report No. CAR 16 (1973).

FUEL COOLING IN ABSENCE OF FORCED FLOW AT SHUTDOWN CONDITION WITH PHTS PARTIALLY DRAINED

L. PARASCA, D. L. PECHEANU
Cernavoda Nuclear Power Plant,
Cernavoda, Romania
Emails: laurentiu.parasca@cne.ro
doru.pecheanu@cne.ro

Abstract

During the plant outage for maintenance on primary side (e.g. for the main Heat Transport System pumps maintenance, the Steam Generators inspection), there are situations which require the primary heat transport system (HTS) drainage to a certain level for opening the circuit. The primary fuel heat sink for this configuration is provided by the shutdown cooling system (SDCS). In case of losing the forced cooling (e.g. due to the loss of SDCS, design basis earthquake-DBE), flow conditions in the reactor core may become stagnant. Inside the fuel channels, natural circulation phenomena known as Intermittent Buoyancy Induced Flow (IBIF) will initiate, providing an alternate heat sink mechanism for the fuel. However, this heat sink is effective only for a limited period of time (recall time). The recall time is defined as the elapsed time until the water temperature in the HTS headers exceeds a certain limit. Until then, compensatory measures need to be taken (e.g. by re-establishing the forced flow or initiate Emergency Core Cooling system injection) to preclude fuel failures. The present paper briefly presents the results of an analysis performed to demonstrate that fuel temperature remains within acceptable limits during IBIF transient. One of the objectives of this analysis was to determine the earliest moment since the reactor shut down when maintenance activities on the HTS can be started such that IBIF is effective in case of losing the forced circulation. The resulting peak fuel sheath and pressure tube temperatures due to fuel heat up shall be within the acceptable limits to preclude fuel defect or fuel channel defects.Thermal-hydraulic circuit conditions were obtained using a CATHENA model for the primary side of HTS (drained to a certain level), an ECC system model and a system model for SDCS. A single channel model was developed in GOTHIC code for the fuel assessment analysis.

1. INTRODUCTION

Currently, the nuclear power industry is undergoing a process of strengthening the nuclear safety boundaries, especially as a response to the Fukushima event. The final goal is to improve nuclear safety, reliability and economic performance.

This paper briefly presents the results of a Channel Cooling analysis in the Absence of Forced Flow (CCAFF) for the Primary Heat Transport System partially drained at shutdown condition in case of losing the main heat sink (e.g. due to a loss of shutdown cooling system or in case of a design basis earthquake-DBE). The presentation is focused on Intermittent Buoyancy Induced Flow (IBIF) phenomenon. The main objectives are to estimate the recall time and to find a threshold for decay power for which temperature of fuel or pressure tube is no longer within acceptable limits for serviceability.

2. METHODOLOGY

The thermal-hydraulic circuit model of the primary heat transport system of a CANDU-6 reactor was built using CATHENA MOD-3.5d rev.3 (Canadian Algorithm for THErmalhydraulic Network Analysis). CATHENA was developed by AECL, primarily for the analysis of postulated upset conditions in CANDU reactors. It is a one-dimensional thermal-hydraulic computer code that solves the one-dimensional transient two phase fluid flow equations in a piping network. CATHENA uses non equilibrium, two-fluid thermal-hydraulic model to describe a two phase fluid flow. In the thermal-hydraulic model, the liquid and vapor phases may have different pressures, velocities, and temperatures. Conservation

equations for mass, momentum and energy are solved for each phase (liquid and vapor), resulting in a 6-equation model.

The circuit model has two loops each consisting of the multiple-average channel model and the above header model. The nodalization of the above header model is shown in Figure 1. Steam generators (SG) U-tube and inlet/outlet SG's are modeled as tanks with initial water level of 0.8 m above the headers elevation. The tank component has a cross sectional area that is a variable function of height. Although an area and volume were specified in the initial tank component, these values were adjusted internally to reflect the entries in a given table. The table values are used in a trapezoidal integration algorithm to construct a height volume table. The calculated total volume from the trapezoidal integration algorithm supersedes the value given in the first tank component record.

The volume above the water level is considered filled with air and D_2O vapor at atmospheric pressure (two SG's remain open during the transient). The CATHENA model does not consider the heat loss to the environment (adiabatic model), but does take into account for the metal mass and the energy stored in the metal (such as piping, fuel, fuel channel, etc.).

A flow path from header to header cannot be established in these conditions because all steam generators U-tubes are vapor/air locked and buoyancy induced flow (driven by density gradients) can not initiate thermo-syphoning (heat exchange) through SG's after the initiating event (DBE). Therefore, the SG secondary side system was not modeled.

In shutdown cooling condition with the HT system partially drained (0.8 m above headers), the pressurizer is expected to be isolated, feed and bleed valve closed. Also the HT system connection to the D2O storage tank is assumed to be closed.

To determine the initial conditions in the circuit at different decay power levels (i.e. decay power at 3 to 60 days after the reactor shutdown) or to determine the initial conditions for specific initial temperatures ($40\ ^0$C or 60^0C) in the headers, a series of steady state simulations were conducted.

After determining the channel group which CATHENA estimates to reach the highest temperature, a supplementary single channel analysis is performed with GOTHIC. The purpose is to obtain more detailed results about the phenomena occurring inside the fuel channel.

GOTHIC (Generation of Thermal Hydraulics inside Containment) is a general purpose IST code developed by NAI (Numerical Applications Inc.) for analysis of ambient conditions inside the containments. The code is capable of solving mass, energy balance, and momentum equations in all three dimensions for liquid, gaseous, droplet and mist phases as well as heat transfer. Though it is originally designed for containment analysis, its flexibility allows for development of models for different applications.

A single channel GOTHIC model has been developed using specific data for CANDU-6 (Fig. 9). While the CATHENA model evaluates the entire reactor core by grouping different fuel channels into several equivalent groups, the GOTHIC model is focused on the evaluation of the conditions inside a single fuel channel such as (but not limited to): liquid and vapor temperature, void fraction, fuel sheath pressure tube temperature. Since the equivalent channel groups in CATHENA use averaged values for heat generation and geometrical data,

it is expected that for a single channel model, GOTHIC will provide more conservative results than CATHENA. In order to have a better evaluation, different channels have been chosen for analysis with GOTHIC, like the channel with the highest power in the reactor core, the channel with the highest power from the channel group indicated by CATHENA where void occurs first.

At 3 days after the reactor shutdown, the average decay power in the channel group where CATHENA predicts the highest sheath temperature is estimated to 13.73 kW. Instead, the GOTHIC model uses the highest channel power in that group, i.e. 16.73 kW.

Additional conservative hypotheses have been assumed for the single channel analysis:

— The heat loss to the moderator and through end fittings and feeders is assumed zero;
— The loss coefficient at the end plates between fuel bundles is considered;
— The metal mass of the end plates is not considered;
— The heat transport circuit is assumed drained down to 0.8 meters above the header elevation, with atmospheric pressure above that level; stagnant conditions are induced in the fuel channel as no other connections are modeled;
— The channel geometry is symmetrical (no creep and no sag).

The fuel channel is divided into 12 volumes, each modeling a fuel bundle and its corresponding pressure and calandria tube sections. The volume inside the pressure tube is divided into cells by a 3x7x7 Cartesian mesh. This allows a model arrangement such that almost every fuel pin fits inside a cell (see Fig. 10). Because GOTHIC only uses Cartesian coordinates, some details of the fuel bundle (such as the end plates or the spacers) are not modeled, though the corresponding loss coefficient is included in the connections between the volumes.

3. ANALYSIS

As a consequence of the initiating event (e.g. DBE), the Shut Down Cooling System pumps are lost. Also the heat sink provided by the SDCS heat exchangers is lost. Following the loss of forced flow circulation in the horizontal fuel channels, the flow in the HT system will start to decrease and oscillate. Eventually the flow through some channels will stop completely. The flow stagnation leads to the Intermittent Buoyancy Induced Flow (IBIF) phenomenon, as it can be seen in Fig. 2.

The decay heat supplied by fuel heats the liquid inventory in the channel. Soon, a slug of hot water is forming in the center of the channel and it gradually grows to the end fittings. Eventually, a small layer of hot liquid escapes through one end fitting (this is called the “no steam vent” mode of IBIF”) and then moves into a feeder, causing a pressure gradient across the channel. As result, cold water enters through the end fitting from the opposite direction. Thereby the single-phase flow is initiated.

The flow through the channels is almost stagnant and consequently, channels reach saturation and a large vapor bubble grows outward from the center of the channel towards the end-fittings. This void generation will begin to uncover the fuel bundles and eventually, the fuel rods will start heating up. According to literature, experiments have shown that after an IBIF transient fuel and fuel channels could be considered fit for service if the maximum sheath and pressure tube temperatures were below 450°C and 400°C, respectively. The

CATHENA code simulation predicts a maximum fuel temperature of 410°C (see Fig. 4) if the initiating event (DBE) occurs 3 days after the reactor shutdown.

The dry out process continues until the steam expands beyond the end-fittings, thereby creating a flow path to the feeders. The bubbles escaping from the fuel channels ("steam-vent") will finally condense in the feeders and headers because of large mass of relatively cold metal and sub-cooled water. The collapsing of the bubble creates a pressure force which sucks in cold liquid from the opposite header and thus the hot fuel is cooled through a quenching process.

After the loss of forced heat removal from the HT system, the D2O inventory will start to swell and consequently levels in all headers will rise slowly from 0.8 m to about 1.5 m.

It is assumed that the heat sink mechanism for this event is effective only until the headers temperature exceeds 90°C (recall time). Till then, operating procedures require to take corrective actions (either by re-establishing forced flow or by manual initiation of ECC injection) to prevent fuel failure.

Fig. 5 shows the evolution of temperature in the outlet headers after the initiatiating event (DBE). At 3 days after the reactor shutdown, for an initial header temperature of 40°C, the estimated recall time is about 50 minutes. If the event occurs at 30 days after reactor shutdown, the recall time increases to around 220 minutes (see Fig. 6).

After initiation of the Emergency Core Cooling System (ECCS), the sub-cooled water flow is injected in the HT system through all headers and all the core channels are eventually flooded. Finally, the injected flow mixes with the D2O inventory and is discharged through the open manholes of both HT system loops (see Fig. 7). The decay heat from fuel is carried out by the discharge flow and a better cooling process is established.

A recall time curve was determined (see Fig. 8) after a series of simulations for different decay power levels (corresponding to 3 to 60 days after the reactor shutdown).

The results of the present analysis contain some uncertainties. However, due to many conservative assumptions used in the simulations, it is expected that the predicted results are still conservative. For further evaluation of the fuel conditions, the GOTHIC analysis was performed.

Though the cooling flow through the fuel channel is much lower in GOTHIC model than CATHENA has predicted, the results show that a natural convection phenomenon occurs inside the channel. The coolant temperature rises a bit faster than predicted by CATHENA (Fig. 11). Also, temperature induced stratification inside the fuel channel (due to differences in density) can be observed. Due to this, the upper half of the fuel channel reaches saturation faster, while the bottom half of the channel remains well below the saturation. Boiling occurs at the middle of the channel, where the highest temperature occurs (Fig. 12). The thermal-hydraulic conditions induce an oscillating flow regime due to expansion and contraction of fluid and vaporization/condensation of vapors until the metal mass reaches the saturation temperature of the vapors. These oscillations continue to provide cold liquid from end fittings, contributing to the fluid stratification. The cold fluid slowly migrates towards the middle of the channel, gaining heat on the way (Fig. 13). The vapors will expand from the center of the channel towards the end fittings. When vapors reach the end fittings, more violent condensation occurs as they meet colder water and mass. The vapors will condense inside the

end fittings, until temperature in this region reaches saturation. Then, they will enter the feeders. The axial velocities inside the fuel channel exceed 3 m/s for short time. This oscillating flow regime can also be observed in the feeders (Fig. 3).

After the upper pins of the fuel are uncovered by water, the heats transfer to the steam decreases. Therefore, the fuel pins begin to heat up and temperature at the sheath surface starts to increase. As expected, the fuel sheath temperature in the GOTHIC simulation increases faster than CATHENA predicted (Fig. 14). The pressure tube temperature increases, but it remains much lower than the fuel sheath tempreture (Fig. 15).

The results presented here show that both codes predict a similar behavior but more single channel simulations are required to reach convergence between the codes.

4. CONCLUSIONS

After losing the primary heat sink (e.g. due to the loss of SDCS, or design basis accident-DBE), a natural circulation phenomena known as Intermittent Buoyancy Induced Flow (IBIF) will provide an alternate heat sink mechanism for the fuel for a limited period of time (recall time).

The maintenance activities which imply draining of HT system to the headers level can be performed only after three days since the reactor shutdown (but this still need confirmation from more single channel analysis). Though the recall time is currently defined as the time elapsed until the headers reach a temperature of 90°C, this might be corrected to a shorter time to limit the sheath temperature to values for which the fuel can still be considered fit for service. This approach not only increases the safety margin, but also reduces the probability for economic penalties.

Though two different codes are being used, they do show a similar behavior and, as expected, GOTHIC is more conservative than CATHEN.

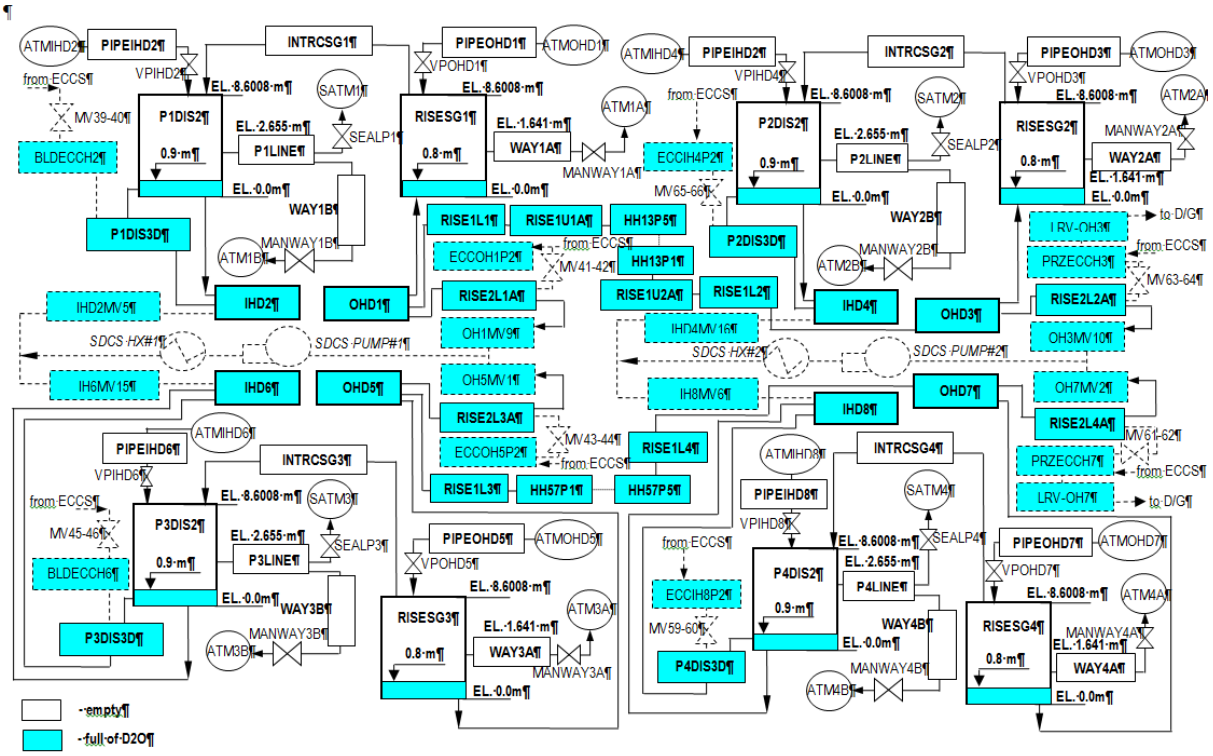

FIG. 1. CATHENA – Above header model for heat transport system in drained configuration (outage).

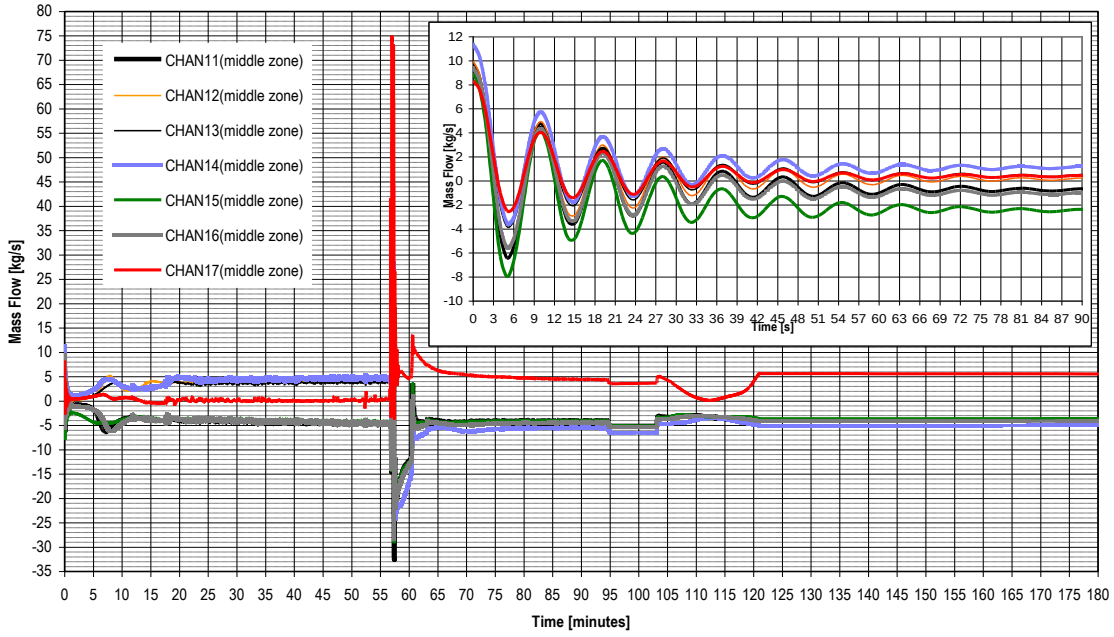

FIG. 2. Core pass 1 flow evolution after a DBE event from decay power at 3 days after reactor shutdown.

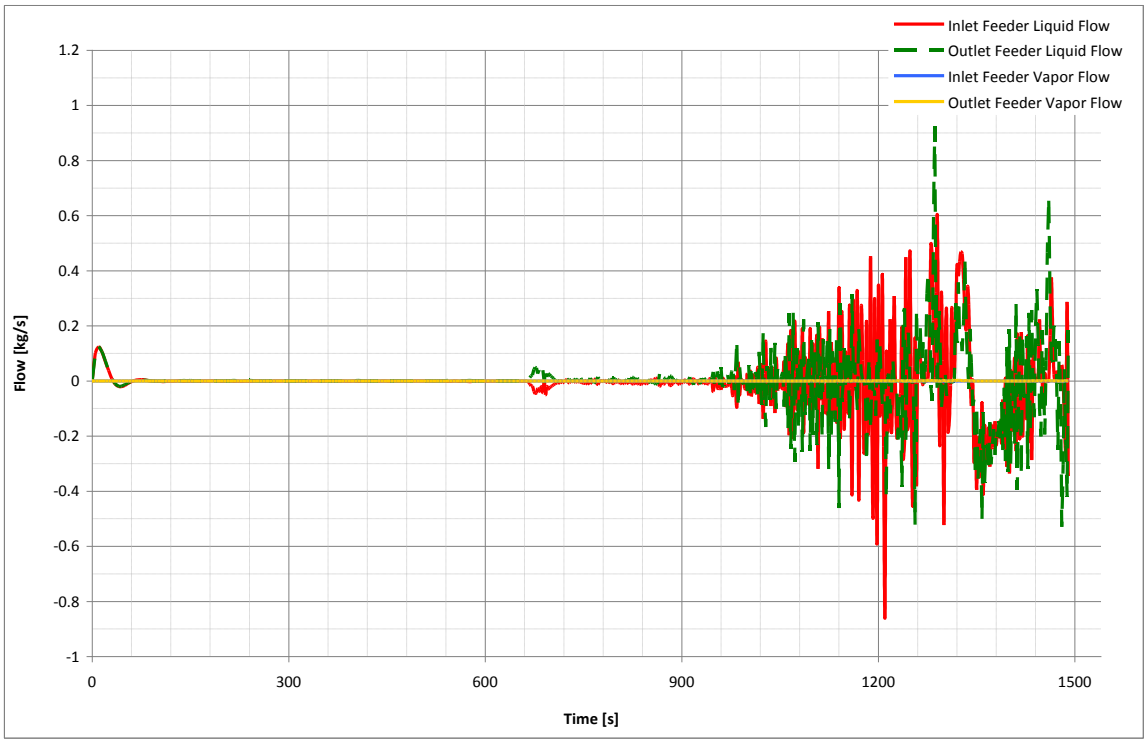

*FIG. **3**. Inlet and outlet feeder flow (GOTHIC prediction for single channel at stagnant conditions).*

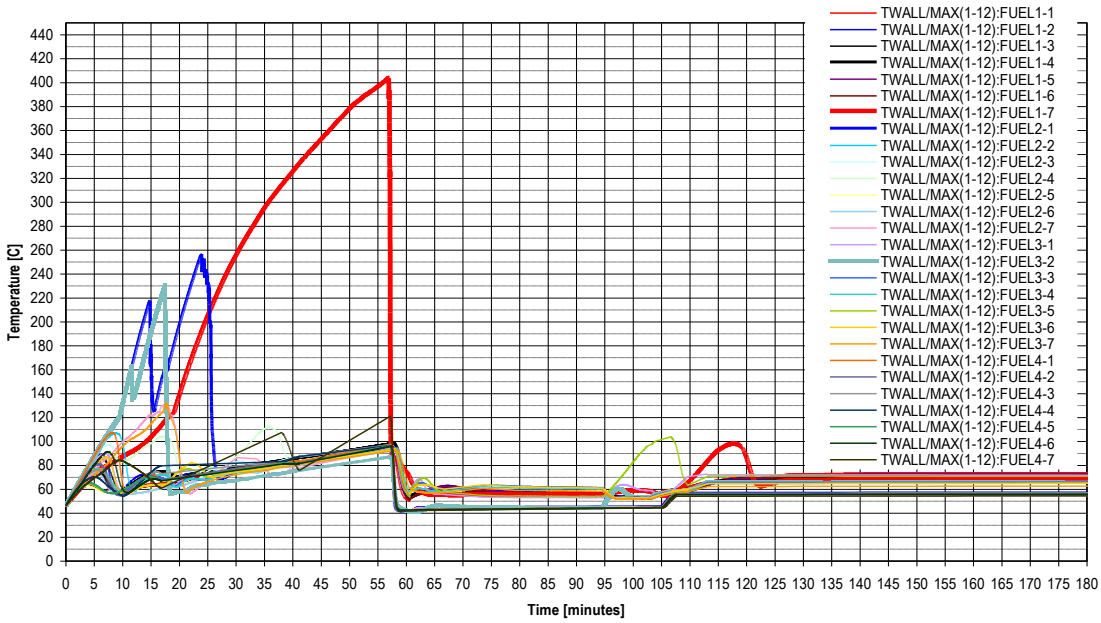

FIG. 4. Maximum fuel sheath temperatures evolution after a DBE event from decay power at the 3 days after reactor shutdown.

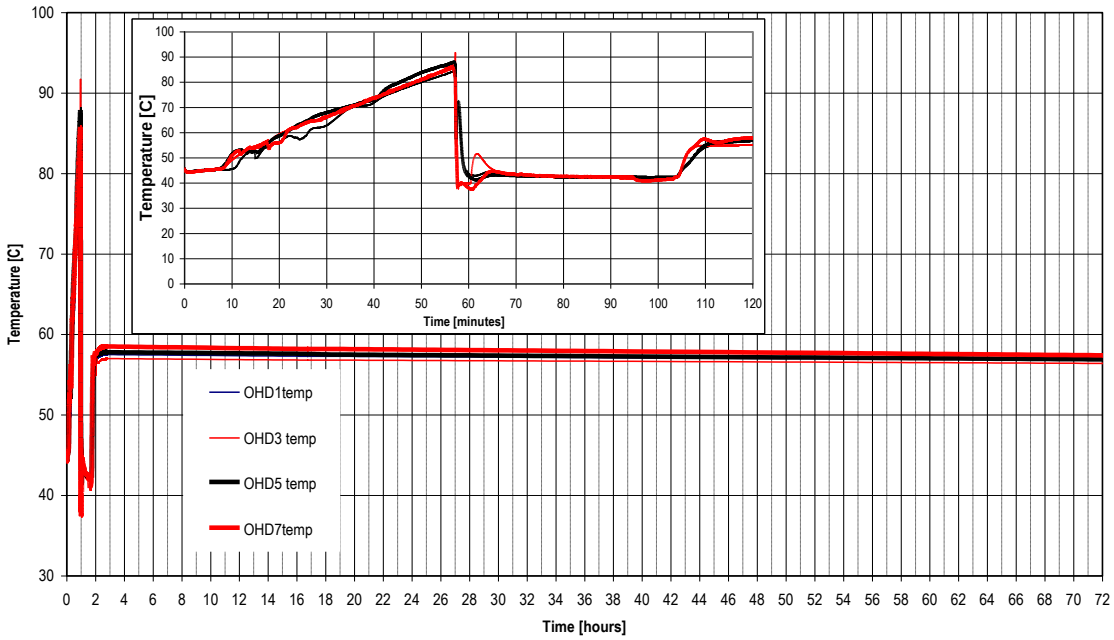

FIG. 5. Reactor outlet headers temperatures evolution after a DBE event from decay power at 3 days after reactor shutdown.

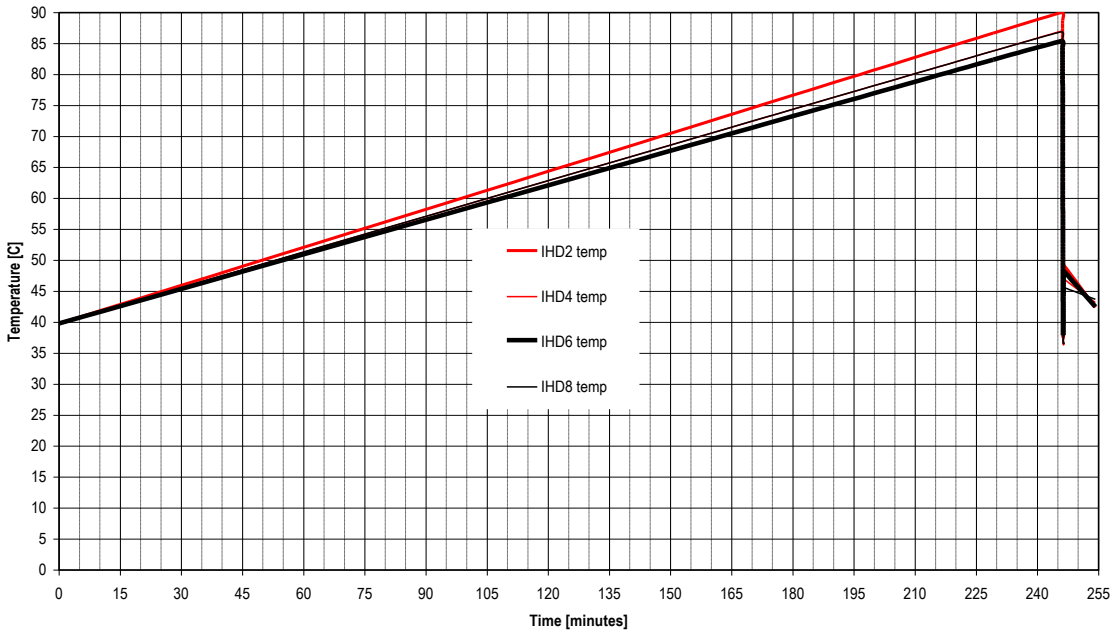

FIG. 6. Reactor inlet headers temperatures evolution after a DBE event from decay power at 30 days after reactor shutdown.

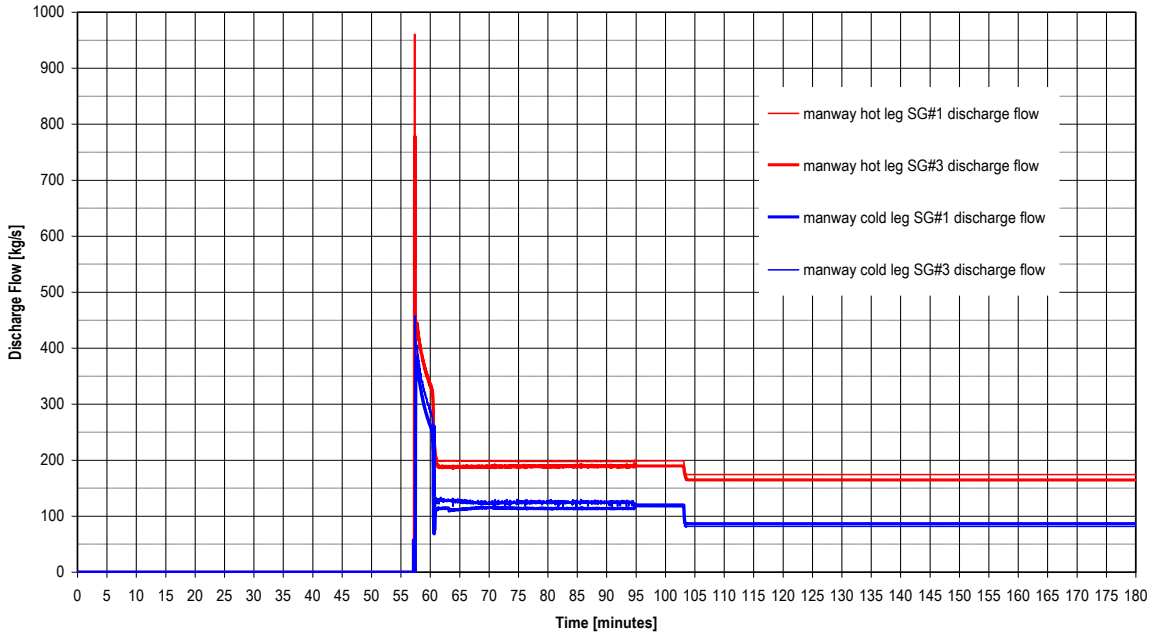

*FIG. **7.** Discharge flow through the open manholes of both HT system loops (after a DBE event from decay power at the 3-rd day of the reactor shut-down).*

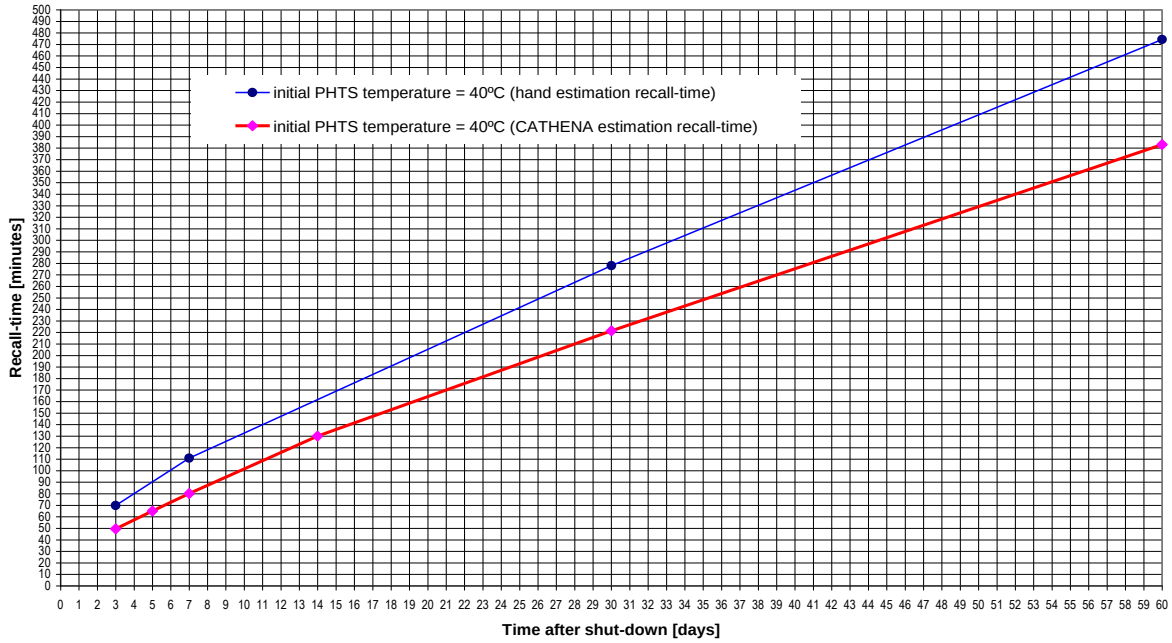

FIG. 8. Recall time curve (PHTS partially drained).

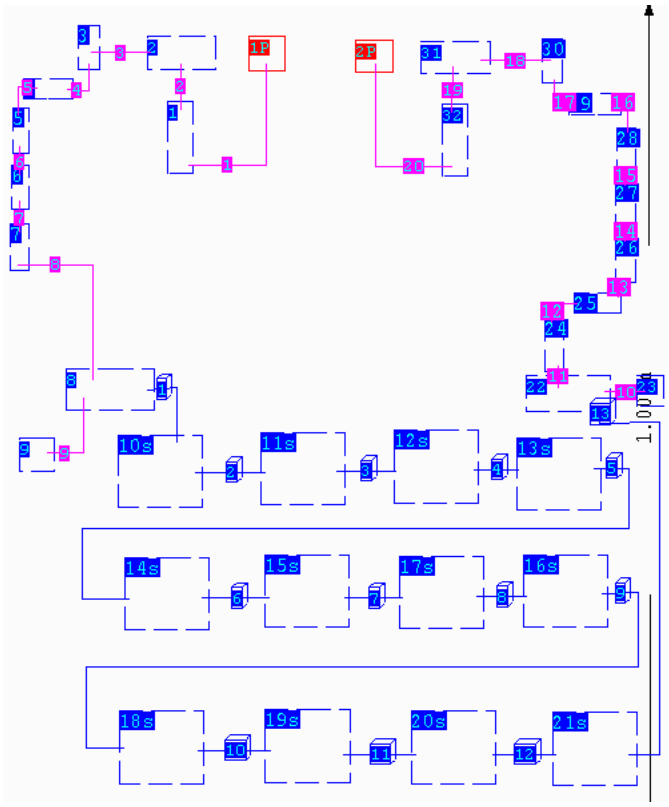

FIG. 9. GOTHIC Single Channel Model.

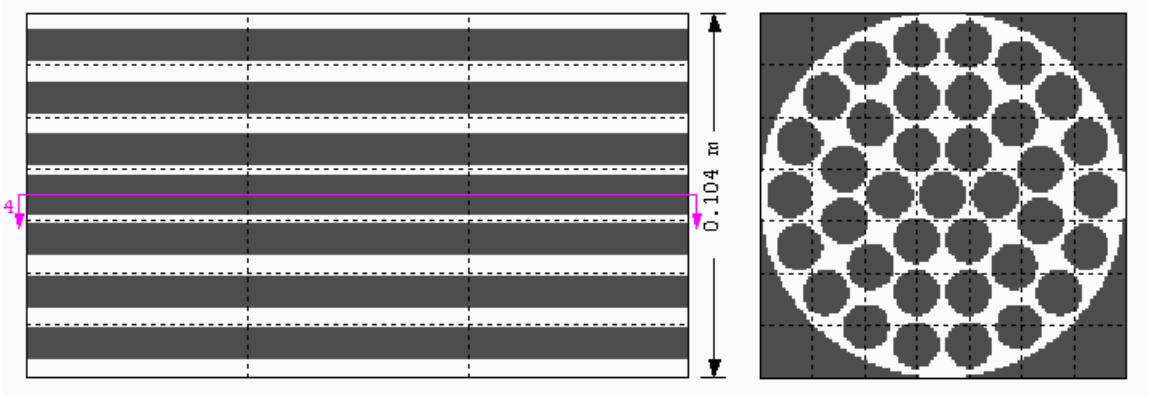

FIG. 10. Geometry of fuel channel model for GOTHIC.

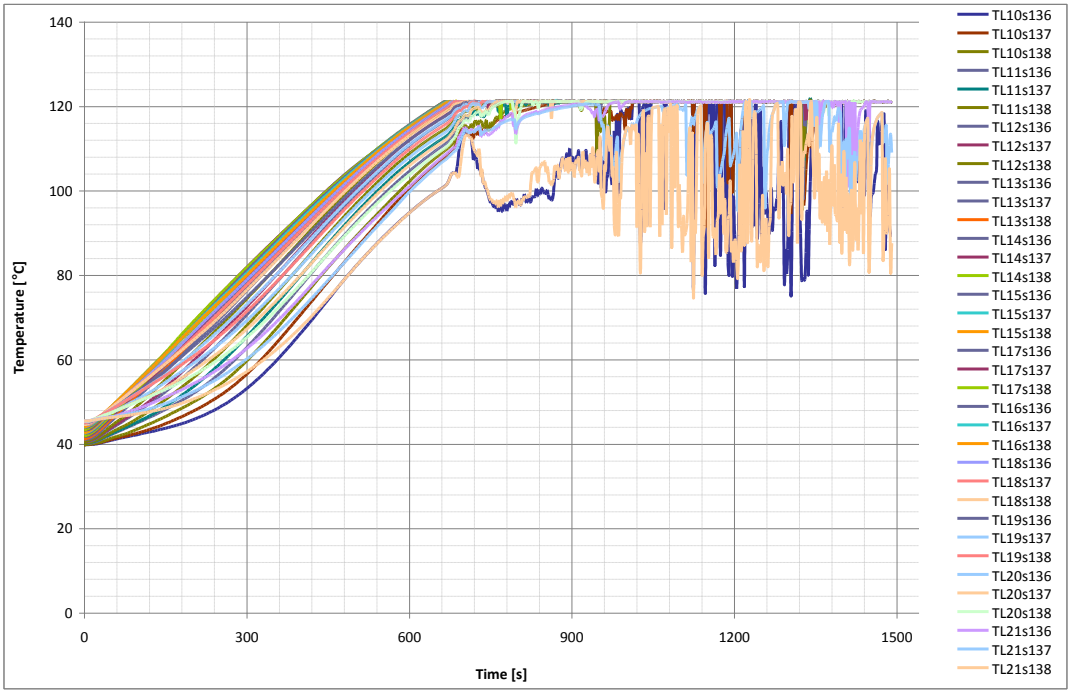

FIG. 11. Liquid temperature at the upper region of the fuel channel (GOTHIC prediction).

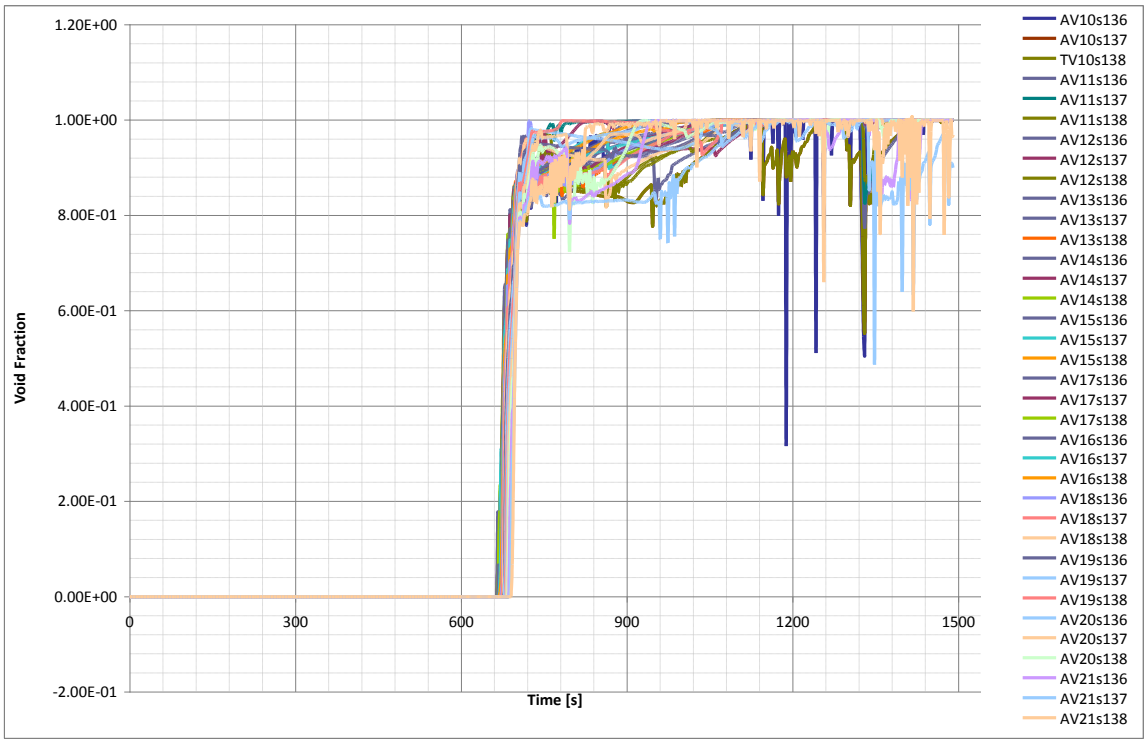

FIG. 12. Void fraction at the upper section of the fuel channel, at the outer ring level (GOTHIC prediction).

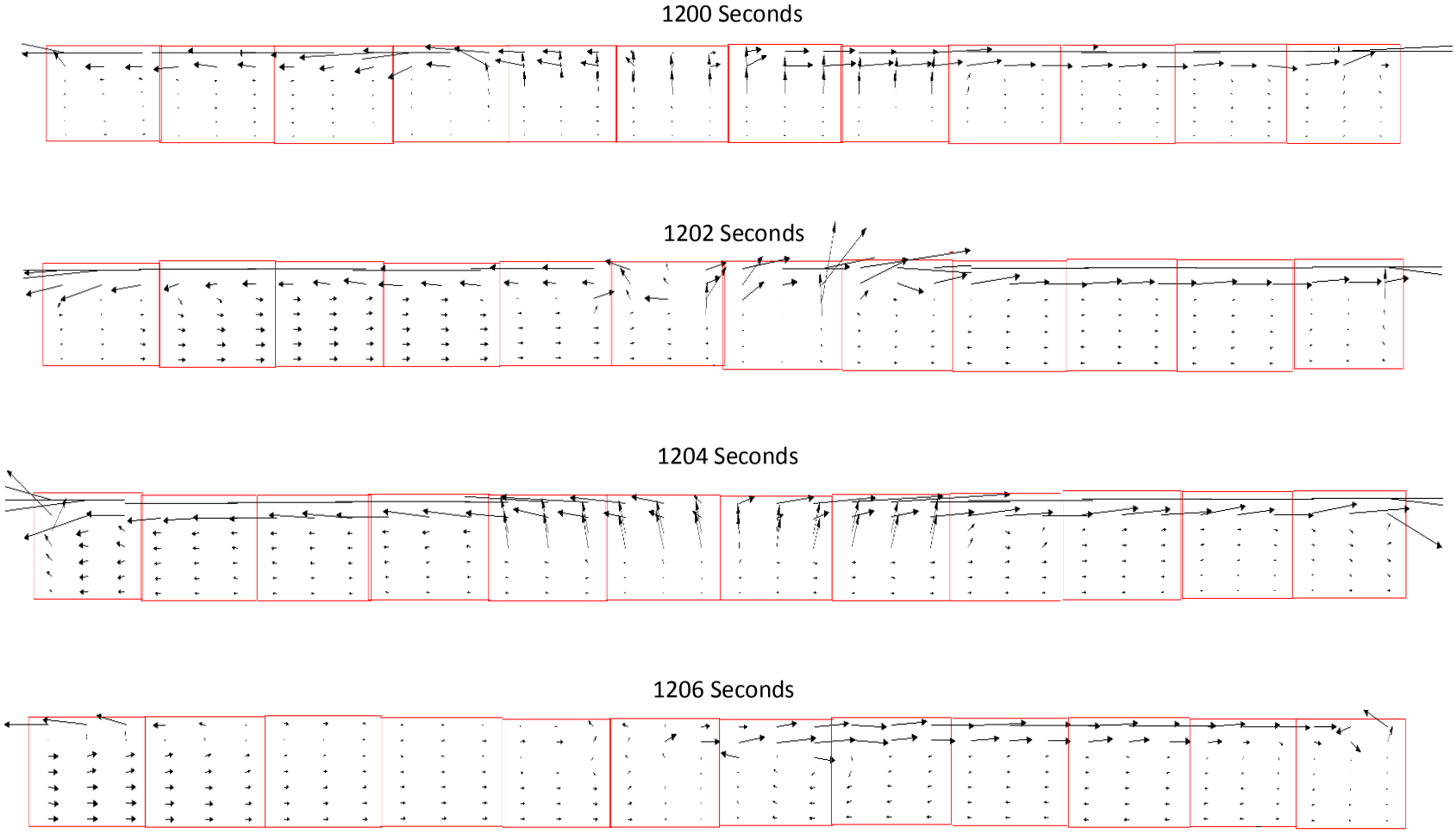

FIG. 13. Fluid oscillating flow inside the fuel channel (GOTHIC prediction).

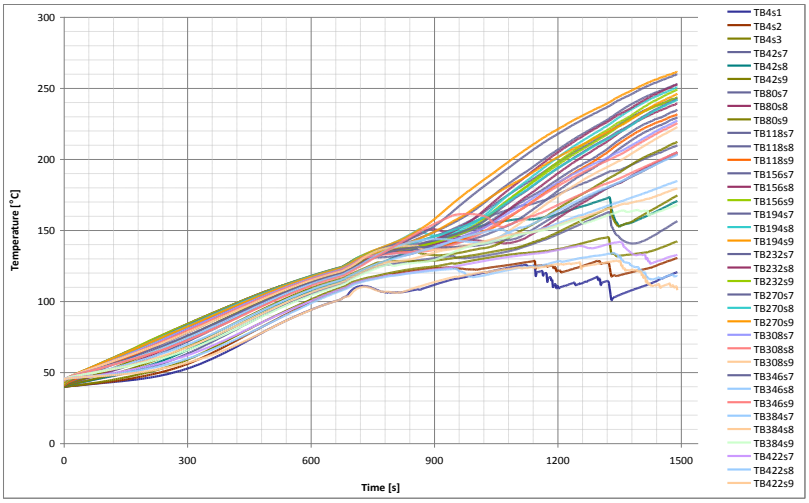

FIG. 14. Upper pin sheath temperature (GOTHIC prediction).

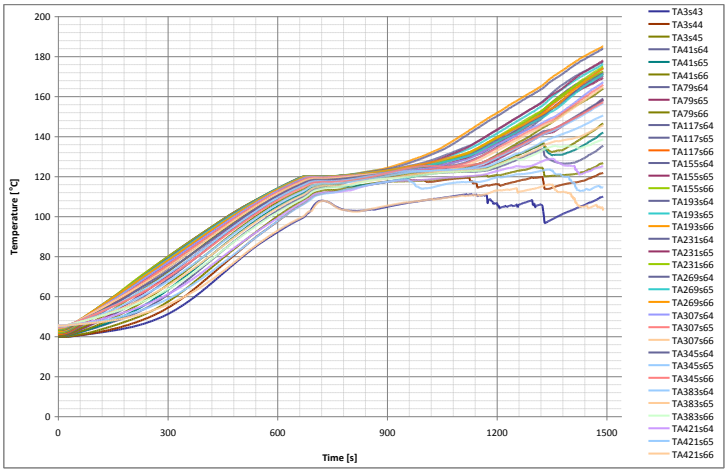

FIG. 15. Pressure tube temperature (GOTHIC prediction).

DEGRADATION MECHANISM OF ZR-4 CLADDING DURING HIGH TEMPERATURE STEAM OXIDATION

T.MELE, D. OHAI
Institute for Nuclear Research,
Pitesti, Romania
Emails: tiberiu.meleg@nuclear.ro
dumitru.ohai@nuclear.ro

Abstract

Isothermal oxidation tests were performed in 873–1673 K temperature range, in mixed argon – steam atmosphere at 1 bar pressure and 28.5ml/min steam flow. From the weight gain curves the kinetic of oxidation were obtained. Below 1073 K the shape of the kinetic curves is cyclic. A theoretical model, those of the dumped oscillator, was proposed to a more accurate description of the kinetic behaviour in the post-transition region. At higher temperatures, over 1173 K, the dumping factor is too high and the post-transition kinetic is near linear. An other important step in interpretation of the kinetic curves, was the development of a thermo-gravimetric method to evaluate the average compressive stress developed in the oxide layer during the oxidation. This allows not only the correlation of the cyclic behaviour with the evolution of the average compressive stress at temperatures below 1073 K, but reveals at higher temperatures also the existence of a cyclic behaviour, at least at the level of stresses. Using this method the classical treatment of the oxidation kinetic laws: parabolic in the pre-transition region and linear in the post-transition one can be refined supposing that the diffusional driving force is the compressive strain gradient in addition to a chemical potential gradient across the oxide scale. Each of these two contributions to the kinetic curve can be treated separately, allowing the evaluation of their dependency of the oxide scale thickness and the evolution in time of both the flows given by the two potential gradients. The shape of the average stress for each isotherm were obtained and discussed .The periodical stress relaxation can be related to the kinetical behaviour and can explain the multilayered structure of the oxide scale .The stress limit obtained at each temperature are presented and discussed. The shape of the stress curves vs.the oxide scale thickness allow to obtainig information's on structural changing and crack formation during the oxidation process.

1. INTRODUCTION

Oxidation kinetics of Zr-4 have been extensively studied in the paste 50 years but a comprehensive understanding is far to be attained. Generally, it is admitted that the isothermal kinetic curve consists of two distinct regions: the first one following a parabolic or cubic law, depending of the temperature, the second one linear or near linear. The transition to a linear kinetic reflects the major changes in the structure of material. An extensive approach to this changes are given in ref. [1], [2], [3]. Because the kinetics of oxidation is governed by the diffusion, the effect of the stress evolution will affect the shape of the kinetic curves.

After an initial parabolic or cubic growth rate up to a transition point, the rate became cyclic, exhibiting a short series of parabolic humps [1]. As an engineering approximation it is assumed that the post transition rate is constant. However the cyclic changes in post-corrosion rate might be related to the micro structural changes in metal. The evolution of the compressive stresses in the growing oxide scale, play a major role in structural changes and consequently in the shape of the kinetic curve. They increase with oxide layer growth, lowering the rate of oxidation, until a plastic deformation of the oxide and the metal take place ([2.]).The high compressive stresses stabilize the tetragonal ZrO_2 close to oxide metal interface. The martensitic transformation of tetragonal ZrO_2 to monoclinic oxide are able to produce small cracks at crystallite. The compressive stress at the oxide –metal interface decreases and may become tensile. The network of cracks favors the transport of the oxidizing

species near to the interface An the other hand the development of a fine porosity throughout the oxide is thought to be the cause of the smoothing of the post-transition curves.

At INR in the past few years, the model of dumped oscillator was developed to a more accurate description of the kinetic behaviour in the post-transition region.

2. RESULTS AND DISCUSSIONS

Isothermal oxidation tests were made on a SETARAM SETSYS EVOLUTION24 thermobalance at temperatures ranging between 873 and1673 K, in steam .The samples used were cylindrical ~20mm height and 13.08 mm diameter, cut from a Zr-4 cladding. For the oxidation a mixed steam – Ar dynamic atmosphere, with the steam flow rate of ~25 ml / min were used at a constant pressure of 1100mbar. Table 1 presents the data related to the samples and the measurements.

TABLE 1. DATA RELATED TO SAMPLES USED AND MEASUREMENTS

Sample nr.	Weight m_0 (g)	Surface S (dm^2)	Temp.T (K)	Duration t (h)	Weight gain Δm (mg)
1	2.2523	0.17423	873	48	96.4
2	2.2359	0.17243	973	2	179.07
3	2.2645	0.17283	1073	6	287
4	2.2830	0.17275	1173	2.5	224.7
5	2.2309	0.17218	1273	2.5	391
6	2.2598	0.17275	1373	2	389
7	2.23933	0.17275	1473	2	390.8
8	2.2378	0.17259	1573	2	381.4
9	2.2639	0.17333	1673	2	389.9

2.1. The dumped oscillator model for the kinetic post-transition

A particular case of kinetic behavior of zirconium alloys at oxidation is the cyclic behavior of the process in the post-transition region. If the pre-transition kinetic follow a parabolic law, the near linear law for the post-transition at a deeper analysis became unsatisfactory. The derivative of the weight gain, much more sensitive to the process, reveal a clearly cyclic shape of the kinetic curve. A typical cyclic kinetic obtained at 873 K is presented in Figure 1.

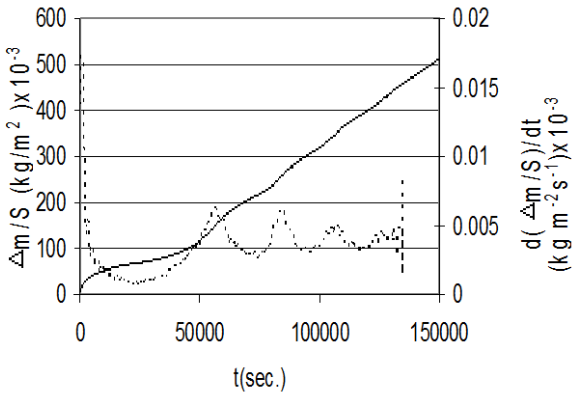

FIG.1. The weight gain per surface, and his derivative at 873K.

The linear fit to the weight gain obtained at this temperature is:

$$\left(\frac{\Delta m}{S}\right) = -77.9 + 0.00402 \cdot t \qquad (1)$$

and can play the role of a zero line. By subtracting this equation from the experimental values on the whole range of post-transition, the shape of the curve obtained is that of a damped oscillation (Fig. 2.)

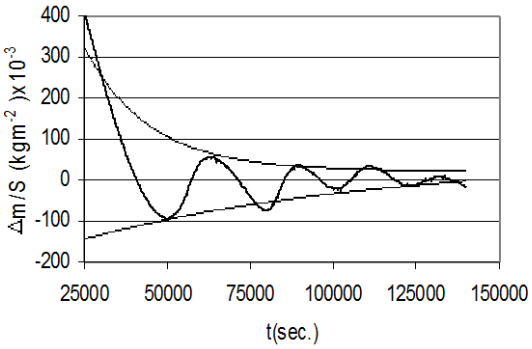

FIG. 2. The kinetic curve and the limiting equations after the zero-line correction.

The equations of the limiting curves are given by the expressions:

$$x = x_{\lim} \pm x_0 e(-\frac{t}{\tau}) \qquad (2)$$

where x_0 and $x_{\lim}$ are the initial and the final value of the amplitude.

From this it can be easily obtained the damping factor $\Gamma=1/\tau$ and also the frequency of the oscillations by measuring the half period. Generally, the frequency have a linear change in time:

$$\omega = \omega_0 + \alpha * t \qquad (3)$$

The equation of the damped oscillations in the general form can be written as follows:

$$x_1(t) = x_0 \cdot e^{-(1/2)\Gamma t} \cdot \cos(\omega\, t + \theta_0) \qquad (4)$$

Figs. 3a and 3b present the wieght gain curves obtained for each sample.

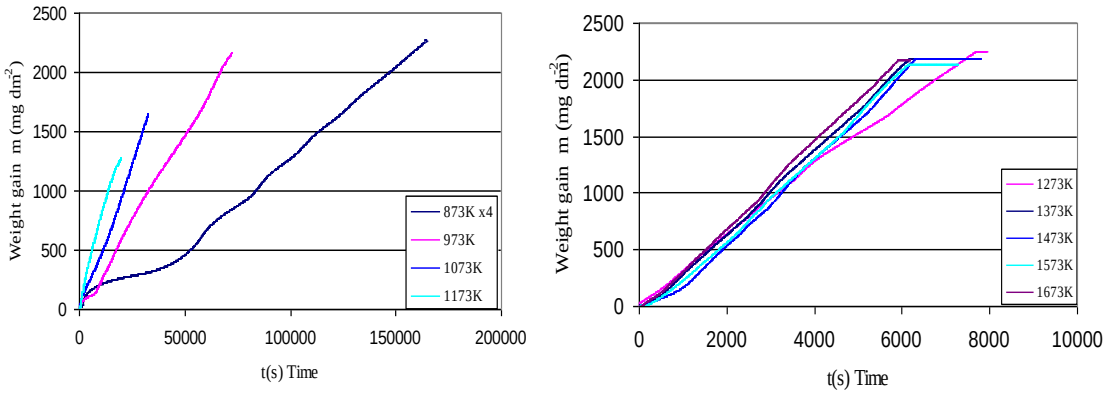

a) b)

FIG. 3. The experimental curves obtained.

The curves obtainei after substracting the zero lines for the post-transition are presented in Figs. 4a and 4b.

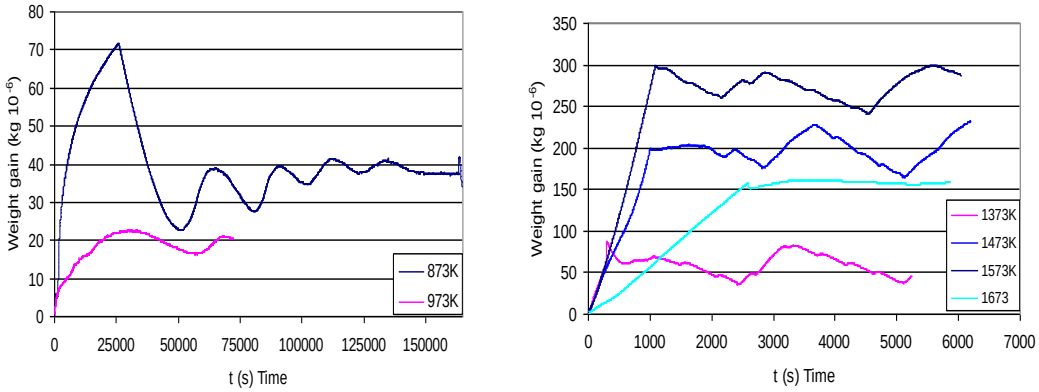

a) b)

FIG. 4. The corrected curves for the zero line.

As can be see the corrected curves for 1073 and 1273K are not presented in this last figure. For this to samples at temperatures of phase transitions(at 1073K the α to β transition of Zr and 1273 themonoclinic to tetragonal transition of zirconia), there are no cyclicity of the post-transition kinetic curves.The data obtained are presented in Table 2 where τ_{break} is the time of kinetic change

x_0: the starting amplitude of oscillation (kg x10^{-6})
ω: the frecvency (rad s^{-1})
Θ_0: the initial phase (rad)
Γ: the dumping factor

For temperatures over 1073 K can't be measured. For this temperature as can be seen in Fig. 4b, the amplitude increases with time.

TABLE 2. DATA OBTAINED FOR THE OSCILLATIONS IN POST TRANSTION REGIONS

T (K)	τ_{break} (s)	x_0 (mg)	Ω (rad s^{-1})	Θ_0 (rad)	Γ (s^{-1})
873	2890	17	2.1 E-7	-2.8	1.66
973	7838	11.5	6.3E-5	-2.2	12.76
1173	2004	8	5.3E-4	-7.56	-
1373	297	23.5	2.8E-3	9.17	-
1473	1001	30	2.73E-3	8.41	-
1573	1097	34	1.65E-3	2.52	-
1673	2589	22	1.8E-3	11.75	-

With theses values obtained, the kinetic equation can be written more generally as:

$$\left(\frac{\Delta m}{S}\right)=\left(\frac{\Delta m}{S}\right)\Big|_0^{\tau}+\left(\frac{\Delta m}{S}\right)_{ech.}+x_0\cdot e^{-\frac{1}{2}\Gamma\cdot t}\cdot\cos(\omega t+\theta)\Big|_{\tau}^{t} \qquad (5)$$

As can bee see , there is an increase of the amplitude and a decrease of the frequency with icreasing temperatures. The damping of the oscillations (at least at temperatures bellow 1073K) can originate in the development of the porosity in the oxide or as is assumed in ref [**2**] the local variation of the corrosion rate became increasingly out of phase with increasing time causing the wight gain curve to approach a smoothed curve. In this hypothesis the the damped oscillator equation must bee replaced with a sum of oscillations with same frequency but with different phases.

For the pre-transition region, a parabolic law was fited:

$$\frac{\Delta m}{S}=kt^{1/2} \qquad (6)$$

The Arrhenius plot of the kinetic coefficient *k* versus 1/T is presented in Fig. 5.

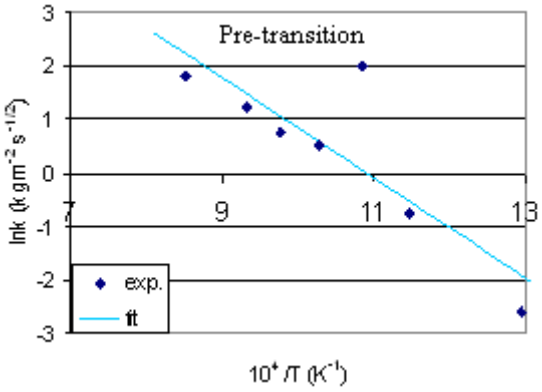

FIG.5. The Arrhenius plot of the kinetic coefficient.

The expression of kinetic coefficient dependency on the temperature obtained by fitting on the experimental results will be:

$$k\ (kgm^2s^{-1/2}) = 10.198 \exp(-0.778 \times 10^5/RT) \qquad (7)$$

2.2. Evaluation of the average compressive stress from the kinetic curves

The development of an oxide on zirconium alloys is governed by the diffusion of the oxygen ions through the oxide scale and growth of compressive stress at the oxide –metal interface. It is admitted that the diffusion driving force is the compressive strain gradient in addition to a chemical potential gradient across the oxide scale.

The thickness of the oxide can be obtained from the weight gain as follows:

$$x = \frac{\Delta m V_m}{2M_O} \qquad (8)$$

where the molar volume $V_m = 2.10 \times 10^{-5}$ m^3mol^{-1} and M_O is the atomic weight of oxygen. From the experimental curves of the weight gain versus time, using expression (8) the thickness dependency of time can be obtained.

To evaluate the average stress, this curves must be calibrated with at least one known value of the stress at a given oxide scale thickness. Dollins and Jursich in their paper [3] assume a linear increase of the stress with the oxide thickness. They give the values of the stress at 2 μm at different temperatures, reported in literature. Figs. 6 and 7 present the evolution for the average stress with the oxide scale growth after the calibration of the thickness change curves.

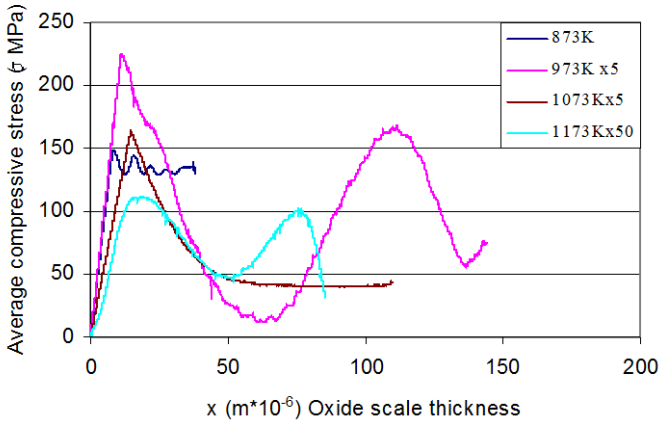

FIG. 6.The average stress evolution with the oxide thickness during the oxidation isotherms at temperatures up to 1173 K.

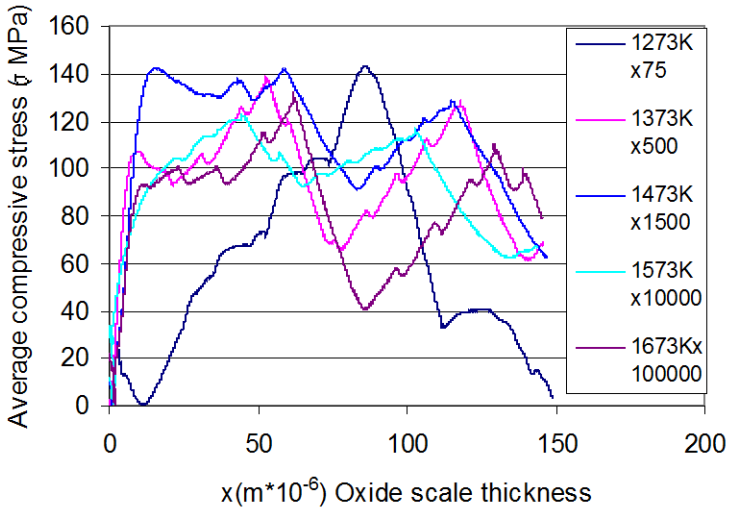

FIG. 7. The average stress evolution with the oxide thickness during the oxidation isotherms at temperatures between 1273 K and 1673 K.

As it can be seen, for the pre-transition region σ have a linear increase. After reaching the stress limit the shape of the curves present successive humps. The stress limits decreases with the temperature from 150 MPa at 873 K to ~30 MPa at 1073 K.

The decrease is exponential and it is given by the relation:

$$\sigma_{rup}=\exp(17.92-0.0142T)\ (MPa) \qquad (9)$$

The frequency of the cyclic decreases with temperature, and at 1073 K it practically disappears. At this temperature the structure changes start for Zr, from α-Zr to β-Zr. Over this temperature the average stress became againe cyclic and more, on each ascending or

descending ramp, small cyclic humps appear's with higher frequency's. A detailed description of the measurements are given in reference [6].

3. CONCLUSIONS

An original approach for the oxidation kinetics of post-transition region was made by the proposed mathematical model of damped oscillator. The paper presents a method for assessing the mean compressive stress evolution with increasing oxide layer thickness from the thermogravimetric curve. Average compressive stress increases linearly in the range of elastic stress (for pre-transition region). After reaching a creep value there are successive regions of drop and linear growth. The testing process of the method was done for isothermal oxidation in steam at temperatures between 873 K and 1673K. The creep stress values for each of these temperatures were determined.

REFERENCES

[2] COX, B., YAMAGUCHI, Y., The development of porosity in thick zirconia films, Journal of Nuclear Materials **210** 303 (1994) 317.

[2] BRYNER, J.S., The Cycle Nature of Corrosion of Zircaloy-4 in 633 K Water, Journal of Nuclear materials **82** 84 (1979) 101.

[3] DOLLINS, C.C., JURISCH, M., A model for the oxidation of zirconium based alloys, Journal of Nuclear Materials, **113** 19 (1983) 24.

[4] HUTCHINSON, LEHTINEN, B., A theory of resistance of Zircaloy to uniform corrosion Journal of Nuclear materials **217** 243 (1994) 249.

[5] YOO, H.-I, et al., A working hypothesis on oxidation kinetics of Zircaloy, Journal of Nuclear materials **299** 235 (2001) 241.

[6] MELEG, T., Thermogravimetric method to evaluate the average compressive stress evolution during Zy-4 oxidation, Journal of Nuclear Reasearch and Development **2** 25 (2011) 28.

DEFORMATION AND BALLOONING OF UNIRRADIATED INDIAN PHWR FUEL CLADDING UNDER TRANSIENT HEATING CONDITIONAAA

T. K. SAWARN, S. BANERJEE, K. M. PANDIT,
S. ANANTHARAMAN, D. N. SAH
BARC,
Mumbai, India
Emails: sawarn@barc.gov.in,
sup@barc.gov.in

Abstract

The high temperature ballooning and deformation behavior of the Zircaloy-4 cladded PHWR fuel pins was investigated. Transient heating experiments were performed in the 5 to 70 bar internal pressure range and 8 to 12oC/sec heating rates. Fuel pins internal overpressure combined with the elevated temperature caused fuel pin claddings to balloon and rupture. The burst data (burst pressure and burst temperature) was recorded while, burst strains, engineering hoop stress and area of burst opening was calculated. Microstructural examinations and SEM fractography were also carried out. This paper presents the details of the experimental procedure and the results obtained**.**

1. INTRODUCTION

The analysis of fuel pin behavior during postulated LOCA condition is an essential part of the defense in depth concept used by the regulators for Indian pressurized heavy water reactors (PHWRs). LOCA is a result of a rupture in the primary heat transport system including the headers, feeders, coolant tubes etc., which leads to coolant depressurization in few seconds, depending on the break size [1–2]. Rapid coolant depressurization results in decrease in heat removal from the fuel and an increase in the internal to external pressure differential across the clad wall. This pressure differential leads to an increased biaxial stress in the cladding [2–4]. With time, the combination of hoop stress and high temperature reaches a point beyond which the fuel cladding begins to deform locally resulting in an increase in diameter due to circumferential strain [2], [4], and [5]. This is known as ballooning. Such deformation can cause partial blockage in the coolant channel which may impair further heat transfer when ECCS comes into operation. The ballooned clad may finally burst when the hoop stress exceeds a critical value called the burst stress of the cladding material. Hence ballooning is identified as one of the well recognized fuel failure mechanisms. Hence the integrity of fuel pins under accident conditions is an important consideration during designing of the fuel element and planning of the reactor safety measures [6]. A careful and systematic evaluation of high temperature deformation of zircaloy cladding is of paramount importance for reactor safety and reliability. Numerous investigations with isothermal and transient heating experiments commencing with the study by Emmerich et. al, have been carried out on single pins as well as multi-rod assemblies [8–16]. Furthermore a number of investigations have been found to be focused on the deformation behavior rather than burst characteristics [15], [16]. Studies have been carried out in steam [8–11] as well as in vacuum and inert atmosphere [12], [13], [16], as during LOCA the clad tube surface may be subjected to a steam starved condition where coolant is partially absent. However, there is no systematic studies had been carried out on the high temperature ballooning and rupture behavior of Indian PHWR fuel cladding. In this background, it has been considered important to generate a database on high temperature ballooning deformation and rupture behavior of Indian PHWR thin cladding. Transient heating experiments on pressurized PHWR fuel cladding, in argon environment, carried out in BARC helped in generating a baseline data in this respect, which will be compared later on with the tests performed in steam.

2. MATERIAL

PHWR fuel pins with zircaloy-4 cladding, having a nominal length, outside diameter and wall thickness of 490 mm, 15.2 mm and 0.4 mm respectively, have been used for this study. The clearance between the inner diameter of the cladding and the outer diameter of the fuel pellet was 40 μm. The dimensional specification of the cladding corresponds to that of 220 MWe Indian PHWR.

3. EXPERIMENTAL

3.1. Experimental set up

A schematic diagram of the experimental set up is presented in Figure 1. Transient heating experiments had been carried out on single fuel pins in a direct electrical heating system, in which a fuel pin is enclosed in a quartz tube, so that it can be heated in a specific environment (inert gas or steam). The fuel pin was held (using copper clamps) between two copper bus bars (at the top and the bottom location) connected with the secondary of a step down transformer. The test apparatus consisted of i) heating system, ii) a programmable power supply, iii) a gas handling system to pressurize the fuel pin, iv) pressure transmitters to measure the internal pressure and v) pyrometers to measure the cladding temperature. The accuracy of the pyrometer was ± (0.3% T_m + 1)^oC, where T_m is the measured temperature. The signals from the pressure transmitters and the pyrometers were continuously monitored and recorded by the data acquisition system. Two pressure transmitters; one in the lower range: 1 to 50 bars and the other for the higher pressure range: 1 to 100 bars have been used during the experiments. The temperatures were recorded along the axial direction at three different locations covering a span of 287 mm length from one end of the fuel pin.

3.2. Experimental procedure

The experiments were limited to two controlled independent variables: internal pressure and heating rate decided by the current. The dependent variables were rupture/burst temperature, time to rupture, circumferential strain, diametral strain, radial strain and area of the rupture opening. The transient heating tests were run on 24 fuel pins at different internal pressures ranging from 5 to 70 bars with a heating rate in the range 8 to 12^oC/s. The test pin was heated directly by passing current through copper bus bar holding the fuel pin.

The volume expansion of the gas resulted in ballooning and deformation of cladding leading to its rupture due to wall thinning. The tests were terminated just after the rupture by switching the power off. The time to failure recorded by the data acquisition system was the time to reach the burst temperature from 350°C due to the limitation of the pyrometer.

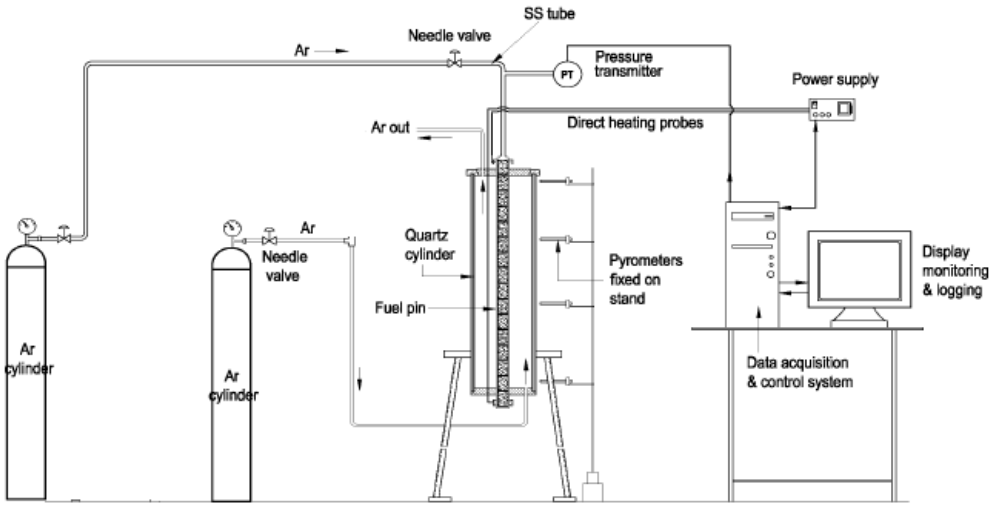

FIG. 1 A schematic diagram of experimental set up.

Three pins were tested at every particular internal pressure and a total of 24 experiments were performed, out of which, one was faulty and hence was not considered for data in this investigation. Details of the independent transient test parameters i.e. initial pressure and heating rates are shown in Table 1.

TABLE 1. TRANSIENT TEST PARAMETERS

$P_{Initial}$ (bar)	5	10	20	30	40	50	60	70
Heating rate (^{o}C/s)	9	8	8	8	8	8	8	12

3.3 Visual examination

The visual appearances of all the tested fuel pins were recorded by a digital camera. Photographs of the burst opening of all the tested cladding were also studied under a macroscope and the burst area was measured with the help of image analysis software.

3.4. Dimensional measurement on ballooned fuel pins

The measurement of diameter along the length of the tested (burst) fuel pins were carried out by a laser based dimension measuring system. The tested pins were then sectioned to remove the fuel pellets. Small rings were subsequently obtained by cutting transverse sections from all the tested pins from the ballooned region of the cladding, at the region of maximum deformation. The ring specimens were then hot mounted in Bakelite and examined under a macroscope. The photomacrographs of the transverse section of the ring specimens were recorded and the circumference at the rupture location was measured by tracing it on the photomacrograph using image analysis software. The samples were also examined under an optical microscope and the wall thickness of the clad ring pieces was measured from the photomicrographs, at the fracture tip of the mounted sample, with the help of image analysis

software. Burst opening area was measured by tracing the area in the recorded stereo microscope photographs of the rupture region with the help of image analysis software.
Diametral strain, circumferential strain, radial strain and engineering hoop stress were calculated in the following ways:

Diametral Strain (%) = $[(D_f / D_i) - 1] \times 100$ …….. (1)
Where, D_f = Final diameter, D_i=Initial diameter
Circumferential Strain (%) = $[(C_f / C_i) - 1] \times 100$ …… (2)
Where, C_f = Final circumference, C_i = Initial circumference
Radial strain (%) = $[(t_f / t_i) - 1] \times 100$ …… .. (3)
Where, t_f = Thickness of the clad at the fracture tip and t_i= Initial clad thickness
Burst Stress $\sigma_B = P_b D_i / 2t_o$ …… (4)
Where, σ_B = Engineering hoop stress (MPa), P_b = Burst Pressure (MPa), D_i = Initial internal diameter (mm), t_o = Initial wall thickness (mm)

4. RESULTS AND DISCUSSIONS

4.1. Visual appearance of the failed pins

The appearance of a few tested pins is shown in Fig. 2. The amount of ballooning at the fracture, shape, size and orientation of the burst opening can be clearly seen from these photographs. The photographs indicate that the expansion was essentially symmetrical about the longitudinal axis (Fig. 2) and most of the fuel pins remained straight after the burst. Bending was observed only in 5 fuel pins which failed at burst temperature and pressure combinations of 640°C & 40 bar, 620°C & 58.4 bar, 654°C & 52 bar, 769°C & 11 bar and 871°C & 21 bar. Some authors attribute bending to two different phenomena: i) jet blast and ii) non-uniform axial contraction [2], [7]. The burst opening was observed to be confined in axial direction in all the cases as circumferential strain takes charge of the axial opening. However in one fuel pin (760°C & 30.6 bar), the expansion of the crack in the axial direction stopped after a certain extent and it changed its orientation in the circumferential direction. This can be attributed to the existence of negative axial strain due to anisotropy [8].

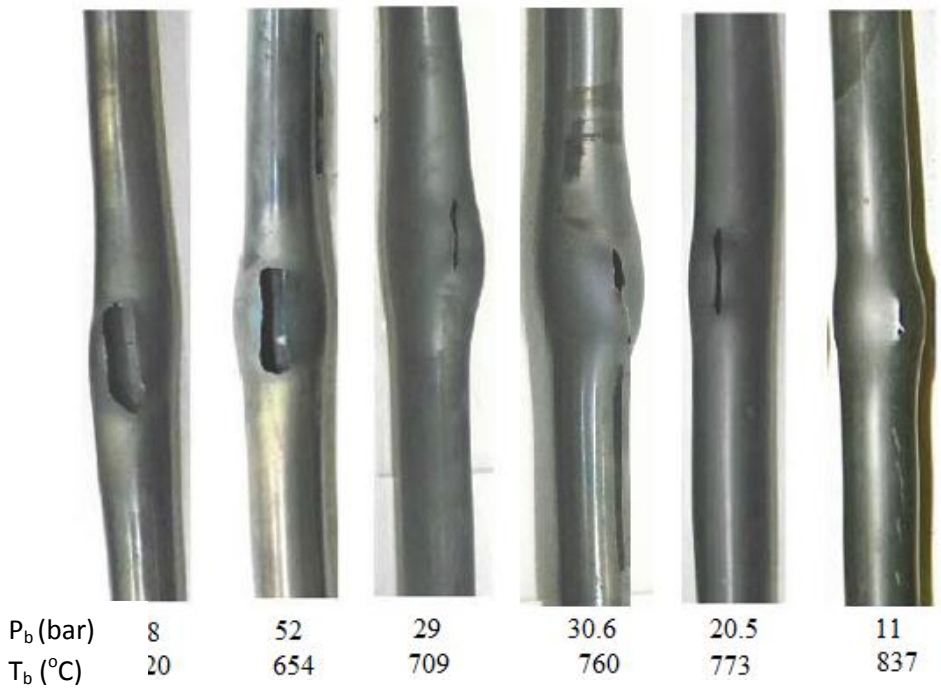

FIG. 2. Failure modes at different burst temperature and pressure.

4.2. Macroview of rupture location

Different types of burst openings varying from rectangular/broad fish mouth type of opening with violent rupture (< 722°C) to narrow crack like opening characterized by 'V' shaped splits at the ends (760 to 920°C) and pinhole type (942°C) were observed during the tests. A few typical burst opening appearances at different burst temperatures as observed under the macroscope are presented by Fig. 3.

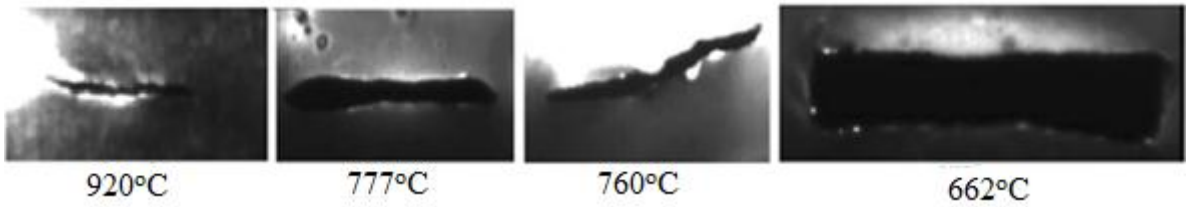

FIG. 3. Appearance of burst opening.

4.3. Area of burst opening as a function of burst pressur

A plot of the measured burst area against the burst pressure is shown in Fig. 4. The measured rupture area was observed to be in the range 2 to 308 mm^2, the minimum and maximum values corresponding to 11 and 42 bar burst pressures. The general trend appeared to be an increase in the area of rupture opening with increase in burst pressure reaching a maximum corresponding to the peak circumferential strain of 82% at 42 bar followed by a decrease in the burst area with an increase in the burst pressure. The area of burst opening is

an important parameter which influences the ingress of steam and the amount of oxidation of inner surface of the cladding as well as the release of fission products to the coolant.

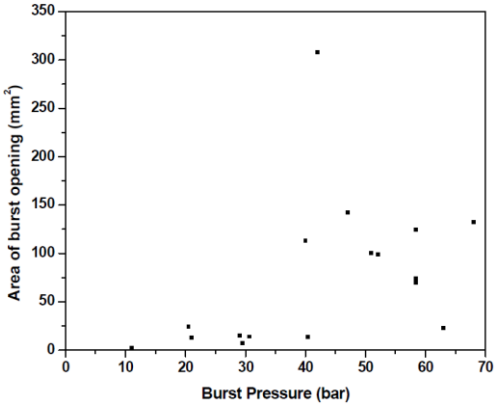

FIG.4. Dependence of the area of burst opening on the burst pressure.

4.4. Burst temperature, hoop stress and time to failure

The burst data, i.e, burst pressure, burst temperature, maximum circumferential strain, maximum diametral strain and radial strains at the rupture location, engineering hoop stress and time to burst, are shown in Table 2. The results show that for the burst pressure in the range of 5 to 70 bar, the corresponding burst temperature was in the range of 942 to 609^{o}C. The engineering hoop stress was determined to be in the range 9 to 131 MPa. The relationship between burst temperatures and hoop stress is presented in Fig. 5. The figure indicates that the fuel pins with high engineering hoop stress burst at lower temperature. Fig. 6 shows the time taken by the test pins to burst as a function of burst pressure indicating a delay in rupture as the pressure decreases.

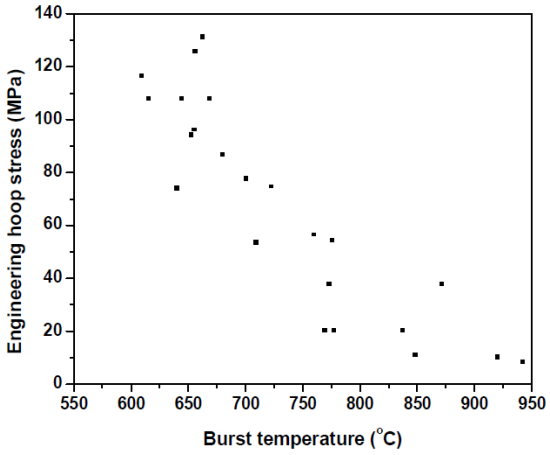

Fig.5. Dependence of burst temperature.

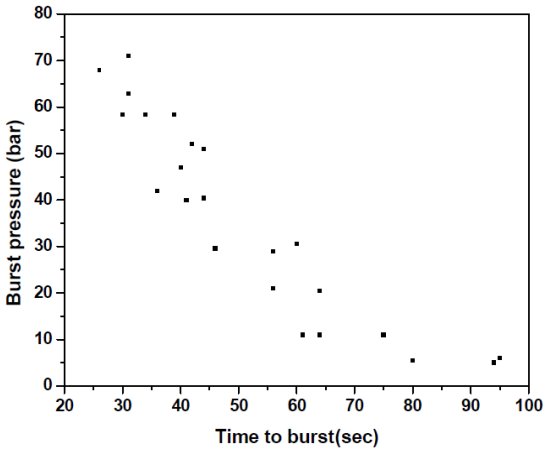

Fig. 6. Time taken by fuel pins to burst at different burst pressures on engineering hoop stress.

TABLE 2. BURST DATA

Test No	Burst pressure (bar)	Burst temperature (^oC)	Maximum circumferential strain (%)	Maximum diametral strain (%)	Rupture radial strain (%)	Engineering hoop stress (MPa)	Time to rupture (sec)
1	6	848	32	37.7	90.4	11	95
2	5.5	920	33	37.7	98	10.2	80
3	5	942	32.3	36	97.4	9	94
4	11	769	18.5	28.3	96	20.4	75
5	11	777	19.5	30	97.3	20.4	64
6	11	837	31	38	97.4	20.4	61
7	21	871	16	29.6	96	39	56
8	20.5	773	22.7	33	89.5	38	64
9	29.5	776	57	71.5	91	54.4	46
10	29	709	51	61	82.5	53.7	56
11	30.6	760	46	62.7	84.4	56.6	60
12	42	700	82	123.6	78	77.7	36
13	40	640	40	59.7	80.6	74	41
14	40.4	722	47	55.4	82	74.7	44
15	47	680	46.5	70.5	80	87	40
16	51	652	39	64.5	80.7	94.4	44
17	52	654	34.5	51.4	78	96.2	42
18	58.4	668	29	51.7	78.7	108	39
19	58.4	620	25	48.5	73.5	108	34
20	58.4	644	30.7	50.2	80	108	30
21	63	609	26	39.4	90	116.6	31
22	71	662	23.5	41.4	80	131	31
23	68	666	39.7	70.2	72	125.8	26

4.5. Effect of burst temperature on radial strain and circumferential strain

The radial rupture strain measured from the reduction in the clad wall thickness as a function of burst temperature is shown in Fig. 7a. Minimum and maximum rupture radial strains were 72% and 98% at temperature of 666^{o}C and 920^{o}C respectively. It was observed that in general, increasing burst temperature was associated with increasing wall thinning.

The circumferential strain was determined to be in the range 16 to 57% which is low compared to other studies [2], [7]. Axial constraint due to the presence of ceramic pellets and localized deformation [13] can be two factors contributing to this. The maximum circumferential expansion as a function of burst temperature is shown in Fig. 7b. The

observed trend is the increase in the circumferential strain reaching a maximum at 776°C, when the cladding is in α phase where deformation is mainly due to the combined action of dislocation glide as well as climb [17]. However a deviation was noticed in one of the fuel pin cladding in which, circumferential strain showed a peak, 82% at 700°C. A near complete uniform clad wall thinning was also observed in this cladding all along the circumference in this fuel pin (Fig. 7c) as against a non-uniform thinning observed over the circumference) in the other fuel pins, two of which are shown in Figs. 7d and 7e. The strain maxima obtained in this study is lower than the value (800°C) reported in the literature.

The maximum circumferential strain vs. burst temperature plot then reached a minimum value at 871°C in the α + β phase which is close to the value (875°C) reported by Chung and Kassner [13] in one of their experiments for a mandrel constrained fuel pin heated in vacuum at a heating rate of 5°C/s. The reason for the observation of the lowest strain in the α + β phase field has been stated in the literature [8] as the prohibition of the α grain growth due to the nucleation of high temperature β phase at α grain boundary reaching the lowest at a temperature where the volume fractions of these two phases are equal.

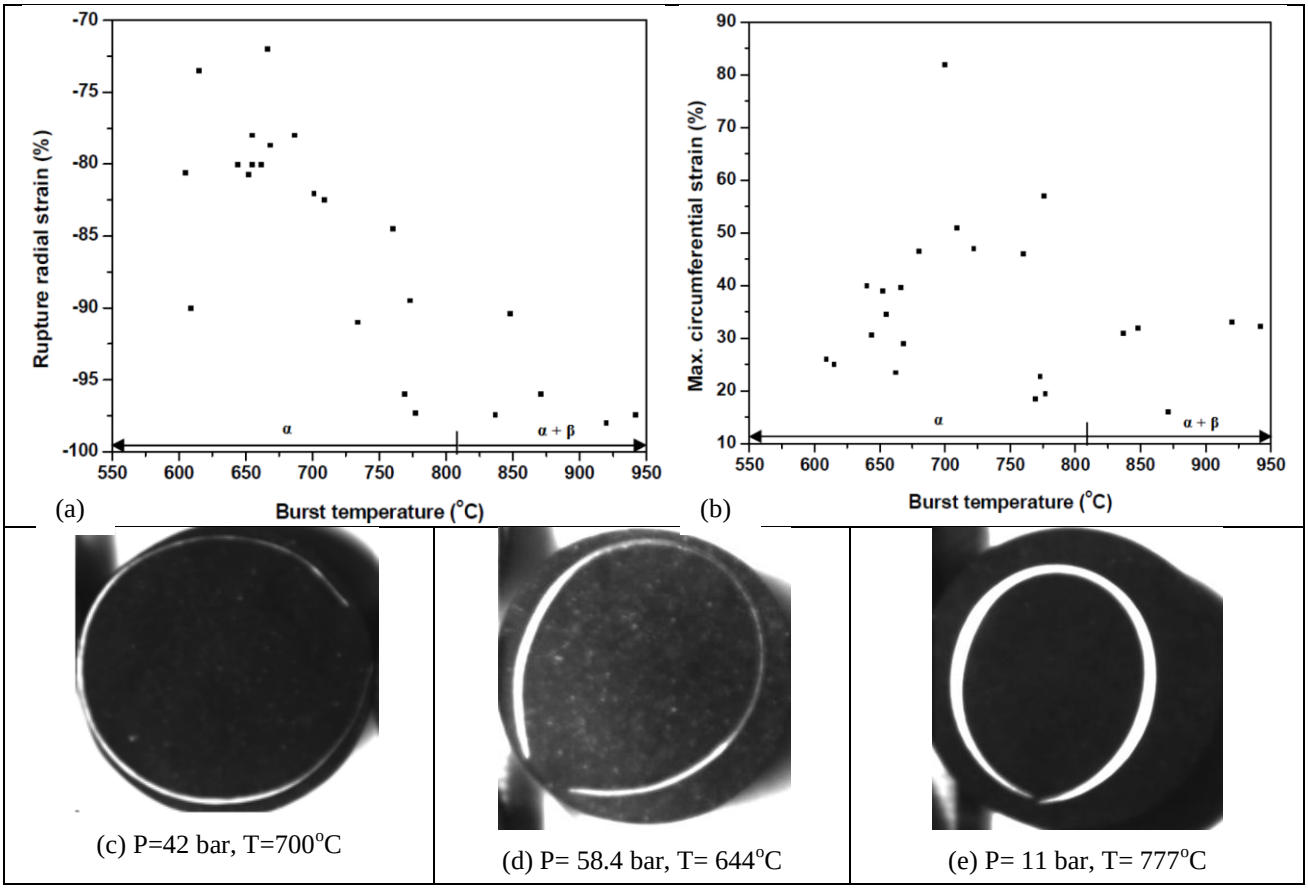

FIG. 7. (a) Plot of radial strain vs. burst temp (b) Plot of circumferential strain vs. burst temp (c) uniform circumferential strain (d) non-uniform circumferential strain (e) localized strain.

The observations revealed that a certain degree of non-uniformity in the circumferential strain was prevalent in almost all the pins in this study. Microstructural examination

confirmed the existence of a temperature variation along the circumference in the cladding in these fuel pins. Hence non-uniformity in circumferential strain is attributed to the azimuthal temperature variation along the cladding.

4.6. Microstructural examination and fractography

Microstructural examination in optical microscope and fractography in scanning electron microscope (SEM) were carried out and the results for a two typical claddings are presented in Fig. 8 and Fig. 9. The cladding ruptured below α/β transition temperature (810^{o}C for alloy containing 0.1wt% oxygen) [13] showed equiaxed grain structure (Fig. 8a). The microstructure of the cladding burst at 942^{o}C showed 'widmanstatten' structure which is commonly observed when zircaloy is cooled from the β phase (Fig. 8c). The rupture edge was observed to be blunt in samples ruptured in the α phase range (Fig. 8b). The rupture edge of the clad fractured at higher temperature was sharp (Fig. 8d). The SEM photographs showed the fracture surface containing dimples, a sign of ductile failure. There is a difference in the size and morphology of the dimples in the two fractographs because at 700^{o}C zircaloy exits as a single phase (α-Zr) while at 920^{o}C it exists as (α + β) phase.

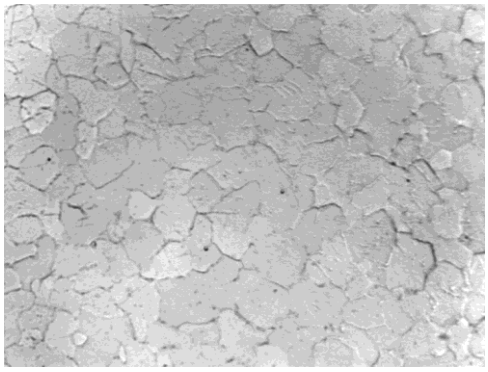

(a) Near the crack tip region.

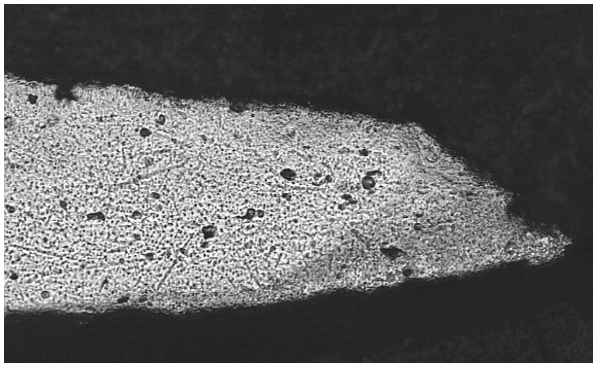

(b) At the rupture edge, failed at 776°C.

Failed below α/β transition temperature

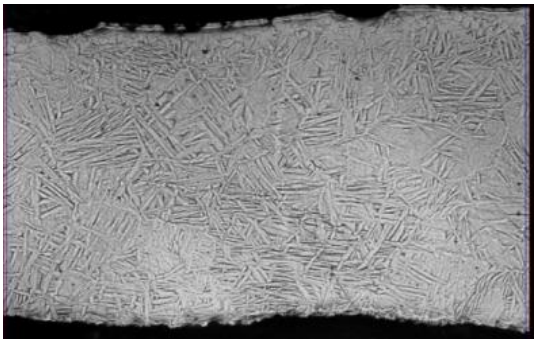

(c) Near the crack tip region.

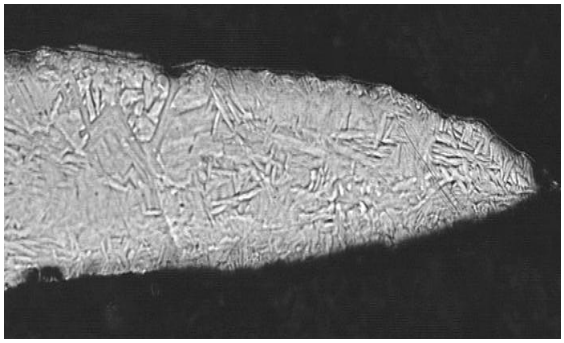

(d) At the rupture edge, failed at 942°C.

Failed above α/β transition temperature

FIG. 8. Microstructures at a magnification (a) 100X (b-d) 20X of 2 different claddings.

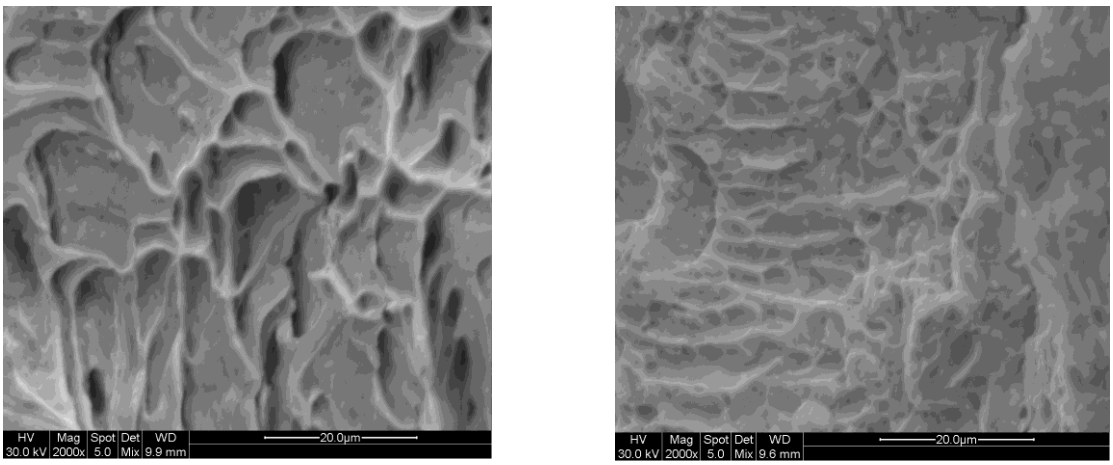

P= 42 bar, T= 700°C P= 5.5 bar, T= 920°C

FIG. 9. SEM fractographs showing characteristic fracture surfaces of the cladding with their respective burst pressure and burst temperature.

5. SUMMARY

Transient heating experiments (at heating rates 8 to 12^{o}C/s) were performed on internally pressurized (5 to 70 bar) pellet constrained zircaloy-4 cladding in argon gas environment in order to understand the high temperature ballooning deformation and burst behavior of Indian PHWR fuel pins. The main findings of these studies are as follows:

— Expansion was symmetrical and the fuel pins remained straight except a few cases where bending was observed;
— The burst opening was observed to be confined to axial direction in all the cases, except the one ruptured at 760^{o}C;
— The rupture area was observed to be in the range from 2 to 308 mm^{2}, the minimum and maximum values corresponding to 11 and 42 bar burst pressure respectively;
— For the burst pressure in the range of 5 to 70 bar, the corresponding burst temperature was observed to be in the range of 942–609^{o}C;
— The circumferential strain was determined to be in the range 16–57% (corresponding burst temperatures of 871 and 776°C). Axial constraint due to pellets inside the cladding appears to be the cause of low ductility. Non uniform circumferential elongation was an important observation in this study, which could be the reason for the observed low ductility;
— The measured minimum and maximum radial strains were 72 and 98% at 666^{o}C and 920^{o}C respectively;
— The difference between our results and those reported in the literature can be attributed to the varying heating rate during the test, presence of azimuthal temperature differences, difficulty in measuring the burst temperature at the exact location as it could not be spotted.

6. CONCLUSION

As various interdependent parameters influence the highest and lowest circumferential strain at different burst temperatures, comparison between the strains obtained in the present investigation with similar single rod tests should be based on the cladding dimension, burst

temperature, heating rate, environment and azimuthal temperature variation. The maximum rupture strain can be reasonably estimated from the present study for different postulated LOCA transient of a PHWR if the azimuthal temperature difference can be predicted from the fuel-modeling codes.

ACKNOWLEDGEMENTS

The authors would like to thank Mr. E. Ramadasan for his critical suggestions during the preparation of this paper. We wish to gratefully acknowledge the assistance rendered by Shri Sourabh Karmakar and Smt. Ujwala Trimbake of PIE Division BARC during the experiment and post test studies.

REFERENCES

[3] BABAR, A.K., SARAF, R.K., KAKODKAR, A., Probabilistic Safety Assessment of Narora Atomic Power Project, DE90602809 (1989).

[2] MARKIEWICZ, M.E., ERBACHER, F.J., Experiments on Ballooning in Pressurized and Transiently Heated Zircaloy-4 Tubes, KfK 4343 (1988).

[3] ERBACHER, F.J., LEISTIKOW, S., A Review of Zircaloy Fuel Cladding Behavior in a Loss-of-Coolant Accident, KfK 3973 (1985).

[4] ALAMA, T. et. al., A Review on the Clad Failure Studies, Nuclear Engineering and Design, **241** 3658 (2011) 3677.

[5] NEITZEL, H.J., ROSINGER, H.E., The Development of a Burst Criterion for Zircaloy Fuel Cladding under LOCA Conditions, KfK-2893 (1980).

[6] KARB, E.H., PRUBMANN, M., SEPOLD, L., HOFMANN, P., SCHANZ, G., LWR Fuel Rod Behavior in the FR2 In-pile Tests Simulating the Heatup Phase of a LOCA, Final Report KfK 3346.

[7] CHUNG, H.M., KASSNER, T.F., Deformation Characteristics of Zircaloy Cladding in Vacuum and Steam under Transient-Heating Conditions: Summary Report, NUREG/CR-1344, ANL.

[8] KIM, J. H., LEE, M. H., CHOI, B. K., JEONG, Y.H., Deformation of Zircaloy-4 Cladding during a LOCA Transient up to 1200°C, Isothermal and Transient in Steam, Nuclear Engineering and Design **234** 157 (2004) 164.

[9] ERBACHER, F., NEITZEL, H. J., WIEHR, K., Studies on Zircaloy Fuel Clad Ballooning in a Loss-Of-Coolant Accident—Results of Burst Tests with Indirectly Heated Fuel Rod Simulators, Zirconium in the Nuclear Industry (Fourth Conference), ASTM STP 681, American Society for Testing and Materials, 429 (1979) 446.

[10] CHAPMAN, R.H., CROWLEY, J.L., LONGEST, A.W., HOFMAN, G.H., Zirconium Cladding Deformation in a Steam Environment with Transient Heating, Zirconium in the Nuclear Industry (Fourth Conference), ASTM STP 681, 393 (1979) 408.

[11] FURUTA, T., KAWASAKI, S., HASHIMOTO, M., Zircaloy-clad Fuel Rod Burst Behavior under Simulated Loss-of-Coolant Condition in Pressurized Water Reactors, Journal of Nuclear Science and Technology **15** 736 (2010) 744.

[12] FIVELAND, W. A., BARBER, A. R., LOWE, A. L., Jr., Rupture Characteristics of Zircaloy-4 Cladding with Internal and External Simulation of Reactor Heating, Zirconium in the Nuclear Industry, ASTM STP 633, American Society for

Testing and Materials 36 (1977) 49.
[13] CHUNG, H.M., GARDE, A.M., KASSNER, T.F., Deformation and Rupture Behavior of Zircaloy Cladding under Simulated Loss-of-Coolant Accident Conditions, Zirconium in the Nuclear Industry, ASTM STP 633, American Society for Testing and Materials 82 (1977) 97.
[14] FERNER, J., ROSINGER, H. E., The effect of Circumferential Temperature Variation on Fuel-Cladding Failure, Journal of Nuclear Material **132** 167 (1985)172.
[15] SAGAT, S., SILLS, H.E., WALSWORTH, J.A., FOOTE, D.E., SHIELDS, D.F., Deformation and Failure of Zircaloy Fuel Sheaths under LOCA conditions, AECL-7754 (1982).
[16] HARDY, D.G., "High temperature expansion and rupture behaviour of zircaloy tubing", ANS Topica1 Meeting on Water Reactor Safety, CONF-730304, Sa1t Lake City, Utah (1973).
[17] FRANKINE, D.G., LUCAS, G.E., BEMENT, A.L., "Creep of Zirconium Alloys in Nuclear Reactors", Vol. 815, ASTM STP, Philadelphia.

POST IRRADIATION EXAMINATION
(Session 3)

Chairman

A. EL JABY
Canada

IRRADIATION BEHAVIOUR OF PHWR TYPE FUEL ELEMENTS CONTAINING UO_2 AND $(TH,U)O_2$ PELLETS

G. HORHOIANU, G. OLTEANUl, D.V. IONESCU
Institute for Nuclear Research,
Pitesti, Romania

Abstract

Two PHWR type fuel elements with reduced length has been irradiated in TRIGA Research Reactor of INR Pitesti. Fuel element A23 has $(Th,U)O_2$ pellets contained in a Zircaloy-4 sheath and the element A24 has UO2 pellets contained in a Zircaloy-4 sheath. The primary objective of the test was to determine the performance of the $(Th,U)O_2$ fuel element comparatively with UO2 fuel element, both irradiated in similar conditions. The fuel elements were irradiated in C1 capsule with a ramp power history. The element A23 achieved a maximum element linear power of 33 KW/m in pre-ramp and 51 KW/m in the ramp. The maximum discharge burnup achieved in A23 fuel element was 189.2 MWh/kgHE. The element A24 achieved a maximum element linear power of 41 KW/m in pre-ramp and 63 KW/m in the ramp. The maximum discharge burnup achieved by A24 fuel element was 207.8 MWh/kgHE. Both elements were destructively examined in Hot Cells of INR Pitesti. Temperature-sensitive parameters such as pellet grain growth, fission-gas release and sheath deformations were analyzed. This paper presents the results of this investigation.

1. INTRODUCTION

INR Pitesti is currently involved in the studies of oxide fuels, as part of a program for advanced fuel cycles for PHWRs [1]. Thoria-based fuel is one of the options under review, having the promise of resource conservation compared with the current natural uranium, once through cycle.

Utilization of ThO_2 based fuel pellets for light water reactor fuels have many performance advantages compared to UO_2 fuel pellets. A review of the open literature has indicated that some of the $(Th,U)O_2$ properties in comparison with those of UO_2 may contribute to the promotion of different fuel rod performance parameters [2], [3]. Some of the more important differences and their comparison with UO_2 are: thermal conductivity-higher; modulus of elasticity-higher; fracture strength-higher at lower temperatures and lower at higher temperatures; creep-thermal component similar to UO_2 and irradiation component considerably less; thermal expansion similar to UO_2. ThO_2 has higher melting temperature and is more corrosion resistant when exposed to reactor coolant. ThO_2 pellets also release less fission gas than UO_2 pellets.

These advantages could be realized in increased steady state power output for a given limiting fission gas release, and indeed some irradiations at steady power have shown the superior characteristics of thoria. However, in others, the performance has been no better than UO_2, possibly due to fuel inhomogeneity [2]. Because of its added fissile component, thoria fuel will experience higher burnup, greater end flux peaking and possibly more severe power ramps than those experienced by natural UO_2 fuel in a PHWR [3]

In order to determine the performance of the PHWR type fuel elements, two types of irradiation tests have been proposed as part of the Nuclear Fuel R&D Programme of INR Pitesti [4]. One type was a declining power irradiation test to a high burnup and the other type was a power ramp irradiation test at low to medium burnup.

In the power ramp irradiation test, presented in this paper, the fuel elements were irradiated in the pre-ramp period at lower power. The power was then increased for ramp at a rate of approximately 0.025 Kw/m·s. The assembly was remained in the high power position for a period of 7 full power days [4] and [5]. The elements were destructively examined in Hot Cells of INR Pitesti. The test results were included in the INR Pitesti "experimental data bank" against which the latest version of ROFEM fuel performance code was recently "fine tuned" [6].

2. FUEL DESCRIPTION

Two fuel elements (coded A23 and A24) with reduced length (A23 has 206.9 mm total length and A24 has 213.3mm total length) were fabricated at INR Pitesti [7]. (Th,U)O_2 fuel element A23 has 5wt% UO_2 (90 % enriched in ^{235}U) and 9.7 gr/cm^3 density contained in a Zircaloy-4 sheath; A24 element has UO_2 pellets contained in a Zircaloy-4 sheath with 5wt% UO_2 (90 % enriched in ^{235}U) and 10.5 gr/cm^3 density. Summary of test fuel elements characteristics are presented in Table 1. The level of fuel enrichment was selected to achieve a high linear power output during the ramp. The elements contain a graphite coating (CANLUB) on the inner sheath surface and have helium at 0.1 MPa as filling gas.

TABLE 1. SUMMARY OF TEST FUEL ELEMENTS CHARACTERISTICS (AVERAGE VALUEA)

1. Pellet	A23	A24
Enrichment U235 (%)	5.0	5.0
Density (g/cm3)	9.7	10.5
Grain Size (μm)	-	9.4
Pellet Geometry		
Pellet O.D. (mm)	12.15	12.15
Length(mm)	12.7	13.5
Land Width (mm)	0.50	0.54
Dishing Depth(mm)	0.24	0.25
Surface Roughness, Ra(μm)	0.62	0.54
2. Cladding		
Cladding I.D. (mm)	12.22	12.22
Wall thickness , (mm)	0.41	0.41
Surface Roughness, Ra(μm)	0.6	0.6
3. Fuel element		
Axial gap (mm)	1.5	2.0
Diametral gap, average (mm)	0.06	0.06
Pellet Stack Length (mm)	178.5	187.3
Number of pellets in stack	14	14
Filling Gas Composition	He	He
Filling gas pressure (MPa)	0.1	0.1
CANLUB layer thickness (μm)	3.9	4.1

3. IRRADIATION CONDITIONS

The fuel elements have been irradiated in capsule C1 of TRIGA research reactor of INR Pitesti in thermal neutron fluxes of $1.8–4.6 \cdot 10^{17}$ n/m^{2}sec [5]. The coolant in the capsule C1 was light water at: 10.6 MPa and 120–173°C. The fuel sheath temperature during irradiation was varied between 110–324°C. The power outputs of each element were determined through calibration of the four flux detectors as power sensors. The capsule operating conditions and the thermal neutron flux are given in reference [5]. The element A23 achieved a maximum element linear power of 33 KW/m in pre-ramp and 51 KW/m in the ramp. The maximum discharge burnup achieved by A23 element was 189.2 MWh/kgHE (Table 2). The element A24 achieved a maximum element linear power of 41 KW/m in pre-ramp and 63 KW/m in the ramp. The maximum discharge burnup achieved by A24 was 207.8 MWh/kgHE (Table 2).

TABLE 2. AVERAGE ELEMENT POWERS AND BURNUPS

Element	Linear Power (Kw/m) *		Discharge burnup (Mwh/KgU) **
	Pre-ramp	Ramp (for 7 days)	
A23	33	51	189.2
A24	41	63	207.8

* Average (on the element length) linear power.
** Uranium isotopic analysis (Cs^{137}) at the middle length of each element.

4. PIE RESULTS

The post irradiation investigation performed in INR Pitesti Hot Cells included both non-destructive examinations (visual, profilometry, axial gamma-scanning, eddy-current testing) and destructive examination (puncturing, fission gas volume and composition, element void volume, chemical burnup determination, metallography/ceramography and mechanical tests) [8], [9].

4.1. Element visual examination

Each element was in good conditions, with no unusual features found on the sheath surface. Typical features that were observed included handling scratches, variations in the zirconium-oxide shading, stains, and white deposits. The visual appearance of the fuel elements shows circumferential ridges on the entire length and distinct ridges at both ends near end caps (Figure 1). The distinct ridges on sheath at pellet interface locations indicated that strong pellet cladding mechanical interaction (PCMI) had occurred.

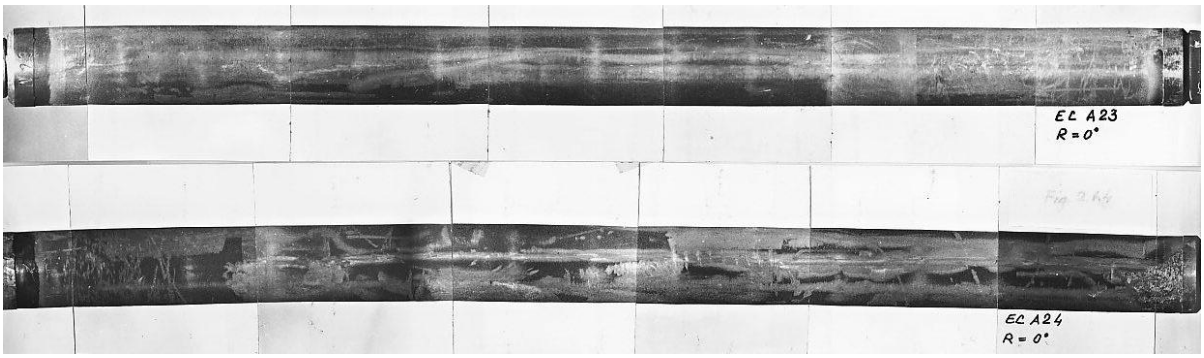

FIG. 1. Fuel elements A23 and A24 after irradiation.

4.2. Element profilometry

The axial profiles of gamma scans are shown in Fig. 2. Intensity dips are seen at the pellet interfaces. The intensity along the fuel stack is uniform, indicating a uniform

distribution of fission products along the fuel stack, and thus a uniform distribution of feed material and fissile distribution in the pellets.

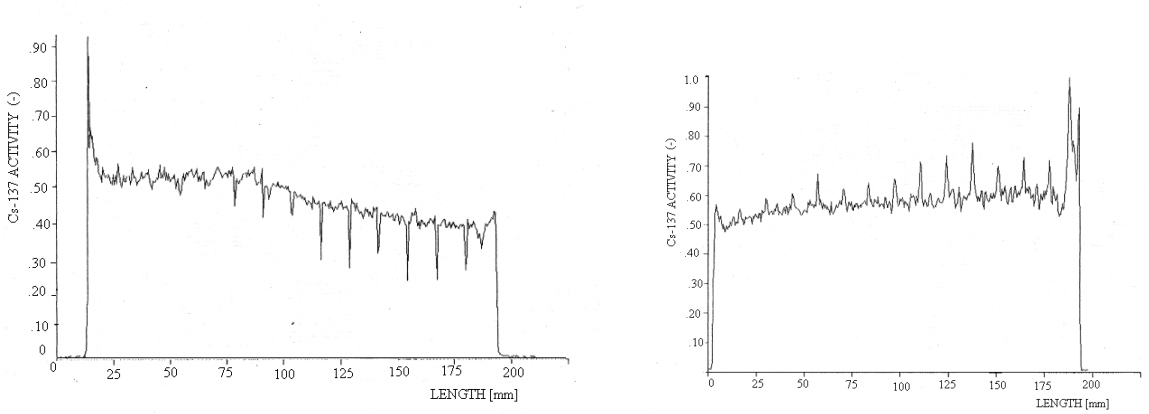

FIG. 2. Axial gamma scan profile after irradiation: a) A23 fuel element, b) A24 fuel element.

Each element was profiled at the 120° positions, thus minimizing gravity effects on the measurements. The element bow at the element centre was 0.08 mm at A23 element and 0.05 mm at A24 element. Fig. 3 shows the cladding deformation profile after irradiation. The lengths of the elements were measured and the calculated axial elongations are recorded in Table 3. The mid-pellet (MP) and pellet interface (PI) residual sheath strain results are also recorded in Table 3. The residual sheath strain at A23 element was slightly higher than at A24 element. The elements showed a significantly greater diameter increase at the high-flux regions (near one endcap) where maximum observed pellet/pellet interface strains were as highs as 1.4% for A23 and 1.1% for A24 element. Measurements of the pellet interface ridge height for each element are summarized in Table 3. The residual sheath strains and ridge height results are within the range observed in similar irradiation tests performed on PHWR type fuel elements in TRIGA Research Reactor [10], [11].

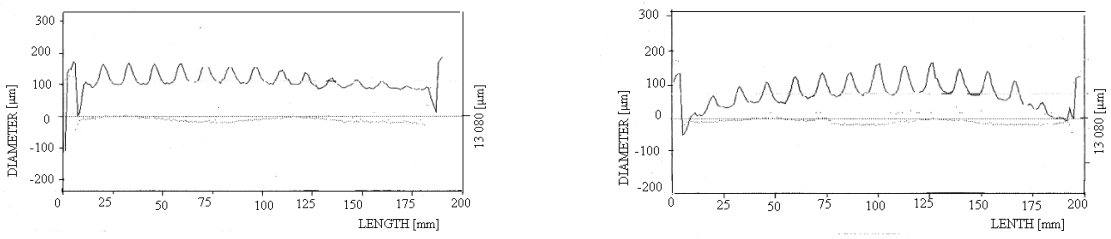

a) b)

FIG. 3. Cladding deformation profile after irradiation: a) A23 fuel element, b) A24 fuel element.

TABLE 3. POST IRRADIATION MEASUREMENTS

Element	Element Bow (mm)	Axial Elongation (mm)	Sheath Oxide Layer(μm)		Residual Sheath Strain* (%)		Ridge Height* (μm)	Gas released
			Outside	Inside	Mid-Pellet	Pellet Interface		Volume** (cm^3)
A23	0.08	0.12	3-9	1-4	0.6	0.9	30	5.5
A24	0.05	0.1	5-26	3-6	0.4	0.7	35	15.9

* Average value at the mid point length region
** STP = **S**tandard **T**emperature and **P**ressure

4.3. Fission-gas release

Gas-puncture analysis was performed on every element. Gas composition was measured, from which the fission-gas release (FGR) was determined. The gas puncture results are summarized in Table 3.

The gas volume was 5.5 cm^3 STP (at A23 element) and 15.9 cm^3 STP (at A24 element). There is a significant differences in fission gas release fraction between (Th,U)O_2 fuel and UO_2 fuel. Fission gas release from (Th,U)O_2 fuel was much lower than that from UO_2 fuel. The results are within the range observed in similar irradiation tests performed in TRIGA Research Reactor [10].

4.4. Metallographic and ceramographic examination

The UO_2 microstructure was examined at three axial locations, for each element. Ceramografic investigation of the grain size in sintered thoria pellets necessitates appropriate surface preparation of the pellets. Conventional etching methods involving either chemical or thermal etching techniques being unsuitable for surface etching of irradiated thoria fuel, transverse section and longitudinal section at the middle length plane of the A23 element are presented in Figs. 4(a), 4(b), 4(c), 4(d) and 4(e). Longitudinal section in the middle length region (Fig. 4c) shows visible pellet interface dish filling. A large number of pores are clearly visible in the (Th,U)O_2 pellets. Many pores appeared at the grain boundaries, looking like pearl necklaces (Figure 4e). The grain boundaries pores seemed to have connected to each other and formed tunnels for FGR paths. Size and number of pores seemed to have gradually increased from outer to inward. Generally, thoria fuel exhibits less microstructural change than UO_2 fuel, primary due to its higher thermal conductivity. The fact that thoria is a more refractory material than UO_2 may also be a contributing factor. Reaction of the (Th,U)O_2 fuel with the Zircaloy end caps was observed at the A23 element (Fig. 4d).

The element A24 had a void at the fuel centre (~2.5 mm diameter at the pellet end cap section where the flux was higher) and around there was no evidence of melting (Figs. 5a and 5b). The central voids in these regions presumably result from migration of lenticular pores in a high thermal gradient. The cracking pattern and grain growth is typical of UO_2 operating at

about 60 Kw/m (radial cracking with some circumferential cracking around a plastic core) [10].

The presence of central region with columnar grains was also observed only in the A24 element (3.5 mm at the end cap, Fig. 6,a). Equiaxed grain growth had occurred in A24 element (Fig. 6b). No grain growth was observed at the pellet periphery of the A24 element. A summary of the ceramografic examination results is given in Table 4.

A continuous layer of oxide with 3-9 μm in thickness was found on the outside sheath surface of A23 fuel element and with 5–26 μm in thickness for A24 fuel element. On the inside sheath, the elements had patches of oxide (2–4 μm in thickness) that covered about 115 μm length at the pellet interface for A23 element while the A24 element had little or no discernable oxide on inside sheath. The Stress Corrosion Cracking (SCC) on the internal sheath surface of the elements was not observed. The CANLUB coating seems to prevent the zircaloy sheath from gettering oxygen that is liberated during fissioning and to mitigate Stress Corrosion Cracking of the sheath following a power ramp.

5. FUTURE WORK

More work remains to be done to demonstrate conclusively the performance capabilities of thoria-based fuels, particularly under off-normal operating conditions and to provide quantitative data required for modeling fuel behaviour for purposes of design and licensing. New power ramp tests are planned in TRIGA Research Reactor on $(Th,U)O_2$ type fuel elements with different microstructures and geometry [1].

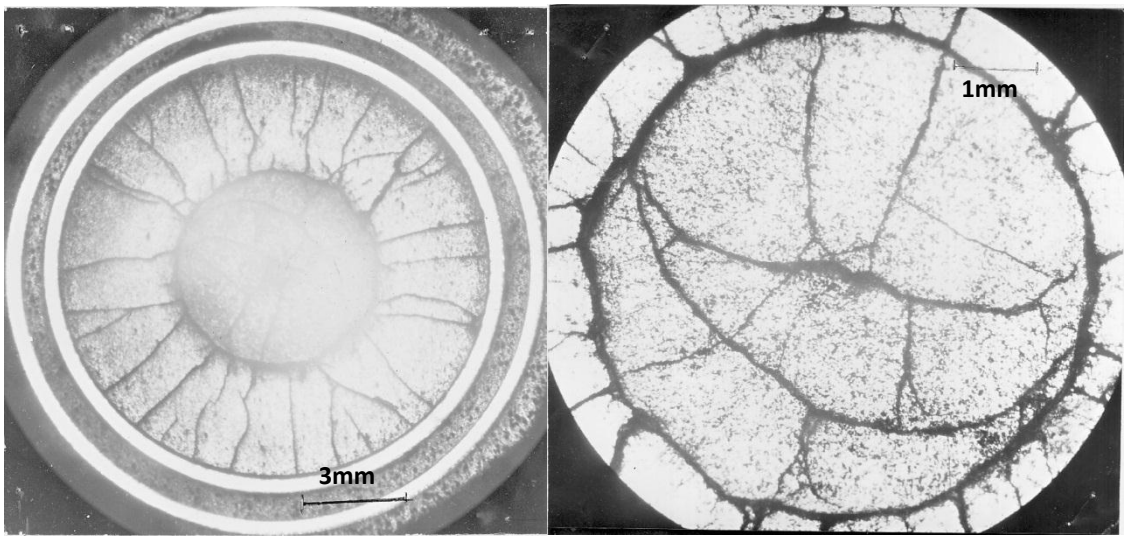

a) b)

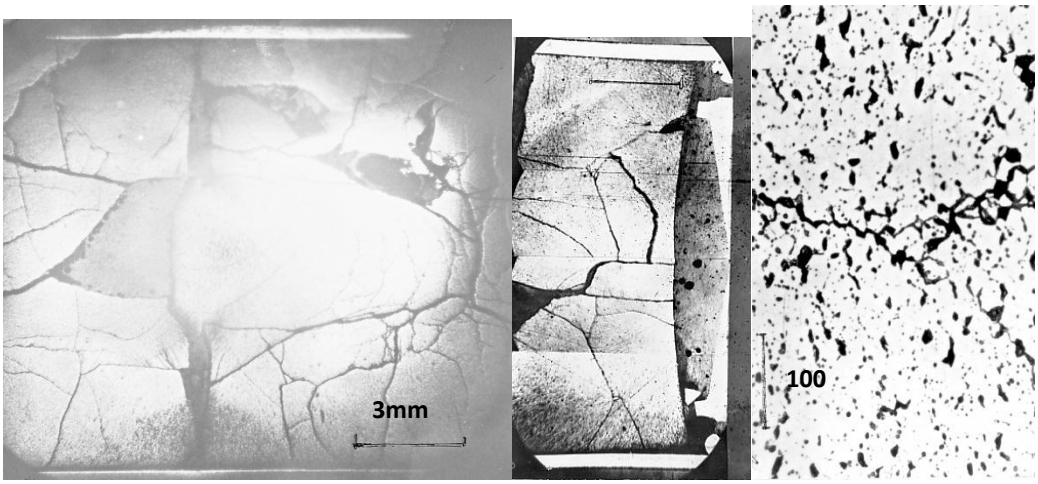

c) d) e)

FIG. 4. Micro structural features of the A23 element: a) Transverse section near the middle length of the element; b) Detail in transverse section (from picture (a)); c) Longitudinal section near the middle length of element showing visible pellet interface dish filling; d) Section near the endcap region; e) porosity in the central zone of the pellet.

6. SUMMARY & CONCLUSIONS

(a) Severe power ramp test performed in TRIGA Research Reactor on PHWR type fuel elements fabricated in INR Pitesti shows no evidence of sheath failure. $(Th,U)O_2$ fuel element operated at lower temperatures in comparison with UO_2 fuel element due to the high thermal conductivity of thoria which is evidenced by various fuel performance parameters;

(b) Profilometry measurements and distinct ridges observed on sheath at pellets interfaces show that both elements experienced high tensile strains at pellet interface regions.

(c) Each fuel element showed a significantly greater diameter increase at the length mid plane position and near one endcap, as effect of the axial flux gradient and flux endcap peaks. Compared to UO_2 fuel element the $(Th,U)O_2$ fuel element exhibited higher sheath strains at both MP and PI locations;
(d) The effect of heat rating on fission product release and sheath strains has been observed. Sheath strains appear to be function of peak heat rating. There was a clear correlation between the release of fission product gas and heat rating;
(e) There is a significant differences in fission gas release fraction between $(Th,U)O_2$ fuel and UO_2 fuel. Fission gas release from $(Th,U)O_2$ fuel was much lower than that from UO_2 fuel;
(f) UO_2 fuel element had a void at the fuel centre near the endcap region, where there was no evidence of melting. The presence of central region with columnar grains was also observed in the UO_2 fuel element;
(g) The SCC was not observed on the internal sheath surface of the elements. This demonstrates the role of CANLUB coating to prevent the Stress Corrosion Cracking of the sheath following a severe power ramp;
(h) The requirement for high density $(Th,U)O_2$ fuel pellets was specified to give high thermal conductivity and minimize in-pile fuel dimensional changes;
(i) The test provides a fully documented irradiation of $(Th,U)O_2$ type fuel experiencing a ramp power history, which may be of use in "fine tuning" and validating fuel performance codes.

To summarize, this preliminary evaluation of the comparison in the performance of the two fuels leads to the conclusion that the performance of the $(Th,U)O_2$ fuel is comparable to, and in main respect superior to that of UO_2 fuel. Although a combination of the thermal conductivity and creep for the $(Th,U)O_2$ fuels would normally tend to produce lower fuel temperatures. Temperature sensitive parameters, including pellet grain growth, residual sheath strain, ridge height and element bow for $(Th,U)O_2$ fuel element were lower than that for UO_2 fuel element. Fission gas releases are lower, thus permitting such fuel to operate at higher power outputs for longer periods without significant physical degradation of the fuel element.

ACKNOWLEDGEMENTS

Many individuals contributed to this investigation. In particular, acknowledgement is made of the personnel of Fuel Technology Section for fuel elements fabrication, the personnel of TRIGA Research Reactor Section who conducted irradiation and of those of Hot Cells Laboratory who carried out the post-irradiation examinations.

REFERENCES

[1] HORHOIANU, G., Nuclear Fuel R&D Program of INR Pitesti for the Period 2011-2015, INR Internal Report No.8779,INR Pitesti (2010).
[2] ZHANG, Z, KURAN, S., "Status of development thorium fuel cycle in CANDU reactors, REUSE 4 Meeting, Missisauga, Ontario, Canada , (2010).
[3] HASTINGS, I.J., et al, Irradiation Performance of $(Th,U)O_2$ Fuel Designed for Advanced Cycle Application, AECL report 7697 (1982).
[4] OLTEANU, G., et al, Test Specification for Irradiation of A23 and A24 Fuel Elements in C1 Capsule of TRIGA Reactor, INR Internal Report No.2247, INR Pitesti (1987).
[5] DRAGOMIRESCU, C., et al, Irradiation of A23 and A24 Fuel Elements in TRIGA

Reactor of INR Pitesti, INR Internal Report No.2608, INR Pitesti (1988).
[6] HORHOIANU, G., et al, Improvement of ROFEM and CAREB Fuel Behaviour Codes and Utilization of these Codes in FUMEX III Exercise, Technical report for IAEA-Vienna Research Contract No.14974, INR Pitesti (2011).
[7] BALAN, V., et al, Fabrication of A23 and A24 Fuel Elements, INR Internal Report No.2307, INR Pitesti (1987).
[8] PARVAN, M., et al, Post-Irradiation Examination Results of A23 and A24 Fuel Elements, INR Internal Report No.2702, INR Pitesti (1989).
[9] POPOV, M. et al, Post-Irradiation Examination Results of A23 and A24 Fuel Elements, INR Internal Report No.2758, INR Pitesti (1989).
[10] HORHOIANU, G., et al., Power Ramp Irradiation Tests on PHWR Type Fuel Elements, KERNTECHNIK journal (2012) (in press).
[11] HORHOIANU, G., PALLECK, S., CANDU Fuel Elements Behaviour in the Load Following Tests, KERNTECHNIK Journal, Vol.76, No.4, 244 (2011) 248.

APPLICATION OF SIPPING AND VISUAL INSPECTION SYSTEMS FOR THE EVALUATION OF SPENT FUEL BUNDLE INTEGRITY

Y.-C. KIM, J.-C. SHIN, S.-K. WOO,
C.-H. PARK, T.-Y. CHOI
KEPCO Nuclear Fuel,
Daejeon, Republic of Korea
Email: yckim@knfc.co.kr

Abstract

When CANDU reactor has defective fuel bundle during its operation, then the defective fuel bundle should be discharged by 2(two) fuel bundles at a time from the corresponding fuel channel until the failed fuel bundle is found. Existing fuel failure detection system GFP(Gaseous Fission Product) & DN(Delayed Neutron) Monitoring System can't exactly distinguish fuel elements failure from each fuel bundle. Because of fuelling machine mechanism and discharge procedure, always two fuel bundles at a time are being inspected. In case visual inspection is available for inspecting fuel elements and suppose that there are no defects and damaged marks on the surface of outer fuel elements, 2(two) defective fuel bundles should be canned and kept in the separate region of spent fuel storage pool. Therefore, the purpose of this study was to develop a system which is capable of inspecting whether each fuel bundle is failed or not. KNF (KEPCO Nuclear Fuel Co. Ltd) developed two evaluation systems to investigate the integrity of CANDU spent fuel bundle. The first one is a sipping system that detects fission gases leaked from fuel element. The second one is a visual inspection system with radiation resistant underwater camera and remotely controlled devices. The sipping technology enables to analyze the leakage of fission products not only in gaseous state but also liquid state. The performance of developed systems was successfully demonstrated at Wolsong power plant this year. This paper describes the results of the development of the failed fuel detection technology and its application.

1. DEVELOPMENT OF SIPPING SYSTEM

The Sipping Technology to inspect defective fuel, generally well known, is divided largely into vacuum sipping, dry sipping, wet sipping or in-mast sipping depending on physical phenomenon and state of fission products which will be detected. KNF adopted a sipping technology that utilizes measurement of the radioactivity of gases and liquid samples holding fission products. This system is classified as a vacuum and canister sipping.

1.1. Canister unit

The canister unit consists of the canister, valve, underwater pump etc. as shown in Figure 1. The canister unit is installed inside the storage pool water to prevent high dose rate from the irradiated fuel contained in the canister. In designing, the structure allowing easy loading and unloading CANDU spent fuel was considered. For waterproof, the lid of the canister is sealed with radioactivity-resistant sealing material. The canister coupled with the valve console is installed on the bottom of the pool of the depth of 5m. The pump and valves of canister are designed to operate remotely by pneumatic process.

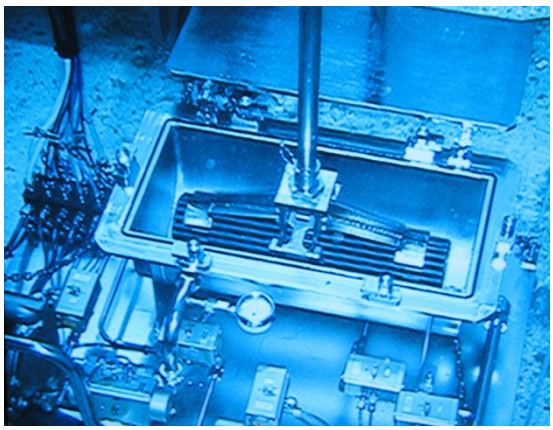

FIG. 1. Canister unit.

1.2. Control unit

The control unit consists of PLC-based control equipment (Touch-screen box, Control panel), a flowchart-diagram display etc as shown in Fig. 2. The control panel, which is a structure of a box shape installed outside the storage pool, includes a local power panel electrically controlling pumps and valves, an air service unit supplying compressed air and a valve controlling fluid flow. The portable touch-screen installed inside the box case performs remote control of the entire system. It carries out the automatic or manual control on its screen by communicating with control panel.

FIG. 2. Control unit.

1.3. Analysis unit

The analysis unit consists of a gamma detector, multichannel analyzer (MCA), sample chamber as shown in Fig.3. The gamma detector and other analysis circuits (amplifier, high voltage PS and multichannel analyzer, etc.) are designed to measure gamma rays from various nuclides. The range of energy to be measured is 50 keV ~ 3.5 MeV, and the entire H/W for radioactivity detection is designed to be automatically controlled by using programmed S/W. MCA built in a computer converts radioactivity to electric signals, to supply high or low voltage, to amplify output signals of the detector and to analyze nuclides.

FIG. 3. Analysis unit.

2. DEVELOPMENT OF VISUAL INSPECTION SYSTEMD

The irradiated fuel released into reception bay by fuel failure detection is loaded onto this visual inspection system through the spent fuel handling tool. The visual inspection system shown in Fig. 4 is installed in underwater of 5 meter deep. This system consists of rack and visual inspection pedestal where the fuel bundle is loaded, rotated and moved forward and backward to inspect surface defect of outer fuel elements, camera and light devices equipped about 700 millimeter away from visual inspection pedestal, and the control system. This system was designed for easy decontamination. This system is minimized to facilitate with adjacent apparatus in the reception bay and the weight of this system is also minimized for easy installation and handling. There are distinctive features in the visual inspection pedestal. Two air motors to drive gear mechanism, enable to move and rotate both X and Y direction with speed control for the movement of spent fuel bundle.

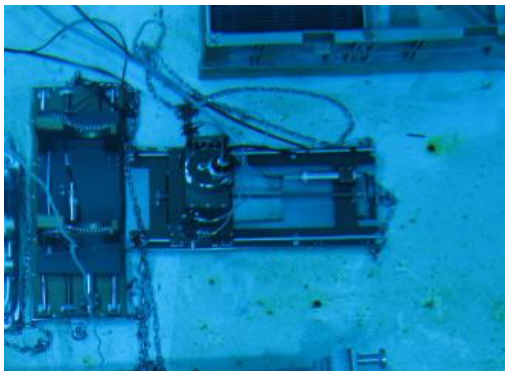

FIG. 4. Visual inspection system.

The radioactive resistant camera which has 100 times zooming ability to inspect the surface of outer fuel elements offers color image with high resolution and the 4 lights around camera are able to give optimized image data. The camera with lead shielding was designed

to resist high level of radiation at closer distance to spent fuel bundle. The control system of the camera governs the camera, lighting device, air motor adjusting components, power supply and air control unit etc. Due to the small volume of control system, it is very easy to scrutinize and install the apparatus as shown Fig. 5.

FIG. 5. Camera controller & monitor.

3. APPLICATION OF THE SIPPING AND VISUAL INSPECTION TECHNOLOGY

3.1. Fuel inspection at Wolsung NPP unit 4

We performed inspection of fuel integrity at the Wolsung unit 4 on February 2012. Four defective spent fuel bundles were inspected for exact distinguishing failed fuel bundles. Visual inspection using underwater camera was carried out on surface of the outer fuel elements. No defective fuel element was found even though there was a little scratch on fuel element surface as shown Fig. 6. The sipping system employed 2 types of the gamma detector to increase measurement reliability and also used vacuum process to easy escape for fission nuclide through defect hole of the fuel element. As the result of sipping inspection, Fig. 7 shows radioactivity of “A” fuel bundle was over one hundred times compared to BKG level in fission nuclides of Xe, Kr etc. Xe-133 nuclide was also detected by gamma detector as shown Fig. 8. Any other fuel bundles of “B”, “C”, “D” have radioactivity value of just two or three times compared to BKG level which is radioactivity level corresponding to intact fuel. And also no fission nuclide was found in any other fuel bundles except activated corrosion product like Ni-57, Cu-61 and Co-56.

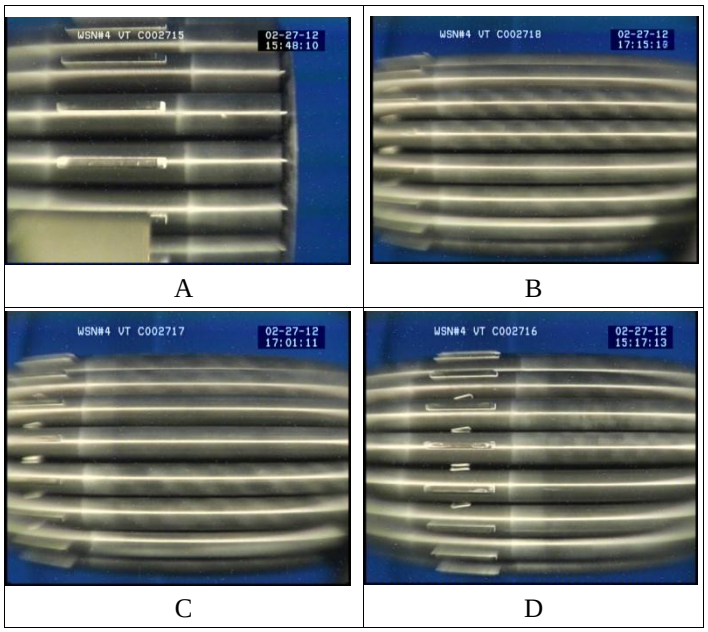

FIG. 6. Visual inspection image of fuel bundles in Wolsung unit 4.

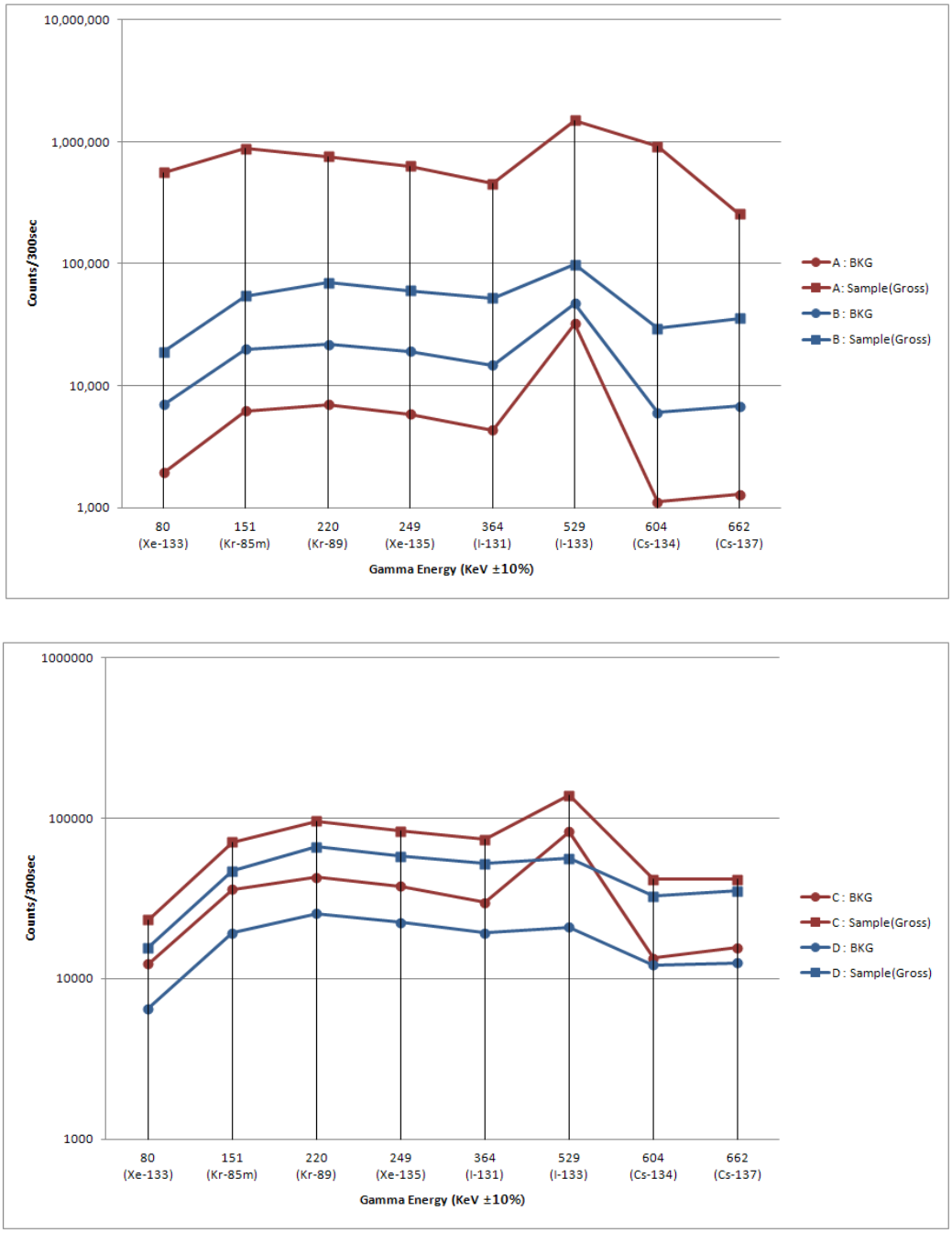

FIG. 7. Sipping inspection results of Wolsung unit 4.

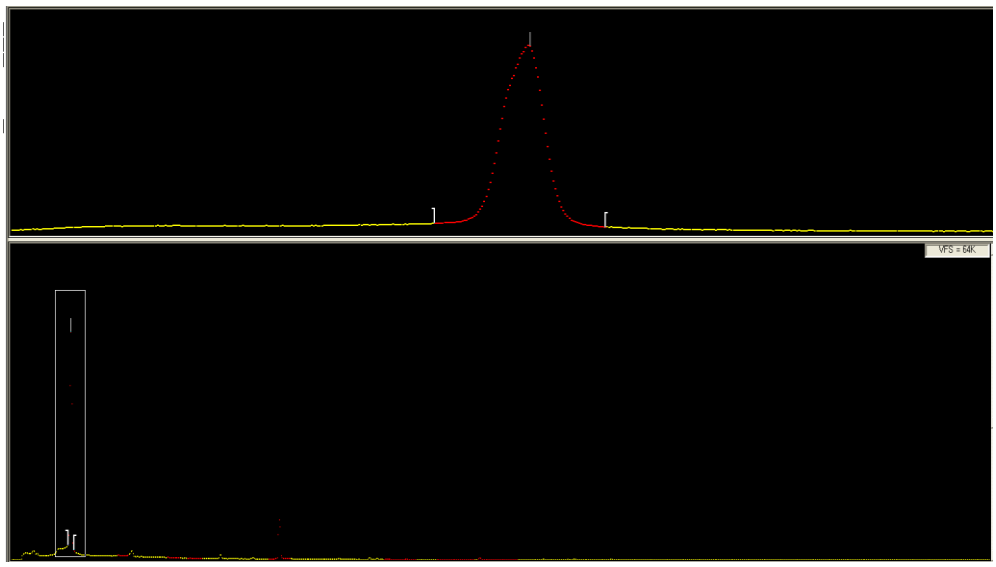

FIG. 8. Xe-133 Fission nuclide spectrum of "A" fuel bundle.

3.3. Fuel inspection at Wolsung NPP unit 2

We also performed inspection of fuel integrity at the Wolsung unit 2 on March 2012. Similarly, four defective spent fuel bundles were inspected for exact distinguishing failed fuel bundle. The sipping system and visual inspection system was applied to inspect fuel integrity. As the results of visual inspection, "H" fuel had a defect on the end plug of the fuel element as shown Fig. 9. Sipping inspection was performed for the fuel bundles just after visual testing. Fig. 10 shows radioactivity level of fuel bundles which was counted for 300 sec but defect fuel bundle "H" was counted for 100 sec by gamma detector because of emitting of too high radioactivity.

The radioactivity levels of "E, F, G" fuel bundles were within two times compared to background value and it was shown radioactivity of intact fuel bundle. In case of "H" fuel bundle, radioactivity level was over thirty times compared to BKG level in fission nuclides of Xe, Kr etc. Xe-133 nuclide was also detected by gamma detector. No fission nuclides were found in any other fuel bundles of "E, F and G".

4. CONCLUSION

The sipping and visual inspection system for evaluation of integrity of CANDU spent fuel bundle has been developed by KNF. These systems were fully utilized to inspect spent fuel bundles in the Wolsung nuclear power plants on February and March 2012. This application successfully proved that sipping technology could effectively determine whether CANDU irradiated fuel bundles are defective or not, even though we could not find out the indication of fuel failure by visual inspection method. We will also set threshold value for discrimination of CANDU fuel failure using the radioactivity data measured on fuel failure inspection. It is anticipated to contribute for reactor operation and the development of the advanced fuel technology of design and manufacturing through the data from evaluation of spent fuel integrity.

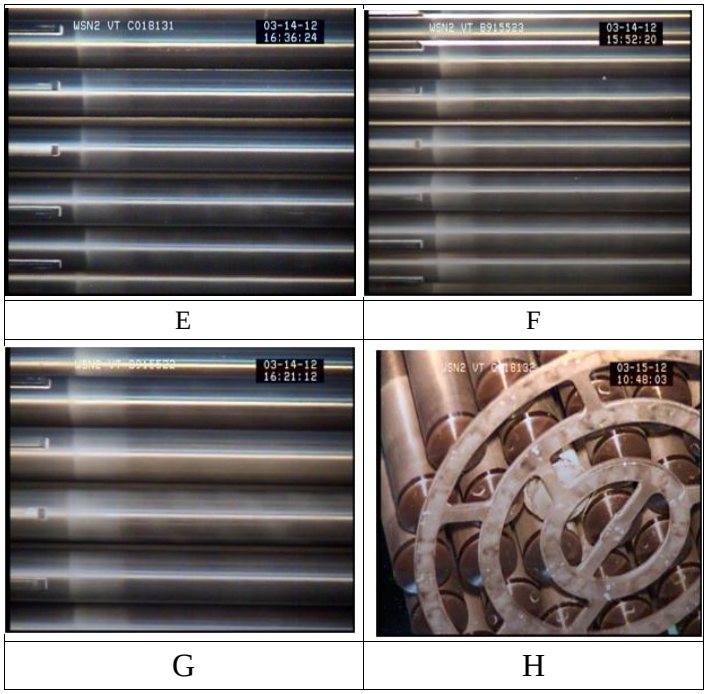

FIG. 9. Fuel inspection image of Wolsung unit 2.

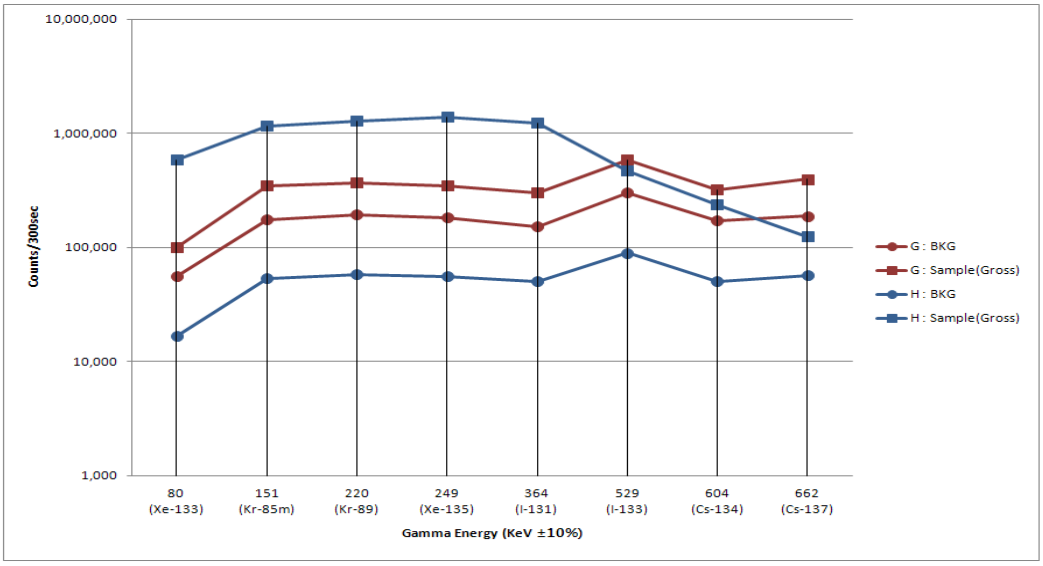

FIG. 10. Sipping inspection results of Wolsung unit 2.

POST IRRADIATION EXAMINATION OF EXPEROMENTAL CANDU FUEL ELEMENTS IRRADIATED IN TRIGA-SSR REACTOR

S. IONESCU, M. MINCU, O. UTA,
C. GENTEA, M.L PARVAN, L. DINU
Institute for Nuclear Research,
Pitesti, Romania

Abstract

The object of this work is the behaviour of CANDU fuel elements under power cycling conditions. The tests were run in the 14 MW (th) TRIGA-SSR (Steady State Reactor) reactor from Institute for Nuclear Research (INR) Pitesti. Zircaloy-4 is the material used for CANDU fuel sheath. The importance of studying its behaviour results from the fact that the mechanical properties of the CANDU fuel sheath suffer modifications during normal and abnormal operation. In the nuclear reactor the fuel elements endure dimensional and structural changes as well as cladding oxidation, hydriding and corrosion. These changes can lead to defects and even to the loss of integrity of the cladding. This paper presents the results of examinations performed in the Post Irradiation Examination Laboratory (PIEL) from INR Pitesti, on samples from a fuel element irradiated in TRIGA-SSR reactor: (i) Dimensional and macrostructural characterization; (ii) Gamma scanning and tomography; (iii) Measurement of pressure, volume and isotopic composition of fission gas; (iv) Microstructural characterization by metallographic analyses; (v) Determination of mechanical properties; amd (vi) Fracture surface analysis by scanning electron microscopy (SEM). The obtained data could be used to evaluate the security, reliability and nuclear fuel performance, and for CANDU fuel improvement.

1. INTRODUCTION

The facilities from INR Piteşti allow the testing, manipulation and examination of nuclear fuel and irradiated materials. The most important facilities are the TRIGA SSR research and material test Reactor and the Post-Irradiation Examination Laboratory (PIEL).

The purpose of this work is to determine by post-irradiation examination, the behaviour of CANDU fuel, irradiated in the 14 MW TRIGA reactor. The results of post-irradiation examination are:

— Visual inspection of the cladding;
— Profilometry (diameter, bending, ovalization) and length measuring;
— Determination of axial and radial distribution of the fission products activity by gamma scanning and tomography;
— Microstructural characterization by metallographic and ceramographic analyzes;
— Mechanical properties determination;
— Fracture surface analysis by scanning electron microscopy.

Dimensional and macrostructural characterization consist of determination of diametrical profile, diametrical increasing, ovality and the arrow of fuel element.

Gamma scanning consists of an axial fuel rod scanning at regular intervals of 0.5 mm. A method of tomographic reconstruction based on a maximum entropy algorithm has been developed.

Microstructural characterization was performed on a LEICA TELATOM 4 optical microscope having a magnification up to x1000. A computer-assisted analysis system is used for the quantitative determination of structural features, such as grain and pore size

distribution. The analyses by optical microscopy provide information concerning the aspect of pellet fissure, the structural modifications of fuel and the sizes of the grains and the thickness of the oxide layer and the cladding hydriding.
Samples prelevated from cladding were tested in order to evaluate the changes of their mechanical properties as a consequence of irradiation. The tensile testing machine used is an INSTRON 5569 model.

After tensile tests the fracture surfaces were analysed by an electron microscop TESCAN MIRA II LMU CS with Schottky Field Emission and variable pressure.
A transportation cask and the necessary devices for bundle handeling were designed and manufacturated at INR Piteşti. The cask will be used for transport the fuel bundles from Cernavoda NPP to Post-Irradiation Examination Laboratory.

The obtained data could be used to evaluate the security, reliability and nuclear fuel performance, and for CANDU fuel improvement.

The irradiation of a fuel element can lead to defects in the cladding. This is due mainly to a combination between a strain quite high and a low ductility of the cladding material. In CANDU reactors, the fuel elements are subjected to power ramps severe enough when reloaded during the functioning of the reactor.

The CANDU reactors from Cernavodă Nuclear Power Plant (NPP) are using as nuclear fuel bundles of 37 elements each, assembled by some edge grids. This bundle has a length of 495 mm, a diameter of 103 mm and weight of 24 kg. The CANDU fuel element contains cylindrical pellets of UO_2 syntherized, placed into a Zircaloy-4 tube (also known as sheath or cladding) closed at both edges with endcaps. It has a length of 492 mm and a diameter of 13.08 mm.

In order to check and improve the quality of the Romanian CANDU fuel, power ramp tests on experimental fuel elements were performed in our TRIGA SSR reactor. The irradiated fuel elements were further subjected to examination in the PIEL laboratory.

During the irradiation, the fuel elements suffer dimensional and structural changes, and also modifications of the cladding surface aspect, as result of corrosion and mechanical processes. This can lead to defects and even the integrity of the fuel element can be affected. The performance of the nuclear fuel is determined by the following elements:

— Status of cladding surface and the effects produced by corrosion;
— Cladding integrity;
— Dimensional modifications;
— Distribution of fission products in the fuel column;
— Pressure and volume of the fission gas;
— Structural modifications of the fuel and cladding;
— Cladding oxidation and hydration;
— Isotopic composition of the fuel;
— Mechanical properties of the cladding.

2. CANDU FUEL CHARACTERIZATION

2.1. The aspect of the cladding surface

After irradiation, the fuel rod was kept in the reactor pool for three months, for cooling. The fuel rod was then transferred to the INR hot cells where it was subjected to detailed examinations.

An image of the fuel element is given in Fig. 1. It was obtained using a periscope, coupled with an OLYMPUS digital camera. The aspect of the cladding surface indicates a normal behaviour of the fuel element.

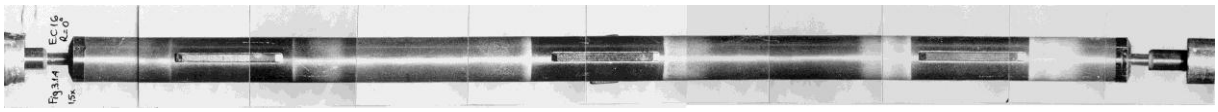

FIG.1. Fuel element CANDU tested in the power ramp.

2.2. Profilometry

The diametrical profile, diametrical increasing, ovality and the arrow of fuel element were determined. In Fig. 2 is presented the average diameter profile of the fuel element. The average diameter is 13 149 mm. The average diametrical increasing is 0,087 mm (0,67 %), with respect to the diameter before irradiation.

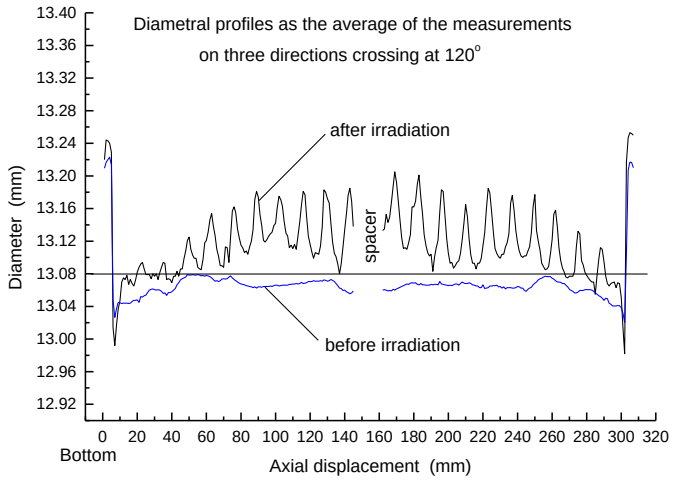

FIG. 2. Average diameter profile after irradiation.

Ovality profiles of the fuel element for two different positions on the vertical axis, Z = 97 mm and Z = 172 mm, are presented in Fig. 3. The graphic representation was made based on the measurements performed at these positions on three directions (0^o, 120^o and 240^o). The profiles of bending are presented in Fig. 4.

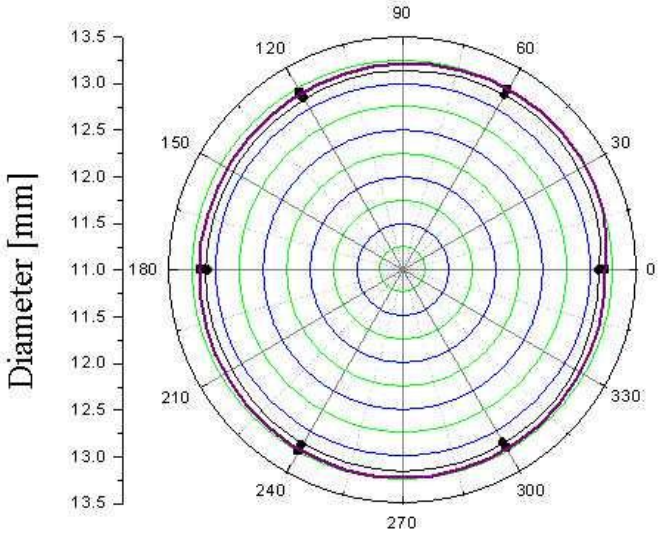

FIG.3. Ovality profiles for Z = 97 mm and Z = 172 mm.

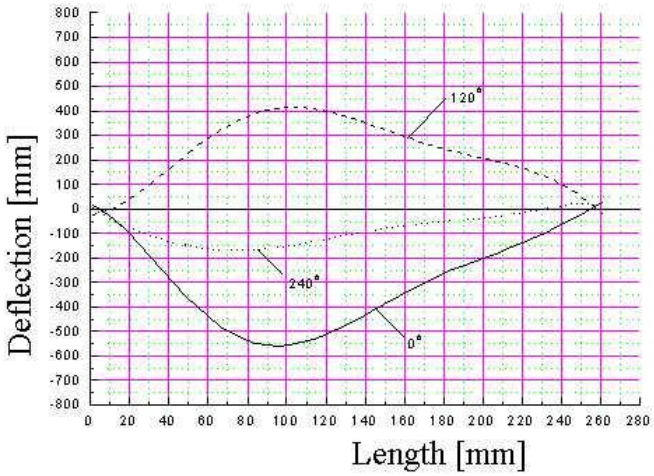

FIG. 4. Profiles of bending after irradiation.

2.3. Gamma scanning and tomography

The gamma scanning equipment consists of a vertical fuel rod positioning machine equipped with SLO-SYN step by step motors, a collimator, in the hot cell shielding wall, a PGT intrinsic Ge detector and a multi channel analyzer.

For axial gamma scanning, the slit of the collimator was horizontal, having an aperture of 0.5 mm. The gamma acquisition along the fuel rod was performed at regular intervals of 0.5 mm; the acquisition time per step was 200s. Fig. 5a shows the fuel rod axial gross gamma activity profile. A prominent depression of count rate at fuel pellet interfaces is observed, which means there is no interaction between the pellets. This gamma activity profile highlights practically a symmetric loading of the fuel rod.

A method of tomographic reconstruction based on a maximum entropy algorithm has been developed as described in ref. [1–2]. The data acquisition was done while the fuel rod was moved transversally step by step at regular intervals of 0.25 mm after every 72º rotation in front of a vertical collimator slit (which is 50 mm high and has a 0.25 mm aperture). Fig. 5b shows, qualitatively, the tomographic image of the radial distribution of ^{137}Cs gamma activity in the cross section of the fuel rod, in the flux peaking area. This tomography indicates that the ^{137}Cs isotope migrated from the middle to the periphery of the fuel rod and was redistributed according to the temperature profile.

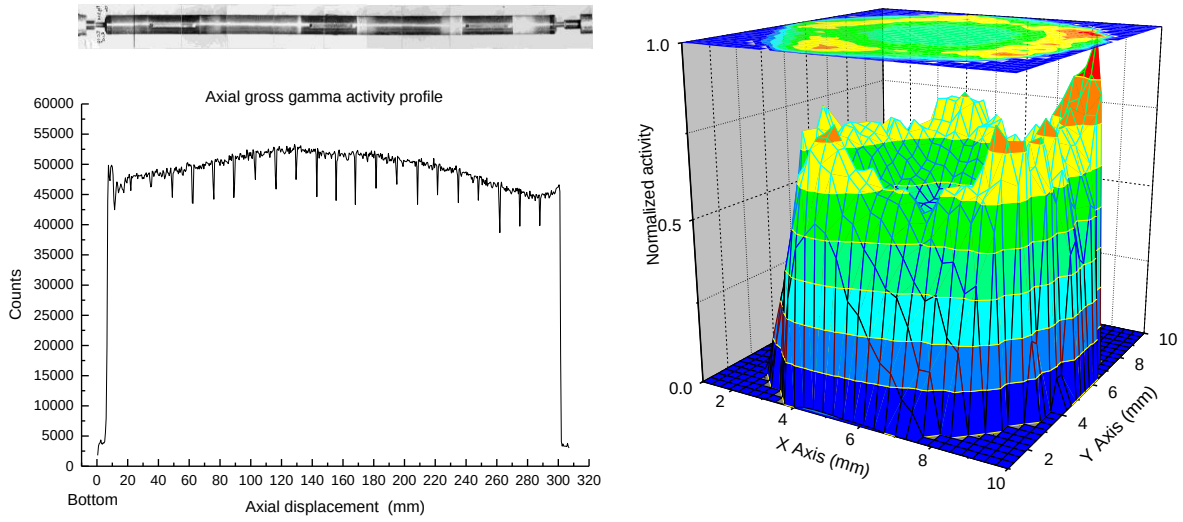

a) b)

FIG. 5. Axial gamma scanning (a) and tomography (b) on a CANDU fuel rod irradiated in the INR TRIGA reactor in a power ramping test.

The ^{137}Cs isotope was used as burnup monitor. For an accurate determination of the burn up, the gamma self-absorption coefficient was calculated using the distribution of ^{137}Cs activity in the cross section of the fuel rod. The burnup of the fuel rod is 8.77 MW·d $(kgU)^{-1}$ (for 192 MeV fission of U). The fuel rod burnup determined by mass spectrometry is 9 MW·d $(kgU)^{-1}$ (for 192 MeV fission of U). These results are in good agreement.

2.4. Metallographic and ceramographic examination

A LEICA TELATOM 4 optical microscope having a magnification up to x1000 was used for macrographic and microstructural analysis of the irradiated fuel rod. A computer assisted analysis system is used for the quantitative determination of structural features, such as grain and pore size distribution.

The preparation of the samples includes precise cutting, vacuum resin impregnation, sample mounting with epoxy resin in an acrylic resin cup, mechanical grinding and polishing, chemical etching [3].

The analyses by optical microscopy provide information concerning:

— The aspect of pellet fissure (Fig. 6);
— The structural modifications of fuel and the sizes of the grains (Fig. 7);
— The thickness of the oxide layer and the cladding hydriding.

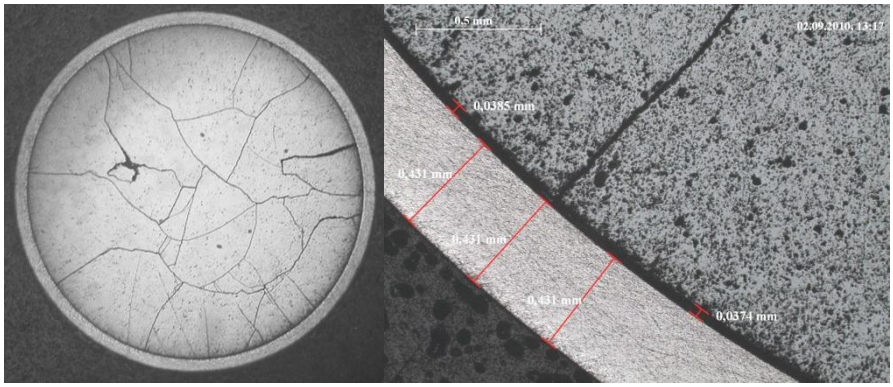

FIG. 6 The cross section of the fuel pellet.

The cross section of the fuel pellet (x8) presents radial and circular fissures on the whole section. The cladding doesn't present nonconformities, the thickness of this being 0,431 mm. There are no visible effects on fuel sheath, due to mechanical or chemical interactions.

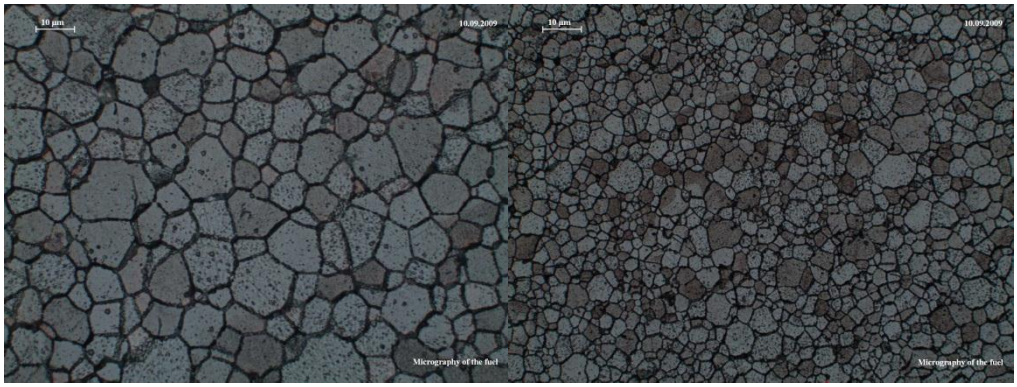

a) Equiaxial grains b) Unaffected grains

FIG. 7. The structural modifications in the fuel pellet.

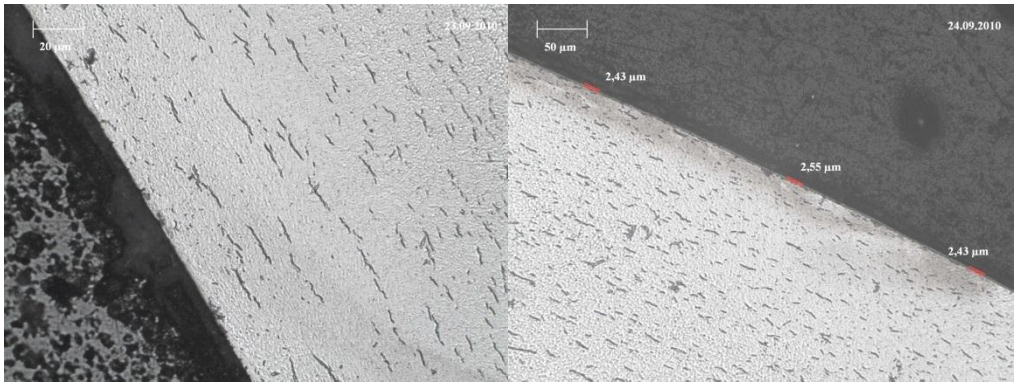

a) Cladding hydrading b) Outer oxide layer on cladding

FIG. 8. Cladding aspect.

The hydride precipitates are orientated parallel to the cladding surface. A content of hydrogen of about 120 ppm was estimated by means of hydriding charts [4] The fuel element presents on the outer side of the cladding a continuous and uniform zirconium oxide layer (Fig. 8). The thickness of the cladding oxide layer is 2.5 µm.

2.5. Determination of mechanical properties

After the preliminary tests, three ring samples (5 mm long each) were cut from the fuel rod, for further tensile tests (Fig. 9). The samples were prepared according to the shapes and dimensions given in ref. [5] and [6].

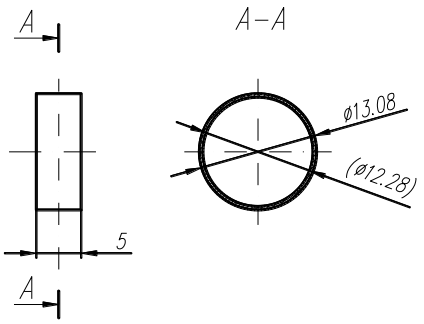

FIG. 9. Ring test sample.

The samples are tested in order to evaluate the changes of their mechanical properties as a consequence of irradiation. The tensile testing machine used is an INSTRON 5569 model. The machine uses the Merlin software for data acquisition and analysis.

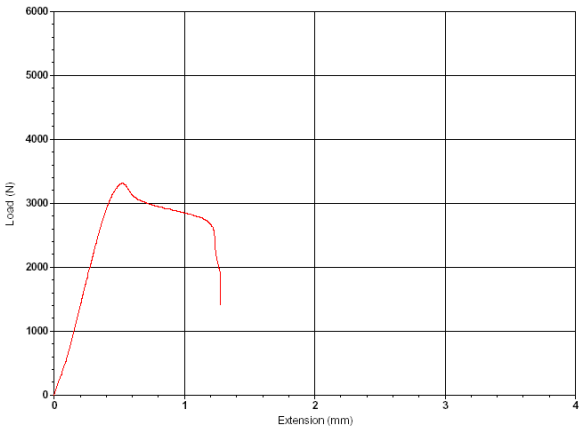

FIG. 10. Load-extension diagram.

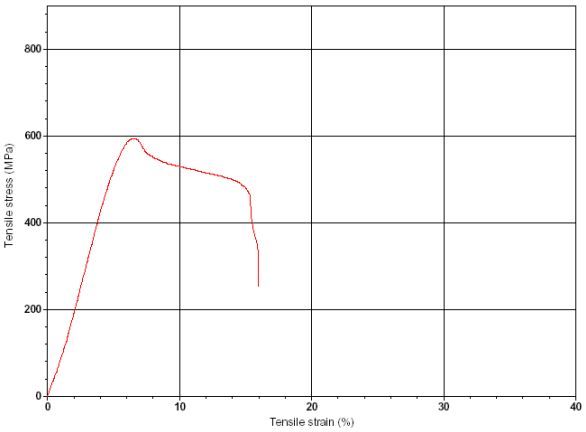

FIG. 11. Strain-stress diagram.

The tests were done under the following conditions: constant testing temperature (300°C), 25N preload and constant tensile strain (v=0, 05 min^{-1}).

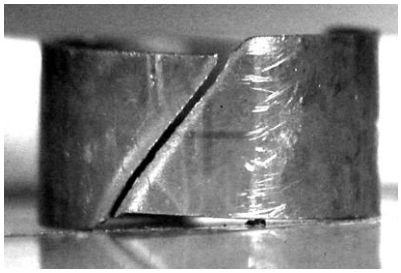

FIG. 12. Ring sample after test.

The tests have been performed in order to record or evaluate the following mechanical characteristics:

— The strain–stress diagrams and load extension (Figs. 10, 11);
— The yield strengths (offset method at 0.2%);
— The elastic limit;
— The ultimate tensile strength of the samples.

The tests were done according to the procedures and standards given in ref. [7] and [8].

The aspect of the ring sample after the test is presented in Fig. 12.

2.6. Fracture surface analysis by scanning electron microscopy (SEM)

For sample analysis an electron microscop model TESCAN MIRA II LMU CS with Schottky Field Emission and variable pressure was used. The magnification range is 4 X ÷ 10 00 000 X. An outstanding depth field, much higher than in the case of optical microscopy

characterizes the scanning electron microscopy (SEM). This makes SEM very appropriate for analyzing fracture surfaces of zircaloy 4 cladding resulted from tensile test.

Because of the ring shape of the sample, for rupture surface visualization, the sample was split in two parts, which were mounted in microscope chamber as in Fig. 13.

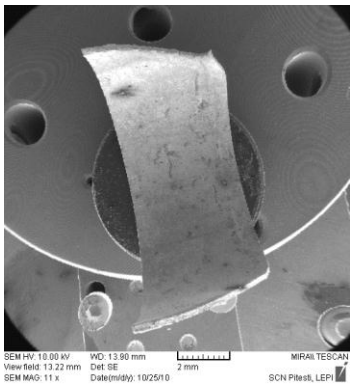

FIG. 13. Sample fixture on the electronic microscope table.

Both sides of the tensile fracture were analysed on each half of the ring. The dimples from the central zone are rather deep, whereas the ones on the outer side are tilted and smaller.

The central zone of the fracture presents equiaxial dimples (Fig. 14).

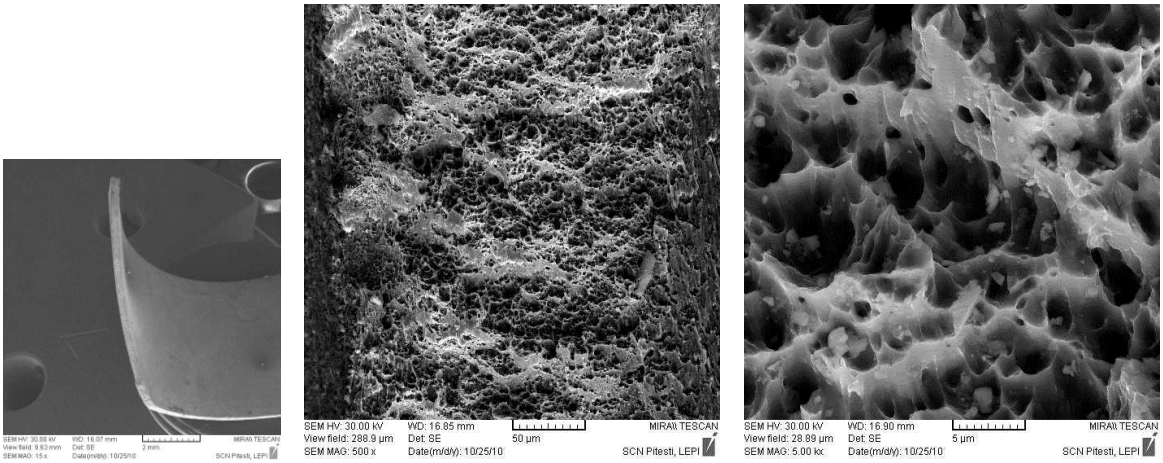

a) general view x15 b) x500 c) x2000

FIG. 14. The aspect of the central zone of the fracture.

2.7. Transportation cask for CANDU fuel

For safe operation of Cernavoda NPP, the examination of spent fuel is necessary, especially of the suspectable one that can present defects. For this purpose, a collaboration contract was drawn up between INR Pitesti and Cernavoda NPP concerning the examination of spent fuel.

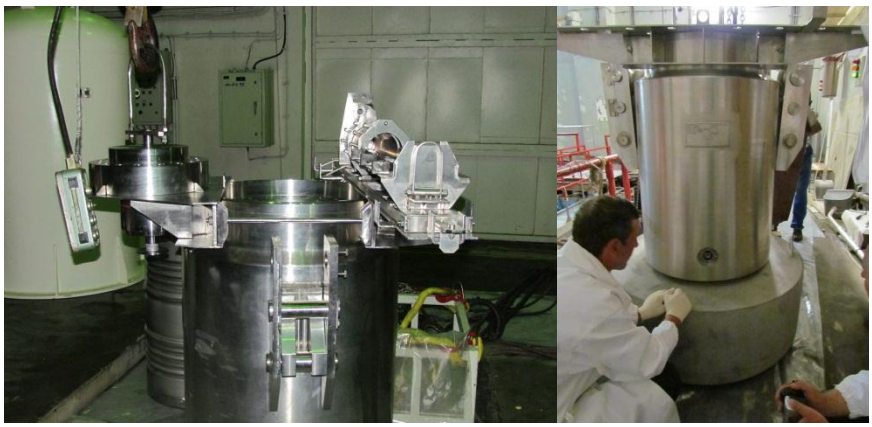

FIG. 15. The transport cask.

A dedicated cask (Fig. 15) was designed and manufactured for spent fuel transportation. All the steps that needed special approval are already past.

All the devices needed to load/unload the fuel bundle into/out of the cask (Fig. 16) were also designed and manufactured at INR Pitesti.

The cask will be loaded at Cernavoda NPP in the fuel storage pool (Fig. 17), after a visual examination of the fuel, performed with a periscope. The cask is then transported at INR Pitesti, where the fuel will be unloaded at PIEL (Post Irradiation Examination Laboratory), in order to be exanimate in the hot cells of PIEL.

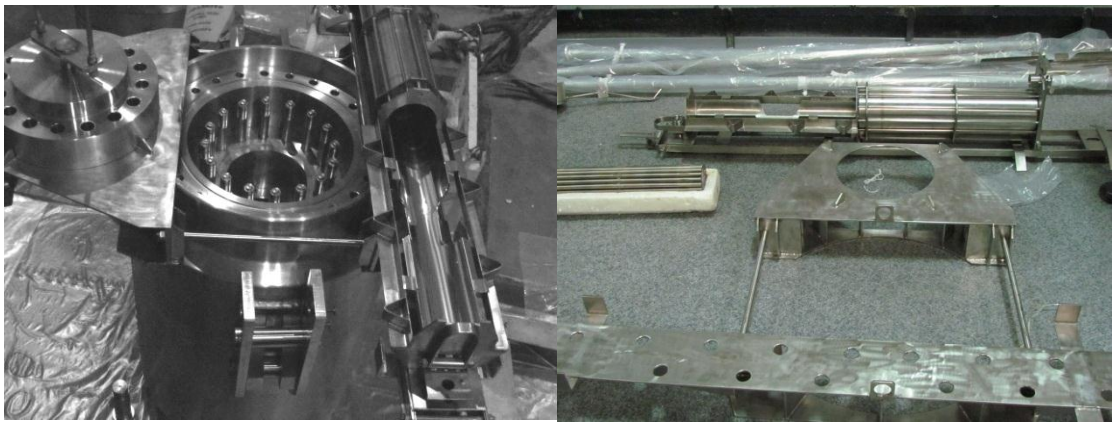

FIG. 16. The devices used to load and unload the cask.

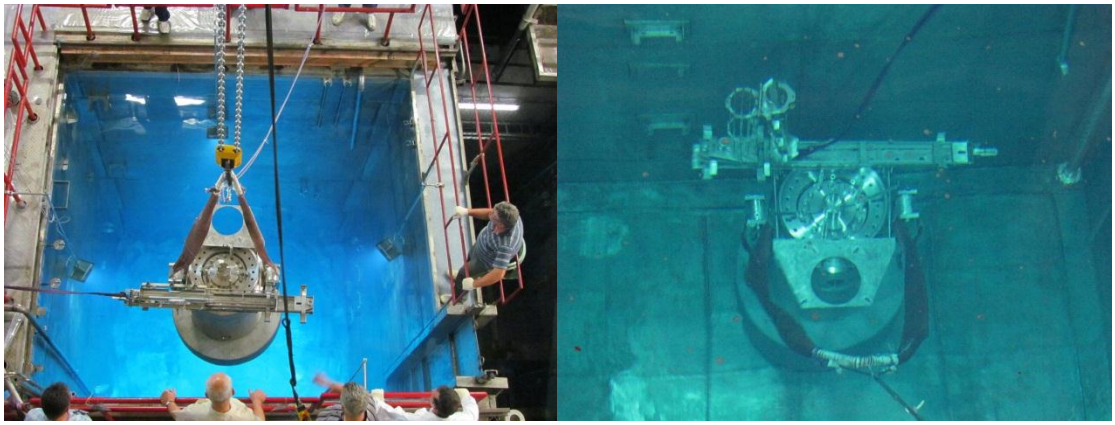

FIG. 17. The cask in the PIEL - INR pool.

All the tests needed to characterize the spent fuel will be performed in PIEL, as described in this work.

3. CONCLUSION

After irradiation, the fuel rod was kept in the reactor pool, for cooling and then it was transferred to the INR-PIEL hot cells where it was subjected to detailed examinations:

- First of all, visual inspection of the cladding was done. The aspect of the cladding surface indicates a normal behaviour of the fuel element;
- The diametrical profile, diametrical increasing, ovality and the arrow of fuel element were determined;
- The tomography indicates that the ^{137}Cs isotope migrated from middle to periphery of the fuel rod and was redistributed according to the temperature profile;
- By metallographic and ceramographic examination we determinated that the hydride precipitates are orientated parallel to the cladding surface. A content of hydrogen of about 120 ppm was estimated. The cladding doesn't present nonconformities. The fuel element presents on the outer side of the cladding a continuous and uniform zirconium oxide layer 2.5 μm thick;
- After the preliminary tests, three ring samples were cut from the fuel rod, and were subject of tensile test on an INSTRON 5569 model machine in order to evaluate the changes of their mechanical properties as a consequence of irradiation;
- Scanning electron microscopy was performed on a microscop model TESCAN MIRA II LMU CS with Schottky FE emitter and variable pressure. The analysis shows that the central zone has deeper dimples, whereas on the outer zone, the dimples are tilted and smaller;
- For safe operation of Cernavoda NPP a collaboration contract was drawn up between INR Pitesti and Cernavoda NPP concerning the examination of spent fuel.

A full set of non-destructive and destructive examinations concerning the integrity, dimensional changes, oxidation, hydriding and mechanical properties of the cladding was performed. The obtained results are typical for CANDU 6-type fuel.

REFERENCES

[1] ALEXA, A., CRACIUNESCU, T., MATEESCU, G., DOBRIN, R., Thetomographic Maximum Entropy Method in the 3-D Analysis of Nuclear Fuel Pins, Journal of Nuclear Materials, **218** 139 (1995)142.

[2] CRACIUNESCU, T, DOBRIN, R., TUTURICI, I. L., The Analysis of Irradiated Failed Nuclear Fuel Rods by Gamma Computed Tomography, Journal of Nuclear Materials, **246** 37 (1997) 42.

[3] AMERICAN SOCIETY FOR TESTING OF MATERIALS, Standard Practice for Preparation of Metallographic Specimens, ASTM E 3-95.

[4] HYATT, B.Z., Metallographic Standards for Estimating Hydrogen Content of Zircaloy-4 Tubing, Report WAPD-TM-1431 (1982).

[5] KITANO, K., Optimization of Sample Geometry in Modified Ring Tensile Test, JAERI (1998).

[6] DAUM, R. et. al., "Mechanical property testing of irradiated zircaloy cladding under reactor transient conditions", 4th Symposium on Small Specimen Test Techniques, Reno (2001).

[7] AMERICAN SOCIETY FOR TESTING OF MATERIALS, Standard Methods for Tension Testing of Metallic Materials [Metric], ASTM E 8M 96.

[8] AMERICAN SOCIETY FOR TESTING OF MATERIALS, Standard Recommended Practice for Elevated Temperature Tension Tests of Metallic Materials, ASTM E 21.

DEFORMATION AND BALLOONING OF IRRADIATED PHWR FUEL PINS SUBJECTED TO ISOTHERMAL HEATING

P. MISHRA, D.N. SAH, S. ANANTHARAMAN
Bhabha Atomic Research Centre,
Mumbai, India
Email: prernam@barc.gov.in

Abstract

Deformation and ballooning of Zircaloy-2 cladding has been studied by isothermal heating of fuel pins taken from irradiated PHWR fuel bundles discharged from operating reactors after attaining fuel burnup up to 15,000MW·D/tU. A small portion (100mm length) of fuel pin at one end was heated in temperature range 700-900^{o}C under an inert gas atmosphere inside the hot cells. Post-test examination included visual examination, leak testing and dimensional measurement on the tested fuel pins and microscopic examination of samples from ballooned and failed region. The study has provided information on deformation and ballooning behavior of irradiated PHWR fuel pins and mode and mechanism of cladding failure during ballooning. The paper presents the details of experiment and results of the study.

1. INTRODUCTION

A PHWR fuel pin consists of solid cylindrical UO_2 fuel pellets hermetically sealed in a thin walled collapsible zircaloy cladding tube. The as-fabricated fuel pin is filled with helium gas at atmospheric pressure. The schematic diagram of the PHWR bundle and fuel pins are shown in Figure 1 [1]. For safety and reliability of nuclear power generation it is essential to assure that fuel pin integrity is maintained during its design life. The behavior of PHWR fuel pins under the normal operating conditions is evaluated through post irradiation examination of irradiated fuel pins discharged from the reactors [2] , [3]. Experimental studies have been initiated in BARC in order to understand the behavior of PHWR fuel pins under postulated accident conditions like LOCA [4–8]. During the irradiation inside the reactor, fission gases like Xe and Kr generated in the fuel are released into the fuel clad gap and the void volume in the fuel pin. Because of this, the internal pressure increases. Measurement of internal gas pressure in the irradiated fuel pins during PIE has shown that the pressure in the PHWR fuel pin can increase up to 5–20 atm (at room temperature) depending on the fuel burnup and the power rating. During normal operation, the external coolant pressure is more than the internal gas pressure in the fuel pins and the cladding remains collapsed on the cladding, experiencing compressive hoop stresses. However, during LOCA, due to the increase in temperature, the internal pressure in the fuel pin increases and the cladding is subjected to high tensile hoop stress at high temperature. Under these conditions the cladding can creep, leading to ballooning and burst [9] of the cladding tube. The ballooning may cause partial blockage of coolant channel affecting the cooling of the fuel assemblies in the channel. One of the major safety requirements during LOCA is the availability of long term cooling for distorted fuel assemblies This limits the extent of allowable deformation like ballooning of individual fuel elements [10].The behaviour of a fuel pin during a loss of coolant accident (LOCA) depends on the temperature of the cladding, the internal gas pressure, extent of oxidation and mechanical properties of the cladding.

Ballooning studies are usually carried out out-of-pile using internally pressurised cladding tubes or using simulator rods. In the present work, isothermal heating tests were carried on irradiated fuel pins inside the hot cells to study the ballooning and deformation behaviour. Irradiated fuel pins takes into account the effects of irradiation fluence, fission gas pressure, cladding corrosion and hydrogen up take. PHWR fuel pins removed from fuel

bundles irradiated up to 15 000 MW·D/tU burnup have been used in this study. The results of deformation, ballooning and failure as function of cladding temperature, internal gas pressure and burnup of the fuel pin and results of microstructural examination of deformed cladding related to the mode and mechanism of creep failure of the cladding are presented in this paper.

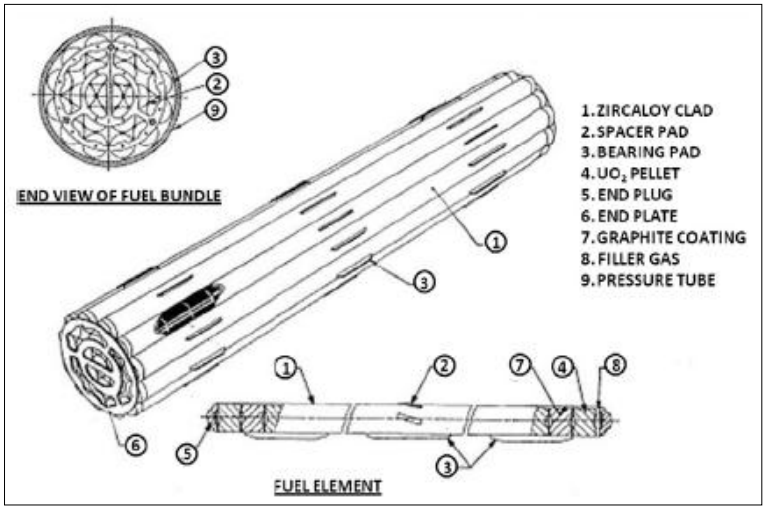

FIG.1. Design details of a PHWR fuel bundle and fuel pin.

2. EXPERIMENTAL

2.1. Irradiated fuel pin heating set up

The in-cell fuel pin heating system consists of a remotely operable electrical furnace capable of heating up to 1350°C under air or argon atmosphere (Fig. 2). The system consists of a closed cylindrical type furnace with an overall length of 750 mm out of which, a constant temperature is obtained over a length of 100 mm. The fuel pins with UO_2 pellets were heated at temperatures from 700 to 900°C under argon atmosphere and held for 10 min at those temperatures, followed by furnace cooling to room temperature. Thoria fuel pins used in the experiment were heated to 900°C. Heating rates used in all the heating experiments were 12°C / min up to the temperature of 800°C and 8°C/min, thereafter, up to 1300°C.

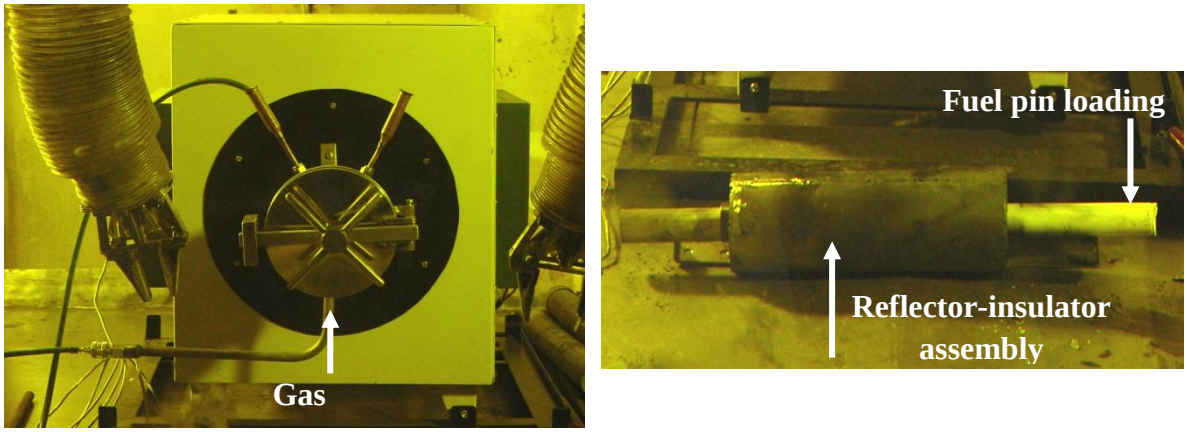

FIG. 2. Furnace inside the hot cell used for the heating experiments.

2.2. Details of the fuel pins used for the study

Fuel pins taken from the outer ring of two irradiated PHWR fuel bundles and one Thoria fuel bundle were used in the tests. Outer fuel pins were selected because they had higher fission gas pressure inside the pins compared to the middle ring pins or the central pin. The details of the fuel pins used in the experiment are given in Table 1.

TABLE 1. CHARACTERISTICS OF IRRADIATED PHWR FUEL PINS

	Parameter	Value
1.	Fuel pin Burnup (MW·d/tM)	7600 - 15,000 for UO_2 pins 11,100 for ThO_2 pins
2.	Pin internal pressure at room temperature (RT) (MPa)	0.55 - 2.4 for UO_2 pins 0.15 for ThO_2 pins
3.	Cladding material	Zr-2/ 4 (Graphite coated)
4.	Cladding ID (cm)	1.44
5.	Cladding OD (cm)	1.52
6.	Clad thickness (cm)	0.04
7.	Void Volume (cm^3)	3
8.	Max. Oxide layer thickness on outer surface (μm)	3.7
9.	Max. oxide layer thickness on inner surface (μm)	5.6
10.	Hydrogen content in cladding (ppm)	47
11.	Irradiation damage in cladding (dpa)	0.8 for 7600 MW·d/tU 1.6 for 15000MW·d/tU

2.3. Post test examination

2.3.1. *Visual examination*

Visual examination on the fuel pins was carried out in the hot cell after the heating test using a wall mounted periscope.

2.3.2. *Dimension measurement*

The outer diameter of the fuel pin was measured along the length of the heated fuel pins, by using a remotely operated stage fitted with a micrometer.

2.3.3. *Leak testing*

After the in-cell heating experiment, leak tests were carried out on the fuel pins to check for cladding failure due to deformation during heating. Leak testing was carried out using liquid nitrogen–alcohol method inside the hot cells.

2.3.4. *Optical Microscopy*

Transverse sections cut from the failed fuel pins from the location showing maximum ballooning and one section taken from other end of the fuel pin, which was not affected by heating were prepared for metallographic examination. Examination of the samples was carried out using a remotised optical microscope first in the as-polished condition and after etching for hydride platelet distribution in the cladding.

2.3.5. *Scanning Electron Microscopy*

The metallographically prepared cladding samples were examined under the scanning electron microscope (SEM) to understand the mechanism of deformation and failure. Fractography of the cladding samples from the ballooned and unballooned region was carried out to study the mode of failure.

3. RESULTS AND DISCUSSIONS

Isothermal heating experiments were carried on fuel pins with burnup from 7600-15000 MW·d/tU. The fuel pins with high internal pressure (2.40 ± 0.30 MPa at RT) had ballooned and failed when heated at 800^{o}C and 900^{o}C for 10 minutes. Fuel pins with lesser internal pressure (0.55 ± 0.05 MPa) ballooned and failed at 900^{o}C when held at that temperature for 15 minutes.

No deformation was observed in UO_2 fuel pins heated at 600 and 700^{o}C. During the test, out of the total 8 fuel pins, 3 pins ballooned and failed while 3 other pins just bulged without failing and 2 pins remained intact without any deformation. ThO_2 fuel pin heated at 900^{o}C did not show any deformation. The details of the fuel pins studied, heating temperature and time and the main observations of the tests are presented in Table 2.

3.1. Appearance of tested fuel pins

Typical appearance of the three high pressure UO_2 fuel pins heated at 700^{o}C, 800^{o}C and 900^{o}C fuel pins after the ballooning test is shown in Fig. 3. Fuel pin which was heated to

700^{o}C did not show any noticeable deformation. Ballooning of the cladding was observed on one end of the fuel pins heated to 800^{o}C and 900^{o}C because this was the portion of the fuel pin heated in the furnace. Heating had not caused any extra oxidation to the surface of the fuel pins but a number of fine cracks were observed on the cladding surface. The ballooned surface of the fuel pin tested at 800^{o}C showed cavity like cracks; whereas the fuel pin tested at 900^{o}C showed cavities, axial cracks and regions of depression on the cladding surface. Profuse bubbling from the ballooned area of the fuel pins observed during leak testing confirmed clad failure in the fuel pin tested at 800^{o}C and 900^{o}C; pin heated at 700^{o}C was intact.

TABLE 2. DETAILS OF FUEL PINS TESTED AND GENERAL OBSERVATION

Sr. No	Fuel pin ID, bundle No, average bundle burn up	Internal pressure (RT), MPa	Temperature, soaking time & environment	Observations
1	Outer pin, fuel bundle 56504, KAPS-1, 14,580 MW·d /tU	2.40 ± 0.30	600°C,10min, Ar	No deformation
2	Outer pin, fuel bundle 56504, KAPS-1, 14,580 MW·d/tU		700°C,10 min, Ar	No deformation
3	Outer pin, fuel bundle 35088, KAPS-2, 15,160 MW·d/tU		800°C,10 min, Ar	Ballooned and failed
4	Outer pin, fuel bundle 56504,KAPS-1, 14,580 MW·d /tU		900°C,10 min, Ar	Ballooned and failed
5	Outer pin, fuel bundle 54505, NAPS-1, 7,670 MW·d/tU	0.55 ± 0.05	800°C,10 min, Ar	Bulging
6	Outer pin, fuel bundle 54505, NAPS-1, 7,670 MW·d/tU		850°C,10min, Ar	Ballooned
7	Outer pin, fuel bundle 54505, NAPS-1, 7,670 MW·d/tU		900°C,10min, Ar	Ballooned
8	Outer pin, fuel bundle 54505, NAPS-1, 7,670 MW·d/tU		900°C,15 min, Ar	Ballooned and failed
9	Outer pin ThO_2 bundle LY-274, KAPS-2 , 11,100 MW·d/t(Th)	0.15 ± 0.05	900°C,10 min, Ar	No deformation

Fuel pin heated at 700°C

Fuel pin heated at 800°C

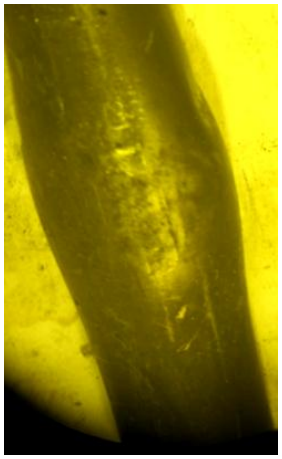

Fuel pin heated at 900°C

FIG. 3. Appearance of UO_2 fuel pins after the heating test.

3.2. Diametral deformation in the cladding

The axial diametral profiles of the failed fuel pins are shown in Fig. 4a. The maximum diametral strain at the failure site was in the range 37.4-41.6% in all the failed fuel pins. The temperature, hot pin pressure and holding time with the resulting diametral strain and clad thinning at the failure location is given in Table 3. The clad wall thinning in the failed fuel pins at the failure location was in the range of 65.5-91%.

TABLE 3. DIAMETRAL DEFORMATION IN THE FAILED PINS

Temperature (°C)	Hot pin pressure (MPa)	Time (min)	Diametral Strain (%)	Clad wall thinning at failure location (%)
800	8.4	10	41.6	91
900	9.4	10	39.8	80
900	2.15	15	37.4	65.5

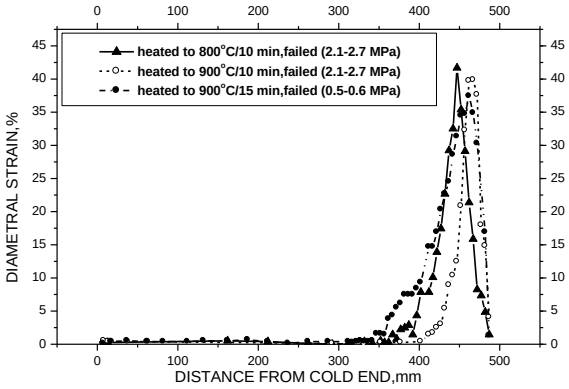

FIG. 4. (a) Axial diametral profile of three fuel pins which failed during heating.

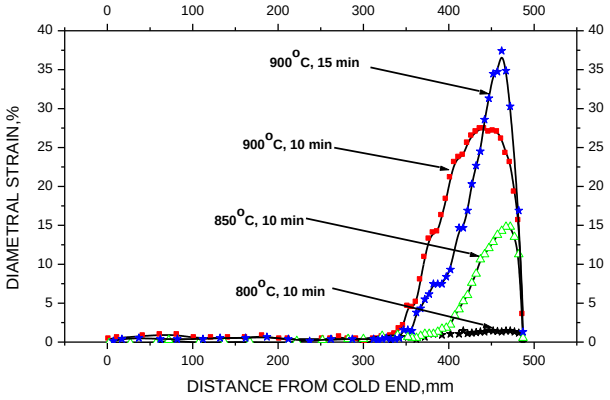

FIG. 4. (b) Effect of time and temperature of heating on axial diametral profile.

Fig. 4b shows the effect of heating temperature and time on the axial diametral profile of the fuel pins having internal pressure of 0.55 MPa. This figure shows that the maximum diametral strain in the fuel pin increases with increasing temperature for constant heating time of 10 minutes. It is also observed that the diametral strain increases by increasing the heating time at the same temperature. This indicates that the deformation is occurring by creep of the cladding.

TABLE 4. HOOP STRESS ON THE CLADDING AND MEASURED CREEP STRAIN RATES

Temperature (^{o}C)	Time of heating (min)	Hoop stress (MPa)	Creep rate (s^{-1})
800	10	34.6	2.4×10^{-5}
850	10	37.0	24.6×10^{-5}
900	10	38.7	45.6×10^{-5}

The creep rate of the cladding in these fuel pins at the location of maximum deformation with the temperature and time of heating and hoop stress on the cladding are given in Table 4. Following correlation for the temperature dependence of creep rate was derived from the data:

$$\text{Creep rate } (s^{-1}) = 2.23 \times 10^{10} \times \exp(-305500/RT) \quad (1)$$

Where, R is gas constant, 8.314 J/mol K and T is temperature in K

3.3. Microstructure of the deformed cladding

Sample from the unballooned region of the cladding revealed a uniform oxide layer at the outer surface of the cladding with an average oxide layer thickness of 3.7 µm. The sample from the ballooned region of the fuel pin tested at 800°C revealed a discontinuous and damaged oxide layer on the outer surface of the cladding (Fig. 5a), whereas oxide layer was absent in the sample from the ballooned region of pin tested at 900°C (Fig. 5b). The oxide layer present on the cladding surface before heating is believed to have damaged at 800°C due to stresses generated during ballooning. Absence of the oxide layer in the sample from the fuel pin heated at 900°C indicates that the oxide had dissolved in the cladding during heating.

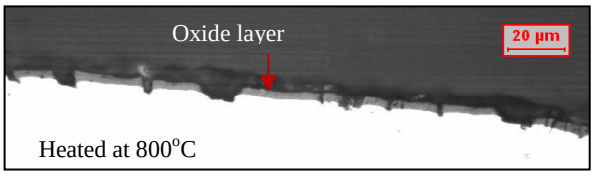

FIG. 5. (a) Damaged oxide layer on the outer surface of the cladding.

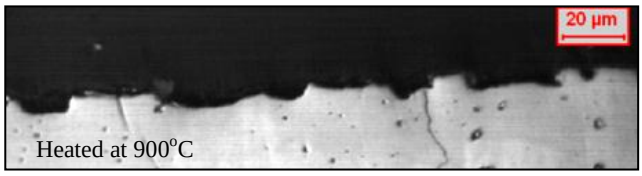

FIG. 5 (b). Oxide layer absent on the outer surface of the cladding after heating.

The microstructure of the cladding from fuel pin heated at 800°C revealed circumferentially oriented hydrides platelets and some fine cavities (along with surface pits probably formed due to chemical etching) as shown in Fig. 6a. The cladding samples taken from the ballooned region of the fuel pin heated at 900°C revealed presence of clearly demarcated equiaxed grains. Hydride platelets were also present on the grain boundary as shown in Fig. 6b.

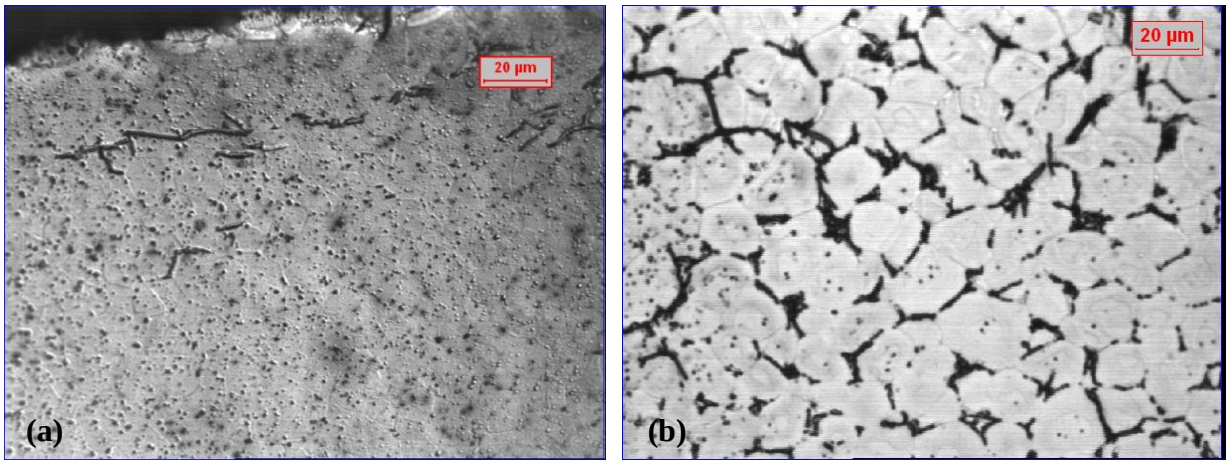

FIG. 6. Microstructure of the cladding in the fuel pin heated at (a) 800°C and (b) 900°C.

3.4. Mode and mechanism of cladding failure

Localised deformation in the form of necking was observed in at the ballooned location of the cladding samples (Fig. 7). The wall thinning at the necking portion was about 90% and 65% in the samples from fuel pins heated at 800^{o}C and 900^{o}C respectively. The necked region of the cladding (900^{o}C test) showed a 100 µm long crack propagating from inner surface to the outer surface.

SEM examination of the metallographic sample from 900^{o}C test showed that the microstructure of the deformed zircaloy cladding consisted of equiaxed grains (Fig. 8). There was no apparent elongation of the grains in the direction of the stress even after a large strain of about 40% (the arrow shows the direction of stress during deformation.)

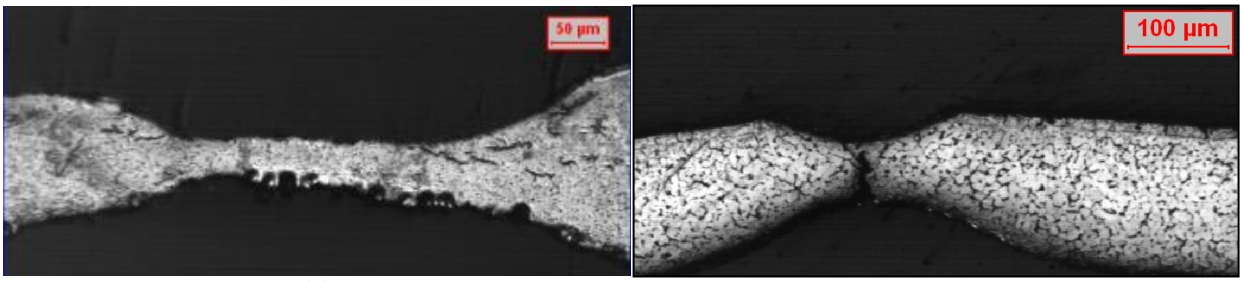

(a) (b)

FIG. 7. Necking in the cladding in the fuel pin heated at (a) 800^{o}C and (b) 900^{o}C.

Cavities and cracks were present on the grain boundaries. These intergranular features on the grain boundaries suggested that grain boundary played a significant role in the deformation. Failure of the cladding occurred by joining of intergranular cracks.

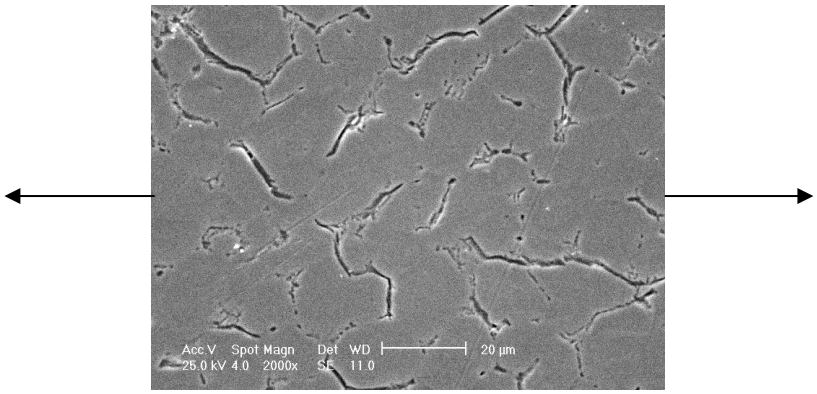

FIG.8. SEM micrograph of cladding showing cracks and cavities on grain boundaries (900^{o}C test).

SEM examination of the outer surface of the cladding revealed a number of axial cracks as shown in the Fig. 9. Fracture surfaces of the cladding obtained by fracturing a piece taken from the unballooned and the ballooned region of the fuel pin are shown in Fig. 10 (a & b).The cladding from the unballooned region showed a typical ductile fracture with dimples on the surface; ballooned region revealed a mixed fracture mode. Fractograph of the cladding taken from the ballooned region revealed presence of cavities and secondary cracks, as shown in Fig. 11a. Magnified view of the cavities is shown in Fig. 11b.

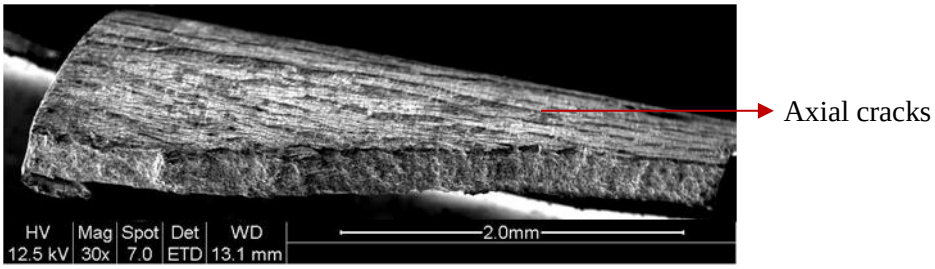

FIG. 9. Axial cracks on the outer surface of the cladding piece removed from ballooned region of the failed fuel pin.

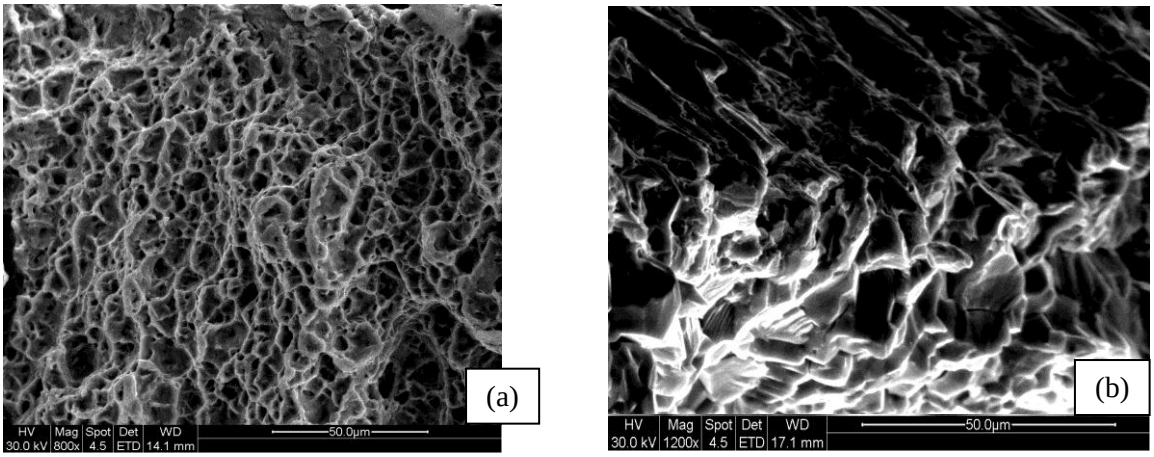

FIG. 10. Fracture surface of the cladding from the (a) unballooned region and (b) ballooned region of the fuel pin heated at 900^{o}C.

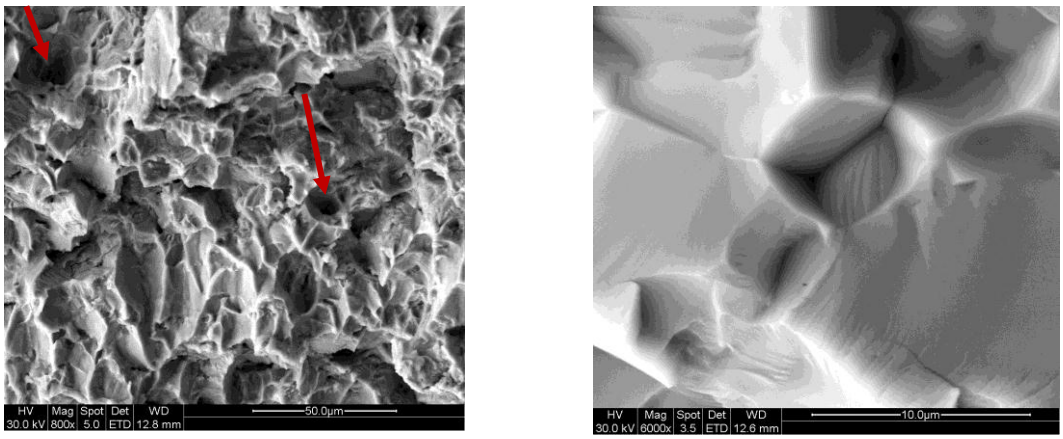

(a) (b)

FIG. 11. (a) Cavities in the fracture surface (b) Magnified view.

4. CONCLUSION

Isothermal heating experiments were carried out in the temperature range of 700–900°C on irradiated UO_2 fuel pins discharged after an average burnup of 7600 MW·d/tU and 15,000 MW·d/tU and having an internal fission gas pressure of about 0.55 MPa and 2.4MPa respectively. The main findings of the examinations carried out on the ballooned fuel pins are as follows:

(1) No deformation or ballooning of cladding occurred in fuel pins on heating at 700°C for 10 min. However, fuel pins heated at 800°C and 900°C for 10 min showed well defined ballooning. ThO_2 fuel pin did not show any deformation even after heating at 900°C for 10 minutes;

(2) Fuel pins with higher fission gas pressure (2.4 MPa) ballooned and failed at 800°C and 900°C when heated for 10 min; but fuel pins with lesser fission gas pressure (0.55 MPa) failed after heating at 900 °C for15 min. The maximum cladding diametral deformation in the ballooned portion of the pin was in the range of 37.4–41.6%;

(3) The temperature dependence of steady state creep rate of Zircaloy-2 cladding at hoop stress of 36 MPa in temperature range 800-900°C can be expressed by the following Arrhenius equation: Creep rate (s^{-1}) = 2.23 x 10^{10} x exp (- 305500/RT);

(4) Failure of the cladding during heating at 900°C occurred at the ballooned location by necking associated with crack propagation through the grain boudaries from the inner surface. The cladding from the 800°C test did not show cracks or cavities in the deformed material. Necking followed by extensive wall thinning of the cladding was observed at the failure location;

(5) Presence of cracks and cavities on the grain boundaries and absence of grain elongation in the direction of the stress indicated that the creep deformation at 900°C was through grain boundary sliding mechanism.

ACKNOWLEDGEMENTS

The authors would like to express their thanks to Shri P.M. Satheesh, Shri V.P. Jathar, Shri S. Katwankar and Shri S.R. Soni of PIE Division for their help in carrying out the experiments and sample preparation inside the hot cell facility. The support provided by Shri J. Banerjee for SEM examination is thankfully acknowledged. The authors acknowledge the keen interest shown by Dr. G.J. Prasad, Director, Nuclear Fuels Group and Shri Arun Kumar, Associate Director, Nuclear Fuels Group in this work.

REFERENCES

[1] SAH, D.N., et. al., J. Nucl. Mater. **383** 144 (2008) 149.
[2] SAH, D.N. et. al., J. Nucl. Mater. **383** 45 (2008) 53.
[3] SAH, D.N. et. al., Post-irradiation Examination of High Burnup PHWR Fuel Bundle 56504 from KAPS-1, BARC Report, BARC/2007/E/002.
[4] SAH, D.N. et. at., "Safety related studies on PHWR fuel cladding and pressure tube material" Proc. International Conference on Advances in Nuclear Material, ANM-2011, Mumbai, India (2011) www.anm2011.org.
[5] SAWARN, T.K., et. al., "Ballooning and deformation behavior of Indian PHWR's fuel cladding under transient heating condition", Proc. International Conference on Advances in Nuclear Material, ANM-2011, Mumbai, India (2011) www.anm2011.org .
[6] VISWANATHAN, U.K., et. al., J. Nucl. Mater. **383** 122 (2008) 127.
[7] SAH, D.N., et. al., Proc. of Theme Meeting on Recent Advances in Post Irradiation Examination (RAP-2008), IGCAR, Kalpakkam, India (2008).
[8] PRENA MISHRA, et. al., Microstructural Examination of High Temperature Creep Failure of Zircaloy-2cladding in Irradiated PHWR Fuel Pins, J. Nucl. Mater, **429** 257 (2012) 262.
[9] TANWEER A., et. al., Nucl. Eng. Des. **241** 3658 (2011) 3677.
[10] CHUNG, H.M., KASSNER, T.F., "Embrittlement Criteria for Zircaloy Fuel Cladding Applicable to Accident Situations in Light Water Reactors", NUREG/CR-1344 (ANL-79-48), US Nuclear Regulatory Commission (1980).

FIPRED (FISSION PRODUCT RELEASE FROM DEBRIS BED) ROMANIAN PROJECT

D. OHAI, I. DUMITRESCU, T. MELEG
Institute of Nuclear Research,
Pitesti, Romania

Abstract

The severe accident scenarios show the evolution of reactor core damage finalized with the corium and debris bed formation. Generally located above the corium, the debris bed has its temperature range evaluated between 1300°C (bottom) and 300°C (top). At the air ingress, in the debris bed the main chemical phenomena contributing to the subsequent degradation and fission products release are: oxidation of the Zircaloy 4 sheaths of the still intact rods, oxidation of the mixtures composed of Zr and UO_2 in the configuration of solid debris (either as relocated drops due to metallic melting or in the form of rubble debris particles) and oxidation of pure UO_2 in the fuel pellets remnants. When air penetrates into the debris bed, the remaining zircaloy4 claddings are oxidized, the oxidation rate decreasing from bottom to top. In the lower part of the debris bed (high temperature) the pins are completely oxidized and may undergo rapid destruction under their own weight, while the pins claddings in the upper part are oxidized with a smaller rate. By the destruction of pins, new sintered pellets with free surface are exposed; part of them remaining in debris bed alongside the material resulted from reactor core relocation and the other part falling down on corium. The oxidation of Zircaloy 4 sheaths is a dynamic process, dependent on the atmosphere, the temperature distribution into the debris bed and the cooling rate of the debris bed. The main objective of FIPRED (Fission Product Release from Debris Bed) Romanian Project is to evaluate the post severe accident fission products release from debris bed in air ingress conditions, tacking in account of UO_2 sintered pellets selfdisintegration by oxidation. The paper presents the scientific objectives and main steps of the project. The equipment (FIPRED EQ), the experimental test matrix and results obtained the mechanism of selfdisintegration of UO_2 sintered pellets by oxidation are presented, also.

1. INTRODUCTION

The physical phenomena involved in severe accidents are extremely complex and demand the development of specific research. The aim of this research is to understand the physical phenomena and reduce the uncertainties regarding their quantification. The final goal is to develop models that can be applied to reactors. These models grouped in computer codes should allow the prediction of severe accident progression. Because in this field it is not possible to conduct experiments on a real world scale, elementary tests must be used. This type of tests allows each physical phenomenon to be studied separately. Then global tests should follow to confirm the interaction between phenomena.

The severe accident scenarios show the evolution of reactor core damage finalized with the corium and debris bed formation. Generally located above the corium, the debris bed has its temperature range evaluated between 1300°C (bottom) and 300°C (top). At the air ingress, in the debris bed the main chemical phenomena contributing to the subsequent degradation and fission products release are: oxidation of the Zircaloy 4 sheaths of the still intact rods, oxidation of the mixtures composed of Zr and UO_2 in the configuration of solid debris (either as relocated drops due to metallic melting or in the form of rubble debris particles) and oxidation of pure UO_2 in the fuel pellets remnants.

The FIPRED (Fission Product Release from Debris Bed) project follows the determination of fission products release from debris bed after core relocation by UO_2 sintered pellets self-disintegration in air ingress condition. This concept can be applied in the severe accident in a spent fuel pool, also.

The oxidation of UO_2 (powder or pellets) has been studied following different objectives. Still 60's a mechanism of UO_2 sintered pellets oxidation versus O_2 diffusion was proposed [1], [2].

In South Korea, during development of DUPIC (**D**irect **U**se of LWR S**p**ent Fuel **i**n **C**ANDU) fuel cycle, many works has been dedicated for obtaining the sinterable powder by oxidation of spent sintered pellets [3] to U_3O_8 and reduction of U_3O_8 to UO_2 by reduction in H_2 atmosphere.

The size distribution of powder resulted by oxidation of irradiated and non irradiated UO_2 samples was studied [4] and fission gases release by oxidation and dissolution of spent fuel was studied, also [5].

2. FIPRED CONCEPT

The main practical objective of FIPRED project is post severe accident evaluation of fission products release from debris bed in air ingress conditions.

2.1. Scientific objectives

— Understanding of in time evolution of debris bed (relocation by pins cracks, temperature evolution, new pellets appearance and distribution between debris bed and corium surface, etc);
— Understanding of the pellets self-disintegration mechanism according to oxidative experimental conditions and pellets characteristics, and modeling of this phenomenon;
— Understanding of fission products release during pellets self-disintegration;
— Modeling of fission products release under destructive oxidation conditions of UO2 pellets;
— Modeling of fission product release from powder and fragments resulted from self-disintegration of pellets come downed on corium surface, in air ingress conditions.

2.2. Main steps of FIPRED project

(a) In time evolution of debris bed:
- Relocation by pins cracks;
- Temperature evolution;
- New pellets appearance and distribution between debris bed and corium surface**,** etc.

(b) $U0_2$ sintered pellets behavior in air and steam atmosphere:
- Design and execution of equipment for experimental activities;
- Oxidation tests of UO_2 pellets under air and steam atmosphere;
- Physical and chemical characterization of powder resulted fromUO_2 pellets disintegration.

(c) Interlinking of granules distribution of powder resulted from self-disintegration of pellets and oxidizing conditions:
- UO_2 sintered pellets self disintegration mechanism;
- Establishing the relations between pellet disintegration rate and experimental parameters;
- Modeling of self disintegration of pellets according to oxidizing conditions.

(d) Evaluation of fission products release by self disintegration of sintered pellets:

- Calculation of fission products distribution in pellets according to burnup and operation conditions;
- Experiments of fission products release using non-irradiated doped pellets according to the calculation of fission products distribution;
- Modeling of fission product release according to fission product distribution and self-disintegration of UO_2 pellets.

(e) Evaluation of fission products release from powder and fragments resulted from self-disintegration of pellets come downed on corium surface, in air ingress conditions;

(f) Evaluation of total fission products release;

(g) Evolution of fission product release post severe accident in containment.

3. EXPERIMENTAL WORKS

The experimental conditions used for UO_2 sintered pellets self disintegration by oxidation studies was the following:

— *Temperature*: 400^0C, 500^0C 600^0C, 700^0C 800^0C, 900^0C, 1000^0C;
— *Atmosphere*: 20%, 40%, 60%, 80% air in N2, 4%, 8%, 12%, 16% O2 in N2 respectively;
— *Flow rate*: 250ml/min.;
— *Sample*: UO_2 sintered pellets, density 10,45g/cm3, and grains diameter 4-5 μm;
— *Samples weight*: around 75 g (5 pellets CANDU type);
— *Equipment*: FIPRED-EQ.

Initially, the samples (UO_2 sintered pellets) were heated to the testing temperature in nitrogen atmosphere, and when the temperature was stabilized, the air-nitrogen mixture introducing started. During the experiment, periodically, the pellets no disintegrated were weighted. When the experiment was finished, the resulted powder and the pellets no disintegrated were weighted. The resulted powder from UO_2 sintered pellets self disintegration by oxidation was sieved by vibration on a sieving equipment having sieves meshes 32-500 μm. The fragments were characterized by SEM, also.

4. RESULTS AND DISCUSSIONS

4.1. Granulometric distributions of resulted powders

The self disintegration rate of UO_2 sintered pellets by oxidation is not dependent of air (O2) concentration if the air (O_2) concentration exceeds 20% (4%). In time, the self disintegration rate of UO_2 sintered pellets by oxidation grow.

The results obtained by sieving the powder resulted from self disintegration of UO_2 pellets by isothermal oxidation at 400°C–1000°C are presented in Fig. 1. The quantity of large fragments dimension increase and small fragments decrease with the temperature increasing.

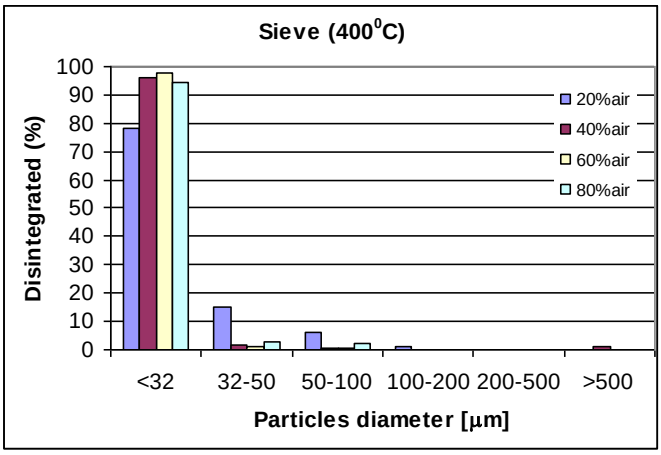
Sieve (400^{0}C)
Disintegrated (%)
100
90
80
70
60
50
40
30
20
10
0
20%air
40%air
60%air
80%air
<32
32-50
50-100
100-200
200-500
>500
Particles diameter [µm]

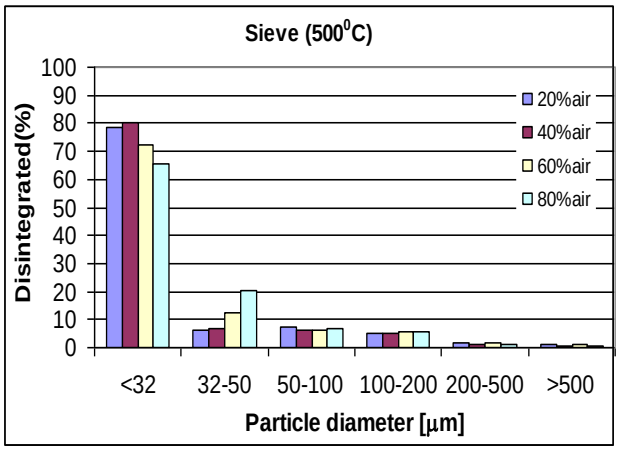
Sieve (500^{0}C)
Disintegrated(%)
100
90
80
70
60
50
40
30
20
10
0
20%air
40%air
60%air
80%air
<32
32-50
50-100
100-200
200-500
>500
Particle diameter [µm]

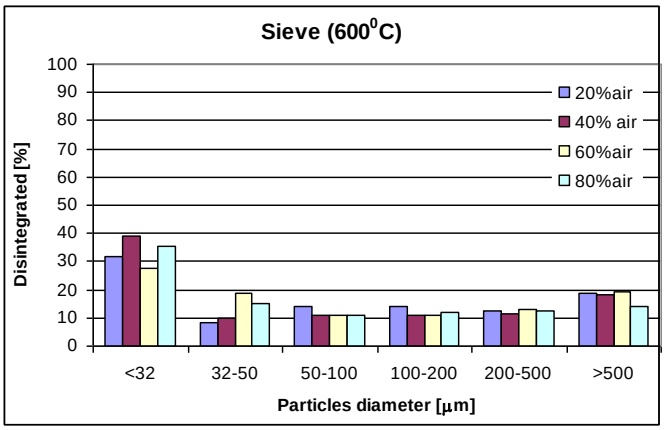
Sieve (600^{0}C)
Disintegrated [%]
100
90
80
70
60
50
40
30
20
10
0
20%air
40% air
60%air
80%air
<32
32-50
50-100
100-200
200-500
>500
Particles diameter [µm]

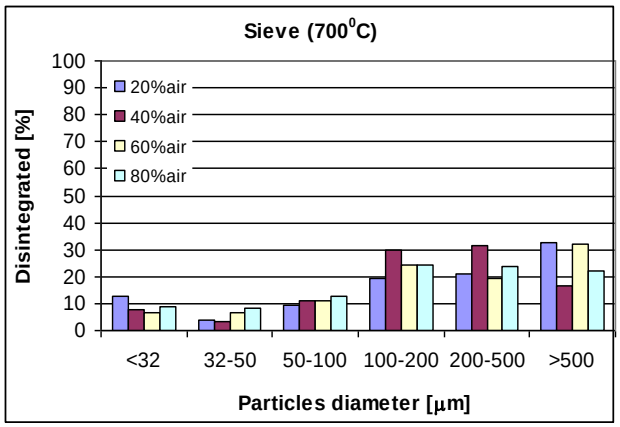
Sieve (700^{0}C)
Disintegrated [%]
100
90
80
70
60
50
40
30
20
10
0
20%air
40%air
60%air
80%air
<32
32-50
50-100
100-200
200-500
>500
Particles diameter [µm]

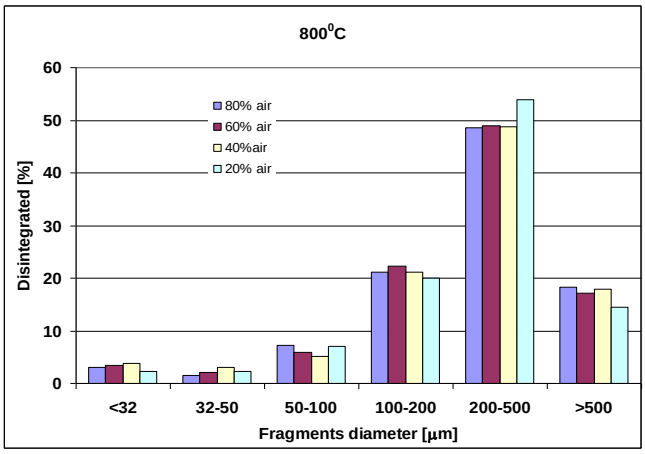
800^{0}C
Disintegrated [%]
60
50
40
30
20
10
0
80% air
60% air
40%air
20% air
<32
32-50
50-100
100-200
200-500
>500
Fragments diameter [µm]

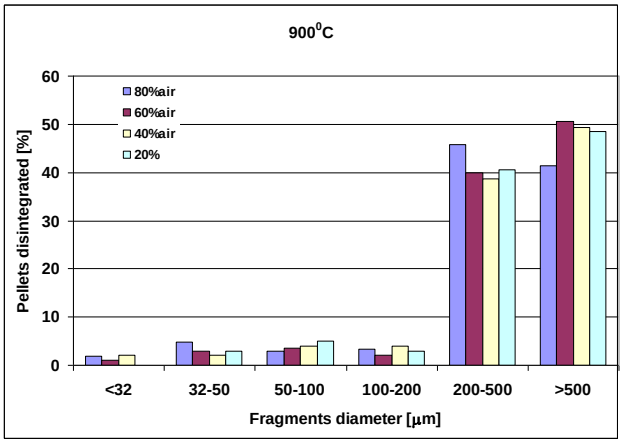
900^{0}C
Pellets disintegrated [%]
60
50
40
30
20
10
0
80%air
60%air
40%air
20%
<32
32-50
50-100
100-200
200-500
>500
Fragments diameter [µm]

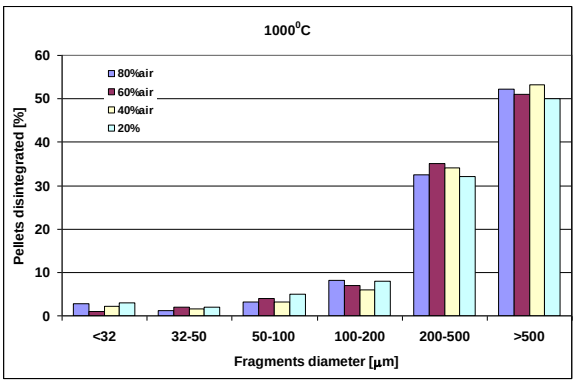
1000^{0}C
Pellets disintegrated [%]
60
50
40
30
20
10
0
80%air
60%air
40%air
20%
<32
32-50
50-100
100-200
200-500
>500
Fragments diameter [µm]

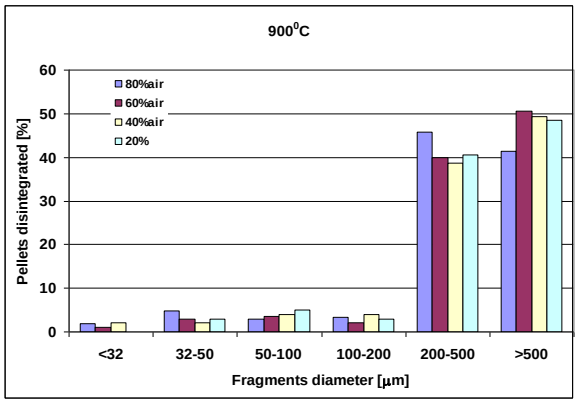

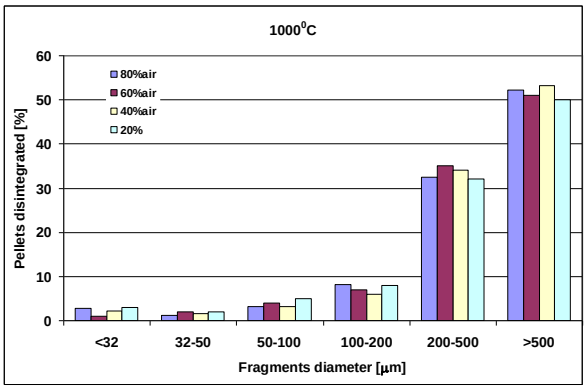

FIG. 1. Powders sieving result.

4.2. Morphology of powders (fragments)

The fragments (powder) resulted from UO_2 pellets self disintegrated by oxidation were examined by Scanning Electron Microscopy (SEM) techniques for morphological characterization. Microscopically aspect of powder resulted by UO_2 sintered pellets self disintegration by oxidation at 400°C is presented in Fig. 2.

The breakage is inter granular and intra granular. The fragments are irregular. The fragments appear as rounded and multi faces bodies, and plaques. All fragments have sharp-edged edge.

The microscopically aspects of powder resulted from UO_2 pellets self disintegrated by oxidation at 500°C are presented in Fig. 3. The inter granular attack is evident.

At 800°C, large fragments appear and the cracks are between groups of initial pellets grain (Figure 4). Parts of cracks are among columnar grains formed inside of fragments. The columnar grains appearance is explained by sintering of U_3O_8 formed by UO_2 oxidation.

At 1000°C–1400°C (Figs 5 and 6), the internal structures of fragments are completely different as initial grains of UO_2 pellets. All grains are columnar, very long and large diameters. The edge and corners are rounded.

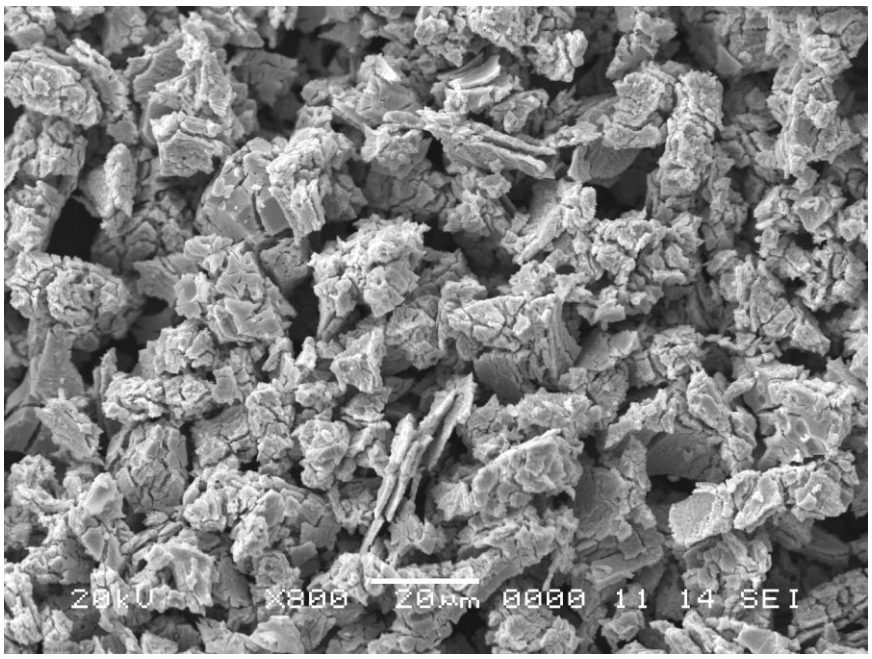

FIG. 2. Powder resulted at 400°C.

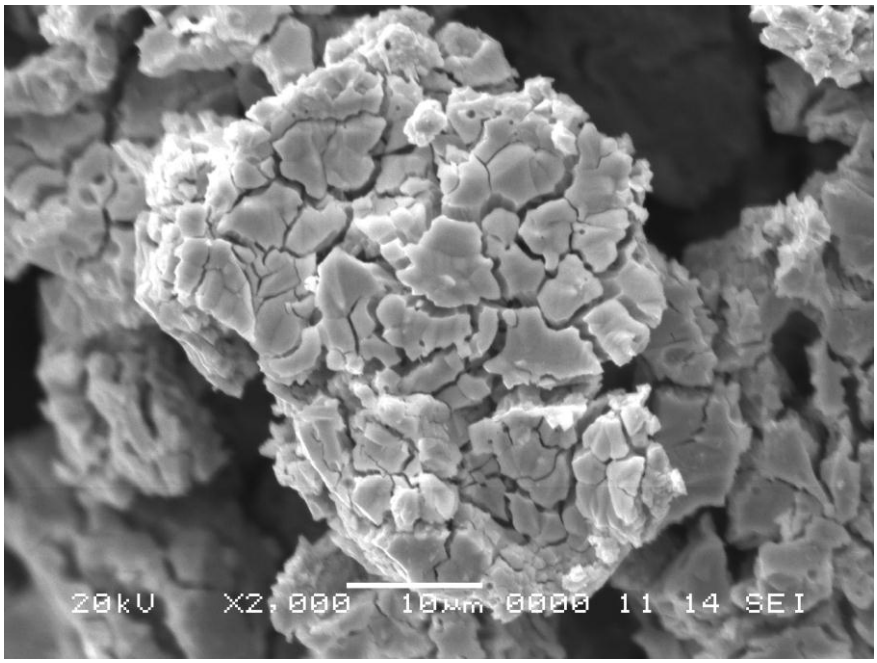

FIG. 3. Powder resulted at 500°C.

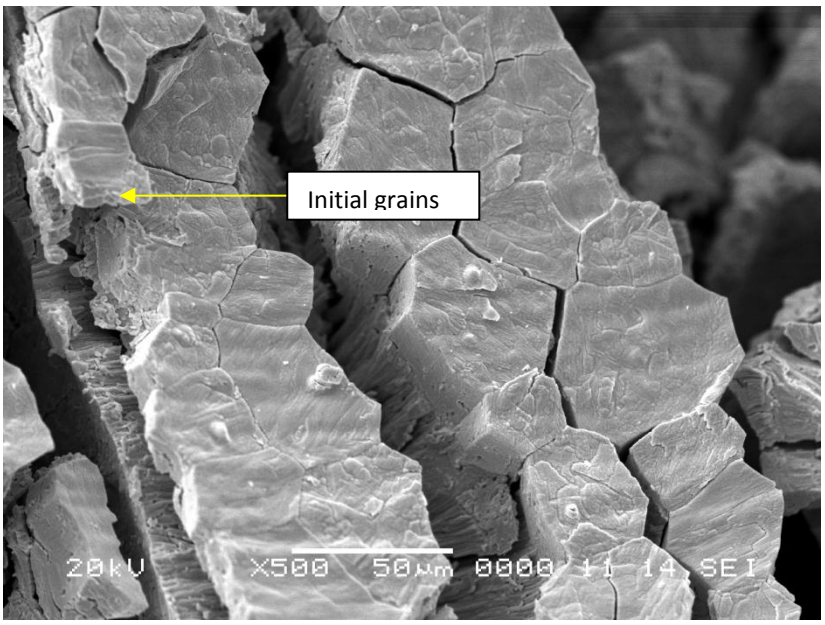

FIG. 4. Fragment resulted at 800°C.

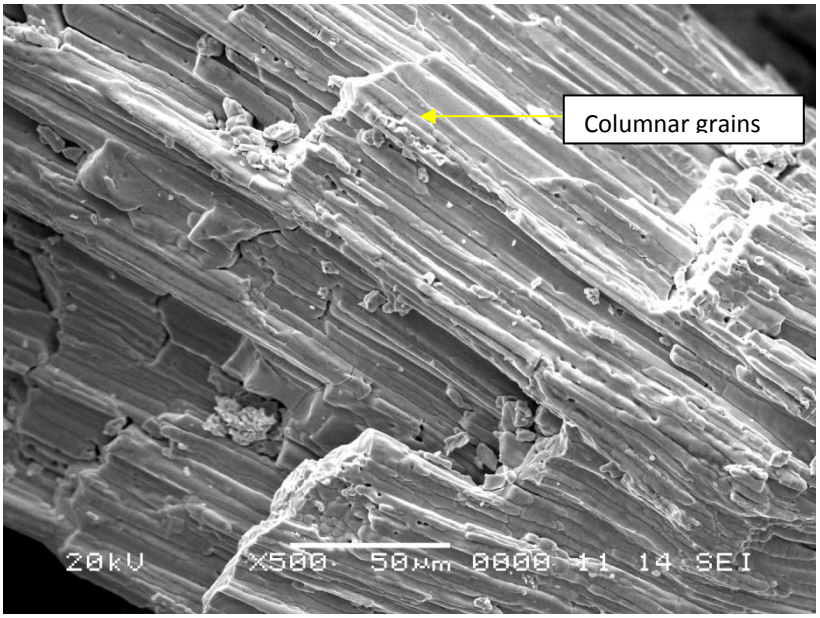

FIG. 5. Fragment resulted at 1000°C.

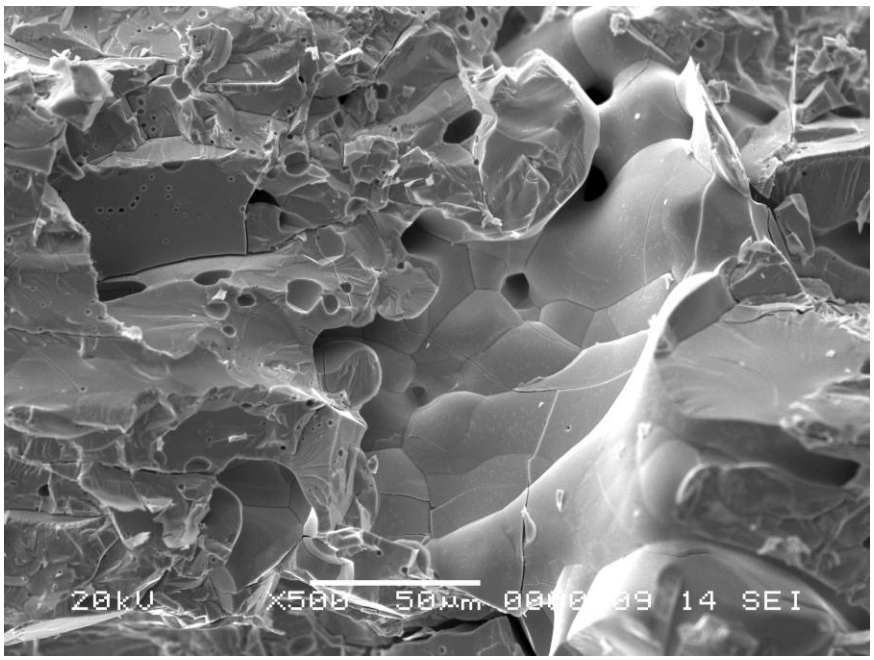

FIG. 6. Inside body aspect at 1400^0C.

4.3. Self disintegration mechanism

Initially, the attack on surface (preferentially to grain limits) of pellet detaches small fragments, only. When the first layer is removed, on the surface appear open pores and cracks. The air (O_2) comes into the open pores and cracks, and the UO_2 is transformed in U_3O_8 inducing very strong strengths. The attack in cracks and pore zones produce dislocations of large fragments with the free surfaces with pores, cracks, corners and edges. Growing surfaces with pores and cracks, the disintegration rate increase. The large fragments are broken in fewer fragments and so on. The UO_2 oxidation rate on new appeared corners and edges increase, also. That contributes to acceleration of self disintegration.

When the temperature grows, a new phenomenon appears: sintering of U_3O_8 formed by UO_2 oxidation. Temperature better 500°C initiate the sintering process of U_3O_8. The sintering rate grows with temperature increasing. Necks and bridges formed by sintering connect the fragments between them and large fragments appear.

During UO_2 pellets oxidation both processes disintegration and sintering work opposite. At low temperature (less 500°C) the disintegration is preponderant and sintering in-significant. When temperature grows, the sintering rate increase and became preponderant. At temperature better 1000°C the disintegration is practically annulated by sintering, the pellets are broken in few pieces, only.

These mechanisms are confirmed by experimental results. The results of oxidation, powder, sieving and microscopically (SEM) characterization of fragments demonstrate that self disintegration and sintering work simultaneously. When UO_2 sintered pellets oxidation is at low temperature (less 500°C), the disintegration is preponderant and fine powder is obtained. When temperature increases (600-1000°C), large fragments appear by sintering of adjacent small fragments. At temperature 10000C better the pellets are broken in few pieces, only. The sintering phenomenon of U_3O_8 is demonstrated by microscopically (SEM)

characterization of fragments:modification of microstructure, grains dimension increasing, columnar grains and necks appearance.

5. REMARKS

The Romanian Project FIPRED is under operation. The step related to UO_2 sintered selfdisintegration by oxidation in air atmosphere is covered by experimental works. The experimental results obtained permitted to propose a mechanism to explain selfdisintegration of sintered pellets by oxidation.

The correlation between temperature, O_2 concentration and resulted particle size distribution was established and the fission product distribution in the irradiated pellets dependent of irradiation condition was calculated, also.

Now, the experimental program related to UO_2 oxidation under steam/steam air atmosphere is under operation.

ACKNOWLEDGEMENTS

The work was funded by EC and Romanian Ministry of Economy under SARNET Project.

REFERENCES

[1] IWASAKI, M., SAKURAI, T., ISHIKAWA, N., KOBAYASHI Y., Oxidation of UO_2 in Air, J. of Nucl. Sc. and Tech. **5** 12 (1968) 48pp.

[2] IWASAKI, M., SAKURAI, T., ISHIKAWA, N., KOBAYASHI Y., Oxidation of UO_2 Pellets in Air, J. of Nucl. Sc. and Tech **5** 12 (1968) 652 pp.

[3] SONG, K., KIM, Y., H., KIM B., G., LEE, J., W., KIM, H., S., YANG M., S., PARK H., S., Effects of High Temperature Treatment and Subsequent Oxidation and Reduction on Powder Properties of Simulated Spent Fuels, J. of Kor. Nucl. Soc., **28** 4 (1966) 366pp.

[4] LIU, Z., COX, D, S., BARRAND, R. D., HUNT C. E. L., "Particle size distribution of U_3O_8 produced by oxidation at 300–900^{0}C", Proceeding of 13th Annual Conference of the Canadian Nuclear Society, Saint John, New Brunswick, Canada, (1992).

[5] KUDO T., KIDA, M., NAKAMURA, T., NAGASE. F., FUKETA, T., Effects of Fuel Oxidation and Dissolution on Volatile Fission Product Release under Severe Accident Conditions, J. of Nucl. Sc. and Tech. **44**, 11 (2007) 1428 pp.

FISSION PRODUCT INVENTORY IN CANDU FUEL

C. ZĂLOG, N. BARAITARU
Reactor Physics and Safety Analyses Group,
Cernavoda Nuclear Power Plant,
Cernavoda, Romania
Emails: czalog@cne.ro
nbaraitaru@cne.ro

Abstract

When the reactor is operated at power, fuel composition changes continuously. The fission reaction produces a large variety of fission fragments which are radioactive and decay into other isotopic species. For different accident analyses or operational events, detailed calculations of the fuel radioactive inventory (fission products and actinides) are needed. The present paper reviews two types of radioactive inventory calculations performed at Cernavoda NPP: one for determining the whole core inventory and one for determining the evolution of the inventory within fuel bundles stored in the Spent Fuel Bay. Two computer codes are currently used for radioactive inventory calculations: ORIGEN-S and ELESTRES-IST. The whole core inventory calculation was performed with both codes, the comparison showing that ELESTRES-IST gives a more conservative result. One of the challenges met during the analysis was to set a credible, yet conservative "image" of the in core fuel power/burnup distribution. Consequently, a statistical analysis was performed to find the best estimate plus uncertainties map for the power/burnup distribution of all in core fuel elements. For each power/burnup in the map, the fission product inventory was computed using a scaled irradiation history based on the Limiting Overpower Envelope. After the Fukushima accident, the problem of assessing the consequences of a loss of cooling event at the Spent Fuel Bay was raised. In order to estimate its impact, a calculation for determining the fission products inventory and decay heat evolution within the spent fuel bundles stored in the bay was performed. The calculation was done for a bay filled with fuel bundles up to its maximum capacity. The results obtained have provided a conservative estimation of the decay heat released and the expected evolution of the water temperature in the bay. This provided a technical basis for selecting the emergency actions required to cope with such events.

1. WHOLE CORE FISSION PRODUCTS INVENTORY FOR CANDU 6

1.1. Introduction

The main task of a Fuel Failure Analysis is to estimate the total radioactive inventory expected to be released during a postulated accident scenario. To accomplish this, besides evaluating the number of fuel elements expected to fail during the transient, one of the main tasks is the computation of fission products inventory within fuel matrix and gap, at the moment of the transient, for the failed fuel elements. Note that, in case of severe accidents, when core melting is presumed, whole core radioactive inventory is needed for assessing the radiological impact to the environment.

1.2. Methodology

When the reactor is operating at power, fuel composition changes continuously due to various nuclear processes such as fission, neutron capture, etc. In addition, fission reactions are producing a large variety of fission product nuclides, which most are radioactive and subsequently decay into other isotopic species. The fuel inventory of any nuclide is generally a balance between the nuclide production and depletion rates, but the calculation is complicated because time and spatial variation in fuel isotopic composition depend on the neutron flux distribution, which itself depends on core composition. Fortunately, changes in core composition are slow and time dependence can be replaced by a sequence of instantaneous static calculations performed at successive time intervals. Also, to account for

the neutron flux spatial variation, the core can be divided into small nodes, and, for each node, calculations are performed using averaged nuclear properties (i.e. cross-sections) and the average neutron flux at that position. Particularly, at CANDU reactors the calculations can be performed, for instance, on each fuel bundle located in core.

A detailed calculation of core fission product inventory at CANDU reactors is even more difficult due to on-power refueling. At CANDU-6 for instance, the core has 380 fuel channels, each loaded with 12 fuel bundles. Daily, few channels are refueled in order to keep the reactor critical at full power. As the nuclear fuel is the standard CANDU 37-element fuel bundle, there is a total of 168720 fuel elements (pins) present inside the core at any moment. If the total core inventory of fission products is needed, then the burnup and power history on each fuel pin are required. Obviously, tracking the power history on each fuel pin since its loading into the core to the moment when the calculation is performed is a difficult task. Instead, the alternative is to derive the most "representative" (i.e. best estimate) power/burnup distribution of the fuel elements within the reactor core by dividing the power and burnup ranges into small intervals (bins) and do a statistical analysis over a reasonably long time period of reactor operation. For instance, an analysis extended over a period of two years operation could give a consistent "image" of the fuel elements distribution within the core at full power, valid at any moment of the reactor life. The maximum linear power on fuel elements from each burnup bin gives the Reference Overpower Envelope. By scaling this curve up such as its peak to correspond to the linear power of a fuel element located on the outer ring of a bundle operating at the license limit, the Limiting Overpower Envelope (LOE) is obtained. Note that the LOE curve covers all possible irradiation histories that an in core fuel element could experience during reactor operation.

At Cernavoda, such an analysis was performed by processing the core tracking simulations done for Unit 1 over a period of two years operation at full power. The burnup range was divided into bins of 10 MWh/kg and the power range, into bins of 1 kW/m. Note that, in order to account for the uncertainty associated to core power distribution calculation, the fuel elements power estimated from core tracking simulations was increased, conservatively, by 3%. The Best Estimate Distribution plus uncertainty (Limit Estimate Distribution – LED, with 95% level of confidence), for 103% FP, is given in Figure 1.

Although the fuel elements within a burnup bin can actually have different irradiation histories, all "real" histories have shapes reasonable close to the Limiting Overpower Envelope curve. Therefore, the irradiation history of each fuel element can be approximated with a curve obtained by scaling down the LOE curve (Fig. 2). This assumption simplifies the inventory calculation. The calculation can be performed for one fuel element form each power/burnup bin. Then, multiplying the result by the average number of fuel elements in each bin and summing the contributions of all bins, total core inventory is obtained.

Calculations can be performed by using either the ELESTRES-IST code [1] or the ORIGEN-S code [2] using the CANDULIB-AECL library of cross-sections [3], specific for CANDU 37-fuel element bundle. Unlike ORIGEN, ELESTRES is a code specialized for studying the performances of CANDU fuel elements under normal operating conditions. Calculations with ELESTRES are performed for 23 isotopes, relevant for safety analyses purposes, while calculations with ORIGEN are performed for almost all possible isotopes produced during fuel irradiation. Note that, among other capabilities, ELESTRES can, also, calculate the gap inventory for the selected isotopes.

1.3. Results and Conclusions

At Cernavoda, the calculations were performed with both codes, ELESTRES and ORIGEN. The results obtained are given in Tables 1 and Table 2. Note that, in case of ORIGEN, the results are presented only for a selection of most important fission products. The comparison between the results given by two codes shows consistency for most of the isotopes with more conservatism from ELESTRES. Thus, for safety purposes, for calculation of the source term in case of severe accidents when core melting is postulated, the total core activity can be taken, in a conservative manner, from both codes results. For the 23 isotopes processed by ELESTRES, inventory values should be taken from ELESTRES simulations, while for the isotopes not processed by ELESTRES, inventory values should be taken from ORIGEN-S simulations.

2. RADIOACTIVE INVENTORY IN THE SPENT FUEL BAY

2.1. Introduction

After discharge from reactor core, spent fuel bundles are transferred to the Spent Fuel Bay for cooling. Following Fukushima accident, the problem of assessing consequences of a loss of cooling event at the Spent Fuel Bay was raised. In order to estimate the impact of such event, it is required to estimate the fission products inventory within the spent fuel stored in a bay filled up to its maximum capacity and to determine time evolution of *decay heat* generated by the spent fuel bundles stored in the bay.

2.2. Methodology

Burnup and irradiation power are the key parameters in obtaining fission product inventory and decay heat for a fuel bundle. Because the spent fuel bundles discharged in the bay have different exit burnups and were irradiated at different powers in the core, it is unreasonable to do inventory and decay heat calculations for each bundle stored in the bay (~ 40,000 bundles). Hence, it is required to define a *typical spent fuel bundle*, representative for all fuel bundles stored in the Spent Fuel Bay. A statistical analysis done on the spent fuel bundles discharged from the core over a period of about five years of reactor operation at full power has shown that, with a 95% confidence level (see Fig. 3.), the *typical bundle* has a discharge burnup of 170 MWh/kgU. Also, it is conservative to assume that this bundle has achieved this burnup operating to the nominal design (peak) power for a bundle of 800 kW.

Calculations were performed with ORIGEN-S computer code both for determining the evolution of its radioactive inventory and decay heat as function of cooling time. In Fig. 4, the decay heat evolution for this *typical spent fuel bundle* is presented for a period of up to 6 years cooling time. As an example, the evolution of I-131 inventory in this bundle is given in Fig. 5. As it can be seen, I-131 inventory is negligible after 600 days of cooling in the bay.

2.3. Results and conclusions

2.3.1. Spent fuel bay decay heat

Decay heat evolution in the Spent Fuel Bay (Fig. 6) is obtained by summing the contributions of all spent fuel bundles stored in the bay. The bay was considered filled to its maximum capacity taking into account the usual refueling rate for a CANDU-6. All bundles in the bay are considered identical to the typical spent fuel bundle and have a continuous decrease in decay heat during storage as shown in Fig. 4. Thus, at any time, while new

bundles, with high decay heat, are discharged in the bay, decay heat from bundles already stored decreases. Even the Spent Fuel Bay was designed with a storage capacity for 8 years of reactor operation at 80% FP, the spent fuel bundles are normally transferred to a dry storage facility after 6 years cooling. Therefore, in our calculations, bundles with more than 6 years cooling time were assumed, conservatively, to have a constant decay heat, equal to the decay heat reached after 6 years cooling. These bundles were considered to remain stored in the pool up to the maximum storage capacity. Fig. 6 shows that, even with these conservative assumptions, the Spent Fuel Bay maximum heat load would be, with a large margin, below the design heat exchangers cooling capacity of 2 MW. Also, it is noticeable that heat load in the bay has a consistent decrease during shutdown periods, when the reactor refueling stops and no bundles are discharged in the bay.

2.3.2. Spent fuel bay fission products inventory

Evolution of fission product inventory in the Spent Fuel Bay is obtained by summing the contributions of all spent fuel bundles stored in the bay. It was assumed a continuous refueling rate of 16 bundles/day (close to the usual value achieved during long time operation of a CANDU-6 unit at full power), until filling the bay to its maximum capacity. All bundles in the bay are considered identical to the typical spent fuel bundle. Fig.7 shows that short-lived isotopes (like ^{131}I) level out in the early stage of bay filling, while total inventory (with prevalent contribution from long-lived isotopes) has a continuous increase, yet with a decreasing slope.

Both decay heat and fission products inventory calculations were used to assess the consequences of a loss of cooling event at the Spent Fuel Bay. The analysis has taken into account volume of water and other structural materials (stainless steel) used to store fuel in the bay. The conclusion is that, if bay cooling is lost, water temperature will increase at a rate of around 1 degree per hour, reaching boiling in about 2.5 days. If cooling is still not restored, the pool water evaporates and, in around two weeks, its level decreases to about one meter above the fuel stack. With one meter of water above fuel stack, staff access is still allowed in the area and it was concluded that, in case of losing cooling at the Spent Fuel Bay, there is enough time (more than two weeks) to take compensatory measures, i.e. to restore an alternative cooling source.

TABLE 1. WHOLE CORE FISSION PRODUCTS INVENTORY OF A CANDU-6 EQUILIBRIUM CORE OBTAINED WITH ELESTRES-IST CODE

Isotope	Total Inventory (TBq)	Gap Inventory (TBq)
Xe-133	4.70E+06	1.66E+04
Xe-133m	1.46E+05	1.64E+02
Xe-135	5.52E+05	8.20E+02
Xe-135m	8.27E+05	6.39E+01
Xe-137	4.69E+06	1.79E+02
Xe-138	4.73E+06	3.50E+02
Kr-83m	2.39E+05	8.40E+01
Kr-85	5.45E+03	1.20E+01
Kr-85m	9.73E+05	3.20E+02
Kr-87	1.89E+06	3.31E+02
Kr-88	2.67E+06	6.91E+02
Kr-89	3.47E+06	1.20E+02
Te-131	1.95E+06	1.04E+03
Te-131m	2.77E+05	1.19E+03
Te-132	3.28E+06	2.17E+04
Te-133	2.99E+06	1.12E+03
Te-133m	2.23E+06	1.76E+03
Te-135	2.59E+06	1.56E+02
I-131	2.10E+06	1.12E+04
I-132	3.32E+06	2.40E+04
I-133	5.16E+06	9.26E+03
I-135	4.84E+06	4.93E+03
I-137	2.55E+06	8.31E+01
Cs-137	5.69E+04	3.67E+03
Sr-89	3.08E+06	3.61E+05
Sr-90	5.63E+04	3.77E+03

TABLE 2. WHOLE CORE FISSION PRODUCTS INVENTORY OF A CANDU-6 EQUILIBRIUM CORE OBTAINED WITH ORIGEN-S CODE

Isotope	Total Inventory (TBq)	Isotope	Total Inventory (TBq)
Kr 85	2.10E+03	I-131	2.00E+06
Kr-85m	6.88E+05	I-132	3.12E+06
Kr-87	1.39E+06	I-133	4.59E+06
Kr-88	1.96E+06	I-134	5.19E+06
Rb-86	2.11E+02	I-135	4.34E+06
Sr-89	1.60E+06	I-137	2.14E+06
Sr-90	1.75E+04	Xe-131m	1.88E+04
Sr-91	3.34E+06	Xe-133	4.30E+06
Y-90	1.75E+04	Xe-133m	1.36E+05
Y-91	1.83E+06	Xe-135	3.89E+05
Zr-95	2.08E+06	Xe-135m	8.97E+05
Zr-97	3.74E+06	Xe-137	4.17E+06
Nb-95	1.22E+06	Xe-138	4.08E+06
Mo-99	4.11E+06	Cs-134	3.54E+03
Tc-99m	3.68E+06	Cs-136	1.57E+04
Ru-103	1.79E+06	Cs-137	2.08E+04
Ru-105	1.60E+06	Ba-140	3.69E+06
Ru-106	1.12E+05	La-140	3.67E+06
Rh-105	1.31E+06	Ce-141	2.67E+06
Te-127	1.31E+05	Ce-143	3.71E+06
Te-127m	7.72E+03	Ce-144	5.65E+05
Te-129	5.87E+05	Pr-143	3.21E+06
Te-129m	8.11E+04	Nd-137	3.21E+06
Te-131	1.85E+06	Np-239	5.98E+07
Te-131m	3.78E+05	Pu-238	1.48E+01
Te-132	3.06E+06	Pu-239	2.35E+02
Te-133	2.54E+06	Pu-240	1.18E+02
Te-133m	2.12E+06	Pu-241	6.98E+03
Sb-127	1.45E+05	Am-241	1.02E+00
Sb-129	6.49E+05	Cm-242	7.94E+01
		Cm-244	2.82E-01

Linear Power	Burnup [MWh/kgU]																									
[kW]	10	20	30	40	50	60	70	80	90	100	110	120	130	140	150	160	170	180	190	200	210	220	230	240	250	260	270
60																											
59																											
58																											
57																											
56	1		1	2	4	2	1	1																			
55	3	4	6	10	10	10	7	3	4		1																
54	11	15	26	27	35	26	20	12	8	5	2	1															
53	30	39	55	63	60	52	48	38	24	16	7	4	2														
52	52	67	61	72	71	75	74	66	57	39	26	16	5	3	2	1											
51	58	78	70	93	80	87	79	77	73	64	55	42	29	11	8	4		2									
50	93	106	116	123	126	103	110	95	87	81	81	64	60	40	27	18	9	3	1								
49	118	141	142	129	138	141	139	124	132	108	95	92	74	72	58	45	22	11	5	2							
48	118	139	140	138	140	146	145	147	135	139	134	113	95	90	73	65	54	30	11	4	1						
47	131	139	155	149	156	162	155	146	152	159	160	151	135	121	99	89	63	40	19	6	2						
46	150	149	150	145	169	199	200	206	193	168	160	155	161	150	134	112	82	43	24	11	3	2					
45	145	130	130	133	150	160	170	185	192	207	201	178	166	164	151	144	109	57	22	11	6	4	2	2	1		
44	125	131	120	120	133	132	148	148	165	187	197	209	197	187	163	140	106	65	29	9	5		3				
43	114	139	129	138	137	139	135	128	136	150	165	183	212	218	209	188	124	71	28	15	8	5	2				
42	120	132	133	144	165	167	151	144	138	133	128	144	169	196	211	195	165	93	50	21	8	5	4	3			
41	150	171	178	192	182	197	191	177	175	148	147	137	141	159	172	165	141	117	85	45	20	7	3	2	3		
40	206	227	234	251	258	241	228	232	216	202	201	181	157	152	128	128	124	99	74	48	31	16	12	5	2	2	1
39	220	219	231	237	238	241	249	248	251	259	252	254	228	180	132	100	95	66	51	36	26	14	12	6	2	1	4
38	229	260	245	258	281	280	263	264	256	271	281	283	287	256	177	131	93	68	34	21	19	12	6	3	5	1	2
37	230	252	234	248	296	298	297	300	303	289	288	306	290	258	193	148	120	84	61	38	21	13	7	2	1	4	4
36	215	241	207	244	252	271	275	289	311	329	335	328	300	257	182	126	119	95	79	66	53	31	16	8	4	2	2
35	197	227	224	236	247	252	267	267	285	307	326	338	326	255	183	131	105	91	70	69	65	65	57	31	20	11	5
34	202	215	235	248	269	258	251	262	274	274	305	306	270	226	178	145	101	76	62	51	58	54	51	44	33	21	13
33	244	263	261	304	307	320	315	289	298	304	291	277	244	184	148	123	98	80	55	51	36	35	27	28	25	21	15
32	258	244	249	288	308	298	311	334	355	366	360	295	219	181	139	101	86	66	49	37	29	20	13	7	5	8	8
31	228	219	225	254	266	275	302	305	341	378	396	364	290	225	154	113	84	70	53	30	18	10	3	3	3	3	2
30	212	236	246	275	283	279	281	307	321	348	350	323	271	230	195	153	125	83	58	37	20	8	2	1	2	2	
29	231	243	245	257	264	283	285	312	338	325	311	256	238	207	185	166	147	139	110	64	27	11	3		1		1
28	222	226	220	246	253	235	258	284	312	334	294	264	208	185	194	185	187	161	124	86	47	18	7	2	1		
27	207	202	208	217	216	232	247	280	321	311	267	237	215	192	174	191	176	179	161	125	84	55	23	8	4	2	
26	182	183	202	220	213	219	225	249	275	259	242	219	207	203	208	182	168	141	143	130	122	101	86	60	36	22	7
25	185	205	220	244	248	243	248	256	254	240	212	216	207	194	167	159	141	120	111	94	80	76	68	66	59	39	28
24	221	229	225	240	244	254	274	278	259	211	210	216	217	226	200	168	107	96	97	81	63	44	27	16	13	15	18
23	194	190	196	214	212	213	227	265	228	212	188	221	256	253	247	184	149	108	82	63	37	21	9	4	1	1	5
22	192	193	204	201	213	212	242	240	215	185	188	203	215	212	209	220	204	171	137	80	40	15	3	1			
21	208	218	221	230	239	248	250	231	184	190	205	222	222	210	174	169	141	138	137	110	65	27	9	2	1		
20	201	194	201	203	212	211	234	226	201	180	209	241	253	229	212	191	155	120	82	53	30	17	4	3	2		
19	153	155	159	175	177	182	184	164	166	184	215	224	238	246	215	186	163	124	90	51	20	7	2	1	1		
18	149	150	147	151	150	162	162	154	137	159	179	177	188	185	178	167	108	82	66	39	16	4	3	1			
17	142	148	149	148	150	154	151	133	134	141	145	165	184	172	146	120	94	70	55	28	8	3		2	2		
16	127	119	118	126	129	129	129	121	114	123	141	141	148	160	134	106	78	59	45	31	12	3					
15	115	114	113	116	122	125	116	106	115	115	118	131	130	124	114	87	70	53	56	34	13	3					
14	135	174	200	204	177	140	109	89	80	85	107	111	123	130	113	84	52	41	37	24	8	5	1				
13	373	382	367	376	268	122	87	69	63	74	79	98	105	113	109	124	107	88	58	36	14	3					
12	304	301	299	286	140	93	70	41	39	56	67	80	89	86	101	166	234	304	330	279	191	97	25	9			
11	457	500	490	389	147	88	71	41	24	30	52	71	110	167	207	226	248	232	193	105	70	45	21	8	10	9	8
10	503	503	511	311	99	78	58	25	15	29	48	79	160	297	448	498	417	269	111	47	14	5	3				5
9	599	580	561	223	69	59	23	12	8	19	71	209	353	439	412	357	246	162	87	35	18	10	4	3			
8	451	454	382	126	62	48	17	3	8	40	122	240	329	327	250	197	185	134	67	21	8	2					
7	446	429	358	86	39	19	4	1	7	31	105	209	261	219	177	185	168	135	76	19	4						
6	438	433	305	60	13	5	1	1	2	19	64	131	188	178	136	104	140	162	96	33	7	3	5	3			
5	398	407	261	16	2	1		1	1	4	38	102	155	174	171	110	104	128	99	36	12						
4	433	437	214	10					1	2	11	54	114	149	179	138	152	210	188	79	31	3					
3	224	212	51	1						1	11	56	135	150	128	91	47	31	25	23	11	1					
2	7	6	1								1	1	3	10	8	1	6	2									
1																											

FIG. 1. Limit estimate distribution for in core fuel elements at 103% FP.

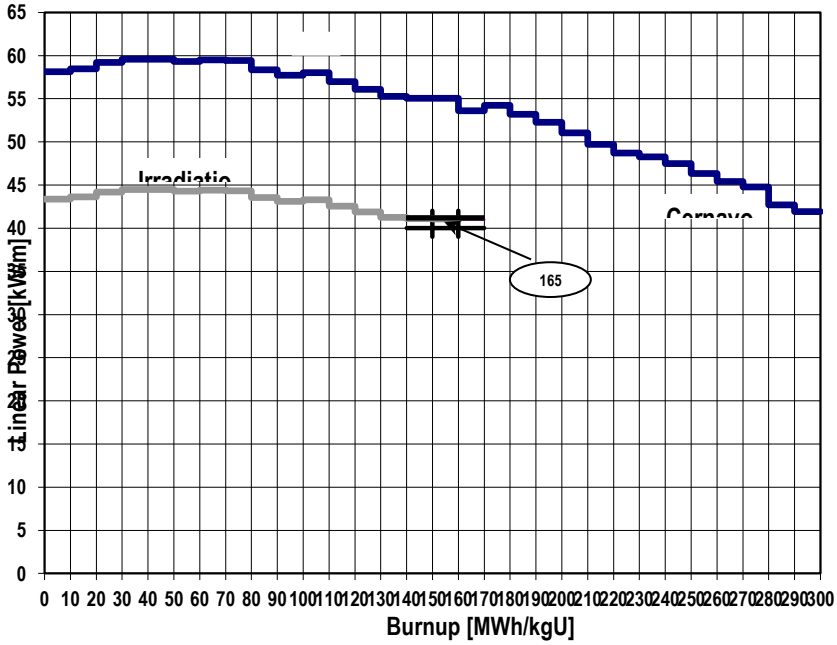

FIG. 2. Limiting overpower envelope for 103% FP.

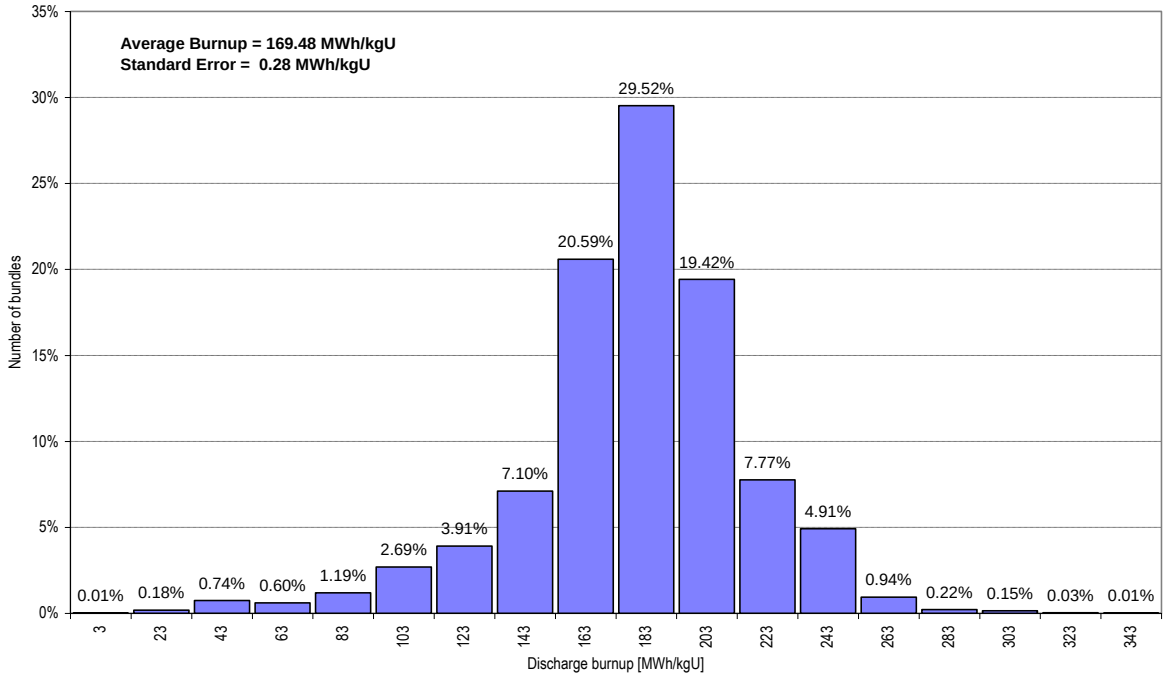

FIG. 3. Statistics on discharged spent fuel bundles.

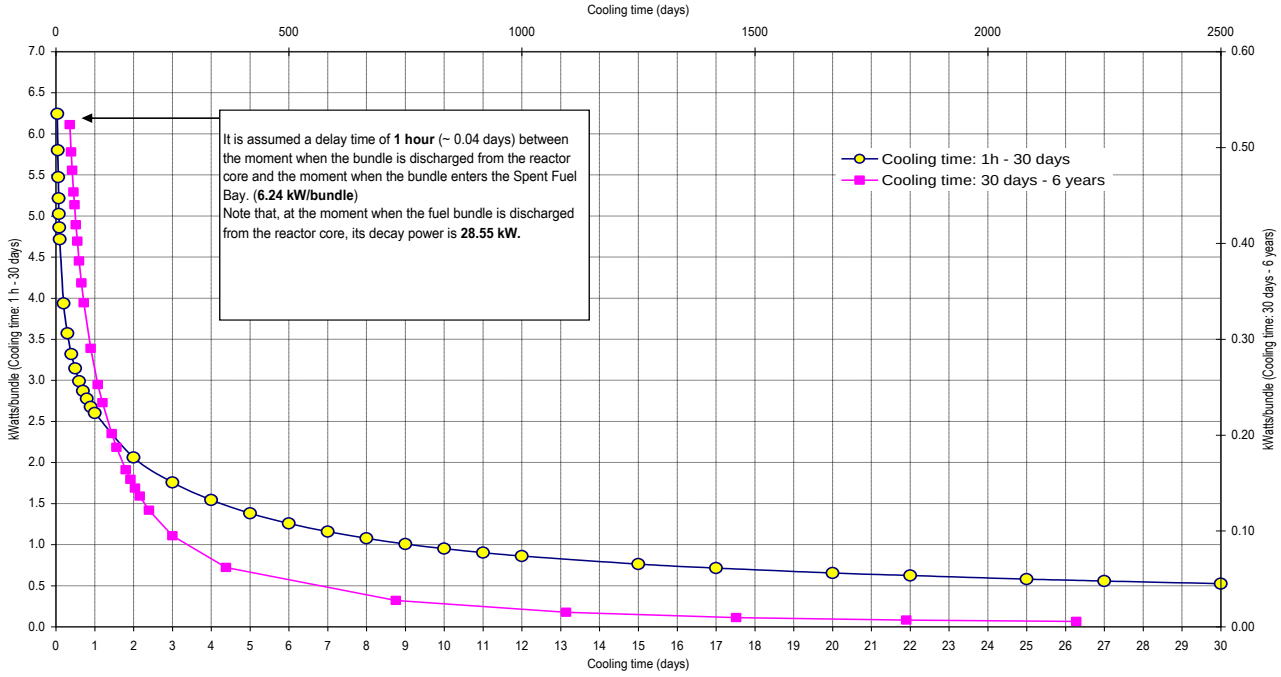

FIG. 4. Decay heat for the typical spent fuel bundle.

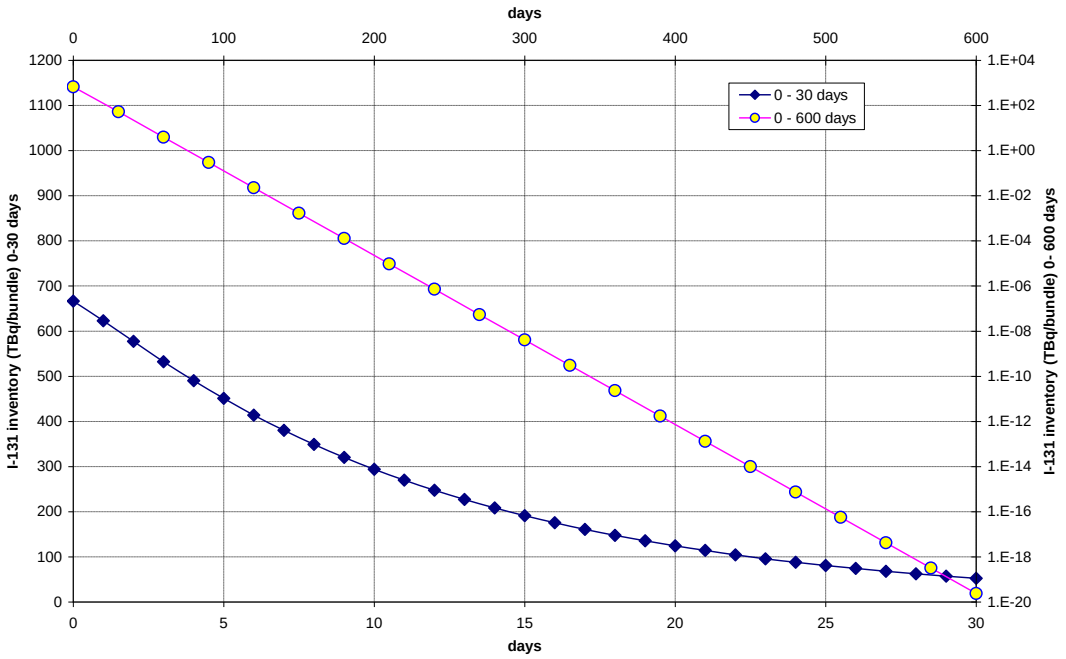

FIG. 5. I-131 inventory for the typical spent fuel bundle.

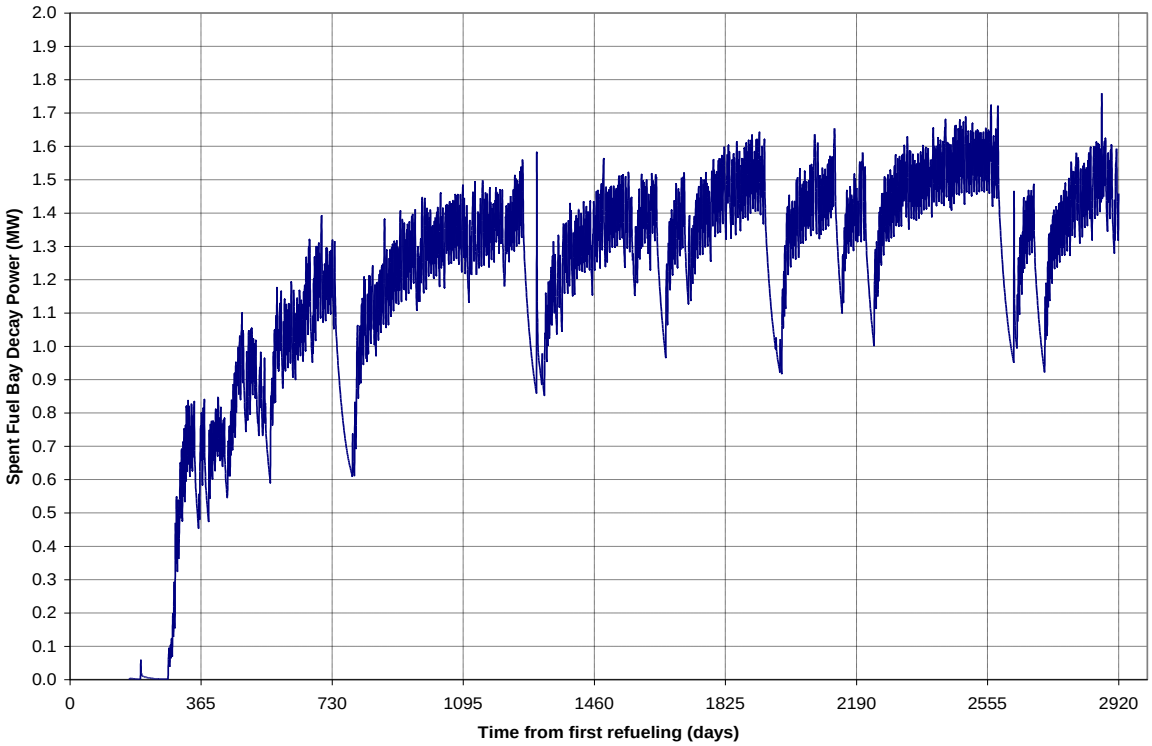

FIG. 6. Spent fuel bay decay heat.

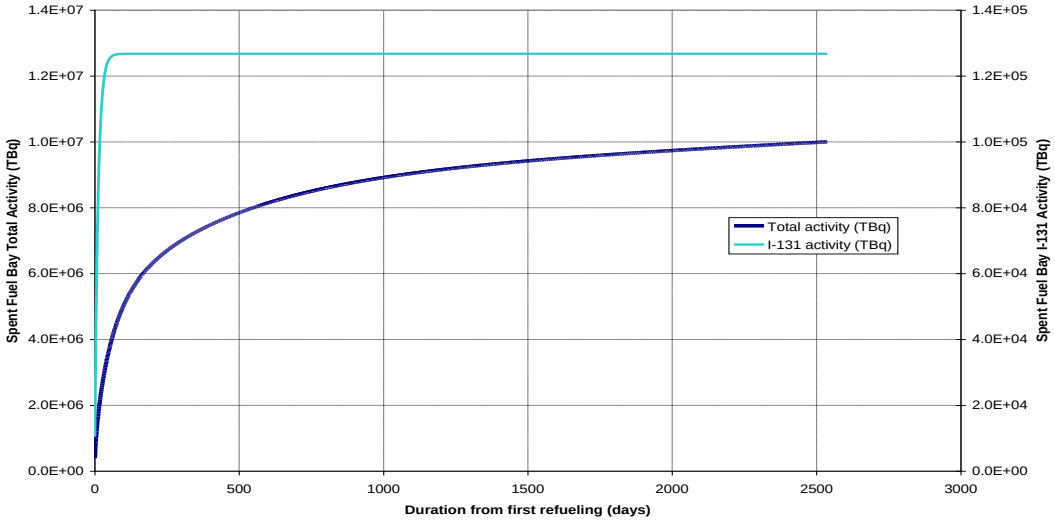

FIG. 7. Spent fuel bay activity.

REFERENCES

[1] CHASSIE, G. G., ELESTRES-IST User's Manual, TTR-733, rev. 1 (2002).
[2] ORIGEN-S User's Manual, Oak Ridge National Laboratory, NUREG/CR-0200, Vol 3.
[3] CANDULIB-AECL: Burnup-Dependent ORIGEN-S Cross-Section Libraries for CANDU Reactor Fuel Characterization, RSICC Data Package DLC-210.

FUEL CODES AND SAFETY
(Session 4)

Chairman

Y. C. KIM
Republic of Korea

DESIGN AND PERFORMANCE OF SLIGHTLY ENRICHED URANIUM FUEL BUNDLES IN INDIAN PHWRS

R. M. TRIPATHI, P. N. PRASAD, A. CHAUHAN
Nuclear Power Corporation of India Ltd,
Mumbai, India

Abstract

Slightly Enriched Uranium (SEU) of 0.9 weight % ^{235}U enrichment is a promising fuel design option for Indian PHWRs. The important component of this option is the improvement in the average discharge burnup from the core. The 19-element fuel bundle with natural uranium currently is being used in all operating 220 MWe PHWRs has been studied for 0.9 weight % ^{235}U by computer code FUDA MOD2. The important fuel parameters such as fuel temperature, fission gas release, fuel swelling and sheath strain have been analyzed for required fuel performance. With 0.9% SEU, average discharge burnups of about 14 000 MW d/TeU can be achieved, improving uranium resource utilization by about 34% relative to that achievable in a natural uranium fuelled PHWR reactor. The FUDA code (Fuel Design Analysis code) MOD2 version has been used in the fuel element analysis. The code takes into account the interdependence of different parameters like fuel pellet temperatures, pellet expansions, fuel sheath gap heat transfer, sheath strain & stresses, fission gas release and gas pressures, fuel densification etc. Thermo-mechanical analysis of fuel element having SEU material is carried out for the bundle power histories reaching up to design burnup 25 000 MW·d/TeU. The resultant parameters such as fuel temperature, sheath plastic strain and fission gas pressure for SEU fuel element were compared with respective thermo-mechanical parameters for similar fuel bundle element with natural uranium as fuel material.

1. INTRODUCTION

Indian nuclear power programme is guided by the limited available natural uranium. Presently 19- element natural uranium fuel bundles are used in 220 MWe (Fig. 1) Indian PHWRs, The core average design discharge burnup for these bundles is 7000 MW·d/TeU and maximum burnup for assembly goes upto of 15 000 MW·d/TeU.

The use of Slightly Enriched Uranium (SEU) with 0.9% ^{235}U by weight is being studied as an attractive fuelling option for Indian pressurized heavy water reactors (PHWR). Due to higher fissile content these bundles will be capable of delivering higher burnup than the natural uranium bundles. The maximum burnup possible with these bundles is 25 000 MW·d/TeU.

The high burnup fuel element development studies for the PHWR fuel bundles and subsequent irradiations have been elaborated in this paper.

2. DESIGN STUDIES

Increase in fuel burnup beyond 15 000 MW·d/TeU using slightly enriched uranium in place of natural uranium in fuel element used in 220 MWe PHWRs is investigated. Performance of the fuel bundles at high burnup is analysed in the report. Due to higher fissile content the bundles will be capable of delivering higher burnup than the natural uranium bundles.

In PHWR fuel elements no plenum space is available and the cladding is of collapsible type. The additional fission product swelling and gas release due to use of SEU fuel in PHWRs, needs to be accommodated within the fuel elements taking into account these factors. Studies have been carried out for different fuel element target burnups with different alternative concepts. Modifications in pellet shape and pellet density are considered.

The element power envelope up to the design burnup for different enrichments generated by reactor physics calculations are utilized for fuel design. The bundle power envelope for SEU is shown in Fig. 2. The peak linear heat rate (LHR) of the element is maintained same as current natural U elements to avoid any thermal hot spots. This has led to increase in residence period corresponding to higher burnups. Following Design studies are carried out for SEU fuel bundle for 220 MWe PHWRs.

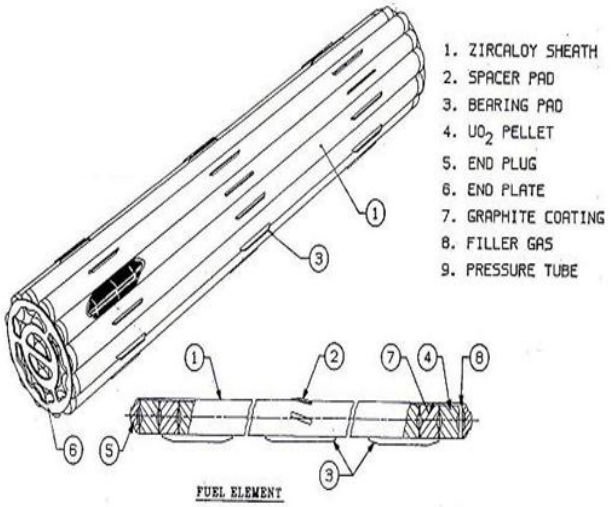

FIG. 1. 19-element SEU Fuel Bundle.

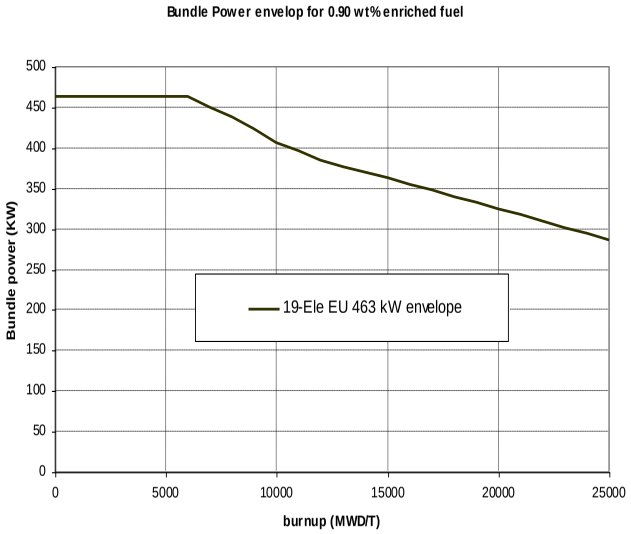

FIG. 2. Bundle power envelope for 0.9% EU bundle.

2.1. Power ramp

Generally 8 bundle fueling scheme is adopted for NU bundles in PHWRs. In the view of power peaking for SEU, Two-Bundle rather than 8-bundle fueling scheme has been adopted. The 2-bundles refueling shift will lead to power ramp on the bundles when bundles in the channel are shifted from 4 to 6th location in the channel. This happens at a relatively high burnup of about 7500 MW·d/TeU, The ability of graphite coating to provide resistance to power ramp at these burnups is one of the main concerns. The irradiation performance of the graphite coated natural U and MOX fuel (Natural UO_2–PuO_2) bundles in the 220 MWe PHWRs gives the confidence that the graphite coated bundles can withstand the power ramps due to neighboring channel fuelling at higher burnups.

2.2. Fuel swelling

At higher burnups, swelling in fuel elements is a concern. To accommodate higher burnups up to 25 000 MW·d/TeU, the fuel (UO_2) density is reduced by 1% i.e. minimum density will be 10.35 gm/cc instead of 10.45 gm/cc for the NU fuels.

2.3. Residence period

The bundle residence period increases for high burnup fuel. This increases oxidation of cladding. The high fuel burnups lead to more residence period in reactor. The higher residence period has effect on:

(1) Low cycle fatigue behavior of fuel cladding & end plate;
(2) Corrosion and hydriding behavior of the fuel cladding and end plate;
(3) Fretting damage of fuel bundle;
(4) Power ramps at higher burnups.

The SEU fuel bundle flux depression factors across the elements are higher compared to natural U bundle. The irradiation experience with both the graphite coated natural U and MOX bundles in the reactors shows that the graphite coating works at the burnups experienced by them and the bundles can withstand the power ramps during refueling. The zircaloy corrosion, hydriding and irradiation embrittlement behavior for the bundle is satisfactory for these extended burnups and powers. Few natural uranium bundles in KAPS-2 were irradiated up to 3.5 years earlier. Also the MOX bundles in KAPS-1 were irradiated up to 2.5 years and irradiation is continuing. The BWR fuel bundles in TAPS-1&2 stay maximum upto 4.5 years under boiling environment. This experience gives confidence that the zircaloy cladding can stay in core for 5 years without any deterioration due to corrosion and irradiation embrittlement.

2.4. Thermo mechanical analysis

2.4.1. FUDA code [1]

The fuel design analysis code (FUDA) MOD2 [2] version has been used in the fuel element analysis. The code takes into account the interdependence of different parameters like fuel pellet temperatures, pellet expansions, fuel-sheath gap heat transfer, sheath strain & stresses, fission gas release and gas pressures, fuel densification etc. Due to this complexity, the code uses mix of empirical, physical and semi-empirical relationships. Finite difference method is used in the calculations to solve differential equation.

The input data requires fuel element material and geometrical parameters and reactor neutronic and thermal hydraulic parameters and element linear heat rating in different burnup

zones. The output data generated by program are radial temperature gradient across fuel and sheath, fuel –sheath heat transfer coefficient, fission gas generated and released, gas pressure, fuel sheath interfacial pressure, sheath stress and strains for different burnup zones [3], [4].

Thermo-mechanical analysis of the fuel element is carried out using fuel design analysis code FUDA for the power envelope up to burnup 25 000 MW·d/TeU respectively. The resultant thermo-mechanical parameters, such as fuel temperature, gas pressure etc, for these high burnup bundles were compared with respect to bundle with current burnups. Typical analysis details are given in Table 1. The studies indicated that, present fuel design is suitable up to 25 000 MW·d/TeU with minor modifications like use of higher grain size, more dish depth etc.

2.4.2. Methodology

Thermo-Mechanical analysis was carried out using FUDA for present design 19-element considering 0.9% enriched uranium as fuel material. In the run power vs. burnup history was utilized as input along with operating parameters of 220 MWe PHWR. The output parameters such as fuel central line temperature, fission gas release, fission gas pressure and clad strain are calculated. The studies indicated that 19-element fuel bundle with 0.9% enrichment and required peak bundle power, needed few design changes to limit the fission gas pressure for the intended burnup of around 25 000 MW·d/TeU. Density and dish depth of the pellet were two parameters, which could be modified in order to limit the fission gas pressure without putting much difficulty in manufacturing. Hence, a parametric study was undertaken for these two parameters, while keeping the other geometric and operating condition same as that of 19-element fuel bundle used in 220 MWe PHWR.

TABLE 1. THERMO MECHANICAL ANALYSIS OF 19- ELEMENT SEU FUEL BUNDLE VIS-À-VIS NU FUEL BUNDLE FOR A BUNDLE POWER ENVELOPE WITH A PEAK POWER OF 508 KW [5]

Properties	NU	SEU
Enrichment	0.7 %	0.9 %
Density (g/cc)	10.6	10.5
Peak bundle Power (kW)	508	508
LHR (kW/m)	60.8	60.8
Burnup (MW·d/TeU)	15000	25000
Fuel Centre Line Peak Temperature (ºC)	2077	2151
Sheath Inner Surface Temperature (ºC)	335	335
Sheath Outer Surface Temperature (ºC)	296	296
Fission Gas Release % (EOL*)	11	10
Fission Gas Pressure (EOL) MPa	9.20	7.29
Maximum Sheath Plastic Strain	0.32	0.21

*EOL: End of Life

3. DESIGN REQUIREMENTS

The design requirements of fuel bundles have been taken into consideration during thermo-mechanical analysis of the peak rated element of fuel bundle. The fuel bundle safety limits and limiting conditions for operation are derived based on the following factors:

(a) Fuel centre line temperature:
Fuel needs to be safe from failure due to excessive thermal expansion. The limiting value on fuel element centre line temperature is the melting point of UO_2 [6] (2840°C). The limiting condition for design is put based on the onset of centre line melting of fuel. This means a large margin is still available from the condition where damage due to fuel thermal expansion may actually take place;

(b) Clad strain:
Fuel cladding fails due to high hoop stress which depends upon internal pressure, temperature of cladding and ductility of cladding. The limiting cladding strain value of 1% is taken as guideline based on data on zircaloy irradiation strain capability. The 1% requirement has come from the ductility requirement of the irradiated fuel;

(c) Fission gas pressure:
Fission gas pressure should be less than the coolant pressure during operation for better gap conductance and structural stability in the view of conservative design.

Following changes in pellet design parameters have been investigated to meet the design requirements of the fuel element:

(a) Pellet density:
Pellet average density of present natural uranium is 10.60 g/cc. A new value of 10.50 g/cc is considered in present analysis;

(b) Pellet dish depth:
Average pellet dish depth of 0.50 mm is considered for SEU instead of 0.25 mm.

4. BUNDLE POWER ENVELOP FOR FUEL FOR FUEL OF 0.9% ENRICHMENT

The bundle power envelope up to the proposed design burnup for 0.9% enrichment generated by physics simulations [7] are utilized as an input for FUDA analysis. Thermo-mechanical analysis was performed keeping the peak bundle power as 508 kW for 19-element fuel bundle. This bundle power is 10% higher than the 220 MWe PHWRs operating limit bundle power. The 0.9% enriched 19-element bundle was analysed up to 25 000 MW·d/TeU. The power burnup histories are obtained from physics simulations.

5. OBERSERVATION & DISCUSSIONS

Maximum center line fuel temperatures are found to be 2151°C SEU fuel bundles. This temperature is much less as compared to the limiting condition of uranium oxide melting point.

Decrease in density results in more porosity but less conductivity. More porosity accommodates more gas. However, it also decreases the thermal conductivity which is found to results in enhanced fuel temperature in present study and consequently more fission gas release. The net effect is found to be decrease in fission gas pressure. The clad strain also decreases with decrease in density.

Fission gas pressure for 19-element 0.9% enriched fuel bundle is maintained with in design limits by increasing dish depth due to more space availability for fission gas accommodation. Reduction in gas pressure leads to decreased clad strain for increased dish depth pellets.

The maximum fission gas pressures are also found to be 7.29 MPa and the peak plastic clad strain values are 0.21 respectively. These values are under the design limit.

6. FABRICATION

The SEU fuel bundles were produced as per the drawings and specifications based on the analysis carried out. The production and quality control plans are similar to 19-elemennt NU fuel bundle fabrication being supplied to all the 220 MWe PHWRs. The bundles were inspected visually and with gauges at site before loading into the fuel transfer system [8].

7. PERFORMANCE

Since June 2009, fifty number of SEU fuel bundles of 0.9% ^{235}U isotopic content was loaded in 14 channels of MAPS-2 unit core. These bundles have seen different bundle power histories and recycled from lower flux region to higher flux region. The channels in which SEU bundles are loaded are kept under watch and the DN Counts of these channels are closely observed. Delayed neutron (DN) monitoring of the channels containing these bundles has not shown any variation. Fifteen numbers of bundles have been discharged from the core at average discharged burnup of 16 750 MW·d/TeU. The maximum burnup is achieved around 23 000 MW·d/TeU.

8. CONCLUSION

For the optimum utilization of available uranium resources in the country, the fuel designs and fuel usage strategies are evolved. In addition to natural uranium bundles, SEU bundles have been designed and test irradiation is carried out in MAPS Unit 2. The performance of these bundles in core is satisfactory and it has given a confidence to usage of fuel having high burnup and high fissile content.

REFERENCES

[1] PRASAD P.N, et al, Computer Code for Fuel Design Analysis FUDA MOD 0, NPC Internal Report, NPC-500/F&S/01 (1991).

[2] FUDA MOD-2 manual, NPC-500/DC/37000/08-Rev-0 (1996).

[3] ORIGEN2, Isotope Generation and Depletion Code, Radiation Shielding Information Center, ORNL, USA, Report No. CCC-371.

[4] NOTLEY, M.J.F, A Microstructure Dependent Model for Fission Product Gas Release and Swelling in UO_2 Fuel, Nuclear Engineering and Design **56** (1980).

[5] TRIPATHI, R. M. et al, "Fuel Element Designs for Achieving High Burnups in 220 MWe Indian PHWRs", Technical Meeting on "Advanced Fuel Pellets Materials and Fuel Rod Designs for Water Cooled Reactors ", PSI, Villigen, Switzerland (2009).

[6] MATPRO-Version 11, A hand book of Material Properties for use in the analysis for light water reactor fuel rod behaviour, TREE-NUREG-1009, USNRC (1976).

[7] MISHRA, S, RAY, S, KUMAR, A. N., The Use of Enriched Uranium Fuel in 220 MWe Reactors, NPCIL Report No. PHY220/01100/M/07 (2008).

[8] CHOUHAN, S.K. et al, “Fuel Design for 0.9% SEU use in 220 MWe Indian PHWRs”, Characterization and Quality Control of Nuclear Fuels (CQCNF)-2012, Hyderabad, India (2012).

CRP FUMEX PHWR CASES A BACO CODE POINT OF VIEW AND ITS RESULTS

A. C. MARINO
Comisión Nacional de Energía Atómica (CNEA),
Centro Atómico Bariloche (CAB),
Bariloche, Argentina

Abstract

The BaCo code was developed to simulate the nuclear fuel rods behaviour under irradiation. BaCo is focussed in PHWR fuel and has good compatibility with PWR, BWR, WWER, among others type of fuels (commercial, experimental or prototypes). The code includes additional extensions for 3D calculations, statistical analysis, fuel design and a full core analysis. The main BaCo features in the area of PHWR nuclear fuel design, the BaCo code results of the PHWR cases included in the Coordinated Projects of the IAEA and an overview of the main findings of our participation of those code comparison is presented in this paper.

1. INTRODUCTION

The BaCo code ("Barra Combustible", Spanish expression for "fuel rod") was developed at the end of the 70´s in CNEA ("Atomic Energy National Commission of Argentina") with the purpose of studying the fuel rod behaviour under irradiation conditions [1], [2]. BaCo currently gives the modelling support for the design of advanced PHWR CARA fuel [3] and innovative PWR fuels as the fuel for the CAREM reactor [4]. The confidence in the results regarding the description of the fuel behaviour under irradiation enables the inclusion of the BaCo code in several international fuel code comparison programs as D-COM [5], CRP FUMEX I [6], II and III [7]. Although the development of BaCo was focused on PHWR fuels [8], as CANDU and Atucha ones, the code holds a full compatibility with commercial –as PWR, BWR, MOX [26], and WWER [9], advanced, experimental, prototypes and/or unusual fuels. The BaCo code includes additional tools as the software package for finite elements 3D calculations [10] and the statistical analysis for advanced fuel designs by taking into account the as fabricated fuel rod parameters and their statistical uncertainties [11]. BaCo allows the calculation of a complete set of irradiations as for example the calculation of a full reactor core [12]. It is of crucial importance nowadays to develop a better experimental and theoretical knowledge of the processes related with the evolution of defects and the accumulation of fission products for modelling the fuel behaviour under different operating conditions and the evolution of a spent fuel over long period of time. The current experimental database could be enough to support empirical correlations and modelling for current fuels [13]. Nevertheless, new approaches are required if the actual fuel computer codes will be used to simulate new materials and extreme situations as ultra high burnup. The unavailable data needed for new fuels development will be obtained through a multiscale modelling (M^3), a methodology that will provide the theoretical approach to model the properties of materials through ab initio, molecular dynamics, kinetic Monte Carlo and finite elements calculations over the relevant length and time scales of each method [14], [25].

2. THE BACO CODE

The BaCo code was developed at CNEA for simulating nuclear fuel rods behaviour under irradiation [1], [2]. The development of BaCo is focused on PHWR fuels, as CANDU [8] and Atucha ones [12], under irradiation and during storage conditions [15-17] but, it keeps

a good compatibility with advanced fuel materials, as for example uranium nitride and carbide at least for illustrative and comparative purpose.

BaCo assumes azimuthal bi-dimensional symmetry in cylindrical coordinates for the fuel rod [1]. Although angular coordinates are not considered explicitly, angular dependent phenomenon, as well as radial cracking, are simulated through the angular averaging method [18]. Also axial pellet cracking and relocation are included in BaCo. The hypotheses of axial symmetry and modified plane strains (constant axial strain) are used in the numerical modelling. The fuel rod is separated in axial sections in order to simulate its axial power profile dependence. Rod performance is numerically simulated using finite time steps (finite differential scheme). The modular structure of the code easily allows the description of phenomena observed in the UO_2 pellet and the zircalloy cladding behaviour. The current version of BaCo can be applied to any geometrical dimensions of cylindrical fuel rods mainly with UO_2 pellets (either compact or hollow, with or without dishing) and zircalloy cladding. However, the code allows us to calculate fuel rods with other materials for the pellets and the cladding as metallic uranium, uranium carbide, uranium nitride (for pellets) and silicium carbide (for cladding), at least for illustrative and comparative purpose, due to the simplicity of the modelling of these materials included in BaCo [14], [25].

Advanced features of BaCo

BaCo 3D tools [10], statistical analysis [11], full core calculations [12] and graphical data post-processing improve the code performance and the analysis of the calculations [2].

Although the BaCo code uses a quasi two dimensional approach, the use of several three dimensional (3D) finite element features allow a complementary analysis of 3D properties, as for example the stress-strain state at a specific period of time during the irradiation [10]. The BaCo code results were enhanced by using “ad hoc” tools developed at the MECOM and SyM³ Divisions (Bariloche Atomic Centre, CNEA) [19]. The temperature profile, the crack pattern and the boundary conditions (as the inner pressure, pellet stack weight, etc.), among others, are calculated with BaCo as the input data to the 3D stress strain state and the deformations of the UO_2 pellet.

For a better understanding of the uncertainties and their consequences, the mechanistic approach must therefore be enhanced by the statistical analysis [11]. BaCo includes a probability analysis within their code structure covering uncertainties in fuel rod parameters, in the code parameters and/or into the fuel modelling taking into account their statistical distribution. As consequence, the influence of some typical fabrication parameters on the fuel cycles performance can be analyzed. It can also be applied in safety analyses and economics evaluation to define the operation conditions and to assess further developments. These tools are particularly valuable for the design of nuclear fuel elements since BaCo allows the calculation of a complete set of irradiations.

3. D-COM & CRP FUMEX I

No CANDU cases or PHWR conditions were included in D-COM [5] and CRP FUMEX I [6].

It is valuable to simulate those cases at least up to the low burnup in comparison of the PHWR fuels.

4. PHWR & CRP FUMEX II

CNEA was a participating member of the IAEA Coordinated Research Project (CRP) on "Improvements of models used for fuel behaviour simulation (FUMEX II)" [22] with the BaCo code. This initiative was an international effort to enhance the knowledge on nuclear fuel behaviour.

The CANDU fuels are characterized by short length (about 0.5 m), thin cladding, no plenum, natural UO_2, normal pressure of the filling gas, horizontal position during irradiation, etc. CANDU is an extremely simple fuel (six pieces, four materials and four types of welding). The burnup at EOL of a CANDU fuel is ~7 MW·d/kgU. The cladding is collapsible due to the low thickness of the cladding and the lack of over pressure inside the rod. As for the PWR, the present trends in the CANDU technology includes the increment of the number of fuel rods (decrement of the linear power) and burnup extension (with SEU), as the CANFLEX and CARA fuels [3]. The starting point of a CANDU code is the assumption of a pellet stack with the clad collapsing over the pellets, and as consequence, it loses a full compatibility with PWR fuels. That is not the situation for the BaCo code because it can simulate all situations, i.e., open and closed pellet cladding gap.

The use of CANDU cases in the CRP FUMEX II was a good challenge for all the participants, not only for the COG ("CANDU Owners Group"). The CRP FUMEX II did not include a real case for CANDU fuel and the two selected cases were simplified ones. Those data were prepared by AECL (Canada) as an exercise of fuel design review and participated in the CRP FUMEX II with the ELESTRES code. Those exercises should be understood as a comparison between the codes of AECL and the rest of the participants, in particular Argentina, Korea, India and Rumania.

4.1. Effect of power on the fission gas release (Case 27 -3a-)

The purpose of this computational experiment was to study the effects of linear rating on fission gas release by comparing the differences between codes via parametric studies. The main aim was to identify regions where models differ significantly. The power histories were a series of constant linear powers in the range 10–60 kW/m up to a burnup of 800 MWh/kgU. It is important to note that the calculated pressure arises over a conservative pressure level if we take into account that the coolant pressure is ~12 MPa (Figure 1). The same trends and values were calculated for Profess –BARC– (Fig. 2), START-3 –VNIINM–and ELESTRESS –AECL– [20]. The calculations were inconsistent due to overpressure above a linear power of ~400 W/cm. The best ways to enhance the design of this hypothetic Hi-Bu CANDU fuel is to increase the plenum volume. Nevertheless a CANDU fuel has no plenum. A final conclusion should be that an increment of the rod free volume could be done just with the increment of the dishing volume or with a special design of the end caps.

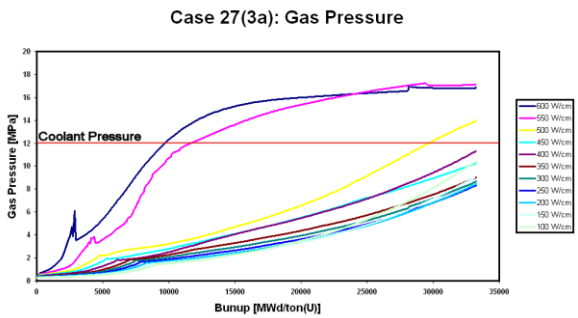

FIG. 1. Internal gas pressure (BaCo, CNEA, Argentina). Coolant pressure as reference.

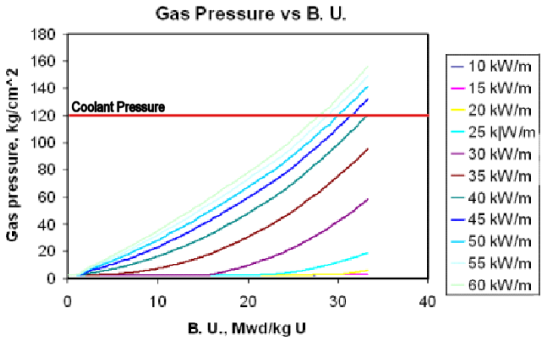

FIG. 2. Internal gas pressure (Profess, BARC, India).

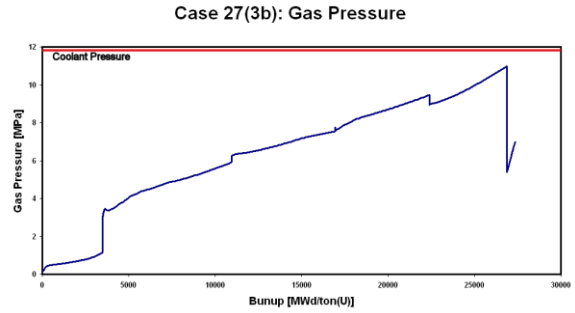

FIG. 3. Internal gas pressure (BaCo, CNEA, Argentina).

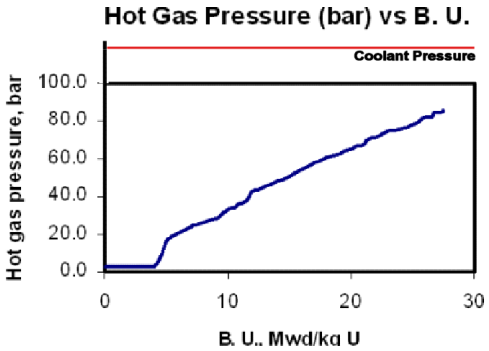

FIG. 4. Internal gas pressure (Profess, BARC, India).

4.2. Effect of power envelope on fuel Performance (Case 27 -3b-)

The objective of this experiment was to examine differences among codes related with the effect of envelope power on fuel performance parameters and the sensitivity to coolant temperature and pressure on fuel during irradiation. The main purposes of this exercise were: to verify that the codes continued showing reasonable trends when element linear ratings changed with time; to identify differences among codes from sensitivity to coolant temperature and pressure; and to analyze the necessary design changes in order to keep the full fuel integrity along the power history. The power history for the second CANDU simplified case was used for fuel design including some power jumps between the nominal design power history and the reference over power envelope. The inner gas pressure was under the coolant pressure value during the irradiation (Fig. 3). The same result was obtained for the Profess code –BARC– (Fig. 4). A low overpressure was calculated for START-3 –VNIINM– and an extreme overpressure for ELESTRESS–AECL– [20].

4.3. Comparison of the simulation of Indian CANDU fuel

A complement of the CRP FUMEX II was carried out with experimental data produced for BARC, India [21]. The fuel of the blind test was a CANDU (a 19 fuel rod bundle irradiated in the Kakrapar Atomic Power Station-I (KAPS-I) up to about 15 000 MW·d/tU and subjected to detailed post-irradiation examination (PIE) in the hot cells facility at BARC).

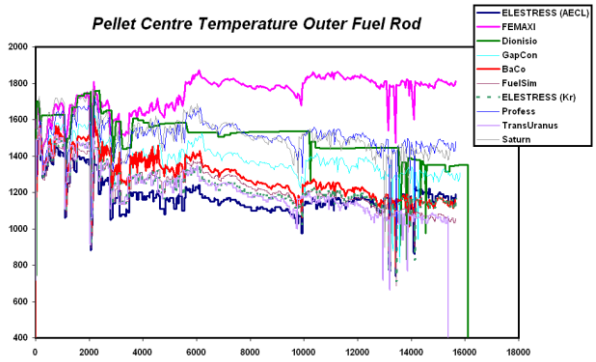

FIG. 5. Code calculations of the pellet centre temperature of an outer fuel rod of the PHWR bundle K1-56504.

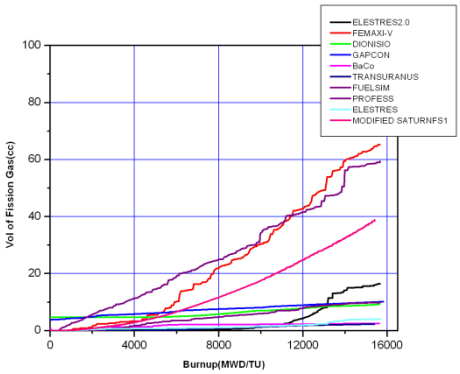

FIG. 6. Code calculations of the volume of fission gas release of an outer fuel rod of the CANDU bundle.

Fig. 5 shows the code simulations results related with the pellet centre temperature versus burnup for the outer fuel rod. The high temperature of the pellet is a consequence of the big diameter of this type of fuels. The results at the EOL are located in a temperature band width of ~700°C. However, the dispersion is only ~400°C if the top curve is disregarded. The increment of the dispersion started at EOL around to ~4000 MW·d/tU. After that value, the dispersion band remains approximately constant.

Fig. 6 shows the volume of the fission gas release (FGR) versus burnup. A great dispersion during the irradiation is observed and an amount of FGR between ~3 to ~65 cm^3 at EOL is obtained. A similar behaviour was observed for the inner gas pressure and a value of ~5 to ~9 MPa [20] at EOL is obtained. The codes with the maximum of FGR are not the same that the codes with the maximum of pressure. That means a different evaluation of the temperature (Fig. 5) and the free volume in the fuel rod.

This exercise is outdated because it was based on an old CANDU fuel with 19 fuel rods. In fact, the present generation of CANDU fuels contain 37 fuel rods (that means a reduction in the linear power) and the projected CANFLEX and CARA [3] fuels are increasing the number of fuel rods, among others improvements.

5. PHWR & CRP FUMEX III

5.1. AECL cases

Prototype CANDU Fuel bundles for the CANDU6 (bundle NR) and Bruce (bundle JC) reactors were irradiated in the NRU experimental reactor at Chalk River Laboratories in experimental loop facilities under typical CANDU reactor conditions, except that they were cooled using light water.

Bundles JC and NR were 37-element fuel assembly prototypes for pressurized heavy water reactor (PHWR). This design utilizes a heavy water moderator and pressurized heavy water coolant. The bundles' elements were coated with a graphite coating. For irradiation in the NRU reactor, the centre fuel element was removed and replaced by a central tie rod for irradiation purposes in the vertical test section. Coolant for the test was pressurized light water under typical PHWR conditions of approximately 9 to 10.5 MPa and 300°C.

No element instrumentation was used during the irradiation. However, the bundle was subjected to extensive Post-Irradiation Examination (PIE) that included dimensional changes, fission gas release, and fuel burnup analysis.

5.2. AECL-JC-bundle

Bundle JC was a prototype 37-element fuel bundle for the Bruce-A Ontario Hydro reactors. The fuel elements used 1.55 wt% ^{235}U in U uranium dioxide fuel and were clad with Zircaloy-4 material. The fuel is somewhat atypical of 37 elements type fuel since the length to diameter ratio (l/d) is large (1.73) due to the pellets being ground down from an outer diameter of 14.3 mm to 12.12 mm. The fuel rod is filled with 90% Ar and 10% He. The outer element burnup averaged approximately 640 MWh/kgU on discharge. Outer element power varied between 57 kW/m at the beginning of life (BOL) to 23 kW/m at the end of life (EOL). Due to the long irradiation, the bundle experienced 153 short shutdowns, and 129 longer duration shutdowns.

5.3. AECL-JC-Bundle during irradiation

Fig. 7 includes the power history of an outer fuel rod of the AECL-JC-Bundle at three axial segments (the fuel length is ~50 cm). The Figure 8 is the BaCo calculations of the fuel pellet centre temperature. It was included the Vitanza threshold in order to take a first approach to the fission gas release (FGR). We find that the curves of temperature for the three axial segments are over the Vitanza threshold. Due to this simple observation we expect a high level of FGR as we observe in the Fig. 9. Fig. 10 includes the evolution of the central hole, the radius of the columnar grains, the equiaxed grains and the zone without restructuring. The Fig. 11 shows the change of the percentage gas composition. The heat transference during irradiation is not optimized due to the use of a 90% of Ar as filling gas. Fig. 12 shows the dynamics of the gaseous fission products inside the fuel rod. We discriminate in this plot the fission gases produced, released, at grain boundary and at the UO_2 matrix following the model of FGR included in BaCo (Hering model). In the Fig. 13, we discriminate the volume of the fission gases released. Fig. 14 shows the inner gas pressure of the fuel rod of the CANDU fuel rod under study and the coolant pressure included as a reference line. The pressure is under the coolant pressure during the entire irradiation as we expect from a conservative point of view.

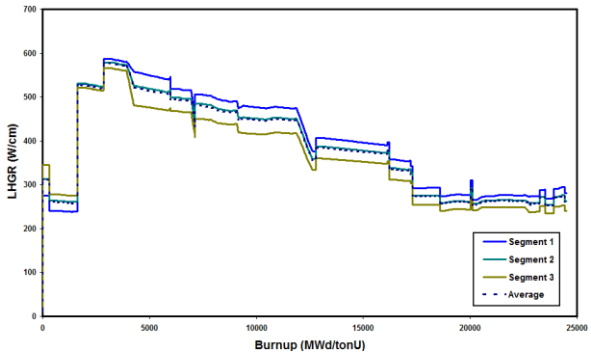

FIG. 7. Linear Heat Generation Rate. Outer fuel rod of the Bundle AECL-JC.

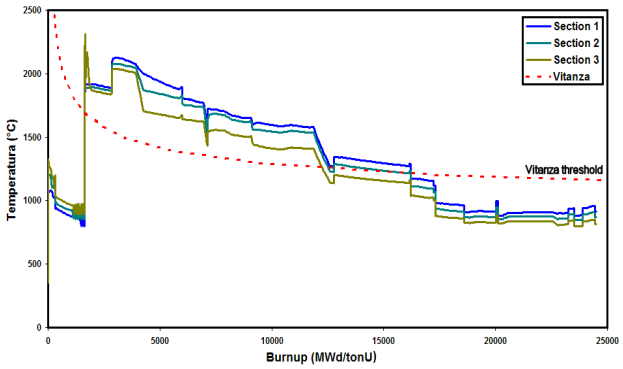

FIG. 8. Fuel pellet centre temperature. Outer fuel rod of the Bundle AECL-JC.

An overview of the mechanical behaviour can be estimated in the Fig. 15 to Fig. 18, where the radius evolution, the pellet cracks opening and the hoop stress are included. Fig. 15 shows the curves of the inner radius of the cladding and the radius of the pellet. We includes the lines of the as fabricated pellet radius and the as fabricated inner cladding radius as a reference. We do not obtain the closure of the gap at BOL ("Beginning of life") like we expect for the CANDU fuels due to the extreme conditions of this experiments. Fig. 16 includes the radial deformation of the outer cladding for the three axial segments of this Bruce CANDU fuel. Most of the cracks were opened during the stage at high power level (Fig. 17). We found stress reversal in the cladding (Fig. 18). The 3D maps of the pellets calculated with BaCo3D are included in the Figure 19 where it were selected: the mesh for the calculation with finite elements, the radial displacements, the von Mises equivalent stress, the hoop stress and the radial profile by using different geometrical points of view in order to illustrate this powerful post processing tool. We obtained the ridge height from this calculation. Those ridges correspond with the most demanding condition –maximum power– and we assume that the cladding is copying the pellet profile, a plastic deformation is done in the cladding and the ridge remains up to EOL. The Table 1 summarized the comparisons between the experimental data and the calculations where a good agreement was found.

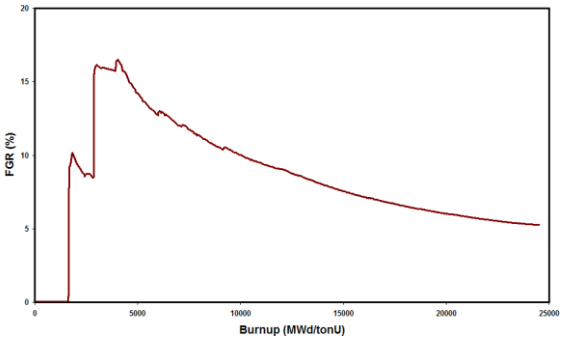

FIG. 9. Fission Gas Release against average Burnup. Outer fuel rod of the Bundle AECL-JC.

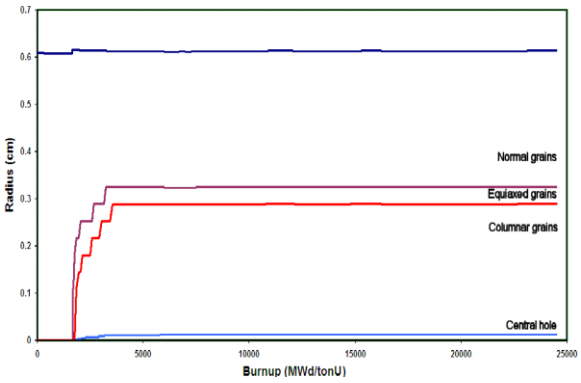

FIG. 10. Grain size evolution. Outer fuel rod of the Bundle AECL-JC.

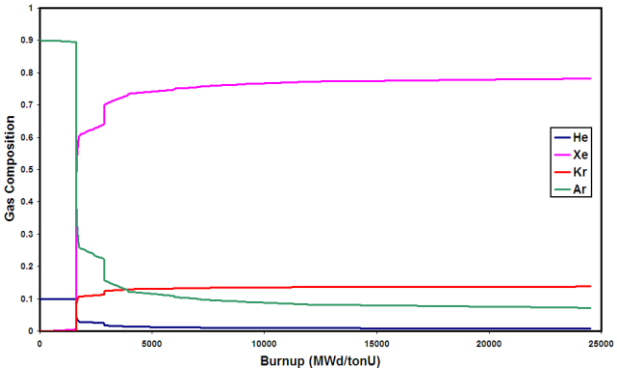

FIG. 11. Relative gas composition versus Burnup. The filling gases were 90% Ar and 10% He.

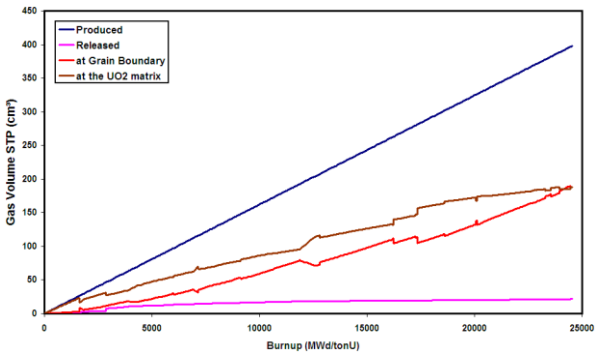

FIG. 12. Fission gases produced, released, at grain boundary and at the UO_2 matrix against Burnup.

TABLE 1. BaCo CALCULATION AND DATA COMPARISON

	AECL JC		AECL NR (plenum: 0 cm³)	
	data	BaCo	data	BaCo
Burnup(av) [MW·d/tonU]	~26600	24500	~26600	24530
FGR(av) [cm³]	~48-60	21 (5.3%)	~39-40	16 (4.0%)
Xe [%]	0.8595	0.784	0.8511	0.769
Kr [%]	0.0753	0.138	0.0993	0.136
He [%]	0.0413	0.0078	0.0496	0.096
Ar [%]	0.0193	0.070	~0.001	-
Diameter(av) [cm]				
up	~1.318	1.3215	~1.311	1.3135
middle	~1.319	1.3523	~1.312	1.3569
lower	~1.318	1.3335	~1.311	1.3237
Length change [mm]	~1.1	1.12	~0.4	0.25
Grain size				
Columnar grain growth fractional radius	~0.47	~0.47	~0.43	~0.41
Equiaxed grain growth fractional radius	~0.56-0.60	~0.53	~0.69	~0.59
Ridge heights [mm]	0,055-0.075	0.045	0.03-0.06	0.04

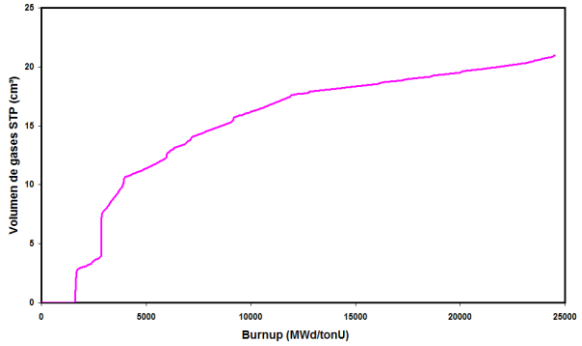

FIG. 13. Volume of fission gases released normalized at STP conditions.

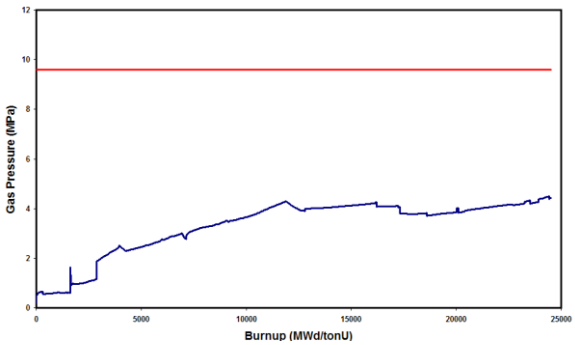

FIG. 14. Inner gas pressure of the fuel rod. Outer fuel rod of the Bundle AECL-JC. Coolant pressure included as a reference line.

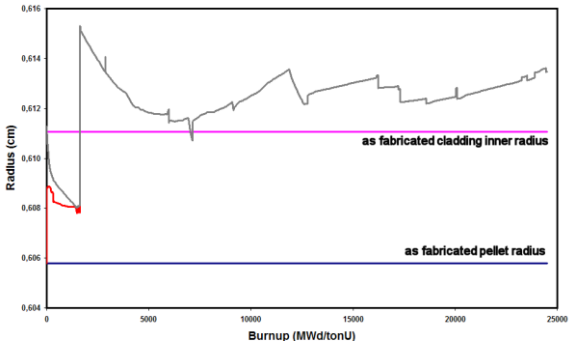

FIG. 15. Pellet and inner cladding radius evolution. Outer fuel rod of the Bundle AECL-JC.

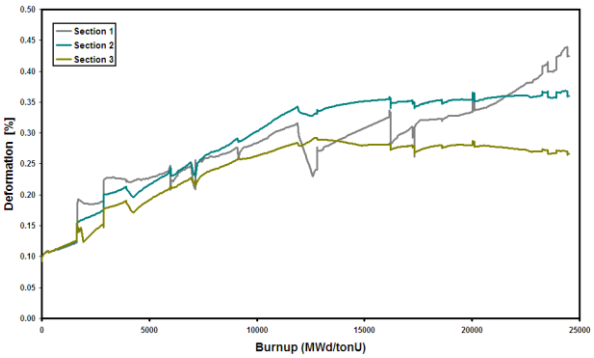

FIG. 16. Outer cladding deformation vs average burnup. Outer fuel rod of the Bundle AECL-JC.

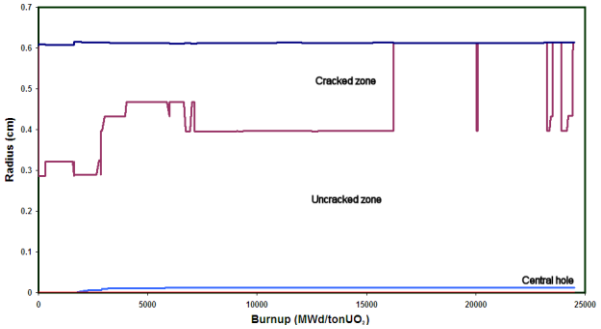

FIG. 17. Cracks opening due to tangential stresses. Outer fuel rod of the Bundle AECL-JC.

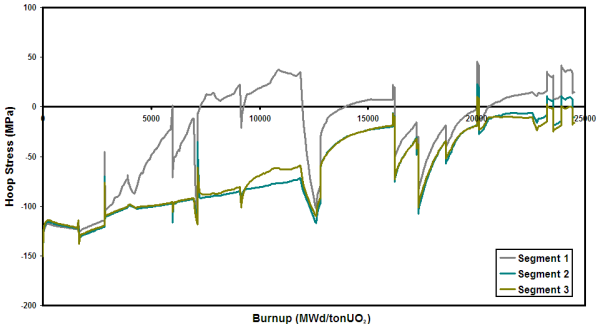

FIG. 18. Hoop stress against average burnup. Outer fuel rod of the Bundle AECL-JC.

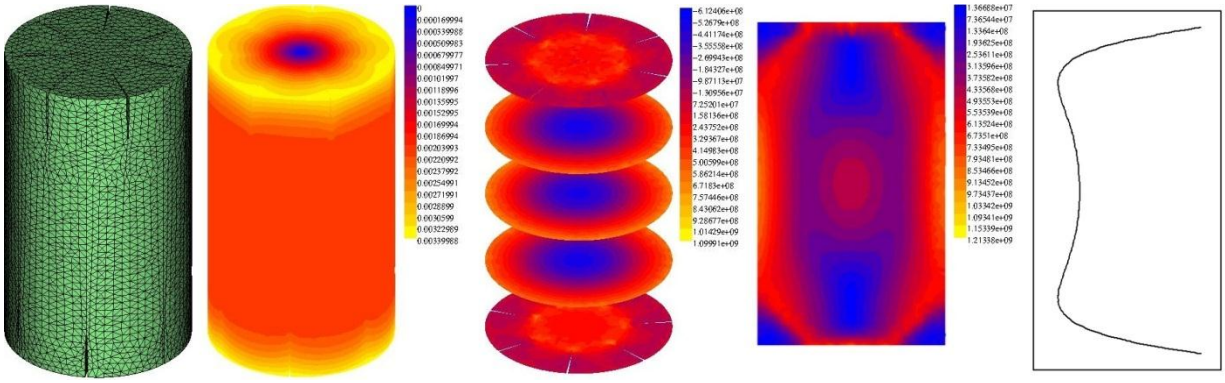

FIG. 19. 3D mesh for finite elements calculation, 3D radial displacement, hoop stress, von Mises equivalent stress and radial profile of the most demanding pellet during the irradiation of the bundle AECL-JC.

5.4. AECL-JC-bundle at dry storage conditions

It is usually accepted that the fuel element must not fail during the operation of the power plant. However, it is emphasized in this work that the fuel integrity must also be kept during the intermediate storage at pools or silos. The simulation of the fuel behaviour under dry storage conditions can be calculated by using the BaCo code as an extension of the normal application of the analysis of nuclear fuel elements under irradiation. The safe conditions of storage, in particular the temperature of the dry storage system, were analyzed and the results are presented in Fig. 20 to Fig. 23.

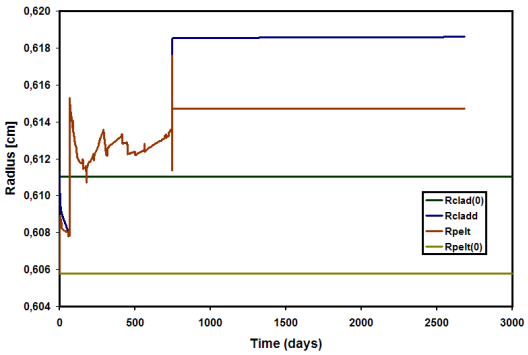

FIG. 20. Pellet and clad inner radius evolution during irradiation and at dry storage conditions. Bundle AECL-JC.

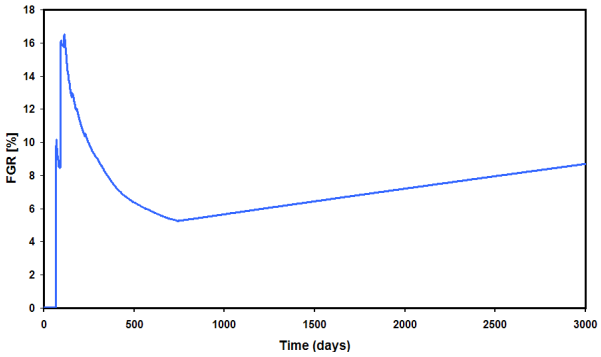

FIG. 21 Fission gas release during irradiation and at dry storage conditions. Bundle AECL-JC.

Fig. 20 shows the evolution of the pellet and cladding radius during irradiation and at the dry storage. We observed the opening of the pellet-cladding gap due to the change of the boundary conditions at EOL; the coolant pressure is present during irradiation and the ambient pressure during storage (approx. 3000 days). Fig. 21 shows the FGR at the same time of the previous plot; it is observed a small release of fission gasses thermally activated. Fig. 22 shows a parametric analysis of the inner gas pressure at four different values of the temperature of the storage device; a statistical analysis is included. The Fig. 23 includes the same analysis for the hoop stress of the cladding of the Bundle AECL-JC.

We found that there is a small increment of stresses and gas pressure into the fuel rod due to a small fission gas release in the presence of the corrosive elements or compounds as I, Cs, CsI, etc. A Stress Corrosion Cracking (SCC) failure could be achieved in the fuel due to the accumulated damage of the cladding during irradiation and the small but constant increment of FGR.

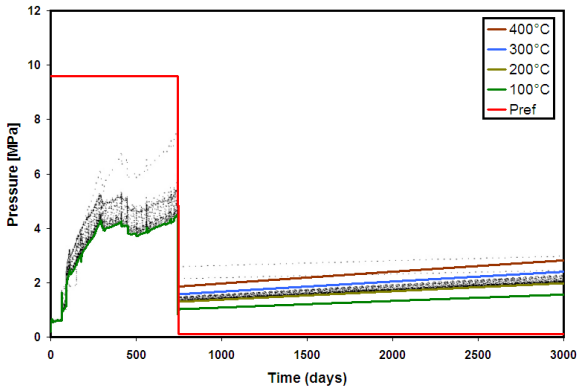

FIG. 22. Fuel rod inner gas pressure during irradiation and at dry storage conditions. Bundle AECL-JC.

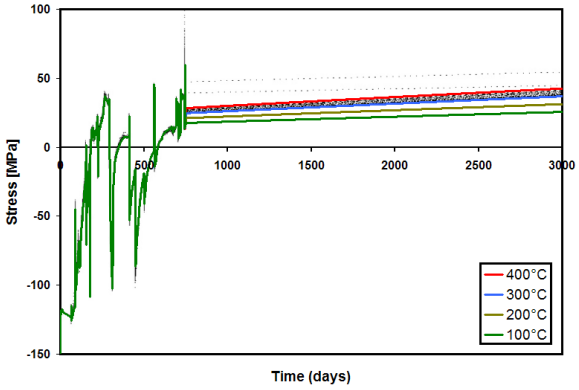

FIG. 23. Hoop stress during irradiation and at dry storage conditions. Bundle AECL-JC.

5.5. AECL-NR-bundle

Bundle NR was a prototype 37-element fuel bundle for the CANDU 600 reactor. The fuel elements used 1.41 wt% ^{235}U enriched UO_2 fuel pellets and were clad with Zircaloy-4 material. Three types of pellet stack to end cap geometries were used for the outer elements: a 350 mm^3 plenum insert (six elements), a 580 mm^3 plenum insert (six elements), and no plenum insert (six elements). Intermediate and inner element rings had no plenum insert. Outer element burnup reached average measured burnup of 235 MWh/kgU. Outer element powers were steady during the irradiation and ranged between 58 and 62 kW/m during the irradiation. The fuel rod is filled with 100% He.

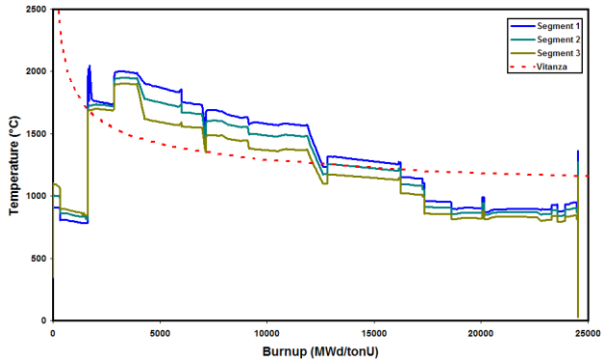

FIG. 24. Fuel centre temperature of an outer rod (with no plenum) of the AECL-NR bundle at three axial sections.

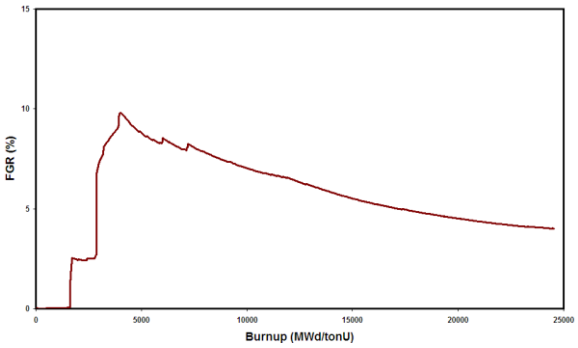

FIG. 25. Fission Gas Release against average Burnup. Outer fuel rod of the Bundle AECL-NR with "no plenum".

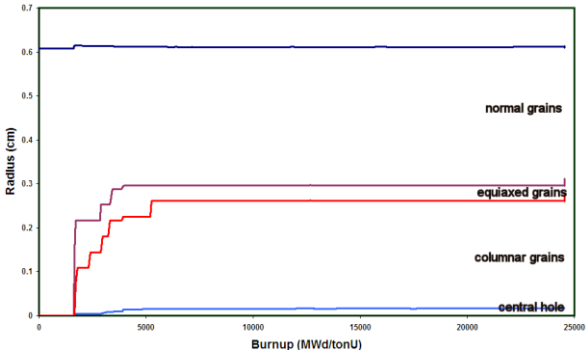

FIG. 26. Grain size evolution. Outer fuel rod of the Bundle AECL-NR without a plenum.

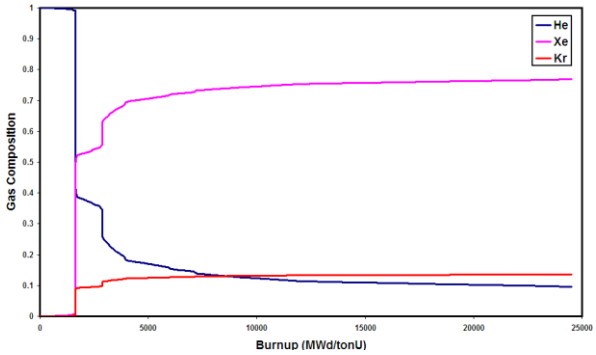

FIG. 27. Relative gas composition versus Burnup. The filling gas was 100% He.

5.6. AECL-NR-bundle under irradiation

The filling gases used for the fuels AECL-JC and AECL-NR are the origin of the main differences of the behaviour during irradiation between both fuels. The analysis is focused in the fuel rod without plenum because that is the most demanding condition for the fuel and this is the most realistic one due to the difficulties to design a CANDU fuel rod with a plenum in order to accommodate the FGR at high burnup. Fig. 24 shows the pellet centre temperature of this fuel. We find a difference of approximately 200°C with previous fuel rod (AECL-JC Bundle –with "no plenum"). By a simple comparison of the Vitanza curve of both fuels we can advise that the FGR of the AECL-NR fuel releases less gas than the AECL-JC (Fig. 25) and less growing of columnar grains (Fig. 26). The change of the filling gasses composition is included in the Fig. 27. The volume of FGR is less than the previous fuel rod due to the reduction of temperature (see the Table 7 and the Fig. 28 where the curve with the volume of FGR is included). The FGR calculated by the BaCo code was under the experimental value nevertheless the set of calculations for the AECL bundle are consistent (Table 7).

The inner gas pressure in the outer fuel rod of the bundle AECL-NR –"no plenum"– is in the Fig. 29 where the value of the coolant pressure is included as a reference line. We find overpressure at 13 000 MW·d/tonU. The measurement of the pressure could be valuable. The usual CANDU fuel accepts by design a small overpressure at EOL but the normal fuel uses natural Uranium and the discard burnup is 7500 MW·d/tonU. Here we have a different situation due to the extension of burnup and the absence of a plenum in order to accommodate the fission gases. A plenum at the right and/or the left of the fuel rod (CANDU fuel is placed inside horizontal channels) is not a practical issue for a commercial CANDU fuel because we will find end peaking in the interface between fuel elements.

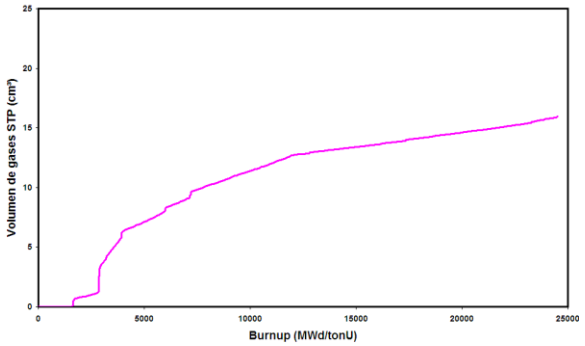

FIG. 28. Volume of fission gases released in the fuel rod without plenum of the bundle AECL-NR.

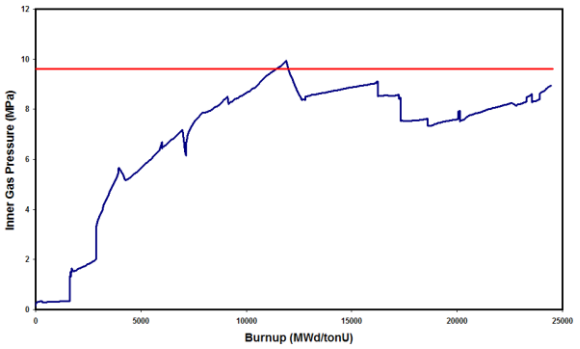

FIG. 29. Inner gas pressure of the fuel rod. Outer fuel rod of the Bundle AECL-NR –"no plenum"–. Coolant pressure included as a reference line.

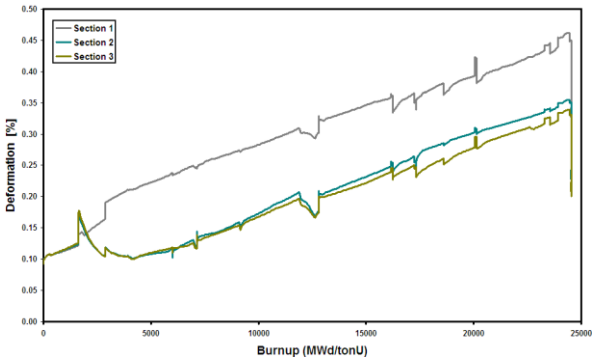

FIG. 30. Outer cladding deformation vs average burnup. Outer fuel rod of the Bundle AECL-NR.

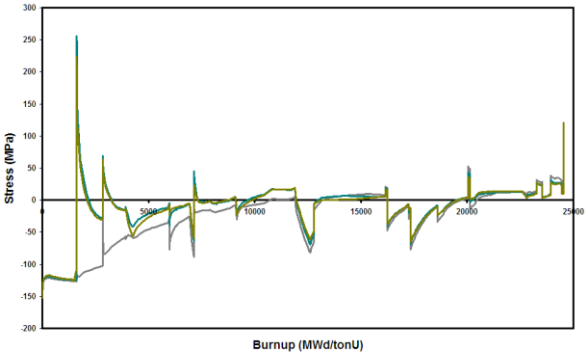

FIG. 31. Hoop stress against average burnup. Outer fuel rod of the Bundle AECL-NR.

Fig. 30 includes the radial deformation of the outer cladding for the three axial segments of this CANDU6 fuel. More events of stress reversal are found in the bundle AECL-NR (Fig. 31).

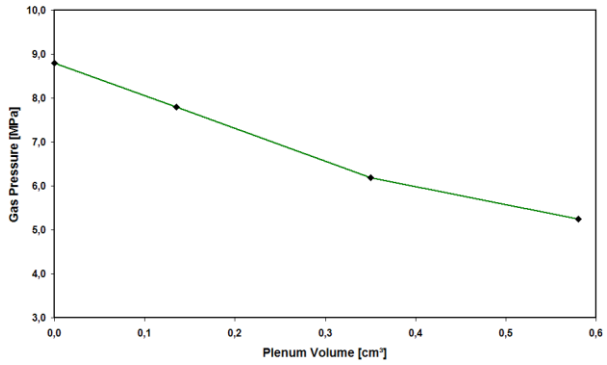

FIG. 32. Gas pressure at EOL of the rods of the AECL-NR Bundle –a parametric analysis of the volume of the plenum–.

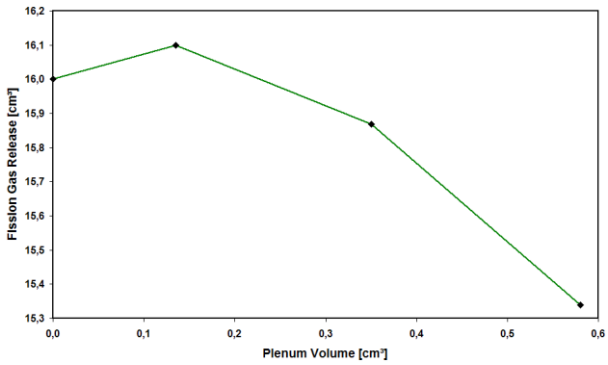

FIG. 33. FGR at EOL of the rods of the AECL-NR Bundle –a parametric analysis of the fission gas release–.

5.7. AECL-NR-bundle parametric study

It is mandatory to define a way to reduce the high value of the inner pressure for these fuel rods. The usual way is to increase the volume of the plenum and that is not easy for CANDU fuels. The experiments were done with the inclusions of two types of fuel rods in the same bundle with a plenum of 350 mm^3 and 580 mm^3. We include a forth calculation with a plenum of 135 mm^3 for an illustrative purpose. Fig. 31 shows the strong reduction of the gas pressure obtained by the increment of the volume of the plenum accompanied for a small reduction of FGR (Fig. 33).

5.8. Behaviour of advanced Argentinian fuels

The advanced fuels under development in Argentina are the CARA [3] fuel and the fuel for the CAREM reactor [4]. The main goal of the CARA fuel is the increment of the number of rods of the fuel assembly. It will produce a decrement in the linear power of a fuel rod as a consequence of the reduction of each fuel rod diameter by keeping constant the total fuel material of the original design of the fuel assembly. The first result is a strong reduction of the fuel pellet temperature. The CAREM fuel assembly has thin fuel rods by design. The BaCo code shows several benefits in the safety and performance of the fuel assembly if the temperature at the pellet centre remains below 1400ºC. Those advantages are: no central hole, no columnar grains, decrement of the FGR, less thermal expansion, reduction in the fuel deformations, no plastic behaviour in the centre region of the pellet, an increment of the pellet cracking with cracks crossing the pellet, increment of the effective pellet radius due to the relocation of pellet fragments, etc. The fuel pellets structure become more uniform but high stresses can be find at the cladding when PCI is attained because a plastic state enough to allow the release of the fuel rod stresses is not achieved in the inner region of the pellet. Those results are among the main findings obtained with the BaCo code when it simulates the expected behaviour of the CARA fuel [3] and of the CAREM reactor fuel [4]. The previous results with the code could be done by the analysis of following plots. Fig. 34 shows the ultimate tensile stress and the elastic limits of the UO_2 by taking into account the range of temperature of operation of several fuel rods. Fig. 35 shows the thermal conductivity of the UO_2 by using the same fuels and range of temperatures.

6. CONCLUSIONS

This work describes briefly the main features of BaCo, as for example: the 3D tools, the statistical analysis, and data post-processing in order to improve the code's performance and the analysis of the results. The modular structure of BaCo easily allows the inclusion of new models and material properties.

The D-COM and the IAEA CRP FUMEX I did not include CANDU cases. Nevertheless, from the point of view of the CANDU fuels, it is valuable to simulate those cases at least up to the low burnup in comparison of the PHWR fuels.

In this work, the BaCo code was applied to simulate the fuel rod behaviour in two selected examples from the IAEA CRP FUMEX II and two strong cases of the 3rd edition of the CRP FUMEX. The first test of the CRP FUMEX II presented in this work was an irradiation computational experiment related with the design of an advanced CANDU fuel. The second one was a comparison between a real experiment of irradiation and the results of BaCo simulations. It is clearly shown the difficulties to obtain a complete set of experimental data in order to cover the development and validation of the fuel behaviour modelling.

The simulations of the PHWR cases of the CRP FUMEX III show the difficulties of the CANDU technology in order to accommodate the FGR at high burnup. It is not easy to design a plenum in the fuel rods without an increment of the end peaking. The results obtained by using the BaCo code are acceptable. We have an under prediction for the FGR by the present modelling of the fission gas release used in the code. We are not including specific issues of high burnup then we obtain a low value of the FGR wit BaCo. A good thermal performance was attained by the code as we observe in the evaluation of the grain structure of the UO_2 pellets. Good results were found for the mechanical issues. We presented the most demanding PHWR case in order to reduce the extension of this analysis.

It is remarkable that one of the CRP FUMEX III cases were a MOX fuel experiment of an Argentinian fuel and that experiment of irradiation were prepared by using the BaCo code [26].

Finally, we are finding that the decrement of the linear power by the reduction of the fuel diameter could lead to a fuel pellet completely brittle with a small capacity to reduce stresses by creep and plastic deformation and to increase the PCI.

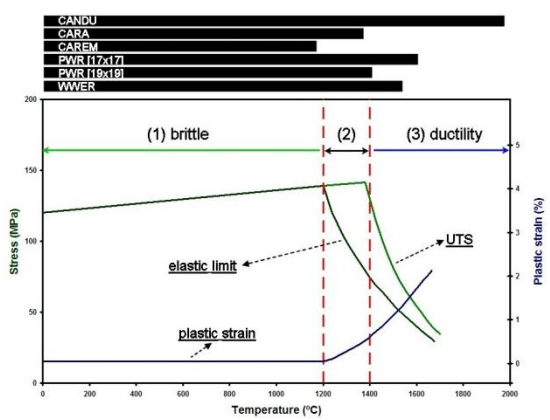

FIG. 34. Fracture and flow characteristics of UO_2 as a function of temperature. At the top the ranges of fuel centre temperature of various fuels are included [23].

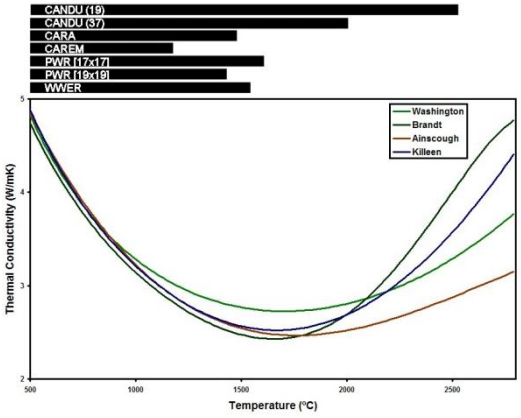

FIG. 35. Modelling the thermal conductivity of UO_2 as a function of temperature [24].

REFERENCES

[1] MARINO, A.C., et al., BaCo (BArra COmbustible) Code Version 2.20: a thermomechanical description of a nuclear fuel rod, Journal of Nuclear Materials, **229** 155 (1996) 168.

[2] MARINO, A.C., "Starting Point, Keys and Milestones of a Computer Code for the Simulation of the Behaviour of a Nuclear Fuel Rod", Science and Technology of Nuclear Installations, Article ID 326948 (2011).

[3] BRASNAROF, D O., et al, "A New Fuel Design for Two Different HW Type Reactors", Science and Technology of Nuclear Installations, Article ID 194650 (2011).

[4] BOADO, M.H., et al, "CAREM Projects Status", Science and Technology of Nuclear Installations, Article ID 326948 (2011).

[5] MISFELDI I., "The D-COM blind problem on fission gas release," IAEA, International Working Group on Fuel Performance and Technology for Water Reactors, OECD-NEA CSNI/IAEA Specialist's Meeting on Water Reactor Fuel Safety and Fission Products Release in Off-Normal and Accident Conditions, RISØ National Laboratory, IWGFTP/16 (1983).

[6] INTERNATIONAL ATOMIC ENERGY IAEA, Report of the Coordinated Research Programme on Fuel Modelling at Extended Burnup - FUMEX, 1993 1996, IAEA TECDOC-998.

[7] KILLEN, J., et al, "Fuel modelling at extended burnup: IAEA coordinated research project FUMEX-II" Proc. International LWR Fuel Performance Meeting, Top Fuel 2006, Salamanca, Spain (2006).

[8] MARINO, A.C., "Computer simulation of the behaviour and performance of a CANDU fuel rod" Proc. 5th International Conference on CANDU Fuel, Toronto, Canada (1997).

[9] MARINO, A.C., "An approach to WWER fuels with BaCo", Proc. 7th International Conference on WWER Fuel Performance, Modelling and Experimental Support, Albena, Bulgaria, (2007).

[10] DEMARCO, G.L., MARINO, A.C., "3D Finite Elements Modelling for Design and Performance Analysis of UO_2 Pellets", Science and Technology of Nuclear Installations, Article ID 843491 (2011).

[11] MARINO, A.C. et al, "Sensitivity analysis applied to nuclear fuel performance related to fabrication parameters and experiments" Proc. 14th International Conference on Structural Mechanics in Reactor Technology, Lyon, France (1997).

[12] MARINO, A.C. et al, High power ramping in commercial PHWR fuel at extended burnup," Nuclear Engineering & Design, **236** 1371 (2006) 1383.

[13] TURNBULL, J.A. et al, "Experimental data on PCI and PCMI within the IFPE database," Proc. International Seminar on Pellet-Clad Interaction in Water Reactor Fuels (PCI '04), Aix-en-Provence, France (2004).

[14] MARINO, A.C. et al, Proc. "Present and Future Trends in PHWR Fuel Material Modelling with the BaCo code", 21st International Conference on Structural Mechanics in Reactor Technology, (SMiRT 21), New Delhi, India (2011).

[15] MARINO, A.C., "PHWR fuel rod behaviour during dry storage", Proc. of the Water Reactor Fuel Performance Meeting, (WRFPM) Paris, France (2009).

[16] MARINO, A.C., "CANDU Fuel Rod Behaviour during Dry Storage", Proc. 11th International Conference on CANDU Fuel, Niagara Falls, Ontario, Canada (2010).

[17] MARINO, A.C., "An overview of the dry storage of nuclear fuels with the BaCo code" Proc. 8th International Conference on WWER Fuel Performance, Modelling and Experimental Support, Helena Resort near Burgas, Bulgaria (2009).

[18] MARINO, A.C., “Crack and dishing evolution models and PCI-SCC considerations for fuel pellets in a quasi-bidimensional environment”, Proc. International Seminar on Pellet-Clad Interaction in Water Reactor Fuels, Aix en Provence, France (2004).
[19] BUSCAGLIA, G. et. al., “Un programa general de elementos finitos en paralelo”, Proc. 6to Congreso Argentino de Mecánica Computacional, MECOM’99, Mendoza, Argentina (1999).
[20] MARINO, A.C. et al., “PHWR fuel rod modelling: a BaCo code point of view”, IAEA Technical Meeting on PHWR Fuel Design, Fabrication and Performance, Buenos Aires, Argentina (2009).
[21] SAH, D.N. et al., “Blind prediction exercise on modelling of PHWR fuel at extended burnup”, Nuclear Engineering & Design **383** 144 (2008) 149.
[22] KILLEEN, J. et al., “Fuel Modelling at Extended Burnup: IAEA Coordinated Research Project FUMEX-II”, 2006 International Meeting on LWR Fuel Performance, “NUCLEAR FUEL: Addressing the future”, Top Fuel 2006, 2006, Salamanca, Spain (2006).
[23] OLANDER, D.R., Fundamental Aspects of Nuclear Reactor Fuel Elements, Energy Research and Development Administration, USA (1976).
[24] MARTIN, D.G., A re-appraisal of the thermal conductivity of UO_2 and mixed (U, Pu)O_2 fuels, Journal of Nuclear Materials **110** 73 (1982) 94.
[25] MARINO, A.C. et. al., “Simulation of Nuclear Materials and Fuels by using the BaCo code and Multiscale Modelling of Materials (M³)”, Proc. Water Reactor Fuel Performance Conference (TopFuel 2012) Manchester, United Kingdom (2012).
[26] MARINO, A.C., ADELFANG, P., PEREZ, E. E., Irradiation of Argentine MOX fuels. Post-irradiation results and experimental analysis with the BACO code, Journal of Nuclear Materials **229**, 169 (1996) 186..

THREE DIMENSIONAL FINITE ELEMENT MODELLING OF A CANDU FUEL PIN USING THE ANSYS FINITE ELEMENT PACKAGE

A. F. WILLIAMS
AECL,
Chalk River Laboratories,
Chalk River, Ontario,
Canada

Abstract

The ANSYS finite element modelling package has been used to construct a three-dimensional, thermomechanical model of a CANDU fuel pin. The model includes individual UO2 pellets with end dishes and chamfers, and a Zircaloy-4 fuel cladding with end caps. Twenty node brick elements are used with both mechanical and thermal degrees of freedom, allowing for a full coupling between the thermal and mechanical solutions under both steady state and transient conditions. Each fuel pellet is modelled as a separate entity that interacts both thermally and mechanically with the cladding and other pellets via contact elements. The heat transfer between the pellets and cladding is dependent on both the interface pressure and temperature, and all material properties of both the pellets and the sheath are temperature dependant. Spatially and temporally varying boundary conditions for heat generation and convective cooling can be readily applied to the model. The model naturally exhibits phenomena such as pellet hour glassing and ridging of the cladding at the Pellet to pellet interfaces, allowing for the prediction of localized sheath stresses. The model also allows for the prediction of fuel pin bowing due to asymmetric thermal loads and fuel pin sagging due to overheating of the cladding, which may occur under accident conditions.

1. INTRODUCTION

One of the greatest challenges in modelling ceramic zircaloy clad nuclear fuels is the strong interaction between the thermal and mechanical behaviour via the pellet-to-clad heat transfer coefficient. This is especially true of CANDU fuels which have a relatively thin zircaloy cladding of around ~0.4 mm, and under normal operation the coolant system pressure causes this zircaloy sheath to collapse into contact with the fuel pellet, enhancing the heat transfer from the fuel. Up until recently, limitations in computing power have restricted fuel models to one dimension (radial). While some computer codes, such as the CANDU fuel analysis code ELESTRES [1], have included limited two-dimensional capability to account for the hour glassing of the fuel pellets, this capability was not fully coupled to the thermal solution.

Now, however, computing power and the capabilities of commercially available finite element modelling tools have reached a stage where it is feasible to construct a detailed three dimensional model of a CANDU fuel pin, which fully captures the local variations in heat transfer due to pellet hour glassing. Such a 3D model also allows for the modelling of other phenomena, such as fuel pin bowing due to dry out under off-normal conditions. These models have the advantage in that the individual pellets are modelled as separate entities that interact with each other and the sheath via contact elements, making it unnecessary to make approximations and assumptions about the composite behaviour of the assembly. The model described here was constructed using ANSYS 13.0.

2. GEOMETRY, ELEMENTS AND MESHING

The CANDU fuel geometry has evolved over time, but the basic geometry and features have remained constant. To aid application of the model to different fuel designs, a reference model was created and meshed in such a way that the node coordinates may be readily scaled to the desired fuel geometry. The model includes all the geometric features of a fuel pellet,

such as the dishes and chamfers. The dishes and chamfers are added to the cylindrical fuel pellet to allow for thermal expansion and reduce ridging of the sheath due to pellet hour glassing. Fig. 1 shows the mesh for a typical pellet with dishes and chamfers included.

FIG. 1. Meshed pellet with dish and chamfer.

The simulations presented here are for a fuel pin of the type used in 37-element bundles. The model consists of individual cylindrical fuel pellets surrounded by a thin fuel sheath sealed with an end cap. The fuel stack is approximately 480mm long with an outside diameter of 12mm. The fuel pellets are approximately 15.5mm long with dishes, but no chamfers.

Both the pellet and the sheath are meshed with twenty node hexahedral finite elements of ANSYS type SOLID226. This element type has the advantage of having both mechanical and thermal degrees of freedom, allowing for direct coupling between the thermal and mechanical solutions. For this model, planes of symmetry are assumed to cut the pin transversally at the midpoint (z=0 plane) and vertically along the longitudinal axis (x=0 plane), as shown in Fig. 2. Fig. 3 shows details of the fuel pellet and sheath mesh. Note that there are three elements across the thickness of the sheath.

Pellet to pellet and pellet to sheath interactions are handled using surface to surface contact and target elements (type CONTA174 and TARG170). These elements are able to transfer both thermal and mechanical loads between components (see Section 4).

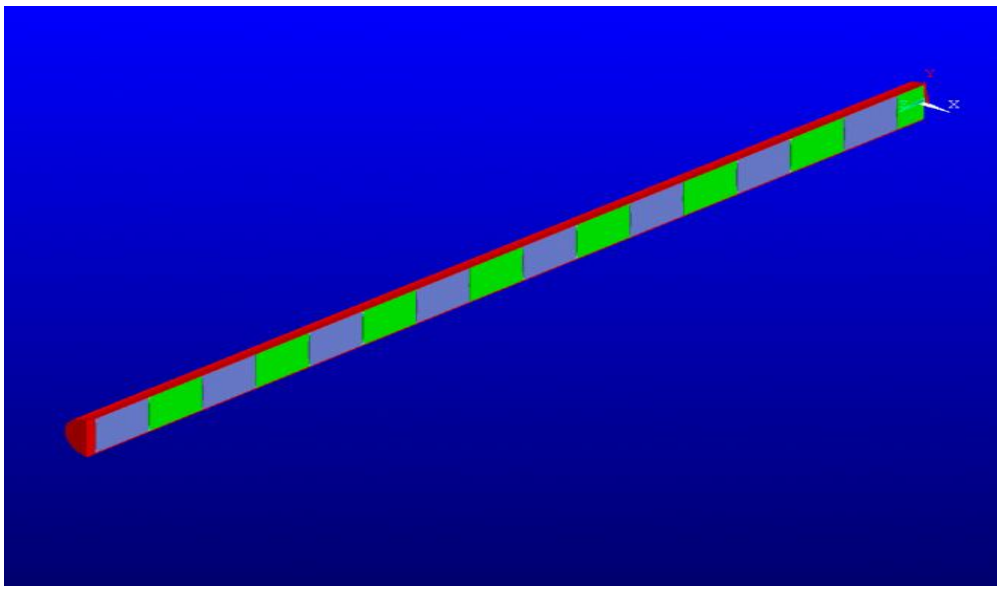

FIG. 2. Schematic of the fuel pin.

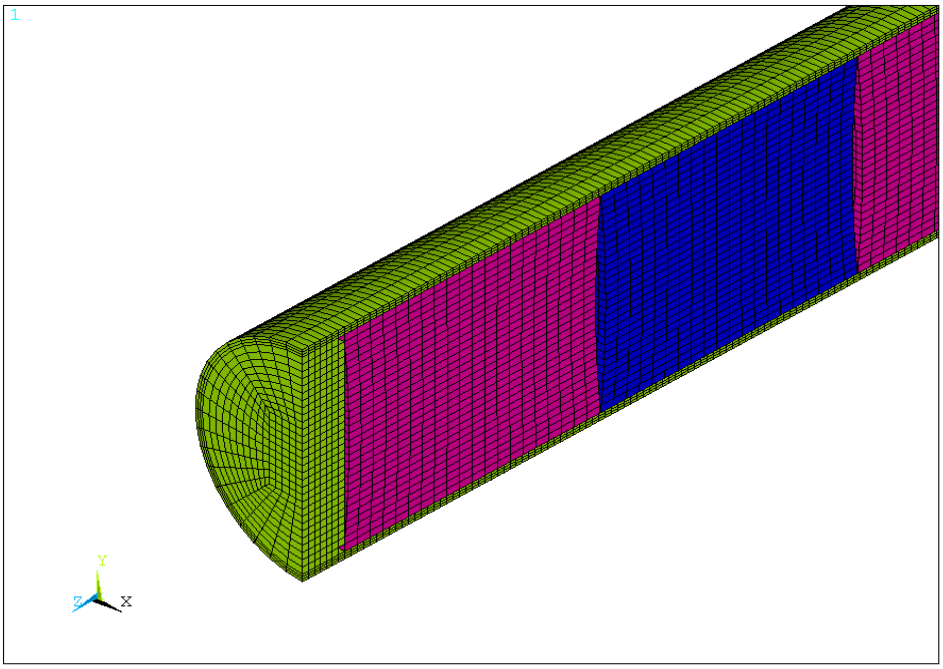

FIG. 3. Detail of the mesh for the pellets, sheath, and end caps.

3. MATERIAL PROPERTIES

The material properties models used are generally temperature dependant and are based on the models currently used in the Canadian Industry Standard Toolset (IST) codes ELESTRES [1] and ELOCA [2]. Relevant material properties include thermal conductivity, specific heat capacity, thermal expansion and Young's modulus for both the UO_2 fuel and the

Zircaloy-4 sheathing. The ELOCA code uses a micro-structure based deformation model [3] for Zircaloy-4 that could not be readily incorporated into the ANSYS model. Instead, a bilinear plasticity model is used and was derived from the viscoplastic model described in the Matpro handbook [4]. Typical stress/strain curves for this model are shown in Fig. 4. Fig. 5 shows the yield stress as a function of the temperature derived from the Matpro model. The tangent modules (Fig. 6) was defined as ultimate tensile strength (UTS) - yield stress/strain at UTS – strain at yield, i.e., the average gradient of the stress strain curve following yield.

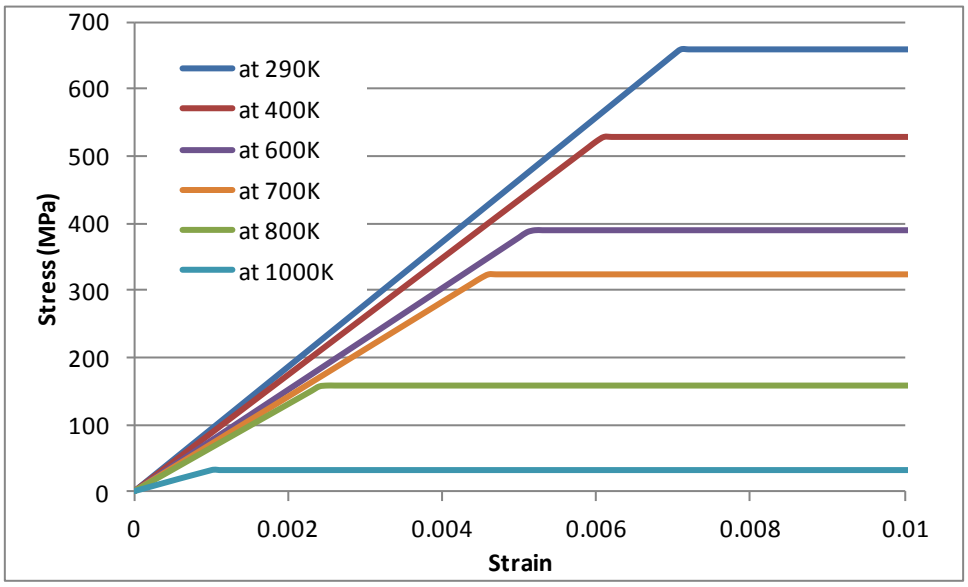

Fig. 4. Bilinear model of zircaloy plasticity.

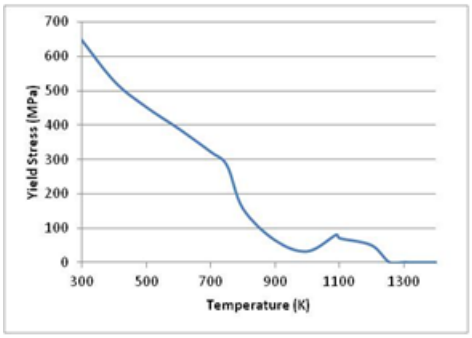

FIG. 5. Zircaloy yield stress (MPa)

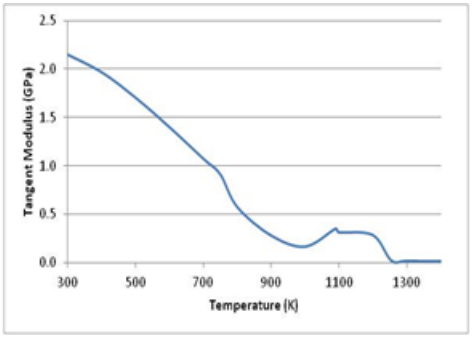

FIG. 6. Zircaloy tangent modulus (GPa)

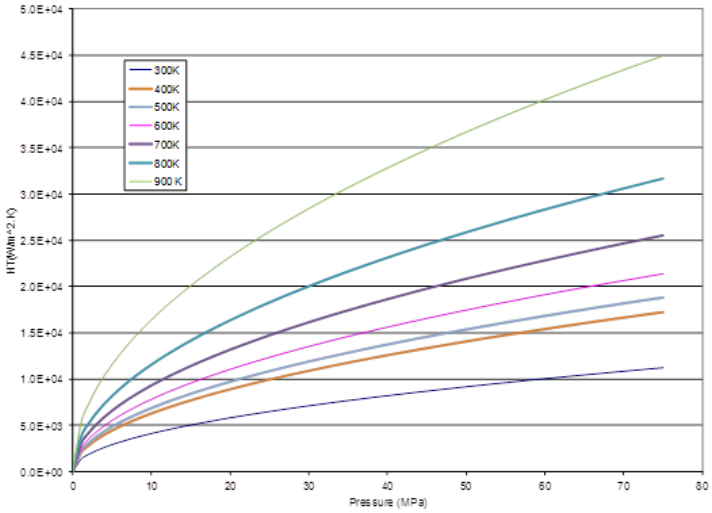

FIG. 7. Fuel-to-sheath heat transfer coefficient

4. CONTACT MODELLING

An important feature of this model is the ability to simulate the thermal and mechanical interactions of the separate components, i.e. the interaction between each pellet and the sheath, and neighbouring pellets. This is achieved using contact and target elements (ANSYS types CONTA174 and TARGE170) between the components. The interface pressure between contacting surfaces is determined using the "augmented Lagrange" option, which is a commonly used penalty-based method documented in the ANSYS user's manual. In general the ANSYS contact model defaults are used including a penalty stiffness factor of 1.0.

The heat transfer between the contacting surfaces is dependent on the contact pressure between the surfaces and the temperature of the contact surfaces. This relationship is defined in the ANSYS model using a lookup table and is shown graphically for several temperatures in Fig. 7. These values are derived from the fuel to sheath heat transfer model currently used in the ELESTRES [1] and ELOCA [2] codes.

5. BOUNDARY CONDITIONS

One of the many advantages of using a commercial finite element package is the flexibility and ease of application of the boundary conditions to the model. For slowly varying conditions such as those experienced by the fuel under normal operation, a steady state solution method may be used which assumes that the fuel pin is in thermal and mechanical equilibrium at all times. Under the fast changing conditions typical of an accident, a fully transient solution method is available.

Spatially and temporally varying boundary conditions applied to this model include, volumetric heat generation rates (including the ability to account for flux depression), convective and radiative heat transfer from the sheath surface to the coolant, external pressure on the outer surface of the sheath (i.e. the system coolant pressure), and mechanical restraints to simulate the attachment points of the pin in the fuel bundle assembly. An internal pressure may also be applied to the sheath to simulate the build-up for internal fission gas (later it is hoped to link this directly to a fission product source term model). Application of a global

gravitational field also allows for the simulation of high temperature slumping. The effects of fuel pin deformation due to localised dry out patches on the sheath surface may also be simulated by applying a localised reduction in the convective heat transfer coefficient, or by directly applying sheath surface temperatures as a boundary condition.

6. EXAMPLE RESULTS

Because of the wide range of possible application of this model, it is difficult to illustrate the full potential within a short paper; however the following figures show how the model captures many of the phenomena observed in irradiated fuel, including hour glassing of the pellets due to the radial temperature gradient. The figures shown here are for a fuel pin operating at a steady state linear power of approximately 35 kW / m with a system pressure of 10 MPa and coolant temperature of 600 K.

Fig. 8 shows the fuel temperatures corresponding to these conditions. Fig. 9 shows the hoop strain in both the pellets and the sheath due to the thermal expansion of the pellets.

Fig. 10 also shows the hoop strain in the pellet, and illustrates the effects of pellet hour-glassing, which causes high hoop strains in the sheath at Pellet to pellet interfaces. These strains have been known to result in stress corrosion cracking and failure of the sheath at the Pellet to pellet interfaces. Fig. 11 illustrates the resulting impact of pellet hour-glassing on the sheath; a phenomenon sometimes called “bambooing”.

Fig. 12 shows the contact status of the contact elements. Note that friction prevents the sheath from sliding against the pellets in areas where the contact pressure is high.

Fig. 13 shows the interface pressure between the pellets and the sheath, (the grey annulus at the Pellet to pellet interface is a region of very high interface pressure where the dished pellets contact each other).

Fig. 14 illustrates how the interface pressure influences the heat transfer. Note that heat flow from the pellet to sheath is negative.

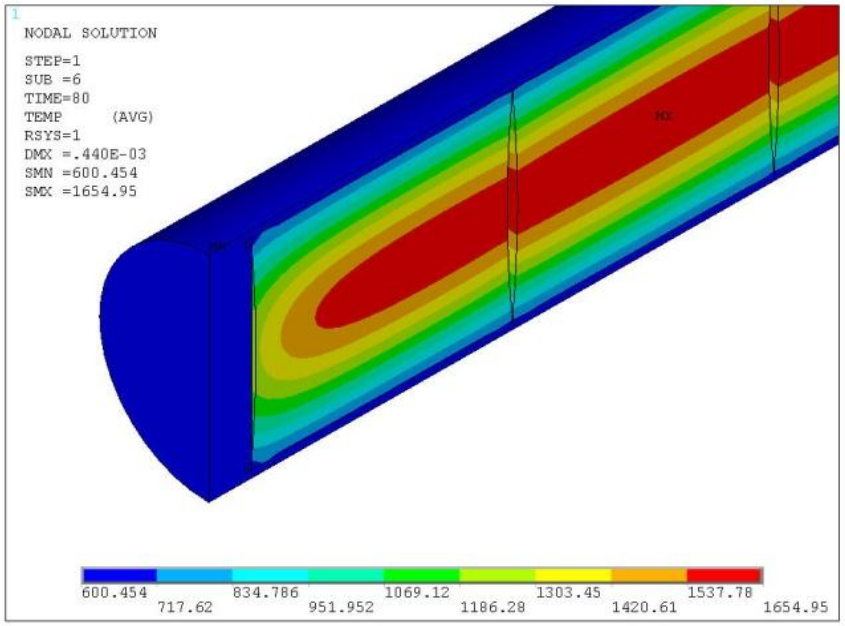

FIG. 8. Fuel temperatures (K).

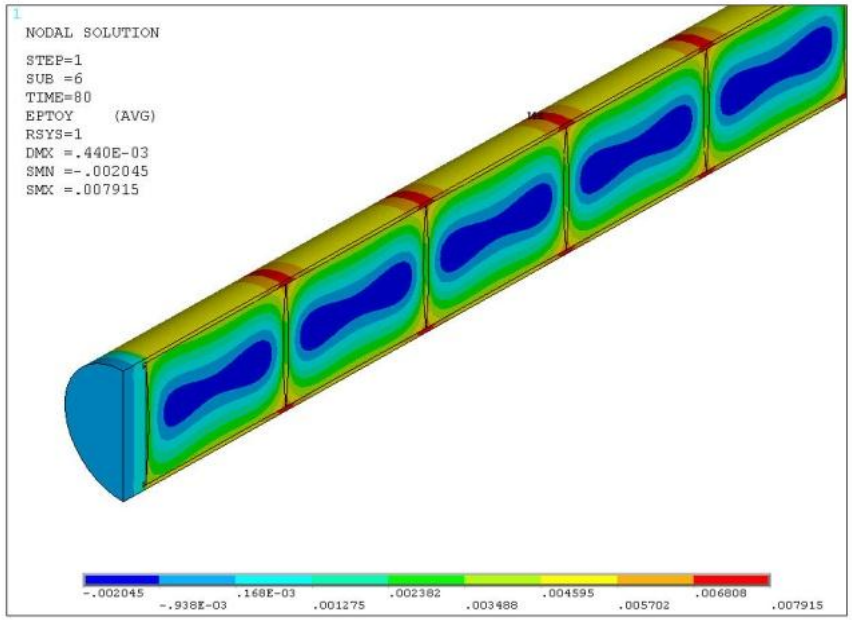

FIG. 9. Hoop strain in pellets and sheath.

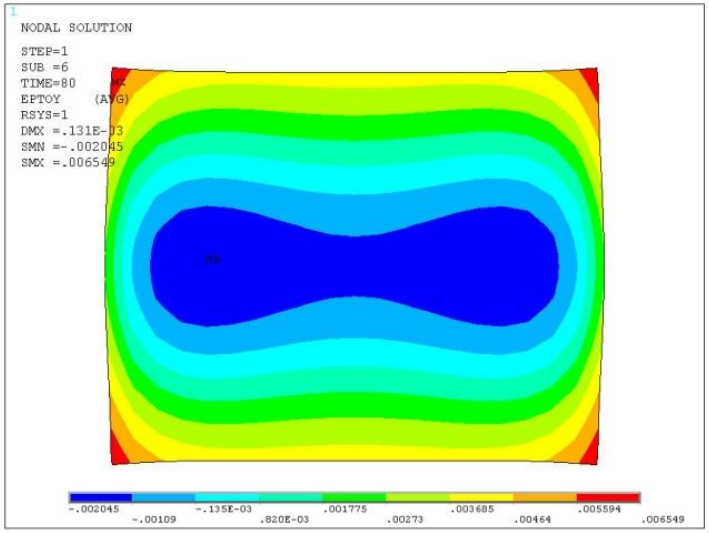

FIG. 10. Pellet strain showing hour-glassing (deformation 10).*

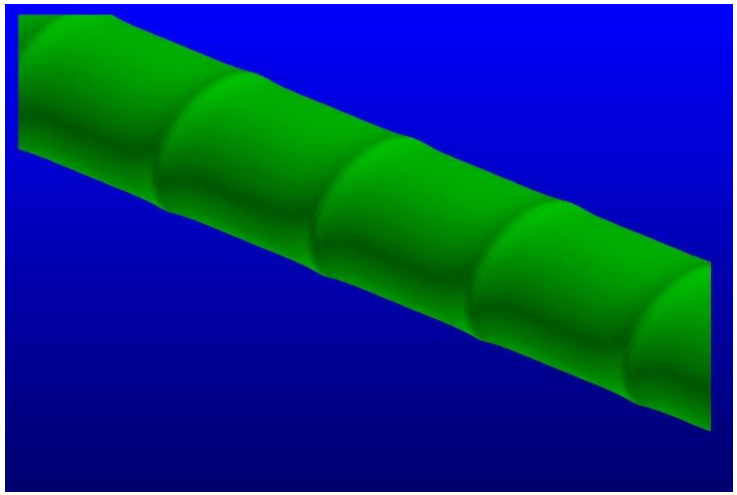

FIG. 11. The effect of pellet hour-glassing on the sheath. (bambooing).

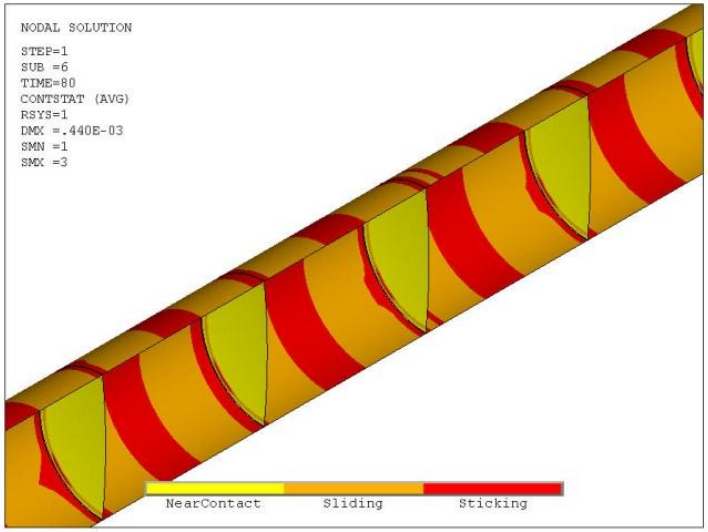

Fig. 12. Contact status between pellets and sheath.

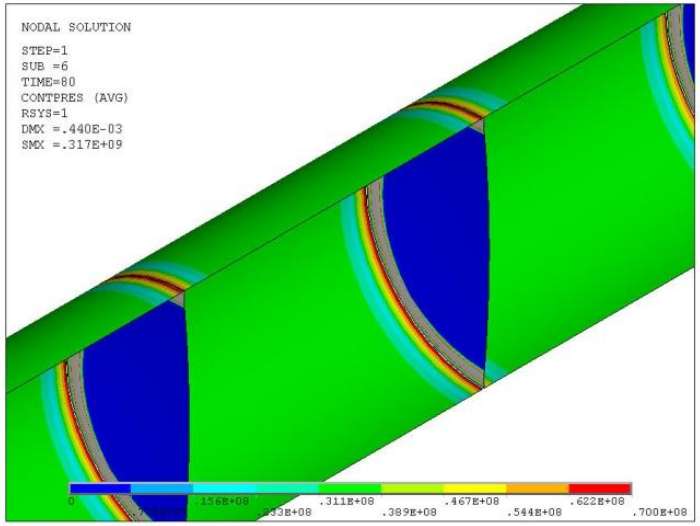

FIG. 13. Interface pressure between the pellets and the sheath.

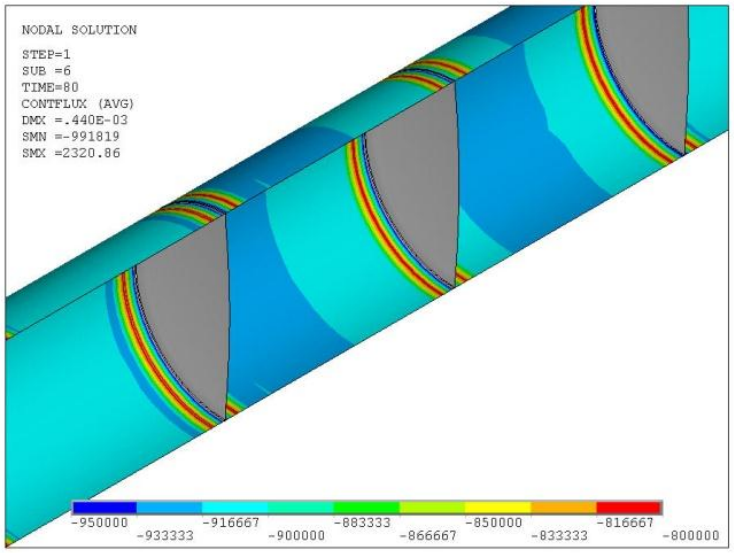

FIG. 14. Heat flux between the pellets and the sheath (W/m^2).

7. FUTURE PLANS

Future plans for this model include implementation of low and high temperature Zircaloy creep models to simulate the creep down of the sheath under system pressure, and the high temperature sagging of the pin under accident conditions. Spacers and bearing pads will also be added to the outer surface of the sheath to assess both the thermal and mechanical impact of these features. There are also plans to couple this model to the IST fission product behaviour code SOURCE IST [5].

REFERENCES

[1] CHASSIE, G.G., SIM, K.S., XU, S., LAI, L.P., XU, Z., "Recent Development of ELESTRES for Applications to More Demanding Reactor Operating Conditions", 10th International CNS Conference on CANDU Fuel, Ottawa, Ontario, Canada (2008).

[2] WILLIAMS, A.F., "The ELOCA fuel modelling code: past, present and future", 9th International CNS Conference on CANDU Fuel, Belleville, Ontario, Canada, (2005).

[3] SILLS, H.E., HOLT, R.A., "Predicting High-Temperature Transient Deformation from Microstructural Models", 4th International Conference of Zirconium in the Nuclear Industry, Stratford-upon-Avon (1978).

[4] SCDAP/REPLAP Code Development Team, "SCDAP/RELAP-3D Code Manual Volume 4: MATPRO – A Library of Material Properties for Light-Water-Reactor Accident Analysis", Idaho National Engineering and Environmental Laboratory Report INEEL/EXT-02-00589, Volume 2, Rev. 2.2 (2003).

[5] BARBER, D.H., ET. A.L., "Source IST 2.0: Fission Product Release Code", 9TH International Conference on CANDU Fuel, Belleville, Ontario, Canada (2005).

ADVANCED FUELS CYCLE CONCEPTS
(Session 1)

Chairman

A. CHAUHAN
India

REVISITING THE EXPERIENCE WITH ADVANCED FUELS IN THE ARGENTINE HEAVY WATER REACTORS

L. ALVAREZ, A. BUSSOLINI and P. TRÍPODI
National Commission on Atomic Energy,
Buenos Aires, Argentina
Emails: lalvarez@cnea.gov.ar
bussolini@cnea.gov.ar
tripodi@cnea.gov.ar

Abstract

Argentina has two Nuclear Power Plants (NPPs) in operation and the construction of a 3rd NPP is almost completed. The first NPP in operation is Atucha-1 (CNA-1), a Siemens/KWU PHWR design of 357 MWe. The second one is known as Embalse or CNE. It has a CANDU-6 type reactor and produces 648 MWe. The 3rd NPP is Atucha-2 (CNA-2). This is also a Siemens/KWU PHWR design that at full power will supply 700 MWe to the grid. The Fuel Assemblies (FA) for the three NPPs are entirely manufactured in Argentina. The original designs of the fuels were supplied by the designers of the NPP. At the present these designs were improved at CNEA and the main driving forces in this process were the results of the operational experience, the evolution of the fabrication methods or the application of advanced fuel cycles to improve the competitiveness of the nuclear generation. The main application of an advanced cycle was performed in Atucha-1 (CNA-1) where an increase of the U enrichment from natural uranium to Slightly Enriched Uranium with 0.85 % ^{235}U (SEU) allowed to increase the average burnup extraction of the fuel from 5900 MW·d/tU to 11 000 MW·d/tU. The main consequence of this improvement is an important reduction of the fuel consumption and a positive impact on the reduction of the cost of generation. Other programs for alternative fuels with evolutionary designs have been successfully applied in both reactors in operation with the same objective. The fuel engineering activities for the advanced or alternative fuel designs have included among other tasks the adjustment of product specifications, the preparation of new drawings, extensive fuel rod thermomechanical design verifications, new safety analysis and the evaluation of the fuel performance of the first series of new fuels. This paper is mainly focused in the above mentioned application in Atucha-1. Information about the current performance of the fuels with the advanced fuels in the Atucha-1 Reactor is also presented.

1. GENERAL INFORMATION

1.2. Nuclear power plants in Argentina

Argentina has two nuclear power plants in operation. The first one is Atucha-1 (Pressurized Heavy Water Reactor – Pressure Vessel) and the second one is Embalse (CANDU-6 reactor – Pressure Tubes). The construction of a third NPP called Atucha-2 (PHWR-Pressure Vessel) is almost completed and the starting and commissioning process was initiated in 2012. Currently all the fuels are loaded into the reactor and the high pressure tests on the primary circuit are in progress.

Tables 1, 2 and 3 describe the main characteristics of these nuclear power plants:

TABLE 1. ATUCHA-1 (CNA-1)

Reactor Designer	SIEMENS-KWU (Germany)
Beginning of commercial operation	1974
Reactor Type	PHWR - Pressure Vessel
Thermal Output	1179 MW
Gross Electrical Output	357 MWe
Coolant And Moderator	D_2O
Fuel Channels	252
Fuel Assemblies	252 (Full Length)
Refueling And Fuel Shuffling	Continuous On-Power
Initial Fuel	Natural Uranium (NU)
Current Fuel	Slightly Enriched Uranium (SEU 0.85% U-235)
Active Length	5300 mm
Total Uranium Loading	38,9 tU
Average Discharge Burnup (NU)	5,9 MW·d/kgU
Average Discharge Burnup (SEU)	11.6 MW·d/kgU
Refueling Frequency (NU)	1.1 FA/Full Power Day
Refueling Frequency (SEU)	0.7 FA/Full Power Day
Pellet Peak Discharge Burnup (NU)	8.4 MW·d/kgU
Pellet Peak Discharge Burnup (SEU)	15.0 MW·d/kgU

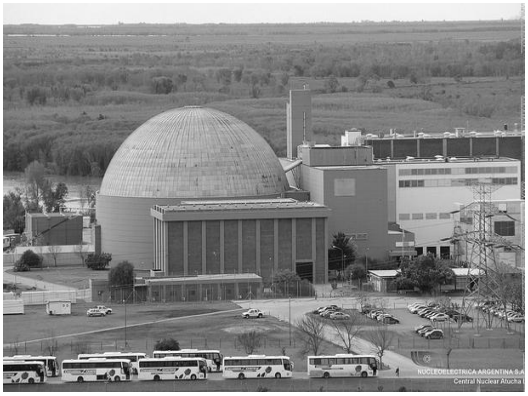

TABLE 2. EMBALSE (CNE)

Reactor Designer	AECL (Canada)
Beginning of Commercial Operation	1983
Reactor Type	PHWR – Horizontal Pressure Tubes
Thermal Output	2109 MW
Gross Electrical Output	600 MWe
Coolant and Moderator	D_2O
Fuel Channels	380
Fuel Assemblies	4560 (Length ~ 50 cm)
Refueling	On-Power
Fuel Shuffling	On-Power (Only along the Fuel Channels)
Fuel	Natural Uranium
Active Length	478.6 mm
Total Uranium Loading	74 tU
Average Discharge Burnup	161 MWh/kgU
Refueling Frequency	17.5 FA/Full Power Day

TABLE 3. ATUCHA-2 (CNA-2)

Reactor Designer	SIEMENS-KWU (Germany)
Reactor Type	PHWR - Pressure Vessel
Thermal Output	2175 MW_t
Gross Electrical Output	745 MWe
Coolant And Moderator	D_2O
Fuel Channels	451
Fuel Assemblies	451 (Full Length)
Refueling And Fuel Shuffling	Continuous On-Power
Initial Fuel	Natural Uranium (NU)
Total Uranium Loading	85 tU
Active Length	5300 mm
Average Discharge Burnup	7.5 MW·d/kgU
Refueling Frequency	1.43 A/Full Power Day

1.3. Organizations in nuclear fuels activities

The main organizations involved in activities associated with the nuclear fuels and their relationships are presented in Figure 1.

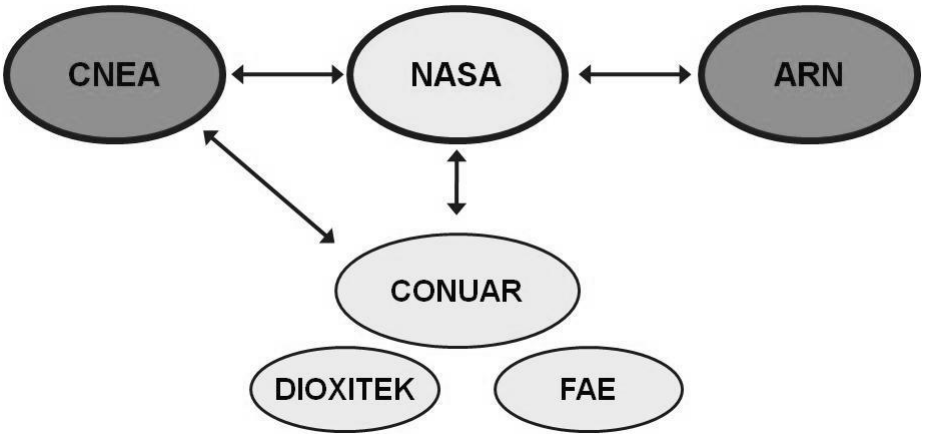

FIG. 1. Main organizations involved in fuel activities in Argentina.

— CNEA provides the fuel design and fuel engineering services to the manufacturer and also to the user of the fuels;
— CONUAR is the fuel manufacturer, DIOXITEK supplies UO_2 powder and FAE fabricates Zry-4 claddings and other structural components;
— Nucleoléctrica Argentina (NA-SA) operates the nuclear power plants and therefore is the user of the fuels;
— ARN is the licensing authority.

Fuel management and neutronic and thermal hydraulic calculations are within the scope of NA-SA activities. Fuel design analysis, non-conformities evaluation and fuel verification are performed by CNEA.

The Fuel assemblies for the three NPP are entirely manufactured in Argentina. The original designs of the fuels were supplied by the designers of the NPP but current designs are the result of improvements performed by CNEA and based on the operational experience, the evolution of the fabrication methods and the application of advanced fuel cycles to improve the competitiveness of the nuclear generation.

2. ADVANCED FUELS IN PHWR

2.1. General concept

Several alternatives of fuels designs different than those originally defined for the Pressurized Heavy Water Reactors have been proposed as Advanced Fuels in the different

countries operating this type of reactors. The IAEA-TECDOC-1686 (see Table 4) identifies the following options of Advanced/Alternative Fuels

TABLE 4. CONVENTIONAL AND ADVANCED FUELS FOR PHWR

Type of reactor	Conventional fuel	Advanced/alternative fuels
Pressurized Heavy Water Reactor (PHWR)		
• Fuel pellets	Natural UO_2	• REPU or SEU in the form of UO_2 • $(U,Pu)O_2$, $(Th, Pu)O_2$ and $(Th,^{233}U)O_2$, containing up to 2% fissile material • PuO_2 in Inert Matrix (SiC) for burning 'Pu'
• Cladding	Zircaloy-4	Zircaloy-4
• Typical Burnup (MW·d/ton HM)	6-7	15–20

2.2. Advanced fuels in Argentine PHWRs

2.2.1. Driving forces

After the deregulation of the Argentine Electricity Market that took place during the 90's the organizations involved in the production of electricity from nuclear energy had to make an effort to improve its competitiveness. The reduction of the contribution of the cost of the fuel on the cost of generation played a key role in this process.

Several fuel modifications were evaluated to reduce the cost of the fuel without affecting its reliability and pursuing at the same time a better utilization of the natural resources. Two main programs were finally applied in Atucha-1. The first program consisted in the replacement of the natural uranium with slightly enriched uranium as raw material to fabricate the fuel pellets. The second one was to introduce design changes in order to increase the U content of the fuel rods. The main target of both programs was to reduce the annual consumption of Fuel Assemblies increasing the dwelling time of the Fuel Assemblies.

2.2.2. SEU experience

The main application of an advanced cycle was performed in Atucha-1 where an increase of the U enrichment from natural uranium to Slightly Enriched Uranium with 0.85 %

U-235 (SEU) allowed to increase the average fuel discharge burnup from 5900 MW·d/tU to more than 11 000 MW·d/tU with a corresponding reduction of the refueling frequency.

A similar program was launched for the CANDU type fuel of the Embalse NPP. Only a first step to demonstrate the integral feasibility of the utilization of SEU 0.9 % U-235 was completed. This study included reactor, fuel and safety aspects. The study showed that this design optimization is possible without affecting significantly the operation of the power station.

Fuel Engineering studies are being conducted to evaluate the feasibility of replacing the Natural Uranium with SEU in the Atucha-2 Fuel. In this case an additional attractive to apply this type of programs is the higher refueling frequency of this reactor and the existence of only one refueling machine.

2.2.3. More-U programs

Within the category of alternative fuels, several design optimizations were proposed and developed to improve the U content of the Atucha-1 Fuel. The main ones were the reduction of the number of internal fuel rod components and their replacement with fuel pellets, the modification of the pellet design and the replacement of the structural tube with a fuelled fuel rod. This complete set of design changes allowed increasing the U content of the fuel in more than 4 %. A similar program allowed increasing the U content of the Embalse fuel in more than 3.5 %.

2.2.4. Other programs

Other studies with more complexities are currently in progress and include the utilization of burnable absorbers like dysprosium and an effort to unify the main components of the different fuels that are used to load the Argentine PHWR.

3. DESCRITION OF SEU EXPERIENCE IN ATUCHA-1

3.1. Atucha-1 fuel

The fuel for CNA-1 is a very stable product with a consolidated and proved design. The initial design was supplied by SIEMENS-KWU. Since 1983 the fuel assemblies are fabricated in Argentina using standardized and reliable manufacturing technologies. The administration of the design, the analysis of non-conformities, the qualification of special manufacturing process and the evaluation of the fuel performance are within the scope of CNEA activities.

The fuel assembly for Atucha-1 reactor consists of 36 fuel rods in an array of three concentric rings and one central fuel rod. A structural tube is placed in one position of the outer ring. The stack of UO_2 pellets is 5300 mm long. An internal tube (gas plenum), a compression spring and isolating pellets complete the internals of the fuel rod.

Rigid Spacer Grids and a Tie Plate located at the top of the fuel assembly keep the fuel rods in their positions. Bearing pads welded to the outer surface of the free standing claddings are set to interact with the spacer grids. Sliding shoes attached to the spacer grids and to the structural tube are used to set the radial position of the fuel assembly into the coolant channel.

Table 5 shows the main characteristic of the CNA-1 fuel assembly.

TABLE 5. CHARACTERISTICS OF CAN-1 FUEL ASSEMBLY

Assembly Geometry	Circular Array
Fuel Rods	36
Supporting Tube	1 (Zircaloy-4)
Rigid Spacer Grids	15 (Zircaloy-4)
Tie Plate	1 (Zircaloy-4)
Cladding Material	Zircaloy-4
Coupling and linkage	Stainless Steel/Zircaloy-4

The following schematic representation shows a description of the Atucha-1 fuel assembly:

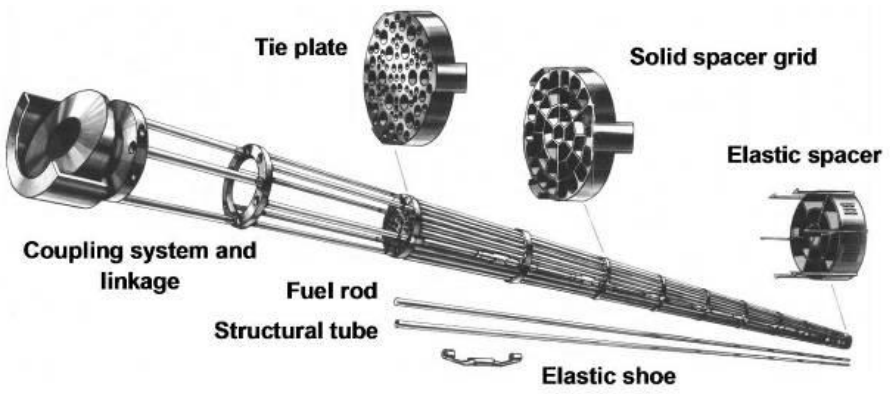

FIG. 2. Description of Atucha-1 fuel assembly.

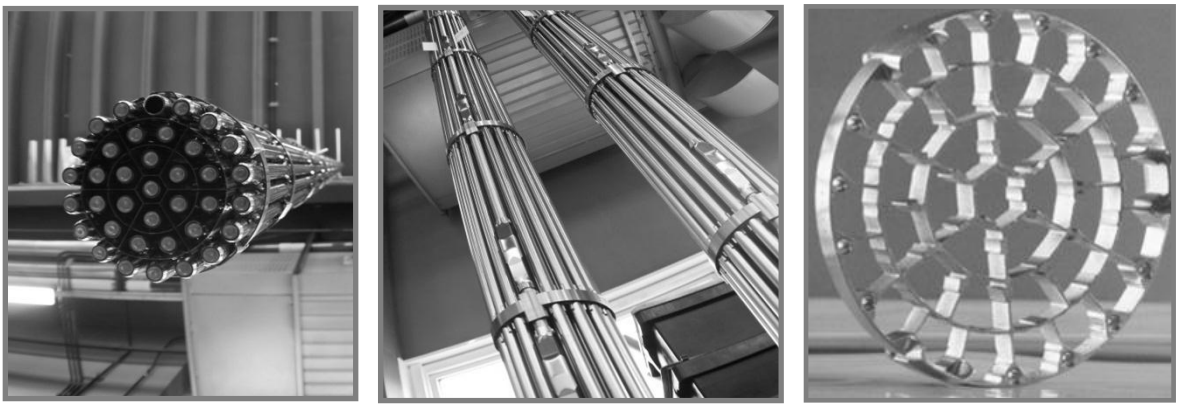

(a) (b) (c)

FIG. 3. Views of fuel assembly and spacer grid.

Figs. 3(a) and 3(b) show the bottom and the lateral view of the fuel assembly. Fig. 3(c) shows a view of the rigid spacer grid. The refueling and reshuffling of the fuel in the core are performed typically in a three zones scheme as is presented in Fig. 4.

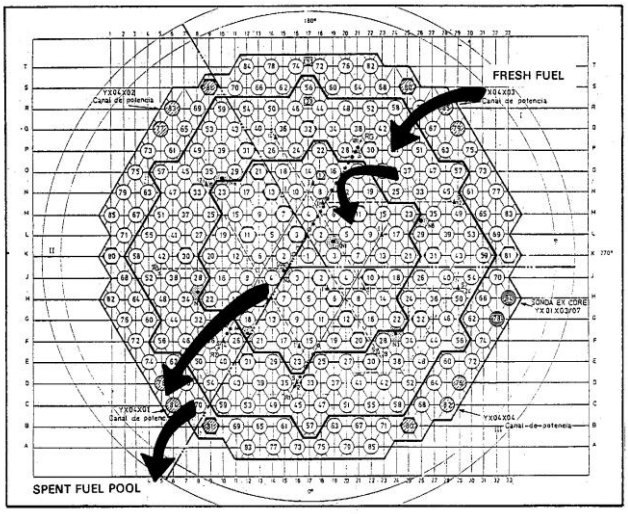

FIG. 4. Scheme for refueling and reshuffling.

3.2. Project to introduce SEU in Atucha-1

A step by step approach was adopted for the replacement of the original fuel material by Slightly Enriched Uranium. The project was divided in different Phases with an increasing upper limit for the quantity of SEU Fuel Assemblies (FA) in the core. Licensing documentation was prepared for each phase and the authorization from the Nuclear Regulatory Authority was required before starting a new phase. A Safety Report was also prepared for each stage of the program.

— **Phase 1** consisted in the introduction of a limited number of SEU FA but not exceeding twelve in the core at any time;
— **Phase 2** was initially defined as the transition period from 12 to 60 SEU FA, but was later extended up to 99 FA;
— **Phase 3** covered the transition from 100 SEU FA to full core.

During Phase 1, the fresh SEU FA was introduced in six predetermined channels that were selected because they had larger margins to the channel power limit. This allowed accommodating the higher power increases that were produced when fresh SEU fuels were introduced in the core. Besides that the channel powers at these positions are relatively high and then the irradiation time until the FA are transferred to other positions are lower than in other channels. The selected positions also had outlet channel temperature measurements and five out of the six had in core detectors in the vicinity. These features allowed comparing coolant temperatures and neutron fluxes obtained from calculations with data obtained from the reactor.

The main objectives of the Phase 1 were:

— To verify the performance of the SEU fuel in the core with discharge burnups close to the values expected for the equilibrium full SEU core and to verify the behavior at power ramps during refueling operations, reactor power increases, and startups from low power;
— To reach discharge burnups of 10000 MW·d/tU;
— To verify predictions of neutronic calculations like reactivity gain, channel power increase and neutron flux increase when introducing SEU fresh FA;
— To test operating procedures developed for SEU fuel.

During Phases 2 and 3, the average discharge burnup of the SEU fuel was increased up to 11 000 MW·d/tU, and the maximum average burnup of the bundles during their irradiation in the center of the core up to 10 000 MW·d/tU. The main objectives for Phases 2 and 3 were:

— To verify the global behavior of the core with a larger fraction of SEU fuel;
— To verify the performance of the SEU fuel at discharge burnups similar to what was expected with full SEU cores and also during reshufflings at conditions typical for a whole converted core;
— To prepare the location of SEU FA in the core for the transition to a full SEU core.

The whole program took almost 6 years. During them the reactor was operating with different mixed cores. At the present and since 2001 the reactor is fully loaded with SEU fuel.

3.3. Design optimizations

Several changes have been introduced to both the fuel rod and fuel assembly designs to keep the impact of the new operating conditions on the fuel performance as low as possible. The main changes were:

— The plenum length was increased to provide more volume for gas release;
— Bearing pads with longer contact surfaces were adopted to provide reliable interaction between spacers and fuel rods during the whole life of the fuel;
— The ductility of the cladding material was increased to reduce the fuel rod susceptibility to PCI failures on power ramps;
— Inconel 718 was used to replace the original material of elastic sliding shoes (SS A286). In addition to its superior spring characteristics Inconel was chosen because of its good resistance against stress relaxation, providing similar safety margin for holding the SEU fuel assemblies in position than the one for the natural uranium fuel. The effect of this modification on the neutron economy is practically negligible.

3.4. Advantages of the SEU fuel in Atucha-1

The main advantages of the utilization of SEU in Atucha-1 are:

3.4.1. Extension of fuel discharge burnup

This is the main advantage of the program. A 20 % increase of the enrichment represents a ≈ 92 % increase of the average discharge burnup and its corresponding reduction

in fuel consumption. Considering the small fabrication scale of this type of fuels the above mentioned burnup extension has a very important impact on the cost of the fuel included in the cost of the electricity. The reduction may reach up to around 40 %.

3.4.2. Savings on the consumption of natural resources

The reduction of Uranium ore consumption resultant from the application of this program may be as high as 50 % depending on how is obtained the SEU.

3.4.3. Reduction of spent fuel volume

The volume of spent fuel discharged to the storage pools is 45 % less with SEU than with NU.

3.4.4. Reduction of on-power refueling frequency

The reduction of the use of the refueling machine is about 41 %.

Table 6 shows a global comparison between the operation of Atucha 1 with NU and the situation with SEU.

TABLE 6. OPERATION OF ATUCHA-1 WITH NU AND SEU

	Natural uranium fuel	SEU fuel 0.85% ^{235}U
Average FA Discharge Burnup [MW·d/tU]	5900	>11000
Pellet Peak Discharge Burnup [MW·d/tU]	8400	>16000
Average FA residence time [fpd*]	195	362
Annual Consumption of FA (F_u: 0.9)	430	230
Average refueling frequency (FA/fpd)	1.3	0.7

*fpd = full power days

3.5. SEU fuel performance

During the three phases of the transition program and also during the operation with full SEU cores no failures associated with the introduction of the SEU with 0.85 % U-235 or with the new operating conditions were reported. The overall failure rates remain very low and in most of the cases the origins of the defects are unknown.

Table 7 shows the evolution of the quantity of failures during the last three years of operation.

TABLE 7. STATUS OF FUEL ASSEMBLY FAILURES

Year	2010	2011	2012
Number of Fuels Discharged	248	213	219
Number of Fuel Assemblies with leaking Fuel Rods	4	0	0

Fuel Discharge Burnups remain stable and close to the average value targeted in the SEU Project as shown in Table 8.

TABLE 8. FUEL DISCHARGE BURNUP IN ATUCHA-1

Year	2010	2011	2012
Average Fuel Discharge Burnup [MW·d/tU]	10563	10649	10696

4. FINAL REMARKS

Competitiveness of the electricity generated in NPP with PHWR requires a constant effort to minimize the cost of the fuel and to improve the utilization of the natural resources. These are the main driving forces for the study and industrial application of the so called advanced fuels in PHWR. One of the most common characteristics of these fuels is that they operate in conditions that are well beyond the ones defined originally for the power reactor under analysis.

This was the situation of the Argentine Atucha-1 NPP where a program for a gradual transition from a natural uranium core to a SEU core (0.85 % ^{235}U) has been completed and has been successfully applied for more than 10 years with cores loaded completely with SEU fuels.

The reduction of the cost of the fuel included in the cost of the electricity is around 40 %. The increase of the average discharge burnup goes from 5900 MW·d/tU (NU) to approximately 11 000 MW·d/tU (SEU) and the reduction of the refueling frequency (fuel consumption) from 1.31 to 0.7 FA per full power day.

The excellent results obtained in Atucha-1 have encouraged NA-SA and CNEA to evaluate the feasibility of applying a same type of conversion to the Embalse NPP. A similar study is being conducted by the Fuel Engineering Department also for the Atucha-2, the third NPP in Argentina which construction is almost completed.

ACKNOWLEDGEMENTS

The authors of this paper would like to express their gratitude to colleagues from NA-SA and from CONUAR that have provided valuable information for this work.

DEVELOPMENT OF ADVANCED 37-ELEMENT FUEL FOR CHF ENHANCEMENT

J. H. PARK and J. YEOBJUNG
Korea Atomic Energy Research Institute,
Daejeon, Republic of Korea
Email: jhpark@kaeri.re.kr

Abstract

A CANDU-6 reactor has 380 fuel channels of a pressure tube type which provides an independent flow passage, and the fuel bundles rest horizontally. Most of the aging effects for a CANDU operating performance originate from creep in a horizontal pressure tube. A horizontal pressure tube can be expanded radially as well as axially owing to its creep behavior during its life time. The creep pressure tube deteriorates the CHF (Critical Heat Flux) of the fuel channel, and finally worsens the reactor operating performance and thermal margin. This paper introduces an increase of the inner ring radius of the standard 37-element fuel bundle to enlarge the peripheral subchannel area adjacent to the center rod because of most CHF locations around the center rod, and to enhance the CHF of a fuel bundle. Subchannel analysis technics using the ASSERT-PV code were applied to investigate the CHF characteristics according to the inner ring radius variation for the uncreep pressure tube. Also the dry out power of the modification of the inner ring radius was compared to the standard 37-element fuel bundle. It was found that the modification of the inner ring radius is very effective in enhancing the dry out power of the fuel bundle through an enthalpy redistribution of the subchannels and change in the local locations of the CHF occurrences.

1. INTRODUCTION

A CANDU-6 reactor has 380 fuel channels of a pressure tube type, which creates an independent flow passage and the fuel bundles rest horizontally. Most of the aging effects for a CANDU operating performance originate from a horizontal creep pressure tube. As the operating years of a CANDU reactor proceeds, a pressure tube experiences high neutron irradiation damage under high temperature and pressure. It is expanded radially as well as axially during its life time, resulting in a creep of the pressure tube which allows a bypass flow on the top section inside of a pressure tube owing to more open space in its top section than the bottom section. Hence, the creep pressure tube deteriorates the CHF (Critical Heat Flux) of the fuel channel and finally worsens the reactor operating performance and thermal margin. This is known to be very important phenomena of a CHF for a horizontal pressure tube owing to the aging effects.

During last three decades, some papers have been published to enhance the Critical Heat Flux (CHF) and/or Critical Channel Power (CCP), which is determined by the dry out and hydraulic characteristic curves of the primary heat transfer system of a CANDU reactor [1, 2, 3, 4]. In the early 1980s, a turbulent promoter was invented to increase the turbulent intensity surrounding the fuel elements in a fuel channel [1]. The axial positions or the number of bearing pad planes were changed, or the number of spacer pad planes were increased to enhance the CHF by means of increasing the turbulent intensity or flow mixing within a fuel passage [2]. These attempts provided a CHF increase, but an adverse effect on the CCP existed to worsen the hydraulic characteristics of the primary heat transfer system when increasing the pressure drop of the fuel channel, as shown in Figure 1 [5].

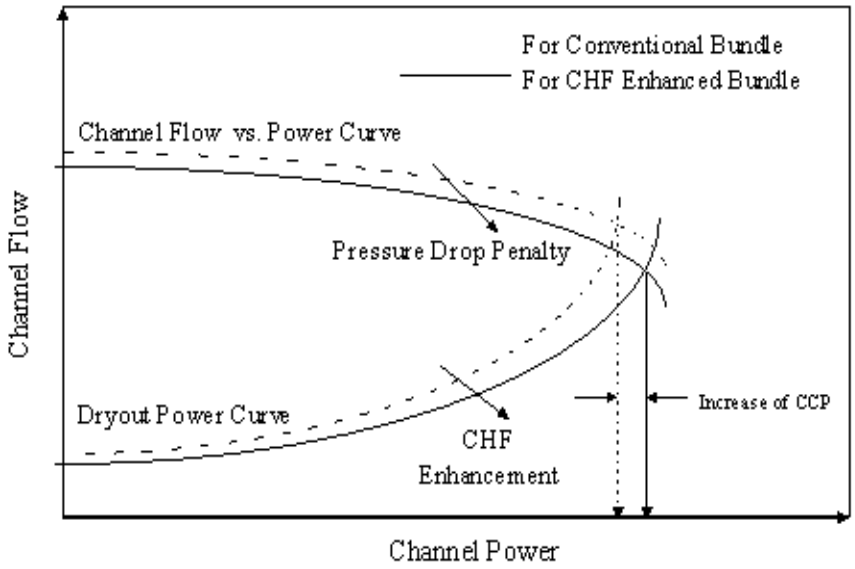

FIG. 1. Relation between hydraulic characteristics and power curves to determine CCP enhnancement [5].

In particular, a 37-element fuel bundle has been used in commercial CANDU reactors for over 40 years as a reference fuel bundle. Most CHF of a 37-element fuel bundle were occurred at the elements in the inner ring at high flows, or in reactor conditions of which the reference flow rate is 24 kg/s in the Fuel Design Manual [6], but at the element in the outer ring at low flows [7]. It is caused that the 37-element fuel has relatively small flow area and high flow resistance at the peripheral subchannels of its center rod compared to the other subchannels. The configuration of a fuel bundle is one of the important factors affecting the local CHF occurrence. Recently, the diameter effect of each rod located in the center, inner, intermediate, and outer rings of the 37-element fuel bundle has been studied [8]. It shows that the dry out power of a fuel bundle has a tendency to increase as the size of the rod diameter decreases. However, a decrease of the rod size of a fuel bundle increases the coolant volume in a fuel channel. Finally, it can deteriorate the safety margin by increasing the coolant void reactivity, etc.This paper introduces the modification of a ring radius, especially an inner ring radius, to increase the CHF. Also, the dry out power and CHF occurrence were analyzed for a standard 37-element fuel bundle with the modified inner ring radius. Also, the effects of the inner ring radius variation on the subchannel enthalpy distribution and dry out power of the proposed modification were examined, and the results were compared to those of the standard 37-element fuel bundle.

2. SUBCHANNEL MODELING

For the sensitivity studies of the effect of an inner ring radius on the CHF or dry out power of a fuel bundle, the subchannel analysis was performed using the ASSERT code [9], which was transferred from AECL to KAERI under a Technology Transfer Arrangement (TCA) between KAERI/AECL. It is known that the subchannel analysis technique is very useful tool to precisely investigate the thermal-hydraulic behavior of a fuel bundle in a nuclear reactor. In the present study, the subchannel analysis for a horizontal flow has been performed with a variation of the inner ring radius of a fuel bundle.

2.1. Geometry of a fuel bundle

Standard 37-element fuel is composed of 37 fuel elements and 4 rings, a center ring, an inner ring, an intermediate ring, and an outer ring and several appendages such as bearing pads, spacer pads, and end-plates to configure a bundle structure as shown in Fig. 2. Also, each ring radius is summarized in Table 1.

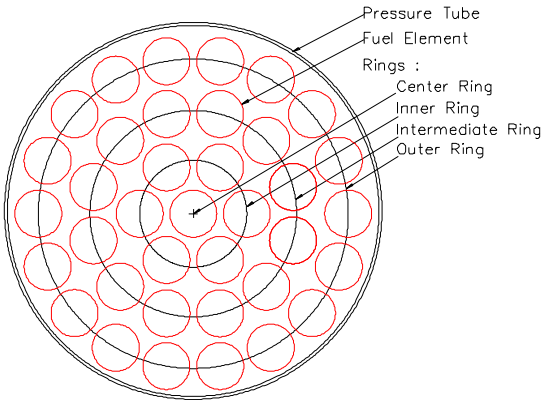

FIG. 2. Cross sectional view of standard 37-element fuel.

TABLE 1. RING RADII OF THE STANDARD 37 ELEMENT FUEL

Ring Identification	Ring radius (mm)	No. of elements
Center	0.0	1
Inner	14.88	6
Intermediate	28.75	12
Outer	43.33	18

From the previous CHF experiments, it is known that most local CHFs of a standard 37-element fuel occurred at the peripheral subchannels of a center rod at high flow [6]. It was caused by the relatively small flow area of the inner subchannels or higher resistance than the other subchannels.

Recently, the modification of standard 37-element fuel was suggested by Ontario Power Generation (OPG) in Canada. The main idea of the modified 37-element fuel (37M fuel) is the size reduction of a center rod to enhance the CHF. The small size of the center rod among 37 elements makes a larger flow area and lower flow resistance of the inner subchannels of a standard 37-element fuel bundle. The CHF experiments of the 37M fuel was performed in Stern Laboratory (ST). It is known that the CHF enhancement was obtained for the uncrept and crept channels, but any information of the specific CHF results for the 37M fuel were not published yet. Even if the 37M fuel has a higher CHF performance than the standard 37-element fuel bundle, it could have an adverse effect on safety, in which the large flow area of the fuel bundle can increase the coolant void reactivity, and the small size of the center rod

can also increase the linear element power of the other rods to achieve the same bundle power.

To overcome the negative safety effects owing to the small size of the center rod of the 37M fuel, this paper proposed an increase of the inner ring radius instead of reducing the center rod diameter. Hence, the peripheral subchannel area adjacent to the center rod can be enlarged and finally enhance the CHF of a fuel bundle without any adverse impact on safety as well as fabrication cost.

A schematic view of the increase in inner ring radius is shown in Fig. 3.

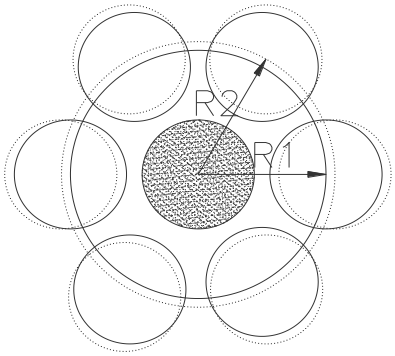

FIG. 3. Schematic diagram of flow area increase around.

R1 and R2 represent the inner ring radii of the standard and modification of a 37-element fuel bundle, respectively as shown in Fig. 3. When increasing the inner ring radius, the minimum gap size between elements or the maximum allowable inner ring radius should be considered from the view-points of the element interference. In the Fuel Design Manual of the standard 37-element fuel [5], it is noted that "The average height reduction on the mating spacer pairs, measured for each bundle, ranged from 0.015mm to 0.035mm after 6178 hours of testing. The maximum height reduction measured was 0.16mm or about 25 percent of the specified minimum height of one inter-element spacer. The minimum height of one inter-element spacer is acceptable since spacer to sheath contact is not like to occur until about 50 percent of the combined spacer thickness is removed." The minimum gap size between elements of the inner and intermediate ring of the standard 37-element fuel bundle was designed as 1.8mm. Hence, the allowable maximum inner ring radius from the above statement in Fuel Design Manual [5] can be found as follows;

— Minimum height of one spacer: 0.64 mm (minimum allowable gap: 1.28 mm);
— Excess gap height : 0.52 mm;
— Allowable maximum inner ring radius: 15.4 mm (14.88 mm + 0.52 mm).

Hence, for the present study, the inner ring radii were considered to be from 14.88 mm to 15.38 mm with 0.1 mm step increase. The increasing ratio of the flow area of the inner subchannels with respect to the standard 37-element fuel bundle is shown in Fig. 4. The subchannel area of the inner ring of the 37M fuel is equivalent to that of 15.18 mm of the inner ring radius, as shown in Fig. 4.

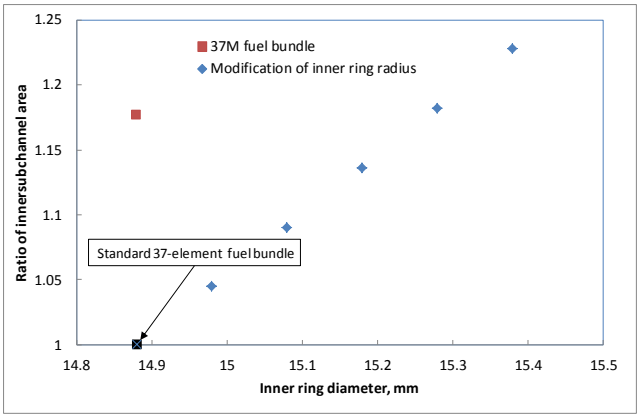

FIG. 4. Variation of the inner subchannel area according to increasing an inner ring radius.

2.2. Modeling of AFD and RFD

A CANDU-6 core is composed of 380 fuel channels, and each fuel channel accommoda tes 12 fuel bundles resting horizontally. Hence, the CHF of a fuel bundle can be affected by th e radial power profile (RFD) of a fuel bundle, as well as the axial power profile (AFD) in a fuel channel. The Figs. 5 and 6 show the typical RFD and AFD of standard 37-element fuel bundle in a fuel channel, respectively. For a subchannel analysis of the standard 37-element fuel bundle and its inner ring radius modification, the same AFD and RFD can be used because the change of the inner ring radius does not affect the AFD and RFD except that the radial position of the inner rods is different, as shown in Fig. 5.

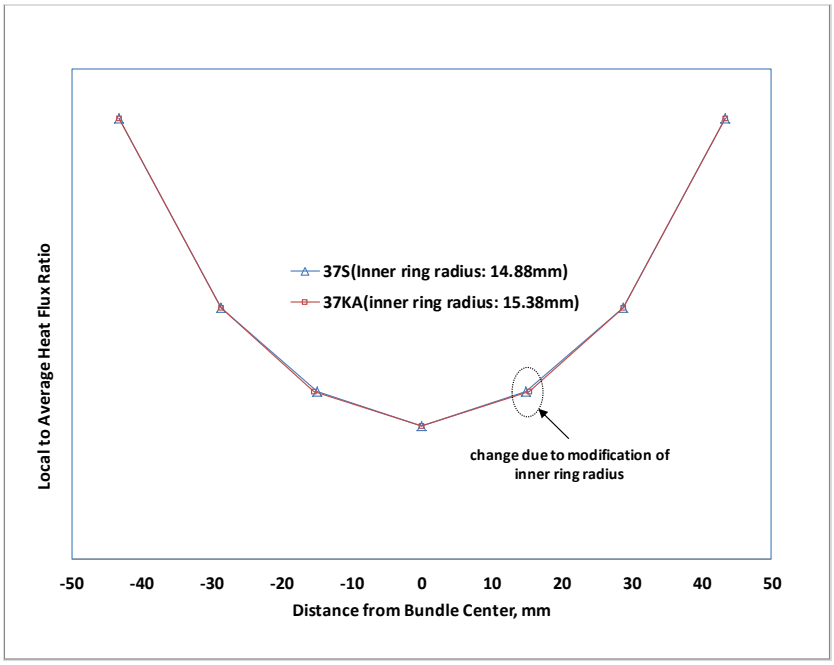

FIG. 5. Comparison of radial heat flux ratios of the standard 37-element fuel bundle and modification of its inner ring radius.

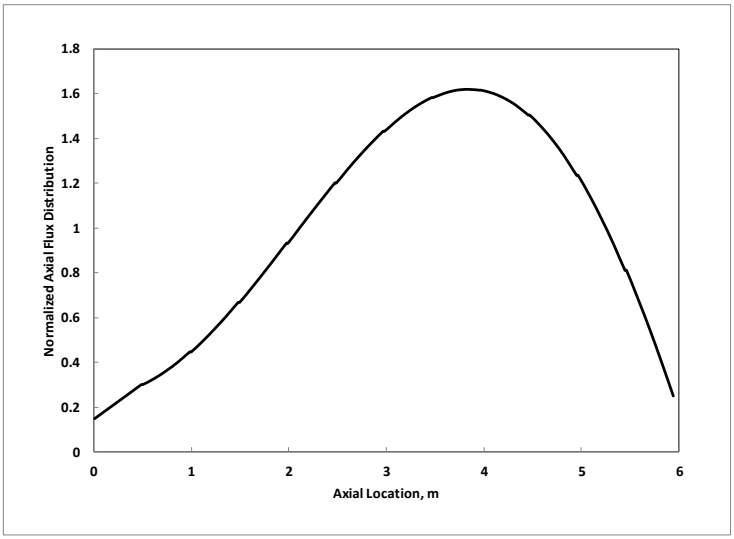

FIG. 6. Normalized axial heat flux distribution for a fuel channel.

3. RESULTS AND DISCUSSION

Subchannel analyses were performed for a standard 37-element fuel bundle with/without the inner ring radius modification using the ASSERT code. To examine the dry out enhancement of the modified inner ring radius, the inlet temperatures were selected 256℃, 262℃ and 268℃, and the inlet mass flow rates were 20kg/s, 24kg/s, and 28kg/s. The inner ring radius of the standard 37-element fuel bundle is increased from 14.88mm to 15.38mm in 0.1mm steps.

Fig. 7 shows the subchannel and rod identification for the subchannel analysis of the ASSERT code. The results of the rod and adjacent subchannel number for the first CHF occurrences are summarized in Table 2. As summarized in Table 2, it was found that all CHF occurrences of the standard 37-element fuel bundle, which has a 14.88mm inner ring radius was located at the peripheral subchannel around the center rod, rod #7 and subchannel #1. These results are the same as the previous CHF experiment of the standard 37-element fuel bundle at high flow [7].

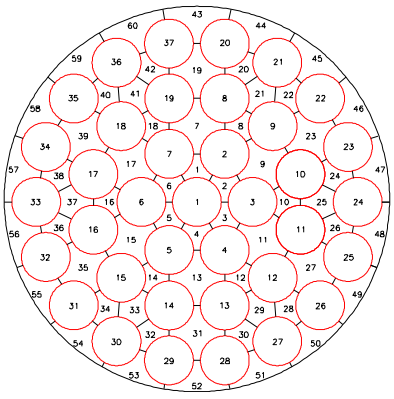

FIG. 7. Rod and subchannel identifications of 37-element fuel bundle.

The axial positions of the CHF occurrences are located before the spacer of the 10^{th} or 11^{th} bundle for all flow rate conditions. It is revealed that the location of the CHF occurrences are moved to the upstream of the fuel channel as mass flow rate increases, while those locations were not changed by the inlet temperature conditions.

TABLE 2. AXIAL AND RADIAL LOCATIONS OF CHF OCCURRENCES UNDER VARIOUS MASS FLOW RATE AND TEMPERATURE

Temp (℃)	Flow Rate (kg/s)	Axial Location	Rod No	Channel No
256	20	508.5	7	1
262	20	508.5	7	1
268	20	503.4	7	1
256	24	466.3	7	1
262	24	466.3	7	1
268	24	466.3	7	1
256	28	459.0	7	1
262	28	466.3	7	1
268	28	459.0	7	1

The dry out powers of the standard 37-element fuel bundle with/without the inner ring modification were calculated and compared under the mass flow rate conditions. The ratio of dry out power of the standard 37-element fuel bundle to that with the ring radius modification is defined as follows:

$$R_{en} = \frac{Dryout\ power\ with\ ring\ radius\ modification}{Dryout\ power\ without\ ring\ radius\ modification}$$

R_{en} were plotted in terms of the various inner ring radii as shown in Figs. 8, 9, and 10 for the mass flow rate conditions of 20 kg/s, 24 kg/s, and 28 kg/s, respectively. As shown in Figs. 8, 9, and 10, R_{en} is not sensitive to the inlet temperature conditions. However R_{en} is revealed differently according to increasing the mass flow rates.

For the mass flow rate of 20 kg/s, the R_{en} is increasing as the inner ring radius increases and is the maximum at 14.98 mm of the inner ring radius. The first CHF occurrence for the standard 37-element fuel bundle was located at rod #1 and subchannel #7, but it was moved to rod #32 and subchannel #30 as the inner ring radius increases, as shown in Fig. 8. It was found that the maximum dry out enhancement was 1.4% for 28kg/s of the mass flow rate and 14.98mm of the inner ring radius.

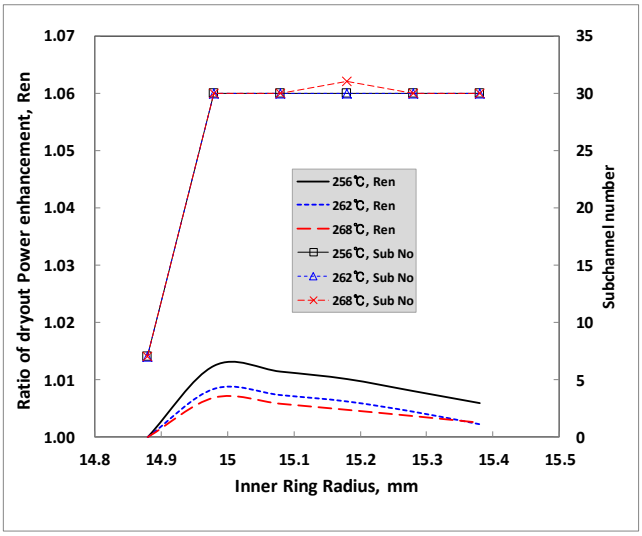

FIG. 8. Dry out power enhancement ratio and corresponding CHF subchannel at 20kg/s.

For the mass flow rate of 24 kg/s, R_{en} has a similar trend at 20 kg/s of the mass flow condition, but the subchannel locations of the CHF occurrences were changed from the inner subchannels to the outer or intermediate rings and returned to the intermediate subchannels, subchannel #12 or #13, for further increase of the inner ring radius, as shown in Fig. 9. The maximum R_{en} is increased to 1.02 at 14.98 mm or 15.08 mm of the inner ring radii.

For the mass flow rate of 28 kg/s, the maximum dry out enhancement was 4.5% at 15.08 mm of the inner ring radius. It was noted that the dry out power for the lager flow area of the inner subchannel could be enhanced more than that for the low mass flow rate conditions. As shown in Fig.10, the locations of the CHF occurrences at 28kg/s of the mass flow rate were moved from the inner subchannels to the outer or intermediate subchannels, like those at 24kg/s of the mass flow rate condition.

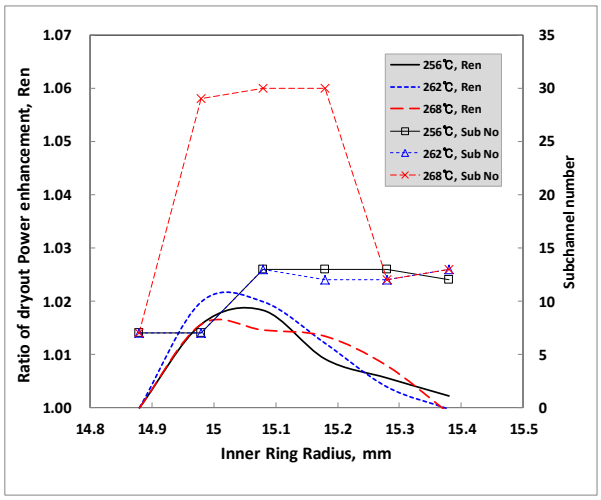

FIG. 9. Ratio of dry out power enhancement under 24 kg / s of mass flow rate condition.

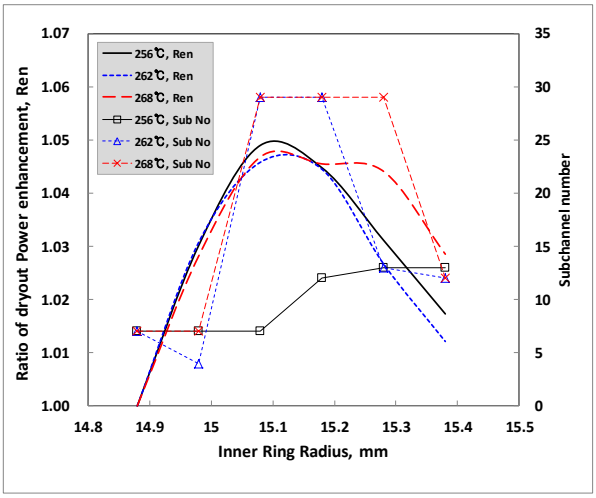

FIG. 10. Ratio of dry out power enhancement under 28 kg/s of mass flow rate condition.

The dry out enhancement ratio for 15.18 mm of the inner ring radius was plotted versus the mass flow rates in Fig. 11. As shown in Fig. 11, the mass flow rate is higher, and more dry out power enhancement can be obtained for the larger inner subchannel area by increasing the inner ring radius.

To compare the enthalpy distributions of the standard 37-element fuel bundle with/without a modification of the inner ring radius, an enthalpy imbalance factor is defined as follows:

$$Ent\ ImbF = \frac{Subchannel\ enthalpy\ specified\ at\ location\ of\ CHF\ occurrence}{Volume\ averaged\ subchannel\ enthalpy\ of\ a\ fuel\ bundle}$$

The imbalance factors of the subchannel enthalpy were plotted versus the subchannel numbers for 24 kg/s of the mass flow rate and 15.18 mm of the inner ring radius in Fig. 12. As shown in Fig. 12, the enthalpy imbalance factors of the inner subchannels of the standard 37-element fuel bundle are much higher than those of the modified inner ring radius. On the contrary, the enthalpy imbalance factors of the intermediate or outer subchannels of the standard 37-element fuel bundle are a little higher than those of the modified inner ring radius. It is noted that the CHF of the standard 37-element fuel bundle occurred at the peripheral subchannel #7 of the center rod, while the CHF for the modified inner ring radius occurred at the peripheral subchannel #12 of rod #12 (see subchannel and rod identifications of Fig. 7).

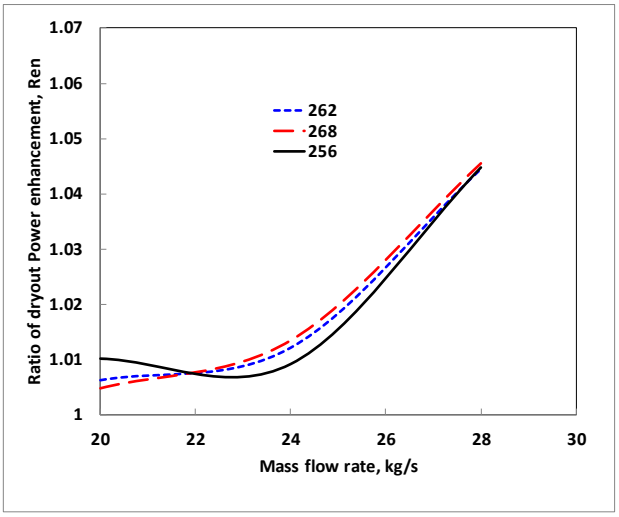

FIG. 11. Ratio of dry out power enhancement according to increasein mass flow rate for 15.18 mm of the inner ring radius.

From the present results of the subchannel analysis, the subchannel enthalpy of a fuel bundle can be more uniform if the ring radius of the standard 37-element fuel bundle is increased. Finally, the dry out power of a modified inner ring radius can be increased.

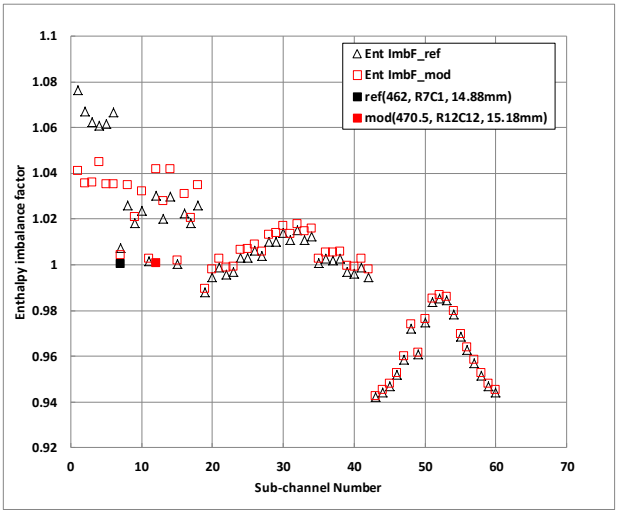

FIG. 12. Comparison of subchannel enthalpy imbalance factors of standard 37-element fuel bundle with/without the inner ring radius modification at the axial CHF location under for 24 kgs.

4. CONCLUSION

A subchannel analysis was performed to investigate the effect of the inner ring radius modification of the standard 37-element fuel bundle on the dry out power. It was revealed that the inner ring radius modification is a very efficient way for the CHF enhancement and can

increase the dry out power of the standard 37-element fuel bundle without any adverse impact on the safety margin or fuel fabrication cost. Also, the enhancement of the dry out power is strongly dependent on the mass flow rate condition but weak dependent on the inlet temperature of the coolant.

As the inner ring radius is increasing, the location of the first CHF occurrence can be moved to the other subchannels. On the other hand, the maximum enhancement of the dry out power was 4.5% at a 15.08mm inner ring radius compared to the standard 37-element fuel bundle, which has a 14.88mm inner ring radius.

Since the present study was performed only for an uncreep pressure tube, further study will be necessary for the creep pressure tubes, such as 3.3% and 5.1% creep, to optimize the inner ring radius to achieve the maximum dry out power enhancement. It is expected that the modification of the inner ring radius can be very effective for the higher creep rate of the pressure tubes.

REFERENCES

[1] GREONEVELD, D.C and GOEL, K. C., A Method of Increasing Critical Heat Flux in Nuclear Fuel Bundles, CRNL-1763 (1978).

[2] McDONALD, A.G AND SUTRADHAR, S.C., CANFLEX Bundle Thermal-hydraulic Experiments, Part 4: Freon CHF Tests on the 37E-Hybrid Bundle, Equipped with Two Space Planes and Four Bearing pad Planes, HPBP-32/ARD-TD-124 (1988).

[3] SUTRADHAR, S.C and GROENEVELD, D.C., CANFLEX Bundle Thermal-hydraulic Experiments: Part 5, Overview of the Effect of Spacer and Bearing-Pad Location on CHF in 37- eleements bundle, ARD-TD-189 (1989).

[4] JUN, J.S AND LEUNG, L.K.H.,J.S., Comparison of Dryout Power Data between CANFLEX MK-V and CANFLEX MK-IV Bundle Strings in Uncrept and Crept Channels, Nuclear Engineering and Technology, **37** (2005).

[5] JUN, J.S, PARK, J.H. AND SUK, H.C., Thermalhydraulic Analysis of the CANDU-6 Channel loaded with CANFLEX Bundle, KAERI/TR-723/96 (1996).

[6] Fuel Design Manual for CANDU-6 reactors, DM-XX-37000-001, AECL (1989).

[7] LEUNG, L.K.H and DIAMAYUGA, F.C.,F.C., Measurements of Critical Heat Flux In CNADU 37-Element Bundle with a Steep Variation in Radial Power Profile, Nuclear Engineering and Design **240** (2010).

[8] JUN HO BAE AND JOO HWAN PARK, The Effect of a CANDU Fuel Bundle Geometry Variation on Thermal-hydraulic Performance, Annals of Nuclear Energy **38** (2011).

[9] CARVER, M.B, KITELEY, J.C, ZOU, R.Q.N, JUNOP, S.V AND ROWE, D.S., Validation of the ASSERT Subchannel Code; Prediction of Critical Heat Flux in Standard and Nonstandard CANDU Bundle Geometries, Nuclear CANDU Fuel Bundle Geometry Variation on Thermal-hydraulic Performance, Annals of Nuclear Energy **38** (2011).

[10] CARVER, M.B, KITELEY, J.C, ZOU, R.Q.N, JUNOP, S.V AND ROWE, D.S., Validation of the ASSERT Subchannel Code; Prediction of Critical Heat Flux in Standard and Nonstandard CANDU Bundle Geometries, Nuclear Technology, **112** (1995).

ADVANCED FUEL BUNDLES FOR PHWRS

R. M. TRIPATHI, P. N. PRASAD, ASHOK CHAUHAN
Nuclear Power Corporation of India Ltd,
Mumbai, India

Abstract

The fuel used by NPCIL presently is natural uranium dioxide in the form of 19- element fuel bundles for 220 MWe PHWRs and 37-element fuel bundles for the TAPP-3&4 540 MWe units. The new 700 MWe PHWRs also use 37-element fuel bundles. These bundles are of short 0.5 m length of circular geometry. The cladding is of collapsible type made of Zircaloy-4 material. PHWRs containing a string of short length fuel bundles and the on-power refueling permit flexibility in using different advanced fuel designs and in core fuel management schemes. Using this flexibility, alternative fuel concepts are tried in Indian PHWRs. The advances in PHWR fuel designs are governed by the desire to use resources other than uranium, improve fuel economics by increasing fuel burnup and reduce overall spent nuclear fuel waste and improve reactor safety. The rising uranium prices are leading to a relook into the Thorium based fuel designs and reprocessed Uranium based and Plutonium based MOX designs and are expected to play a major role in future. The requirement of synergism between different type of reactors also plays a role. Increase in fuel burnup beyond 15 000 MW·d/TeU in PHWRs, using higher fissile content materials like slightly enriched uranium, Mixed Oxide and Thorium Oxide in place of natural uranium in fuel elements, was studied many PHWR operating countries. The work includes reactor physics studies and test irradiation in research reactors and power reactors. Due to higher fissile content these bundles will be capable of delivering higher burnup than the natural uranium bundles. In India the fuel cycle flexibility of PHWRs is demonstrated by converting this type of technical flexibility to the real economy by irradiating these different types of advanced fuel materials namely Thorium, MOX, SEU, etc. The paper gives a review of the different advanced fuel design concepts studied for Indian PHWRs.

1. INTRODUCTION

Indian nuclear power program is guided by the limited available natural uranium. As the available reserve is less in comparison of the power requirement of the country, the feasibility of advanced/alternate fuel material is always worked out. Indian PHWRs facilitates us to use various types of fuel bundles inside the core to irradiate and consequently power production is achieved. In view of this, in past fuel bundles of fertile material like Thorium, MOX-7 and Slightly Enriched Uranium (SEU) of 0.9 weight % ^{235}U enrichment fuel bundles were irradiated in 220 MWe Indian PHWRs.

Presently 19 element natural uranium fuel bundles are used in 220 MWe Indian PHWRs (Figure 1). The core average design discharge burnup for these bundles is 7000 MW·d/TeU and maximum burnup for assembly goes up to of 15 000 MW·d/TeU.

The PHWRs use natural uranium in oxide form as fuel. So far, more than 600 000 number of 19-element fuel bundles have been irradiated in the 16 Pressurized Heavy Water Reactors and more than 20 000 number of 37-element fuel bundles in the 2 units of Tarapur Atomic Power Station Units (540 MWe) PHWRs. The fuel performance in Indian reactors has progressively improved over the years. Efforts have been put to improve the fuel bundle utilization by increasing the fuel discharge burnup of the natural uranium bundles. The discharge burnup of all the reactors have increased in the last 3 years.

In addition to natural uranium bundles, other types of bundles are also irradiated time to time based on the specific requirement/ situation. Short length fuel bundles and on-power refueling provision in PHWRs provides flexibility to use variety of fuel loading patterns and different fuel types and consequently permits optimum use of fuel in the reactor and allows generation of full power all the time. Using this flexibility, alternative fuel concepts are tried

in Indian PHWRs.

The use of Slightly Enriched Uranium (SEU) with 0.9% ^{235}U by weight is being studied as an attractive fuelling option for Indian pressurized heavy water reactors (PHWR). Due to higher fissile content these bundles will be capable of delivering higher burnup than the natural uranium bundles. The maximum burnup possible with these bundles is 25 000 MW·d/TeU.

The different fuel types tried are depleted uranium bundles, dummy aluminum bundles, Thorium bundles and MOX bundles. This paper gives the design, development, fabrication and operating experience of the SEU, Thorium and MOX fuel bundles in PHWRs. Following paragraphs cover the alternative fuel designs used in Indian PHWRs.

The high burnup fuel element development studies for the PHWR fuel bundles and subsequent irradiations have been elaborated in this paper.

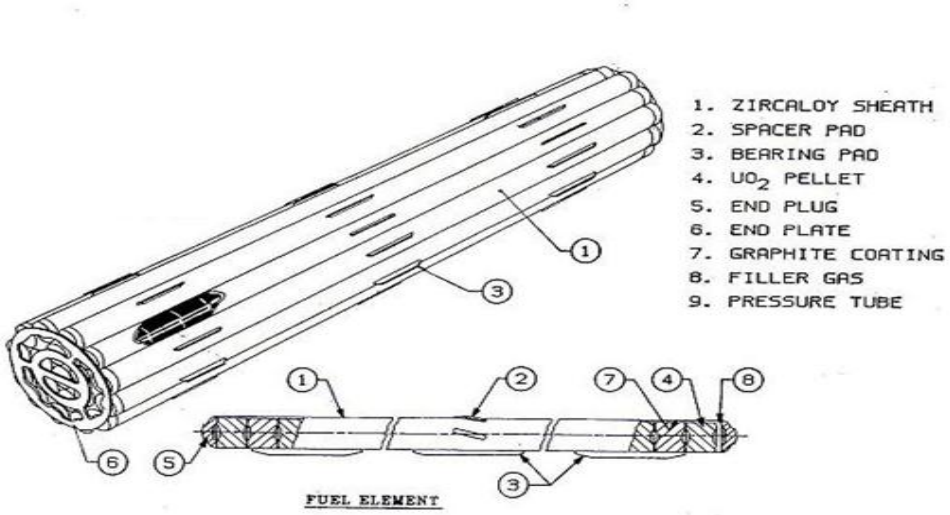

FIG. 1. 19-element fuel bundle.

2. SEU FUEL BUNDLES

2.1. Design studies

Increase in fuel burnup beyond 15 000 MW·d/TeU using slightly enriched uranium in place of natural uranium in fuel element used in 220 MWe PHWRs is investigated [1–2]. Performance of the fuel bundles at high burnup is analysed in the report. Due to higher fissile content, the bundles will be capable of delivering higher burnup than the natural uranium bundles.

In PHWR fuel elements no plenum space is available and the cladding is of collapsible type. The additional fission product swelling and gas release due to use of SEU fuel in PHWRs, needs to be accommodated within the fuel elements taking into account these

factors. Studies have been carried out for different fuel element target burnups with different alternative concepts. Modifications in pellet shape and pellet density are considered.

The element power envelope up to the design burnup for different enrichments generated by reactor physics calculations are utilized for fuel design. The peak linear heat rate (LHR) of the element is maintained same as current natural uranium elements to avoid any thermal hot spots. This has led to increase in residence period corresponding to higher burnups. Following Design studies are carried out for SEU fuel bundle for 220 MWe PHWRs:

2.1.1. Power ramp

Generally 8 bundle fueling scheme is adopted for NU bundles in PHWRs. In the view of power peaking for SEU, Two-bundle rather than 8-bundle fueling scheme has been adopted. The 2-bundles refueling shift will lead to power ramp on the bundles when bundles in the channel are shifted from 4 to 6^{th} location in the channel. This happens at a relatively high burnup of about 7500 MW·d/TeU, The ability of graphite coating to provide resistance to power ramp at these burnups is one of the main concerns. The irradiation performance of the graphite coated natural U and MOX fuel (Natural UO_2-PuO_2) bundles in the 220MWe PHWRs gives the confidence that the graphite coated bundles can withstand the power ramps due to neighboring channel fuelling at higher burnups.

2.1.2. Fuel swelling

At higher burnups, swelling in fuel elements is a concern. To accommodate higher burnups up to 25 000 MW·d/TeU, the fuel (UO_2) density is reduced by 1%.

2.1.3. Residence period

The bundle residence period increases for high burnup fuel. This increases oxidation of cladding. The high fuel burnups lead to more residence period in reactor. The higher residence period has effect on:

(1) Low cycle fatigue behavior of fuel cladding & end plate;
(2) Corrosion and hydriding behavior of the fuel cladding and end plate;
(3) Fretting damage of fuel bundle;
(4) Power ramps at higher burnups.

The SEU fuel bundle flux depression factors across the elements are higher compared to natural U bundle.

2.1.4. Thermo mechanical Analysis (FUDA code) [3]

The FUDA code (Fuel Design Analysis code) MOD2 [4] version has been used in the fuel element analysis. The code takes into account the interdependence of different parameters like fuel pellet temperatures, pellet expansions, fuel-sheath gap heat transfer, sheath strain & stresses, fission gas release and gas pressures, fuel densification etc. Due to this complexity, the code uses mix of empirical, physical and semi-empirical relationships. Finite difference method is used in the calculations to solve differential equation.

The input data requires fuel element material and geometrical parameters and reactor neutronic and thermal hydraulic parameters and element linear heat rating in different burnup zones. The output data generated by program are radial temperature gradient across fuel and

sheath, fuel –sheath heat transfer coefficient, fission gas generated and released, gas pressure, fuel sheath interfacial pressure, sheath stress and strains for different burnup zones.

Thermo-mechanical analysis of the fuel element is carried out using fuel design analysis code FUDA for the power envelope up to burnup 25 000 MW·d/TeU respectively. The resultant thermo-mechanical parameters, such as fuel temperature, gas pressure, etc. for these high burnup bundles were compared with respect to bundle with current burnups. Typical analysis details are given in Table 1. The studies indicated that, present fuel design is suitable up to 25 000 MW·d/TeU with minor modifications like use of higher grain size, more dish depth, etc.

TABLE 1. THERMO-MECHANICAL ANALYSIS OF 19- ELEMENT Fuel BUNDLE [5]

Properties	NU	SEU
Enrichment	0.7 %	0.9 %
Density (g/cc)	10.6	10.5
LHR (kW/m)	60.8	60.8
Burnup (MW·d/TeU)	15000	25000
Fuel Centre Line Peak Temperature (ºC)	2080	2150
Fission Gas Release % (EOL*)	11	10
Fission Gas Pressure (EOL) MPa	9.20	7.29

*EOL: End of Life

2.1.5. Design requirements

The design requirements of fuel bundles have been taken into consideration during thermo-mechanical analysis of the peak rated element of fuel bundle. The fuel bundle safety limits and limiting conditions for operation are derived based on the following factors:

2.1.6. Fuel centre line temperature

Fuel needs to be safe from failure due to excessive thermal expansion. The limiting value on fuel element centre line temperature is the melting point of UO_2 (2840^0C). The limiting condition for design is put based on the onset of centre line melting of fuel. This means a large margin is still available from the condition where damage due to fuel thermal expansion may actually take place.

2.1.7. Clad strain

Fuel cladding fails due to high hoop stress which depends upon internal pressure, temperature of cladding and ductility of cladding. The limiting cladding strain value of 1% is taken as guideline based on data on zircaloy irradiation strain capability. The 1% requirement has come from the ductility requirement of the irradiated fuel.

2.1.8. Fission gas pressure

Fission gas pressure should be less than the coolant pressure during operation for better gap conductance and structural stability in the view of conservative design.

Following changes in pellet design parameters have been investigated to meet the design requirements of the fuel element:

2.1.9. Pellet density

Pellet average density of present natural uranium is 10.60 g/cm^3. A new value of 10.50 g/cm^3 is considered in present analysis.

2.1.10. Pellet dish depth

Average pellet dish depth of 0.50 mm is considered for SEU instead of 0.25 mm.

2.1.11. Bundle power envelope for SEU fuel

The bundle power envelope up to the proposed design burnup for SEU fel generated by physics simulations are utilized as an input for FUDA analysis. Thermo-mechanical analysis was performed keeping the peak bundle power as similar to 19-element NU fuel bundle. This bundle power is 10% higher than the 220 MWe PHWRs operating limit bundle power at higher burnups. The SEU 19-element fuel bundle was analysed up to 25 000 MW·d/TeU. The power burnup histories are obtained from physics simulations.

2.1.12. Observations & discussion

Maximum center line fuel temperatures are found to be about 2150^{0}C for SEU fuel bundles. This temperature is much less as compared to the limiting condition of uranium oxide melting point.

Decrease in density results in more porosity but less conductivity. More porosity accommodates more gas. However, it also decreases the thermal conductivity which is found to results in enhanced fuel temperature in present study and consequently more fission gas release. The net effect is found to be decrease in fission gas pressure. The clad strain also decreases with decrease in density.

Fission gas pressure for 19-element SEU fuel bundle is maintained with in design limits by increasing dish depth due to more space availability for fission gas accommodation. Reduction in gas pressure leads to decreased clad strain for increased dish depth pellets.

2.1.13. Fabrication

The SEU fuel bundles were produced as per the drawings and specifications based on the analysis carried out. The production and quality control plans are similar to 19-elemennt NU fuel bundle fabrication being supplied to all the 220 MWe PHWRs. The bundles were inspected visually and with gauges at site before loading into the fuel transfer system.

2.1.14. Performance

Since June 2009, fifty numbers of SEU fuel bundles of 0.9% ^{235}U isotopic content was loaded in 14 channels of MAPS-2 unit core. These bundles have seen different bundle power histories and recycled from lower flux region to higher flux region. The channels in which SEU bundles are loaded are kept under watch and the DN Counts of these channels are closely observed. Delayed neutron (DN) monitoring of the channels containing these bundles has not shown any variation. Fifteen numbers of bundles have been discharged from the core at average discharged burnup of 16 750 MW·d/TeU. The maximum burnup is achieved around 25 000 MW·d/TeU.

3. THORIUM BUNDLES [6]

India has a long-term strategy of use of thorium in its nuclear power programme. An advanced heavy water reactor is being designed, in addition to deploying Thorium in FBRs in future. It was thus planned to have experience of irradiation of thorium in present power reactors.

3.1. Proposal and design studies

It was planned to use Thorium bundles for flux flattening in the initial core such that the reactor could be operated at rated full power in the initial phase. The Thorium bundle was a 19-element fuel bundle with thorium dioxide as fuel in pellet form. The pellet shapes used were both flat and single dish type. The bundle power of these bundles gradually increases with irradiation exposure time due to production of fissile isotope ^{233}U. The fuel element thermo-mechanical analysis was carried out for elements operating on such an envelope. The elements are designed for a peak linear heat rating of 57.5 KW/m and burnup of 15 000 MW·D/TeHE. The Thorium dioxide pellet specification was evolved which consists of chemical content, density, shape specifications. High density ThO_2 pellets suitable for PHWR were developed at Bhabha Atomic Research Centre, Mumbai, India. The fuel element axial and radial gaps had been suitably specified. By carrying out minor modification in their bearing pad positions, proper identification of these bundles was provided. The fuel bundles were fabricated by Nuclear Fuel Complex, Hyderabad, India.

3.2. Test irradiation

Initially four lead thorium bundles were irradiated in MAPS-1 reactor during the eighties. Subsequently, 35 Thorium bundles have been used as a part of initial charge fuel in the 220 MWe PHWRs for flux flattening in the initial core such that the reactor can be operated at rated full power in the initial phase. These bundles are distributed throughout the core in different bundle locations, both in the high power and low power channels. The criterion used for selection of these locations is such that the worth of the shutdown systems was unaffected. This loading was successfully demonstrated in KAPS-1 and subsequently adopted in the initial reactor loading of KAPS-2, KGS-1&2 and RAPS 3&4.

3.3. Irradiation experience and performance

Numbers of thorium dioxide bundles had been successfully irradiated in different reactors. The maximum fuel bundle power and burnups seen are 408 KW and 13000 MW·d/TeTh respectively. These bundles withstood the power ramps normally experienced in reactor while the typical power envelope of thorium fuel is such that power increases with irradiation. Out of the loaded thorium bundles, one bundle was suspected to have failed during operation at relatively low burnup. The thorium dioxide fuel bundle fabrication and

irradiation had provided valuable experience. Two of these irradiated thorium bundles were under Post Irradiation Examination (PIE) at BARC hot cells.

4. MOX-7 BUNDLES [6]

It was planned to load mixed oxide (MOX) fuel in one of the existing PHWRs. For this purpose, MOX-7 bundle design has been evolved, which is a 19-element cluster, with inner seven elements having MOX pellets consisting of Plutonium dioxide mixed in natural uranium dioxide and outer 12 elements having only natural uranium dioxide pellets. Fig. 2 shows typical MOX fuel bundle.

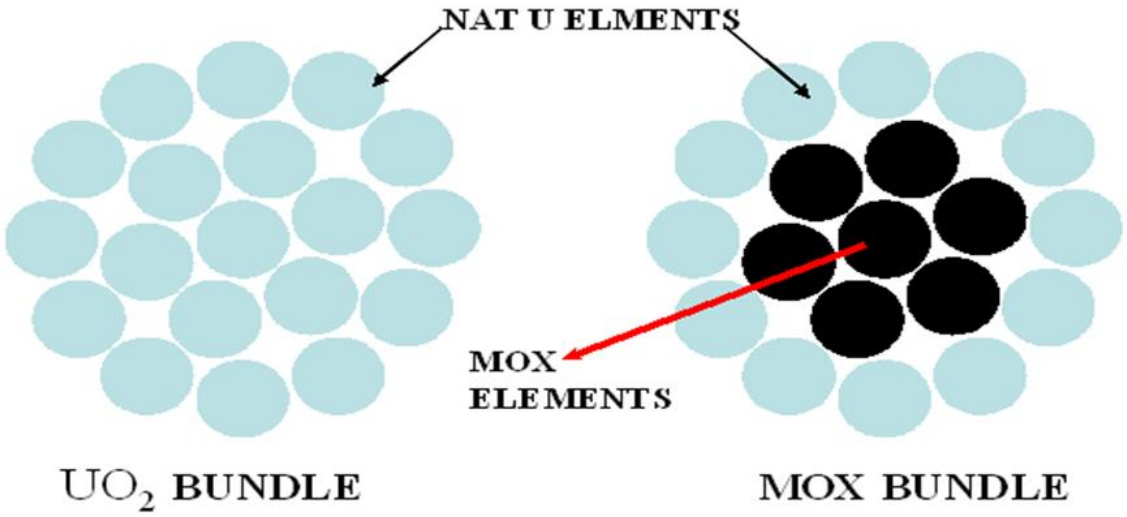

FIG. 2. Natural uranium and MOX 19 element fuel bundles.

Large scale utilization of such bundles leads to substantial savings in the usage of natural uranium bundles. The core average discharge burnup increases to 9000 MW·D/TeHE with this scheme. Due to this, the fueling rate came down from 9 bundles/FPD to 7 bundles/FPD.

Based on detailed studies, an optimized loading pattern and refueling scheme has been evolved for loading initially 50 lead MOX bundles in an existing operating reactor.

The MOX-7 fuel bundle design has been carried out. Maximum linear heat rating (LHR) for MOX bundle occurs for the inner ring MOX elements (Fig. 3). The LHR for these elements are maintained similar to the 19-element natural uranium bundle outer elements. Based on this concept, the fuel bundle power burnup envelope for MOX-7 bundle was evolved. The variation of plutonium content possible in MOX lots is taken into account in this.

4.1. Analysis

The fuel bundle subchannel analysis and thermo-mechanical analysis had been carried out to check for dry out margins for channel loaded with 12 MOX fuel bundles and the thermo-mechanical parameters of the fuel elements respectively. The results show that adequate margins existed for the design parameters of MOX bundles to reach their respective limiting values.

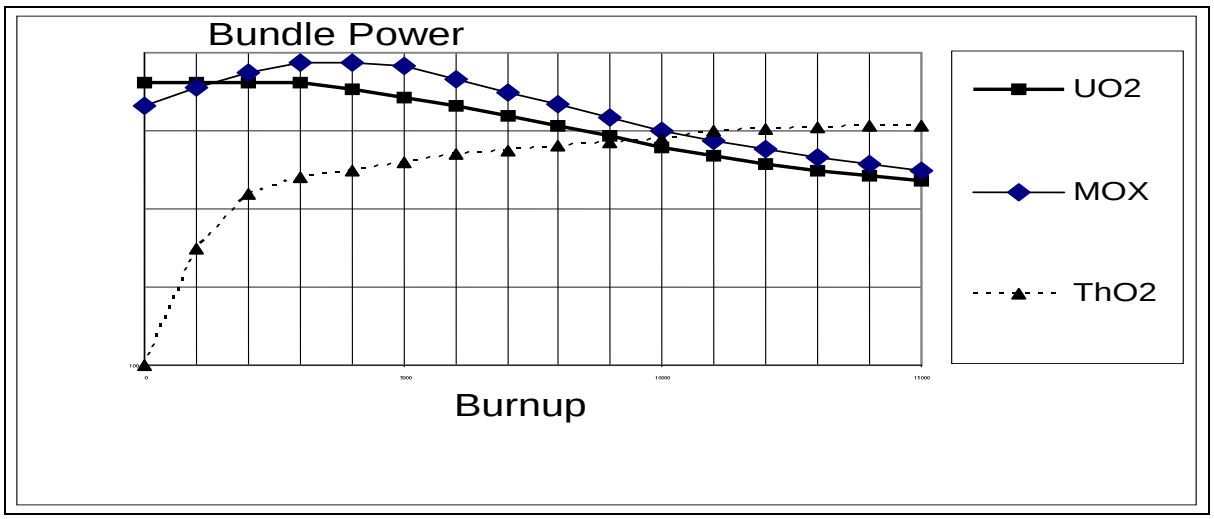

FIG. 3. Bundle power vs burnup for different types of fuel bundles for 220 MWe IPHWRs.

The structural design of end plates was evaluated with respect to strains induced due to difference in power ratings of inner ring of MOX bearing elements as compared to present all natural uranium elements. Due to this, the different elements of bundle expand differently in axial direction. These elements with differential expansion will try to bend the end plates. This gives rise to bending stresses on the end plates of the bundle. There will be cyclic variation of these bending stresses because of bundle power cycling. Analysis was carried out to estimate the stresses in end plate and calculate the number of fatigue cycles, which the fuel bundle can withstand. It was found that present bundle design qualifies the analysis.

4.2. Design and fabrication

Subsequently the fuel bundle drawings and fabrication specifications had been prepared. Provision for identification of bundles provided. The specific requirements for MOX fuel pellet and element fabrication were included. Earlier experience of MOX fuel fabrication and irradiation experience in the BWRs has provided valuable feedback for this purpose. For initial trial irradiation 50 number of MOX-7 bundles have been fabricated by BARC and NFC. Unlike natural uranium bundles, elements of these bundles were seal welded by TIG welding. The pellets were of single dish pellets.

4.3. Irradiation up to higher burnup

These 50 MOX bundles were loaded in the KAPS-1 reactor in different locations in the year 2004. In each refueling four MOX, bundles are loaded in the bundle locations 5 to 8 of the channel. In few channels MOX bundles were loaded in 4^{th} location and subsequently

shuffled to 8th location in the same channel. In order to obtain higher bundle power production from MOX bundles and achieve desired burnup at the earliest, bundles producing about 300 KW in low power channels were recycled to central channels at a burnup of about 2000 MW·D/TeHE. These bundles successfully withstood the power ramps. The performance was good. The DN counts of these channels were steady, indicating good fuel performance of those bundles. The iodine activity in the coolant was maintained quite low. The discharged bundles were sniffed in spent fuel bay and found non defective.

5. CONCLUSIONS

Indian nuclear power program is based on optimum utilization of available uranium and thorium resources in the country. The fuel designs and fuel usage strategies are evolved based on this objective. In addition to natural uranium bundles, the different alternative fuel designs irradiated namely Thorium bundles and MOX bundles have performed well.

For the optimum utilization of available uranium resources in the country, the fuel designs and fuel usage strategies are evolved. In addition to natural uranium bundles, Thorium and MOX-7 bundles; SEU bundles have been designed and test irradiation was carried out in MAPS- Unit 2. The performance of these bundles in core was satisfactory and it has given a confidence to usage of fuel having high burnup and high fissile content.

REFERENCES

[1] TRIPATHI, R.M. et al, “Fuel Element Designs for Achieving High Burnups in 220 MWe Indian PHWRs”, Technical Meeting on Advanced Fuel Pellets Materials and Fuel Rod Designs for Water Cooled Reactors , 23-26 November 2009, PSI, Villigen, Switzerland (2009).

[2] CHOUHAN, S.K. et al, “Fuel Design for 0.9% SEU use in 220 MWe Indian PHWRs”, Characterization and Quality Control of Nuclear Fuels (CQCNF), February 2012, Hyderabad, India (2002).

[3] PRASAD, P.N. et al, “Computer Code for Fuel Design Analysis FUDA MOD 0”. NPC Internal Report, NPC-500/F&S/01 (1991).

[4] FUDA MOD-2 manual, NPC-500/DC/37000/08-Rev-0 (1996).

[5] TRIPATHI, R.M. et al, “Design and Performance of Slightly Enriched Uranium Fuel Bundles in Indian PHWRs”, Technical Meeting on Fuel Integrity during Normal Operating and Accident Conditions in PHWR, 24–27 September 2012, Bucharest, Romania (2012).

[6] PRASAD, P.N. et al, “Design, Development and Operating Experience of Thorium and MOX Bundles in PHWRS”, in Proc. International CANDU Fuel Conference, (2005).

INR RECENT CONTRIBUTIONS TO THORIUM-BASED FUEL USING IN CANDU REACTORS

I. PRODEA, C. A. MĂRGEANU, A. RIZOIU, G. OLTEANU
Institute for Nuclear Research Pitesti
Mioveni, Romania
Email: iosif.prodea@nuclear.ro

Abstract

The paper summarizes INR Pitesti contributions and latest developments to the Thorium-based fuel (TF) using in present CANDU nuclear reactors. Earlier studies performed in INR Pitesti revealed the CANDU design potential to use Recovered Uranium (RU) and Slightly Enriched Uranium (SEU) as alternative fuels in PHWRs. In this paper, we performed both lattice and CANDU core calculations using TF, revealing the main neutron physics parameters of interest: k-infinity, coolant void reactivity (CVR), channel and bundle power distributions over a CANDU 6 reactor core similar to that of Cernavoda, Unit 1. We modelled the so called Once Through Thorium (OTT) fuel cycle, using the 3D finite-differences DIREN code, developed in INR. The INR flexible SEU-43 bundle design was the candidate for TF carrying. Preliminary analysis regarding TF burning in CANDU reactors has been performed using the finite differences 3D code DIREN. TFs showed safety features improvement regarding lower CVRs in the case of fresh fuel use. Improvements added to the INR ELESIM-TORIU-1 computer code give the possibility to fairly simulate irradiation experiments in INR TRIGA research reactor. Efforts are still needed in order to get better accuracy and agreement of simulations to the experimental results.

Key words: Thorium, CANDU, SEU-43, WIMS, DIREN, ELESIM.

1. INTRODUCTION

The paper presents INR Pitesti contributions and latest developments to the Thorium-based Fuel (TF) using in present CANDU-PHWR nuclear reactors. Also, it continues earlier studies dedicated to the using alternative fuel cycles in CANDU reactors based on SEU, RU and MOX fuels. Despite the fact that Romanian Nuclear Energy Strategy foresees other two units to be commissioned in Cernavoda NPP by the end of actual decade, the lack of strategic in investors led to the slow advancement of the nuclear new builds program.

Face to actual situation, Romanian scientific nuclear energy community is mandated to conduct the research directed to alternative fuel cycle, possible to be used in existing CANDU- reactors. It is clear that this would surely be more cost effective than the build of new units. Advanced knowledge and research along with experimental work are to be performed in order to evaluate the suitability of one or another fuel cycle.

Someone may wonder why CANDU instead of, let say, a new Gen. III+ or IV project? Despite of its relatively older technology, in the light of Fukushima accident, Romanian CANDU reactors have passed successfully the "stress test". The stress test performed by an interdisciplinary team of experts, concluded in [1] that Romanian CANDU reactors have sufficient safety margins and high robustness in order to cope with extremely weather conditions, like those underwent by Fukushima-Daiichi NPP.

In this paper we investigate through the performing both lattice and CANDU core calculations the influence of different Thorium-based fuels on the main neutron physics parameters of interest: k-infinity, coolant void reactivity (CVR), channel and bundle power distributions over a CANDU 6 reactor core similar to that of Cernavoda, Unit 1 [2].

We modelled the so called Once-Through-Thorium (OTT) fuel cycle, proposed by AECL [3], in both mixed-core and mixed fuel bundle approaches using the 3D finite-differences DIREN code, developed in INR [4]. The INR flexible SEU-43 bundle design (Figures 1 & 2) [5] was the candidate for fuel carrying the Th-based fuels.

A major challenge was underlined in [6] and it rises from dependence of ^{233}U generating from ^{232}Th by neutron flux level. The process is similar to that of ^{239}Pu generation from ^{238}U, but while Pu equilibrium concentration is 0.4% from that of ^{238}U concentration, ^{233}U equilibrium concentration is about 1.5% of that of ^{233}U. That means the flux level should be taken into account in estimation of ^{233}U final concentration [6].

In the final part of the paper, experimental results from nuclear fuel element A23 irradiation in INR TRIGA reactor is described.

2. FUEL BUNDLE DESIGN AND LATTICE BURNUP AND CORE METHODOLOGY

The Th-based fuel compositions by inner rings (Central Element=CE, R1, R2, R3), considered in our study are presented in Table 1, below.

TABLE 1. THORIUM BASED FUEL BUNDLE COMPOSITION DESIGNS

Th-based fuel design	Composition by inner rings	Th232 (kg)	U235 (kg)	U238 (kg)	Gd (kg)	Total mass Th/U HE (kg)
OTT-1	CE: ThO2	0.51	0	-	-	
	R1: ThO2	3.59	0	-	-	4.1 / 14.2
	R2: 1.8% SEU	-	0.102	5.58	-	18.3
	R3: 1.8% SEU	-	0.153	8.37	-	
OTT-2	CE: ThO2	0.51	-	-	0.030	
	R1: ThO2	3.59	-	-	-	4.1 / 14.2
	R2: 1.8% SEU	0	0.102	5.58	-	18.3
	R3: 1.8% SEU	0	0.153	8.37	-	
OTT-3	CE: ThO2	0.51	-	0	-	
	R1: ThO2	3.59	-	0	-	15.85 / 1.09
	R2: 1.8% SEU	4.7	0.087	0.349	-	16.94
	R3: 1.8% SEU	7.05	0.131	0.523	-	

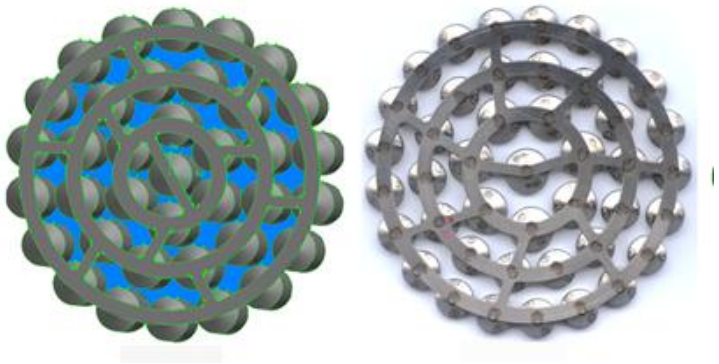

FIG. 1. 37-NU (left) face to SEU-43 (right) Bundle Designs, [7].

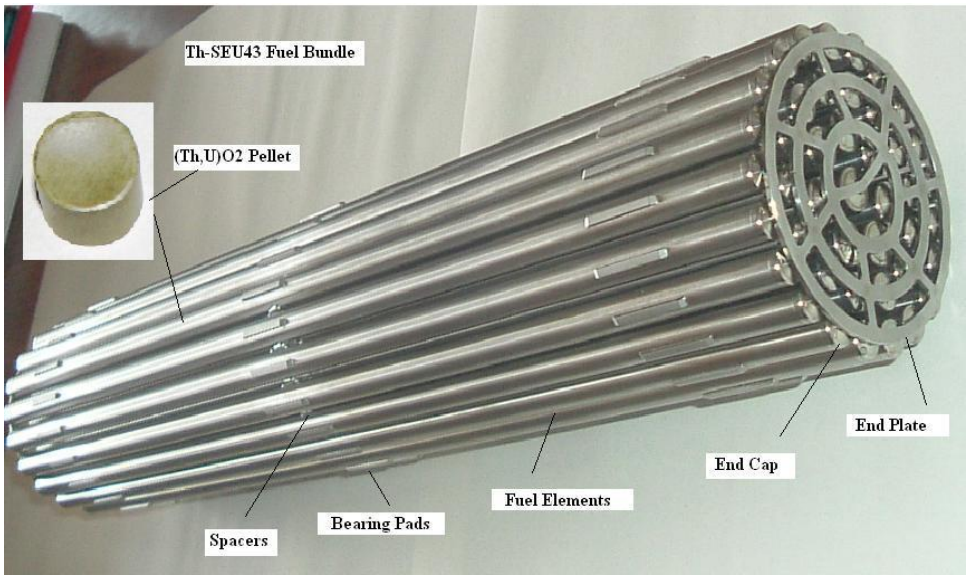

FIG. 2. SEU-43 Bundle Design filled with (ThU)O_2 fuel, [8].

First of all, lattice burnup calculations have been performed with the WIMS-D5B code [9] and associated IAEA nuclear data library [10], in order to generate macroscopic cross sections tables with respect to the burnup, up to 38-40 MW·d/kgU. Then, with these data and using a standard CANDU 6 core model [2], [11] adapted to the DIREN input, we performed a suite of *time average* calculations to find out reference data for refuelling: reference burnup and channel power distributions along with ZCU reference radial power distribution, (in %). Varying the discharge burnup values on the burnup regions as shown in Figs. 3 and 4, we should achieve a symmetric ZCU radial powers and a maximum channel power value around of 6.5 MW. Two core approach options were taken into account, as in Figs. 3 and 4. The burnup regions are denoted by digits (1, 2, 3, 4, 5) while the different fuel channel composition is underlined in Figure 4, by different pattern colours (brown=inner core (124 channels), yellow=middle core (196 channels), white=peripheral core (60 channels).

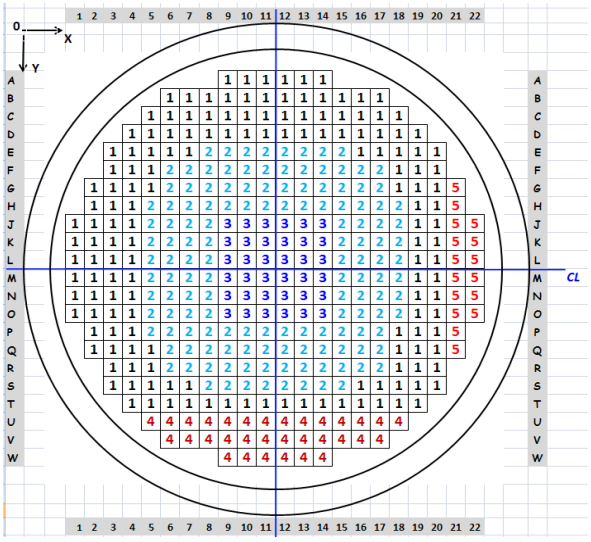

FIG. 3. Core Th-1 option (OTT1 fuel design overall the core).

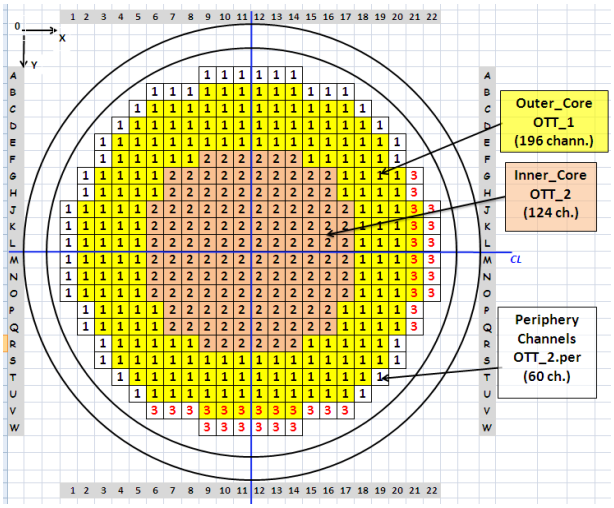

FIG. 4. Core Th-2 option (mix of OTT-1, OTT-2 and OTT- 3 fuel designs).

The first core approach (Th-1) assumes feeding the entire core with OTT-1 fuel design with 5 different fuel burnup regions in order to achieve requested symmetric ZCU power distribution and a Maximum Channel Power (MCP) around of 6.5 MW.

The second core approach (Th-2) is based on different core compositions: in the inner 124 channels OTT-2 fuel design is used (with 6% Gd in the CE), in the intermediate 196 channels OTT-1 is used and in the outermost 60 channels OTT-3 is used, see Table 1.

3. RESULTS

The first results are presented in Fig. 5 in form of k-inf variation with respect to fuel burnup for the three Th-based fuel design from Table 1.

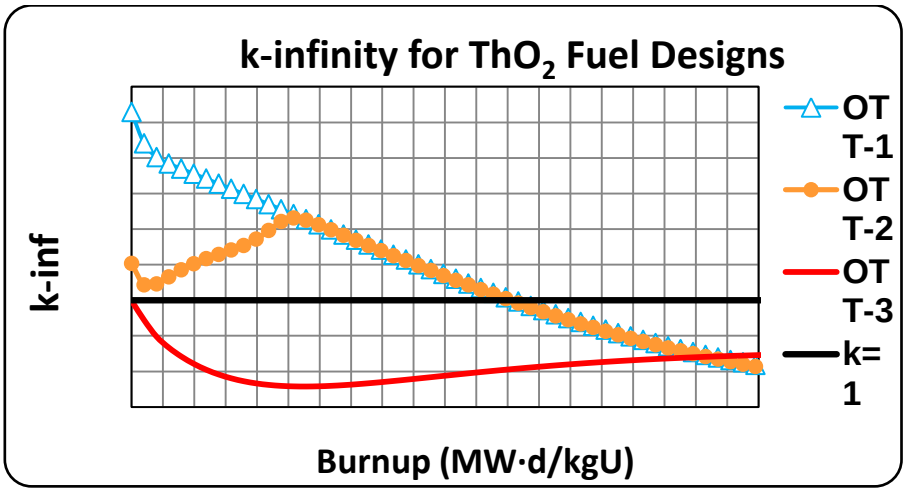

FIG. 5. Lattice k-inf variation with respect to the burnup.

It can be observed that the presence of Gd absorbent in the CE (orange curve) limits the initial reactivity excess face to OTT-1. As Gd burnable absorber is consuming, the reactivity build-up until the burnup attains 5 MW·d/kg, then it starts to decrease following the standard decreasing law, as in OTT-1. Regarding OTT-3 Th fuel design, despite of its k-inf under 1, it can be taken into account for differentiated core region composition approach (peripheral channels), as in Th-2 core option.

The first core results are presented in form of channel power maps corresponding to the well known and documented *time/average* calculations [12].

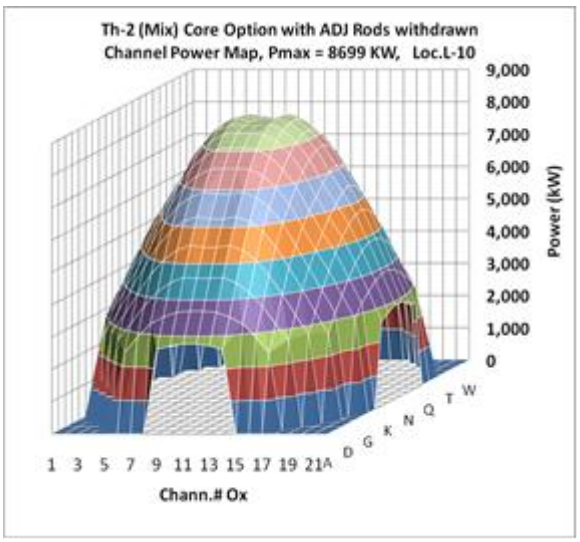

FIG. 6. Th-1 channel power map, Pmax.

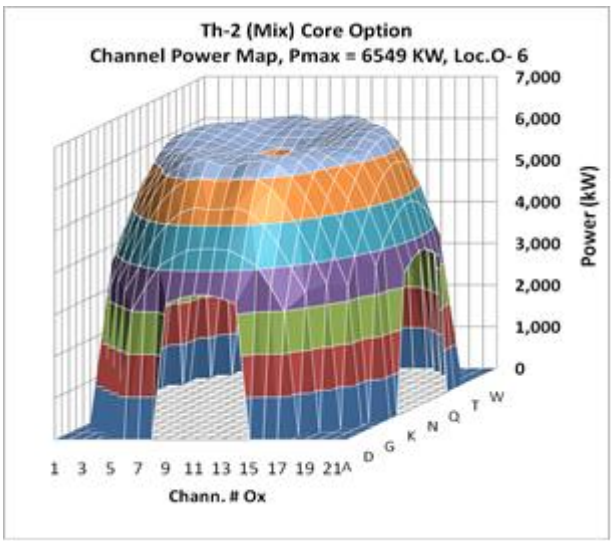

FIG. 7. NU channel power map.

A very well flattening of power for Th-1 and Th-2 core options can be observed in Figs. 6 and 8, similar to that of NU standard CANDU-6 core shown in Fig. 7, for comparison.

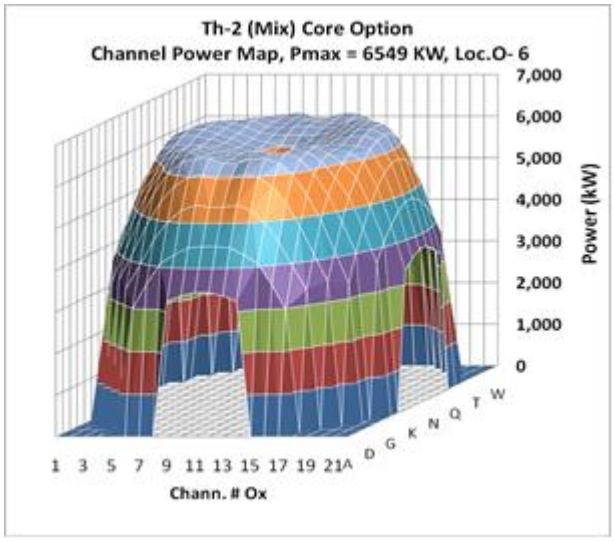

FIG. 8. Th-2 channel power map (ADJ rods in).

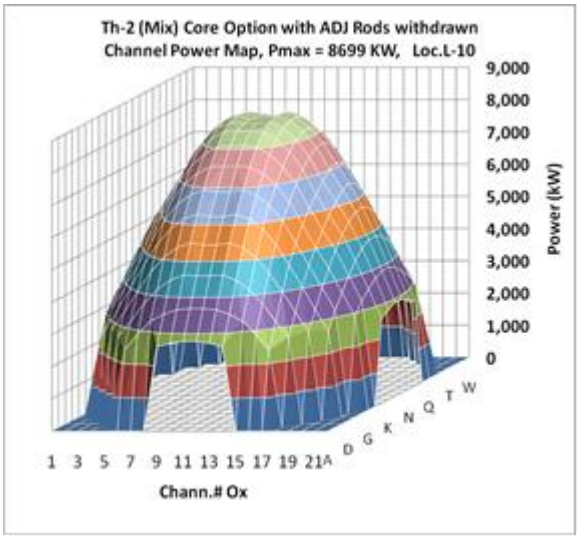

FIG. 9. Th-2 channel power map (ADJ rods out).

Also, for comparison purpose, in the Th-2 mixed core option adjuster rods (ADJ) removing was simulated, the corresponding channel power map being presented in Fig. 9. The flattening feature offered by ADJ system is very well emphasized.

Core integral parameters supplied by Th-1 and Th-2 core options in time/average approximation are presented in Table 2, comparatively to those supplied by NU based one.

TABLE 2. TIME AVERAGE CORE NEUTRONIC CHARACTERISTICS

Core Parameter	NU option (std. 37 el. fuel bundle)	Th-1 (OTT-1 fuel bundles)	Th-2 (mixed core)
ZCU powers (%)	16.69 12.96 12.95 14.96 12.94 12.92 16.58	16.83 12.85 12.85 15.00 12.77 12.80 16.89	16.8 13.05 13.00 14.32 13.03 13.01 16.8
Burnup on the four regions (MW·d/kgU)	*1 2 3 4* 6.35 7.0 6.5 5.95	*1 2 3 4 5* 16.8 21.3 21.2 16.2 16.4	*1 2 3 4* 17.7 15.5 17.37 17.4
Average Discharge Burnup (ADB) (MW·d/kgU))	6.65	19.12	16.65
Max. channel power and location	6.54 MW P-8	6.54 MW M-14	6.55 MW O-6
Max.bundle power and location	804 kW S 11 - 6	731 kW M-14- 4	869 kW O- 6- 6
k-effective	1.000066	1.000342	1.000154
Core reactivity (mk)	0.07	0.3	0.15
Bundle shift scheme	8-bundle	2 bundle	2 bundle
Channel refuelling time (days)	207	127	113

As it can be seen, all the mandatory conditions (core criticality range of ±0.5 mk, ZCU power good symmetry and maximum channel power around of 6.5MW) in order to (eventually) start core-follow simulations have been accomplished. Of interest is the Average Discharge Burnup (ADB) evaluated through time/average (TA) calculations. As expected, both Th-based option fuel designs supplied an ADB significantly larger than that of NU: 19.2 MW·d/kgU and 16.65 MW·d/kgU face to 6.65 MW·d/kgU. Regarding the refuelling time, despite the fact that it is smaller than that of NU, we must observe that refuelling scheme for Th option supposed only two bundle using per operation. That means 8 fuel bundles will be refuelled in about 4 times longer period than channel refuelling time estimated by code, i.e for Th-1 option in about 4* 127=508 days. The choosing of two bundle scheme has been done in order to have more flexibility in the planned refuelling calculations, instead of minimizing fuelling machine usage.

The first refuelling calculations have been performed for Th-1 core option, specific results being presented in Figs. 10 and 11.

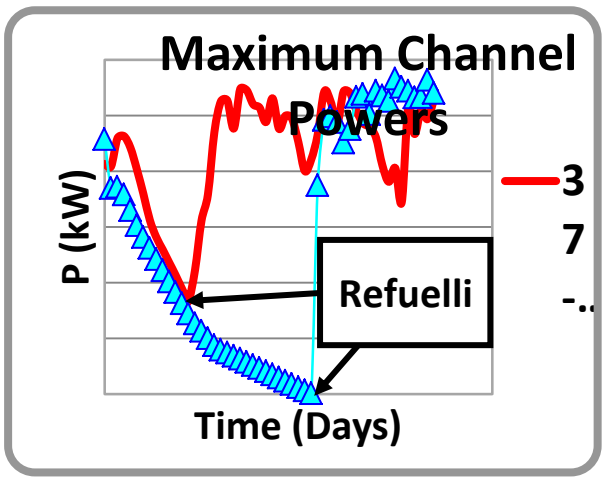

Fig. 10. Th-1 &NU Max. channel power in the first 500 days of core-follow simulation.

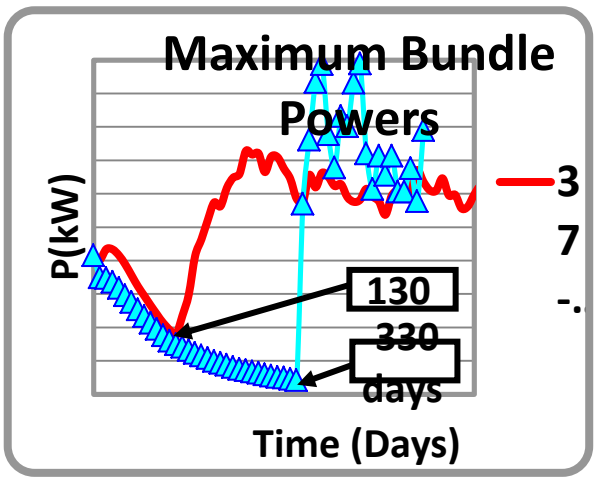

Fig. 11. Th-1 & NU Max. bundle power in the first 500 days of core-follow simulation.

Figs. 10 and 11 illustrate the maximum channel power (MCP) and maximum bundle power (MBP) evolutions during a 500 days interval, simulated for Th-1 and NU core designs. The refuelling is started at 130 days for NU and 330 days for Th-1 based fuel. While the imposed values for MCP are not override, in the case of MBP, some peaks over 1000 kW are revealed for Th-1 core option. Limiting of these effects can only be assured if the reactor power is reduced to 80% in the corresponding period of simulation. Improvements in DIREN modelling are still needed, in order to take into account for flux level dependence on previous step simulated, as is suggested in [6]. This work is planned to be accomplished up to the next IAEA event dedicated to PHWR, or in the frame of another collaborative project, in which, eventually Romania would be part.

TABLE 3. CORE INTEGRAL PARAMETERS GENERATED BY DIREN REFUELLING CALCULATIONS

Parameter	NU-37, [13] (0.72%U235)	RU-43, [13] (0.96%U235)	Th-1 (1.8% U235 in U mass 1.39% U235 in HE mass, see Table 1)
Discharged Bundles	6520	3228	1596
FPD	500	500	500
#Bundles/FPD	13.04	6.46	3.19
HE bundle mass (kg)	19.3	18.6	18.3
HE consumption = #Bundles/FPD HE bundle mass (kgHE/FPD)	251.3	120.3	58.4
Daily Energy (DE) = Fission Power(MWt) 1 Day	2156 MW·d	2156 MW·d	2156 MW·d
Refuelling Average Burnup (RAB) = DE/HE consumption (MW·d/kgHE)	8.58	17.9	36.9

In Table 3, core integral parameters generated by DIREN refuelling calculations in the case of Th-1 option (the same bundle composition overall the core) are presented, comparatively to those corresponding to 37-rods Natural Uranium fuel bundle (37-NU) and Recycled Uranium (RU-43) bundle options [13].

The lack of Th-1 refuelling results beyond 500 days, determined this comparison to be based only on the first 500 of evolution. It must be underlined that all Refuelling Average Burnup (RAB) values are a coarse estimation of HE consumption. It depends on the number of FPD considered in simulation. For example in [13], NU-37 core option supplied an RAB of about 7 MW·d/kg throughout of 700 FPD, while RU-43 core option supplied about 14 MW·d/kg throughout of 900 FPD. Anyway, we consider that the results from Table 3 are proportional, despite of systematic overestimation. A gross doubling of RAB value is shown by Th-1 option compared to that of RU-43 option, accordingly, we think, to about up to twice higher enrichment.

Safety aspects of Th-based, RU, SEU and MOX fuel have been evaluated through the lattice CVR calculation. CVRs were estimated by simply and uniformly reducing the coolant density. The results are presented in Table 4 and Fig. 12.

TABLE 4**.** CVR FOR ADVANCED FUEL DESIGNSTO BE USED IN CANDU REACTORS

Parameter	CVR for Fresh fuel (mk)	CVR for Equilibrium fuel (mk)
37-NU	15.5	10.6 (6.5 MW·d/kgHE)
RU-43 (0.96%)	13.9	10.5 (9.5 MW·d/kgHE)
SEU (1.1%)	12.8	8.5 (6.5 MW·d/kgHE)
MOX*	-8.4 [6]	40.5[6] (120 MW·d/ bundle)
OTT-1	6.2	9.7 (6.5 MW·d/kgHE)
OTT-2 (*with Gd*)	-16.3	10.4 (6.5 MW·d/kgHE)
OTT-3	6.3	10.4 (6.5 MW·d/kgHE)

*MOX Fuel is based on 210 g Pu in an inert matrix of Si_4C with 60g of Gd, see [14]

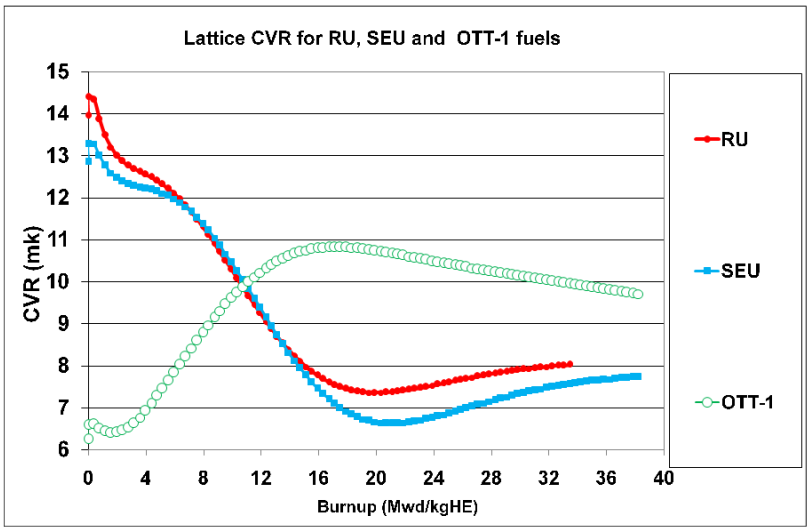

FIG. 12. CVR for RU, SEU and OTT-1 fuels.

Despite of the fact that Th-based fuel CVR values still remain positive in all configurations, their values for fresh fuel are significantly lower than that of NU, RU and SEU, showing improved safety features.

Recent INR Pitesti experimental developments in the frame of Th-based fuel testing consisted in irradiation of experimental nuclear fuel elements **A23** and **A24** along with experiment simulation with *ELESIM-TORIU-1* computer code [8].

Fuel design

The A23 fuel element (Fig. 13) contains pellets with mixed oxide of Thorium and Uranium (5 % ^{235}U) while A24 contains only UO_2 pellets (5% ^{235}U). The nominal design characteristics of A23 and A24 elements have been underlined in a paper presented in September 2012 at another IAEA meeting in Bucharest [15].

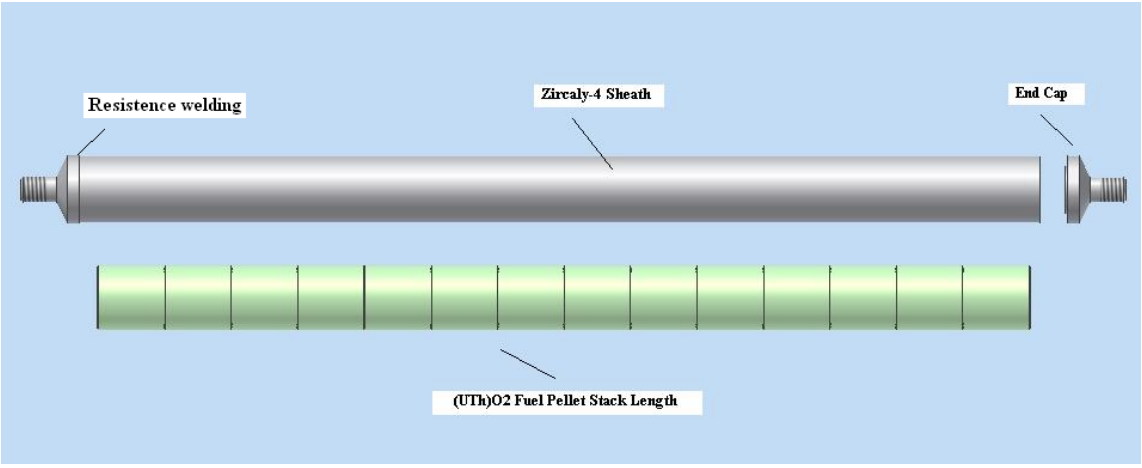

FIG. 13. Experimental fuel element A23 design.

Also, irradiation conditions have been well described in [15] according to Table 5.

TABLE 5. AVERAGE A23 ELEMENT POWERS AND BURNUPS

Experimental element	Linear power [Kw/m]		Discharge burnup [Mwh/Kg H.E.]
	Pre-ramp	Ramp (for 7 days)	
A23	33	49.8	189.2

The experiment simulation with ELESIM-TORIU-1 computer code is the main advancement since Sep. 2012 IAEA meeting. An improved version of the ELESIM computer code (ELESIM-THORIU-1) developed by Nuclear Fuel Performance Division was used. This version includes improvements, among which we mention: theoretical density depending on composition, higher melting point ($3370 \pm 20^{o}C$), temperature threshold of plasticity, thermal conductivity of $(Th,U)O_2$, coefficient of thermal expansion, equi-axed grain growths, columnar grain growths, fuel densification, fission gas release, fission gas release and burnup dependence implementation.

Irradiation history

As actual variant of code does not allow more than 50 data blocks, the real history of irradiation has been processed. Nuclear fuel irradiation history is presented in Fig. 14. ELESIM-THORIU-1 input data file was done on the basis of its original documentation [15, 16, 17] and included both geometry (pellet/sheath) and irradiation data (irradiation history). The ELESIM-THORIU-1 results are shown in Figs. 14–17.

TABLE 6. FISSION GAS RELEASE OBTAINED AFTER POST IRRADIATION ANALYSIS

Experimental fuel element	Filling gas volume [cm^3 at STP]
A23	5.5
A24	15.9

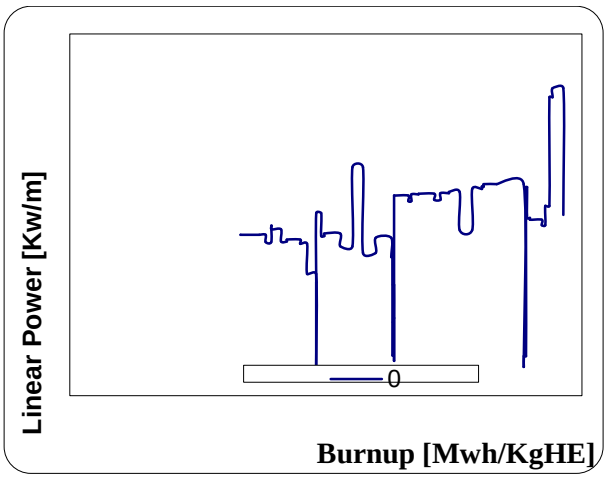

FIG. 14. Irradiation history of A23 experimental fuel element.

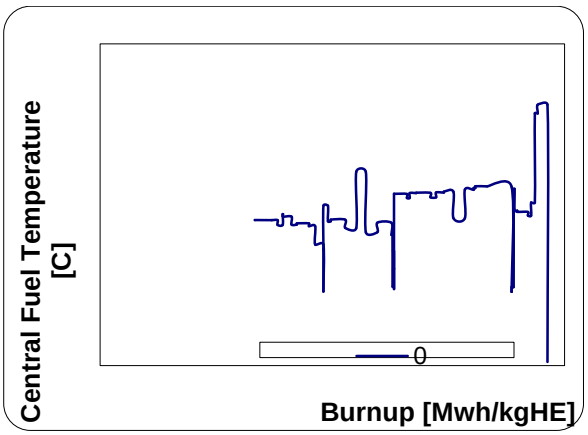

FIG. 15. Evolution of fuel centre temperature.

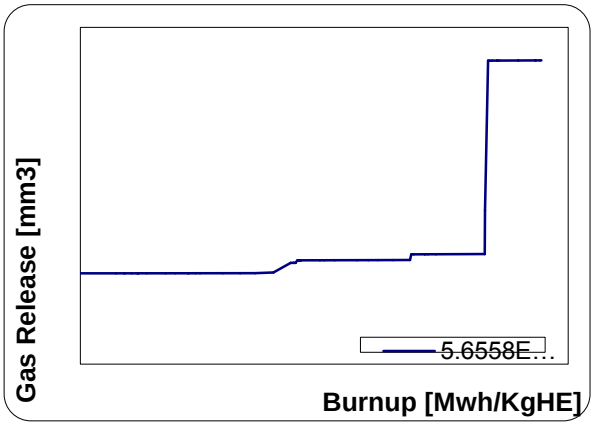

FIG. 16. Gas Release Volume for A23 element.

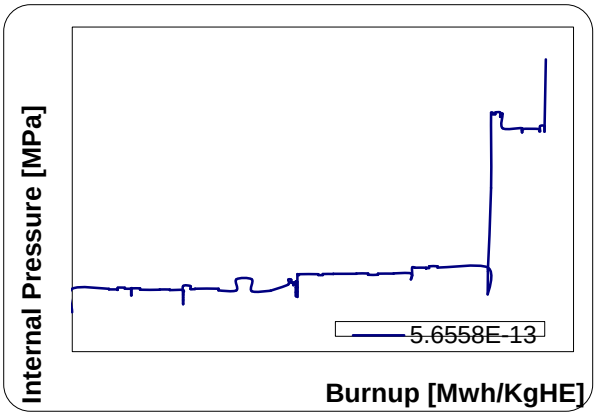

FIG. 17. Internal pressure profile for experimental fuel element A23.

The maximum central pellet temperature is around of 1460^{o}C (Fig. 15) and the temperature on the surface pellet achieves a maximum value of 396^{o} C. The volume of gas released rises up to 3.6 cm^{3} and the pressure gas, inside the element, attains a value of 1.8 MPa (Figs. 16 and 17). Because of the low value of the temperature obtained in the central pellet (1460 ^{o}C), the metallography analysis should come in support of certification the obtained value.

The volume of fission gas release, obtained with ELESIM-THORIU-1 code (3.6 cm^{3}), is in a fair accordance with the value obtained from post irradiation examination (5.5 cm^{3}, see Table 6).

4. CONCLUSIONS

Preliminary analysis regarding Th-based fuel burning in CANDU reactors can be performed using the finite differences 3D code DIREN. Better core refuelling simulations can

also be possible after DIREN algorithm improvement in order take into account for peculiar burnup of Th-based fuels.

Th-based fuels showed safety features improvement regarding lower CVRs at fresh fuel using.

Some improvements added to the ELESIM-TORIU-1 computer code give the possibility to fairly simulate irradiation experiments in INR TRIGA research reactor. Efforts are still needed in order to get better accuracy and agreement of simulations to the experimental results.

ACKNOWLEDGEMENTS

The main author thanks the IAEA, especially the Nuclear Fuel Cycle and Waste Technology Division (Nuclear Energy Dept.), for supporting this work and his participation in the Technical Meeting on "Advanced Fuel Cycles in PHWR", in Mumbai, India, on 8-11 April 2013.

REFERENCES

[1] NATIONAL COMMISSION FOR NUCLEAR ACTIVITY CONTROL, National Report on the Implementation of the Stress Tests (2011) http://www.cncan.ro/assets/stiri/ROMANIA-National-Report-on-NPP-Stress-Tests

[2] BARAITARU, N., A New core model for neutronic calculations with RFSP-IST (CV03M4.0), Cernavoda NPP Unit-1, Reactor Physics and Safety Analysis Group, IR-03310-34, Rev.0 (2004).

[3] INTERNATIONAL ATOMIC ENERGY IAEA, Thorium fuel cycle - Potential benefits and challenges, IAEA-TECDOC-1450 (2005).

[4] PATRULESCU, I., Developing of DIREN code for Multigroup Core Calculations, Internal Report no. 5120, INR Pitesti (1997).

[5] HORHOIANU, G. et al., Development of Romanian SEU-43 fuel bundle for CANDU type reactors, Annals of Nuclear Energy, **25** 1363 (1998) 1372.

[6] PATRULESCU, I. DOBREA, G., Evaluation of Reactor Physics Implication at the Using of Advanced Fuel Cycles based on RU, SEU, MOX and Th in CANDU Reactors, INR Pitesti, IR-8001 (2007).

[7] CATANA, A., Thermalhydraulics Advanced Methods for Nuclear Reactors (CFD and Subchannel Analyses for CANDU 600 Core), PhD Thesis, POLITEHNICA University of Bucharest, Power Engineering Faculty (2010).

[8] MARGEANU, C. A., RIZOIU, A., OLTEANU, G., Th-based mixed with Pu and U Oxides Fuel Behaviour Evaluation in CANDU Reactors, INR Pitesti, IR-9495 (2012).

[9] WIMSD5B - NEA1507/03 Package, http://www.nea.fr/dbprog

[10] WLUP-WIMS Library Update Project, http://www-nds.iaea.org/wimsd/download/iaea.zip

[11] BARAOTARU, N., Description and Material Structure for Reactivity Devices and Other Components present inside a CANDU-600 Core, Cernavoda NPP Unit-1, Reactor Physics and Safety Analysis Group, IR-03310-17 (2000).

[12] ROUBEN, B., "Fuel Management in CANDU", Presented at Chulalongkorn University Bangkok, Thailand, 1997, https://canteach.candu.org/Content%20Library/20043404.pdf.

[13] PRODEA, I., HORHOIANU, G., OLTEANU, G., “Recovered Versus Natural Uranium Core Fuel Management Study in a CANDU 6 Reactor”, SIEN 2011, Bucharest, Romania (2011).
[14] INTERNATIONAL ATOMIC ENERGY IAEA, “Heavy Water Reactors: Status and Projected Development", Technical Report Series no.407 (2002).
[15] HORHOIANU, G., OLTEANU, G., “Irradiation Behaviour of PHWR Type Fuel Elements Containing UO_2 and $(Th,U)O_2$ Pellets”, IAEA Meeting on Fuel Integrity during Normal Operations and Accident Conditions in PHWR, September 24–27, 2012, Bucharest, Romania (2012).
[16] OLTEANU, G., et. al., Test specification for Irradiation of A23 and A24 Fuel Elements in C1 Capsule of TRIGA Reactor, INR Internal Report No. 2247/1987, INR Pitesti, Romania.
[17] DRAGOMIRESCU, C., et. al, Irradiation of A23 and A24 Fuel elements in TRIGA Reactor of INR Pitesti, Internal Report No. 2608/1988, INR Pitesti.
[18] BALAN, V., et. al, Fabrication of A23 and A24 Fuel Elements, INR IR-2307/1987, INR Pitesti, Romania.

UTILISATION OF THORIUM IN AHWRS

V. SHIVAKUMAR, V. VAZE, V. JOEMON, P.K. VIJAYAN
Bhabha Atomic Research Centre,
Mumbay, India
Email: vshiv@barc.gov.in

Abstract

Advanced Heavy Water Reactors (AHWRs) based on thorium fuel cycle are being designed at BARC. These reactors are vertical pressure tube type, boiling light water cooled, and heavy water moderated reactors. AHWR will use (Th-Pu) MOX and (Th-233U) MOX fuels. The fissile 233U for this reactor will be obtained by reprocessing its spent fuel, while plutonium will be provided from reprocessing of the PHWR spent fuel. The adoption of closed fuel cycle in AHWR helps in generating a large fraction of energy from thorium. A co-located fuel cycle facility is planned along with the reactor and it will have facilities for fuel fabrication, fuel reprocessing and waste management. AHWR300-LEU will use (Thorium-LEU) MOX as fuel with LEU (Low Enriched Uranium) having 235U enrichment of 19.75%. The reactor is being designed based on open fuel cycle. A provision is however being made for long-term storage of the spent fuel which will keep open the option of reprocessing the spent fuel at a later date. The AHWRs will provide a platform for demonstration of technologies required for thorium utilisation. This paper briefly describes the major challenges in large-scale utilisation of thorium and the fuel development programmes being carried out at BARC on the thoria based MOX fuels.

1. INTRODUCTION

Thorium is three to four times more abundant than uranium and is widely distributed globally. This led to a lot of worldwide focus on thorium fuel based systems during the early years of nuclear energy development. A major difference between the two nuclear energy resources is that thorium has to be converted to fissile ^{233}U for its use as fuel. The initial enthusiasm to supplement uranium with thorium in view of the predictions of uranium shortage waned later among the developed nations, due to discovery of new deposits of uranium and saturation in their electricity demand. In recent times, there has however been a renewed global interest in thorium-based fuels due to the need for some of the advantages it offers like greater proliferation-resistance, potential for higher fuel burnup, and improved waste form characteristics. ^{233}U in comparison to the other two fissile materials ^{235}U and ^{239}Pu is the best in terms of neutronics in power reactors. For thermal or epithermal neutron energies, the eta (ratio of neutron yield per fission to neutrons absorbed) is higher to that of ^{235}U or ^{239}Pu. ^{233}U therefore has the required physics characteristics for use in any (Th-^{233}U) based reactor system and as a sustainable option. [1]

In the context of Indian nuclear programme, thorium has always had a prominent place due to our unique resource position of having large thorium deposits, but limited uranium reserves. A three stage programme has been devised to effectively utilize the available resources. The first stage involves utilisation of natural uranium in PHWRs (Pressurised Heavy Water Reactor). The second stage involves the utilisation of plutonium obtained from reprocessing the spent PHWR fuel in fast reactors. The second stage will also provide the required ^{233}U for the third stage which involves the Th–^{233}U cycle based reactor system. The large-scale utilisation of thorium will require the adoption of closed cycle which poses several challenges. The development studies in India for the use of thorium in reactors have focused on both front end and back end of fuel cycle. To provide impetus to this programme, the thorium fuel cycle based advanced heavy water reactor (AHWR) has been conceptualized.

Besides AHWR, the high temperature reactors (HTRs) being developed by India also aims to utilize thorium in a big way [2].

This paper brings out the history of thorium utilization in power reactors, the Indian advanced reactor designs utilizing thorium and some of the challenges in utilizing thorium.

2. INDIAN EXPERIENCE IN THE USE OF THORIUM

In India, work on thorium fuel has been carried out right from the inception of our nuclear programme. Studies have been carried out on all aspects of thorium fuel cycle: mining and extraction, fuel fabrication, utilisation in different reactor systems, evaluation of its various properties and irradiation behaviour, reprocessing and recycling [3–4].

Thoria fuel assemblies known as 'J' rods were irradiated in the reflector region of research reactor CIRUS. Thoria fuel assemblies were also loaded in research reactor Dhruva during its initial days of operation to take care of the excess reactivity of the initial core. These assemblies were similar in design to that of the natural uranium assemblies of the reactor. The irradiated thoria has been reprocessed to recover ^{233}U and used in KAMINI reactor. Thoria fuel bundles have been irradiated in PHWRs for initial core flux flattening. The design of these thoria fuel bundles was identical to that of the urania fuel bundles to ensure compatibility with other reactor systems. A total of 232 thoria bundles have been irradiated in PHWRs. The details of the loading of fuel bundles in different reactors and their irradiation history are given in the below Figure 1.

Reactor	No. of bundles
MAPS- I	4
KAPS - I	35
KAPS - II	35
RAPS - II	18
RAPS - III	35
KGS - II	35
RAPS - IV	35
KGS- I	35

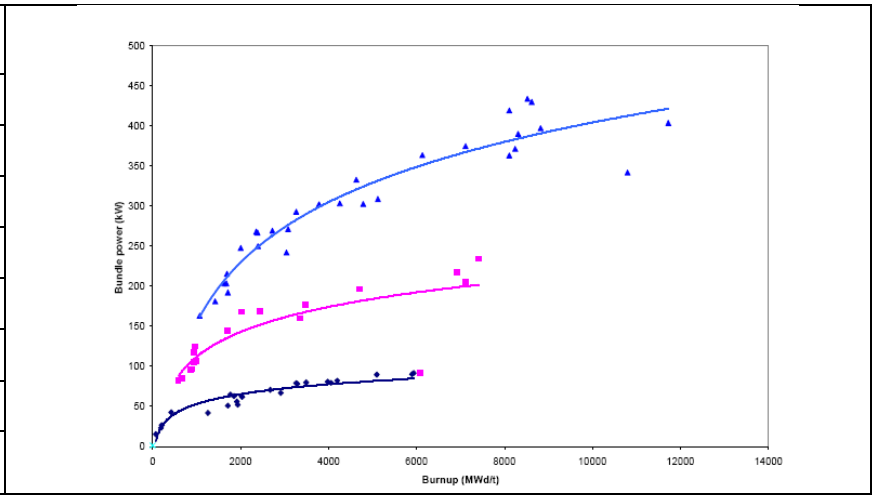

FIG. 1. Details of thoria fuel bundles loaded in different PHWRs.

Thoria based (Th-Pu) MOX fuels have been test irradiated in the Pressurised Water Loop (PWL) of CIRUS reactor and Dhruva. The different fuel pins are:

(1) (Th-4%Pu) MOX of TAPS-BWR fuel design;
(2) (Th-6.75%Pu) MOX of PHWR fuel design;
(3) (Th-8%Pu) MOX of AHWR fuel design;
(4) (Th-1%Pu) MOX of AHWR fuel design.

Post Irradiation Examinations (PIE) was carried out on these thoria based fuels. The PIE results for these test irradiations were found to be consistent with the better thermo-physical properties and better fission gas retention capability of the thoria based fuels. The fuel

temperatures for the thoria based fuels based on microstructure examinations were found to be lower than that observed for the urania fuel pins. The fission gas release was also found to be considerably lower than that observed for the urania fuel pins.

The high density thoria fuel pellets used in PHWRs (Fig. 2a) and research reactors was fabricated by the conventional powder metallurgy technique of cold compaction and high temperature sintering in reducing atmosphere. The fabrication experience generated during the campaign for PHWRs provided an insight into the large tonnage scale production of thoria fuel. Moisture absorption on powder due to high surface area, caking of powder during milling, die wall lubrication during powder compaction, defects in green compacts, attainment of high density of greater than 96% TD, reject recycling, control of aerosol generation were some of the major difficulties experienced during production campaign. The (Th-Pu) MOX fuel for the various irradiation experiments were fabricated in glove box fuel fabrication facility as shown in Fig. 2b. The experience of fabricating the test fuel pins was useful in the development of fabrication flow sheet for the MOX fuel.

FIG. 2(a). Thoria fuel pellets.

FIG. 2(b). Glove-box facility.

3. REACTOR DESIGNS

Thorium fuel cycle can be adopted in all thermal reactors and fast reactors [5]. It is also feasible to use thorium in the existing reactors without major modifications in the engineered systems. Some of the power reactor concepts studied for thorium fuel cycles include Light water reactors (LWRs), pressurised heavy water reactors **(**PHWRs), gas turbine-modular helium reactors (GT-MHRs), pebble bed modular reactors (PBMRs); accelerator driven systems (ADS) and fusion breeders.

In India, advanced reactors AHWR and AHWR300-LEU are being designed at BARC to provide impetus to the large scale utilisation of thorium. These are 300 MWe, vertical, pressure tube type, boiling light water cooled, and heavy water moderated reactors. A schematic of the various reactor systems and the general arrangement of the fuel assembly are given in Fig. 3 and Fig. 4 respectively. These reactors are being set up as a technology demonstration reactor keeping in mind the long term deployment of thorium based reactors in the third phase of our nuclear power programme. It will provide a platform for demonstration

of technologies required for thorium utilisation. AHWR will use (Th-Pu) MOX and (Th-^{233}U) MOX types of fuel. The fissile ^{233}U for this reactor will be obtained by reprocessing its spent fuel, while plutonium will be provided from reprocessing of the spent fuel of PHWRs. The adoption of closed fuel cycle in AHWR helps in generating a large fraction of energy from thorium. A co-located fuel cycle facility (FCF) is planned along with the reactor and it will have facilities for fuel fabrication, fuel reprocessing and waste management. AHWR300-LEU will use (Thorium-LEU) MOX as fuel with low enriched uranium (LEU) having ^{235}U enrichment of 19.75%. The reactor is being designed based on once-through fuel cycle during its life time. A provision has therefore been made for long-term storage of the spent fuel along with monitoring and retrieval. These provisions during storage will keep open the option of reprocessing the spent fuel at a later date, if required.

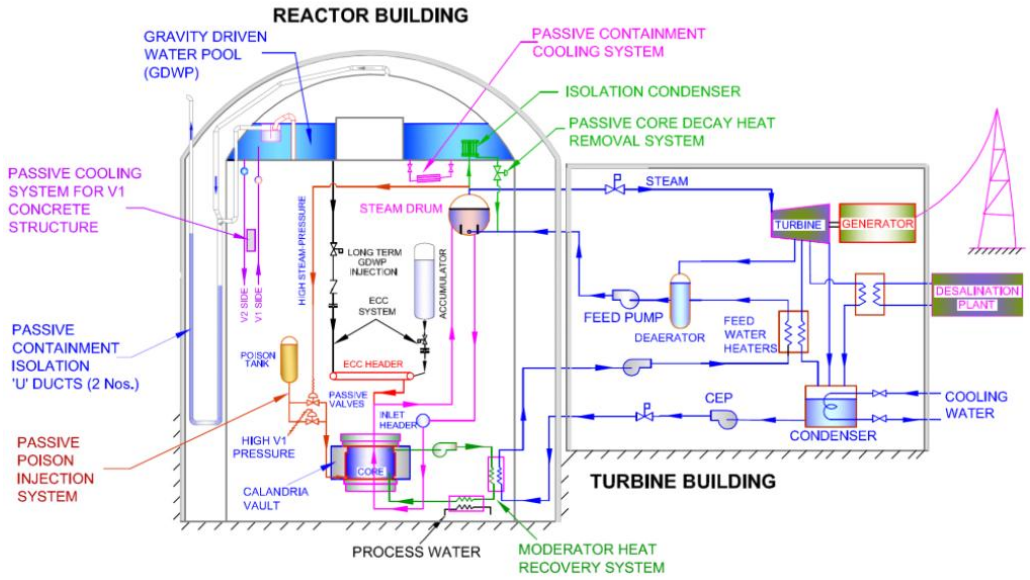

FIG. 3. Schematic of the different systems of AHWR.

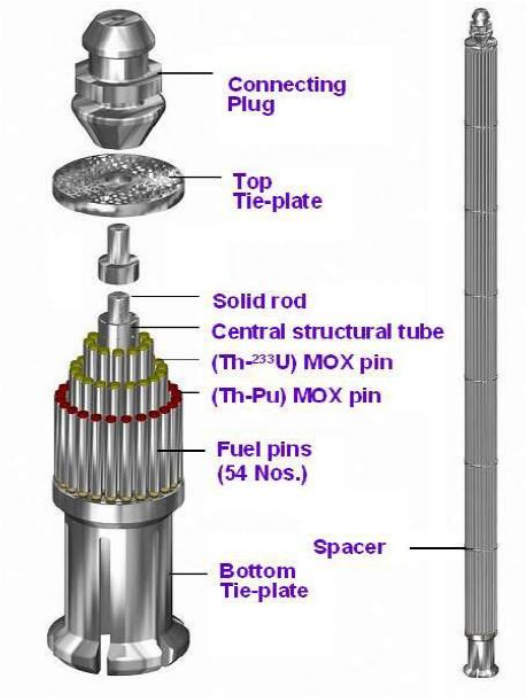

FIG. 4. General arrangement of fuel assembly.

4. FUEL CYCLE ASPECTS

4.1. Comparison of thorium with uranium

The assessment carried for thoria based fuels show that their thermo-mechanical performance will satisfy the safety limits used for uranium-based fuels and provide a better scope for operating successfully to higher burnup. A comparison of the properties of thorium dioxide and uranium dioxide shows thorium dioxide to be superior from the point of view of fuel performance in the reactor and are brought out below [6]:

(a) ThO_2 is a highly stable stoichiometric oxide and therefore has better dimensional stability. There is also less concern of the fuel reacting chemically with the clad material around it or with the coolant in case of clad failure;
(b) ThO_2 has higher thermal conductivity and lower coefficient of thermal expansion than UO_2. This will result in lower fuel temperatures and induce lower strains on the cladding and therefore allow operating for longer in-reactor residence time;
(c) The melting point of ThO_2 is about 500°C higher than that of UO_2. This difference provides an added margin of safety in the event of a temporary power surge or loss of coolant;
(d) ThO_2 has a lower fission gas release rates, which result in slower fuel deterioration;
(e) The amount of higher actinides (such as neptunium, plutonium, americium and curium) produced in Th-U fuels per unit of energy generated is less due to the lower mass number of ^{233}U The lower production of higher actinides results in a reduced toxicity of waste from thorium fuel.

Despite thorium fuel cycle having a number of attractive features, there are several challenges for its use in a closed fuel cycle mode. The highly stable thoria posses problems in dissolution in pure nitric acid for reprocessing the spent fuel This problem is mitigated by addition of small amounts of HF, which enhances the corrosion of stainless steel which is used as the material of construction for the various equipments. Another major concern with the thorium fuel cycle is the presence of ^{232}U along with ^{233}U. The daughter products of ^{232}U, ^{212}Bi and ^{208}Tl are emitters of hard gamma rays. This requires the fuel fabrication and recycling of uranium to be carried out in shielded hot-cells remotely and with considerable automation. These two aspects however provide a high level of proliferation resistance to the thorium fuel cycle. These two aspects have been however providing the major global attraction for the use of thorium [7].

5. CONCLUSIONS

The use of thorium is necessary from long-term objective of sustainability of energy resources. The thorium fuel cycle technologies which are being developed for AHWR will demonstrate the capability for large-scale thorium utilisation in the third stage of Indian nuclear power programme. The co-located Fuel Cycle Facility (FCF) planned for the thoria based Advanced Heavy Water Reactor (AHWR) will have facilities for fuel fabrication, fuel reprocessing and waste management. The programme for AHWR-FCF will provide an impetus for the development of technologies to overcome the challenges posed by thorium fuel cycle. Some of the technologically challenging issues are handling of the highly radioactive fresh fuel, the requirement of remote fuel fabrication and carrying reprocessing by dissolution of the stable thoria matrix. Many development programmes are being pursued at BARC to develop technologies for overcoming these challenges. The AHWR300-LEU which is designed for operation in the open fuel cycle mode will provide the globally recognised features of thorium fuel cycle like the advantage of having greater proliferation resistance, improved waste management and better safety with higher fuel burnups.

REFERENCES

[1] ANANTHARAMAN, K., VASUDEVA RAO, P.R., Global Perspective on Thorium fuel, Nuclear Energy Encylopedia, Wiley Series on Energy, 89-100.

[2] SINHA, R.K., KAKODKAR, A., Design and Development of AHWR – The Indian Thorium Fuelled Innovative Nuclear Reactor, Nuclear Engineering and Design, **236** 683 (2006) 700.

[3] ANANTHARAMAN, K, SHIVAKUMAR, V., SAHA, D., Utilisation of Thorium in Reactors, Journal of Nuclear Materials, **383** 119 (2008) 121.

[4] SHIVAKUMAR, V et. al., 'Fuel Irradiation Experiments for AHWR and CHTR', Paper F6-C3, Theme Meeting on Recent Advances in Post-Irradiation Examination, (RAP 2008), Kalpakkam, India (2008).

[5] VIJAYAN, P.K., SINHA, R. K., 'Thorium Utilization in Advanced Reactor Designs', The 2nd International Workshop on Accelerator-Driven Sub-Critical Systems and Thorium Utilization, 12–14 December 2011, Mumbai, India (2011).

[6] LUNG, M, GREMM, O, Perspectives of the Thorium Fuel Cycle, Nuclear Engineering and Design **180** 133 (1998) 146.

[7] SHIVAKUMAR, V., et. al., "Thoria based Fuel Cycle for AHWR - An Overview", Proc. International Conference on Peaceful Uses of Atomic Energy, 29 September – 1 October 2009, New Delhi, India (2009).

FUEL DESIGN AND DEVELOPMENT
(Session 2)

Chairman

P.N. PRASAD
India

PRELIMINARY DESIGN STUDIES FOR UTILIZATION OF SLIGHTLY ENRICHED URANIUM IN ATUCHA-2 FUEL RODS

A.A. BUSSOLINI, P. TRIPODI, L. ALVAREZ
National Atomic Energy Commission (CNEA),
Buenos Aires, Argentina
Email: bussolini@cnea.gov.ar

Abstract

At the present there are two nuclear power plants in operation in Argentina, one is Embalse (CNE), a CANDU-6 design, and the other is Atucha-1 (CNA-1), a Siemens/KWU PHWR design. Fuel assemblies for CNE and CNA-1 are entirely manufactured in Argentina and over the years their designs have been improved as the result of the operational experience, the fabrication evolution and because of both, technical and economic needs. One of the main modifications was the utilization of Slightly Enriched Uranium (SEU) in CNA-1 to replace the natural uranium considered initially in the design of this power plant. This design modification and the introduction of the SEU fuel were performed between the years 1995 and 2000. Since then only SEU fuel is in use. The fuel engineering activities for the SEU fuel were performed by the Fuel Engineering Department of the National Atomic Energy Commission (CNEA) and have included among other tasks the preparation of drawings, the adjustment of product specifications, extensive fuel rod thermo-mechanical design verifications and the performance evaluation of the first SEU fuel series. Nowadays the construction of Atucha-2 (CNA-2), the 3rd Argentine Nuclear Power Plant of Argentina, is almost completed. The fuel assemblies have been loaded in the reactor and the commissioning phase of the project has already started. Atucha-2 is also a Pressurized Heavy Water Reactor designed by SIEMENS-KWU. The fuel assembly is a 37 fuel rods circular arrange with PWR type spacer grids. The initial fuel material is natural uranium. Because of the similarities between CNA-1 and CNA-2 fuels and considering the excellent result of the utilization of SEU fuel in CNA-1 a program to evaluate the feasibility of the application of a similar fuel design modification in CNA-2 is being performed by CNEA. Preliminary design criteria for CNA-2 SEU fuel rods were established to assure the correct behavior during normal operating conditions and initial fuel rod thermo-mechanical calculations were performed. The objective of this paper is to summarize the advantages of the utilization of SEU fuel in CNA-2 and to present the most relevant design challenges and the calculations performed for a preliminary initial assessment of the fuel rod performance in the new operating conditions. Some minor fuel rod design modifications that might be required are also described.

1. INTRODUCTION

Argentina has two nuclear power plants in operation, one is Embalse (CNE), a CANDU-6 design, and the other is Atucha-1 (CNA-1), a Siemens/KWU PHWR design. Currently, the construction of Atucha-2 (CNA-2), the 3rd nuclear power plant of Argentina, is almost completed and the commissioning phase of the project has already started. This third reactor was also designed by Siemens/KWU. The construction started in the 80's, halted in the 90´s and was re-launched in 2006.

Fuel assemblies for CNE and CNA-1 are entirely manufactured in Argentina and over the years their designs have been improved as result of operational experience, fabrication evolution and technical and economic needs. The first core for CNA-2 was fabricated by the same national manufacturer.

The Fuel Engineering Department of the National Commission on Atomic Energy (CNEA) has performed the engineering activities for the CNA-2 fuel assemblies with a strong emphasis on those aspects associated with the fuel reliability. This is the first time that Argentina is in charge of the engineering and manufacturing of the first core for a nuclear power plant.

1.1. Fuel Assembly Descriptions of ATUCHA-2

Atucha-2 is a 745 MWe (2160 MWt) nuclear power plant with pressure vessel design and moderated and cooled using D2O. The reactor core is approximately cylindrical in shape and consists of 451 natural uranium fuel assemblies located in the same number of coolant channels. A diagram of CNA-2 pressure vessel and core is shown in Figure 1. Table 1 summarizes some key characteristics of CNA-2.

Each fuel assembly consists of 37 fuel rods arranged in three concentric rings and a central fuel rod. The assembly also includes a tie plate, thirteen sheet spacer grids and a coupling system to connect the fuel assembly with the reactor internals. Each fuel rod consists of a stack of uranium dioxide pellets enclosed by a thin walled zircaloy-4 canning tube with welded end plugs at both ends to make it gas tight.

The fuel assemblies are removed on-line from the coolant channels during reactor operation by a refueling machine. The coolant channels are surrounded by the moderator, which is contained in the moderator tank.

The CNA-2 fuel assembly design is based on the one used in CNA-1, including the cladding free standing concept. Fuel assembly details are shown in Fig. 2. Table 2 shows some key characteristics.

1.2. Description of ATUCHA I and similarities with CNA-2

CNA-2 was designed and built based on the design and experience of CNA-1 but scaled in size and power. CNA-2 delivers approximately twice the power of CNA-1. This power increase is mainly due to the use of more FA in the core thus a greater amount of uranium. Some characteristics comparing both NPP are listed in Table 1.

The fuel assembly for CNA-1 has the same geometrical arrange of the CNA-2 FA but consists of 36 fuel rods and one structural tube that occupies one position in the outer ring. The fuel rods are kept in their positions using zircaloy-4 rigid spacer grids. The main CNA-1 fuel details are shown in Fig.s 3 and Fig. 4 and listed in Table 2.

The internal designs of CNA-1 and CNA-2 fuel rods are very similar. Each fuel rod has a 5300 mm long stack of UO_2 pellets, isolating pellets, a gas plenum and a compression spring. The most significant differences between CNA-1 and CNA-2 FA are listed in Table 3.

2. UTILIZATION OF SEU FUEL IN CNA-2

Based on the NPP and FA similarities between CNA-1 and CNA-2, the excellent results obtained with the implementation of the SEU program since 1995 in CNA-1 and the extensive experience acquired in this process, the preliminary feasibility of a similar SEU program in CNA-2 is evaluated in this paper.

Furthermore, based on the few FA design differences listed in Table 3 between CNA-1 and CNA-2, it is considered that the CNA-2 FA is better prepared than the CNA-1 FA to implement a SEU program upgrade.

2.1. Design criteria

The CNA-2 fuel rod is designed to fulfill specific certain design criteria during normal operation in order to prevent excessive fuel temperatures, excessive internal fuel rod gas pressure and excessive cladding stresses and strains.

The design criterions have been established following the recommendations of NUREG-0800 [5] and [6], reviewed in [7] and [8]. These design criterions are associated with the main SEU life limiting aspects. The main design guidelines for SEU FA are [3]:

— Maintain the fuel ability to operate reliably to extended burnups levels;
— Avoid the introduction of new power operation restrictions;
— Maintain the present margins of safe operation of the reactor.

The influence of parameters like pellet size and density, clad/pellet gap, gas plenum size, cladding dimension, and helium pre-pressure are considered among others in fuel design calculations. Models for density changes, fission gas release, cladding creep, radial relocation of pellet fragments and other physical effects are also considered.

The criterions and limits [9] considered in this preliminary study of SEU fuel rods in CNA-2 are indicated in Table 4.

2.2. Calculations

Calculations were performed using a computer code especially prepared to simulate the thermo-mechanical behavior of the CNA-2 fuel rod during irradiation. This computer code simulates the whole rod in its radial and axial extensions and is applicable to pelletized oxide fuel in metal cladding tubes irradiated in water reactors. The individual power histories of the fuel rods during its total in-reactor lifetime including power changes due to refueling are considered in the design analysis.

2.3. Input data

Selected conservative power histories obtained from the NPP operational simulation were extended up to 16 000 MW/tU to simulate the fuel rod behavior in case of SEU utilization. Data input were selected to assure the most conservative conditions in each study (MAX fuel rod internal pressure and MAX PCMI). Nominal conditions were also considered as a reference. The data input and the limiting parameters are listed in Tables 5 and 6. In Fig. 5 shows the power histories used for these calculations.

2.4. Results

The main results obtained are shown in Fig. 6 to Fig. 9. From the results analysis arises that the critical parameters continue to satisfy the design limits.

2.4.1. Burnup

Fig. 6 illustrates the evolution of the calculated burnup associated with the power histories used in this study. For a residence time of 500 days the burnup is around 16 000 MW·d/kgU. This is approximately twice the original burnup for the natural uranium CNA-2 fuel (Table 1).

2.4.2. Center line fuel temperature

Fig. 7 illustrates the evolution of the calculated fuel center line temperature with the fuel residence time. The results show that the case that maximizes the fuel rod internal pressure exhibit the higher center line fuel temperature. Nevertheless the maximum temperature is far below the UO_2 melting temperature (2800°C).

2.4.3. Fuel rod internal pressure

Fig. 8 illustrates the evolution of the calculated fuel rod internal pressure with the fuel residence time. In the nominal and MAX PCMI cases the pressure shows a stable evolution around 60 bar. Instead, in the case that maximizes the fuel rod internal pressure it increases with the residence time up to 105 bar but it still remains below the design limit (Table 4).

2.4.4. Fuel and cladding relative deformations

Fig. 9 illustrates the evolution of the calculated fuel and cladding diameters with the fuel residence time for the case that maximizes the pellet cladding mechanical interaction at the central segment of the fuel rod. Close to the final stage of the residence time it is observed hard contact between the fuel pellet and the cladding, however there is no stress inversion in the cladding so it remains within the design limits (Table 4).

Axial relative deformations were not verified because they are less sensitive than in CNA-1 because CNA-2 fuel rod has no bearing pads to interact with the spacer grids.

3. FINAL REMARKS AND DESIGN MODIFICATIONS

The results obtained in these preliminary studies together with the excellent results obtained with the SEU program in CNA-1, allow to anticipate that no systematic failures in the Atucha-2 fuel rods due to the implementation of a SEU program are expected and no major design modifications arise to be necessary.

This is the first step in a much extensive study and design verification for SEU utilization in CNA-2 and its main aim was to demonstrate that no draw backs are expected in connection with the fuel rod thermomechanical behavior.

Further steps will include more extensive Fuel Assembly studies evaluating the higher relaxation produced by the increase in neutron fluence in the elastic spacer grids and particularly in their cantilever springs. These studies will also include the effect of potential power ramps at burnups over 8000 MW·d/tU.

Based on CNA-1 experience [1–2], some minor design modifications in the fuel rod like an increase of plenum void and a slight decrease of the filling gas pressure have to be evaluated to optimize them for SEU requirements.

These and other extensive studies of SEU utilization in CNA-2 must be performed with more representative power histories of a realistic SEU fuel management.

TABLE 1. CNA-2 AND CNA-1 NUCLEAR POWER PLANTS DATA [1–3], [10]

General operating conditions	CNA-2	CNA-1 (SEU)	Unit
Thermal reactor power	2160	1179	MWth
Net electric power	692	335	MWe
Average specific fuel rod power	232.8	232.0	W/cm
Fuel burnup at equilibrium	7500	11400	MW·d/Mg
Number of fuel assemblies in the core	451	253	-
Refueling	on power	on power	-
Primary system pressure	115,0	112,8	bar
Coolant channel inlet temperature	277,8	261,7	ºC
Mean coolant channel outlet temperature	314,6	296,1	ºC
Internal pressure vessel diameter	7368	5360	mm
Coolant and moderator	D_2O	D_2O	-

TABLE 2. CNA-2 AND CNA-1 FUEL ASSEMBLY DESIGN SUMMARY [3], [10]

	CNA-2	CNA-1
FUEL ASSEMBLY:		
Number of fuel rods per fuel assembly	37	36 (+1 structural rod)
Length (from the bottom end to the top of the coupling)	6028 mm	6028,5 mm
Outside diameter (without elastic shoe)	107,8 mm	107,8 mm
Type of spacer grids	Elastic (Raw material: sheet)	Rigid (Raw material: bar) + 1 elastic at the lower end
Number of spacer grids	13 (12 from Zry-4 and 1 at the lower end from Inconel 718)	16 (15 from Zry-4 and 1 at the lower end from Inconel 718)
FUEL ROD:		
Cladding material	Zircaloy-4	Zircaloy-4
Cladding outside diameter	12.90 mm	11,9 mm
Fuel column length	5300 mm	5300 mm
Fuel rod length	5566.4 mm	5566,4 mm
Fuel pellets		
Material	Uranium dioxide	Uranium dioxide
Form	Cylindrical pellets with dishing on both end faces	Cylindrical pellets with dishing on both end faces
Density of the pellets	10,55 g/cm3	10,60 g/cm3
Enrichment	Natural	SEU (0,85 w% U235)

TABLE 3. FUEL ASSEMBLIES OF CNA-2 AND CNA-1 FA

	CNA-2	CNA-1
Type of spacer grids (Fig. 4)	Elastic (fabricated from Zry-4 sheets)	Rigid (fabricated from Zry-4 bars)
Linkage between the fuel rods and the spacer grids	Friction between fuel rod and the cantilever springs of the elastic spacer grid.	Bearing pads welded to the outer surface of the sheaths interact with the solid spacer grid.
Uranium enrichment	Natural uranium	SEU (0,85 w% ^{235}U)

TABLE 4. CNA-2 FUEL ROD LIFE LIMITING ASPECTS

Parameter	Criteria	Design Limit
Internal Pressure	Prevent the increase of the fuel/clad gap	115 bar
Maximum fuel temperature	Prevent melting of the UO_2	2800ºC
Total cladding diametric strain	Avoid cladding damage due to PCMI (long-term interaction)	2.5%

TABLE 5. MAIN INPUT DATA FOR MAX FUEL ROD INTERNAL PRESSURE

Parameter	Value
Pellet diameter	Min
Dishing volume	Min
Fuel swelling	Min
Overpower (fp)	1.12

TABLE 6. MAIN INPUT DATA SET FOR MAX PCMI

Parameter	Value
Pellet diameter	Max
Dishing volume	Max
Cladding outer diameter	Min
Cladding inner diameter	Min
Plenum volume	Max
Filling gas pressure	Min
Fuel densification	Min
Fuel swelling	Max

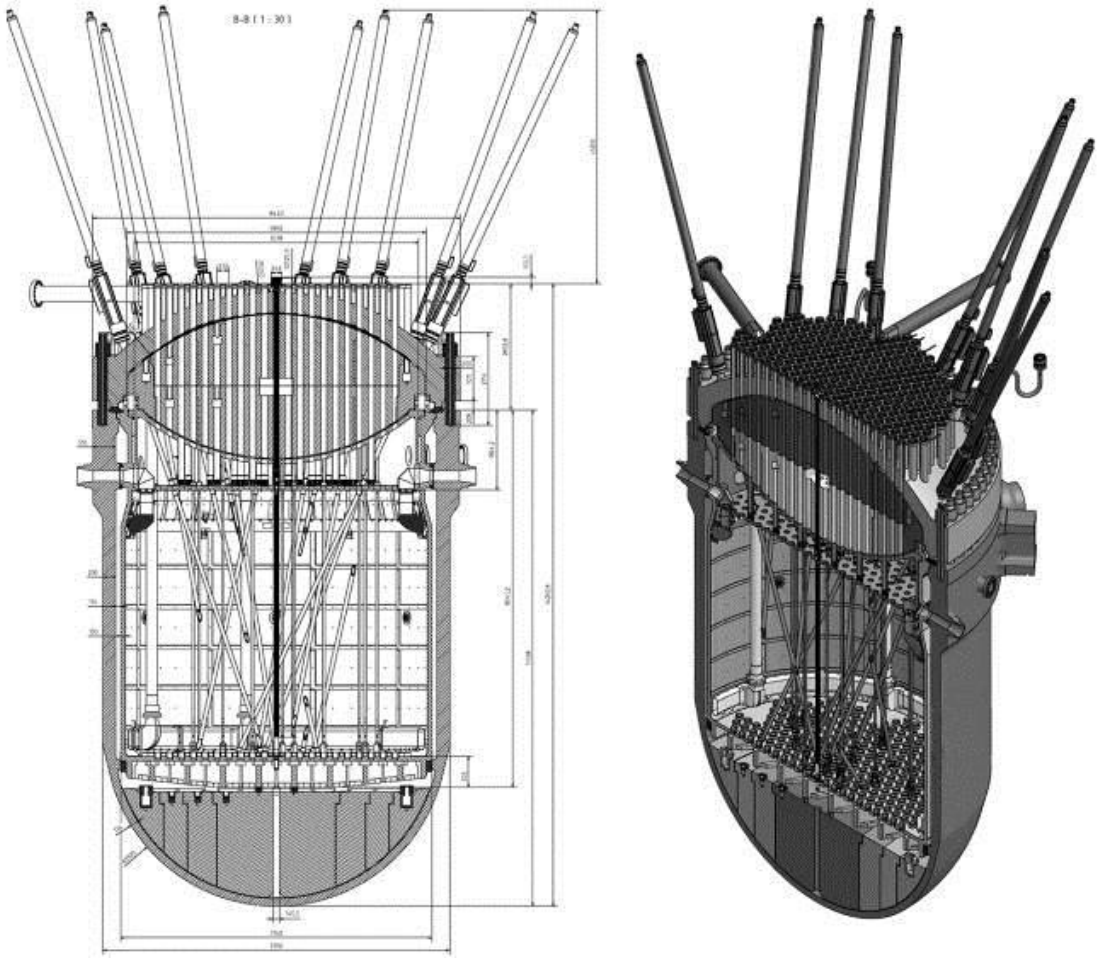

FIG. 1. Diagram of CNA-2 pressure vessel and core [11].

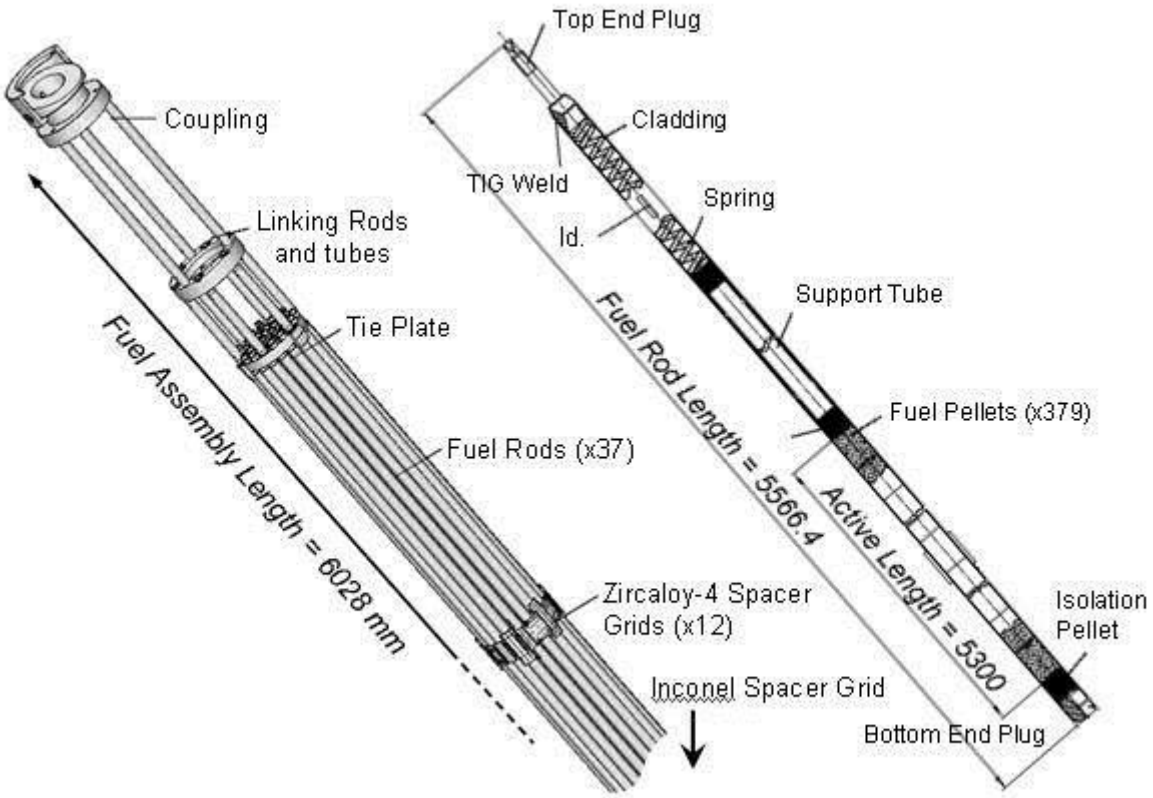

FIG. 2. CNA-2 fuel assembly design and fuel rod details [9].

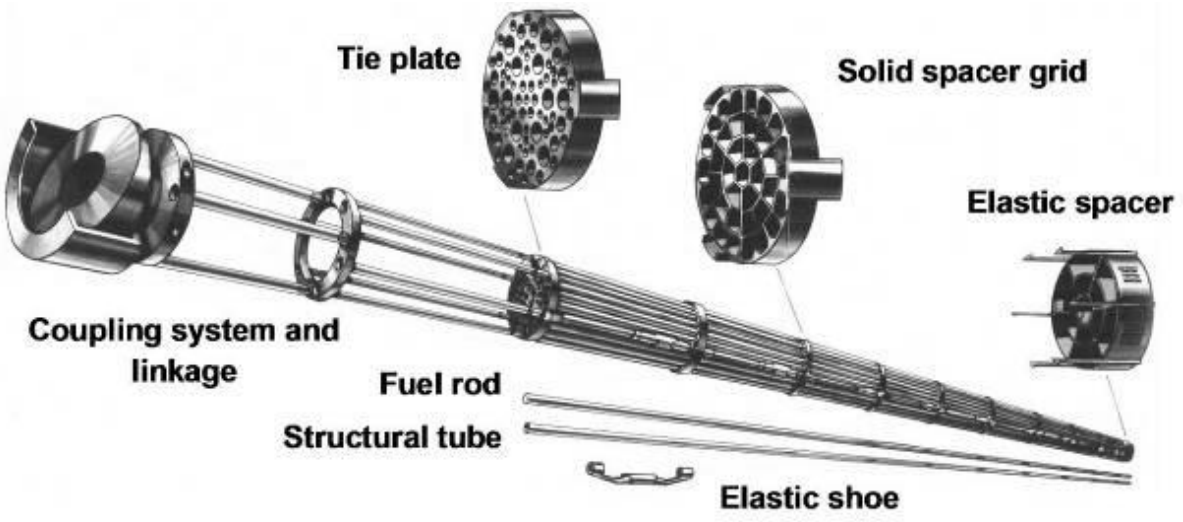

FIG. 3. CNA-1 fuel assembly design [4].

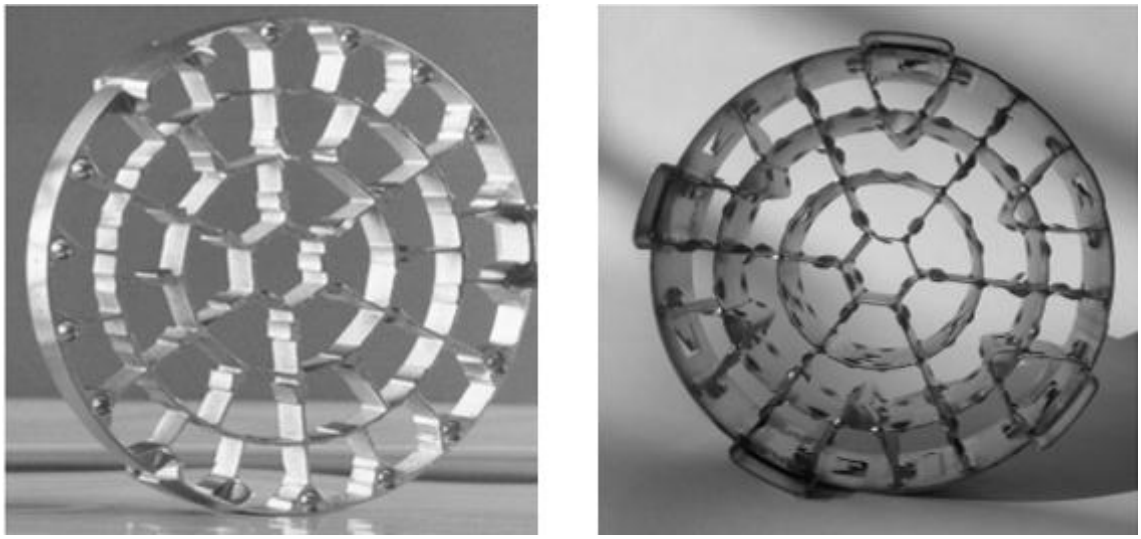

FIG. 4. CNA-1 and CNA-2 spacer grid (4).

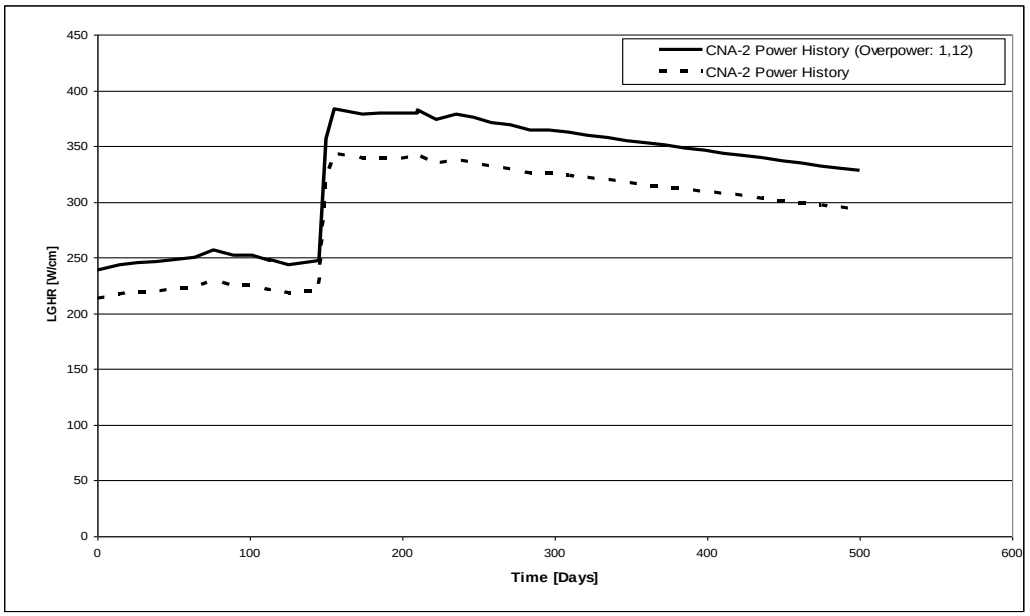

FIG. 5. Power histories used for calculatios.

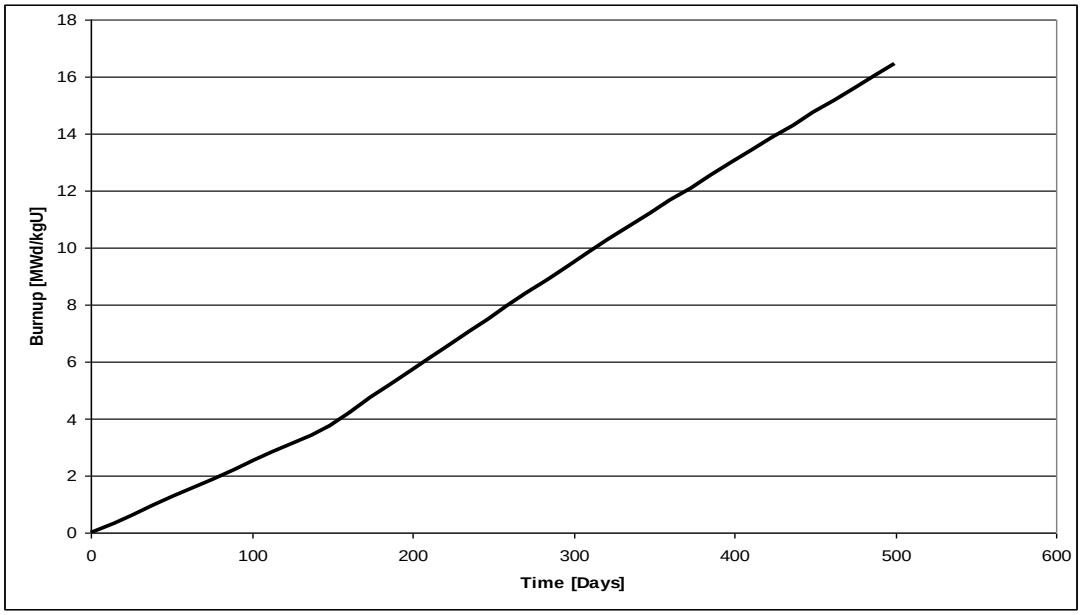

FIG. 6. Evolution of calculated burnup.

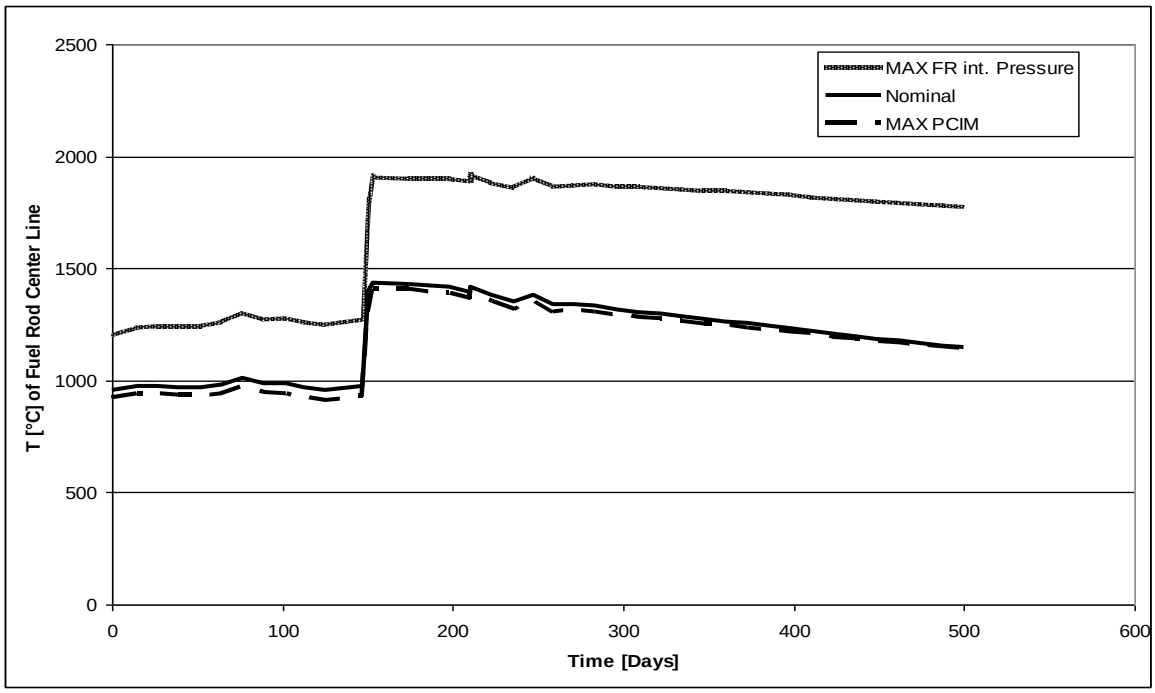

FIG. 7. Evolution of calculated center line fuel temperature.

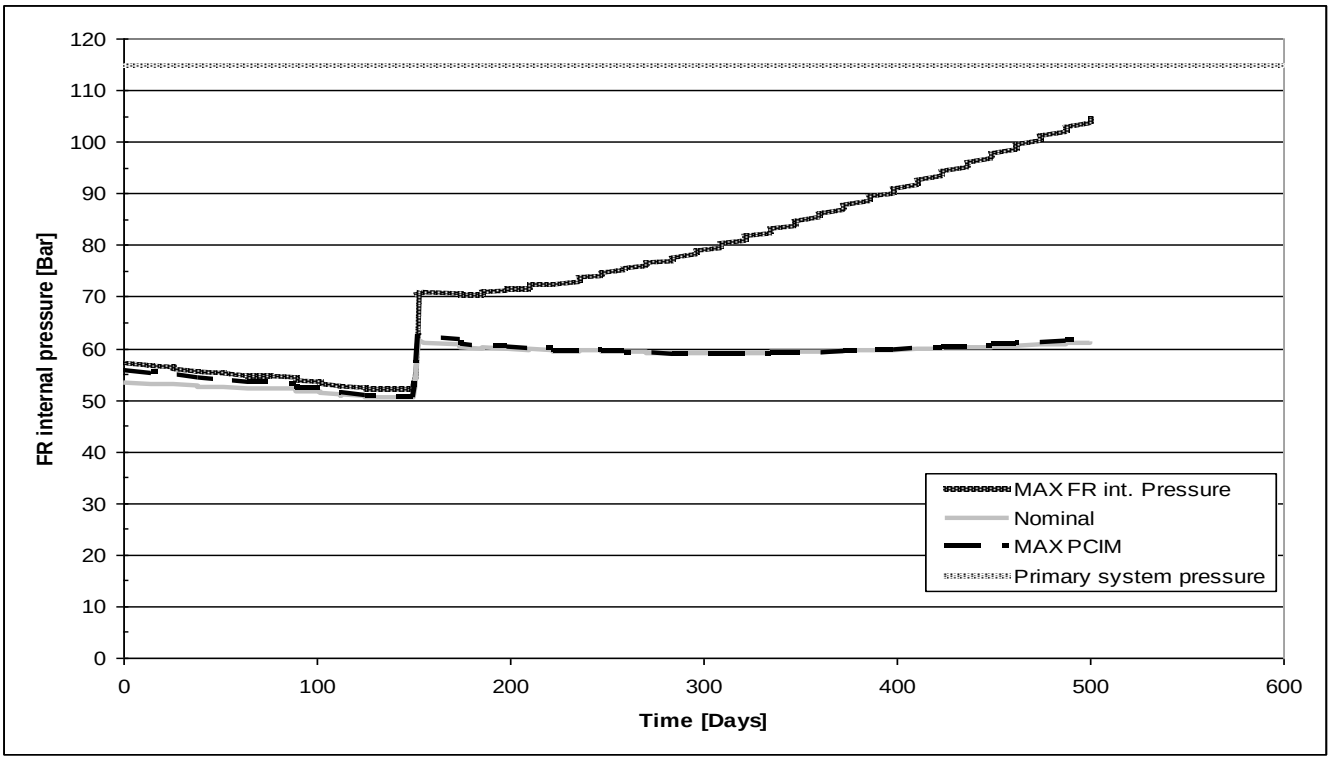

FIG. 8. Evolution of calculated fuel rod internal pressure.

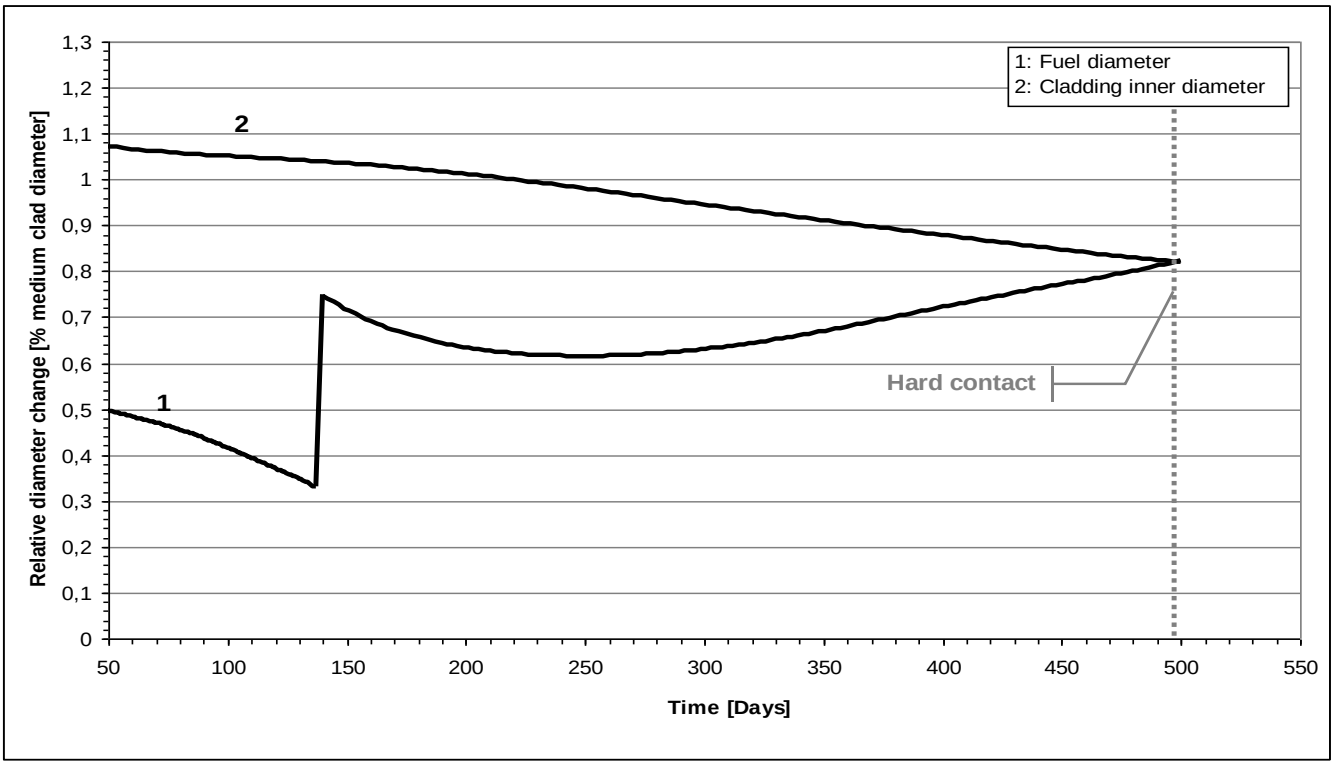

FIG. 9. Evolution of calculated relative diameters of fuel and cladding for MAX PCMI study (central segment).

REFERENCES

[1] FINK, J.M., et. al., "Overview of the SEU Project for Extended Burnup at the Atucha-I NPP. Four Years of Operating Experience", Technical and Economic Limits to Fuel Burnup Extension, Bariloche (1999).

[2] ALVAREZ, L., et. al., "Extended Burnup with SEU Fuel in Atucha-1 NPP". Technical and Economic Limits to Fuel Burnup Extension, Bariloche (1999).

[3] CASARIO, J.A., ALVAREZ, "Developments in Slightly Enriched Uranium for Power Reactor Fuel in Argentina". Impact of Extended Burnup on the Nuclear Fuel Cycle, IAEA Technical Meeting, Vienna (1991).

[4] LEMOS, L. S., VALESI, J. A., "Zircaloy-4 Spacer Grids for CAN-2 Fuel Element". IAEA Technical Meeting on PHWR Fuel Design, Fabrication and Performance, Buenos Aires, Argentina, 2009.

[5] NUCLEAR REGULATORY COMMISSION, USA, "NUREG-0800: Standard Review Plan".

[6] INTERNATIONAL ATOMIC ENERGY IAEA, "Design of the Reactor Core for Nuclear Power Plants", IAEA Safety Guide NS-G-1.12.

[7] INTERNATIONAL ATOMIC ENERGY AGENCY, "Analysis of Differences in Fuel Safety Criteria for WWER and Western PWR Nuclear Power Plants", IAEA TECDOC-1381.

[8] NUCLEAR ENERGY AGENCY, Fuel Safety Criteria Technical Review,. NEA/CSNI/R (1999) 25pp.

[9] CASTANIZA, S., ALVAREZ, L., "Simulation of CAN-2 Fuel Rod Behavior under Normal Operation". IAEA Technical Meeting on PHWR Fuel Design, Fabrication and Performance, Buenos Aires, 2009.

[10] BUSSOLINI, A.A., CASTANIZA, S., ALVAREZ, L., "Atucha-2 fuel Cladding Design Criteria and Requirements for Normal Operating Conditions". IAEA Technical Meeting on Fuel Integrity during Normal Operating and Accident Conditions in Pressurized Heavy Water Reactors, Bucharest, 2012.

[11] MAZZANTINI, O., et. al., A Coupled Calculation Suite for Atucha II Operational Transients Analysis, Science and Technology of Nuclear Installations, Article ID 785304 (2011).

CARA FUEL: AN ADVANCED PROPOSAL FOR PHWR

A. C. MARINO, D. O. BRASNAROF, C. MUNOZ, G. DEMARCO,
H. AGUEDA, L. JUANICO, J. LAGO FERNANDEZ, H. LESTANI,
J. E. BERGALLO, G. LA MATTINA
Comisión Nacional de Energía Atómica,
Bariloche, Argentina
Email: marino@cab.cnea.gov.ar

Abstract

A new fuel element (called CARA –"Combustible Avanzado para Reactores Argentinos", Spanish expression for "Advanced Fuel for Argentine Reactors"–) designed for two different heavy water reactors (HWR) is presented. CARA could match fuel requirements of both Argentine HWR reactors (one CANDU and two unique Siemens's designs as Atucha I and II). It keeps the heavier fuel mass density and hydraulic flow restriction in both reactors together with improving both thermo-mechanic and thermal-hydraulic, safety margins of present fuels. In addition, the CARA design could be considered as another design line for the next generation of CANDU fuels intended for higher burnup.

1. INTRODUCTION

Argentina has two pressurized heavy water reactor (PHWR) nuclear power plants (NPP) in operation (Atucha I and Embalse) since 1974 and 1984 respectively, operated by the same national utility (N.A.S.A.) and has another one under construction projected to be connected to the grid in 2013 (Atucha II). Although both of them are cooled by pressurized heavy water, designed to be fuelled with natural uranium and are moderated with heavy water, they have strongly different designs. Embalse is a standard CANDU-6 [1–2], horizontal pressure-tubes typical Canadian reactor. Atucha I and II have a unique Siemens' design: vertical fuel channels inside a pressure vessel reactor [3]. Fuels for Atucha I and II have small dimensional differences for the rod diameter and structural spacer grids.

Both nuclear power plants use on-line refuelling, but they differ in the length and number of their fuel elements (FE). Embalse uses a short FE with a length of 0.5 meter [4], and so, the horizontal 6-meter-long fuel channel is filled with twelve FE. The vertical channel of Atucha is filled by one FE of 5.3 meters active length [3]. Both fuels use 37 fuel rods arranged in a circular cluster array but with different designs of cladding:

(1) Atucha has self-supporting rods and one structural rod without fuel, following PWR design [5];
(2) Embalse has collapsible rods, following the well-known CANDU design [4].

The Atucha's fuel uses structural rigid spacer grids at intermediate positions like in PWRs [5]. The fuel of Embalse follows the principle of the CANDU series: a cluster of collapsible rods supported on its extremes by two structural plates (end plates). It uses middle plane appendages welded on cladding to avoid fretting between contiguous rods (spacers) and between rods to pressure tube wall (bearing pads). Both reactors use 37 fuel rods of similar diameters (1.0% greater the Embalse one), and therefore, they have similar uranium mass linear density. Their fuel channel diameters are similar, being slightly greater in Atucha (4%) that in Embalse, and therefore they have hydraulic similarity too. Unfortunately, their fuel cost is not similar, being the fuel cost in Atucha higher than in Embalse.

The fuel cost of Atucha I electrical energy was strongly reduced by the use of slightly enriched uranium (SEU) since 1998 up today. The burnup of design (for natural uranium)

achieved was around 6000 MW·d/THM, but through this program it was increased up to 11,400 MW·d/THM by using an enrichment level of 0.85% 235U [45]. This program illustrates the efforts pushed by the markedly high fuel costs of Atucha I. This economic performance is mainly due to the unique characteristics of the Siemens design of Atucha, in which a "PWR fuel" is used for a natural-uranium reactor. The low scale of the fuel supplier company (CONUAR), with two different manufacturing lines for feeding only two medium-size reactors, appears like the main drawback of the Argentine nuclear fuel cycle, regarding its economical competitiveness. This performance could be ideally improved by using the same FE on both reactors.

A project was started in 1997 for dealing with this challenge: to design a single FE for fuelling both Argentine reactors and at the same time enhancing their fuel performance, by considering the improvement reached by the use of SEU [6]. So, let us describe both FE involved. While Embalse's fuel has a robust and simple design, the Atucha's fuel has greater fuel costs due to its more complex mechanical solution related to its design of a long bundle. From this point the CARA was designed ("Combustible Avanzado para Reactores Argentinos", Spanish expression for "Advanced Fuel for Argentine Reactors") within "a CANDU concept", that is by using collapsible short rods.

The 37-rods fuel has been the commercial technology for CANDU-6 for the last thirty years [4]. It was designed for natural uranium low burnup (6,700 MW·d/THM). This technology is now evolving towards advanced fuel designs in order to get extended burnup by using SEU [6–7]. Nowadays, a new generation of FE (CANFLEX®) is being developed by AECL jointly with KAERI, expecting to reach higher burnup with higher fuel rod number and consequently lowering the linear power of a fuel rod and the central temperature [8].

By considering the similarities (geometric, hydraulic and neutronic) between Atucha and Embalse, the feasibility of filling the Atucha fuel channel with ten FE of Embalse will be considered, keeping the uranium mass and the hydraulic similarity, and fastening the assembly by means of a circumferential external tube. Then, after having demonstrated this point, a completely new fuel design will be developed under this ideal (but then realistic) scenario.

2. FEASIBILITY ANALYSIS

In order to carry out a preliminary feasibility assessment of the Embalse based concept for designing the new fuel element, the behaviour of a CANDU-6 fuel chain into Atucha was studied. This theoretical exercise is useful for understanding the handicaps and drawbacks of CANDU fuel under the Atucha operating conditions.

2.1. Hydraulic analysis

For performing the preliminary hydraulic analysis, a one dimensional model was used. The hydraulic modelling of the CANDU-6 rod was done by extracting their concentrated and distributed pressure-drop coefficients, obtained from critical heat flux (CHF) experimental data performed in a Freon loop [9] and from monothermic endurance tests performed in a water loop [10]. In his work [9], Dimmick measured the pressure drop along the fuel channel, and from this, the distributed and concentrated pressure drop terms were calculated, that were checked against Chung´s data [10] and other data obtained at Argentine test facilities [11]. The concentrated pressure-drop terms are produced on every pair of contiguous end-plates and middle planes (with spacers and bearing pads) of every FE and also, on the fuel chain

inlet and outlet. The distributed pressure drop term is related to friction along the whole fuel channel.

First, by taking into account the distributed pressure drop along one FE, the Darcy coefficient (f) and the equivalent cladding roughness (ε) were calculated by using the flow Reynold number (Re); showing that the distributed pressure drop can be evaluated by means of simple one-dimensional correlation for circular tubes [12]. Subtracting the distributed term from pressure drop measurements between every local restrictions, the hydraulic coefficient of spacer (Ksp), inlet and outlet channel (Ki and Ko), and end-plates junction (Kend) could be determined, as showed in Table I. The hydraulic restriction of end-plates junction is a function of its misalignment angle, in accordance with this degree of freedom characteristic of CANDU reactors, in which FEs rest on the channel inner wall placed randomly in the fuel chain.

Hence, for a given N-elements FE chain and a coolant flow, the pressure drop (Δp) can be estimated from the hydraulic coefficients that characterize the CANDU fuel by using the classic hydraulic one-dimensional model, by Eq. 1:

$$\Delta p = \tfrac{1}{2} [K_i + K_o + (N-1)*K_{end} + N*K_{sp} + f*L/D_h] * \rho * V^2 \qquad (1)$$

Where L, Dh , V and r are the fuel chain length, hydraulic diameter, average flow velocity and liquid density respectively.

TABLE 1. FRICTION TERMS OF CANDU FUEL IN EMBALSE CONDITIONS

ε	2.16 μm
f	0.01505
Re	513,000
K_{sp}	0.12
K_i	0.39
K_o	0.36
K_{end}	0.34 (full alignment, minimum)
	0.60 (average misalignment)
	0.72 (full misalignment, maximum)

The model and the hydraulic parameters of the CANDU FE were validated with the experimental results for a 12 FEs chain for the most probable misalignment CANDU-6. The model predictions and experimental data are within a 10% error bandwidth.

By using this model (Eq. 1) for appropriate flow conditions, and by considering the end plate average misalignment value for Kend , the fuel pressure drop was calculated for Embalse and for this preliminary Atucha case study filled with ten CANDU FEs (see Table 2). For the Atucha reactor conditions, a two phase correction is not necessary since the flow remains in single phase along the whole channel, and so, this model can be directly used.

The estimated pressure drop obtained (by means of this conservative homogeneous model) with ten CANDU FE is lower than the actual pressure drop of Atucha I (600 KPa)

[14]. This pressure drop margin enables us to design a circumferential external tube as the assembly system for Atucha. So, the mechanical compatibility with Atucha's refuelling machine is ensured (note: the Atucha's fuel is hanged up from the top pressure vessel lid, inside the vertical fuel channels).

In order to study the hydraulic compatibility of an assembly system, a 1 mm thick solid tube was adopted (a realistic input value considering its mechanical feasibility) deployed at the maximum external radius, and so, the diameter (106.2 mm) of channel is reduced. By using this hydraulic model, a new pressure drop value was obtained, which is slightly higher (576 KPa) but still compatible with the reactor conditions, in the case of (minimum pressure drop) fully aligned FE. In Table 3, it the overall fuel channel pressure drop is shown for ten CANDU-37 FEs assembled inside a circumferential tube estimated as function of the tube thickness and the alignment angle (considering average misalignment and fully aligned conditions). It shows that circumferential tube thicknesses up to 0.5mm are compatible with a chain of randomly misaligned fuels (the simplest mechanical design) but up to about 1.2 mm thickness if fully alignment is imposed, which in turn implies a more complex mechanical design.

TABLE 2. HYDRAULIC PARAMETERS OF THE HOTTEST (DESIGN CASE) FUEL CHANNEL

Reactor Data		
	Embalse [13]	CANDU in Atucha I
Mass flow	23.94 Kg/s	32.90 Kg/s
Average liquid density (ρ)	800 Kg/m3	832 Kg/m3
Channel diameter	103.8	108.2
Fuel chain length (L)	6 m	5 m
FEs chain number (N)	12	10
Results		
Average velocity (V)	8.57 m/s	9.36 m/s
Hydraulic diameter (D_h)	7.56 mm	9.08 mm
Fuel chain pressure drop (Dp)	608 KPa	539 KPa

TABLE 3. ATUCHA PRESSURE DROP CHANNEL FOR AVERAGE MISALIGNMENT OR FULLY ALIGNED Fes PREDICTED FOR TEN CANDU FUELS ASSEMBLED BY MEANS OF A CIRCUMFERENTIAL TUBE

Tube thickness (mm)	Velocity (m/s)	ΔP average (KPa)	ΔP minimum (KPa)
0.0	9.36	539	456
0.5	9.75	602	512
1.0	10.17	675	576

TABLE 4. ATUCHA I AND CANDU-6 CORE DATA

	Atucha I	Embalse
Thermal Power	1179	1992
Fuel channels	250	380
Core length	5.3	5.95
Core diameter	4.4	5.9
Rods per FE	37	37
Fuel rod Linear Uranium density [kgUO_2/m]	0.91	1.16

Considering now its thermal hydraulic behaviour, this basket reduces the circumferential "water bypass" originated by the greater channel diameter of Atucha I. This water bypass decreases the overall flow restriction, particularly at the end-plates junction, but in turns it reduces the flow within inner subchannels, a bad behaviour for the cooling of rods. This kind of analysis must be quantified on a more detailed study performed by using a subchannel numerical code or by means of experimental data, since it implies momentum and energy balances between coupled subchannel flows. This analysis was performed using the COBRA code, as it will be shown in section 2.3.

2.2. Neutronic analysis

Both Argentine reactors are designed for natural uranium fuel and heavy water coolant and moderator, having a core built by many channels with similar pitch and length. Besides, its fuels have similar diameters and an equal number of fuel rods with just slightly different diameters and thus have similar linear mass densities (see Table 4). These core and fuel design similarities allow to consider, at this early state of the CARA development, that it could exists a neutronic compatibility between both reactors.

The core extraction burnup could be estimated for continuous refuelling core (like Atucha I and Embalse) if the cell calculation is performed with geometrically buckling (including reflector saving to achieve core length and diameter) by calculation of the extraction burnup, as the burnup that equalize the area between a given excess reactivity for the core and the reactivity calculated with the code [14]. The same code and method have been used in order to obtain the reactivity for each fuel and its reactor. As the burnup depends on the core reactivity value used in the calculation, the value for each reactor was calculated by the present fuel and present extraction burnup, also calculated with the same code, nuclear data, and number of energy group and cell options.

Considering the fuel rod characteristics, the corresponding power densities, dimensions and geometrical buckling were used as the WIMS D5 input to estimate the CANDU in Atucha I neutronic behaviour (see Table 5) [4], [15–16]. In particular, the radial buckling was not changed, as it is related with the core radii. The change in core length was considered for the axial buckling calculation and the power density was scaled by considering the difference in fuel rods and UO_2 mass. The maximum linear power ratio was analyzed in relation to the maximum power peaking factors for the four pin annulus during the burnup.

By comparing the results shown in Table 5, under Atucha I conditions, the CANDU fuel has higher linear power values than the Atucha natural uranium (NU) (6%) and similar in

respect to the CANDU-6 reactor. Moreover, the use of SEU in Atucha I enable the power radial core flattening and the reduction of the maximum linear power ratio.

2.3. Thermal hydraulic analysis

The COBRA is a well-known subchannel code used for CHF estimation on PWR, BWR [5], [17–20] and PHWR reactors [21]. By using COBRA, the DNB (Departure of Nucleated Boiling) margin for a CANDU fuel chain filling the Atucha fuel channel was calculated and compared with the present Atucha's fuel, showing the new fuel is better. The peripheral water bypass caused by its smaller fuel diameter is avoided by using an outer tube, for which two different thicknesses are studied (see Table 6). The COBRA capabilities allow us to calculate the channel pressure drop and herein, the hydraulic compatibility estimated with the one dimensional model was checked. The outer tube increases the pressure drop but increases the DNBR margin; even in the worst case (using water by pass) this margin is better than the present condition.

TABLE 5. NEUTRONIC MAXIMUM ROD POWER RATIO AND BURNUP FOR EMBALSE AND ATUCHA I

Characteristic	CANDU 37	Atucha I - NU	Atucha I – SEU (0.85%)	CANDU in Atucha I
Burnup [MW·d/TonU]	7300	5900	11 800	5700
Core peak factor	1.843	2.03	1.87	2.03
Max bundle peak factor	1.1261	1.096	1.0996	1.1234
Maximum rod linear power ratio [W/cm]	595	550	508	586

TABLE 6. THERMAL HYDRAULIC MARGIN AND PRESSURE DROP MODEL COMPARISON

Fuel element and reactor	DNBR	□P 1-D model (KPa)	□P COBRA (KPa)
Atucha FE in Atucha I	3.41	608	601
10 Embalse FE in Atucha I	3.88	539	518
10 Embalse FE + tube of 1 mm in Atucha I	4.14	675	630

TABLE 7. FLOW EXCITATION PARAMETERS IN BOTH REACTORS

Bundle	Reactor	Tube thickness (mm)	Velocity (m/s)	$\rho * V$ (Kg/m^2 s)	*Re* (x10^5)
CANDU-37	CANDU 6	----	8.57	6859	5.13
Atucha I	Atucha I	----	7.78	6477	7.34
		0.0	9.36	7790	6.80
CANDU-37	Atucha I	0.5	9.75	8116	6.81
		1.0	10.17	8466	6.83

2.4. Mechanical analysis

The CANDU fuels use many weldings on pads and spacers of cladding to ensure the gap between rods, which implies higher costs to certify the whole assembly is manufactured right. On the other hand, since the pads are the single restriction to rod displacement, the rods bow under axial load. Hence and regarding the vertical position in Atucha and their higher axial and turbulence loads, the CANDU mechanical solution becomes inappropriate for this case. Therefore the mechanical requirements of Atucha will be used as the design base for the new FE and the proposed external tube could help to fit CANDU fuels in vertical channels. On the other hand considering fuel elements of PWR that use spacer grids to keep fuel rods positions, they not use welding on clad sheath. Let us remember that these fuels reach burnup several times higher than CANDU ones, which are designed for natural-uranium [5] fuels.

2.5. Dynamical analysis

The most important dynamical requirement in CANDU-6 and Atucha is flow-induced vibrations by turbulence [22] that could induce fuel rods failures by wear, fretting and fatigue cracking [23]. The dynamical behaviour of CANDU fuel under both reactor conditions can be studied by comparing their flow-induced excitations, which is proportional to the product □*V, while its deviation is proportional to the flow turbulence intensity, given by the Reynolds number [22–23]. Table 7 shows these parameters for the CANDU-37 FE in Embalse, the original Atucha FE in Atucha, and ten FE chain of CANDU-37 FE with three different assembly tube thicknesses for Atucha I conditions. It can be seen in Table 7 that the original Atucha I has nearly the same □*V product than CANDU-37, both in their original reactors, but having a significant difference (43% higher) for the Reynolds number. When the CANDU-37 conditions at Atucha is compared with respect to CANDU-6, the Atucha flow excitation is appreciably higher (□*V up to 123%, Reynolds up to 133%) than the operation condition of CANDU fuel.

2.6. Thermomechanical analysis

The thermomechanical compatibility between both reactor conditions can be studied in a first order analysis by studying their central pellet temperatures and power history. The steady state central pellet temperature is proportional to the linear power. In section 2.2 it was shown that for the CANDU FE inside the Atucha I operating condition, the estimated rod maximum linear power ratios were similar to those in Embalse (CANDU-6 reactor), but the power transient during Atucha refuelling is higher than in Embalse [14] ,[15]. Therefore the

thermomechanical requirements for fuel rods in Atucha I will be adopted as the design base for the new FE. This implies that a new CANDU fuel must be an enhanced design, thus lowering its linear power density. But this requirement does not match easily with others boundary conditions, as keeping the total hydraulic restriction [14].

2.7. CANDU fuel comparison

A new fuel requires improving its thermalhydraulic, neutronic, mechanical and thermomechanical behaviours, which are coupled and have opposite trends. For example, if the rod cluster is more spread out (by using smaller diameters) but keeping the total fuel mass (by increasing the rod number), its hydraulic restriction should be increased and consequently, the coolant flow (and so, thermalhydraulic safety margins) would be decreased. Thus, this trial and error process must be guided by a merit figure. A dimensionless parameter, Ndg, is useful to compare the "dispersion grade" of different fuel element designs. This parameter is defined as the heated and fuel cross section areas ratio, normalized for the heated length per meter of the fuel channel. At higher values of Ndg better thermo-hydraulic and thermo-mechanical behaviours are obtained, according to:

$$Ndg = \frac{\pi N_b \phi_b L_h}{\frac{\pi}{4} N_b \phi_p^2} \qquad (2)$$

Where:

ϕb = rod outside diameter
ϕp = pellet diameter
Lh = heated length per channel length unit
Nb = number of fuel rods

By regarding the evolution of the fuel series on CANDU reactors, a continuous growing on Ndg values is noted from the first seven-rod (N.D.P. reactor) fuel element up till now (CANFLEX), shown in Table 8 [1], [24]. This trend is also observed within PWR fuel elements. The historical evolution of this technology has also followed an increase in the number of the fuel rods per element [5], [24].

TABLE 8. DISPERSION GRADE OF CANDU FUEL ELEMENT SERIES

Fuel element type	*Nb*	*Ndg*
N.D.P.	7	176
Douglas Pt.	19	295
Pickering	28	302
Bruce	37	354
CANFLEX ®	43	377

3. CARA DEVELOPMENT

3.1. Initial criteria for the new bundle design

The new fuel, called CARA, must keep the same operational conditions for both NPP. They are the coolant flow, total hydraulic channel pressure drop, and the mechanical compatibility with the refuelling machine of each NPP.

The feasibility of our fuel concept has already been analyzed in previous sections, based on the hydraulic, thermalhydraulic and neutronic compatibilities; the need to enhance their mechanical and thermomechanic performance was also shown. Now, as a starting point for the CARA development the CARA fuel has been designed to improve the major fuel performance of both reactor types. This FE was set up with the following objectives:

(1) Mechanical compatibility with both NPPs;
(2) Hydraulic compatibility (hydraulic pressure drop of each NPP core);
(3) Just one fuel rod diameter;
(4) Higher thermal-hydraulic safety margins;
(5) Lower fuel pellet-centre temperatures;
(6) Higher linear uranium mass density;
(7) No welding on cladding sheath;
(8) Allowing extended burnup;
(9) Lower energy fuel cycle cost.

But these objectives go in opposite directions: for example, increasing the number of fuel rods increases the heated perimeter and, as a consequence, increases the hydraulic pressure drop due to the distributed friction, and increases the number of welding appendages. Thus, the need to keep similar core pressure drops leads to the CANFLEX® solution that looses the possibility of using a single fuel rod diameter, in order to keep the hydraulic cross section. Moreover, CANFLEX® keeps welding pads in the clad and even increases its number, which is not desirable for extending burnup [25]. Hence, it is clear that to simultaneously solve these conditions, the CARA fuel must explore new options.

The key of CARA design is to double the length of present CANDU fuels, eliminating in this way an end-plates junction. This solution is compatible with CANDU refuelling machine (that manages the FE always by pairs) and enables:

(1) To eliminate the intermediate end-plates and hence their local pressure drop;
(2) To use this handicap to balance the whole hydraulic restriction (#2) at the same time increasing the heated perimeter (#4);
(3) To use spacer grids instead of classical CANDU spacer pads welded on the cladding sheath to eliminate its welding and simplifying the manufacturing process (#7);
(4) To increase the number of rods by creating a new FE with many thin rods of a single diameter (#3), so that the fuel centre temperature is decreased (#5);
(5) To reach higher burnup can be reached (and so, lower specific fuel cost, #9), due to the lower thermomechanical behaviour (#8).

The mechanical compatibility is obtained by using the slightly greater channel diameter of Atucha I (5 mm greater than Embalse, which is 103 mm), in order to assemble five FEs within a basket assembly compatible with the refuelling machine (#1). The hydraulic

compatibility with Atucha is achieved by tuning the assembly pressure drop with the basket geometry and the choosing the angular misalignment between contiguous FEs.

3.2. Fuel rod definitions

For a given encapsulated cross section of a fuel bundle, the wet surface is proportional to rod number. Regarding the 37-rods CANDU FE in which the pressure drop (Dp) is related to end plates [26], the double-length CARA FE reduces the Dp by eliminating the intermediate end-plate junction and so, this handicap could be used to balance by its higher friction loss. Besides, this reduction on end plates and plugs increase noticeably the volume filled with uranium.

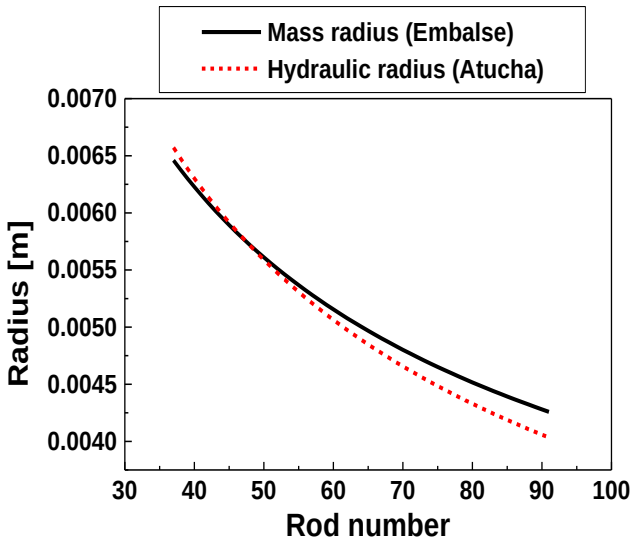

FIG. 1. Fuel rod radii for keeping 1) hydraulic similarity; 2) fuel mass similarity.

On the other hand, by increasing the number of rods the rod diameter decreases with the constrain of keeping the linear mass density, but the total external perimeter of fuel rods is increased and thus the pressure drop, so for the condition of keeping pressure drop, the rod diameter must be lower than the value obtained by keeping linear mass density. Clearly both curves decrease for higher rod numbers.

The CARA FE must be compatible with the most restrictive curve for both reactors. Taking into account that Embalse is the FE with higher linear mass, and Atucha I has the higher hydraulic constrain when an external tube is used, the design criteria are the Embalse mass curve and the Atucha Δp curve. Having in mind that if a double length bundle is used, an intermediate end-plate junction and plugs can be removed, the uranium mass can be increased. This approach can be checked by plotting two types of curves against the number of rods (Fig. 1), one curve keeping the uranium linear mass density and the other one keeping the hydraulic pressure drop by using very simple analytical models, which are crossing at 50 rods for 1-m bundle.

3.3. Bundle geometry

Different bundle geometries were studied and the 52-rod assembly was chosen due to good symmetry and compactness. This geometry (shown in Figure 2) has rings with 4, 10, 16 and 22 rods. This bundle has one symmetry axe and one mirror symmetry axe. The CARA rod diameter and thickness are similar to the smallest CANFLEX ® rods [9]. Table 9 shows the characteristics of three CANDU FEs regarding their uranium cross section; both CANFLEX ® and CARA have values 2% smaller than the 37-rod FE.

TABLE 9. BUNDLE CHARACTERISTICS OF CANDU FEs.

Bundle type	Rod number	Rod outer Diameter (mm)	Clad thickness (mm)	Inner cross Section (mm^2)	Relative Inner volume
CANDU 37	37	13.08	0.42	4,354	1
CARA	52	10.86	0.35	4,216	0.98
CANFLEX ®	35	11.5	0.33	4,256	0.98
	8	13.5	0.36		

3.4. Mechanical design

All CANDU fuels use pads welded to the clad sheath in order to ensure the clearance between neighbour rods. The sheath microstructure surrounding the welding zone is modified by the thermal load during the welding process. Despite the complexity inherent to this process and its manufacturer QA, the mechanical integrity margins of this rod can be considered as lower than another one without weldings. In addition, the use of welded pads for cluster geometry implies to deal with different rod types, due to different height of pads needed.

Instead of the use of the standard CANDU approach for ensuring rods position, CARA uses the spacer grid concept, as used in PWRs, adapted to the cluster geometry. This implies that all fuel rods are identical without any welding to the clad sheath and it simplifies the manufacturing process.

The CARA is designed to reach higher extraction burnups by using SEU and keeping the original microstructure to avoid clad failure during irradiation (due to pellet clad interaction by swelling and external cyclic mechanical load due to turbulence).

The CARA FE has 52 diameter fuel rods of the same diameter and of about 1 meter length (see Fig. 2) fastened by three self-supported spacer grids (see Figs. 3 –first version of the spacer– and 4 –a present development–) and welded to end-plates of low hydraulic restriction (see Figs. 5, 6 and 7). Every spacer grid has two rigid plates joined by a tube with external bearing pads, each rod position has a transversal spring made of Inconel (see Fig. 4). This is useful in order to use them in vertical channels. In PHWR with horizontal fuel channels (like CANDU ones), the CARA fuel laying on the pressure tube by several bearing pads are built on the outer surface of the spacer grids, whereas the CANDU bearing pads are

welded onto outsider rods. Fig. 6 shows a detail of the new endcap and Fig. 7 the socket between that endcap and the grid.

FIG 2. CARA rod bundle.

FIG. 3. First version of the CARA fuel element.

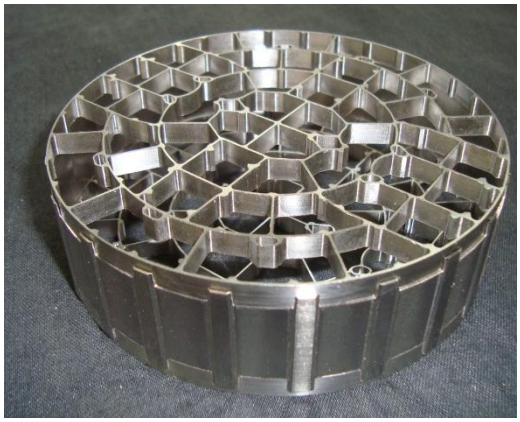

FIG. 4. Second version of the CARA Spacer grid [41].

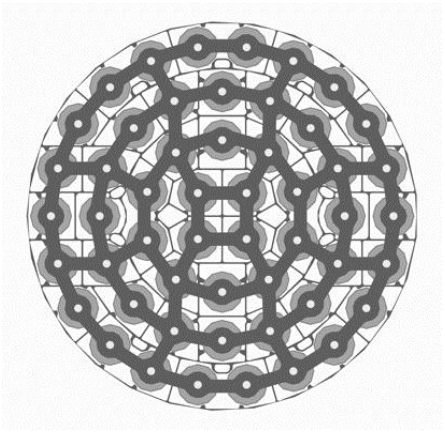

FIG. 5. Third version of the CARA end plate.

FIG. 6: present CARA fuel rod, end cap and end plate.

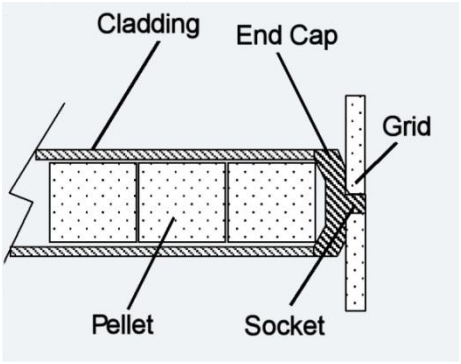

FIG. 7: Socket between fuel rod and grid.

FIG. 8. Inner view of an external assembling tube for using in Atucha I.

FIG. 9. CARA Atucha FE assemblies.

TABLE 10. FLOW EXCITATION PARAMETERS FOR CARA FUEL

Reactor	Tube thickness (mm)	Velocity V (m/s)	$\rho * V$ (Kg/m^2 s)	Reynolds number
CANDU	----	8.21	6567	4.51 E5
Atucha I	0.5	9.40	7817	5.99 E5
Atucha I	1.0	9.78	8141	6.00 E5

The assembly system was designed to be loaded by the top side in Atucha and is built in Zircaloy to provide low neutron absorption (see figs. 8 and 9). It has flexible sliding shoes to fix the FE assembly relative position to the channel. By considering that the radial displacement of the assembly system is limited by flexible sliding shoes, and the whole systems is hanged by the upper end, the effects of flow induced vibrations in the amplitude of cycling stress will be below the fatigue design limit of the sliding shoes.

3.5. Preliminary vibration analysis

Considering the CARA under Atucha I and Embalse operating flow conditions, the value of the dimensionless velocity coefficient for the fluid-elastic instability are 0.46 for Atucha I and 0.42 for Embalse. These analyses were done considering a conservative case of non collapsible effects on Young module, and since these values are less than the unit, concerns of fluid-elastic instability are negligible.

The fuel rod natural frequencies mainly depend on mass, length and cross-section moment of inertia. The CARA fuel cladding was designed to collapse over the fuel pellets at the reactor operational pressure. Therefore the moment of inertia is related to the shear stress between the cladding and the fuel pellet. For understand this complex behaviour,

experimental studies using different metallic pellets inside claddings were performed to simulate collapsible conditions. It was found that Euler-Bernoulli model described the phenomena of collapsible fuel rods by using a Young module 50% higher than the clad value. In this case the pellet has major contributions to the rod stiffness, which is not the PWR (Atucha) case, having self-supporting cladding.

As was already seen, the CARA mechanical design must fit the flow induced vibration at Atucha I conditions, while CANDU-6 conditions are less demanding (see Table 10). Due to its fuel rods similarities the CARA FE can be compared with the actual CANDU-37 FE in the CANDU-6 reactor. For this case the CARA flow excitation is lower (the product □*V decreasing up to 95%, Reynolds decreasing up to 88%) than for the CANDU fuel in CANDU 6 reactor. When the CARA FE with an outer tube of 1 mm thickness in Atucha I reactor is compared with the actual CANDU-37 FE in the CANDU-6 reactor, the CARA flow excitation is higher (the product □*V increasing up to 119%, Reynolds increasing up to 117%) than the CANDU fuel situation, but not excessively.

For a preliminary analysis, it is useful to do a comparative study including other reactors and their FEs. By comparing Atucha I fuel against CARA, both have three intermediate spacer grids per meter of length, but while Atucha fuel has a single long rod (5, 25 m) the CARA uses short rods (1 meter length), and then, its natural frequencies are at least about five times higher than Atucha ones, without considering collapsible effects, using the Euler Bernoulli model for beams [27].

The three spacer-grids of CARA are placed in order to increase the frequencies of its natural transversal vibration modes and bending constrains for mechanical compatibility in horizontal refuelling. One is fixed at the middle and the others are placed symmetrically at one sixth from each extreme. The distance among spacer grids is 333 mm, similar to PWR [5] and Atucha fuels. This distance is less than the minimum conservative value for mechanical buckling stability without considering collapsible effects.

The spacer grids design consider the elastic springs behaviour, especially the residual force at the end of life following the PWR concept (fuel rod always in contact with the spacer grid dimples, see Figure 4). Thus, the clad and spacer-grid interaction (fretting) do not produce any significant wearing effect during irradiation [28]. The designed CARA discharge burnup (about 18 000 MW·d/THM) is less than one half of actual PWR (38 000 MW·d/THM) burnup, and nearly one third of the advanced PWR (55 000 MW·d/THM) burnup [5].

The CARA has fixed extremes (end plates) every 1m long, and uses collapsible fuel rods, which shows that the CARA rods are more binding that PWR fuel ones and its natural frequencies are at least 5 times higher, together with shorter irradiation time compared with PWR.

A preliminary analysis was carried out without considering the collapsible effects on the stiffness of the fuel rod, which is a conservative assumption. The natural frequencies considering the mechanical constrains due to spacer grids and end plates, were calculated by a computational code. Considering the Atucha and Embalse operating conditions, the hydrodynamic mass (added mass which increase the weight of vibrating body due to surrounding water) was calculated [29], getting 4 times the water mass in the fuel rod volume. The CARA natural frequency results are: F1 = 73.9 Hz, F2 = 92.9 Hz, F3 = 212.6 Hz.

The turbulence induced vibration was estimated in a conservative approach with the paidoussis formula (without considering the collapsible effect) having for the CARA FE a

zero-peak vibration amplitude of 0.155 mm for Atucha and 0.118 mm for Embalse [23]. This is compatible with the maximum acceptance criterion, which is 2% in diameter (0.22 mm).

In accordance with the previous discussions, it was estimated that the mechanical design of CARA could be considered as conservative for CANDU-6 reactors, and as feasible for Atucha ones.

3.6. Hydraulic design

Due to their concepts, the CARA and present CANDU fuels have different balances of concentrated and distributed hydraulic losses. Since only distributed losses are strongly dependent of the flow regime (that is, Reynolds number), they have different hydraulic performance in reactor conditions (at very high Reynolds numbers) than in low-pressure test facilities (at moderately high Reynolds numbers). Hence, for hydraulic similarity objectives, it is important to model the Reynolds dependence of the fuel hydraulic loss, in order to extrapolate experimental data obtained at low-pressure test facilities.

3.6.1. End plates modelling

In the CANDU reactor the fuel chain is loaded with random different azimuthal angles. The end plates junction hydraulic loss depends on the misalignment angle. To evaluate the channel average hydraulic pressure drop it is necessary to measure this dependence. This behaviour can be used to tune the channel pressure drop in the Atucha by fixing their relative angular position with the assembly system.

An analytical model of pressure drop for the misalignment angle of junction between neighbour fuels has been developed and tested using published [28] and CNEA experimental data. The excellent agreement between the model and published experimental data for CANDU 37-rod and CANFLEX fuel elements are shown in Figs. 10 and 11 respectively.

The general concept of the CARA end-plate was chosen by following the CANDU 37-rod and CANFLEX 43-rod bundles. The hydraulic pressure drop produced on every contiguous pair of endplates is a function of the misalignment angle, as it can be observed from these two FEs. Then, it is useful to develop a rational base model for this term at the early stage of the CARA design development, for the hydraulic design of the new end-plate geometry. This model provides a useful tool for analyzing the trade-off between mechanical requirements (that claims for thicker and wider bars) and hydraulic pressure-drop requirements (that claims for the opposite trends).

A simple model was developed for estimating the end-plate hydraulic restriction, based on a detailed calculation of the cross flow section variation through the conical plugs (gradual expansion and contraction terms) and end-plate width (sudden contraction and expansion terms) [29–30]. This model was adjusted by using CANDU-37 rod data (Fig. 10), and validated against CANFLEX data showing a good accuracy (deviation lower than 10%) as it can see in Fig. 11. Thus this model was used for the pressure drop CARA end-plate coefficient prediction, as it is illustrated in Fig.12. The most probable, minimum (fully aligned) and maximum values obtained are 0.60, 0.32 and 0.68 respectively. This model predictions were verified with experimental data obtained in a hydraulic low pressure loop within a 10% error bandwidth.

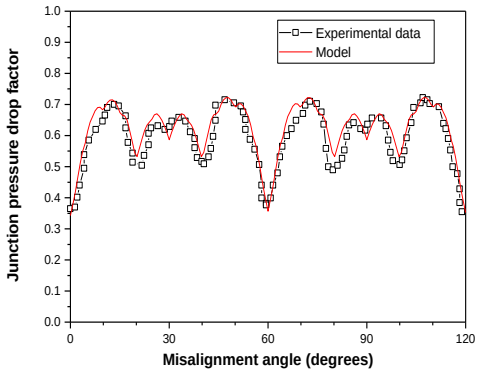

FIG. 10. CANDU junction pressure drops.

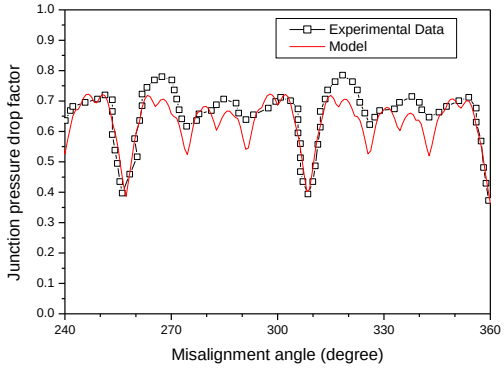

FIG. 11. CANFLEX junction pressure drops.

In order to extrapolate the experimental results to reactor conditions, a sequence of test were done varying the Reynolds number between 5 x 104 and 1.6 x 105, by changing the flow velocity. These tests were useful for end plate modelling as much as grid spacer and friction hydraulic modelling. By considering the experimental findings, it was shown that the Reynolds dependence of endplate junction is negligible (in agreement with our model), within 5% of accuracy band error, and so, those model predicted values can be considered satisfactory.

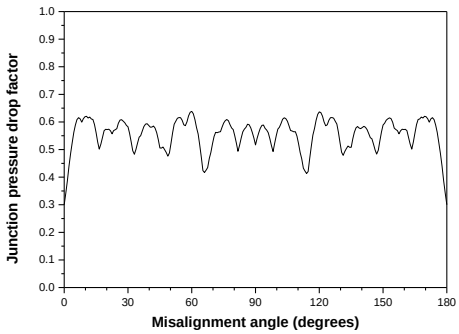

FIG. 12. CARA junction pressure drop predicted by model.

3.6.2. Spacer grid modelling

Several designs of spacer grids could be used. The first design provides a good performance in both reactors from a hydraulic standpoint. This design, included in Figure 3, was tested in hydraulic tests loops.

The hydraulic pressure drop of grid spacers depends on flow Reynolds number, as is well known from published models [31–32] and experimental data, due to friction on spacer wall and changes in flow cross section. Our experiments confirm this behaviour; thus, the extrapolations for CARA conditions in both reactors are showed in Table 11, where Ksg is the hydraulic coefficient for the spacer grid, having considered an external circumferential tube of 1 mm.

TABLE 11. FLOW PARAMETERS FOR CARA IN BOTH REACTORS

Reactor	*Re* (x 10^5)	*Ksg*
CANDU-6	4.51	0.68
Atucha	6.00	0.65

3.6.3. Distributed friction modelling

The Steggeman's correlation [33] is used in order to consider the dependence of the Darcy coefficient with the hydraulic diameter and the flow Reynolds number. By using this, the f factor for CARA fuel in each reactor was estimated and is shown in Table 12, considering an assembly tube of two different thicknesses for Atucha I.

The distributed friction factor from experimental data is compared with the classical well-known Moody correlation [12], and the specific correlation developed for fuel rod PWR arrays [39] in Fig. 14, showing good agreement within 10% deviation. A new specific cluster correlation using the experimental data was built with least square fitting. In Fig. 15, the total spacer grid loss coefficient was adjusted from the experimental data showing good agreement [11].

3.6.4. Overall hydraulic modelling

Using the previous hydraulic restriction coefficient, the overall fuel channel pressure drop can be calculated by using Eq. 1, with the right numbers of end-plate junction and spacer grids in each case, obtaining the results shown in Table 13. These results show that even a 1 mm thickness assembly tube can be acceptable by using the fully aligned configuration. Let us remark that besides this one, an assembly tube with openings has been designed (instead of a solid one as we have consider here), that is expected to produce a still lower pressure drop (see in Fig. 10 the first prototype tested on the low-pressure loop test facility of CNEA).

TABLE 12. FLOW PARAMETERS FOR CARA IN EACH REACTOR

Reactor	Tube thickness (mm)	*Re* (x 10^5)	Hydraulic Diameter (mm)	*f*
Candu-6	----	4.51	6.96	0.0157
Atucha	0.5	5.99	8.01	0.0147
	1.0	6.00	7.70	0.0145

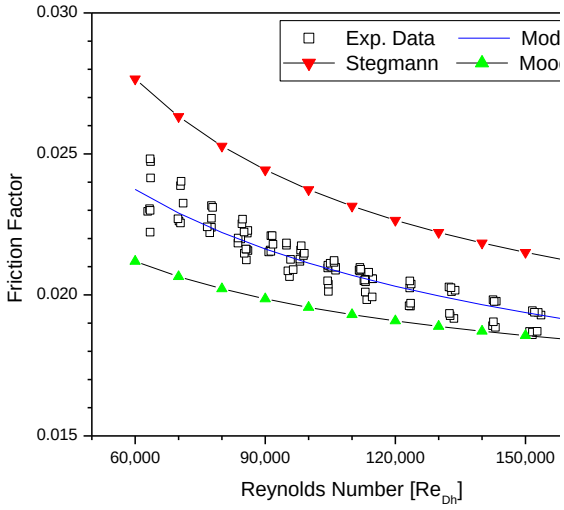

FIG. 14. Distributed fiction loss coefficient.

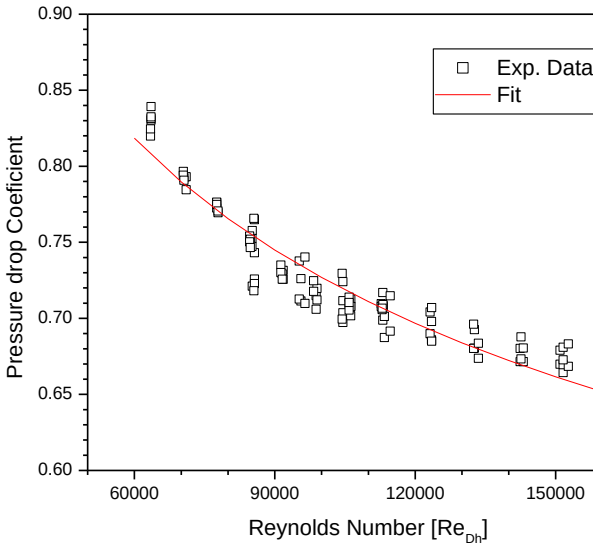

FIG. 15. Spacer grid loss coefficient.

TABLE 13. ESTIMATED CARA FUEL CHANNEL PRESSURE DROP UNDER DIFFERENT CONFIGURATION

Reactor type	Tube thickness (mm)	K_{end}	Pressure drop (KPa)
Candu-6	-------	Average	562
Atucha	0.5	Average	510
		Fully aligned	472
	1.0	Average	624
		Fully aligned	580

TABLE 14. WIMS RESULTS, NEUTRONIC DIFFERENCES BETWEEN CARA CANDU AND ATUCHA I

Characteristic	CANDU 37	Atucha I	CARA (In Embalse)	CARA (In Atucha I)
Natural Uranium -				
Burnup [MW·d/ton·UO_2]	7500	6100	7529	6368
Peak Factor	1.1261	1.0936	1.1359	1.1483
SEU (0.9%) -				
Burnup [MW·d/ton·UO_2]	14 537	13 466	14 576	14 524
Peak Factor	-	-	1.1484	1.1577

4. FUEL PERFOMANCE MODELLING

4.1. Neutronic behaviour

The neutronic behaviour of the CARA fuel element was calculated by using the code WIMS D/4 [27]. Considering the materials of the fuel element and reactor core geometry, the burnup could be estimated by using the cell reactivity evolution, as well as the power peak factor (highest to average power ratio) [34]. The burnup was calculated as the value that equalized the mean core reactivity of an average cell to the required excess reactivity for operation [14].The beginning of life (BOL) excess reactivity, power peaking factor and burnup level can be seen in Table 14 and the crown rod power distribution in Table 15, for natural uranium and SEU fuels respectively, for each reactor. Using the power evolution, burnup level and peaking factor calculated with WIMS, together with all the geometry and compositions, the complete thermo-mechanical behaviour could be calculated for the most demanded CARA rods.

TABLE 15. WIMS RESULTS FOR THE CARA ROD POWER DISTRIBUTION FOR 0.9 % SEU AT BOL

Crown	CARA (in Embalse)	CARA (in Atucha I)
1	0.8098	0.8045
2	0.8499	0.8433
3	0.9474	0.9439
4	1.1411	1.1476

4.2. Thermomechanical behaviour

The analyses of the thermomechanical behaviour and the fuel rod design were performed by using the BaCo code [35–36]. BaCo was developed at CNEA for the simulation of the behaviour of nuclear fuel rods under irradiation. BaCo is a code for the simulation of the thermo-mechanical and fission gas behaviour of a cylindrical fuel rod under operation. The development of BaCo is focused on PHWR fuels as the CANDU and Atucha ones but it keeps full compatibility with PWR, BWR, WWER and PHWR MOX fuels, among advanced and experimental fuels. A specific version of BaCo was developed and validated for the CARA fuel. The BaCo present version includes post processing tools for statistical improvement [37] and 3D enhancements [38–39]. BaCo was part of the CRP FUMEX II of the IAEA, and at present is part of the CRP FUMEX III of the IAEA in order to continue the validation and experimental support of fuel simulations by means of BaCo [40].

The major changes in the models of the code for CARA were not significant because BaCo was originally designed for Atucha and CANDU fuels. Two specific techniques for fuel design were developed: parametric (or sensibility) analysis and probabilistic (or statistical) analysis among the normal (or standard) analyses and the "extreme cases analysis".

5. CARA FUEL ROD BEHAVIOUR

The power history for an Atucha I fuel used for calculation is included in Fig. 15. The power history sketched reaches high power (and then high temperature). This hypothetical, but realistic, power history was defined for real demanding conditions of irradiation for a fuel element and for the BaCo code simulation. Starting with that power history we extrapolate the respective history for the equivalent CARA fuel conditions in the Atucha I NPP correcting by the neutronic cell calculation model. The use of an extra crown of rods, by reducing the rod diameter, produces a decrease in the power level. The extrapolation is based on the burnup extension and the adaptation of linear power levels of the CARA fuel. In order to use a proper power history for the Atucha I fuel we extend the scale of burnup of a power history of an Atucha I fuel keeping the corresponding power level. The extension in burnup is ~14 750 MW·d/tonUO_2 and the linear power is reduced up to a 72 % of the original value, due to the new geometry of the CARA fuel. Fig. 15 represents the local power history of the seventh axial segment of a 5 meter long Atucha I fuel element (numbering from the top of fuel and taking into account ten axial segments). The seventh segment is the most demanded axial section during irradiation; as it includes a maximum power level of 547 W/cm. The CARA fuel extrapolation corresponds to the fourth module of a CARA assembly in Atucha I (the fourth CARA module is equivalent with the seventh Atucha segment). The burnup at end of life is ~14 750 MW·d/tonUO_2 and the power level is reduced a 73.4 % of the original Atucha fuel value. The maximum calculated pellet temperature for the Atucha fuel is ~1850°C during the maximum power level (see Fig. 16). The temperature for the equivalent CARA module is ~1350°C, thus, a decrease of ~500°C respect of the normal Atucha I fuel.

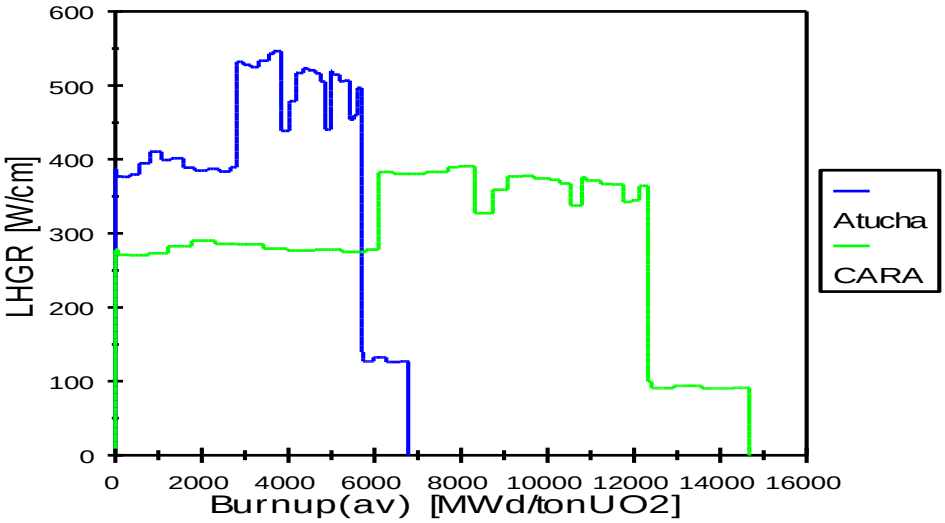

FIG.15. Local power history for the 7th segment of a fuel rod of the Atucha I NPP and a CARA fuel at that axial position in the channel.

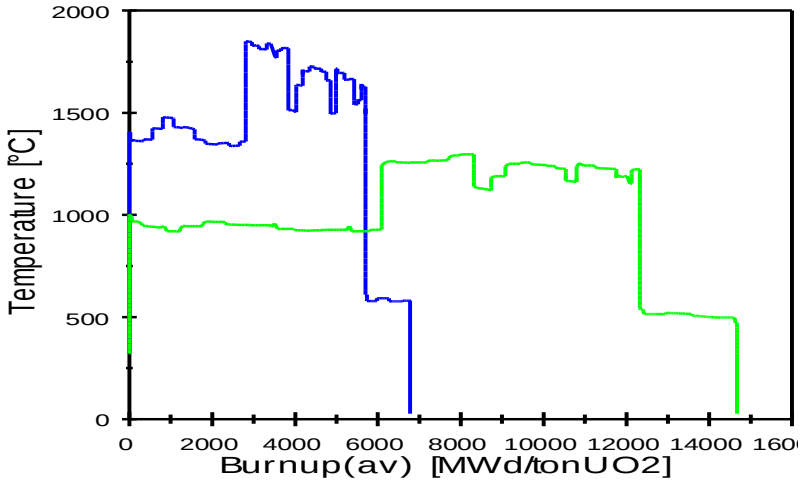

FIG. 16. Local temperature in the 7th segment of a fuel rod of the Atucha I NPP and a CARA fuel at the 7th axial position in the channel.

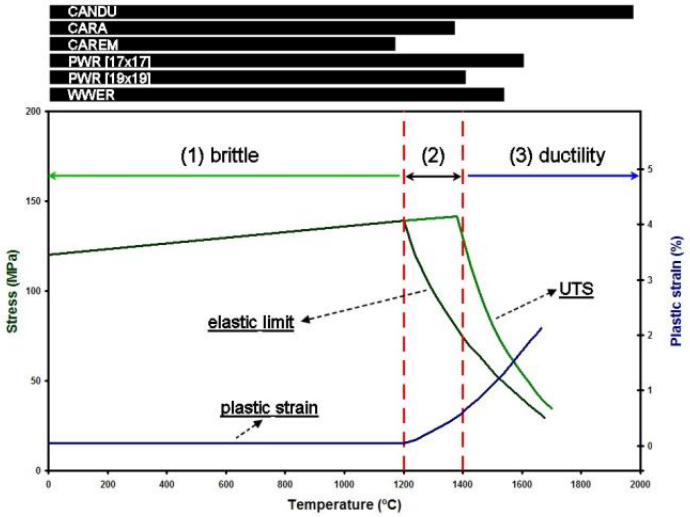

FIG. 17. Fracture and flow characteristics of UO_2 as a function of temperature, at the top the ranges of fuel centre temperature of various fuels are included [42].

TABLE 16. ARGENTINE PHWR FUELS COMPARISON

	Embalse	Atucha I	Atucha II
	CANDU NU	SEU 0.85%	U. Natural
Max. power [W/cm]	*600*	*550*	*596*
Peak factor	*1.12*	*1.11*	*1.10*
Burnup EOL	*7500*	*11700*	*7500*
# Fuel rods	*37*	*36*	*37*
DNBR	*3.27/2.05*	*3.41*	*3.5*
	CARA SEU 0.9%	CARA SEU 0.9%	CARA SEU 0.9%
Max. power [W/cm]	450 (75%)	400 (78%)	435 (73%)
Peak factor	1.15 / 0.95	1.16 / 0.94	1.13 / 0.96
Burnup EOL	14000	13350	~14000
DNBR	4.22/3.00 (129%)	5.61 (164%)	

The decrease in the linear power of the fuel rods is due to the increment of the number of rods of the fuel assembly. That is a result of the fuel rod diameter reduction in order to keep constant the total fuel material in the fuel assembly. The first consequence of the previous features is a strong reduction of the fuel pellet temperature. The BaCo code simulations show several benefits in the safety and performance of the fuel assembly if the temperature at the pellet centre remains below 1400ºC. Those advantages are: no central hole,

no columnar grains, decrement of the FGR, less thermal expansion, reduction in the fuel deformations, no plastic behaviour in the centre region of the pellet (see Fig. 17), an increment of the pellet cracking with cracks crossing the pellet, increment of the effective pellet radius due to the relocation of pellet fragments, etc. The fuel pellets structure become more uniform but high stresses can be find at the cladding when PCI is attained because a plastic state enough to allow the release of the fuel rod stresses is not achieved in the inner region of the pellet (see Fig. 20). Those results are among the main findings obtained with the BaCo code when it simulates the expected behaviour of the CARA fuel and of the CAREM reactor fuel [43].

6. CARA CVN (NEGATIVE VOID COEFFICIENT)

The CARA fuel element was originally intended with SEU 0.9%. With this uniform enrichment the void coefficient became positive.

Table 16 shows a final comparison of the CARA fuel and the common argentine PHWR fuel elements (Embalse CANDU-, Atucha I and II). The CARA Project became interesting due to the advantages included in the Table 16, in particular the trend for a less demanding conditions of irradiation for the fuel and the economy due to the extension in burnup [44–47].

A new version of the CARA fuel element, named CARA CVN, was designed with an academic purpose in order to establish the basis of a safest design of this fuel. The first design is included in Table 17 and Fig. 18 where the objective was attained by using differential enrichment in the three crowns of the fuel and natural o depleted Uranium plus Dysprosium in the four central rods.

TABLE 17. BASIC CHARACTERISTICS AND RESULTS OF THE CARA CVN

Ring # 1 (4 FRs)	7 – 7.5% Dy + UN
Ring # 2 (10)	1.4 – 1.7 ULE
Ring # 3 (16)	1.7 – 2.0 ULE
Ring # 4 (22)	1.45 – 1.60 ULE
Peak	1.19 – 1.22
Lin. Power	491- 506 (600) W/cm
α_v med	-1.7 – -2.4 mk
Burnup	16700 – 20800 MW·d/TU

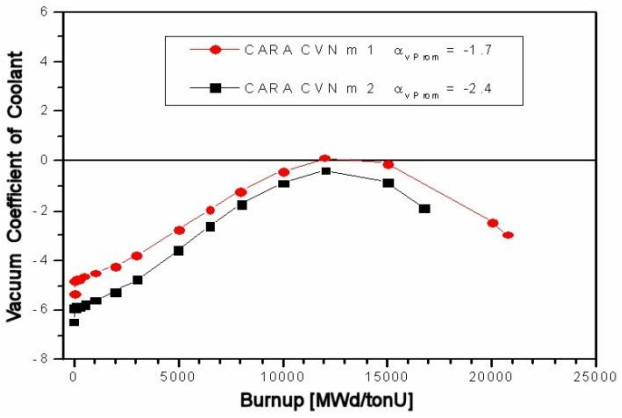

FIG. 18. An academic comparison of the Vacuum coefficient of coolant, α_V, of CARA CVN in the Atucha II NPP

7. CONCLUSIONS

The development of the CARA fuel element, intended for use in two different PHWR was presented, showing its design criteria and the way in which they were reached. The mechanical solution proposal by CARA is very innovative (doubling length and using this hydraulic advantage for adding spacer grids and for eliminating weldings on cladding) relative to the evolutionary solution proposal of CANFLEX for CANDU reactors, allowing extended burnup by the use of SEU, and with good thermal hydraulic margins using a single fuel rod diameter. From the point of view of designer, the CARA approach could be considered as another design line for new advanced CANDU fuels intended for higher burnup.

Different CARA fuel elements prototypes were hydraulically tested in a low-pressure loop. The experimentally validated models show the CARA hydraulic similarity with respect to CANDU fuel in Embalse. An additional assembly system enables the use of CARA in the vertical channels of Atucha. The mechanical feasibility for Atucha and Embalse, and hydraulic compatibility were checked, verifying that the CARA fuel can fit the unique Argentine challenge: a single fuel element for two different HWRs. The CARA could comply with all the design requirements, and with its implementation, SEU fuel element can be used in the Argentine NPPs at competitive values, an essential task for economic production in Argentina.

The BaCo code calculations shows: temperature decrease, smaller fission gas release, no restructuring and no central hole, lower thermal expansion, and finally a better tolerance of the dimensional parameters of CARA. This allows improving the manufacturing tolerance with an improvement in the dishing and shoulder of the pellet, and a smaller plenum. Similar results were found for a CARA FE in a CANDU NPP.

REFERENCES

[1] TORGERSON, D.F, SHALABY, B.A. AND PANG, S, S. CANDU Technology for

Generation III+ and IV Reactors, Nuclear Engineering and Design, **236** 1565 (2006) 1572.
[2] NGUYEN, T., et al, "Development of Severe Accident Management Guidance for the Canadian CANDU 6 Nuclear Power Plants", Nuclear Engineering and Design, **238** 1093 (2008) 1099.
[3] PRATO, C.A., et al, Full Scale Dynamic Tests of Atucha II NPP, Nuclear Engineering and Design, **179** 225 (1998) 243.
[4] JEONG, C.J., CHUN SUK, H, Assessment of Core Characteristics during Transition from 37-Element Fuel to CANFLEX-NU Fuel in CANDU 6, Annals of Nuclear Energy **29** 1721 (2002) 1733.
[5] TONG, L.S, WEISMAN, J., "Thermal Analysis of Pressurized Water Reactors", Proc. American Nuclear Society, La Grange Park, Illinois USA (1996).
[6] LEUNG, L.K.H., et al, Thermalhydraulics Studies Examining the Feasibility for Introducing Slightly Enriched Uranium Fuel into the Embalse CANDU Reactor, Nuclear Engineering and Design, **237** 1628 (2007) 1638.
[7] SHAN, C. Li, LEUNG, L.K.H., Subchannel Analysis of CANDU-SCWR fuel, Progress in Nuclear Energy, **51** 799 (2009) 804.
[8] DUTTON, R., et al, Advanced Technologies for CANDU Reactors, Nuclear Engineering and Design, **144** 269 (1993) 281.
[9] DIMMICK, G.R., et.al., "Full Scale Water CHF Testing of the CANFLEX Bundle", Proc. 6th CANDU Fuel Meeting, Niagara Falls, Canada 103 (1999) 113.
[10] CHUNG, C.H., et al, "Performance of the CANFLEX Fuel Bundle under Mechanical Flow Testing", Proc. 6th Int. Conference on CANDU Fuel, Toronto, Canada 60 (1999) 69.
[11] BRASNARO, D., et al, "CARA Development: an Argentine Fuel Cycle Challenge", Proc. 9th International Conference on CANDU Fuel, Ramada on The Bay, Belleville, Ontario, September 2005.
[12] WHITE, F., Fluid Mechanics, 3rd edn., McGraw-Hill, New York (1994).
[13] CLAYTON, F. T., "Station Data Manual, L6K 1B2", Central Nuclear Embalse, Córdoba.
[14] FLORIDO, P., et al, "CARA Fuel Bundle: A New Concept for HWR Present Situation", Proc. 6th International Conference on CANDU Fuel, Ontario, Canada 258 (1999) 267.
[15] INTERNATIONAL ATOMIC ENERGY IAEA, Technical and Economic Limits to Fuel Burnup Extension, Bariloche, Argentina, Nov. 1999.
[17] REDDY, D.G. AND FIGHETTI, C.F., "Parametric Study of CHF Data: A Generalized Subchannel Correlation for PWR and BWR Fuel Assemblies", Heat Transfer Research Facility, Dep. of Chemical Engineering, Columbia University, 1983.
[18] STEWART, C.W., et. al., "COBRA IV Development and Applications", Battelle, Pacific Northwest Laboratories, 1977.
[19] GLUCK, M., Validation of the subchannel code F-COBRA-TF: Recalculation of Single-Phase and Two phase Pressure Loss Measurements, Nuclear Engineering and Design, **238** (2008) 2308–2316.
[20] GLUCK, M., Subchannel Analysis with F-COBRA-TF – Code Validation and Approaches to CHF Prediction, Nuclear Engineering and Design, **237** (2007) 655–667.
[21] DAVERIO, H., JUANICO, L AND DELMASTRO, D., "COBRA Code Assessment for Dry Out of Advanced CANDU Fuels", Proc. 12th International Conference on Nuclear Engineering ICONE 12, Arlington, Virginia, USA, April 2004.
[22] PAIDOUSSIS, M., An Experimental Study of Vibration of Flexible Cylinders

Induced by Nominally Axial Flow, Nuclear Science and Engineering, **35** (1969).
[23] PETTIGREW, M.J AND TAYLOR, C., Two phase Flow-Induced Vibration: An Overview, Journal of Pressure Vessel Technology, **116** (August) 1994.
[24] NUCLEAR ENGINEERING INTERNATIONAL, Fuel Review 2004.
[25] LANE, A., GRIFFITHS, J. AND HASTINGS, I. "The Role of the New Canflex Fuel Bundle in Advanced Fuel Cycles for CANDU Reactors", Proc. 10th Annual Conference, CNS, 1989.
[26] MACDONALD, I.P., "Enhancement of critical heat flux in CANDU 37 Element Bundles", Proc. 8th Annual Conference, CNS, 1987.
[27] TIMOSHENKOET, S., et. al, "Vibration Problems in Engineering", Ed. Wiley & Son, pp 420-426, N.Y., USA, 1974.
[28] CHEN, S., "Flow-Induced Vibration of Circular Structures", Ed. Hemisphere Pub., NY, USA, 1987
[29] BRASNAROF, D. AND DELMASTRO, D., "CARA Fuel Pressure Drop Characterization", Informe Técnico CNEA–CAB–62/17/98, in XXV Reunión Científica de la Asociación Argentina de Tecnología Nuclear, Buenos Aires, Argentina, 1998.
[30] INTERNATIONAL ATOMIC ENERGY IAEA, "CARA Fuel Assembly Development", in Technical Meeting on Fuel Assembly Structural Behaviour, Cadarache, France, November 2004.
[31] NAE-HYUN KIM, LEE, S AND MOON, S., Elementary Model to Predict the Pressure Loss Across a Spacer Grid Without a Mixing Vane, Nuclear Technology, **98** (1992) 349–353.
[32] REHME, K., Pressure Drop Correlations for FE Spacers, Nuclear Technology **17** (1973) 15–23.
[33] STEGEMANN, D., "Diseño de Centrales Nucleares", Ed. by Centro Atómico, San Carlos de Bariloche, Falicov's Library, 1982.
[34] MARINO, A., SAVINO, E AND Marino, HARRIAGUE, S., BaCo (Barra Combustible) Code Version 2.20: a Thermo Mechanical Description of a Nuclear Fuel.
[35] MARINO, A., SAVINO, E AND Marino, HARRIAGUE, S., BaCo (Barra Combustible) Code Version 2.20: a Thermo Mechanical Description of a Nuclear Fuel Rod, Journal of Nuclear Materials **229** (1996) 155–168.
[36] INTERNATIONAL ATOMIC ENERGY IAEA, "Probabilistic Safety Criteria on High Burnup HWR Fuels", Technical Committee Meeting on "Technical and Economic Limits to Fuel Burnup Extension, Bariloche, Argentina, 1999.
[37] MARINO, A AND FLORIDO, P., High Power Ramping in Commercial PHWR Fuel at Extended Burnup, Nuclear Engineering and Design, **236** (2006) 1371–1383.
[38] INTERNATIONAL ATOMIC ENERGY IAEA, "An Approach to the 3D Modelling of the UO_2 Pellets Behaviour Under Irradiation Conditions", Technical Meeting on Fuel Behaviour Modelling Under Normal, Transient and Accident Conditions, and High Burnup, Kendal, U.K., September 2005.
[39] MARINO, A, DEMARCO, G, FLORIDO, P, "3D Assessments for Design and Performance Analysis of UO2 Pellets", Proc. 9th International Conference on CANDU Fuel, Belleville, Canada, September 2005.
[40] KILLEEN, J et al, "Fuel Modelling at Extended Burnup: "IAEA Coordinated Research Project FUMEX-II", Proc. Top Fuel 2006, Salamanca, Spain, October 2006.
[41] Brasnarof D.O. et al, "Diseño CARA CVN: Elemento Combustible Inherentemente Seguro Para Centrales PHWR y Propuesta Para Atucha II", in XXXIV Reunión Científica de la Asociación Argentina de Tecnología Nuclear, Buenos Aires,

Argentina, 2007.
[42] OLANDER, D. R., “Fundamental Aspects of Nuclear Reactor Fuel Elements”.
[43] BOADO, H. et al, “Project Report: CAREM Project Status”, Science and Technology of Nuclear Installations, Article ID 140373 (2011).
[44] INTERNATIONAL ATOMIC ENERGY IAEA, “Revisiting the experience with Advanced Fuel Cycles in Argentine Heavy Water Reactors”, Technical Meeting on Advanced Fuels for PHWRs, Mumbai, April 2013.
[45] BRASNAROF, D., et al, “A New Fuel Design for Two Different HW Type Reactors” Science and Technology of Nuclear Installations, Article ID 194650 (2011).
[46] LESTANI, H., et al, “Conceptual Engineering of CARA Fuel Element with Negative Void Coefficient for Atucha II”, Science and Technology of Nuclear Installations, Article ID 264235 (2011).
[47] BRASNAROF, D., et al, “Diseño CARA CVN: Elemento Combustible Inherentemente seguro para centrales PHWR”, XXXIV Annual Meeting of AATN, November 19–23, 2007, Buenos Aires, Argentina.

FUEL FABRICATION AND PERFORMANCE
(Session 3)

Chairman

J. H. PARK

Republic of Korea

SEU FUEL FABRICATION FOR PHWR 220 UNITS - MANUFACTURING EXPERIENCE

U. K. AROR, SHEELA, N. SAIBABA
Nuclear Fuel Complex,
Hyderabad, India

Abstract

Nuclear Fuel Complex (NFC), an industrial unit of the Department of Atomic Energy, has been manufacturing, natural and enriched uranium oxide fuels for all the water-cooled nuclear power reactors in India. Natural Uranium Di Oxide powder is converted to high density sintered pellets for Pressurized Heavy Water Reactors (PHWRs). The pellets are fabricated from nuclear grade UO2 powder, produced through ammonium di-uranate (ADU) precipitate route followed by the standard "powder-pellet" route involving pre-compaction, granulation, cold compaction and high temperature sintering. Sintered pellets are ground using centreless grinders to required size and to attain uniform diameter along the length. Slightly Enriched Uranium (SEU) is one of the probable options, can be used as advance fuel to enhance burnup of existing PHWRs. NFC has manufactured fuel pellets of different designs, in close coordination with Nuclear Power Corporation of India Ltd (NPCIL). SEU pellet design is modified version of existing Natural Uranium Oxide pellet design, with the consideration of higher burnup and higher residence period. Specified sintered density for SEU pellets is lower than Natural Uranium (NU) Di Oxide pellets with the aim of additional porosity. The stack of pellets, used in fuel element, is combination of SEU and NU. Natural Uranium Oxide pellets are specially fabricated for this purpose, having lower L/D ratio compared to NU pellets, being used in PHWR assemblies. The paper deals with manufacturing experience of SEU pellets and fuel elements. It describes about process modifications carried out to meet design and specification of these pellets.

1. INTRODUCTION

Nuclear Fuel Complex (NFC), an industrial unit of the Department of Atomic Energy, manufactures natural and enriched uranium oxide fuels for all the water-cooled nuclear power reactors in India. Powder metallurgy route has been established to convert Uranium Di Oxide Powder (UO_2) into very high density sintered fuel pellets. These sintered products are cylindrical in shape and required to be ground using CNC operated centreless grinders to met dimensional requirements. The virgin UO2 powder is produced through Ammonium di-Uranate (ADU) precipitate route. The powder is not free flowing, hence required to be pre-compacted and granulated before final compaction operation.

Pre-compaction & granulation is carried out in special purpose roll compactor, designed for ceramic UO_2 powder. Green pellets are formed by cold compaction using CNC hydraulic presses. The pre-compaction pressure is generally kept lower than the final compaction pressure, to collapse these granules easily, during final compaction operation.

Granulated powder is filled simultaneously, in die block having multiple die sleeves, using specially designed powder feeder. Twelve pellets are compacted in each compaction stroke. The purpose of compaction is to obtain the required shape and density. It imparts adequate strength to compacts for subsequent handling and processing. Compaction cycle consists of multiple steps namely die filling, under filling, compaction, dwell and ejection. Each step has its own importance with respect to compact characteristics, particularly in double acting compaction.

Density of green pellet is measured at regular interval to monitor required compact quality. Geometric method is used to determine green density and is used as process control parameter. Weights of individual pellets are also monitored, to check proper and consistent

die filling. Sintered density of the pellets shall be in the range of 10.45 to 10.75 gm/cc. Sintering operation is carried out in reducing atmosphere at 1700°C.

All the Pressurized Heavy Water Reactors (PHWRs) in India are operating with natural uranium oxide fuel. Nineteen (19) element fuel bundles are used in 220 MWe reactors and average exit burnup of this design is approximately 6800 MW·d/TeU. It was envisaged to utilize fuel with 0.9 % enrichment in existing 220 MWe PHWRs on experimental basis, to enhance exit average burnup. Expected exit burnup with 0.9 % enrichment was approximately 14 000 MW·d/TeU. It was proposed to manufacture minimum 50 fuel bundles with available enriched fuel as a campaign.

2. MODIFIED SEU PELLET DESIGN AND PELLET STACK CONFIGURATION

Proposed pellet design for Slightly Enriched Uranium (SEU) was different with respect to dish depth and sintered density requirement. These modifications were proposed by NPCIL considering expected higher exit burnup. The stack of pellets, used in fuel element, was combination of SEU and natural uranium (NU) Oxide pellets. End pellets of stacks were NU oxide pellets having lower average L/D ratio of 0.70. Pellet stack configuration is shown in Figure 1.

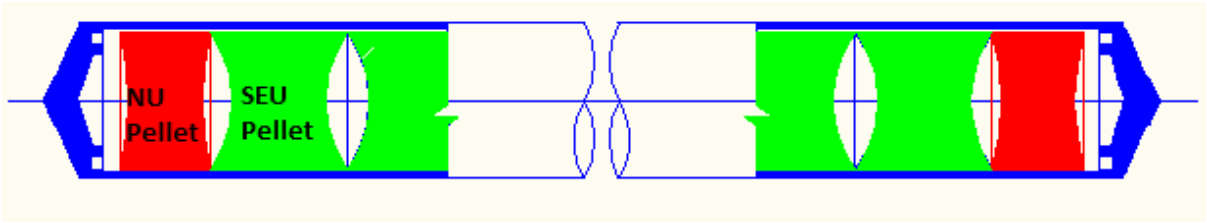

FIG. 1. Pellet stack configuration.

Comparison of existing pellet design for NU and modified design for SEU is mentioned in Table 1.

TABLE 1. PELLET DESIGN COMPARISON

S. No.	Design Parameter	NU Oxide Pellet	SEU Oxide Pellet
01	Average dish depth at each end	0.25 mm	0.50 mm
02	Sintered density range	10.45-10.75 gm/cc	10.35 – 10.65 gm/cc

Comparison of pellet stack configuration is mentioned in Table 2.

TABLE 2. PELLET STACK CONFIGURATION COMPARISON

S. No.	Stack configuration parameter	NU oxide pellet stack	SEU oxide pellet stack
01	Number of pellets	26-31	26-31
02	Average L/D ratio of end pellets	1.15	0.7
03	Average L/D ratio of other pellets of stack	1.15	1.15

3. MANUFACTURING OF SEU OXIDE PELLETS AND LOW L/D RATIO NU OXIDE PELLETS

It was challenging to manufacture pellets with new design specification, considering limited quantity of available SEU oxide powder. Following were the major tasks involved for manufacturing SEU oxide pellets:

(a) Design and fabrication of new punches for compaction press;
(b) Validation of new punch design;
(c) Experiments to establish compaction parameters.

In order to manufacture NU oxide pellets with lower L/D ratio, in the range of 0.65 to 0.75, new set of compaction parameters were required to be established.

3.1. Design and fabrication of new punches for compaction press

Pellet dish depth at each end of the pellet is desired for axial thermal expansion during in the reactor. The required dish depth for SEU oxide pellet was 0.50 mm compared to 0.25 mm for NU oxide pellets being manufactured regularly. New set of punches were designed and fabricated for increased dish depth. Typical punch end is shown in Fig. 2.

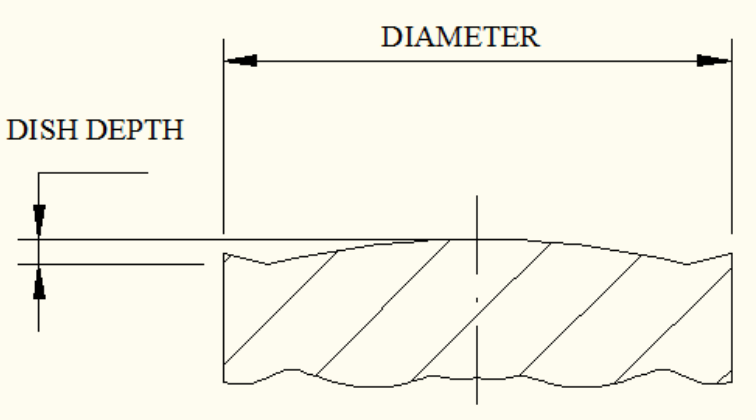

FIG. 2. Typical punch end.

3.2. Validation of new punch design

Punch design was required to be validated before starting manufacturing SEU oxide pellets. Validation was carried out by manufacturing NU oxide pellets with new set of punches. The UO_2 powder characteristics like specific surface area and O/U ratio also affect shrinkage behaviour of the pellets. NU oxide powder lot selected for validation was having almost similar physical characteristics as that of SEU oxide powder. Comparison of powder characteristics are shown in Table 3.

TABLE 3. COMPARISON OF POWDER CHARACTERISTICS

S.No.	Powder characteristic	NU Oxide powder	SEU Oxide powder
01	BET specific surface area (m^2/gm)	2.80	2.80
02	Bulk density (gm/cc)	1.90	1.92
03	O/U ratio	2.05	2.05

Thirty pellets were compacted and sintered. Dish depth of both the ends of all the pellets was measured. Minimum, maximum and average value is tabulated in Table 4.

TABLE 4. DISH DEPTH WITH NEW PUNCH DESIGN

S.No.	Dish depth	Top end	Bottom end
01	Minimum value (mm)	0.457	0.452
02	Maximum value (mm)	0.533	0.534
03	Average value (mm)	0.494	0.492

3.3. Experiments to establish compaction parameters:

It was desired to reduce sintered density range of SEU oxide pellets in comparison with NU oxide pellets. Sintered density can be reduced by (i) using dopant or by (ii) reducing density at green stage. Since very small change in sintered density was desired and very limited quantity of pellets had to be manufactured, second option was selected.

The required range of green density to be maintained, to get required quality of pellets, depends on shrinkage pattern. Green pellets were formed using different compaction pressures. The compaction pressure was varied from 80 bar to 200 bar in the step of 10 bar. The sample pellets were sintered in six zones, high temperature sintering furnace under reducing atmosphere. Sintered density was measured by immersion as well as geometrical

method. Green density of pellets increases with increase of compaction pressure. Beyond 180 bars, increase in green density is minimal.

Relation between green density and compaction pressure is shown in Fig. 3. Relation between sintered density and compaction pressure is shown in Fig. 4. The effect of compaction pressure on sintered density and green density is similar. Based on these results compaction pressure was selected as 130 bar and average green density was maintained at 5.70 gm/cc.

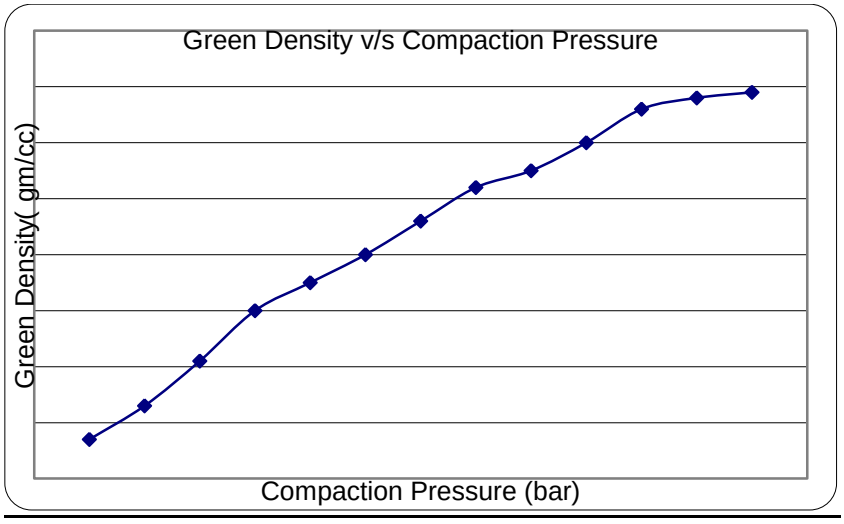

FIG. 3. Green density vs compaction pressure.

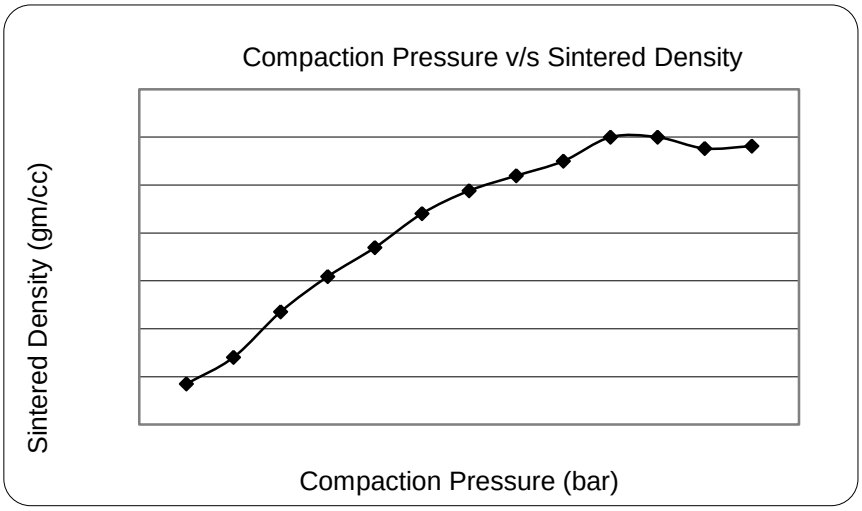

FIG. 4. Compaction pressure vs sintered density.

3.4. Fabrication of low L/D ratio NU oxide pellets

Length/diameter (L/D) ratio of NU oxide pellets being fabricated on regular basis for is in the range of 1.1 to 1.2. The desired L/D ratio of NU oxide pellets, to be used as endpellets of pellet stack of SEU fuel bundle was in the range of 0.65 to 0.75. Die fill depth of compaction press was modified to obtain required range of L/D ratio. Weight of green pellets was used as process check parameter. Sintered pellets were ground on centre less grinding equipment with additional support to pellets in order to avoid toppling of pellets while grinding.

After establishing modified compaction process for SEU oxide pellets and low L/D ratio NU oxide pellets, SEU powder was released for production. Pellets were fabricated to meet requirement of 51 fuel assmblies. All the 51 fuel assemblies were dispatched to reactor site for testing.

4. SUMMARY

(a) Green density has a well defined relation with sintering behaviour and physical characteristics of sintered pellets;
(b) Manufacturing of required SEU oxide pellets with limited quantity of available SEU oxide powder was successfully carried out by modifying die design and optimizing compaction parameters;
(c) Process of fabrication and grinding of low L/D ratio pellets was established;
(d) Process for manufacturing SEU fuel assemblies has been established successfully and can be utilized for mass scale production.

ACKNOWLEDGEMENTS

The authors would like to thank our colleagues of the Production and Quality Assurance Group for their valuable suggestions and active participation in establishing process and system.

REFERENCES

[1] NPCIL Report “Design Note on Use of SEU Fuel Bundle in 220 MWe PHWRs
[2] SEROPE KALPAKJIAN, “Manufacturing Process for Engineering Materials”, PEARSON Education 635 (2007) 645.
[3] ASM Handbook, “Powder Metal Technologies and Applications”, Volume 7, 1998.

RESEARCH ON SOL–GEL MICROSPHERE PELLETIZATION OF UO_2 FOR PHWR FUEL IN INDONESIA

M. RACHMAWATI, SARJONO, TRI YULIANTO,
B. HERUTOMO, B. BRYATMOKO
Center for Nuclear Fuel Technology,
National Nuclear Energy IAEA (BATAN),
Jakarta, Indonesia

Abstract

In this study, sol-gel precipitation using external gelation for Sol Gel Microsphere Pelletization (SGMP) of UO_2 pellet for PHWR will be conducted. Suitable feed compositions along with the calcination and reduction steps of heat treatment have been chosen to optimize the properties of the dry gel microspheres. The composition in this work is viscosity 40–60 Cp, Uranyl nitrate 0.6–0.9 mol U/l, Tetrahydrofurfurilyalcohol (43–47)% volume, Polyvinyl alcohol 10–15 g/l. The feed will be heated before feeding into drop formation and gelation column that converts the feed solution into gels. The gels are then dried and heat treated at 85°C and 200°C respectively. After that the gels are calcined in O_2 at 500°C followed by reduction in H_2 and N_2 mixture at 600°C to obtain UO_2 microspheres with certain specific surface area and O/U ratio. The UO_2 microspheres are characterized with respect to the dimensions, sphericity, surface area, tap density, crush strength, and O/U ratio. The UO_2 microspheres then are pelletized in a hydraulic press to produce the green pellet densities about 55% T.D. The green pellets are sintered in H_2 and N_2 mixture at 1100°C for 6 hours. The sintered pellets are characterized with respect to the density and their microstructure. The results show that the microspheres have average size of 900 µm, tap density 1.90 g/cm^3, specific surface area 6 m^2/g, and crush strength 2.0 N/particle. The compaction of the microsphere gives the green density result 55% T.D at compaction pressure 300 MPa. and sintering of the green pellet give sintered density about < 90% T.D. The dimension (900 µm) and sphericity (1.10), tap density (1.9 g/cm^3), O/U (2.37), specific surface area (6 m^2/g), and crush strength (2.0 N/particle) of the microspheres give a better feed for direct compaction into green pellet. The use of the microsphere as compaction feed have important advantages in comparison with the use of powder metallurgical process techniques, where the dust generation and flowability problems necessitate supplementary precautions in view to minimize the exposure of personnel to radiation and this means more operation steps which complicate the process.

1. INTRODUCTION

Indonesia has the facilities for research and development in nuclear fuel fabrication technology for power reactors: the Experimental Fuel Element Installation to produce power reactor fuel and Power Ramp Test Facility (PRTF) to test the fuel performance. The R and D activities in fabrication technology have been conducted using a conventional powder metallurgical processing including UO_2 pellets with large grain size by addition of small amount of dopant for high burnup by decreasing fission products and increasing thermal stability as well as $(Th,U)O_2$. An innovative fuel pellet, UO_2-metal cermet pellet fuel, has been developed using the same method. The purpose is to improve the thermal conductivity of a UO_2 pellet. The main difficulty in performing the research mentioned above is to obtain microhomogeneity; especially in the manufacture of MOX such as $(Th,U)O_2$. Besides, the National Nuclear Energy IAEA (BATAN) has also been doing a research on fuel fabrication technology of high temperature gas reactor (HTGR). One of the process steps in the HTGR fabrication, which is sol – gel precipitation process, was found to be attractive for sol gel microsphere pelletization (SGMP) of UO_2 and MOX fuel mainly in obtaining microhomogeneity [1].

The name sol-gel process is a generalized heading for chemical routes which involves the gelation of a droplet of sol or solution of the desired fuel material into a gel microsphere [2]. Recently, gel microspheres derived from the sol – gel process are used as press feed material of the pellet type fuel fabrication. The combination of front end HTR fuel fabrication

with established technology of standard pelletization process called Sol gel microsphere pelletization (SGMP). In general, the advanced SGMP methods for fabrication of fuel pellet type have the following features: 1) microspheres of being practically dust free; 2) their use as press feed eliminates dust generating steps from the pelletizing process; 3) the free flowing property of microspheres allows important process line simplifications; 4) sol-gel microspheres of mixed fuel have a homogeneous composition resulting from co-precipitation of heavy metals. This facilitates the solid solution formation of mixed oxides which is an important prerequisite to obtain good pellets in the sintering step of the process; 5) minimize open porosity but having homogenously distributed closed pores which improve performance in the reactor; 6) SGMP technique is particularly attractive for mixed oxide fuel because it gives a high degree of micro-homogeneity of uranium and thorium or plutonium in the solution stage. The prolonged ball milling of oxide powders for achieving good micro-homogenization in the standard powder pellet route is unnecessary. The disuse of the powder mixing step prevents build-up of radioactive dust in the glove box, minimizing the dose related problems to the operating personnel. The potential of the sol-gel precipitation method becomes a driving force to do a research in application of the method for production of pellet fuel for LWR and PHWR reactor.

In the present work, a SGMP process has been developed for producing UO_2 pellet by merging external gelation of uranium has been adapted for producing gel microsphere which are suitable as press – feed material. The distinguishing feature of this method is that a water soluble organic polymer is added to the heavy metal solution or sol. The polymer supports the particle spherical shape while amonia diffusee into the gel sphere and precipitates the heavy metal. One of the most attractive features of the original method was that no pretreatment of uranium solution was required. The necessary chemicals were simply added to the uranyl nitrate solution to prepare the broth, which is very stable and can be stored for days or weeks. High acid and electrolyte concentrations are tolerated [3].

2. EXPERIMENTAL PROCEDURE

The flow chart of SGMP for oxide pellets is given in Figure 1. Suitable feed or broth compositions along with the calcination and reduction steps of heat treatment have been chosen to optimize the properties of the dry gel microspheres that suitable to merge with pelletization of UO_2 pellets using powder metallurgical process. The compositions suitable for the SGMP are having higher molarity of uranium in feed solution. The pressed pellets are sintered at desired temperature to make high density pellets.

The process comprises feed or broth preparation, droplets formation and gelation, washing of gel particles, drying and heat treatment of the gel microspheres. Then the dried microspheres are calcined in O_2 at 500°C followed by reduction in H_2 and N_2 mixture at 600°C to obtain UO_2 microspheres with certain surface and O/U ratio.

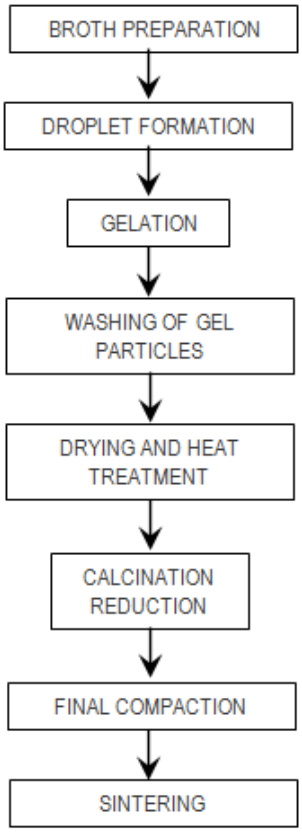

FIG. 1. Flow sheet of SGMP Process.

The UO_2 microspheres then are pelletized in a hydraulic press to produce the green pellets density about 50% T.D. The green pellets are sintered in H_2 and N_2 mixture at 1100°C for 6 hours [1]. The sintered pellets are characterized with respect to the density and microstructure.

2.1. Broth preparation

Various methods of broth preparation for external gelation have been reported previously [4]. Fig. 2 shows the flow diagram of broth preparation used in this work [5]. One of the most attractive features of the broth preparation used for external gelation is that no pretreatment of uranium solution was required. The necessary chemicals were simply added to the uranyl nitrate solution to prepare the broth, which is very stable and can be stored for days or weeks. High acid and electrolyte concentrations are tolerated [3].

The process comprises of adding tetrahidrofurfuril alcohol (THFA) separately into both uranyl nitrate solution (mixture 1) and polivynil alcohol solution (PVA) (mixture 2), and subsequently both mixture 1 and mixture 2 are mixed to form the broth. Then the broth will be heated before feeding into drop formation and gelation. The gels then are washed, dried and heated at 400°C in air.

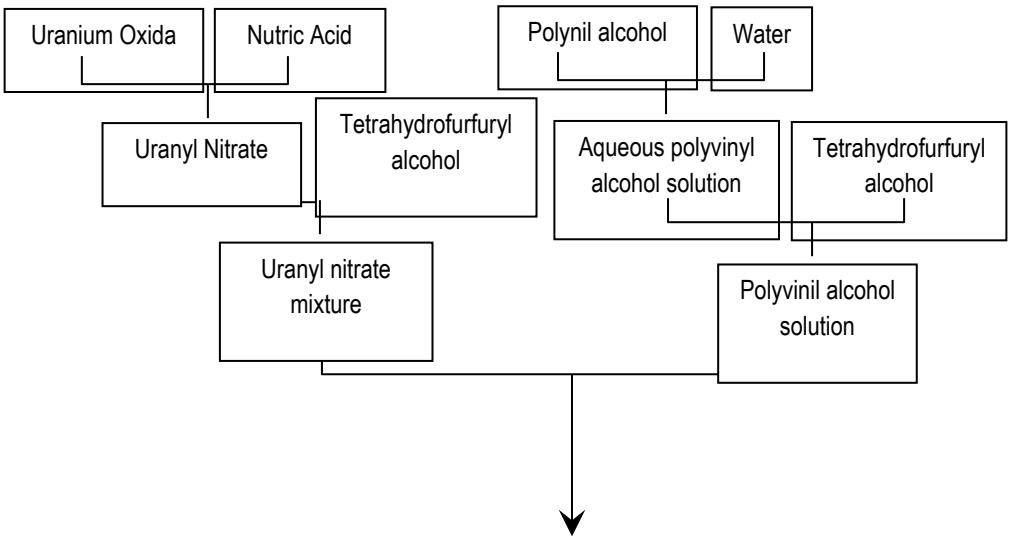

FIG. 2. Preparation of Broth [5].

The broth composition having uranyl nitrate 0.6 – 0.9 mol U/L, THFA 43 – 47% volume, PVA 10 – 15 g/L, and viscosity between 40 – 65 cp [5].

2.2. Droplet formation and gelation

Droplets were prepared by forcing the broth solution through nozzle having a diameter of 1.0 mm. To control the breaking up of the fluid stream into droplets of uniform size, the dispertion nozzle was vibrated at 150 Hz with the electromagnetic vibrator. Formation of microspherical drops in an NH_3-free environment and brief exposure to ammonia in the same phase to form a thin skin and fix the shape of the drop. Transfer of the partially gelled microsphere through an interface into the gelating solution (usually concentrated NH_4OH) by free fall through the gelating solution for several seconds and aging in this solution for several minutes or hours. The droplets entered the gelation medium, gelled in a few seconds and transferred to the wash tank. Fig. 3 shows the sol – gel precipitation column used in this work.

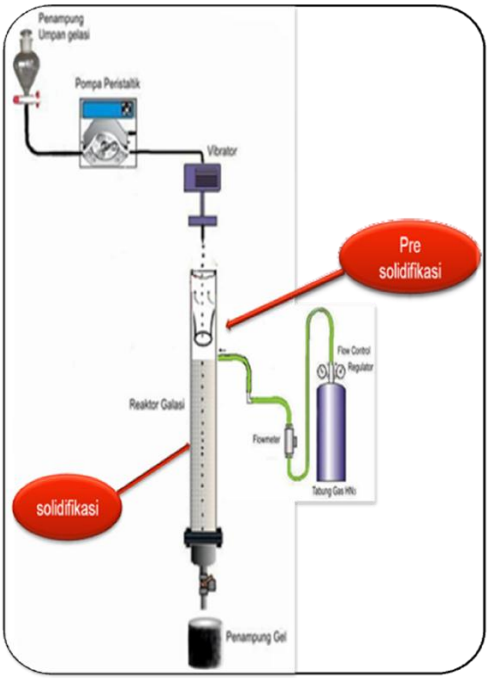

FIG. 3. Schematic diagram of sol – gel precipitation.

2.3. Washing, drying and heat treatment of microspheres

The formed gel microspheres were placed in the wash tank and were washed 4 times with diluted NH_4OH to remove NH_4NO_3 formed from the precipitation reaction which causes serious problems in the further heat treatment steps [1].

To obtain soft microsphere for easy pelletization, the water in the gel microspheres was replaced by isopropyl alcohol by heating in a dryer at 85°C. The gel microspheres after washing were heat-treated at 220°C for two hours.

2.4. Calcination and reduction

Dried microspheres were calcined in muffle furnace at 500°C for 1 hour in a continuous flow of air and cooled to room temperature in the same atmosphere.

$$3\ (NH_4)_2U_2O_7 \rightarrow 6\ UO_3 + 6\ NH_3 + 3\ H_2O$$

$$6\ UO_3 \rightarrow 2\ U_3O_8\ + O_2$$

The calcined microspheres were characterized with respect to optical microscopy, tap density, crush strength, O/U ratio, and surface area.

An important parameter of the experiment was the specific surface (m^2/g) of the microspheres used for pellet production. In principle, the specific surface can be adjusted either prior to reduction (U_3O_8 state) or after reduction (UO_2 state) [6]. So, reduction of the microspheres is conducted in this work. The calcined particle were reduced to UO_2 at 600°C for one hour in a continuous flow of hydrogen and cooled to room temperature in the same atmosphere.

$$U_3O_8 + 2\,H_2 \rightarrow 3\,UO_2 + 2\,H_2O$$

$$UO_{2+xx} + H_2 \rightarrow UO_{2+x}$$

The microspheres suitable for pressing and sintering should have a specific surface area and O/U ratio in the range of 2 – 13 m^2/g and 2.34 – 2.55, respectively [6]. In general, microsphere of low O/U ratio revealed high specific surface area and vice versa for getting good pellets [6].

2.5. Characterization of microspheres

The UO_2 microspheres are characterized with respect to the dimensions and sphericity, tap density, O/U ratio, surface area, and crush strength. The dimension of the microspheres was measured using an optical stereo microscope using image analyzer software. For determination of tap density, the microspheres were filled in a measuring cylinder of 100 cc volume up to the mark. The weight of the microspheres was noted and the volumetric flask was fitted to the tap density apparatus. The flask was tapped vertically to a pre-set value and, after completion of the tapping, the volume of the product was recorded. The ratio of weight of the product to the volume obtained after tapping gave the tap density.

The O/U ratio was measured by calcination at 900°C for four hours. The specific surface area of the microshere was measured using using multipoint BET method. The crush strength of the microsphere was determined using a crush strength apparatus universal testing machine. A single microsphere was placed in the sample table of the apparatus and the load road was moved and pressed the microsphere. When the microsphere breaks, the unit displays the load required to break the microsphere in terms of newtons per particle.

2.6. Pelletizing and sintering

The UO_2 microspheres were compacted in a hydraulic press double action floating dies system. The compaction pressure varied from 200 to 500 MPa. For comparison, the compaction of UO_2 powder with the same compaction condition was conducted. The geometry (L/D), green densities of the green pellets were measured and subsequently the pellets were sintered in N_2 and H_2 mixture atmosphere at 1100°C for six hours. The sintered pellets density and microstructure were characterized.

3. RESULT AND DISCUSSION

The results show that the microspheres have average size of 900 μm, tap density 1.90 g/cm^3, O/U ratio 2.37, specific surface area 6 m^2/g, and crush strength 2.0 N/particle. Fig. 4 show process apparatus involving the sol-gel process in the front end of fuel fabrication merged with the pellet making process called Sol-gel microsphere pelletisation (SGMP) process developed in this work.

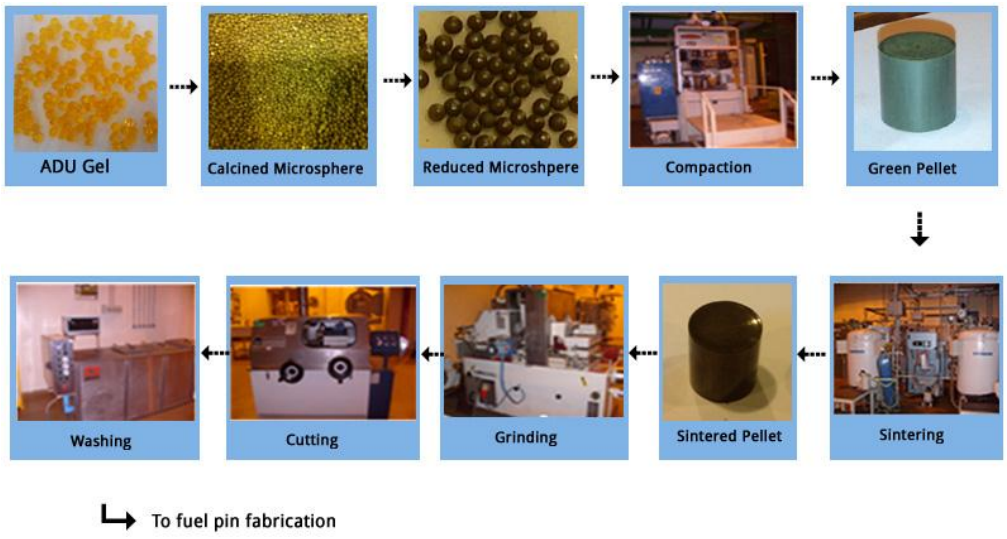

FIG. 4. SGMP process stages.

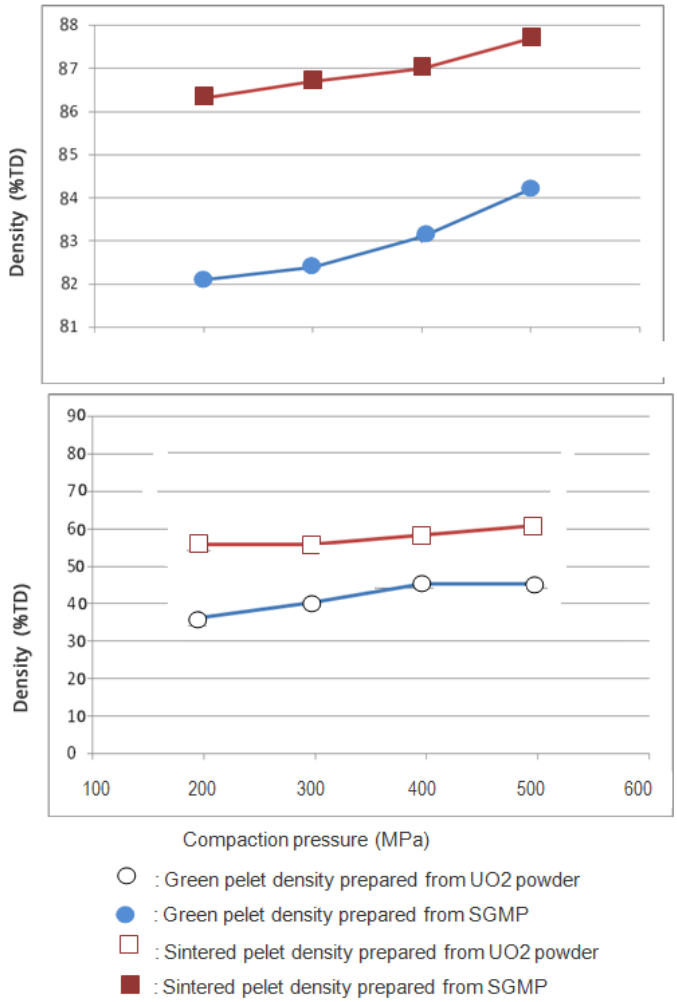

FIG. 5. Green and sintered density of pellet prepared from conventional pelletization and SGMP.

As seen in Fig. 5, green pellet densities increase with increasing compaction pressure. Although the green pellets were intact, the sintered pellets derived from 400 – 500 MPa were cracked. It desired that the green density of the pellets about 55% of the theoretical density. The compaction pressure chosen in this work is 300 MPa.

In comparison to powder, the microsphere had a very different pelletizing and sintering behavior. Fig. 5 shows, at the same compaction pressure, the green density of UO_2 microsphere feed compaction are higher than the green density of UO_2 powder feed compaction**.** The morphology of the microsphere, tap density, O/U, specific surface area, and crush strength value give a better feed for direct compaction into green pellet. This result is in a good agreement with previous research [1].

During sintering, suitable properties of the microspheres give a good sinterability/shrinkage capability between and within microsphere. Fig. 5 shows, sintered density of the pellets from UO_2 microsphere are higher than sintered density of UO_2 pellets from UO_2 powder.

Fig. 6 shows a typical optical micrograph of fracture surface of a pellet shows that the densification and sintering have not completed yet. It also shows that the blackberry structure do not detectable, the pellets have practically no microsphere boundaries.

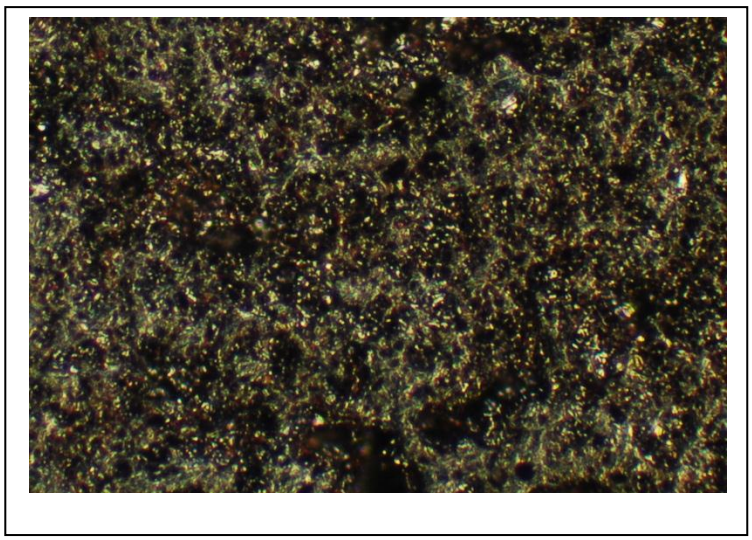

FIG. 6. The microstructure of fracture surface of UO_2 pelet from SGMP showing no blackberry structure

These results is in a good agreement with previous research reported that the sintered pellets prepared by SGMP process have been reported to have a low density (≤ 85%) and blackberry structure with significant quantities of open pores[7,8]. The low crushing strength of the microspheres disintegrated completely and lost their individual identity during pellets pressing, hence avoiding the blackberry structure of the sintered pellets [9]. Sintering temperature at 1100°C for 6 hours has not given sintered pellet with high density and good microstructure. It is necessary to investigate the sintering conditions in order to reach high densities of UO_2 pellets (≥ 95% TD) and their microstructure.

4. CONCLUSION

The morphology the microsphere, tap density, O/U, specific surface area, and crush strength values give a better feed for direct compaction into green pellet with the compaction pressure of 300 MPa. Sintering temperature at 1100^{o}C for 6 hours has not give sintered pellet with high density and good microstructure. It is necessary to investigate the sintering conditions in order to reach high densities of UO_2 pellets (>95% TD) and their microstructure.

The use of microspheres as press feed possesses undoubtedly important advantages in comparison with the classical powder techniques, where the dust generation and flowability problems necessitate supplementary precautions in view to minimize the exposure of personnel to radiation and this means more operation steps which complicate the process

REFERENCES

[1] TEL, H., ERAL, M., ALTAS, Y., Investigation of Production Conditions of ThO2 – UO3 Microsheres via the Sol-gel Process for Pellet Type Fuels, Journal of Nuclear Materials **256** 18 (1998) 24.

[2] INTERNATIONAL ATOMIC ENERGY IAEA, Proceedings of the Panel on Sol-gel Processes for Ceramic Nuclear Fuels, IAEA, Vienna, 1968.

[3] HASS, P.A., NOTZ, K.1., SPENCE, R.D., "Application of Gel Microsphere Processes to Preparation of Sphere-Pac Nuclear Fuel", Annual Meeting of the American Ceramics Society, May 6-11, 1978, Michigan,USA.

[4] HTGR Generic Technology Program, General Atomic Company, Semi-annual Report for the Period Ending September 30, 1980 HTGR.

[5] TAKAHASHI, M., "Method of Preparing Feedstock Liquid, Method of Preparing Uranyl Nitrate Solution, and Method for Preparing Polyvinyl Alcohol Solution", Nuclear Fuel Industries Ltd, Tokyo, Japan, 8 Dec. 2009.

[6] HASS, P.A., BEGOVICH, J.M., RYON, A.D., VAVRUSKA, J.S., Chemical Flowsheet Conditions for Preparing Urania Spheres by Internal Gelation, ORNL, Tennessee, USA, 1979.

[7] TIEGS, M., HASS, P.A., SPENCER, R.D., ORNL/TM–6906 (1979).

[8] MATHEWS, R.B., HART, P.E., J. Nuclear Material **92** (1980) 207pp.

[9] GANGULY, C., LANGEN, H., ZIMMER, E., MERZ, E., Nuclear Technology **73** (1986) 84pp.

PERFORMANCE OF SLIGHTLY ENRICHED URANIUM BUNDLES LOADED IN MAPS-2 EQUILIBRIUM CORE

S. RATHAKRISHNAN, J .K. SAHU, R. GEORGE,
D. RAJENDRAN, R. K. GUPTA, T .J. KOTTEESWARAN
Nuclear Power Corporation of India Limited,
Madras, India

Abstract

To obtain feedback on the performance of SEU bundles prior to its large scale use in 220Mwe reactor, 51 SEU bundles have been loaded in Unit-2 core of Madras Atomic Power Station (MAPS-2) for trial irradiation. The dimension of SEU bundles is same as that of 19 element Natural Uranium (NU) bundle used in Indian 220 MWe Pressurized Heavy Water Reactor (PHWR). Locations of these bundles have been selected in such a way that reactor should be operating at rated power without violating limits on maximum bundle powers and maximum channel outlet temperature. Initially these bundles were loaded in the low flux location. Later on after achieving a bundle burnup of more than 5000 MW·D / TeU, they were recycled to high flux location to see the performance of the SEU bundles with power ramp. Out of the 51 SEU bundles loaded, 47 bundles have already been discharged and the remaining 4 bundles are still in the core. The maximum discharge burnup of the SEU bundles is about 24770 MW·D/TeU. The performance of the SEU bundle is excellent and so far no SEU bundle is failed. Based on this experience, converting a natural uranium core to SEU core by full core loading of SEU bundles in the Indian 220MWe PHWR, has been studied.

1. INTRODUCTION

The reactor core of 220MWe Indian Pressurized Heavy water Reactor (PHWR) consists of 306 horizontal fuel channels, 12 fuel bundles reside in each such channel and heavy water coolant flows through the channel to carry the heat produced by the fuel. Since Natural Uranium (NU) bundles are used as a fuel, there is a little excess reactivity in the equilibrium core. Hence ON Power refueling is done with 8-Bundle Shift scheme (BSS) to compensate daily reactivity loss due to operation.

The direction of the coolant flow in adjacent channel is opposite in direction. Thus out of 306 fuel channels, 153 channels have the coolant flow in one direction and other 153 channels have flow in opposite direction. Refueling is also done according to the direction of coolant flow. This helps in achieving axial flux flattening. For the required radial flux flattening to operate the reactor at 100% FP, differential refueling scheme is followed. To adopt this, the core is divided into two zones namely inner zone and outer zone. The inner zone consists of 78 channels where the discharge burnup of the fuel bundle is kept as high as 10 000 MW·D/TeU and outer zone consists of 228 channels where the discharge burnup of the fuel bundle is kept as low as 5500 MW·D/TeU. The required rate of refueling is 1.1 channels per full power day (FPD) which is equivalent to 9.16 bundles for the equilibrium core configuration with core excess reactivity of 12mk in the form of adjuster rods. The design average discharge burnup for the core is 6300 MW·D/TeU.

For extending the discharge burnup for better fuel utilization, different countries conceived new fuel design, like CANFLEX 43-element fuel bundle with 0.9 to 1.2 % enrichment for CANDU PHWRs, usage of enriched Uranium fuel (EU) of 0.85 wt% ^{235}U in Atucha-1 vertical type PHWR in Argentina. In India, Irradiation of NU bundles in two channels to a burnup of around 22 000 MW·D/TeU was already carried out in KAPS-2 during

the years 1999–2003 [3]. The trial irradiation of 50 Mixed Oxide Fuel (MOX) was also done in KAPS-1 [1–2].

In order to improve fuel burnup using advanced fuel, NPCIL is also exploring the feasibility of loading of Slightly Enriched Uranium (SEU) bundles (up to 1.1 wt% ^{235}U) for whole core in 220 MWe PHWRs with maximum achievable discharge burnup of 25 000 MW·D/TeU [4]. Before going for a large scale usage of SEU bundles in Indian PHWRs, it was planned to have a trial irradiation of 51 SEU bundles in Madras Atomic Power Station unit-2 (MAPS-2) equilibrium core. Trail irradiation of SEU bundles is aimed to ascertain the capability of these bundles in withstanding higher burnups of the order of 25 000 MW·D/TeU and ability of graphite coating to withstand power ramps at high burnups.

2. SEU BUNDLES' DESIGN

The SEU bundle dimensions like diameter, length etc is same as that of present 19-element NU fuel bundle. To accommodate extra fission gas release up to the burnup of 25 000 MW·D/TeU, the pellet dish depth was increased slightly. To minimize the axial end flux peaking of SEU bundles, end pellet configuration of the pellet stack in each element of the bundle was modified. The design bundle burnup of SEU bundles is 25 000 MW·D/TeU unlike 15 000 MW·D/TeU for NU bundles. The bundle power envelope for SEU bundle is similar to that of NU bundles up to 2800MW·D/TeU burnup and after that the SEU bundle power envelope has 6 to 7 % more margin than that of NU bundles [5].

3. SEU BUNDLES' IRRADIATION CAMPAIGN

The necessary fuel bundle design analysis, reactor physics estimations and safety margin estimations were carried out and regulatory approval of the proposal for the trial irradiation of 51 SEU bundles in MAPS-2 was obtained. Trail irradiation of SEU bundles is aimed to ascertain the capability of these bundles in withstanding at higher burnup of the order of 25 000 MW·D/TeU and also at higher power ramp due to global power raise, refueling and recycling, and adjuster rod movements.

After obtaining the required regulatory clearance from Safety Committee, loading of SEU bundles was started on 6th June 2009 and by 24th August 2009, 51 SEU bundles have been loaded in 14 channel of MAPS-2 core. Out of 51 SEU bundles, 46 SEU bundles have 0.93 wt% ^{235}U and remaining 5 have 0.8 wt% ^{235}U. For loading of the SEU bundles, channels were selected uniformly through out the core. Initially these bundles were loaded into the low flux location and later on, after achieving a bundle burnup of more than 5000 MW·D/TeU, these bundles were moved to higher flux location for further irradiation to study their performance in higher flux location. Maximum burnup of about 24 770 MW·D/TeU was achieved. The total irradiation plan can be broadly divided into four phase as described below.

Phase 1

51 SEU bundles were initially loaded into 14 low flux location channels. The bundles are loaded by following 8 BSS with a combination of SEU and NU fuel bundles. Out of the 14 channels, 11 channels were refueled by 8 BSS with four SEU bundles in the 5th to 8th string position, one channel was refueled by 8 BSS with three SEU bundles in the 2nd to 4th string position and two channels were refueled by 8-BSS with two SEU bundles in the 2nd and 3rd string position. The delayed neutron (DN) count rate and channel outlet temperature (COT) were monitored for these channels during the loading of SEU bundles. The detail of

channels loaded with SEU bundles is given in the Fig. 1. The variation of DN ratio before and after refueling and increase in COT of each channel is given in Table 1.

From the Table 1, it is observed that the estimated value of the increase in COTs of the SEU loaded channel were in good agreement with observed increase in COTs. Also the DN ratio of the channels before and after refueling with SEU bundles showed that the loaded SEU bundles were healthy.

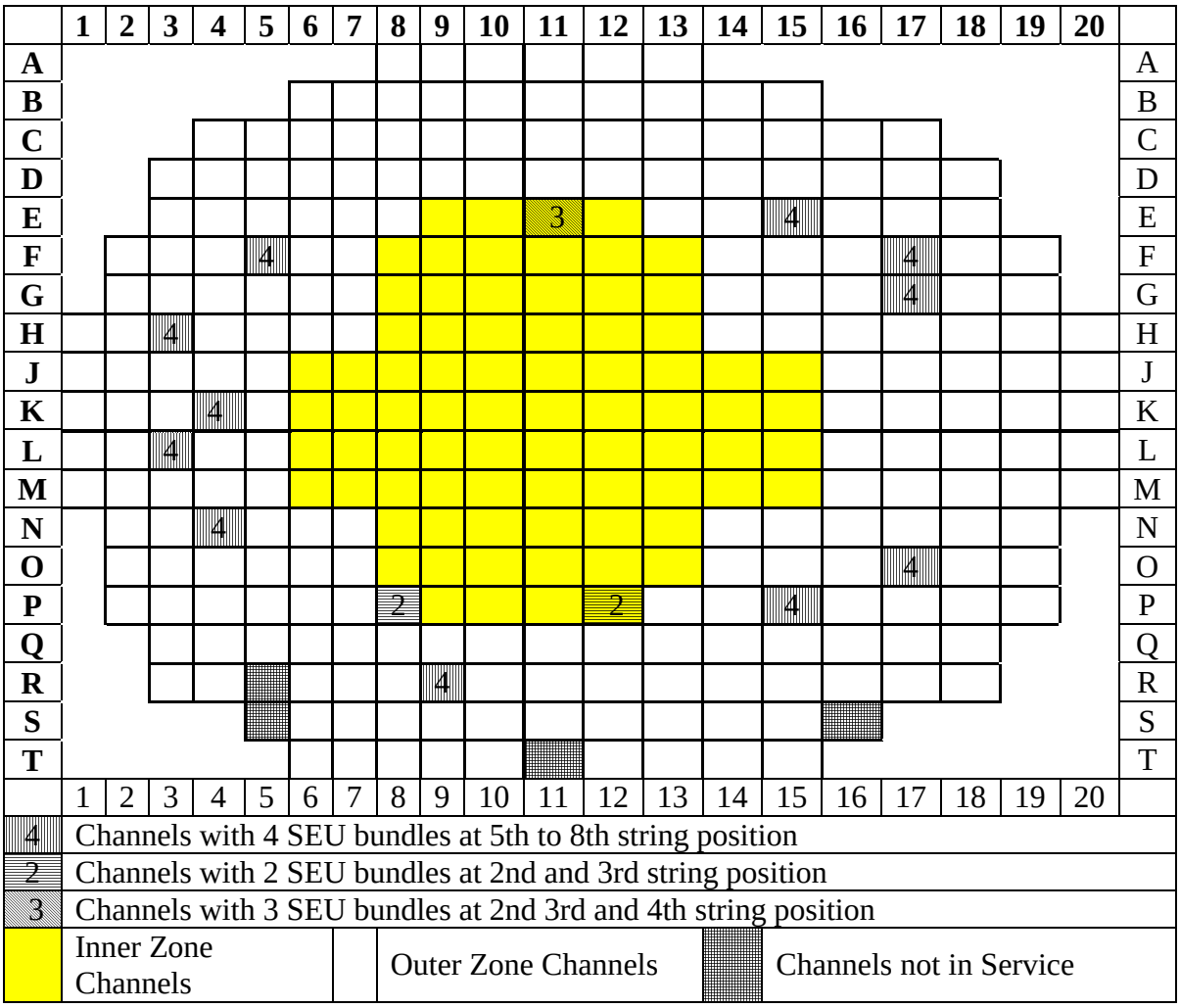

FIG.1. Channels loaded with SEU bundles.

TABLE. 1 DATE OF REFUELING, VARIATION OF DN RATIO BEFORE AND AFTERREFUELING AND INCREASE IN COT OF EACH CHANNEL LOADED WITH SEU BUNDLES

Sl. No.	Date	Channel ID	No. of SEU bundles loaded with string position	DN ratio		Increase in COT (0C)	
				Before refueling	After refueling	Observed	Estimated
1	6-Jun-09	G-17/S	4 (5th to 8th)	1.1	1.1	6.0	6.4
2	8-Jun-09	O-17/N	4 (5th to 8th)	0.9	0.9	5.5	5.0
3	9-Jun-09	E-15/S	4 (5th to 8th)	1.1	1.0	5.3	4.2
4	10-Jun-09	F-17/N	4 (5th to 8th)	1.2	1.1	5.8	5.3
5	15-Jun-09	H-03/N	4 (5th to 8th)	1.0	0.9	6.2	6.4
6	16-Jun-09	L-03/S	4 (5th to 8th)	1.1	1.1	6.6	5.6
7	17-Jun-09	N-04/N	4 (5th to 8th)	1.0	1.0	7.4	6.7
8	20-Jun-09	F-05/N	4 (5th to 8th)	1.1	1.1	4.6	4.7
9	23-Jun-09	R-09/S	4 (5th to 8th)	0.9	0.9	4.7	4.9
10	27-Jun-09	P-15/S	4 (5th to 8th)	1.0	1.0	8.7	9.0
11	29-Jun-09	P-08/N	2 (2nd & 3rd)	0.9	0.9	3.3	3.8
12	18-Jul-09	K-04/S	4 (5th to 8th)	1.0	1.0	8.2	7.8
13	20-Aug-09	E-11/S	3 (2nd to 4th)	1.1	1.0	4.9	5.7
14	24-Aug-09	P-12/N	2 (2nd & 3rd)	1.0	0.9	3.1	2.7

Phase 2

After achieving a minimum burnup of 5000MW·D/TeU, the SEU bundles from lower flux regions were radially recycled to higher flux regions for further irradiation to study their performance in the higher flux location. Similarly the channels having two and three SEU bundles were refueled by 4 BSS to move the SEU bundles to the high flux location of the

channel. The location of the channels having SEU bundles after recycling is given in the Fig. 2. The burnup at the time of recycling and bundle power before and after recycling for each string positions of channels loaded with SEU bundles is given in Table 2. The maximum burnup of SEU bundle at the time of recycling to inner channel was 9190MW·D/TeU from the channel H-03 to G-09. The Power ramp capability of the bundles to withstand this ramp is explained in section 3.2.

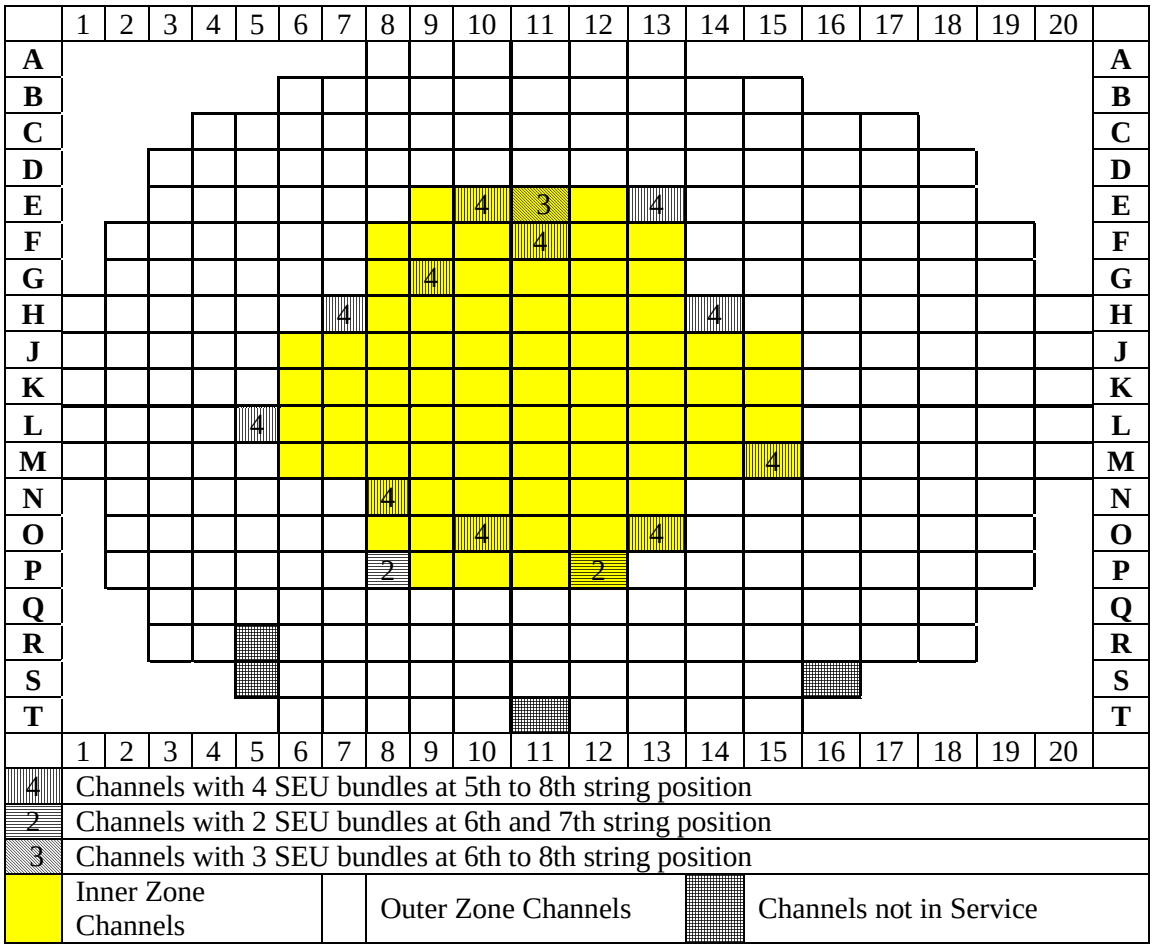

FIG.2. Channels Loaded with SEU bundles.

Phase 3

Nearly after 2 years of loading of 51 SEU bundle into the core, the average burnup for the SEU bundle has reached around 15 000 MW·D/TeU. At this time it was decided to retain only 20 SEU bundles in the existing inner zone location for further irradiation up to 25 000 MW·D/TeU. Among the rest of the SEU bundles, some bundles were planned to be recycled and the remaining SEU bundles were to be discharged.

As per the above plan, SEU bundles from the channels M-15, E-10, P-12, H-07, P-08 and E-11 were discharged to Spent Fuel Store Bay (SFSB) and SEU bundles from the channels H-14, L-05 and E-13 were recycled to the peripheral channels B-15, A-10 and A-12 respectively. The average burnup for the discharged bundles was 16400MW·D/TeU and same

for the recycled bundle was 154 00 MW·D/TeU. The detail of channels having SEU bundles at the end of this phase is given in the Fig. 3.

TABLE 2. DATE OF RECYCLING, BURNUP AT THE TIME OF RECYCLING, BUNDLE POWER BEFORE AND AFTER RECYCLING FOR EACH STRING POSITIONS OF CHANNELS LOADED WITH SEU BUNDLES.

Date of recycling	Burnup (MW·D/TeU)	Bundle Power (kW)		Initial channel	Final channel
		Initial	Final		
22-Feb-10	5303	259	356	K-04	F-11
	5847	280	328	K-04	F-11
	5767	274	317	K-04	F-11
	5135	245	355	K-04	F-11
17-Apr-10	6123	227	349	G-17	H-07
	6868	256	337	G-17	H-07
	6918	259	325	G-17	H-07
	6270	234	343	G-17	H-07
19-May-10	6177	213	362	E-15	M-15
	6572	228	316	E-15	M-15
	6576	227	324	E-15	M-15
	6289	211	363	E-15	M-15
28-May-10	5653	195	322	R-09	E-10
	6087	209	291	R-09	E-10
	6031	203	290	R-09	E-10
	5503	181	323	R-09	E-10
31-May-10	1428	69	363	P-12	P-12
	3449	160	348	P-12	P-12
1-Jun-10	5230	223	282	E-11	E-11
	3574	155	327	E-11	E-11
	1457	65	341	E-11	E-11
3-Jun-10	1825	70	334	P-08	P-08
	4318	156	307	P-08	P-08
2-Jul-10	7145	204	345	L-03	N-08
	7875	223	305	L-03	N-08
	7715	219	320	L-03	N-08
	6831	196	353	L-03	N-08
8-Jul-10	7654	220	322	P-15	O-13
	8084	217	296	P-15	O-13
	8122	217	302	P-15	O-13

Date of recycling	Burnup (MW·D/TeU)	Bundle Power (kW)		Initial channel	Final channel
		Initial	Final		
	7804	218	323	P-15	O-13
13-Jul-10	7504	226	325	N-04	L-05
	8155	245	283	N-04	L-05
	8017	244	293	N-04	L-05
	7190	220	330	N-04	L-05
21-Jul-10	7306	215	301	O-17	E-13
	8172	234	272	O-17	E-13
	8133	234	264	O-17	E-13
	7324	214	297	O-17	E-13
24-Jul-10	6937	195	368	F-17	H-14
	7746	216	339	F-17	H-14
	7725	217	325	F-17	H-14
	6966	198	362	F-17	H-14
15-Sep-10	8195	235	367	F-05	O-10
	8834	256	327	F-05	O-10
	8773	256	335	F-05	O-10
	8087	234	372	F-05	O-10
13-Oct-10	8372	204	370	H-03	G-09
	9190	219	333	H-03	G-09
	8953	215	354	H-03	G-09
	7910	192	381	H-03	G-09

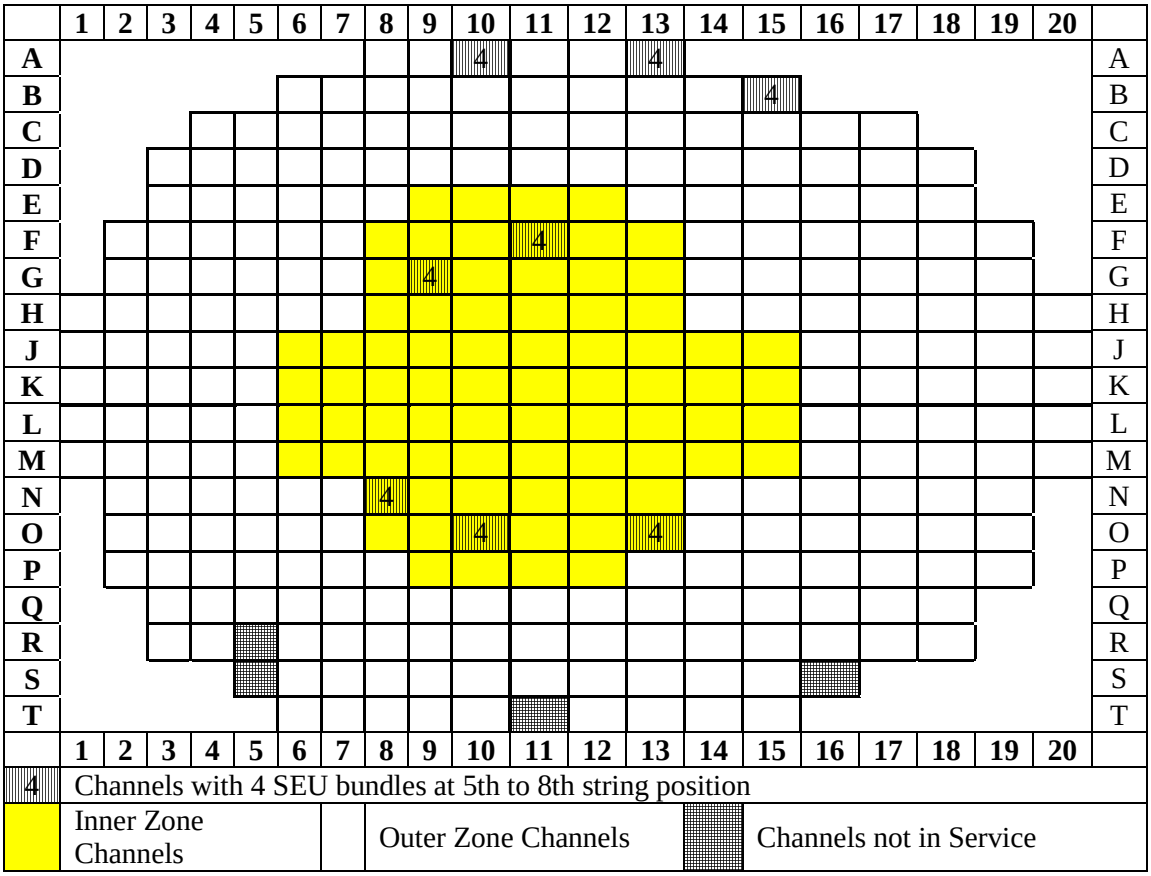

FIG. 3. Channels Loaded with SEU bundles.

Phase 4

After achieving a burnup of around 20 000 MW·D/TeU for the 20 SEU bundles kept in the inner zone channels, it was planned to discharge these bundles at different ranges of exit burnup. Accordingly, 20 SEU bundles with different burnup ranges from 20 000 MW·D/TeU to 24 770 MW·D/TeU were discharged to SFSB. Similarly out of 12 SEU bundles kept in the outer zone channels, so far 8 bundles were discharged to SFSB. Currently only 4 SEU bundles are in the channel A-10. The DN count rate during the refueling of channel for the discharge of SEU bundles was monitored and also wet sniffing for some of the discharged fuel bundles were carried out. The results are given in Table 3. The wet sniffing results were found to be normal. No SEU bundle has failed in core.

The burnup of SEU bundles which were discharged as well as present currently in the core is given in the Table 4. The maximum and average burnup of the SEU bundles discharged to SFSB is around 24 770 MW·D/TeU and 19 466 MW·D/TeU respectively and the same for the SEU bundles present in the core is around 20 370MW·D/TeU and 20 038 MW·D/TeU respectively.

3.1. Bundle power of SEU bundles

Bundle Powers (BP) of all SEU bundles were within the envelope. The bundle power envelop for the some SEU bundles is shown in Fig. 4.

TABLE 3. DATE OF DISCHARGE, VARIATION OF DN COUNT AND RESULT OF WET SNIFFING FOR EACH OF CHANNELS LOADED WITH SEU BUNDLES

SEU bundles loaded channel	Number of SEU bundles	Average burnup of the SEU bundles (MW·D/TeU)	Date of discharge	Variation of DN count during refueling (CPS)			Wet sniffing result
				Initial	Final	% Variation	
M-15/N	4 (5^{th} to 8^{th})	16667	5-Aug-11	90	74	17.8	Normal
E-10/N	4 (5^{th} to 8^{th})	15665	9-Oct-11	98	80	18.4	Normal
P-12/N	2 (6^{th} & 7^{th})	14321	5-Dec-11	81	70	13.6	Not Done
H-07/N	4 (5^{th} to 8^{th})	19856	9-Dec-11	77	67	13.0	Normal
P-08/N	2 (6^{th} & 7^{th})	15025	7-Dec-11	88	80	9.1	Not Done
E-11/S	3 (6^{th} to 8^{th})	15728	9-Mar-12	88	88	0.0	Not Done
G-09/S	4 (5^{th} to 8^{th})	21075	7-Jun-12	73	62	15.1	Not Done
O-10/S	4 (5^{th} to 8^{th})	22052	3-Jul-12	81	65	19.8	Normal
F-11/N	4 (5^{th} to 8^{th})	23137	23-Jul-12	66	56	15.2	Normal
A-12/N	4 (5^{th} to 8^{th})	17370	6-Aug-12	74	68	8.1	Not Done
B-15/N	4 (5^{th} to 8^{th})	17694	7-Aug-12	79	78	1.3	Not Done
N-08/N	4 (5^{th} to 8^{th})	24474	11-Sep-12	108	97	10.2	Normal
O-13/N	4 (5^{th} to 8^{th})	24272	5-Oct-12	89	79	11.2	Normal

TABLE 4. BURNUP (MW·D/TeU) FOR SEU BUNDLES

SEU Loaded Channel	String Position in the Channel				Maximum Burnup	Average Burnup	Remarks
	5	6	7	8			
A-10/N	19820	20220	20370	19740	20370	20038	SEU Bundles present inside the core
H-07/N	19747	20028	19928	19721	20028	19856	
M-15/N	16427	16976	16886	16377	16976	16667	
E-10/N	15429	15739	15912	15580	15912	15665	
P-08/N	-	14179	15871	-	15871	15025	
P-12/N	-	13572	15070	-	15070	14321	
E-11/S	-	14563	16104	16517	16517	15728	SEU bundles discharged to SFSB. Burnup of the bundle given here is just before discharge to SFSB
G-09/S	21226	21205	20855	21013	21226	21075	
O-10/S	21947	22247	22161	21854	22247	22052	
F-11/N	22700	23371	23550	22927	23550	23137	
A-12/N	17168	17671	17522	17117	17671	17370	
B-15/N	17624	17728	17717	17708	17728	17694	
N-08/N	24225	24571	24770	24330	24770	24474	
O-13/N	23976	24637	24519	23955	24637	24272	

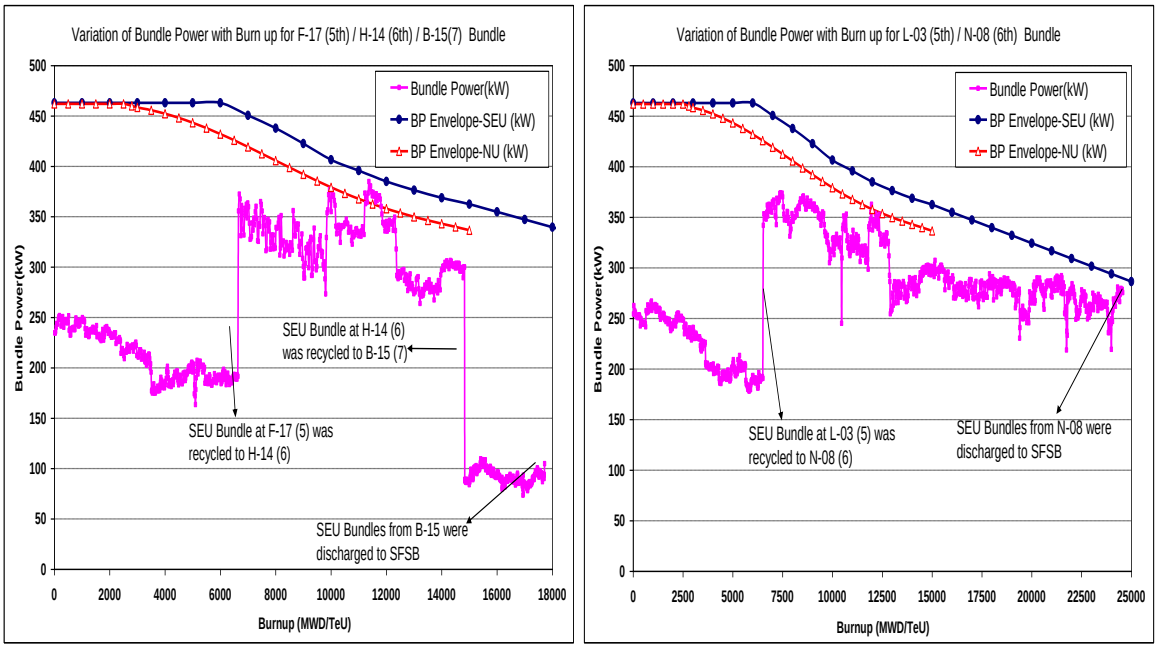

FIG. 4. Variation of BP with burnup.

3.2. Power ramp experienced by SEU bundles

The power ramp failure probability of the fuel bundles in core due to different power increases including effect due to radial recycling was monitored. For this purpose, the validity of power ramp equation is assumed beyond the regular burnups, upto 25000 MW·D/TeU burnups. The maximum of the calculated power ramp failure probability was observed to be 9.49E-03 for the 7th bundle of H-14. For all other bundles, the calculated maximum value of failure probabilities are less than 9.49E-03. During this period, the maximum value of fuel failure probability for the NU bundles was found to be 3.11E-04 for the 6th bundle of L-13 having burnup of 9728 MW·D/TeU. As can be seen the estimated fuel failure probability for SEU bundles is 30 times more than that of NU bundle and these SEU bundles with their graphite coating performed well at these higher power ramp vulnerabilities.

3.3. PHT system iodine activity

The variation of ^{131}I activity in the PHT system from just before the commencement of SEU loading to February 2013 is given in the Fig. 5. Even though 5 NU fuel bundles have been failed during this period, not a single SEU bundle has failed. The healthiness of the SEU bundles was very good.

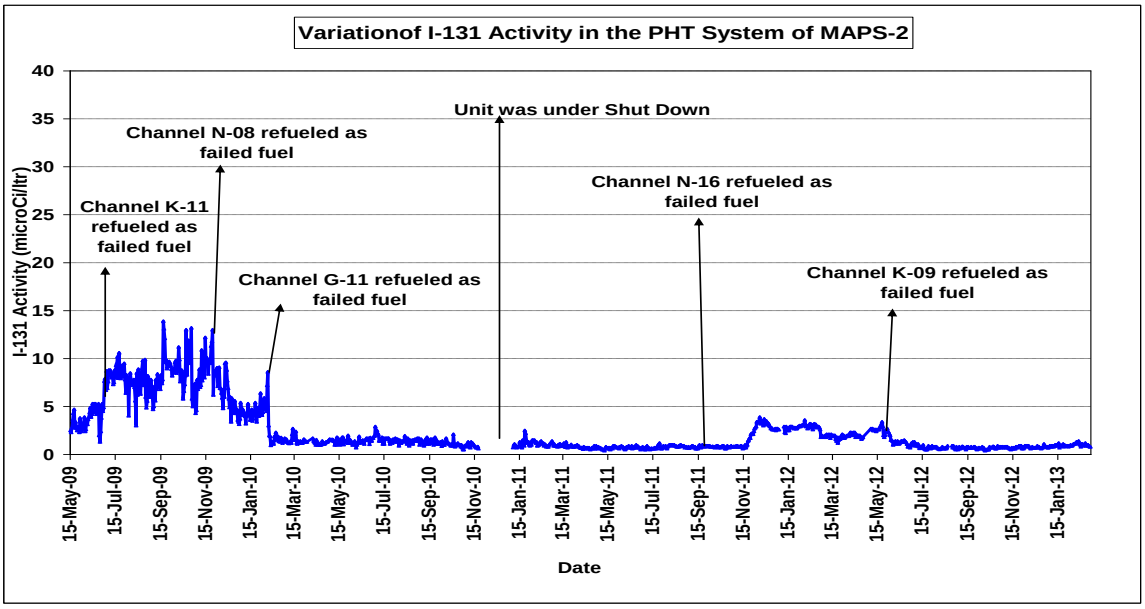

FIG. 5.Variation of I-131 Activity in the PHT system.

4. ANALYSIS FOR CONVERSION TO FULL SEU CORE

Presently all 220 MWe Indian PHWRs are operating in equilibrium core condition with NU fuel. The good performance of the 51 SEU bundles motivated us to carry out an analysis for the conversion of the NU equilibrium core to SEU equilibrium core. Since the channel coolant flow in the core is designed for the existing NU equilibrium core power distribution, it is required to keep the power distribution of SEU core close to this to avoid restriction on reactor power by Maximum Channel Outlet Temperature (MCOT) or Maximum Bundle Power (MBP). Hence the variations of core parameters like MBP and MCOT during the transient phase of the conversion of NU core to SEU core as well as in the equilibrium SEU core condition are studied in this analysis. The salient feature of the analysis and results are discussed below.

Analysis is carried out with 19 element SEU fuel bundles having 0.93wt% of U-235. The normal 8 BSS refueling adopted in the existing NU core could not be followed as the bundle power of the SEU bundle is higher than NU bundle. After the preliminary analysis carried out with 6, 4 and 2 BSS, it was decided to adopt 4 BSS for the outermost 67 channels and 2 BSS in the rest of the channels for the first time refueling with SEU bundle. This sequence is followed to reduce the overall rate of refueling and also to avoid the restriction on operating power by MBP in the inner channel. In the subsequent refueling, 2 BSS is followed in all channels including the 67 outermost channels to avoid MCOT of these channels going beyond 299^0C. From the second time refueling onwards, the core is divided into two burnup zone: 86 channels form inner zone and the rest of the channels in the core form outer zone. The refueling ratio (i.e. ratio of the number of inner channels refueled to the number of outer channels refueled) is also suitably adjusted while moving the core condition from transient phase SEU-NU core to equilibrium SEU core to minimize the constraints on reactor power due to MCOT and MBP.

The time gap between the successive refueling (del-FPD) of a channel is optimized such that it minimizes the possibility of exceeding MBP limit by avoiding a very low burnt fuel

bundle moving to higher flux location in a channel and at the same time it does not allow the refueling rate to be too high. Initially this gap is kept at 50FPDs and 40FPDs for the inner and outer zone channel respectively. During the transient period, the Del-FPD gap for inner zone channel is slowly increased in smaller step for every successive refueling to a value of 150FPDs in an equilibrium core. Similarly for the outer zone channel, it is increased from 40FPDs to the final value of 90FPDs.

It takes around 1100 FPDs of operation to convert the existing NU equilibrium core to SEU equilibrium core. Number of SEU bundles present in the core at different cumulative FPDs is given in the Table 5 and the result of the analysis both in the transient phase of core and at equilibrium core in the interval of 100 FPDs is summarized in the Table 6. Similarly the variation of in core and discharge burnup is given in the Fig. 6.

TABLE 5. TOTAL NUMBER OF SEU BUNDLE PRESENT IN THE CORE

Cumulative FPDs	Number of SEU bundles in the core	Cumulative FPDs	Number of SEU bundles in the core
1600	0	2306	3242
1804	1312	2406	3416
1904	1730	2505	3542
2004	2158	2604	3596
2105	2582	2706	3672
2205	2984		

TABLE 6. FUEL CONSUMPTION, AVERAGE DISCHARGE BURNUP, REFUELING RATE, RATIO AND MINIMUM ALLOWED POWER IN THE INTERVAL OF 100 FPD

FPD interval	Fuel consumption		Avg. discharge BU (MW·D/TeU)			Refueling rate (channel per FPD)	Refueling ratio		Minimum allowed power (% FP)	
	Bundle per FPD	kg/MU	Inner zone	Outer zone	Full core		Inner zone	Outer zone	by MBP	by MCOT
100	8.48	24.41	9458	4598	5561	3.72	1.00	2.29	98.1	99.0
100	4.54	13.07	8786	4847	5515	2.27	1.00	3.20	98.2	98.8
100	4.22	12.15	9622	6577	7157	2.11	1.00	2.20	100	98.2
100	4.28	12.32	12241	7968	8594	2.14	1.00	2.69	100	99.2
100	4.16	11.98	14446	9257	10120	2.08	1.00	2.78	100	97.0
100	4.08	11.75	14688	10106	10938	2.04	1.00	2.46	100	99.4
100	3.94	11.34	15120	11597	12491	1.97	1.00	2.94	100	99.4
100	4.02	11.57	15875	12457	13324	2.01	1.00	2.94	100	100
100	3.98	11.46	17121	13049	14113	1.99	1.00	2.83	100	100
100	3.98	11.46	18183	13397	14599	1.99	1.00	2.98	100	100
100	3.98	11.46	18618	13635	14937	1.99	1.00	2.97	100	100

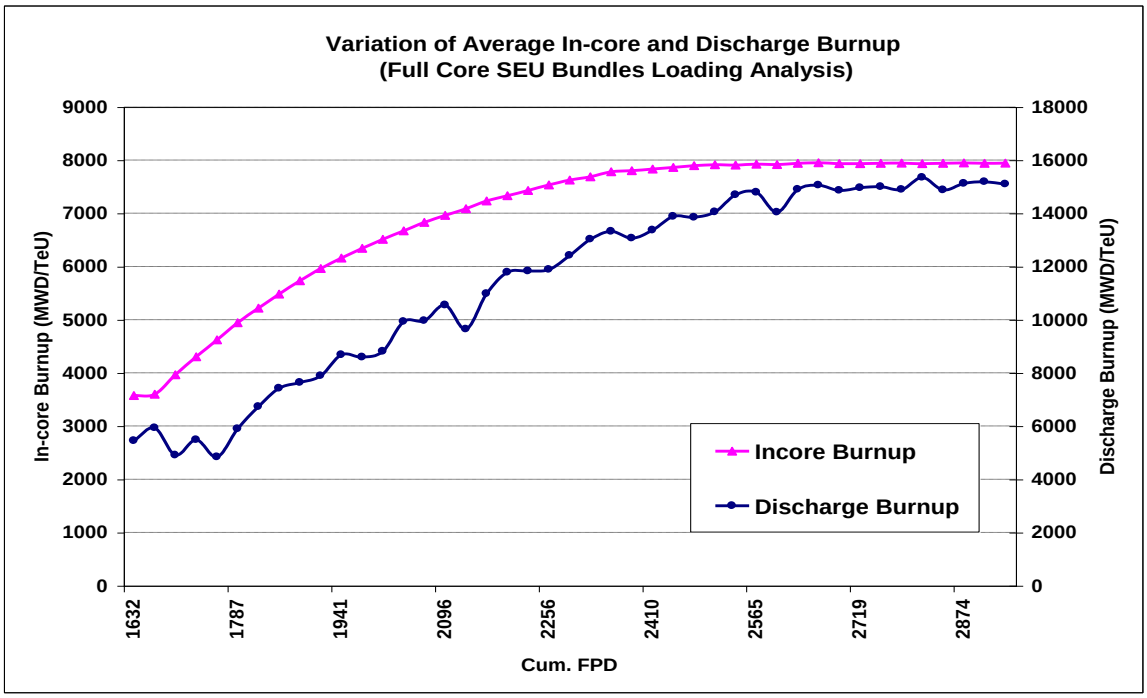

FIG. 6 Variation average in core and discharge burnup.

5. CONCLUSION

5.1. Trial irradiation of SEU bundle in MAPS-2 core

51 SEU bundle were loaded initially at the low flux location in 14 channels. The DN count and COT was monitored during loading of all SEU bundles. After achieving a minimum burnup of 5000 MW·D/TeU for the SEU bundles, recycling of SEU bundles from low flux to high flux location were started and up to a maximum SEU bundle burnup of 9190 MW·D/TeU were recycled to ascertain the fuel integrity after giving power ramp. After achieving burnup of around 15 000 MW·D/TeU, partial recycling and discharge of SEU bundles were carried out. Ultimately only 20 SEU bundles were kept in the core for achieving burnup of more than 20 000 MW·D/TeU. The failure probability due to power ramp was close to 1% for the 7th bundle of H-14 and the same for 15 bundles is higher than 0.01%. However wet sniffing results for these bundles after discharge to SFSB were found to be normal. The observed COTs for the SEU loaded channel are also in good agreement with the predicated COT.

Till now, 47 SEU bundles with different range of burnup were discharged from the core. The maximum and average burnup of the SEU bundles discharged to SFSB are around 24 770 MW·D/TeU and 19 466 MW·D/TeU respectively. Presently only 4 SEU bundles at 5th to 8th string position of the channel A-10 are residing in the core and the maximum and average burnup of these SEU bundles are around 20 370 MW·D/TeU and 20 038 MW·D/TeU respectively. The DN count and DN ratio of the SEU loaded channel are slightly higher than that of NU loaded channel connected to a particular DN counter. This is due to high burnup of SEU bundles of the SEU loaded channel in comparison with low burnup of NU bundles of the non–SEU loaded channels.

The trial irradiation of 51 bundles is successfully done. No SEU bundle has failed so far and the performance of the SEU bundles is quite satisfactory.

5.2. Analysis for converting all NU equilibrium core to all SEU equilibrium core

Analysis was done for converting NU equilibrium core to SEU equilibrium core. As the coolant flow are fixed for the current NU core power distribution, the initial refueling is done by 4BSS for 67 outermost channels and by 2 BSS in the rest of the channels to avoid high refueling rate and restriction on reactor power due to MBP for the inner channels. For the successive refueling, 2 BSS was followed for all channels. The refueling Del-FPD gap for successive refueling was slowly increased from 50 to 150 and 40 to 90 for inner zone and outer zone channels respectively. Similarly the refueling ratio was suitably adjusted while moving from transient phase of SEU-NU core to equilibrium SEU core to avoid the restriction on operating power due to MCOT and MBP.

The restriction on reactor power for few occasions during transient phase of core, mainly due to MCOT, was observed in the analysis. It takes around 1100FPDs of operation to convert the existing NU equilibrium core to SEU equilibrium core. The average in core and discharge burnup for the SEU equilibrium core is expected to be around 8000 MW·D/TeU and 15 000 MW·D/TeU respectively compared to that of 3700 MW·D/TeU and 6300 MW·D/TeU for the NU core. No restriction on reactor power due MCOT or MPB is expected in the SEU equilibrium core.

ACKNOWLEDGEMENTS

The authors would like to acknowledge their sincere thank to Shri P.N. Prasad, ACE (Fuel Cycle), Nuclear Power Corporation of India Limited, Mumbai, for his constant support and valuable suggestion through out the trial irradiation campaign of SEU bundles.

REFERENCES

[1] PRADHAN, A. S., SHERLY, R., PARIKH, M. V., KUMAR, A. N., “MOX–Equilibrium Core Design and Trial Irradiation in KAPS # 1”, OPENUPP-200, Mumbai, India (2000).

[2] PRASAD, P.N. et. al., “Design, Development and Operation Experience of Thorium and MOX-7 Bundles in PHWRs”, Proc. 9th International Conference on CANDU Fuel, Canadian Nuclear Society, 18-21 September 2005, RAMADA On The Bay, Belleville, ON, Canada.

[3] BHARDWAJ, S.A., “Design, Development and Performance of Advanced Fuels in PHWRs”, Proc. CQCNF-2012, Hyderabad, India, 27-29 February 2012.

[4] MISHRA, S., RAY, S., PRADHAN, A.S., KUMAR, A.N., “Design Note on the use of Enriched Uranium Fuel in 220-MWe Reactor”, Design Note Number-RSA/DN/01100/03, NPCIL (2008).

[5] TRIPATHI, R.M., PRASAD, P.N., CHAUHAN, A., “Design & Performance of Slightly Enriched Uranium Fuel Bundles in Indian PHWRs”, Technical Meeting on Fuel Integrity during Normal Operating and Accident Conditions in PHWR", Bucharest, Romania, 24–27 September 2011.

UTILIZATION OF RECYCLED URANIUM IN INDIAN PHWRS

S. MISHRA, S. RAY
A. S. PRADHAN, H. P. RAMMOHAN
Nuclear Power Corporation of India Limited,
Mumbai

M. V. PARIKH
Kakarapar Atomic Power Station, NPCIL,
Gujarat

India

Abstract

Presently India is having 7 small sized 220 MWe pressurized heavy water reactors (PHWRs) under safeguards and 2 more PHWR units will be brought under safeguards in near future. These reactors are operating using internationally available Natural Uranium (NU). Each reactor is discharging about 45 tons of irradiated fuel to spent fuel bay every year. The piling inventory of this safeguarded discharged fuel material is a matter of great concern because of limited storage capacity of spent fuel bay. Reprocessing these safeguarded material and recycle back into the existing safeguarded reactors may be considered as one of the possible solution to this problem. This recycling will not only help in conserving the Uranium reserve but also reduce the volume of the radioactive waste substantially. The present study is aimed to check various options to reuse the reprocessed safeguarded fuel back into safeguarded PHWRs in such a manner that it does not require any engineering changes in the existing hardware. This paper presents the analysis carried out for various possible fuel designs by mixing reprocessed PHWR uranium with reprocessed light water reactor (LWR) uranium in different proportions. Two kinds of fuel bundle designs are proposed which have almost similar characteristics to that of NU bundles and hence can readily be used in the existing PHWRs.

1. INTRODUCTION

The PHWRs are operating with flattened flux distribution obtained by differential burnup zone scheme with the average discharge burnup of about 7000 MW·D/TeU. At 7000 MW·D/TeU discharged burnup the content of uranium and plutonium is about 99.3%. From the burnt fuel, Uranium and Plutonium can be extracted by chemical extraction processes and if they can be further used as fuel material then the nuclear waste (consists of fission products and other actinides) is reduces to 0.7% only. The isotopic content in 7000 MW·D/TeU discharged fuel bundle are given below in Table 1.

TABLE 1. ISOTOPIC CONTENT IN 7000 MW·D/TeU DISCHARGED BURNUP

	content gm/kg		% content in Uranium			% content in Plutonium			
Burnup	net U	net Pu	U235	U236	U238	Pu239	Pu240	Pu241	Pu242
7000	989.1	3.7	0.248	0.071	99.681	68.841	24.205	5.546	1.322

The average discharge burnup of light water reactor (LWR) is about 30000 MW·D/TeU and the isotopic content in 30000 MW·D/TeU discharged fuel bundle are given below in Table 2.

TABLE 2. ISOTOPIC CONTENT IN 30000 MW·D/TeU DISCHARGED BURNUP

	content gm/kg		% content in Uranium			% content in Plutonium			
Burnup	net U	net Pu	U235	U236	U238	Pu239	Pu240	Pu241	Pu242
30000	963.0	6.0	0.900	0.45	98.65	61.0	29.1	9.1	3.8

Various fuel cycle options to reuse the reprocessed safeguarded fuel back into safeguarded PHWRs are studied and the suitable options are proposed which does not require any engineering changes in the existing hardware. The aim of the present study is to propose fuel bundle design using reprocessed uranium from PHWRs (denoted as RU) and from LWRs (denoted as SEU) which should essentially have all the characteristics closer to NU bundles.

2. ANALYSIS

The following options are studied using the transport theory code CLUB [1]:

(1) The RU from PHWR contains 0.25% U^{235} and 0.27% fissile Plutonium (^{239}Pu + ^{241}Pu). The RU (having both UO_2 and PuO_2) can be mixed with natural uranium (0.711% ^{235}U) to increase the ^{235}U content and used as fuel material. The variation in effective multiplication factor with burnup is shown in Figure 1. The required proportion of natural uranium is very high which makes this design unattractive;

(2) The UO_2 and PuO_2 from RU of PHWRs are separated out. The extracted PuO_2 can be mixed with ThO_2 in the ratio of 0.02:0.98 and be used as fuel material. The variation in effective multiplication factor with burnup is shown in Fig. 2. The very high excess reactivity of fresh bundle may invite many other issues which make the design impractical;

(3) The SEU from LWR contains about 0.9% ^{235}U and 0.42% fissile Plutonium (^{239}Pu + ^{241}Pu). The SEU of LWR can be mixed with RU of PHWR in following ways:

- The SEU (having extracted UO_2 only) of LWR mixed with RU (having extracted UO_2 only) of PHWR can be used as fuel material. The variation in effective multiplication factor with burnup for mixture in different proportion is shown in Fig. 3a. The bundle having SEU and RU in the ratio 0.72/0.28 can be considered as a good alternative. However, requirement of higher proportion of SEU may provide practical limitation on use of this design;
- The SEU (having extracted UO_2 only) of LWR mixed with RU (having both extracted UO_2 and PuO_2) of PHWR can be used as fuel material. The variation in effective multiplication factor with burnup for mixture in different proportion is shown in Fig. 3b. The mixture in the ratio of 0.5/0.5 appears to be promising fuel material;
- The SEU (having both extracted UO_2 and PuO_2) of LWR mixed with RU (having both extracted UO_2 and PuO_2) of PHWR can be used as fuel material. The variation in effective multiplication factor with burnup for mixture in different proportion is shown in Fig. 3c. The mixture of SEU and RU in the ratio of 0.2/0.8 may be considered, however, initial very high reactivity will create operational difficulties on refueling;
- The SEU (having both extracted UO_2 and PuO_2) of LWR mixed with RU (having extracted UO_2 only) of PHWR can be used as fuel material. The variation in effective multiplication factor with burnup for mixture in different proportion is

shown in Fig. 3d. The mixture of SEU and RU in the ratio of 0.42/0.58 may be considered, however here also initial high reactivity may create operational difficulties on refueling;

(4) The UO_2 and PuO_2 from RU of PHWR are separated out. The ratio of PuO_2 and UO_2 in RU is 0.00375/0.99625. The fissile content can be increased by remixing the extracted PuO_2 with extracted UO_2 in the ratio of 0.006/0.994 and use as fuel material. The variation in effective multiplication factor with burnup is shown in Fig. 4. The multiplication factor at low bunrup is very high and it reduces drastically with burnup, which lowers the attractiveness of this type of bundle design;

(5) There are nineteen pins in 220 MWe fuel bundles arranged in three rings. The inner ring has single pin, intermediate ring has 6 pins and outer ring has 12 pins. A MOX mixture with separated (extracted) PuO_2 & UO_2 from RU of PHWR and remixed in the ratio of 0.0055/0.9945 or 0.006/0.994 can be used in inner pins. The variation in effective multiplication factor with burnup is shown in Fig. 5. The study shows that a bundle having MOX (ratio 0.0055 / 0.9945) in inner seven pins and NU in outer twelve pins are most suited as a fuel in PHWR;

(6) In order to reduce the reactivity gain due coolant void, ThO_2 can be used in innermost pin, MOX mixture (extracted PuO_2 & UO_2 ratio 0.009/0.991) from RU of PHWR in six intermediate pins and NU in twelve outer pins. Though the reactivity gain due to void in coolant reduces, the higher intermediate pin power ratio makes bundle design impractical.

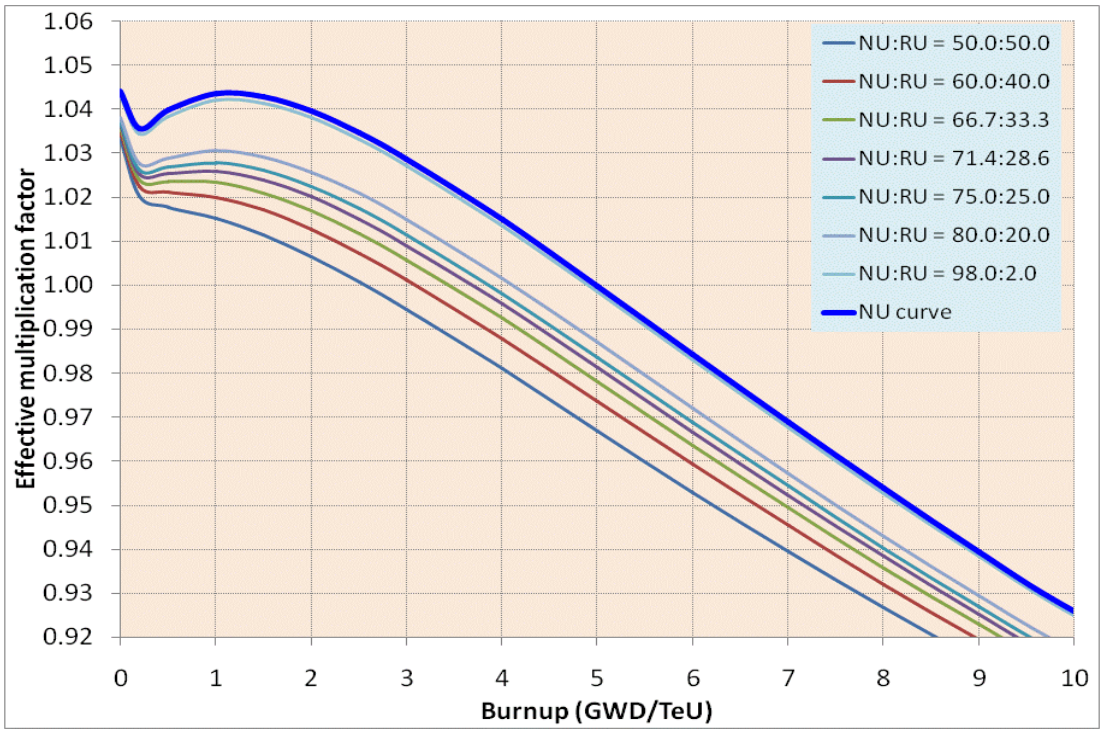

FIG. 1. PHWR RU mixed with natural uranium.

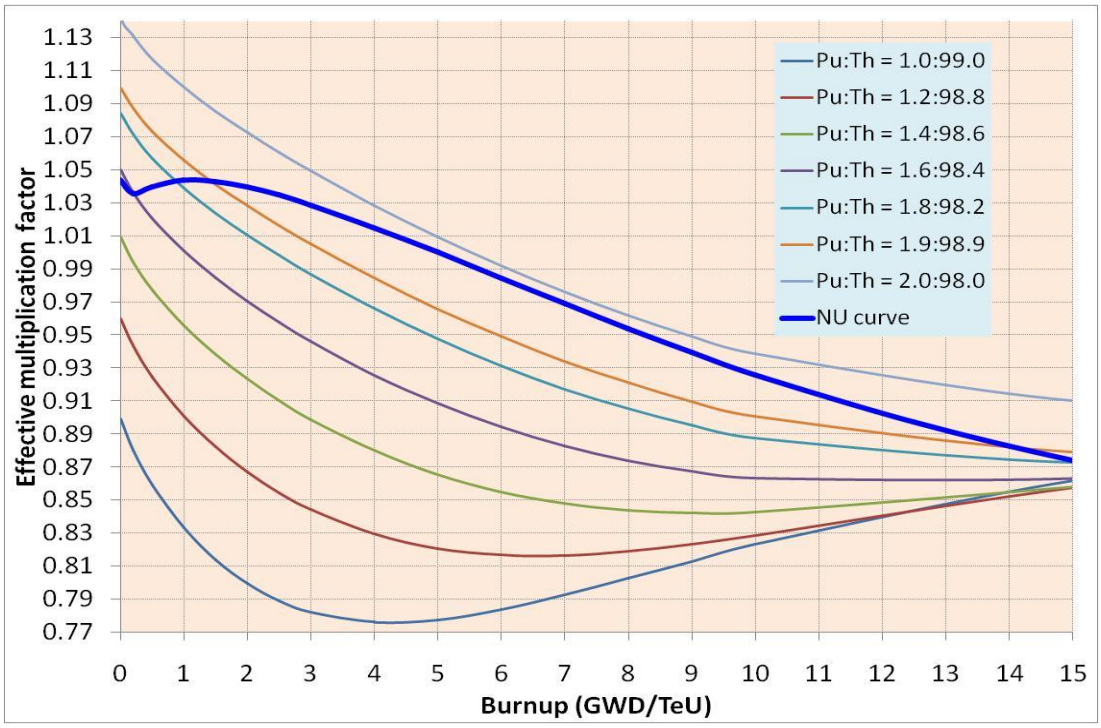

FIG. 2. Extracted PuO_2 from RU of PHWR mixed with ThO_2.

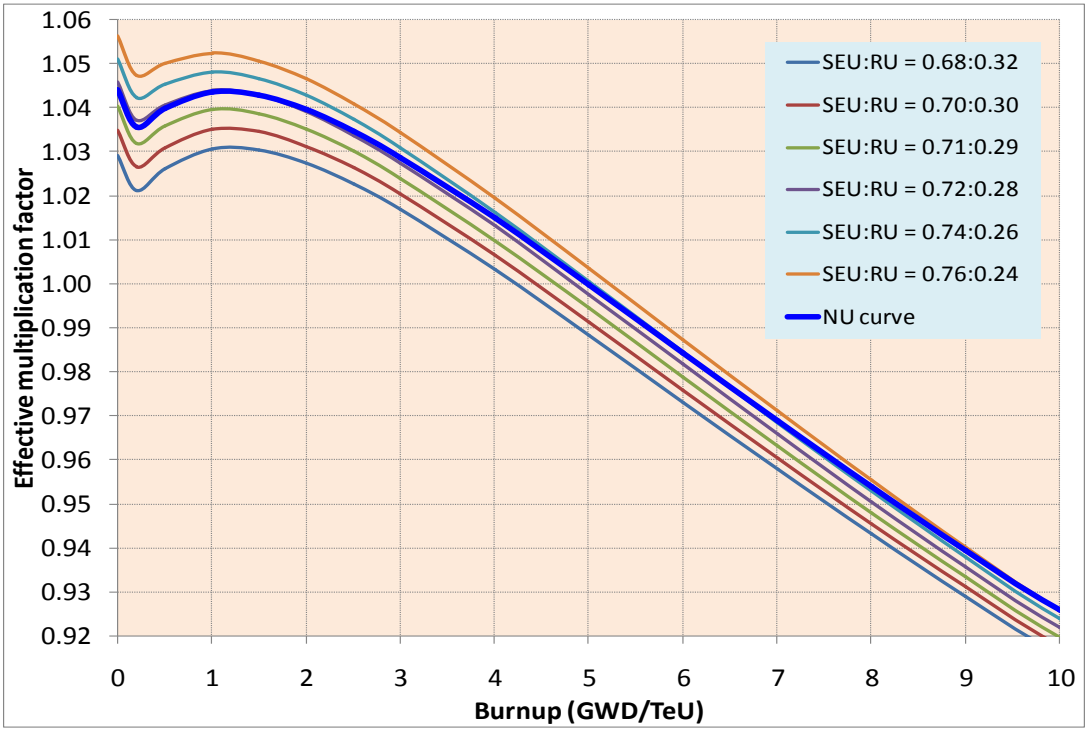

FIG. 3a. RU (only UO_2) of PHWR mixed with SEU (only UO_2) of LWR.

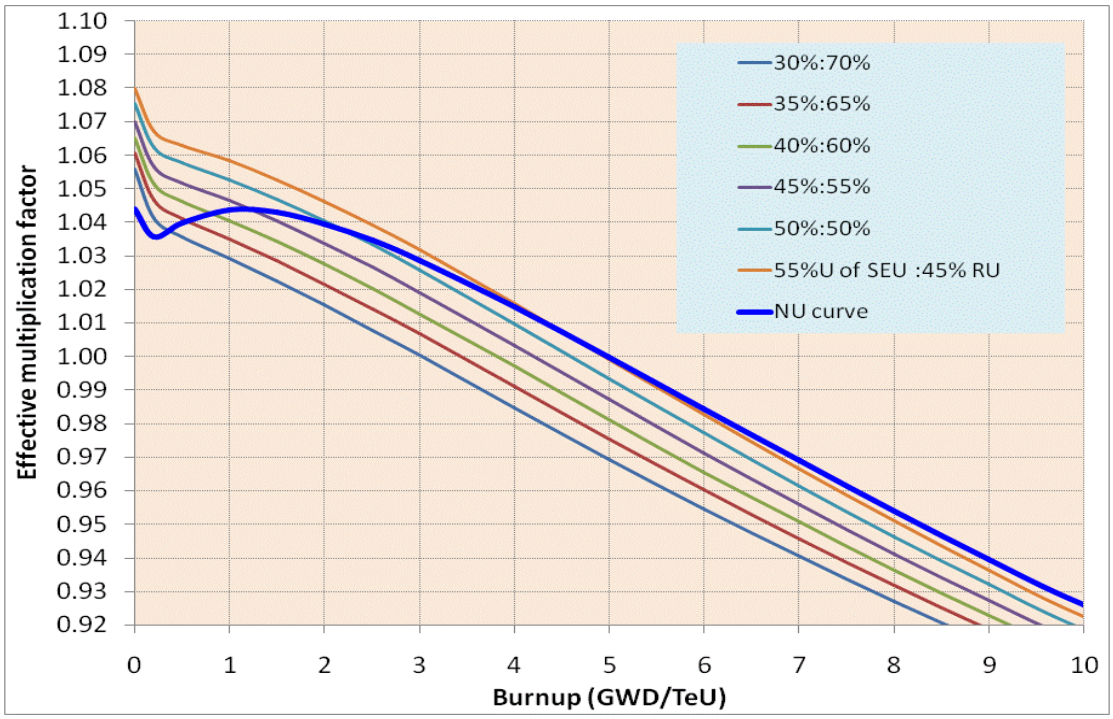

FIG. 3b. RU (having both UO_2 and PuO_2) of PHWR mixed with SEU (only UO_2) of LWR.

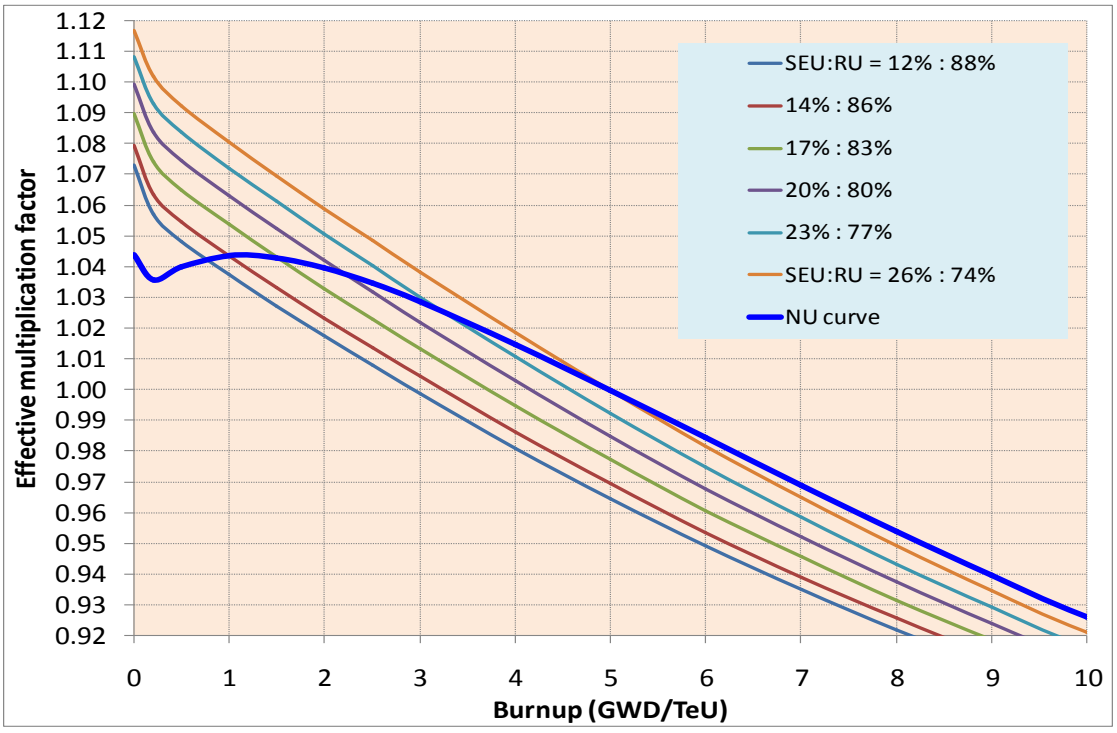

FIG. 3c. RU (having UO_2 & PuO_2) of PHWR mixed with SEU (having UO_2 & PuO_2) of LWR.

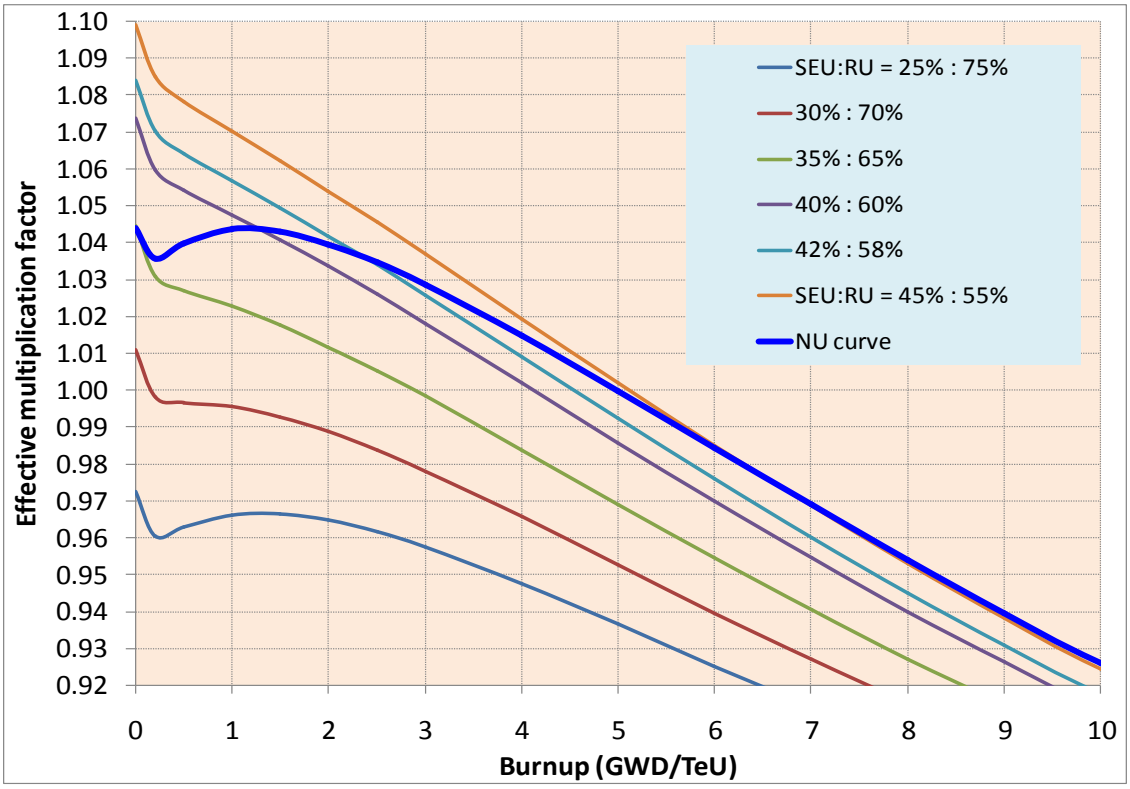

FIG. 3d. RU (only UO_2) of PHWR mixed with SEU (having both UO_2 and PuO_2) of LWR.

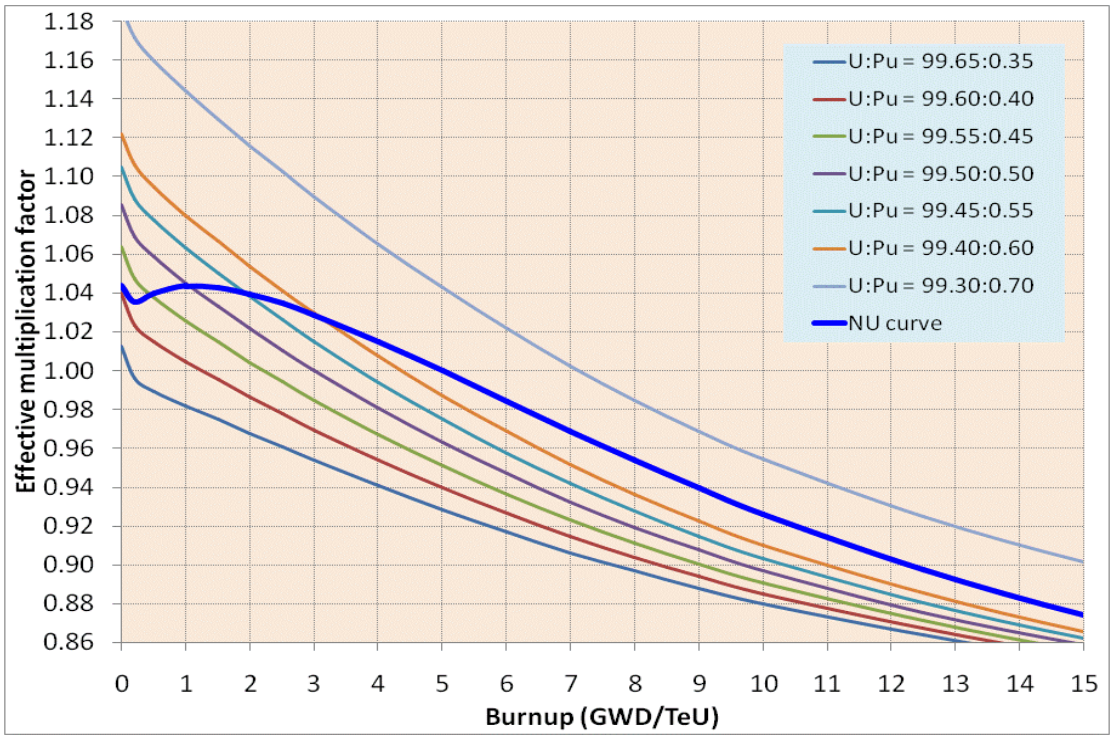

FIG. 4. Extracted PuO_2 & UO_2 from RU of PHWR separated & remixed.

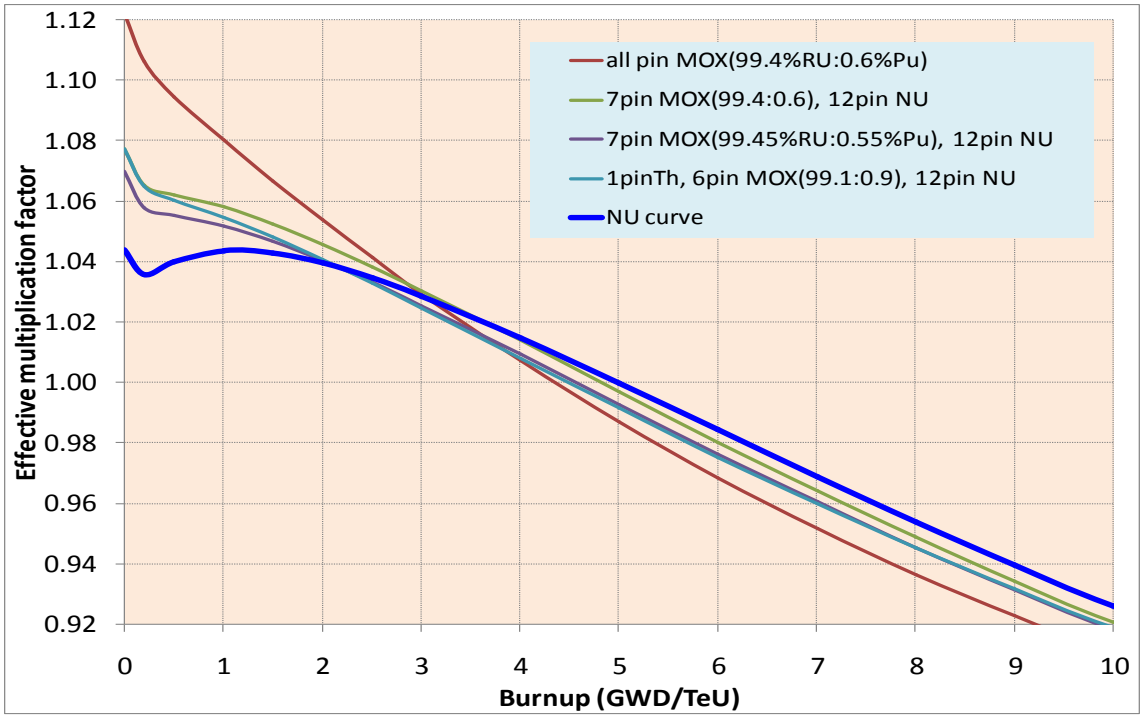

FIG. 5. RU (having both PuO_2 & UO_2) of PHWR in inner 7 pins and NU in outer 12 pins.

3. DISCUSSIONS

Based on the above analysis following two fuel designs are proposed:

(1) The RU (having both UO_2 and PuO_2) of PHWR and SEU (having only UO_2) of LWR mixed in the ratio of 50% / 50%. During further discussion this bundle will be called RU+SEU bundle;

(2) A bundle with outer 12 pins NU and inner 7 pins MOX (mixed oxides). The MOX contains PuO_2 / UO_2 as 0.55% / 99.45% extracted from RU of PHWR (separated and remixed). During further discussion this bundle will be called MOX-7 bundle.

Using code TAQUIL [2] the time averaged feed rate, maximum bundle power (MBP) and maximum channel power (MCP) for both the above proposed fuel bundle are derived and compared with NU bundle in Table 3. The worth of shutdown systems (14 primary shutoff rods and 12 secondary liquid poison tubes) is also provided for comparisons. It can be seen that both the fuel design is having close similarity to NU bundles including the worth of shutdown systems.

TABLE 3. COMPARISON OF FEED RATE, MBP, MCP AND SHUTDOWN SYSREM WORTH

Type of bundle	Burnup (MWD/TeU)			Feed rate (bundle/day)			MBP	MCP	14PSS	12SSS
	Inner	Outer	Average	Inner	Outer	Total	(kW)	(MW)	(mK)	(mK)
NU	10700	6100	7008	1.7	6.8	8.5	423	3.07	38.0	31.2
RU+SEU	10500	6300	7147	1.7	6.6	8.3	422	3.07	36.2	32.4
MOX-7	10400	6200	7045	1.7	6.7	8.4	422	3.07	36.6	32.9

The Isotopic composition with burnup of bundle is given below in Table 4. Since the reduction in fissile content is low, 2–3 such cycles are possible with increase in the ratio of UO_2 of LWR from 50% to 55%.

TABLE 4. ISOTOPIC COMPOSITION OF RU + SEU BUNDLE

Burnup	Isotopic composition (gm/kg)						
	U235	U236	U238	Pu239	Pu240	Pu241	Pu242
0	5.729	2.595	989.800	1.295	0.455	0.104	0.025
5000	2.831	2.986	985.100	2.541	1.025	0.260	0.098
6000	2.446	3.033	984.130	2.636	1.157	0.294	0.121
7000	2.107	3.073	983.140	2.706	1.288	0.328	0.148
10000	1.328	3.154	980.090	2.816	1.653	0.423	0.244

The Isotopic composition with burnup of MOX bundle will be different for 7 inner pins and 12 outer pins as given below in Table 5a and 5b respectively. While reprocessing, the NU pins can be reprocessed separately to continue the cycle.

TABLE 5a. ISOTOPIC COMPOSITION FOR 7 INNER MOX PINS

Burnup	Isotopic composition (gm/kg) for MOX [extracted PuO2 & extracted UO2 in 0.0055:0.9945]						
	U235	U236	U238	Pu239	Pu240	Pu241	Pu242
0	2.466	0.696	991.340	3.789	1.332	0.305	0.073
5000	1.285	0.861	986.780	3.225	2.015	0.512	0.226
6000	1.113	0.884	985.800	3.161	2.113	0.543	0.268
7000	0.961	0.903	984.800	3.109	2.200	0.570	0.312
10000	0.608	0.944	981.740	3.000	2.412	0.632	0.459

TABLE 5b. ISOTOPIC COMPOSITION FOR 12 OUTER NU PINS

Burnup	Isotopic composition (gm/kg) for NU burnt bundle						
	U235	U236	U238	Pu239	Pu240	Pu241	Pu242
0	7.110	0.000	992.890	0.000	0.000	0.000	0.000
5000	3.319	0.574	987.970	2.289	0.585	0.122	0.019
6000	2.854	0.642	986.980	2.447	0.744	0.164	0.032
7000	2.449	0.701	985.970	2.564	0.902	0.207	0.049
10000	1.528	0.831	982.870	2.754	1.347	0.329	0.124

The pin power distribution derived using CLUB is shown in Table 6.

TABLE 6. COMPOSITION OF PIN POWER DISTRIBUTION WITH BURNUP

Burnup	NU bundle			RU+SEU bundle			MOX-7 bundle		
(MWD/TeU)	Inner	Interme	Outer	Inner	Interme	Outer	Inner	Interme	Outer
0	0.821	0.883	1.074	0.812	0.877	1.077	0.952	1.048	0.980
1500	0.820	0.883	1.074	0.815	0.880	1.075	0.880	0.957	1.032
4000	0.835	0.894	1.067	0.832	0.892	1.068	0.841	0.904	1.061
6000	0.847	0.902	1.062	0.844	0.900	1.063	0.836	0.893	1.067
10000	0.860	0.910	1.057	0.858	0.908	1.058	0.844	0.896	1.065

The pin power distribution is identical for NU and RU+SEU bundle whereas the pin power distribution of MOX-7 is having typical behavior. Though at lower burnups the intermediate pins have higher pin power ratio, it is still lower than that for NU bundle outer pins which indicates that the MOX-7 bundle will have higher bundle power limit at lower burnups. However at higher burnups outer pins for MOX-7 bundles have higher pin power which may call for slightly lower Bundle power envelop limit for burnup > 5000 MW·D/T.

In Fig. 6, variation of reactivity change with burnup due to change in fuel temperature from 271^{0}C (0 % FP) to 771^{0}C (100 % FP) is shown. It is seen that for equilibrium core, the fuel temperature coefficient is almost same for all the three fuel bundles.

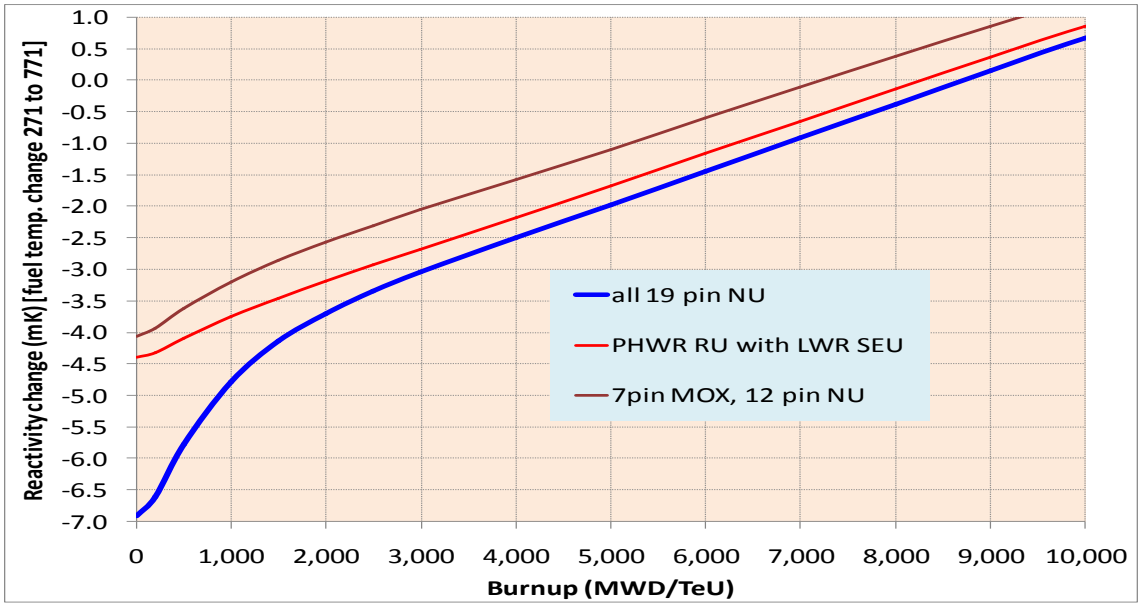

FIG. 6. Variation of reactivity change due to change in fuel temperature from 271°C to 771°C for NU, RU+SEU and MOX-7 bundle.

The reactivity gain due to voiding in coolant is shown in Fig. 7. The Void coefficient for both the proposed fuel design is less positive than the NU bundle which is a desirable feature.

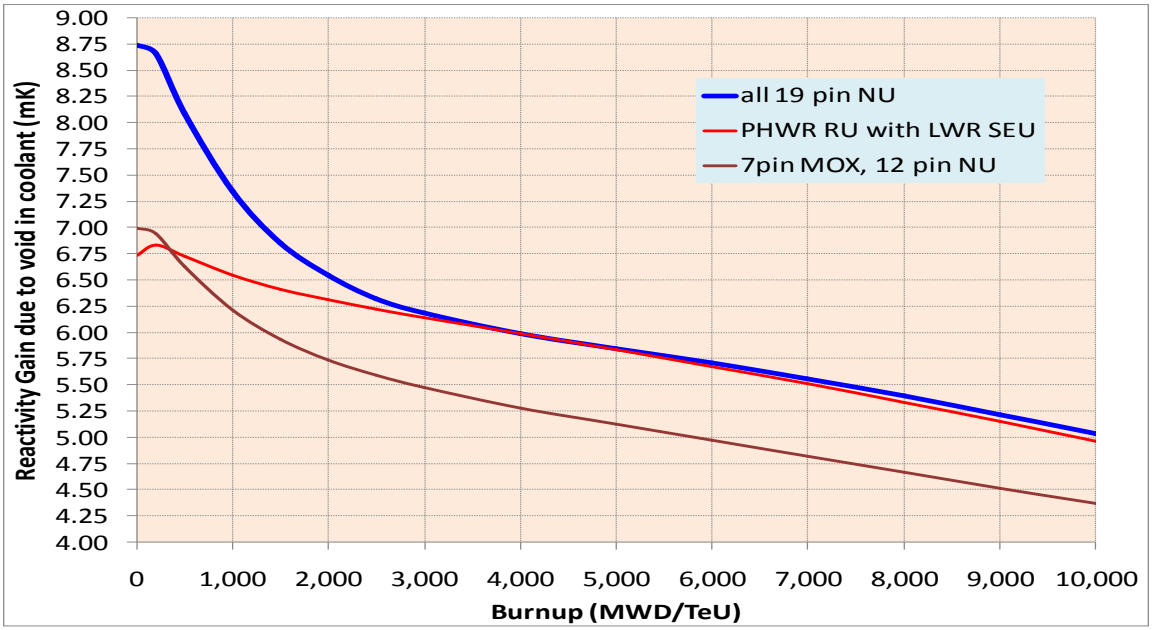

FIG. 7. Variation of Void reactivity gain (mK) for NU, RU+SEU and MOX-7 bundle.

Variation of kinetics parameters viz. delayed neutron fraction and prompt neutron life time for both the fuel designs along with NU bundle with burnup is provided in Figs. 8 and 9 respectively. It can be seen that for equilibrium core, the kinetics parameters are comparable for all the three fuel bundles.

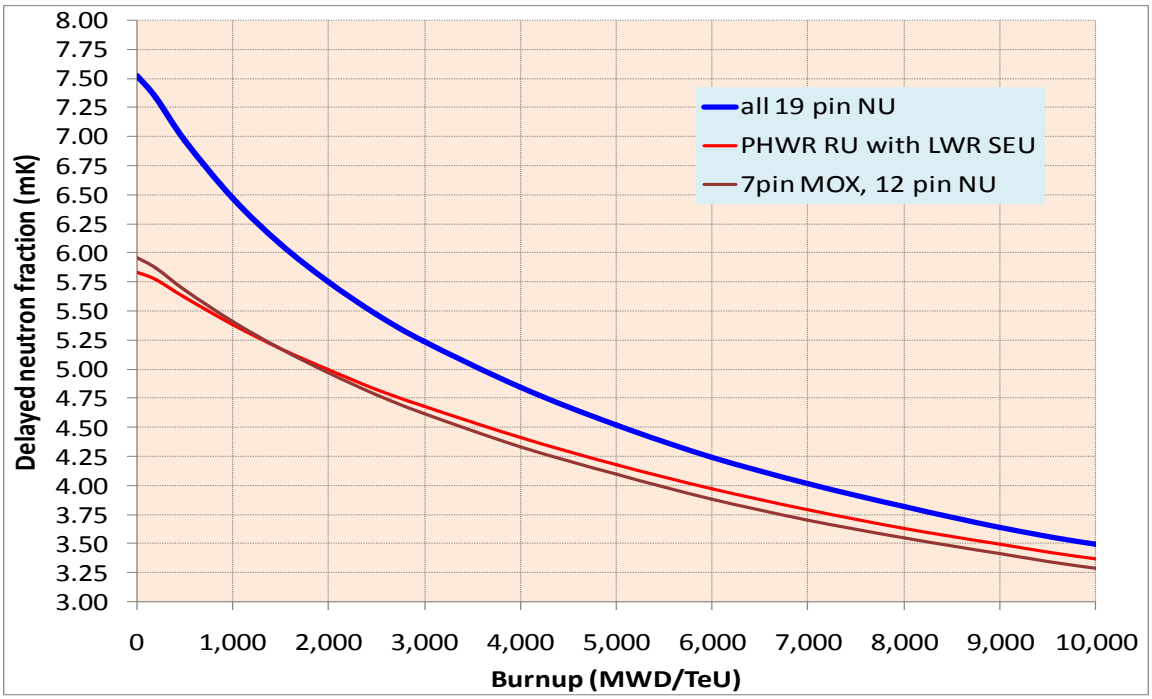

FIG. 8. Variation of delayed neutron fraction (mK) for NU, RU+SEU and MOX-7 bundle.

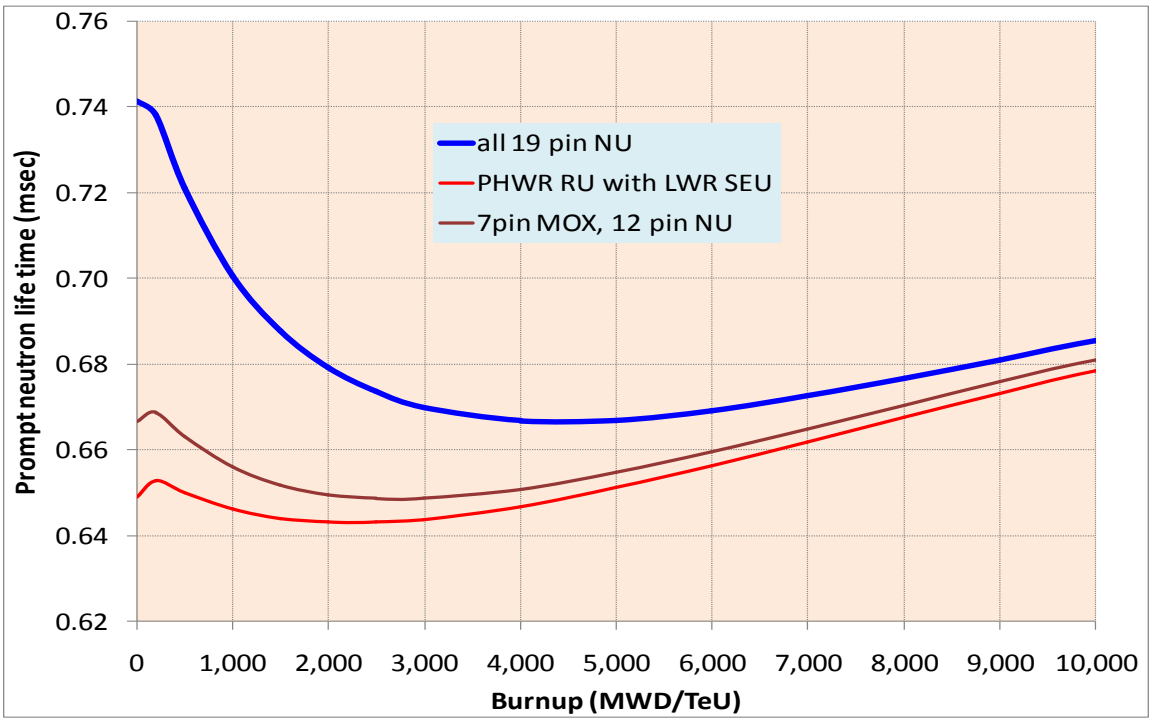

FIG. 9. Variation of prompt neutron life time (msec) for NU, RU+SEU and MOX-7 bundle.

To find the effect of loading the proposed fuel bundle on operational parameter like channel outlet temperature the deviation in equilibrium channel power distribution with respect to NU core is given below in Fig. 10. It can be seen that the deviation in channel power is within the operational margin however, the MOX-7 core is relatively closer to NU core.

	10	9	8	7	6	5	4	3	2	1
A	1.4	1.5	1.8							
B	0.7	0.8	1.1	1.7	2.3					
C	0.0	0.2	0.6	1.2	1.7	2.2	2.7			
D	-0.8	-0.5	0.0	0.6	1.3	1.7	2.2	2.8		
E	-2.5	-2.2	-0.7	0.1	0.9	1.4	1.9	2.6		
F	-3.3	-3.0	-2.3	-0.5	0.4	1.1	1.7	2.2	2.9	
G	-4.0	-3.6	-2.9	-1.0	0.1	0.8	1.5	2.1	2.6	
H	-4.4	-4.1	-3.3	-1.4	-0.4	0.6	1.3	1.9	2.4	3.1
J	-4.7	-4.4	-3.7	-2.7	-1.6	0.3	1.2	1.8	2.3	2.9
K	-4.8	-4.5	-3.8	-2.8	-1.7	0.2	1.1	1.8	2.3	2.9
L	-4.6	-4.3	-3.7	-2.7	-1.6	0.3	1.2	1.8	2.3	2.9
M	-4.3	-4.0	-3.3	-2.4	-1.3	0.6	1.3	2.0	2.5	3.2
N	-3.7	-3.4	-2.7	-0.9	0.1	0.9	1.6	2.2	2.8	
O	-2.9	-2.6	-2.0	-0.2	0.6	1.3	1.9	2.4	3.0	
P	-2.0	-1.7	-0.3	0.5	1.2	1.7	2.2	2.7	3.3	
Q	-0.1	0.1	0.5	1.1	1.7	2.2	2.6	3.1		
R	0.7	0.9	1.2	1.8	2.2	2.6	3.0	3.5		
S	1.4	1.6	1.8	2.3	2.7	3.3				
T	2.2	2.3	2.5	2.8	3.4					

% change in Channel Power for RU+SEU core

	10	9	8	7	6	5	4	3	2	1
A	0.9	1.0	1.2							
B	0.4	0.5	0.7	1.1	1.5					
C	0.0	0.1	0.4	0.7	1.1	1.4	1.7			
D	-0.5	-0.4	0.0	0.4	0.8	1.1	1.4	1.7		
E	-1.5	-1.3	-0.4	0.1	0.6	0.9	1.2	1.6		
F	-2.0	-1.8	-1.4	-0.3	0.3	0.7	1.0	1.3	1.8	
G	-2.4	-2.2	-1.7	-0.6	0.0	0.5	0.9	1.2	1.6	
H	-2.7	-2.5	-2.0	-0.9	-0.2	0.3	0.8	1.1	1.5	1.9
J	-2.9	-2.7	-2.2	-1.6	-0.9	0.2	0.6	1.0	1.4	1.8
K	-2.9	-2.7	-2.3	-1.7	-1.0	0.1	0.6	1.0	1.4	1.7
L	-2.9	-2.6	-2.2	-1.6	-1.0	0.2	0.7	1.1	1.4	1.8
M	-2.6	-2.4	-2.0	-1.4	-0.7	0.3	0.7	1.1	1.5	2.0
N	-2.3	-2.1	-1.6	-0.5	0.1	0.5	1.0	1.3	1.7	
O	-1.8	-1.6	-1.2	-0.1	0.4	0.8	1.1	1.5	1.8	
P	-1.2	-1.0	-0.2	0.3	0.8	1.1	1.3	1.6	2.0	
Q	-0.1	0.0	0.3	0.7	1.1	1.3	1.6	1.9		
R	0.4	0.6	0.8	1.1	1.4	1.7	1.9	2.2		
S	0.9	1.0	1.1	1.5	1.7	2.1				
T	1.4	1.5	1.6	1.8	2.2					

% change in Channel Power for MOX-7 core

FIG. 10. Deviation in channel power distribution with respect to NU core.

4. CONCLUSION

The proposed use of MOX-7 and/ or RU + SEU in PHWRs will not only help in conserving Natural Uranium but also provide a good alternative to reduce the problem of storage of discharged fuel especially for the safeguarded reactors. The nuclear waste material can also be reduced drastically. This fuel clusters provide almost similar characteristics to that of NU bundles and hence can readily by introduced in the existing PHWRs without facing any operational difficulties or compromising in the safety requirements. Based on the present study, it can be concluded that the MOX-7 design is more attractive and preferable.

REFERENCES

[1] KRISHNANI, P.D., CLUB – A Multi Group Integral Transport Theory Code for Lattice Calculation of PHWR cells, BARC Report Number BARC/1992/E/017 (1992).

[2] SRINIVASAN, K.R., TAQUIL & TRIVENI – Computer Codes for Fuel Management of PHWRs, BARC Report Number PHWR-500/PHY/18 (1986).

STATUS OF CANDU6 FUEL IN KNF

C.-K. SUK, B.-J.-LEE, C.-H. PARK
Kepco Nuclear Fuel,
Daejeon, Republic of Korea

Abstract

Kepco Nuclear Fuel (KNF) has been producing CANDU 6 fuel for 14 years since 1998. Its fabrication process includes from powder preparation to fuel assembling with about 400MTU/year capacity. Some of the key manufacturing equipment has been developed to improve productivity and quality. New tack and brazing machine to join appendages on cladding surface use a vacuum system instead of argon gas flow in order to reduce inert gas cost. New graphite coating process is fully automated to improve productivity. Beside these developments, the overall fabrication technologies of CANDU6 fuel have been enhanced. Furthermore, KNF developed CANFLEX-NU(CANDU Flexible –Natural Uranium) fuel from 2000 to 2004. KNF fabricated around 150 CANFLEX fuel bundles to develop manufacturing process and demo irradiation in Wolsung power plant. 24 CANFLEX fuel bundles were successfully demo irradiated and there was no indication of any defect or unusual fuel rod power history in the demo irradiation. Recently, KNF decided to develop 37M(modified-37 CANDU6) fuel as a countermeasure for power derating due to reactor aging. In this presentation, status of CANDU6 fuel in KNF will be introduced.

1. MANUFACTURING PROCESS IN KNF

Figure 1 shows a flow diagram of pellet manufacturing process. UO_2 powder is imported from foreign supplier. Because of poor flow ability, powder preparation is for fabricate
ng granule in order to improve flow ability of powder. After powder preparation, make green pellet to have uniform size, shape and density by using press machine then, make sintered pellet by heating up to 1600°C for 6 hrs. Finally centerless grinding is carried out to get specified diameter and surface roughness.

Beryllium is used for brazing as a filler metal. Beryllium is deposited on one side of the strip for the subsequent brazing operation. In order to evaporate beryllium to the strip, strip needed to be rough surface for adherence of the beryllium coating, so blast one side of strip using oxide particle. The coated strips are loaded into an automatic punch press which punches appendages from the strips. The appendages are electric resistance welded on the cladding surface to have specified position and an induction heating coil surrounding the cladding tubes heats the appendages, the gap between beryllium coating layer and cladding tubes to form the braze joint. Graphite is deposited on the inside of the fuel cladding tubes by graphite coating machine. The graphite coat forms a barrier to corrosive fission gases generated in the fuel pellets during irradiation. The coated claddings are dried in air and then cured in a bake oven. Both ends of the cladding tubes are brushed in the inside and outside to clean the cladding tube ends for the end closure welding operation. The claddings are trimmed to an exact length. Fig. 2 shows the above manufacturing process.

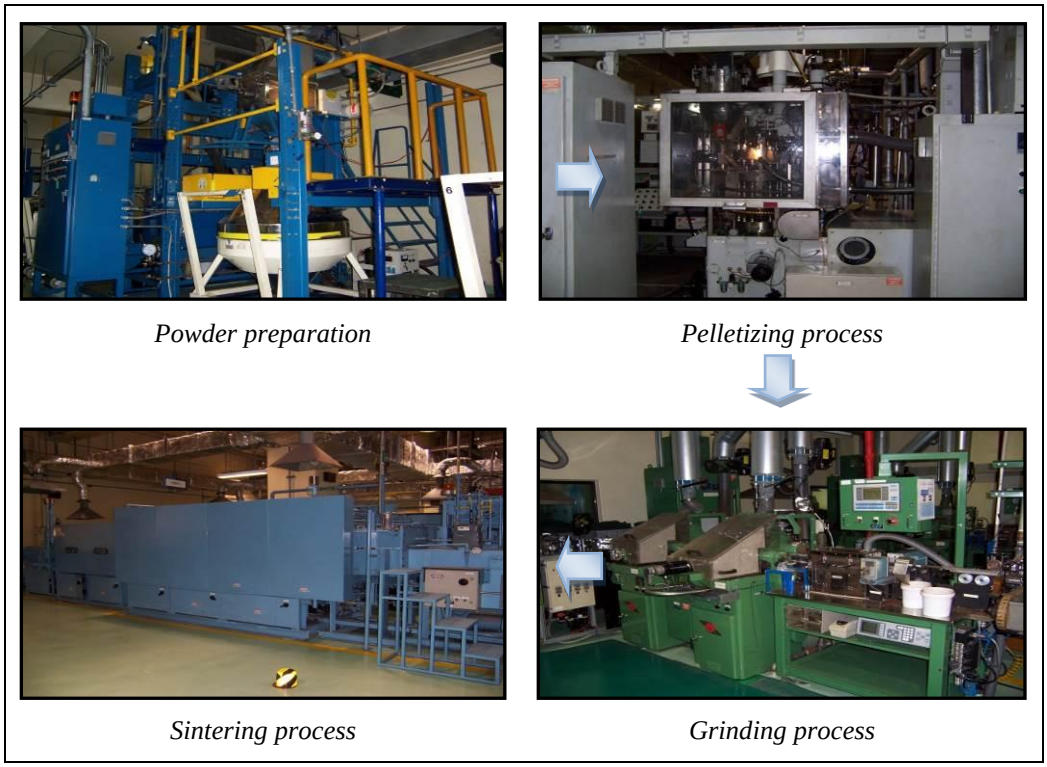

FIG. 1. UO_2 Pellet manufacturing process.

Bar stocks for end plugs are ultrasonically tested for defects inspection. End plugs are turned to the correct shape in automatic screw machines and lathes. The end plugs are cleaned in a cleaning solution and sample end plugs are checked for dimensions. Incoming skids of pellets are stored on storage racks. The pellet stacks are loaded into the cladding tubes. End plugs are joined to each end of the cladding tubes by an electric resistance welding. A small amount of helium is injected into the cladding tubes before the final end closure weld for subsequent leak testing of finished fuel bundles. Fuel rod is assembled into fuel bundle fixture. End plates are punched from strip in a progressive punching operation. The end plates are then flattened and cleaned. Sample end plates are checked for dimensions. The end plates are electric resistance welded with fuel rods in sequence. KNF tested fuel bundles using helium detector. And washing and packing them. That is overall fabrication process shown in Fig. 3.

2. DEVELOPMENT OF FABRICATION EQUIPMENT

Vacuum system of Beryllium coating M/C is improved to reduce cycle time. KNF redesigned substrate holding fixture to hold more substrates to improve productivity. Punching press M/C was newly built last year and optimized hydraulic control and cylinder itself so the punching speed was enhanced. Fig. 4 represents the developed manufacturing equipment. As a result, the cycle time was reduced.

The tack and brazing M/C has two distinctive improvements. Argon gas was being used in this process to protect heat affected zone (HAZ) oxidation. However, newer developed brazing is carrying out under the vacuum instead of argon gas flow. So the inert gas cost is reduced. On the other side for tacking process, using ceramic tacking fixture instead of

anodizing fixture to have better insulation as a result the tacking quality is improved and malfunction is reduced. Furthermore, to increase productivity, appendages supplying mechanism is changed with a rotation table. Lots of appendages are tack welded and brazed on the cladding. It is not easy for workers to inspect all appendages on cladding. So, automatic vision system finds defects on brazing joint using vision camera with light reflection one by one and image software evaluate image data as shown in Fig.5.

FIG. 2. Appendage brazing and graphite coating process.

Former graphite coater was a semi-automatically operated. But, in the newly designed graphite coater as shown in Fig. 6, from inserting cladding tubes to graphite head to move to first dryer chain are fully automated by automatic pneumatic actuators. So, the number of operators was reduced.

End plug welding M/C is improved on weld flash removal system. The former one couldn't control RPM and feeding speed of cutter. But new one can control RPM and feeder speed. So, fuel rod has better quality of cutting surface.

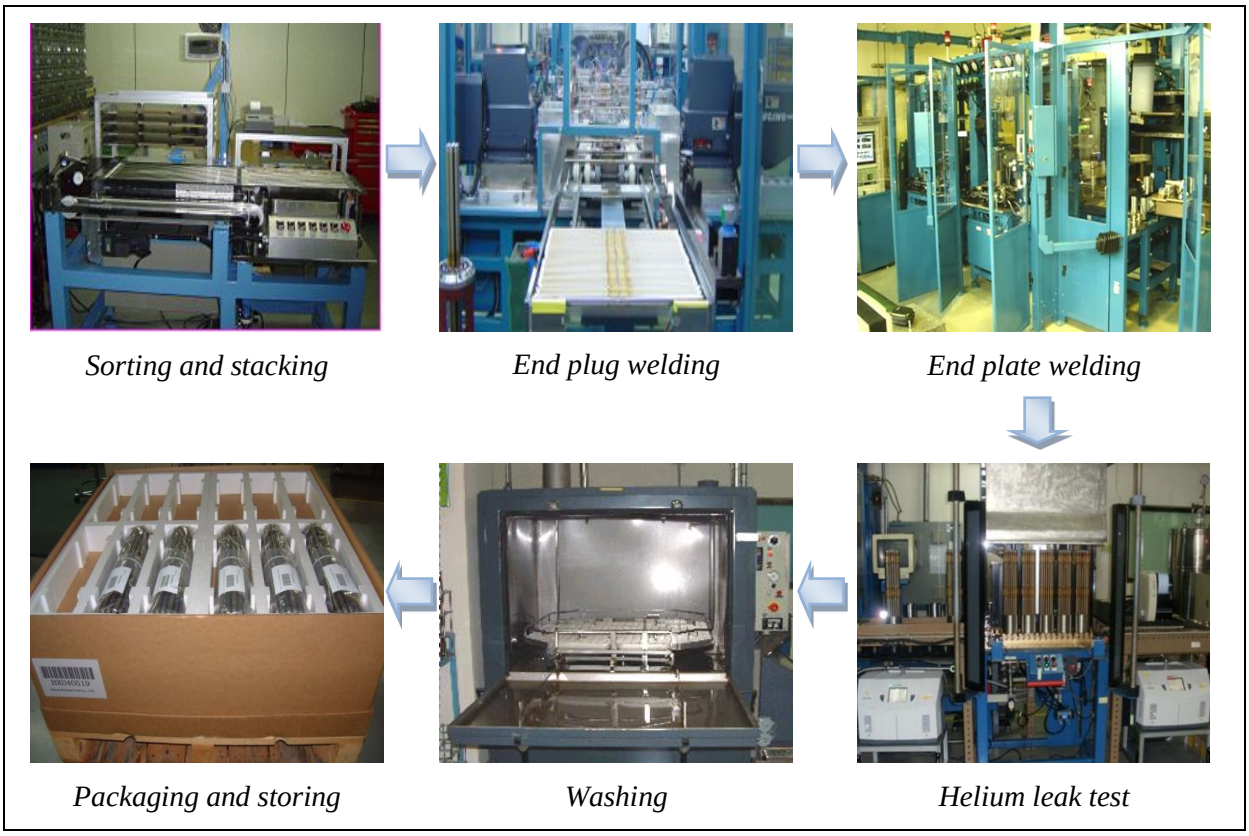

FIG. 3. Fuel rod and fuel bundle manufacturing process.

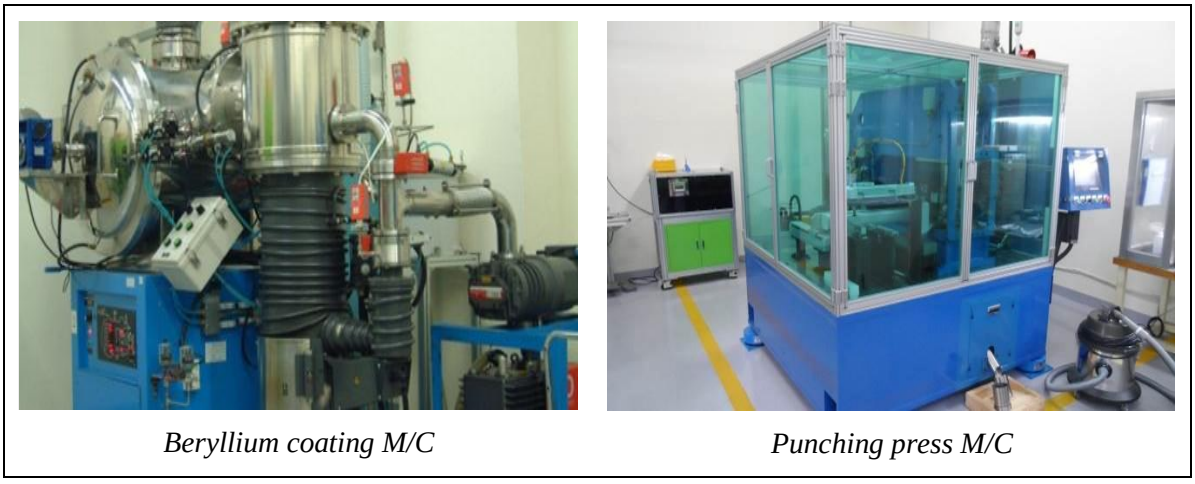

FIG.. 4. Developed appendage manufacturing equipment.

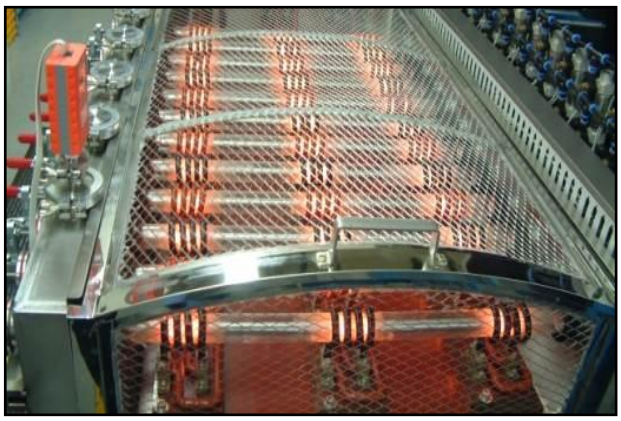

Tack and brazing M/C

Vision system of tack and brazing M/C

FIG. 5. Developed tack and brazing machine.

Graphite coater

End plug welding M/C

FIG. 6. Developed graphite coater and end plug welding machine.

Pellets sort and stack M/C was being done at separate location. It is not efficient to divide two processes for sorting and stacking so, it is combined two processes to one. So operators can do sorting and stacking pellets at the same location as shown in Fig. 7

Before

After

FIG. 7. Developed sort and stack machine.

3. EXPORTED ITEMS

Figs. 8 and 9 are ceramic J-Plate that is used in fuel bundle welding process. The purpose of this tooling is to give insulation during welding current flows. Even though ceramic material has a little difficulty in mechanical machining, welding quality and duration is even better. KNF exported ceramic J-plate to GHNEC in 2007.

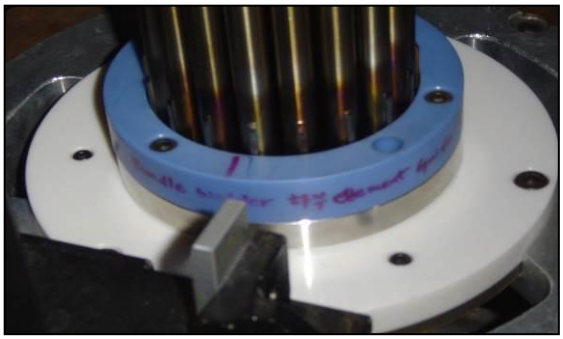

FIG. 8. J-Plate for end plate welding machine.

FIG. 9. Ceramic J-plate.

Fig. 10 is bearing pad and spacer pads fixture for tacking process and Fig. 11 is Pyrex tube for brazing. KNF modified dimple angle of Pyrex tube which is for supporting claddings during brazing in order to maintain straightness after brazing. KNF exported both parts to Argentina CONUAR last year.

FIG. 10. Bearing/spacer pads fixture.

FIG. 11 Pyrex tube.

4. CANFLEX-NU DI PROGRAM

CANFLEX-NU DI program carried out under the cooperation of KHNP/KAERI/AECL/KNF. Its objective is to establish CANFLEX fuel strategies in Korea. In order to achieve the goal, KNF developed manufacturing process and reviewed how to prepare commercial production. Fuel bundles were fabricated for Demonstration Irradiations, 3 fuel bundles were supplied to AECL for evaluation purpose in 2003. 16 fuel bundles were demonstration irradiated at high power channel and 8 fuel bundles at low power channel at Wolsong plants from 2002 to 2004 as shown Fig. 12. KNF manufactured about 150 CANFLEX fuel bundles for process qualification and out pile tests.

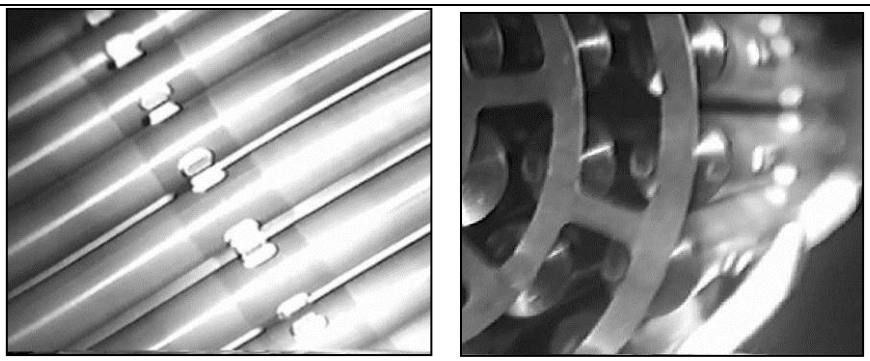

FIG. 12. In-bay visual examination.

5. RELIABILITY OF CANDU6 FUEL IN KNF

KNF has been supplying CANDU6 fuel from 1998 and the total amount of supplying is around 5,565MTU. Bundle defect rate is below 0.005%. This is far below the accepted performance target 0.05%.

6. DEVELOPMENT OF SIPPING SYSTEM

The Sipping Technology to inspect defective irradiated fuel bundle, generally well known, is divided largely into vacuum sipping, dry sipping, wet sipping or in-mast sipping

depending on physical phenomenon and state of fission products which will be detected. KNF adopted a sipping technology that utilizes measurement of the radioactivity of gases and liquid samples holding fission products. This system is classified as a vacuum and canister sipping. KNF introduced the sipping technology at IAEA TM in Romania in 2012 as shown Fig. 13.

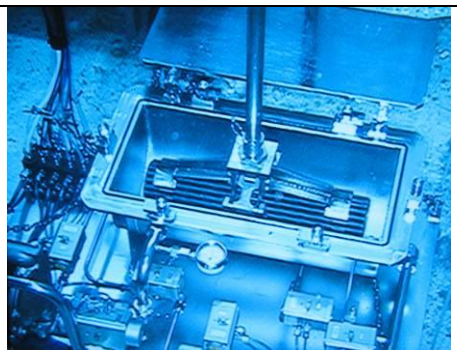

FIG. 13. Sipping System

7. FUTURE PLAN

KHNP has a plan to utilize 37 Modified CANDU6 fuel around 2016. In order to supply 37M fuel, development of manufacturing technologies will be carried out. KNF is planning to produce CANDU6 fuel cladding tubes and now, reviewing the feasibility of CANDU6 fuel cladding tube production.

POST IRRADIATION EXAMINATION
(Session 4)

Chairman

S. ANANTHARAMN
India

METALLOGRAPHIC STUDIES ON IRRADIATED PHWR FUELS

P. MISHRA, V. P. JATHAR, J. BANERJEE S. ANANTHARAMAN
Bhabha Atomic Research Centre,
Mumbai, India
Email: prernam@barc.gov.in

Abstract

Metallography/Ceramography during post irradiation examination (PIE) provides valuable information on the in-reactor behaviour of the fuel and plays an important role in failed fuel investigation. Microstructural studies have been carried out on natural UO2 fuel bundles in the burnup range of 400-15000 MW·d/tU irradiated in various Indian PHWRs. The primary cause of fuel failure in the fuel bundles has been identified as fabrication related defects and handling defect. The small primary defects caused hydriding of the cladding resulting in large secondary defects. The discharge burnup of the failed fuel bundles was much less than the average burnup of 7,000 MW·d/tU. The results of PIE of the two high burnup (15,000 MW·d/tU) fuel bundles have demonstrated the capability of these bundles to sustain such burnups. The techniques involved in metallographic studies include optical microscopy, scanning electron microscopy, microindentation studies, β-γ autoradiography and α-autoradiography. This paper presents the observations on the fuels examined and the conclusion drawn.

1. INTRODUCTION

Metallography plays a vital role in the post irradiation examination of irradiated nuclear fuels and provides valuable information on the in-reactor performance of the fuel and in failed fuel investigations. Metallographic examination provides information on the microstructural changes in the fuel and cladding as well as the fuel-clad and coolant-clad interactions. The microstructural studies on fuels are used to evaluate the extent of restructuring in the fuel, radial temperature profile in the fuel pellet [1], densification, cracking morphology in the pellet, fission product distribution and extent of corrosion and hydriding of the cladding.

There is a need to increase the discharge burnup of PHWR fuels by using slightly enriched uranium or mixed oxide to reduce the cost of fuel and also to reduce the volume of discharged fuel to be stored. With this in view, some of the PHWR fuels that have been irradiated to a burnup of around 15,000MW·d/tU against the average discharge burnup of 7,000 MW·d/tU to study their performance at extended burnup. The main issues related to high burnup fuel performance is fission gas release [2, 3] due to the absence of any fission gas plenum in the standard PHWR fuel pin. Apart from this, cladding corrosion, the corrosion at the crevice of the bearing bad and fuel swelling are also a matter of concern at high burnups. Metallographic studies are useful to show the region of the fuel that contributed to the fission gas release and estimate the fuel centre temperature, which is the governing factor for the fission gas release [4]. Examination of the fractured fuel faces indicates the mechanism responsible for the fission gas release.

During these years there has been a considerable improvement in the fuel performance with the fuel failure rate of < 0.1%. Still some of the bundles fail at burnups lower than the average discharge burnup. To understand the cause of low burnup fuel failure, metallographic examination was carried out on some of the failed bundles.

Microstructural studies have been carried out on natural UO_2 fuel bundles in the burnup range of 400-15000 MW·d/tU irradiated in various Indian PHWRs [5, 6]. The techniques involved in metallographic studies include optical microscopy, scanning electron microscopy, microindentation studies, β-γ autoradiography and α-autoradiography. This paper presents the observations on the fuels examined and the conclusion drawn.

2. FUEL DESCRIPTION

The details of the fuel bundles subjected to metallographic studies are given in Table 1.

TABLE 1. DETAILS OF THE FUEL BUNDLES EXAMINED

S. No.	Bundle No.	Reactor	Discharge burnup (MW·d/tU)	Residence time (days)	Remarks
1	56504	KAPS-1	14580	708	High burnup fuel bundle
2	35088	KAPS-2	15160	765	
3	82505	KAPS-1	4409	710	Failed fuel bundles
4	102653	KAPS-2	1188	64	
5	108305	KAPS-2	387	17	

3. RESULTS AND DISCUSSION

3.1. High burnup PHWR fuel bundles

Two fuel bundles which had accumulated an average burnup of 15 000 MW·d/tU, which is more than twice the designed discharge burnup of 7000 MW·d/tU were examined. The bundles were of the 19-element design with natural UO_2 fuel pellets encapsulated in Zircaloy-2 cladding. The results of the PIE carried out on the high burnup fuel bundles are given in reference [5].

Metallographic samples taken from the outer, intermediate and central fuel pins of the bundle were prepared in the hot cells and examined under a remotised microscope. Examination of the fuel revealed a dark region at the centre of the fuel section extending up to 55% of the fuel radius in the outer pin as shown in Figure 1a. The dark region covered 15% of the fuel radius in the intermediate pin and was negligible in the central pin.

Observation of the dark porous region at higher magnification revealed interconnected pores/bubbles on the grain boundaries (Fig. 1b). Different microstructural parameters like grain size at the centre, cladding corrosion, porosity in the fuel along with the fission gas analysis results evaluated to assess the performance of the different pins of the bundle are shown in Table 2. Fractured surface of the fuel from the central region of the outer fuel pin revealed fission gas bubbles formed at the grain surface and tunnel formed by inter-linking of the bubbles along the edge of the grain as shown in Fig. 2. Majority of the bubbles were in the size range of 0.5 to 1.5 μm and the fission gas bubble density on the faces of the grain was found to be in the range of 0.1×10^8 to 0.5×10^8 bubbles per cc of the fuel matrix.

Since the extent of clad corrosion and the crevice corrosion near the spot welds of bearing pads and other appendages are a cause of concern at high burnups for a PHWR fuel, these areas were examined. Examination of the section through the spot weld of the bearing

pad indicates uniform corrosion of the clad and the weld region without any evidence of crevice corrosion.

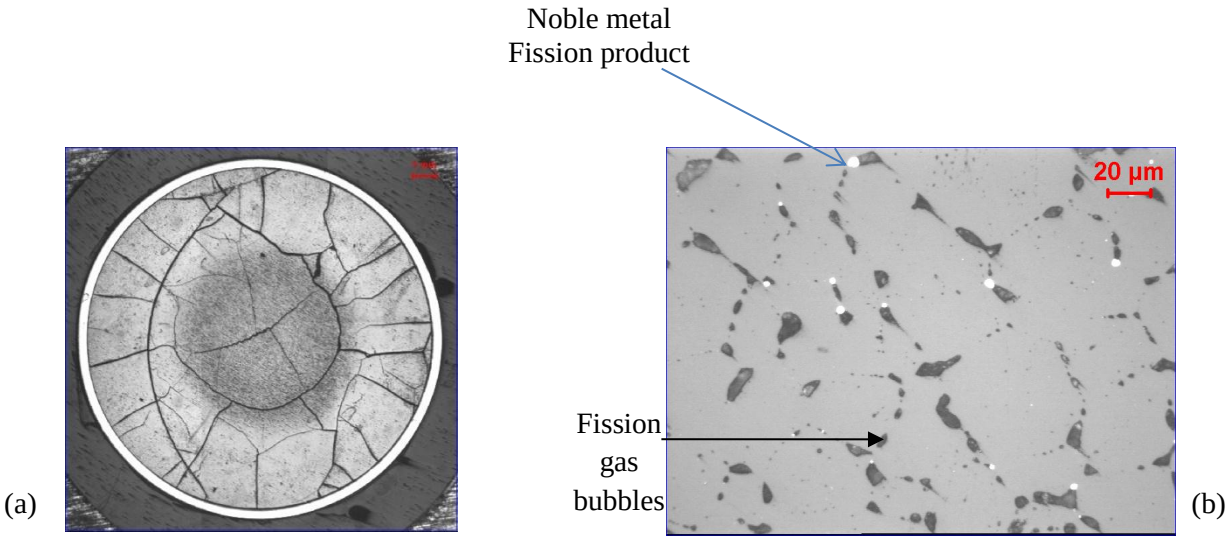

FIG. 1 (a) Photomacrograph and (b) Microstructure at centre of a fuel section from the outer fuel pin

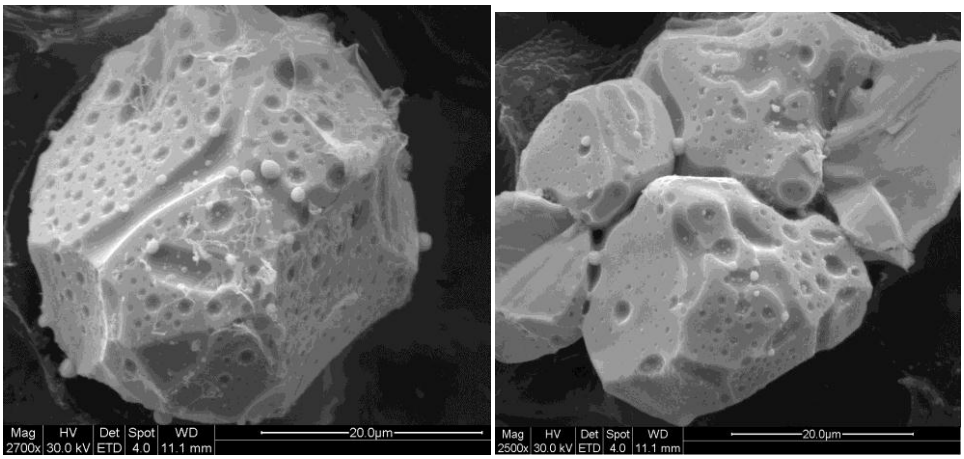

FIG. 2. Grains of UO_2 from the central region of the fuel from outer fuel pin.

TABLE 2. METALLOGRAPHIC DETAIL OF THE HIGH BURNUP FUEL BUNDLE

Parameter	Outer pin	Intermediate pin	Central pin
Fission gas release, %	20	2	0.7
Fission gas pressure, kg/cm^2	28	4.3	3.2
Fuel central temperature, ºC	1600	1250	1170
Grain size, µm	33	19	15
Pellet-clad gap, µm	32	27	16
Oxide layer thickness (ID), µm	5	Discontinuous	0
Oxide layer thickness (OD), µm	2.7	2.4	2.4
Oxide layer thickness (bearing pad), µm	3.7	—	—

3.2. Failed fuel bundles

Case 1:

Fuel bundle no. 82 505 in Kakrapara Atomic Power Station unit #2 reactor failed and was discharged after accumulating a burnup of 4400 MW·d/TU. The details of the failure investigation carried out on the failed fuel pin are given in reference [7]. The primary cause of failure of a fuel pin in the bundle was a lack of fusion defect in the end plug to clad tube weld which was detected during ultrasonic testing of the weld and confirmed by metallographic examination. The defect opened up during operation and lead to the entry of coolant into the fuel pin. The water entering the fuel pin flashed into steam causing oxidation of the fuel and cladding and produced hydrogen. Oxidation of the fuel alters the stoichiometry profile in the fuel pellet, which reduces the fuel thermal conductivity. Also, presence of steam in the fuel clad gap reduces the gap conductance. Combination of these effects leads to a rise in the fuel centre temperature. These processes lead to degradation of the fuel and cladding in the form of (i) extensive fuel restructuring due to temperature escalation (ii) fuel oxidation (iii) cladding oxidation and fuel-clad interaction (iv) secondary hydriding (v) hydride blister formation and cladding failure.

Degradation of the fuel and the cladding was observed during metallographic examination of the samples taken from different axial locations of the fuel pin. Extensive restructuring of fuel like formation of central void, columnar grain growth (CGG) and equiaxed grain growth (EGG) was noticed in the fuel close to the end plug weld having the defect and the extent of restructuring decreased with increase in the distance from the defective end plug weld region as shown in Fig.3. Fuel centre temperature (FCT) was estimated from the restructuring of fuel and found to increase from 1500^{o}C at the colder end to 2500^{o}C near the defective end plug.

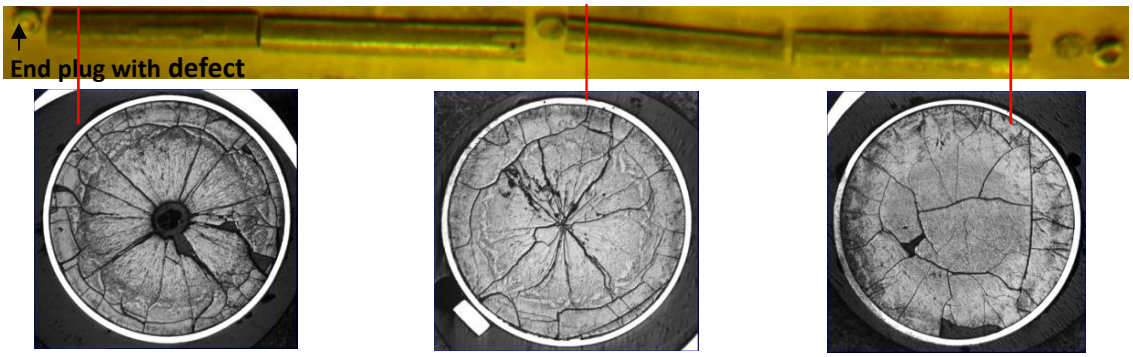

FIG. 3. Photomacrographs showing restructuring in the fuel at different axial locations.

Thick oxide layer and fuel clad interaction (FCI) layers were observed on the inner region of the clad (Fig. 4) near the defective end plug and their thickness variation along the fuel pin length is shown in the Fig. 5.

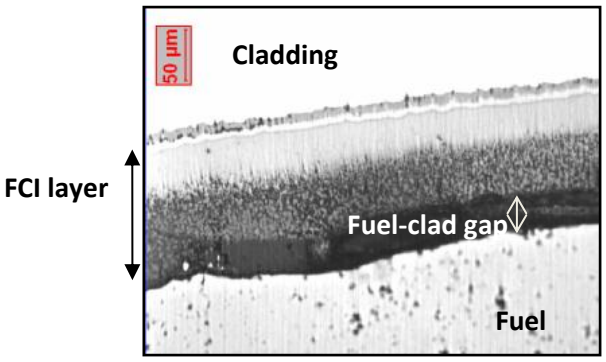

FIG. 4 Oxide layer and fuel-clad interaction (FCI) Layer on the inner side of the clad.

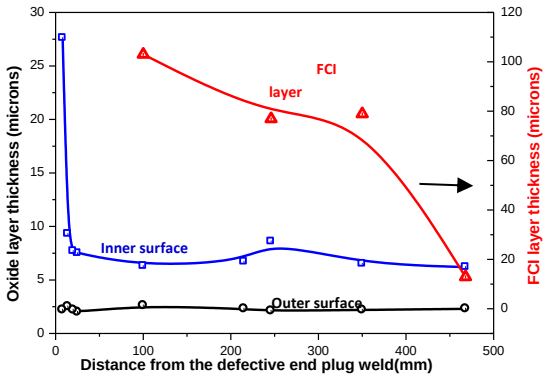

FIG. 5. Oxide layer and fuel-clad interaction layer thickness variation along the fuel pin.

Secondary hydriding in the form of massive hydride blister was observed at two locations of the fuel pin. Sectioning along the blister revealed sunburst hydride formed in the cladding as shown in Fig. 6. The size of the blister was 6mm diameter and 0.4mm depth.

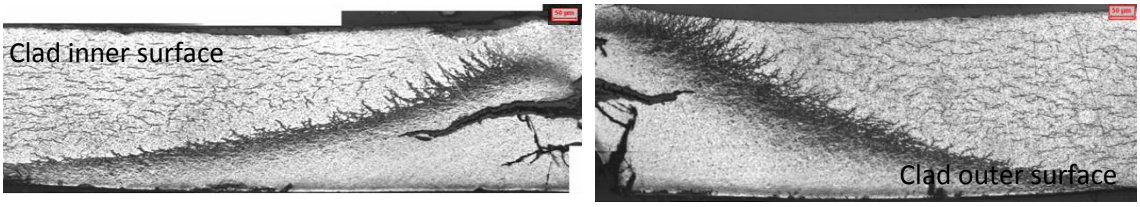

FIG. 6. Sectional view of the "sunburst" hydride blister.

Case 2

The results of metallographic examination on a 19-element PHWR fuel bundle that had failed at a burnup of 387 MW·D/TU within 17 days of residence in the reactor are presented. Of late, fuel failures at such low burnups are rare. Two outer fuel pins from the bundle had multiple axial cracks on the cladding. Fig. 7a shows one of the axial cracks that were observed in one of the outer elements.

The photomacrograph of the fuel section from the failed pin shows restructuring of fuel (Fig. 7b). From the observed metallographic features, the fuel centre line temperature was estimated to be 2100^{o}C. The photomacrograph of the fuel section from an unfailed pin does not show restructuring of fuel and the fuel centre temperature was estimated to be less than 1300^{o}C. This ruled out any power ramps that the fuel might have undergone during its loading into the reactor.

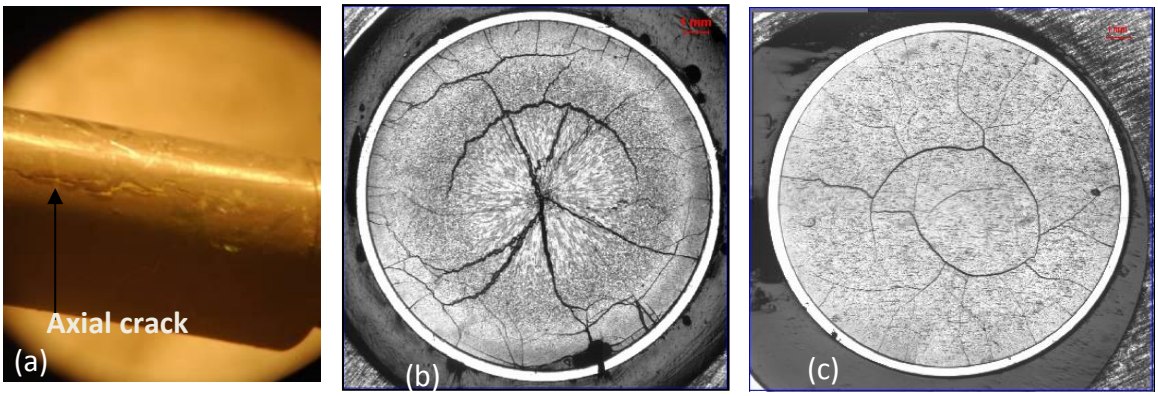

FIG. 7. (a) Failed fuel pin showing axial crack on the cladding. Photomacrograph of a fuel section from (b) the failed pin and (c) an intact pin.

Examination of the cladding revealed multiple failure sites. Micro-blisters of zirconium hydride were observed at several sites (Fig. 8a) along with some partially penetrating radial cracks in the clad. Average length and depth of the observed micro-blisters were 300µ and 50 µm respectively. A through-wall crack was observed, through which a significant amount of fuel had leached out. Examination of the clad after etching revealed presence of hydride platelets at all the crack tips (Fig. 8b). The hydrogen content in the cladding of the failed fuel pin was 42 ppm.

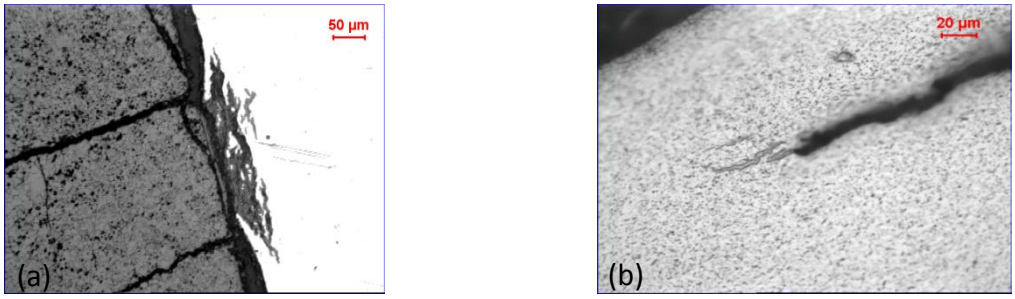

FIG. 8. (a) Micro-blister in the clad with close fuel-clad contact (b) Hydride at the tip crack in the clad.

The hydride platelets observed in the cladding ahead of all the cracks in the cladding indicates that the crack propagation has taken place by delayed hydride cracking (DHC) mechanism. A piece of the clad with a partially propagated in-reactor crack was completely opened through the thickness by fracturing in the laboratory and the fracture surface was examined under scanning electron microscope SEM). The Photomacrograph of the fracture surface showed two regions of in-reactor fracture and laboratory fracture as shown in Figure 9a. The in-reactor fracture region shows layer/step type morphology, similar to a typical DHC fracture surface, but examination at higher magnification revealed the surface to be covered with oxide (Fig. 9b). A typical ductile mode of fracture was observed in the region of the clad fractured in the laboratory (Fig.9c). Fracture surface of the cladding which failed through the wall thickness in the reactor revealed columnar type of grain morphology (Fig. 9d).

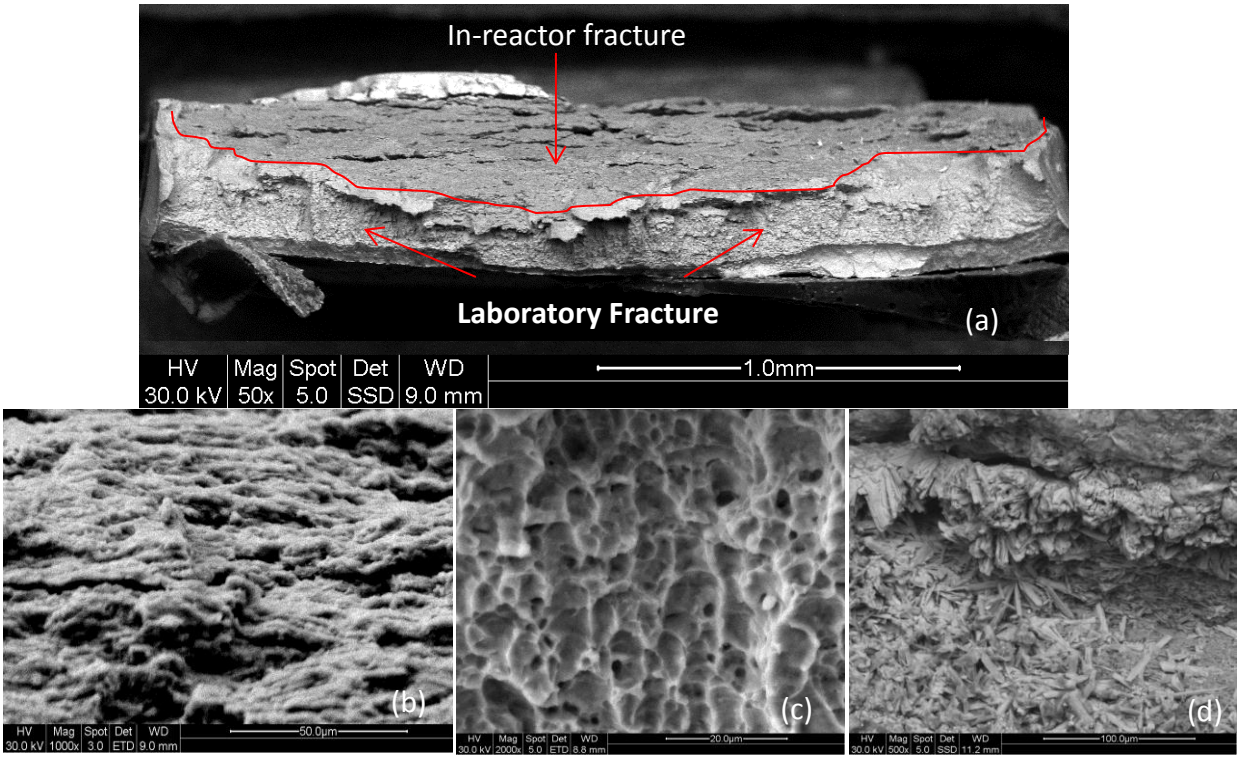

FIG. 9. (a) SEM picture of the fracture surface of the clad with partially penetrated crack. Magnified view of the region of (b) in-reactor fracture (c) Laboratory fracture (d) Oxide morphology on the through-wall cracked clad.

Investigations to ascertain the primary cause of failure of two pins of the bundle are going on. Post irradiation examination being carried out on the second failed fuel pin, may throw light in determining the root cause of failure of the fuel pins.

Case 3:

PIE was carried out on the failed fuel bundle no. 102 653 received from Kakrapara Atomic Power Station (KAPS-2) after an irradiation period of 64 days and burnup of 1188 MW·D/TU. It was found during the visual examination that a bearing pad of one of the outer pins had been deformed and dislodged from its position leaving a hole in the clad at the spot weld (Fig. 10a). The other pins in the bundle were intact with all their welded appendages in position.

A sample was taken from the failed outer element and the structure was examined at the failure location (Fig. 10b). Cracks in radial and circumferential directions were observed in the fuel cross sections. It was also found that the central region of the samples was darker than the peripheral brighter region. Quite an amount of fuel had leached out at the region adjacent to clad failure. The grains boundaries in the central region of the fuel were decorated by pores. As fabricated grains (grain size of about 10 µm) was observed at periphery of the fuel. Larger grains (about 25 µm) with inter-granular porosity were observed at the center. It was found that the clad had failed by ductile shearing of the spot welded region. No other defects were observed in the fuel clad. Effect of the reaction of water with the fuel and clad could be observed in the microstructure. The clad inner side had extensively oxidized. The oxide layer thickness on the outer surface of the cladding was around 3 µm and the inner surface had a non-uniform oxide layer varying from 4 to 14 µm. The oxide on the inner surface revealed presence of double layers (revealed by two gray levels) at some locations (Fig. 10c).

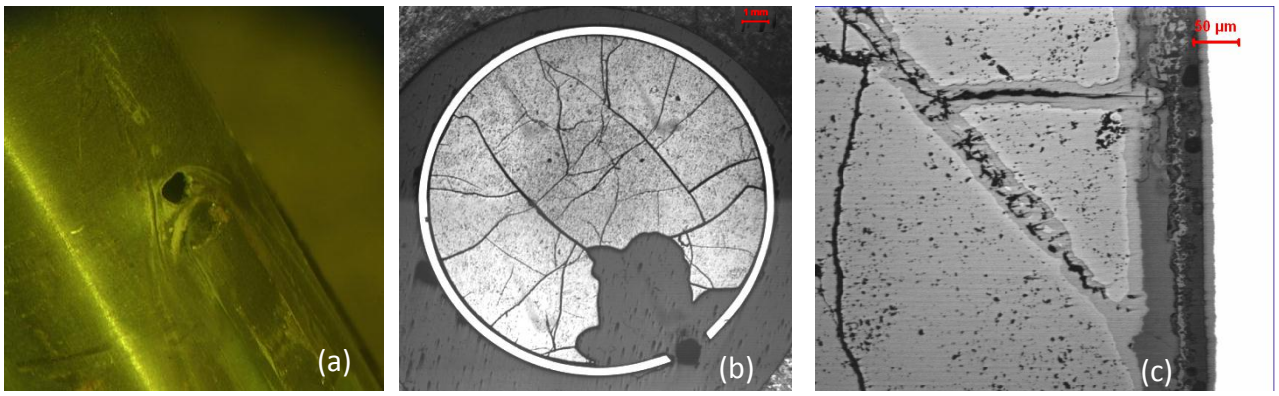

FIG. 10 (a) Failed pin with a perforation in the clad (b) Photomacrograph of the fuel section from the failed pin (c) Fuel-coolant interaction along the cracks

Insignificant hydriding in the clad and bearing pad indicated that the failure of the pin is not related to hydriding phenomena. Also, uniform corrosion at the crevice of the bearing pad confirms that the failure is not due to localized corrosion at the crevice of the bearing pad. The pin appears to have failed due to mechanical pullout of the bearing pad during loading in the reactor and the observed features are secondary effects.

4. CONCLUSIONS

(a) PHWR fuel bundle irradiated to extended burnup performed very well under normal operating conditions. No abnormal corrosion or PCI was observed. The extent of fission gas release, confirmed by the dark porous region and fuel centre temperature in the outer fuel elements of fuel bundle was higher compared to the fuel pins from the intermediate and the central rings. Suitable design modifications may be required to take care of this if the design burnup is to be extended;

(b) One of the main causes of failures in the fuel pins of power reactors were identified as end-plug weld defects. These failures have been eliminated by stringent quality control of welds. Hydriding in the form of massive hydride blister formation and crack propagation by DHC are secondary effects. Handling related defects leading to perforation in the cladding has been observed in one of the fuel pins. Improvements in the alignments during fueling have eliminated such instances of fuel failures.

ACKNOWLEDGEMENTS

The authors would like to thank Shri Shailesh Katwankar and Shri S.R. Soni of the Hot Cells Facility of Post Irradiation Examination Division, BARC, for their assistance during the course of this work. The authors are also thankful to Shri S.K. Swarnakar for the support in SEM examination.

REFERENCES

[1] OLANDER, D.R., Fundamental Aspects of Nuclear Reactor Fuel Elements, TID 26711 (1976).

[2] SAH, D.N., Basic Mechanism of Fission Gas Release and High Burnup Issues, Metals, Materials and Processes, **18** (2006) 27pp.

[3] VISWANATHAN, U K, ANANTHARAMAN, S., SAHOO, K.C., "Measurement of Fission Gas Release from Irradiated Nuclear Fuel Elements", B.A.R.C/2005/E/026,Bhabha Atomic Research Centre, Mumbai (2005).

[4] SAH, D.N., MISHRA, P., UNNIKRISHNAN, K., A model for Calculation of Fission Gas Release from Restructuring Observed in Fuel, Metals, Materials and Processes, **18** 35 (2006) 40.

[5] SAH, D.N et. al.,"Post-Irradiation Examination of High Burnup PHWR Fuel Bundle 56504 from KAPS-1", B.A.R.C/2007/E/002, Bhabha Atomic Research Centre, Mumbai (2007).

[6] MISHRA, P., et. al., "Post Irradiation Examination of a failed PHWR Fuel Bundle from KAPS-2", B.A.R.C/2006/E/019, Bhabha Atomic Research Centre, Mumbai, (2006).

[7] MISHRA, P., et. al., In-Reactor Degradation of Fuel and Cladding in Fuel Pins Operated with Weld Defects, Journal of Nuclear Materials (in press).

POST IRRADIATION EXAMINATION OF TH-PU AND U-PU MOX FUELS

S. ANANTHARAMAN, P. MISHRA, V.P. JATHAR,
R.S. SHRIWASTAW, H.N. SINGH, P.M. SATHEESH,
P.B. KONDEJKAR, G.K.MALLIK, J.L. SINGH
Bhabha Atomic Research Centre,
Mumbai, India
Email: prernam@barc.gov.in

Abstract

Thoria based mixed oxide is the candidate fuel for the Advanced Heavy Water Reactor (AHWR) being developed in India for thorium utilisation. An experimental fuel pin cluster comprising of twelve Zircaloy-2 clad fuel pins of nominal diameter 15mm and 0.4mm wall thickness containing fuels of different chemical compositions namely, UO_2, ThO_2, (Th-6.75%Pu)O_2 and (U-3%Pu)O_2 was irradiated in the pressurized water loop (PWL) of CIRUSreactor for assessing their irradiation performance. The nominal burnup of the fuel pin during irradiation was 10 200 MW·d / t (HM). After irradiation, the fuel pins were examined using various non-destructive and destructive techniques.No abnormality or defect was observed on the cladding of the fuel pins. The difference in the compositions of the fuel pins and their position in the core resulted in the variation of ^{137}Cs activity observed during the axial gamma scanning of the fuel pins. The fission gas release in the fuel pins was low. Metallographic examination did not reveal any restructuring of fuel, but the observed microstructure could not be explained.This paper describes the post-irradiation examinations carried out and presents the results and conclusions.

1. INTRODUCTION

India has limited uranium, but vast thorium reserves. Hence, thorium utilisation is the long term core objective of the Indian Nuclear Power Programme. The third stage of the Indian Nuclear Power Programme is based on the thorium based fuels. Unlike natural uranium which contains fissile isotope, ^{235}U, thorium does not contain any fissile isotope. Its usage in the initial stage requires the aid of fissile material from the uranium cyclein the form of a mixed oxide (MOX) fuel. Since very little database exists on irradiation behaviour of the thoria based fuels; irradiation testing of thoria based fuels was initiated. In order to study the performance of mixed thoria-plutonia and urania-plutonia fuel during irradiation, an experimental fuel pin cluster comprising of twelve fuel pins of PHWR design with fuelpellets of different chemical compositionswas irradiated in the pressurized water loop (PWL) of CIRUS. The fuel pinsin the cluster contained pellets of UO_2, ThO_2, (Th 6.75%Pu)O_2 and (U 3%Pu)O_2 encapsulated in collapsible Zircaloy-2 cladding. As a part of post irradiation examination (PIE), visual examination, dimension measurement, gamma scanning, fission gas release measurement and microscopic examination on the fuel pins of the fuel clusterhave been carried outinside the hot cells.

2. EXPERIMENTAL FUEL CLUSTER FABRICATION DATA

PHWR-type fuel pins with fuel pellets of different chemical compositions were assembled in a two-tier cluster with each tier having six fuel pins. Tier-1 constituted of two natural UO_2fuel pins, two (U,Pu)O_2 fuel pins and two (Th,Pu)O_2 fuel pins whereas, tier-2 had fuel pins containing ThO_2 fuel pellets. The schematic arrangement of the fuel pins in tier-1of the cluster is given in Figure 1. The fuel pellets were encapsulated in graphite coated Zircaloy-2 clad with wall thickness of 0.38 mm. Helium was used as the filler gas in all the fuel pins. Table 1 provides the fabrication details of the fuel pins of the cluster.

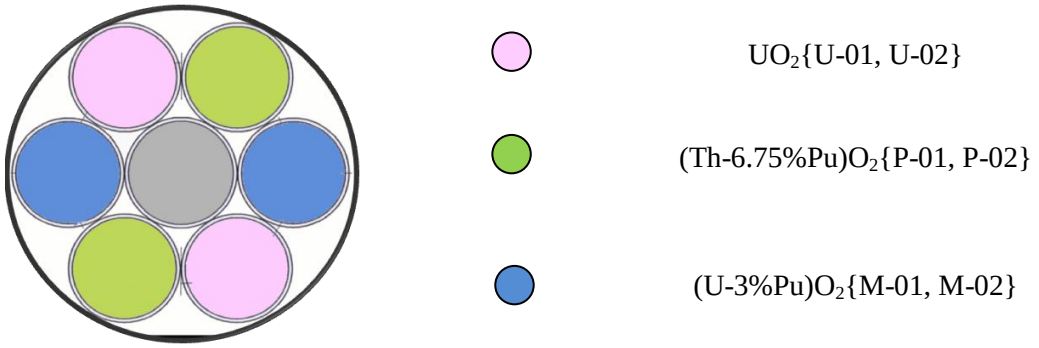

FIG. 1. Arrangement of the fuel pins in the cluster.

The fuelpin M-02 from the cluster consisted of (U-3%Pu)O_2 fuel pellets with normal grain size (4-12 µm) and large grain size (~40 µm). Large grain size pellets were fabricated by addition of 0.05 wt% TiO_2. The fuel pellets were fabricated by powder metallurgy route involving cold compaction and high temperature sintering. The sketch of a typical fuel pin from BC-8 cluster is shown in Fig. 2.

TABLE 1. DETAILS OF FUEL PELLETS IN BC-8 CLUSTER

Pin identification	P-01, P-02	M-02	U-01, U-02
Pellet composition	(Th-6.75%Pu)O_2	(U-3%Pu)O_2	UO_2
PuO_2 enrichment	6.75%	3%	Nil
Pellet diameter	14.3 mm	14.2 mm	14.3 mm
Pellet length	13.9 mm	13.9 mm	14.7 mm
Pellet density	94.6 %	96.4 %	96.3 %
Cladding outer wall diameter	15.26 mm	15.25 mm	15.25 mm
Grain size in the pellet	-	Normal grain size (4-12 µm) and Large grain size (`40 µm)	

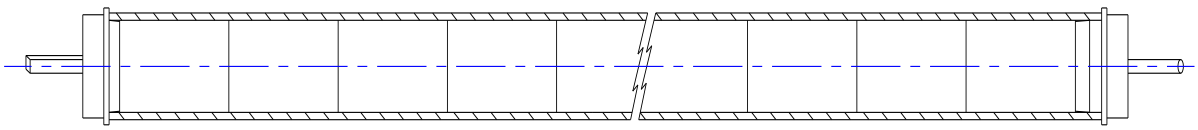

Top end plug (Square) Bottom end plug (Round)

FIG. 2. Schematic of a fuel pin of the BC-8 cluster.

3. IRRADIATION HISTORY

The experimental fuel pin cluster was irradiated in the PWL of CIRUS research reactor. The tier 1 of the cluster containing the MOX and natural urania pins was located above the mid flux zone of the reactor and the tier 2 containing thoria pins was located at the mid flux zone of the reactor, below the tier 1. The nominal thermal neutron flux in the loop was 5×10^{13} n/cm^2/sec and the temperature and pressure of the light water coolant in the loop was 240^{o}C and 105 kg/cm^2 respectively. The peak linear heat rating of the fuel pins was 42 kW/m. The fuel pin cluster was irradiated up to a calculated burnup of 10.2 GW·d / t. After irradiation, and cooling for 13 years, the fuel pin cluster was transported to the hot cell facility for post irradiation examination.

4. PIE RESULTS

The post irradiation examination of the fuel pins of the cluster was carried out at BARC hot cells using different non-destructive and destructive techniques:

(a) Visual examination and dimension measurement:

Visual examination was carried out on the individual pins using a wall mounted periscope. No abnormality or surface defect of any type was visible on the surface of the cladding of the fuel pins. Diameter of the fuel pin was measured using a remotely operated dial gauge. Three sets of readings were taken at each axial location and measurements were taken at an interval of 1cm along the length of the fuel pin. The standard deviation in the diameter readings was 0.02 mm. Reduction in the diameter of the fuel pins was observed in all the 12 fuel pins when compared with their as-fabricated diameter. The results of the diameter measurement in comparison with the as-fabricated data are plotted and shown in Fig. 3. The maximum clad collapse was observed for (U-Pu)O_2 MOX and UO_2 pins, ThO_2 pins showed minimum collapse with (Th-Pu)O_2 in between, as shown in Fig. 4.

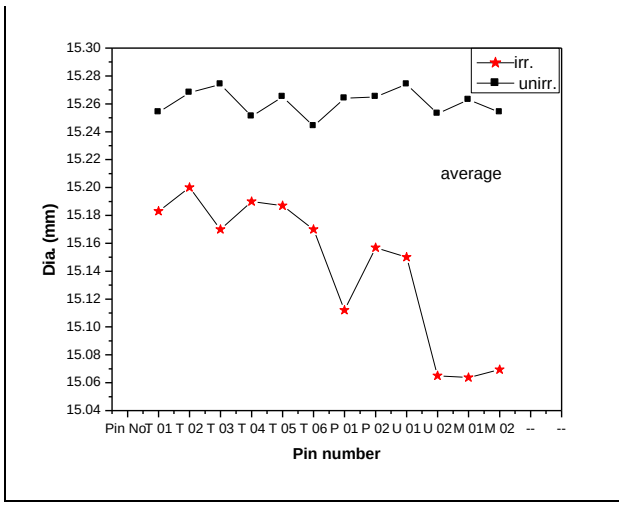

FIG. 3 Average diameter of the fuel pins before and after irradiation.

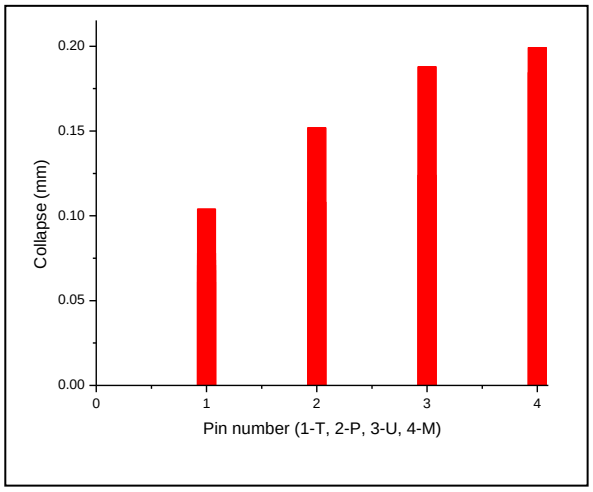

T- ThO_2 fuel pins, **P-**(Th-6.75%Pu)O_2 fuel pins,
U- UO_2 fuel pins, **M-** (U-3%Pu)O_2 fuel pins

FIG. 4 Collapse observed in the fuel pins of the cluster.

(b) Gamma Scanning:

A liquid nitrogen cooled HPGe detector and a PC based multichannel analyzer (MCA) were used for gamma spectroscopy and isotopic gamma scanning. The detector had 40% efficiency with an energy resolution of 1.8 keV FWHM at energy 662 keV. The collimator used for gamma scanning was fitted to the 1.2 meter thick hotcell shielding wall. The front end of the collimator was 50 cm long and is made out of lead. The lead collimator had a slit of 0.5 mm width and 19 mm height which defines the beam geometry. The axial gamma scanning was carried out using multichannel analyzer working on multichannel scaling (MCS) mode in which the accumulated counts are stored in subsequent channels and are displayed on computer monitor as the fuel pin was translated across the collimator. The scanning speed of fuel pin was set at 0.034 mm / sec and the counts accumulated under the set photo peak area were integrated after counting for a period of 6 sec.

The gamma-ray spectrum obtained from the spent fuel with a cooling time of about 13 years showed intense gamma ray peaks of ^{137}Cs (661 keV) and ^{134}Cs (604 and 796 keV) and ^{60}Co (1170 and 1330 keV) in almost all types of fuel pins (Fig. 5 & 6) .The presence of 2.6 MeV energy from ^{208}Tl was observed mainly in ThO_2 and (Th-6.75%Pu)O_2 fuel pins (Fig. 5).

The sloping nature of the gamma activity profiles for the MOX pins are indicative of the shape of the neutron flux profile at the irradiation location of tier 1. However, a similar profile was not observed in case of pure urania pins, though they shared the same tier. The gamma activity profiles of thoria containing pins were flat indicating the reasonably flat nature of the neutron flux profile at the irradiation location of tier 2.

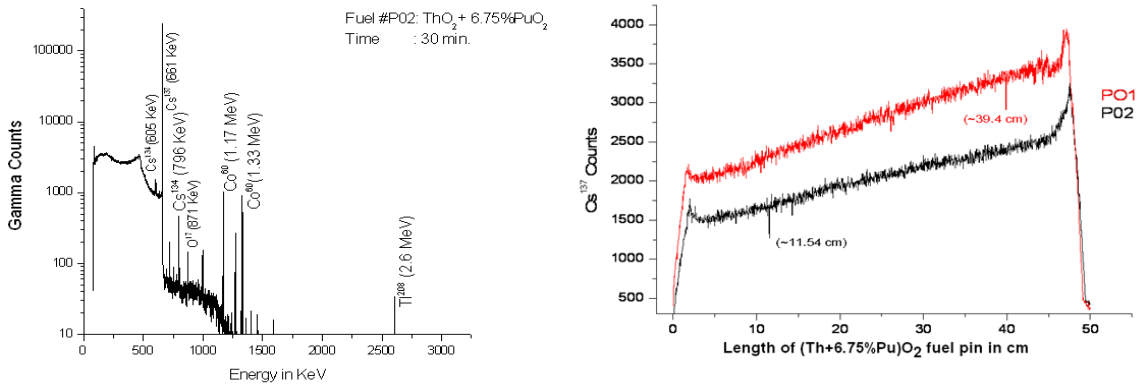

FIG. 5. Gamma spectrum for (Th-6.75%Pu)O_2 fuel (#P02) and axial gamma scanning of #P01 and #P02.

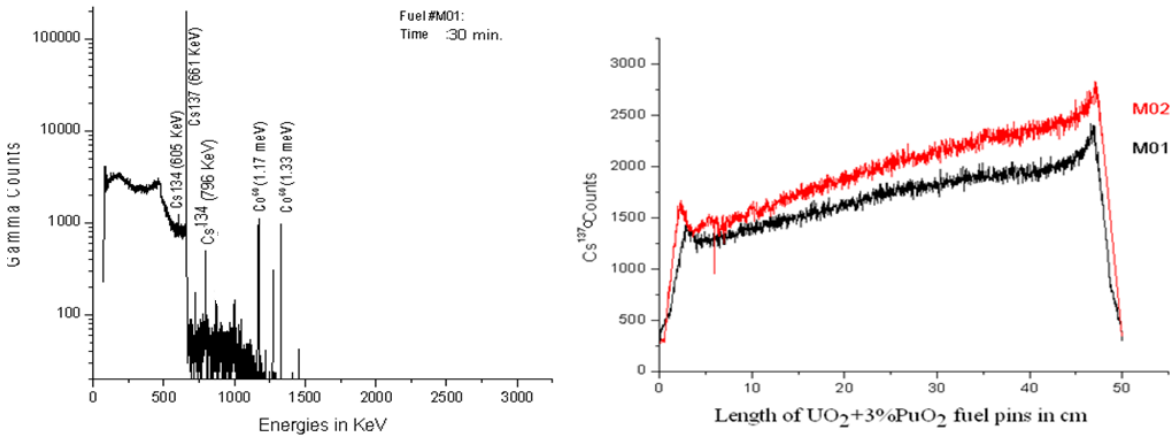

FIG. 6. Gamma spectrum of (U-3%Pu)O_2 fuel (#M-01) and axial gamma scanning of fuel pins#M-01 and #M-02.

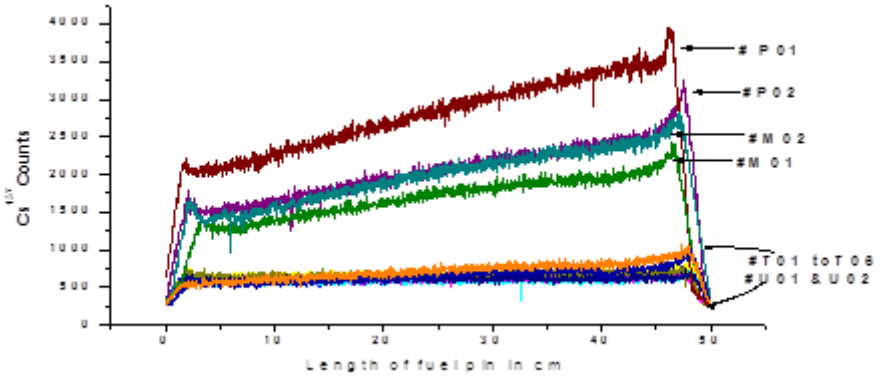

FIG. 7. Gamma activity profile of #U-01, #U-02, #T-01 to #T-06, #M-01,# M-02, #P-01 and #P-02.

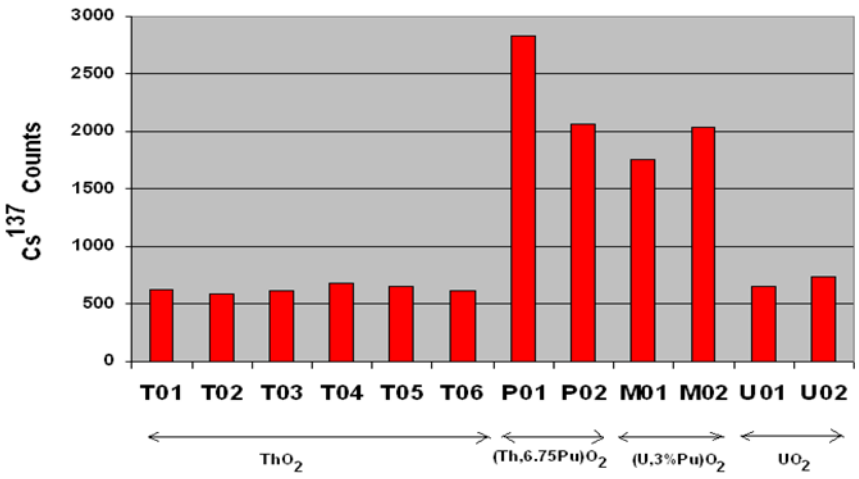

FIG.8. Comparison of average ^{137}Cs activity for all fuel pins.

Results of gamma scanning carried out on all the fuel pins showing the relative counts of ^{137}Cs along the length of the fuel pin are shown in Fig. 7. A relative comparison of the average ^{137}Cs activity of all fuel pins is shown in Fig. 8. This indicates that the contribution to the cluster burnup was in proportion to the fissile element content of the individual fuel pins.

Fission gas release

Measurement of released fission gases on the irradiated fuel pins were carried out by puncturing individual pins under vacuum and collecting the gases. The chemical composition of the released gases was measured using a gas chromatograph. Void volume inside the fuel pin was measured to arrive at the internal pressure of the fuel pins. The results of fission gas release measurements ratio are given in the Table 2. The values of burnup given in the table are estimated from the relative gross gamma activity of the fuel elements and the nominal burnup estimated from reactor operation.

From the table it can be observed that the volume of fission gases released was in proportion to the fissile element content of the fuel pins. The effect of relative locations of the fuel elements on the release has yet to be looked into. The reason for the apparent higher percentage release of fission gases observed in case of pure thoria pins is to be looked into, when the confirmation of the estimated burn ups through radiochemical analysis become available.

TABLE 2. RESULTS OF FISSION GAS RELEASE MEASUREMENTS

Pin ID	Fuel Composition	Burnup (GW·d/t)	Void Volume (cc)	Internal pressure (atm)	Volume of fission gases at STP (cc)	Kr (%)	Xe (%)	Fission Gas Release (%)	Xe/Kr
M-01	UO_2-3.25%PuO_2	7	3.25	1.33	0.07	0.8	1.1	2.8	1.4
M-02	UO_2-3.25%PuO_2	7	2.62	1.59	0.03	0.2	0.7	2.6	3.7
P-01	ThO_2-6.75%PuO_2	12	0.66	2.87	0.75	20.8	23.1	0.8	1.1
P-02	ThO_2-6.75%PuO_2	12	2.25	1.52	0.87	9.9	18.1	1.4	1.8
U-01	UO_2	5	2.25	1.99	0.02	0.3	0.2	3.9	0.7
U-02	UO_2	5	2.57	1.40	0.02	0.3	0.3	3.2	0.9
T-01	ThO_2	4	1.83	2.00	0.02	0.3	0.2	4.4	0.8
T-03	ThO_2	4	2.32	1.53	0.02	0.4	0.3	4.2	0.9
T-04	ThO_2	4	2.71	1.11	0.01	0.3	0.2	3.6	0.8
T-06	ThO_2	4	1.44	2.43	0.03	0.4	0.5	4.3	1.1

Microstructural examination

Metallographic examination has been carried out on samples taken from UO_2, U-Pu MOX and Th-Pu MOX fuel pins designated as U-02, M-02 and P-02 respectively. Metallographic samples were prepared inside the hot cells and examined using a remotised metallograph.

4.1. Pin P-02

The photomacrograph, β-γ autoradiograph and α- autoradiograph of the fuel section taken from the mid-location of the fuel pin are given in Fig. 9. Macroscopic examination of the fuel sections of the fuel pin revealed fine radial cracks. White particles were observed all over the fuel cross sections. The white particles were of different sizes and shape with the largest size being about 800 µm in the fuel section taken from the top end of the fuel. The β-γ autoradiograph of the fuel section revealed low fission product activity from the region of the white particles as compared to the nearby areas. α- autoradiograph of the fuel section revealed lower Pu activity from the white particles. The porosity observed at the periphery and centre of the fuel sections was 6.5% and 6.1 % respectively as compared to 5.4% in the as-fabricated fuel.

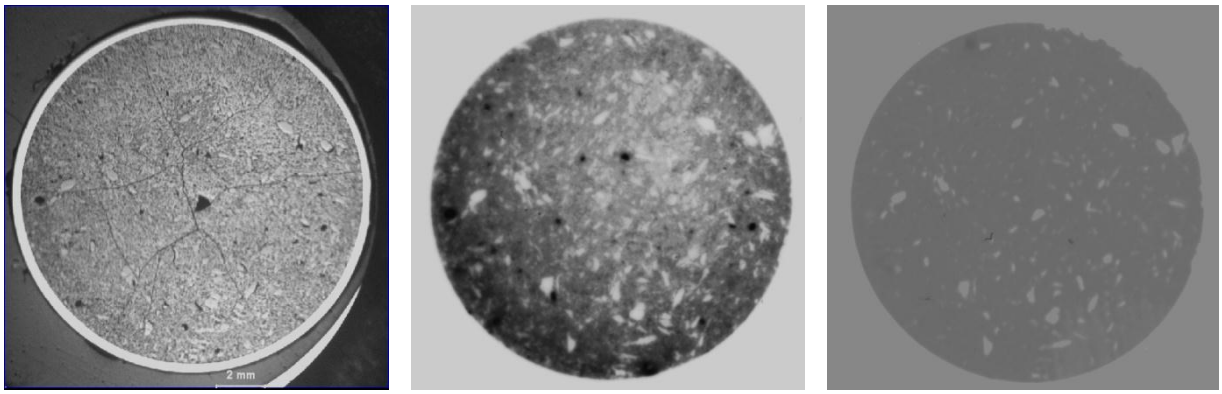

FIG. 9. Photomacrograph, β-γ autoradiograph and α- autoradiograph of the fuel section from P-02.

Continuous oxide layer was observed on the outer surface of the clad with an average thickness of 1.8 µm (Fig. 10a). Oxide layer on the inner surface of the clad was observed at a very few locations with the average thickness1.2 µm (Fig. 10b).

Replicas prepared from the fractured surfaces of the fuel were examined under a scanning electron microscope to measure the grain size in the fuel (Fig. 11). The average grain size in the fuel was 30 µm. Fig. 12a shows a grain of the Th-Pu MOX fuel with one of the grain faces covered with fission gas bubbles. Microstructure of the face of the grain decorated with fission gas bubbles observed at a higher magnification is shown in Fig. 12b.

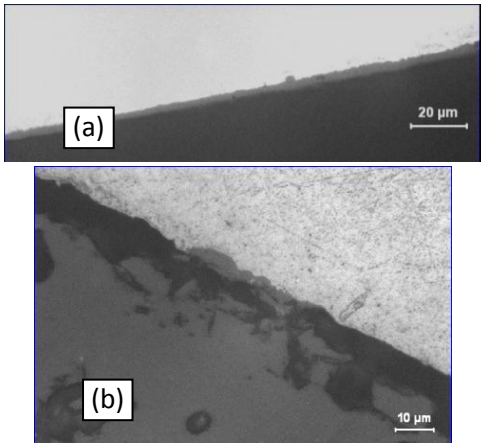

FIG. 10. Oxide layer revealed on the (a) outer and (b) inner surface of the cladding.

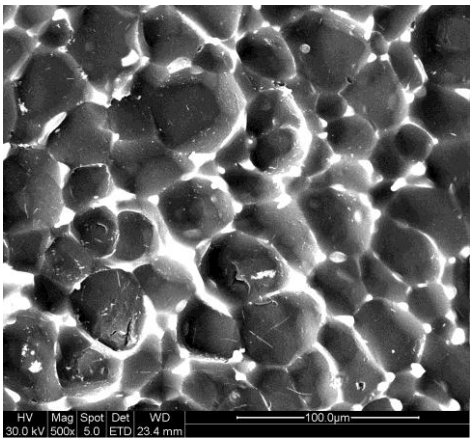

FIG. 11. Replica of the fractured piece of fuel from pin P-02.

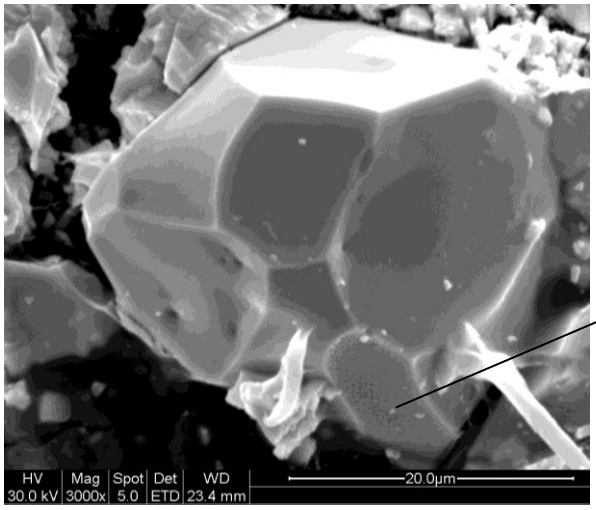

FIG. 12. (a) Single grain of the Th-Pu MOX fuel.

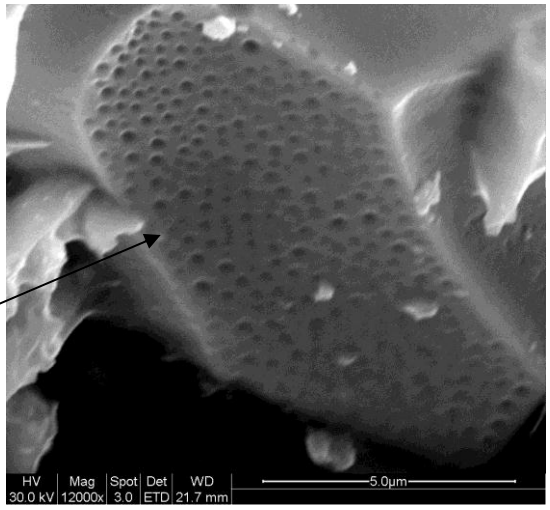

FIG. 12. (b) Face of the grain covered with fission gas bubbles.

4.2. Pin M-02

Macroscopic examination of the fuel sample from the fuel pin M-02 from the normal grain size pellet revealed a number of radial cracks and white spots in the fuel section in the as-polished condition (Fig. 13). The white spots observed in the photo-macrograph correspond to the area of absence of β-γ activity and α activity in the β-γ autoradiograph and the α-autoradiograph, respectively of the fuel section as shown in the Fig. 13. The porosity in the centre and periphery of the fuel section was 4.3 % and 3.7% respectively, which is comparable to the porosity in the as-fabricated fuel.

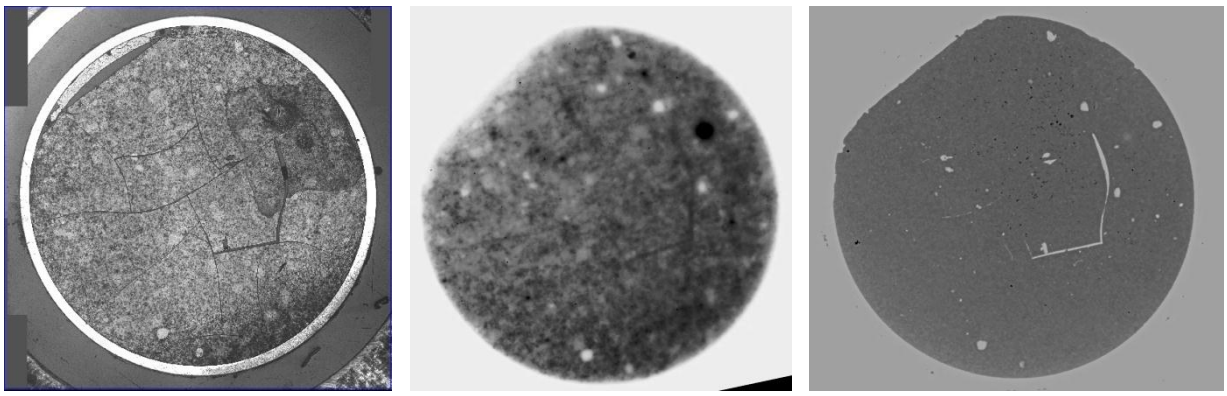

FIG. 13. Photomacrograph, β-γ autoradiograph and α- autoradiograph of the fuel section from pin M-02.

Microscopic examination of the fuel section revealed pores surrounded by a small bright region followed by a dark region. At higher magnification, as shown in Fig. 14, it was observed that the area near the pores was covered by bigger grains of size 12 to 18 µm. These grains were surrounded by smaller grains of size 3–5 µm.

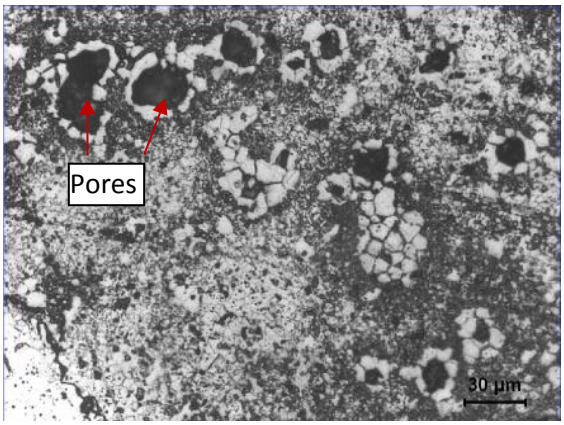

FIG. 14. Pores surrounded by big and small grains.

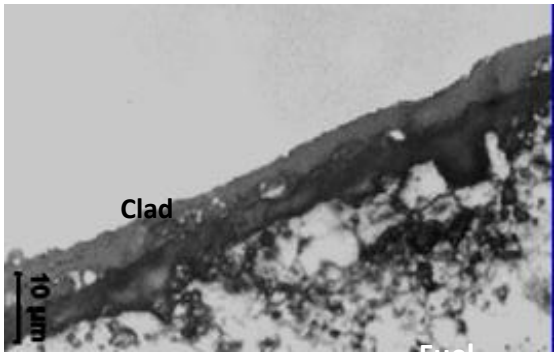

FIG. 15. Oxide layer on the inner surface of the cladding.

Continuous oxide layer was observed on the outer and inner surface of the clad. Average oxide layer thickness on the inner and outer surface of the clad was 3.3 µm and 2.5 µm respectively. Oxide layer on the inner surface of the cladding is shown in Fig. 15.

Examination of the fuel cross section from the large grain size pellet shows a few fine cracks in the fuel and white spots. Fig. 16 shows the photo-macrograph and α-autoradiograph of the sample from a large grain size pellet. General microstructure of the fuel shows bright

and dark patches in the fuel cross section (Fig. 17). Porosity at the centre and periphery of the fuel section was 4.3% and 3.8% respectively as compared to 3.6% in the as-fabricated fuel.

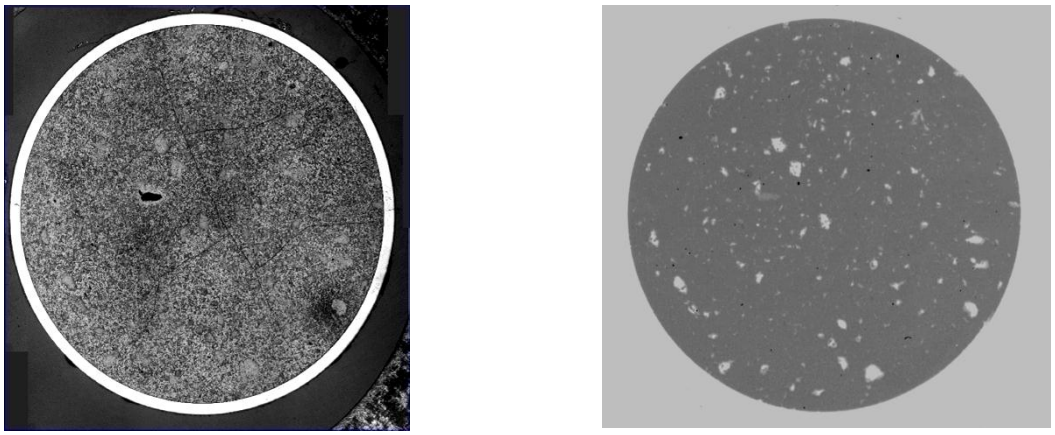

FIG. 16. Photomacrograph and α- autoradiograph.

Examination at higher magnification revealed larger grains with an average size of 30 µm in the bright regions of the fuel and fine grains of the size 5 µm in the dark regions. Larger grains are observed in the vicinity of pores (Fig. 18). The average size of the pore was ~16 µm.

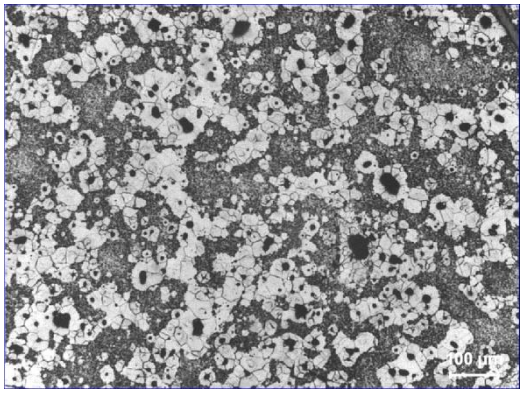

FIG. 17. Bright and dark regions and pores in the fuel.

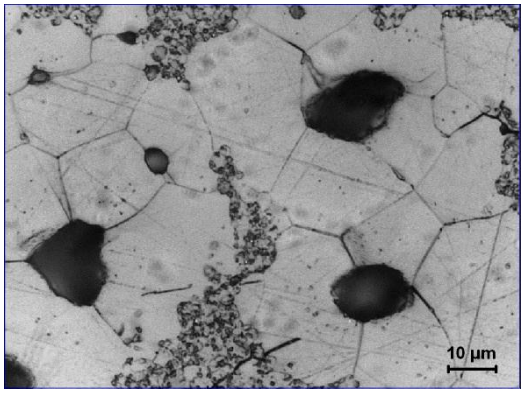

FIG. 18. Pores and large grains.

Continuous oxide layer was observed on the outer and inner surfaces of the clad. Average oxide layer thickness on the inner and outer surface of the clad was 9 µm and 2.3 µm respectively.

5. SUMMARY AND CONCLUSIONS

a) Post irradiation examination of ThO_2-6.75%PuO_2 and U-3%PuO_2 MOX fuel pins of BC-8 cluster irradiated in pressurized water loop of CIRUS up to a nominal fuel burnup of 10.2 GW·d/t has been carried out to assess the irradiation performance of fuel;

b) All the pins were found to be intact after irradiation without any abnormal corrosion;

c) Reduction in the diameter of the fuel pins was observed as compared with their as-fabricated diameter. The maximum clad collapse was observed for (U-Pu)O_2 MOX and UO_2 pins, ThO_2 pins showed minimum collapse with (Th-Pu)O_2 in between;

d) The gamma-ray spectrum obtained from the spent fuel with a cooling time of ~13 years showed intensive gamma ray peaks of ^{137}Cs (661 keV) and ^{134}Cs (604 and 796 keV) and ^{60}Co (1170 and 1330 keV) in almost all type of fuel pins. $^{60}Co$is an activation product present in the clad of the fuel pin. The presence of 2.6 MeV energy from ^{208}Tl was observed mainly in ThO_2 and (Th-6.75%Pu)O_2 fuel pins. The gross gamma activity of the pins indicated that the contribution to the cluster burnup was in proportion to the fissile element content of the fuel pins;

e) PIE observations showed that fission gas release in the fuel pins was in proportion to the fissile element content of the fuel. The reason for the apparent higher percent release of fission gases observed in case of pure thoria fuel elements is to be looked into;

f) Average oxide layer thickness on the outer surface of the cladding was 1.8 µm and 2.5 µm for (Th-Pu)O_2 and (U-Pu)O_2 fuel pins respectively. Oxide layer of about 1.2 µm was observed a very few locations on the inner side of the clad of (Th-Pu)O_2 pin whereas 3.3 µm oxide layer was observed in the (U-Pu)O_2 fuel pin.

MECHANICAL PROPERTY EVALUATION OF HIGH BURNUP PHWR FUEL CLADS

P. K. SHAH, R.S. SHRIWASTAWA, J.S. DUBEY, S. ANANTHARAMAN
Bhabha Atomic Research Centre,
Mumbai, India
Email: pritik@barc.gov.in

Abstract

Assurance of clad integrity is of vital importance for the safe and reliable extension of fuel burnup. In order to study the effect of extended burnup of 15,000 MW·d/tU on the performance of Pressurised Heavy Water Reactor (PHWR) fuel bundles of 19-element design, a couple of bundles were irradiated in Indian PHWR. The tensile property of irradiated cladding from one such bundle was evaluated using the ring tension test method. Using a similar method, claddings of mixed oxide (MOX) fuel elements irradiated in the pressurized water loop (PWL) of CIRUS to a burnup of 10,000 MW·d/THM were tested. The tests were carried out both at ambient temperature and at 300°C. The paper will describe the test procedure, results generated and discuss the findings.

1. INTRODUCTION

Zircaloy (earlier Zircaloy-2 and presently Zircaloy-4) is widely used as cladding alloy for nuclear fuel elements in pressurized heavy water reactors (PHWRs). Fast neutron irradiation and corrosion in the reactor change the mechanical properties of the clad. The performance of fuel depends to a great extent upon the successful performance of the cladding because it is the primary barrier between fuel and the coolant. Mechanical property changes in irradiated cladding can be estimated by several methods e.g. tension test, burst test, ring tension test etc [1]. The stress experienced by the cladding is predominantly hoop stress developed due to internal fission gas pressure and therefore, circumferential strength and ductility of the nuclear fuel claddings are measured to assess their performance in the reactor. As ductility in the circumferential direction of the Zircaloy clad is very important for in-reactor operation, the tension test in this direction can be carried out only by flattening the clad tube section which may not be possible without cracking the tube. Burst test can provide the value for circumferential ductility. However, one needs to utilize a minimum 200 mm length of specimen to obtain a single value of ductility. Ring tension test, in addition to providing a measure of transverse ductility, can yield a better measure of variations in ductility along the 200 mm length, as it requires a ring of around 5 mm width. This ring tensile testing is more suitable for testing of irradiated cladding. This method combines the ease of de-fuelling and relatively lower radiation level with the added advantage of being able to assess local variations in clad properties, e.g. locations with high hydrogen contents.

The normal discharge burnup of a PHWR fuel containing natural UO_2 is about 7,000 MW·D/tU. Use of slightly enriched uranium or mixed oxide fuels will help to extend the discharge burnup leading to better fuel economy. However, increase in burnup leads to higher residence time which means higher corrosion rate and hydrogen pick up of the Zircaloy cladding [2]. The fuel bundle structural components (like spacers) may have to withstand higher fretting. Also, the bundles at high burnup have to face the consequences of power ramps and higher fission gas release and clad local stresses [2].

In order to know the effect of extended burnup on the performance of fuel bundles of current design, a few bundles were irradiated to an extended period in Indian PHWR.

Detailed post irradiation examination (PIE) of one of these fuel bundles (bundle No. 56504 of KAPS-1) was carried out in Post Irradiation Examination Division (PIED) of Bhabha Atomic Research Centre (BARC), India to generate data on the performance at extended burnup, with respect to fuel restructuring, fission gas release, pellet-clad interaction and cladding corrosion and is presented in reference [3]. This paper includes the mechanical property evaluated on the cladding of this fuel bundle. This bundle was loaded in the reactor in November 1995 in the channel L-11 at the 7th string position and had experienced a bundle averaged burnup of 15 000 MW·D/TeU. The total in-reactor residence time was 708 days. The bundle was of the standard 19-element design with natural UO_2 fuel, cladded in Zircaloy-2.

India's nuclear programme envisages a large scale utilisation of thorium, as it has limited deposits of uranium but vast deposits of thorium. As a precursor to the thorium fuel cycle fuels with thorium and mixed oxide fuel materials that can be irradiated to burnups of 20 000 to 50 000 MW·d/TeHM were developed [2]. Such experimental thoria based MOX fuels and thoria were irradiated in Pressurised Water Loop (PWL) of CIRUS reactor [4]. These irradiations were carried with short-length fuel pins of about 500 mm length under simulated power reactor operating conditions. The fuel pin was of PHWR type i.e made of collapsible Zircaloy-2 tube of 15.2 mm OD and 0.4 mm thickness.

2. EXPERIMENTAL

2.1. Material

Mechanical properties were evaluated for Zircaloy-2 (Zr-2) clad material in both unirradiated and irradiated conditions. Irradiated clad tubes were from two different fuel bundles. One fuel bundle had natural UO_2 as fuel and was irradiated in Indian PHWR power reactor KAPS-1 up to a burnup of around 15,000 MW·d/tU. One clad tube (irrd1) from this bundle was tested by ring tension test method.

The second type was an experimental fuel cluster, containing PHWR type fuel elements with collapsible Zircaloy-2 cladding of 15.2 mm OD and 0.4 mm wall thickness, irradiated in the PWL of Indian research reactor CIRUS upto a burnup of around 10,000 RMW·d/tHM. This cluster consisted of twelve fuel elements containing thoria and other types of mixed oxide fuels and also UO_2 fuels. The fuels were arranged in two tiers of six elements each, one below the other. The top six element cluster was in the mid plane of the reactor. This tier had three groups of two fuel elements, each group containing UO_2, UO_2–3%PuO_2, ThO_2–6.75% PuO_2 fuels. The bottom six element cluster had pure ThO_2. Two pins were tested from the experimental fuel cluster out of which one pin (irrd2) was from lower tier having ThO_2 fuel pellets while the other pin (irrd3) was from upper tier having ThO_2-6.75%PuO_2 fuel pellets. Table1 gives the details of the fuel and burnup of the clad tubes tested.

TABLE 1: DETAILS OF THE FUEL PIN FOR CLAD TUBE TESTING

Clad tube ID	Burnup	Fuel
Unirradiated	-	-
Irrd1	15 000 MW·d/TU	Nat. UO_2
Irrd2	10 000 MW·d/THM	ThO_2
Irrd3	10 000 MW·d/THM	ThO_2-6.75%PuO_2

The production of clad tubes involves operations like casting of Zr-2 ingots, hot extrusion, cold pilgering, vacuum annealing. The tensile property requirement was UTS > 483 MPa, YS > 293 MPa and elongation 20% [5] for the Zircaloy-2 clads used in this study.

2.2. Tension test

The estimation of mechanical properties of the fuel cladding was carried out using the ring tension test method on the ring specimens prepared from the fuel pins. The rings of width around 3.0 mm were cut using a slow speed diamond cut-off wheel inside the hot cell. The fuel was removed from the cut rings and the empty clad rings were ground to get rings of uniform width. The ring specimens were then tested in uniaxial tensile loading mode using specially designed grip with two semi-circular mandrels attached to a screw driven machine inside the hot cell. Tests were carried out at room temperature and at 300^0C inside a furnace in air atmosphere at a crosshead speed of 0.25 mm/min.

2.3. Hydrogen analysis, metallographic and SEM study

The fracture surfaces of some of the tested rings were studied in Scanning electron microscope (SEM) and some portion of tested specimens were cut to measure hydrogen content in it.

3. RESULT AND DISCUSSION

Ring tension test was carried out on unirradiated Zircaloy-2 clad as well as on one of the outer fuel pins of fuel bundle 56504 from KAPS1 and two fuel pins from experimental cluster irradiated at CIRUS. Figure 1a shows the typical load-displacement plot obtained in ring tension test of unirradiated clad. The load and crosshead displacement record obtained from the tests were analysed to get the stress-strain data and plot. Typical engineering stress-strain diagrams obtained in testing the unirradiated and irradiated specimens tested at room temperature are shown in Fig. 1b.

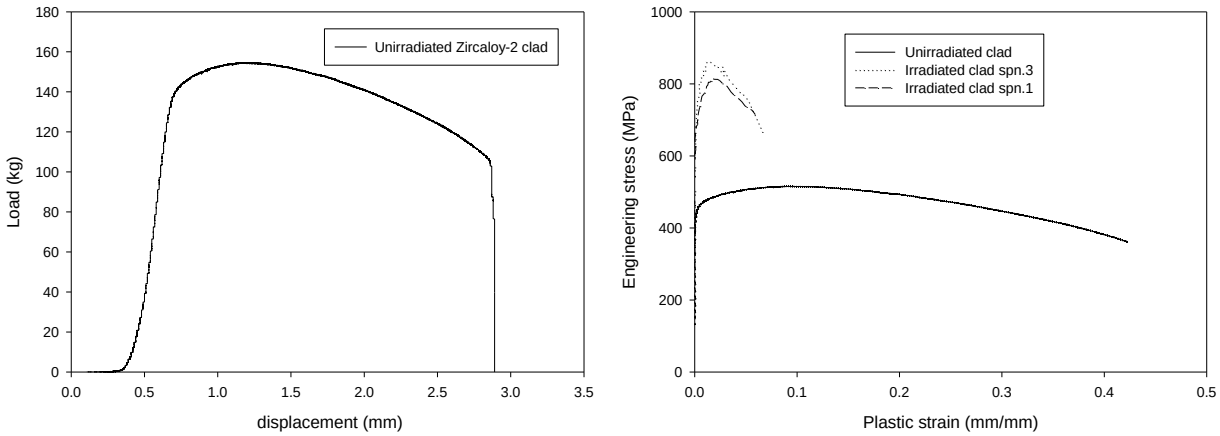

(a) (b)

FIG. 1. (a) Typical load-displacement plot in ring tension test of unirradiated clad and (b) typical engineering stress-strain plot of unirradiated and irradiated clad.

Considering that the irradiated clad specimens have been prepared from the reactor operated fuel elements, the clad has been subjected to factors like oxidation, hydriding, fission product corrosion and these factors are likely to be responsible for the scatter in the irradiated strength values. RTT tests gave good estimate of all the tensile properties. The circumferential tensile properties at room temperature obtained from the ring tension tests are shown in Fig. 2 for the unirradiated and irradiated Zircaloy-2 clad specimens. As seen in the figure it is clear that there is an increase in strength by around 60% and a decrease in ductility by around 80%. Fig. 3 shows the experimental tensile property data obtained in the ring tension test of irradiated and unirradiated Zircaloy-2 clad specimens tested at 300^0C.

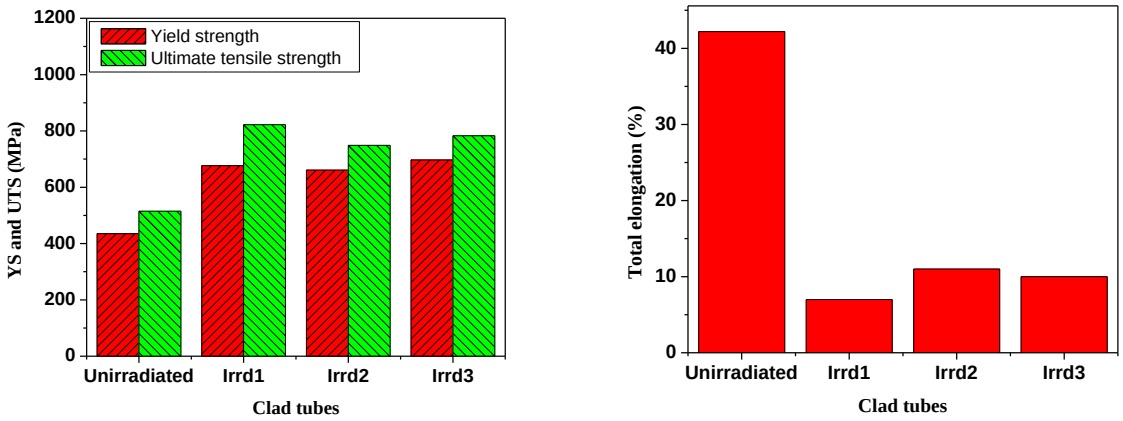

(a) (b)

FIG..2. Room temperature (a) strength and (b) elongation of unirradiated and irradiated clads.

Strength decreased with increasing test temperature for both unirradiated and irradiated clads. When comparing the tensile properties at 300^0C between the unirradiated and irradiated clads, it was found that high burnup clad from PHWR (irrd1) showed 110% higher strength and 30% lower elongation whereas the clads from the experimental fuel bundle showed 60% higher strength and 60% lower elongation compared to the unirradiated clads. It has been observed that unirradiated, irrd1 and irrd2 showed 30% decrease in strength at higher temperature while irrd1 showed 10% decrease in strength compared to their room temperature strength values. When elongation is compred between room temperature and at 300^0C, it was observed that unirraidiated clad didn't show much variation with increasing test temperature while irrd1 showed more than 300% increase in elongation, the clads from experimental cluster (irrd2 and irrd3) showed 90% higher elongation at high temperature compared to their room temperature elongation values. The reason for this difference in high temperature tensile properties between irradiated clads from PHWR (Irrd1) and that from experimental cluster (irrd2 and irrd3) is yet to be analysed. The hydrogen content and the fracture surface of clad from experimental cluster are also yet to be studied.

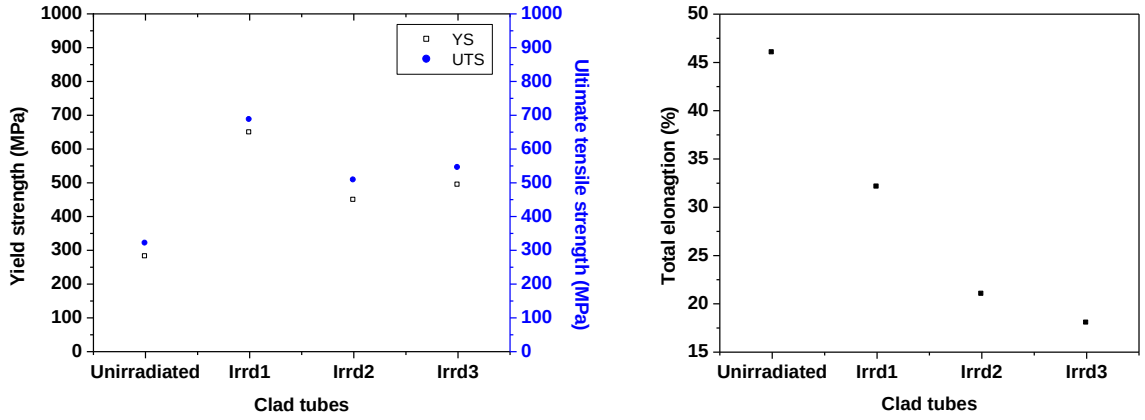

FIG. 3. a) Strength and (b) elongation of unirradiated and irradiated clads at 300^0C.

Fig. 4 shows the photographs of the typical tested ring specimens of unirradiated and irradiated Zr-2 clad. In unirradiated specimen there is pronounced necking along with cup and cone type of fracture indicating ductile failure of the clad. In irradiated specimen the fracture surface is at 45^0 which is also a ductile mode of failure though there is not much necking. Narrow width of the ring specimen often induces a plane stress state across the width which results in a 45^0 shear fracture. In the unirradiated specimen necking is clear at the other side i.e unbroken side of the specimen while necking is not visible at that side in the irradiated specimen.

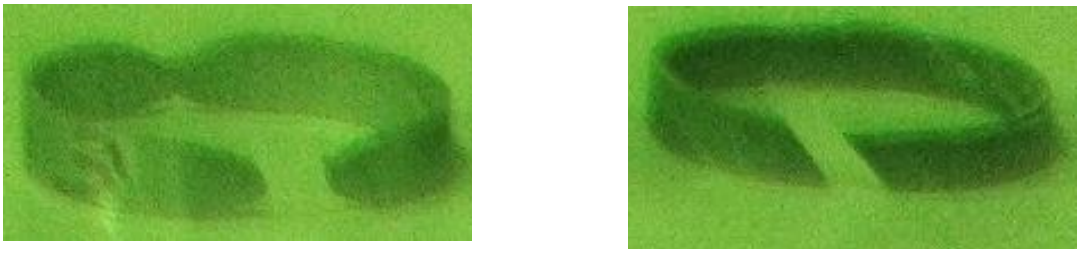

(a) (b)

FIG. 4. Fracture pattern of (a) unirradiated and (b) irradiated (irdd1) tested clads.

In the SEM study, both unirradiated and irradiated clad fracture surface were revealing ductile type fracture the ductility being more in unirradiated clad. Fig. 5 shows the fracture surface of unirradiated and irradiated clad (irdd1) under SEM.

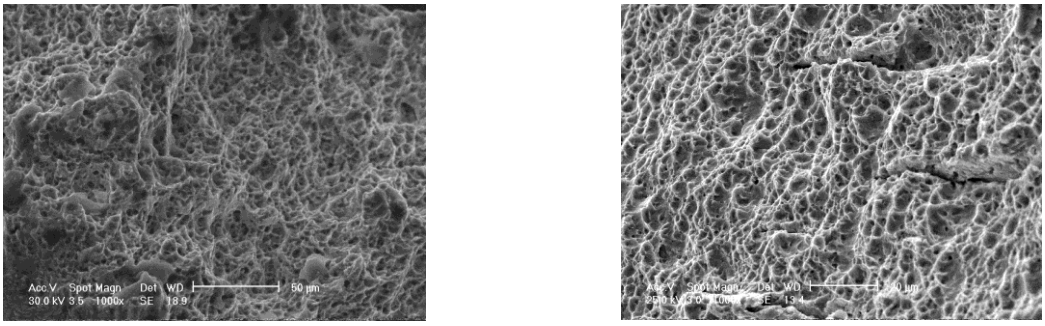

(a) (b)

FIG .5. Fracture surface of (a) unirradiated and (b) irradiated clad (irdd1) specimens under SEM.

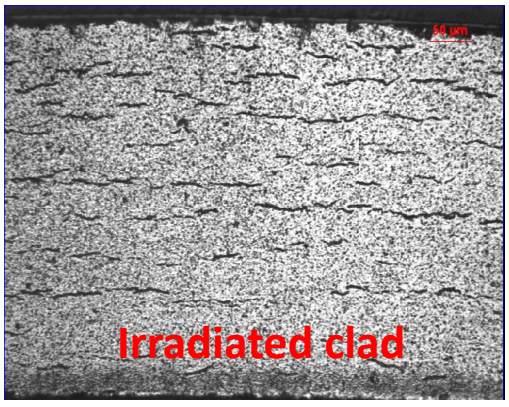

FIG. 6. Circumferential hydrides in the irradiated clad (irdd1).

Circumferentially oriented hydride platelets were observed in the cladding of the high burnup fuel (irdd1) as shown in Fig. 6. The hydrogen content was around 25 ppm in the unirradiated clad and it increased upto 45 ppm in the irradiated clad (irdd1). Average oxide layer thickness at the outer surface of the irradiated cladding was 2.8 μm.

4. CONCLUSIONS

(a) Ring tension test provides useful information on tensile properties of unirradiated and irradiated zircaloy clads;
(b) The ring tension tests on the irradiated cladding indicated that the strength increased by around 60% and the ductility decreased by around 80% at room temperature;
(c) At higher test temperature the strength decreased and elongation increased compared to their room temperature values. The percentage change in properties between room temperature and high temperature was different for clads studied in this experiment;
(d) Hydrogen concentration in the PHWR irradiated clad was around 45 ppm and hydrides were uniformly distributed and circumferentially oriented.

ACKNOWLEDGEMENTS

The authors wish to acknowledge the dedicated support provided by Shri K. B. Gaonkar, Shri H. N. Tripathy and Shri S. B. Deherkar in specimen preparation inside the hotcell remotely. We also acknowledge the contribution of Smt. Prerna Mishra for metallographic study, Shri V. D. Alur for hydrogen estimation and Shri Sunil Kumar for SEM study on irradiated clads.

REFERENCES

[1] CHATTERJEE, S., et. al., Ring Tensile Testing of Irradiated Clad Materials, Report BARC/I-643 (1981).
[2] DWIVEDI, K.P., et. al., "Performance of Zircaloy Cladding in PHWR Fuel Assemblies", Proc. of Theme Meeting in High Burnup Issues in Nuclear Fuels (2005).
[3] SAH, D.N., et. al., "Post-Irradiation Examination of High Burnup PHWR Fuel Bundle 56504 from KAPS-1", Report, BARC/2007/E/002 (2007).
[4] ANANTHARAMAN, K., et. al, Utilisation of Thorium in Reactors, Journal of Nuclear Materials **383** 119 (2008) 121.
[5] MISTRY, R.K., et. al., "Quality Control and Inspection on PHWR Cladding Tubes Made by Hot Extrusion and Cold Pilgering Process", Proc. Symp. on Zirconium Alloys for Reactor Components, ZARC-91 (1991).

ABBREVIATIONS

ADB	Average discharge burnup
AHWR	Advanced heavy water reactor
AM	Analysis margin
AR	Analysis results
BDBA	Beyond design basis accident
BEAU	Best estimate and analysis uncertainty
BFP	Barrier failure point
BOL	Beginning of life
CAA	Composite analytical approach
CGG	Columnar grain growth
CHF	Critical heat flux
CNSC	Canadian nuclear safety commission
CVR	Coolant void reactivity
DAC	Derived acceptance criteria
DBA	Design basis accident
DEGB	Double ended guillotine break
DN	Delayed neutron
ECCS	Emergency core cooling system
EGG	Eqiaxed grain growth
EOL	End of life
FCF	Fuel cycle facility
FCT	Fuel centre temperature
FEM	Finite element method
FGR	Fission gas release
FUDA	Fuel design analysis
HAZ	Heat affected zone

HTR	High temperature reactor
IBIF	Intermittent buoyancy induced flow
KANUPP	Karachi nuclear power plant
KNF	Korea electric power nuclear fuel
LLOCA	Large loss of coolant accident
LOCA	loss of coolant accident
LOE	Limit of operating envelope
LWR	Light water cooled reactor
LVRF	Low void reactivity fuel
MAPS	Madras atomic power stations
MOX	Mixed uranium plutonium oxide
MTF	Margin to failure
MW·d	Mega watt day
NU	Natural uranium
NUE	Natural uranium equivalent
PHTS	Primary heat transport system
PHWR	Pressurized heavy water reactor
PRTF	Power ramp test facility
PVA	Poly vinyl alcohol
RIH	Reactor inlet header
ROH	Reactor outlet header
RU	Reprocessed uranium
SCC	Stress corrosion cracking
SDCS	Shut down cooling system
SEU	Slightly enriched uranium
SGMP	Sol gel microsphere palletisation
SM	Safety margin

LIST OF PARTICIPANTS

Alvarez L. A.	Commission Nacional de Energia Atomica, Argentina
Ananthraman S.	Bhabha Atomic Research Centre, India
Anuradha T.	Nuclear Fuel Complex, India
Armando C. M.	Comision Nacional de Energia Atomica, Argentina
Arora U. K.	Nuclear Fuel Complex, India
Banerjee J.	Bhabha Atomic Research Centre, India
Banerjee S.	Bhabha Atomic Research Centre, India
Baraitaru N.	S.N. Nuclearelectrica S.A, Romania
Basak U.	International Atomic Energy IAEA, Vienna
Bhatt R.	Bhabha Atomic Research Centre, India
Bussolini A. A.	Commission Nacional de Energia Atomica, Argentina
Chauhan A.	Nuclear Power Corporation of India Ltd, India
Chouhan S. K .	Nuclear Power Corporation of India Ltd, India
Das R.	Nuclear Power Corporation of India Ltd, India
El-Jaby A.	Canadaian Nuclear Safety Commission, Canada
Fernando M. P. S.	Nuclear Power Corporation of India Ltd, India
Frigea B.	S.N. Nuclearelectrica S.A, Romania
Gautam A. P.	Nuclear Power Corporation of India Ltd, India
Guo Y.	Canadaian Nuclear Safety Commission, Canada
Gupta L. K.	Nuclear Power Corporation of India Ltd, India
Ionescu S. I.	Institute of Nuclear Research, Romania
Kansal M.	Nuclear Power Corporation of India Ltd, India
Kim Y.-C.	Kepco Nuclear Fuel, Republic of Korea
Kumar A.	Bhabha Atomic Research Centre, India
Kumar A.	Nuclear Power Corporation of India Ltd, India

Kutty P. S.	Bhabha Atomic Research Centre, India
Meghani P. C.	Nuclear Power Corporation of India Ltd, India
Meleg T.	Institute of Nuclear Research, Romania
Mishra A. K.	Bhabha Atomic Research Centre, India
Mishra P.	Bhabha Atomic Research Centre, India
Mishra S.	Nuclear Power Corporation of India Ltd, India
Mohd A.	Bhabha Atomic Research Centre, India
Mukherjee D.	Bhabha Atomic Research Centre, India
Nema A. K.	Nuclear Power Corporation of India Ltd, India
Ohai D.	Institute of Nuclear Research, Romania
Ojha B. K.	Indira Gandhi Centre for Atomic Research, India
Olteanu G.	Institute of Nuclear Research, Romania
Pandey Y. K.	Nuclear Power Corporation of India Ltd, India
Pandit B.	Nuclear Power Corporation of India Ltd, India
Park C.-H.	Kepco Nuclear Fuel, Korea, Republic of
Park J. H.	Korea Atomic Energy Research Institute, Republic of Korea
Parasca L.	S.N. Nuclearelectrica S.A, Romania
Parikh M. V.	Nuclear Power Corporation of India Ltd, India
Pecheanu D.	S.N. Nuclearelectrica S.A, Romania
Prasad P. N.	Nuclear Power Corporation of India Ltd, India
Prodea I.	Institute of Nuclear Research, Romania
Priti Kotak S.	Bhabha Atomic Research Centre, India
Purandare A. K.	Nuclear Power Corporation of India Ltd, India
Rachjmawati M.	Centre for Nuclear Fuel Technology, Indonesia
Ravi M.	Nuclear Power Corporation of India Ltd, India
Rathakrishnan S.	Nuclear Power Corporation of India Ltd, India
Reddy P. V. R.	Nuclear Fuel Complex, India

Reddy D. M.	Nuclear Fuel Complex, India
Rizoiu A.	Institute of Nuclear Research, Romania
Sebastian M. C.	Commission Nacional de Energia Atomica, Argentina
Sheela	Nuclear Fuel Complex, India
Setty D. S.	Nuclear Fuel Complex, India
Shivakumar V .	Bhabha Atomic Research Centre, India
Sowrinathan C. R.	Indira Gandhi Centre for Atomic Research, India
Suk C.-K.	Kepco Nuclear Fuel, Korea, Republic of
Tasneem F.	Karachi Nuclear Power Plant, Pakistan
Tripathi R. M.	Nuclear Power Corporation of India Limited, India
Trpathi M.	Nuclear Power Corporation of India Ltd, India
Vinay V.	Bhabha Atomic Research Centre, India
Williams A. F.	Atomic Energy Canada Limited, Canada
Yadav S. K.	Nuclear Power Corporation of India Ltd, India
Zalog C.	S.N. Nuclearelectrica S.A, Romania

Technical Meetings

Bucharest, Romania: 24–27 September 2012

Mumbai, India: 8–11 April 2013